STAR (1+32)

NASA CONTRACTOR
REPORT

NASA CR-171317

(NASA-CR-171317) RESEARCH REPORTS: 1984 NASA/ASEE SUMMER FACULTY FELLOWSHIP PROGRAM (Alabama Univ., Tuscaloosa.) 776 p HC A99/MF E03 CSCL 05I G3/80

N85-22210 THRU N85-22242 Unclas 14501

RESEARCH REPORTS - 1984 NASA/ASEE SUMMER FACULTY FELLOWSHIP PROGRAM

The University of Alabama
Tuscaloosa, Alabama
and
The University of Alabama in Huntsville

January 1985

Prepared for

NASA-GEORGE C. MARSHALL SPACE FLIGHT CENTER
Marshall Space Flight Center, Alabama 35812

RESEARCH REPORTS

1984 NASA/ASEE SUMMER FACULTY FELLOWSHIP PROGRAM

George C. Marshall Space Flight Center
The University of Alabama

and

The University of Alabama in Huntsville

EDITORS:

Dr. L. Michael Freeman
Assistant Professor of Aerospace Engineering
The University of Alabama

Mr. T. Leroy Osborn
Office of University Affairs
Marshall Space Flight Center

Dr. James B. Dozier
Director, Research and Technology Office
Marshall Space Flight Center

Dr. Gerald R. Karr
Professor of Mechanical Engineering
The University of Alabama in Huntsville

NASA CR - 171317

TECHNICAL REPORT STANDARD TITLE PAGE

1. REPORT NO.	2. GOVERNMENT ACCESSION NO.	3. RECIPIENT'S CATALOG NO.
NASA CR-171317		

4. TITLE AND SUBTITLE	5. REPORT DATE
1984 NASA/ASEE Summer Faculty Fellowship Program	January 1985
	6. PERFORMING ORGANIZATION CODE

7. AUTHOR(S)	8. PERFORMING ORGANIZATION REPORT #
Editors: M. Freeman, L. Osborn, J. Dozier, and G. Karr	

9. PERFORMING ORGANIZATION NAME AND ADDRESS	10. WORK UNIT NO.
The University of Alabama Tuscaloosa, Alabama and The University of Alabama in Huntsville	11. CONTRACT OR GRANT NO. NGT-01-002-099

12. SPONSORING AGENCY NAME AND ADDRESS	13. TYPE OF REPORT & PERIOD COVERED
National Aeronautics and Space Administration Washington, D. C. 20546	Contractor Report
	14. SPONSORING AGENCY CODE

15. SUPPLEMENTARY NOTES

16. ABSTRACT

For the twentieth consecutive year, a NASA/ASEE Summer Faculty Fellowship Program was conducted at the Marshall Space Flight Center (MSFC). The program was conducted by the University of Alabama and MSFC during the period May 29, 1984, through August 3, 1984. Operated under the auspices of the American Society for Engineering Education, the MSFC program, as well as those at other NASA Centers, was sponsored by the Office of University Affairs, NASA Headquarters, Washington, D.C. The basic objectives of the programs, which are in the twenty-first year of operation nationally, are (1) to further the professional knowledge of qualified engineering and science faculty members; (2) to stimulate an exchange of ideas between participants and NASA; (3) to enrich and refresh the research and teaching activities of the participants' institutions; and (4) to contribute to the research objectives of the NASA Centers.

The Faculty Fellows spent ten weeks at MSFC engaged in a research project compatible with their interests and background and worked in collaboration with a NASA/MSFC colleague. This document is a compilation of Fellows' reports on their research during the summer of 1984. The University of Alabama Report No. BER-332-94 presents the Co-Directors' report on the administrative operations of the program. Further information can be obtained by contacting any of the editors.

17. KEY WORDS	18. DISTRIBUTION STATEMENT
Data base management, Composite materials, computational fluid dynamics, mass spectrometry, robot arc welding, space debris, expert systems, optimization of resources, cryogenics, brittle materials, atmospheric models, atomic oxygen exposure, germanium thermometers, solar wind gradients, x-ray gratings	Unclassified - Unlimited W. T. Carey, Director, Executive Staff — 1/30/85 Date

19. SECURITY CLASSIF. (of this report)	20. SECURITY CLASSIF. (of this page)	21. NO. OF PAGES	22. PRICE
Unclassified	Unclassified	775	NTIS

MSFC - Form 3292 (Rev. December 1972)

For sale by National Technical Information Service, Springfield, Virginia 22151

PREFACE

For the twentieth consecutive year, a NASA/ASEE Summer Faculty Fellowship Program was conducted at the Marshall Space Flight Center (MSFC). The program was conducted by the University of Alabama and MSFC during the period May 29, 1984, through August 3, 1984. The program was operated under the auspices of the American Society for Engineering Education (ASEE). The program at MSFC, as well as those at other NASA Centers, was sponsored and funded by the Office of University Affairs, NASA Headquarters, Washington, D. C. The basic objectives of the programs, which are in the twenty-first year of operation nationally, are:

a. To further the professional knowledge of qualified engineering and science faculty members;

b. To stimulate an exchange of ideas between participants and and NASA;

c. To enrich and refresh the research and teaching activities of participants' institutions; and,

d. To contribute to the research objectives of the NASA Centers.

The Faculty Fellows spent ten weeks at MSFC engaged in a research project compatible with their interests and background and worked in collaboration with a NASA/MSFC colleague. This document is a compilation of Fellows' reports on their research during the summer of 1984. The University of Alabama Report No. BER-332-94 presents the Co-Directors' report on the administrative operations of the program. Further information can be obtained by contacting any of the editors.

TABLE OF CONTENTS

1984

NASA/ASEE SUMMER FACULTY RESEARCH FELLOWSHIP PROGRAM

MARSHALL SPACE FLIGHT CENTER
THE UNIVERSITY OF ALABAMA

USING A DATA BASE MANAGEMENT SYSTEM FOR MODELLING SSME TEST HISTORY DATA

Prepared By:	Kenneth Abernethy, Ph.D.
Academic Rank:	Associate Professor
University and Department:	Furman University Computer Science
NASA/MSFC:	
Laboratory:	Structures and Propulsion
Division:	Propulsion
Branch:	Liquid Engine
NASA Counterpart:	Jan Monk
Date:	August 10, 1984
Contract No.:	NASA-NGT-01-002-099 (The University of Alabama)

Acknowledgements

The author would like to express his appreciation for the opportunity to participate in the NASA/ASEE 1984 Summer Faculty Fellowship Program at Marshall Space Flight Center. Much credit is due Mike Freeman, Jim Dozier and Leroy Osborn for their excellent administration of the program and their sincere efforts to make the experience a professionally stimulating one. The author is especially grateful to his NASA counterpart, Jan Monk, for suggesting a meaningful and challenging project and for providing the necessary help and advice for the project's successful completion.

D1

Using a Data Base Management System for Modelling SSME Test History Data

Kenneth Abernethy
Associate Professor of Computer Science
Furman University
Greenville, South Carolina

ABSTRACT

This report summarizes the results of a study whose primary purpose was to assess the usefulness of a data base management system (DBMS) for modelling historical test data for the complete series of static test firings for the Space Shuttle Main Engine (SSME). From an analysis of user data base query requirements, it became clear that a relational DBMS which included a relationally complete query language would permit a model satisfying the query requirements. Furthermore, it was determined that significant percentages of the user query set could be satisfied by network or hierarchical models with somewhat weaker query languages. Representative models and sample queries are discussed in this report.

A list of environment-particular evaluation criteria for the desired DBMS was constructed; these criteria include requirements in the areas of user-interface complexity, program independence, flexibility, modifiability, and output capability. Relative to these criteria, several DBMS's currently available at Marshall Space Flight Center were evaluated, and the results of these evaluations are given in this report. The evaluation process included the construction of several prototype data bases for user assessement. The systems studied, representing the three major DBMS conceptual models, were: MIRADS, a hierarchical system; DMS-1100, a CODASYL-based network system; ORACLE, a relational system; and DATATRIEVE, a relational-type system. MIRADS and DATATRIEVE prototypes allowed users to make some meaningful evaluations concerning user-interface complexity, and to make recommendations concerning the particular data chosen for data base inclusion.

Some conclusions are drawn that support the feasibility of implementing a full-scale historical test data DBMS model. Recommendations are offered concerning general requirements and constraints to be placed on such a DBMS. Finally, the capabilities and usefulness of the particular systems studied are summarized and compared, and specific recommendations are made concerning the desirability of these systems for the SSME historical test data DBMS.

Note: MIRADS is a Marshall Space Flight Center developed DBMS.
DMS-1100 is a registered trademark of Sperry Rand Corporation.
ORACLE is a registered trademark of Relational Software Incorporated.
DATATRIEVE is a registered trademark of Digital Equipment Corporation.

Introduction

This report summarizes the results of a study whose primary purpose was to assess the usefulness of a data base management system (DBMS) for modelling historical test data for the complete series of static test firings for the Space Shuttle Main Engine (SSME). This assessment required answers to two major questions. First, could a DBMS support, in a high level interactive mode, the kinds of queries which must be made against the historical test data base? Assuming an affirmative answer to this question, which of the several distinct conceptual models of DBMS's available would be best suited for the required data base/query system?

In order to answer the first of these questions, a study was made of various user requirements, and a list of sample queries was constructed. Using the collected query set, several alternate models of the historical data base were considered. From this analysis, it became clear that a relational DBMS which included a relationally complete query language would certainly permit a model satisfying the query requirements. Furthermore, it was determined that significant parts of, and in some cases all, the query set could be satisfied by network or hierarchical models with weaker query languages. Representative models and sample queries are discussed in sections 3-6.

The second question mentioned above is by its nature a subjective one. To provide an objective framework for attempting an answer, a list of evaluation criteria for the desired DBMS was drawn up. These criteria include requirements concerning user-interface complexity, program independence, flexibility, modifiability, output capability, and current system compatibility. Evaluation, relative to these criteria, was then undertaken for several systems currently available at MSFC. Results of the evaluation of four systems, representing the major data base conceptual models, are presented in this report. In section 3, MIRADS, a hierarchical system, is evaluated; in section 4, DMS-1100, a CODASYL-based network system, is evaluated; ORACLE, a relational system, is examined in section 5; finally, DATATRIEVE, a relational-like system is investigated in section 6. A comparative analysis of these four systems is then done in section 7. Summary conclusions and recommendations are included in a final section.

It was decided that a prototype historical test data DBMS model would be useful for several reasons: to provide users an opportunity to experiment with a DBMS model and thus participate more meaningfully in the DBMS choice process; to provide first hand evaluation of the particular system chosen; and to minimize any potential user resistance to the eventual "production" system. Such a prototype was constructed using DATATRIEVE, and supporting user documentation was written and distributed to users, so that an evaluation of the system could be made. The details of this implementation and a system User's Guide can be obtained from the author or his NASA counterpart.

Objectives

The primary objective of this study is to draw some conclusions concerning the feasibility of implementing a data base management system (DBMS) for the management of SSME historical test data . In addition, an analysis is planned to identify the general requirements and constraints that should be placed on such a system, as well as to examine the capabilities and usefulness of several particular DBMS's. Specific recommendations are planned concerning the desirability of these systems for the implementation of a SSME historical test data DBMS. A prototype data base is envisioned using one of the particular systems studied in order to provide for user evaluation. However, the major emphasis is to be placed on the more general, product-independent recommendations for several reasons. First, these recommendations should be valid guidelines not only for the present DBMS choice, but also for later DBMS update/change decisions; second, there is an active MSFC request-for-proposal for a major new addition in computer hardware, and it seems reasonable that no final decision be made on a particular DBMS until the identity and DBMS support capabilities of the new hardware is known.

1. DBMS Feasibility.

In this section, we address the question of whether a DBMS is an appropriate system for handling the data storage and retrieval which is characteristic of the applications using the historical SSME test data. At first glance, the answer appears to be affirmative based on two observations.

The first observation is that the storage/update requirements placed on the historical SSME data are well matched to the capabilities of a typical DBMS. In particular, the format of the data is reasonably consistent over a long period of time, and the kind of updating involved doesn't require any restructuring of data storage, but rather is dominated by simple insertions of new data. Second, the required information retrieval is highly variable and unpredictable. Each test firing produces a unique set of questions, many of which have not been previously posed. A traditional data file scheme could be accessed for this information, but almost always at the cost of either modifying or writing new procedural language programs. Not only the direct cost but the time involved in such program writing/updating is prohibitive. The fourth generation query languages provided with most DBMS's would seem to be a ready solution to the problem of providing quick responses to diverse, unpredictable queries.

However, one important question remains before we can confidently say that a DBMS is the preferred tool for handling the historical SSME data storage/retrieval. Would a DBMS and its query language support the range of queries to be made against the given data? In order to answer this question, a list of queries, representing a wide range of conceptually different retrievals, was constructed and analyzed.

Before looking at the query list, we must discuss the contents of the data base itself. The data is collected and organized by test number. For each test number is recorded several categories of information: the engine number of the engine tested, the date of the test, the programmed and actual durations of the test, the total amount of time the engine was operating at or above certain power levels, serial numbers and unit numbers of various parts and subassemblies of the engine, values and descriptions of certain fixed (pre-set) parameters, and observations of some 300 or so test parameter values at times spaced as little as .01 seconds apart. Each test could produce several hundred thousand distinct data observations, depending upon its duration. Several hundred tests are done each year, and test records which are several years old are frequently consulted during queries. The total data volume for the entire series of SSME tests would be measured in billions of bytes, most of which would consist of observations of test parameters at various times.

Fortunately, not all of the data collected is needed for the SSME historical data base. Indeed, only a small percentage of the data described above is needed. In particular, the vast amount of data

collected on each test parameter can be replaced in the historical data base by values which represent that data in highly condensed, summarized form (maximum values, minimum values, averages, values at particular times, etc.). Also, the number of test parameters of long-term interest is considerably smaller than the total number of test parameters. When these factors are considered, the physical size of the historical data base becomes much more manageable.

Now that we have described the data contents of the historical test data base, we will construct a list of queries that illustrates a range of conceptually different questions that could be asked about this data. We will then address the question as to whether this query list could be satisfied by a DBMS and a fourth generation query language. In order to describe how the queries in the query set differ conceptually, we first put the data into several natural categories. Then we can formulate the queries in terms of these categories to make their distinctions clearer.

Category A will contain for each test number the information related to that test which is "one of a kind" data, i.e. which is not part of a "group" of like data for that test. Categories B.1, B.2, B.3, and B.4 all contain natural groupings of like data for a given test. The different B categories are not related directly to each other, but are indirectly linked by belonging to the same test number in category A. Figure 1.1 illustrates these categories and their data contents.

Category A
Test number
Engine number
Date of test
Cut-off method
Programmed duration
Actual duration
Time < RPL
Time >= RPL
Time >= FPL

Category B.1	Category B.2	Category B.3	Category B.4
Fixed parameter id number	Part serial number	Variable parameter id number	Comments
Fixed parameter value	Part description	Units of measurement	
	Part unit number	Maximum value	
		Minimum value	

FIGURE 1.1
Data Categories

We will classify a given query based upon two factors: in which category the desired information is qualified (determined), and from which category it is actually retrieved. For example, we will call a retrieval a 'B.1 to A' retrieval if the qualification is done in category B.1 and the information is retrieved from category A. Graphically we would illustrate this query by placing an arrow from B.1 to A of the form o⟶ . The queries have been kept as simple as possible, and are not to be taken as examples of queries that actually might be required for any particular application. More complex queries can be built from these basic queries as we will see later.

Query 1.1 Find the test numbers and engine numbers for all tests for which the actual duration is larger than 300 seconds.

A to A query :  (qualification/retrieval on same record)

Query 1.2 For all tests on engine #2208, report the maximum value of variable parameter #260.

A to B.3 query: A o⟶ B.3

Query 1.3 For all tests using engine #2208, report the maximum value of variable parameter 260, the value of fixed parameter #10, and HPOTP serial number.

A to B.1, B.2, B.3 query: 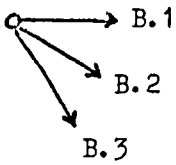

Queries 1.4-1.6 are all 'B to A' queries. They differ in the way the qualification in B is accomplished.

Query 1.4 Find test numbers and engine numbers for all tests where the maximum value of variable parameter #260 exceeds 120.6.

B.3 to A query: A ⟵o B.3 (simple qualification in B.3)

Query 1.5 Find engine numbers for all tests in which variable parameter #260 exceeds 120.6 or #270 exceeds 100.

B.3 to A query: A ⟵o B.3 (or qualification in B.3)

Query 1.6 Find engine numbers for all tests in which parameter #260 exceeds 120.6 and #270 exceeds 100.

B.3 to A query: A ⟵o B.3 (and qualification in B.3)

Queries 1.7 and 1.8 exhibit qualifications involving several B categories at once, connected by 'or' and 'and'.

Query 1.7 Find the engine numbers for all tests where variable parameter #260 exceeds 120.6 and fixed parameter #10 has value 'A603'.

B.1,B.3 to A query:

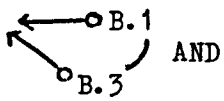

Query 1.8 Find engine numbers for all tests where variable parameter #260 exceeds 120.6 or fixed parameter #10 has value 'A603".

B.1,B.3 to A query:

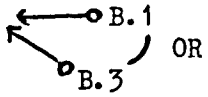

Query 1.9 Find the serial numbers of HPOTP for all tests in which variable parameter #260 exceeds 120.6.

B.3 to B.2 query: (through A by test number)

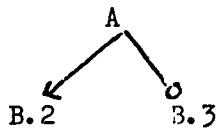

Query 1.10 Find the maximum value of variable parameter #260 for all tests in which the maximum value of parameter #270 exceeds 108.6.

B.3 to B.3 query: (through A)

(qualification/retrieval on different records)

There are, of course, other queries that can be made against the above data, but queries 1.1-1.10 represent a wide conceptual range of queries which includes the conceptual equivalents of all queries deemed likely to occur in current applications of the SSME historical data base. Taking an easily derived, natural relational data base model (very similar to the category structure above), it can be shown that a relationally complete query language will satisfy all of the queries in the above list. We verify this by writing all the above queries in SQL in section 5. In fact, we will illustrate the query set for each of the models in our comparative study in sections 3-6.

2. DBMS Evaluation Criteria.

In the previous section, it was established that a DBMS could provide the functions needed in accessing and effectively using a SSME historical data base. As mentioned in the Introduction, there are three essentially different data base conceptual models. The question as to which of the models might best meet the SSME historical data base needs is difficult to answer because of the many subjective decisions to be considered. In order to better attempt an answer to this question, and also to make comparisons among various particular DBMS's (even of the same conceptual type), we will develop a set of criteria which are especially tailored to the applications and environment relevant to the SSME historical data base. After some preliminary observations, we list the criteria decided upon, broken into several broad categories.

First, we note that there are several query language capabilities which are particularly important for the intended application. Since much of the data involved is numerical, it would be very advantageous to have both a computational capability and a graphical output capability within the query language. Additionally, as we discussed in section 1, the nature of the queries change rapidly, and also the intent of many of the queries is exploratory. Consequently, the capability of storing queries as "procedures" or "subroutines" that could be called by passing parameters, and thus changing the query, would be a very valuable feature. Since most of the procedural language applications programs currently in use with the SSME historical data are written in FORTRAN, it is desirable that the DBMS have a reasonably comprehensive and easy to use FORTRAN interface capability. However, the importance of a FORTRAN interface would be inversely proportional to the strength and flexibility of the query language in such areas as procedure-definition and graphical output capabilities. Finally, since system start-up and maintenance must be accomplished by staff already obligated to ongoing projects, the complexities of system implementation/maintenance and use must be minimized.

Taking into account the above environment-particular factors as well as factors applicable to most any environment, the criteria list given in Table 2.1 was constructed. The reader will notice the absence of any performance related or concurrency criteria in Table 2.1. With many DBMS implementations, system performance is an overriding concern; however, in the applications of the SSME historical data base, performance parameters of the DBMS are relatively unimportant. The anticipated density of SSME data base queries is relatively small (less than 100 per day, maximum), and the likelihood of concurrent updating/reading is small. Consequently, the performance and concurrency control capabilities of any commericially available DBMS would probably be more than adequate for this environment. However, benchmark information should be sought for confirmation of performance adequacy before any final implementation decision.

Evaluation Criteria for SSME Historical Data DBMS

A. Query Language.
   1. Is the query language interface user-friendly?
   2. Does the query language have computational capability?
   3. Does " " " " data update " ?
   4. Does " " " " graphical output capability?
   5. Can queries be nested?
   6. Can query sets be saved as parameter-accepting procedures?
   7. What is the retrieval power of the language?

B. Procedural Language Interface.
   1. Is a FORTRAN interface available?
   2. How complex is the interface?
   3. Is the embedded data manipulation language (DML) non-navigational?
   4. Does the DML require complex currency indicator awareness by the user?
   5. Does the DML allow program independence of the physical data base storage?

C. Implementation/Maintenance Complexity.
   1. Is the data definition language (DDL) easy to use?
   2. How complex are content updating procedures?
   3. How " " data dictionary updating procedures?
   4. How " " file reorganization " ?
   5. How " " index reorganization " ?

TABLE 2.1

3. MIRADS Evaluation.

MIRADS (Marshall Information Retrieval and Display System) is a data management system developed at Marshall Space Flight Center, implemented on the UNIVAC 1108. It uses a hierarchical data model; no secondary hierarchies are allowed. In this section we evaluate MIRADS using the evaluation criteria of Table 2.1. This evaluation along with similar evaluations of DMS-1100, ORACLE, and DATATRIEVE will be summarized in Table 7.1.

Query Language. The MIRADS query language is relatively user-friendly and it includes a reasonable computational capability. There is also an update capability within the query language, and query sets may be saved for later use. However, these saved query sets may not have parameters passed to them. Partial parameter-passing capability may be achieved by saving a part of the total query set and then inserting the parameter-dependent part of the query set at execution time. Nested queries are not allowed, and there is no graphical output option available. The query language is not relationally complete. In fact, the retrieval capabilities of the language depend explicitly upon the particular hierarchical data base structure chosen; but, no matter

how this structure is chosen, there are some of the queries in query set 1.1-1.10 that can not be satisfied. We illustrate at the end of this section.

Procedural Language Interface. The MIRADS procedural language interface capability is quite primitive. There are two ways to accomplish this interface. The first way is by saving the hitfile (the file of retrieved records under some query) from a query set and accessing it from within the procedural language. Since the query set construction and execution is completely external to the procedural language program, the "interface" is extremely weak, and this would not appear to be a very useful feature for most applications. The true interface is accomplished by an embedded data manipulation language (DML). However, this DML is very limited, consisting basically of two routines, WRITES and READS. The WRITES routine is used to write the original data to the MIRADS master file. The READS routine does provide a way to extract information from the data base from within a FORTRAN program, but it depends upon having the record number of the sought record passed to it as a parameter. Hence, the DML is navigational in the extreme; the user must know the internal location of the record he wishes to extract. Of course this also means that changes in the data base physical storage (a record insertion/deletion, for example) would likely force changes in procedural language applications programs using READS, a situation which is highly undesirable.

Implementation/Maintenance Complexity. The data definition facility in MIRADS is not complicated and is quite easy to use. The data dictionary is constructed by a MIRADS subroutine acting on a user-supplied input file, which contains the relevant field and hierarchy information. The construction of the input file is straightforward. The loading of the original data base contents from a data file(s) requires a user-written program calling the MIRADS routine WRITES, but the use of WRITES is reasonably direct. One limitation is that record hierarchy families must be written to the data base in the proper order, but this is standard for most hierarchical systems. Other details such as word alignment of numeric fields, do have to taken into account, but the level of complexity is not overly burdensome. A major shortcoming is the lack of a secondary hierarchy capability, which places severe limitations on the retrievals that are possible (as we will see below). Index reorganization and file reordering are accomplished fairly easily using MIRADS supplied routines. Data base content updating is managed by on-line (query language) updating together with subsequent index and file reorganization using the MIRADS routines, or can be done by "re-implementing" the data base from data input files, which is not too difficult. However, file structure reorganization and data dictionary updating can not be done automatically within MIRADS, and require coordinated updating of the user-written loading program and data dictionary input file.

Query Set 1.1-1.10 in MIRADS. The most natural hierarchy of files for the SSME data would be one very similar to the above category structure (Figure 1.1). In particular, we take the structure given in the conceptual hierarchy in Figure 3.1 as our underlying hierarchy.

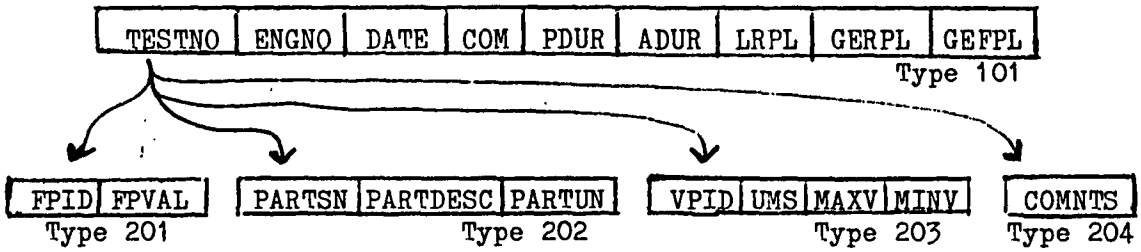

Field-name Key:

TESTNO=Test number
ENGNO=Engine number
DATE=Date of test
COM=Cut-off method
PDUR=Programmed duration
ADUR=Actual duration
LRPL=Time below RPL
GERPL=Time at/above RPL
GEFPL=Time at/above FPL
FPID=Fixed parameter id number
FPVAL=Fixed parameter value
PARTSN=Part serial number
PARTDESC=Part description
PARTUN=Part unit number
VPID=Variable parameter id
UMS=Units of measurements
MAXV=Maximum value of VPID
MINV=Minimum value of VPID
COMNTS=Comments

FIGURE 3.1
MIRADS Hierarchy

We will see that this "natural" hierarchy limits the information retrievals that we can make in MIRADS quite severely. Unfortunately, there is no satisfactory way to remedy this. In the MIRADS version of query set 1.1-1.10 given below, and in later sections, the field-name key in Figure 3.1 will be used.

Query 1.1-M (we will not restate the queries- refer to section 1)

```
QUERY, ADUR>300
PRINT, TESTNO,ENGNO
```

Query 1.2-M

```
QUERY, ENGNO=2208 AND VPID=260
PRINT, MAXV
```

Query 1.3-M This query would have to be broken into three separate queries with the MIRADS hierarchy as in Figure 3.1. The reason is that MIRADS does not allow simultaneous qualification on "peer" records, i.e. records from the same level, in a single query. Several nested queries would easily solve the problem, but MIRADS does not allow nested queries.

```
QUERY, ENGNO=2208 AND VPID =260
PRINT, MAXV
QUERY, ENGNO=2208 AND FPID =10
PRINT, FPVAL
QUERY, ENGNO=2208 AND PARTDESC='HPOTP'
PRINT, PARTSN
```

Query 1.4-M

```
QUERY, VPID=260 AND MAXV >120.6
PRINT, TESTNO,ENGNO
```

Query 1.5-M

```
QUERY, (VPID=260 AND MAXV>120.6)  OR
       (VPID=270 AND MAXV>100)
PRINT, ENGNO
```

None of queries 1.6-1.10 can be achieved in MIRADS with the hierarchy as structured in Figure 3.1. The reason is the peer-access problem mentioned in the discussion of query 1.3-M above. Because of the way MIRADS buffer areas are implemented, there can be no simultaneous qualification on two records at the same level. Actually the restriction is even more severe: two records on the same level from the same hierarchy chain of records (for example two records from type 201) cannot be accessed simultaneously; neither can two records (regardless of level) from two different record chains be accessed simultaneously.

By some restructuring of the hierarchy in Figure 3.1, we could provide limited forms of some of the queries 1.7-1.10. For example, in order to satisfy query 1.9, we could place the information about the part HPOTP in the level 100 record type, or in a level between the two levels in Figure 3.1 (i.e. move the current 200 level record types to the 300 level and insert a new 200 level record type). However, the kind of information that could be moved would be "piece-by-piece" information and not entire files; hence this approach is obviously quite limited. With any reasonable restructuring of the hierarchy, queries like 1.10 would still be unavailable in MIRADS.

To briefly summaraze MIRADS, we could say that its strengths lie in its relatively user-friendly query language, the simplicity of its underlying structure and updating techniques, and its straightforward start-up and initial data base loading. However, the structural simplicity carries a large price in lack of query retrieval power and flexibility, which is a major weakness for the SSME environment. In addition, the MIRADS procedural language interface and query language procedure capability are both quite weak.

4. DMS-1100 Evaluation.

DMS-1100 is a Sperry developed data base management system implemented on the UNIVAC 1100 computer series. It uses a CODASYL-based network model. QLP (Query Language Processor) is implemented with DMS-1100 at MSFC to provide a high-level query language capability.

Query Langauage. DMS does not include a query language, but QLP is interfaced with DMS to provide a query language capability. The use of QLP is straightforward in many cases; however, in order to make certain kinds of QLP retrievals, network details, such as path access identification, must be included in the QLP commands (this will be illustrated in the query set at the end of the section). Thus an element of navigation is present in QLP, which creates some difficulties for the non-programmer user. QLP does contain a computational capability; additionally, control statements such as DO-loops and IF-constructions are allowed. Procedures using parameters may be defined in QLP. An updating capability is included, although its use requires some network detail maintenance. There is no graphical output capability.

Procedural Language Interface. The DMS procedural language interface is accomplished by an embedded CODASYL-modelled DML. The level of complexity is typical of a CODASYL DML and is non-trivial. A FORTRAN version of the DML is available. The DML is, of course, navigational and requires considerable knowledge of the data base network structure on the part of the user. The usual CODASYL currency indicator awareness is also required. Independence of accessing programs and the physical data base is provided.

Implementation/Maintenance Complexity. Network model data bases are typically more difficult to implement and maintain than hierarchical or relational data bases; DMS-1100 is no exception. The data schema must be processed first by the data definition language (DDL) processor, and then by the subschema processor (SDDL) before access can be granted to a user. The DDL is necessarily more complicated than in the other models because of the network mechanics which must be defined. For example, owner/member relationships (set occurences), which are communicated in MIRADS by physically placing the children records and parent records together in storage, must be described conceptually via the DDL in the network model. One reason for this is that a "child" record may have more than one "parent" record associated with it in a network; hence physical record placement is an inadequate method for modelling the relationships that exist. Additional network information such as path access control, prime paths, path level specification, etc. must also be specified via the DDL or SDDL. Through the SDDL, different "views" of the data base may be set up for different users, but even if the entire data base is to be used, a subschema must still be processed using the SDDL.

Maintenance complexity is influenced directly by the underlying network complexity. To insert a record requires inserting not only the record itself, but also placing that record in the appropriate owner/member sets and performing the corresponding maintenance on the

effected paths. Deletions require similar actions. Some of the path maintenance can be done automatically, but the user must supply a significant amount of this kind of information. To use the QLP update commands, familiarity with details of the DMS schemas and subschemas is often required.

Query Set 1.1-1.10 in DMS-1100. For each of MIRADS, ORACLE, and DATATRIEVE, sample data bases were constructed and the relevant version of query set 1.1-1.10 was tested. Time did not permit the construction of a DMS sample data base. Consequently, the QLP queries in this section have not been tested. The network structure, including paths, used in the query set, is given below in Figure 4.1.

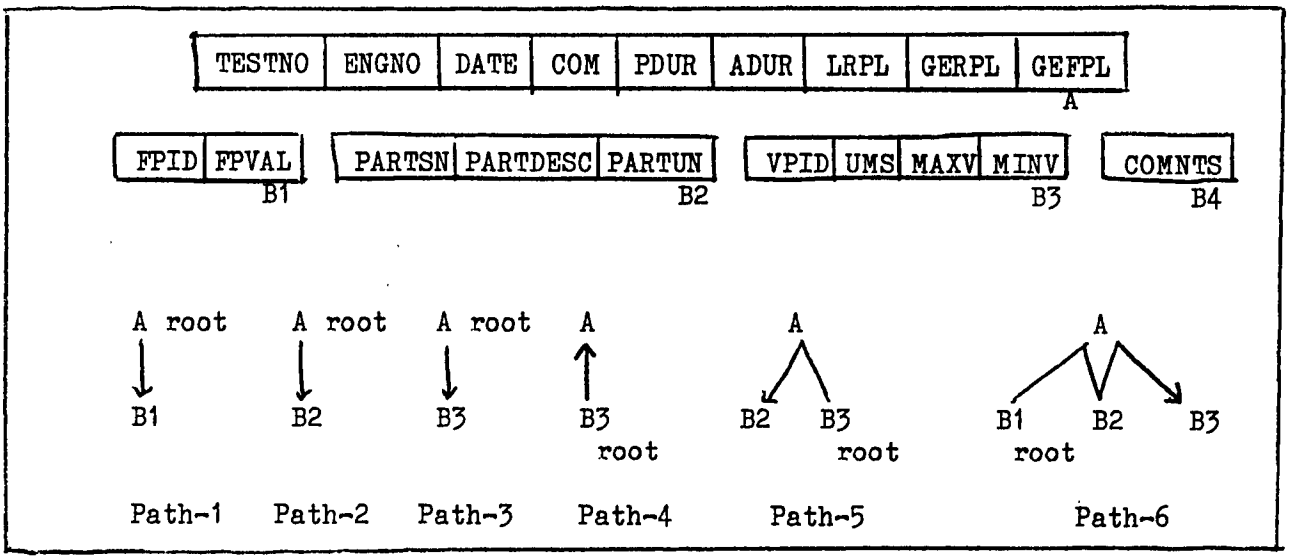

FIGURE 4.1
DMS-1100 Network

Query 1.1-DMS (refer to section 1 for query definitions)

```
LIST TESTNO,ENGNO
     WHERE ADUR>300
```

Note: The "path" needed here is a trivial one since only one file is used.

Query 1.2-DMS

```
LIST MAXV
     WHERE ENGNO=2208 AND VPID=260
```

Note: The path used is Path-3. Since it is the only path which contains the data requested, it need not be mentioned explicity.

Query 1.3-DMS

```
LIST MAXV,FPVAL,PARTSN
     WHERE FPID=10 AND ENGNO=2208 AND VPID=260
           AND PARTDESC='HPOTP'
     VIA PATH-6
```

Note: The path designation is actually optional here since DMS could find Path-6 on its own. However, in more complex networks there may be multiple paths available and the selection of the correct path may be crucial to the meaning of the query. Even in this case, there would be a gain in efficiency of query execution by specifying the path. We give the path in each of the queries that follow.

There is more complexity than meets the eye in path designation, as in query 1.3-DMS. Suppose we desire the same information as above except for the FPID information. Then our path would actually need to start at B2 rather than B1. The options available are to have defined in the subschema a separate path B2-to-A-to-B3 or to use Path-6. In order to use Path-6 we must enter the path at the root file, B1; thus we would have to include a "dummy" qualifier on file B1 (FPID>0, for example) in order to enter the root of the path. Both these approaches have drawbacks. In a large complex network, to specify all possible paths through the network is burdensome at best; additionally, users are required to keep track of and use this multitude of paths. On the other hand, forcing the user to specify "dummy" qualifiers imposes an unnatural constraint on query construction. These considerations are especially important in the SSME environment because of the unpredictable nature of the desired queries, and hence the need to have almost total network access.

Query 1.4-DMS

```
LIST TESTNO, ENGNO
     WHERE VPID=260 AND MAXV>120.6
     VIA PATH-4
```

Query 1.5-DMS

```
LIST ENGNO
     WHERE (VPID=260 AND MAXV>120.6)
        OR (VPID=270 AND MAXV>100)
     VIA PATH-4
```

Queries 1.6 and 1.10 can be made in DMS, but require control statements beyond the scope of this section, and so, are omitted.

Query 1.7-DMS

```
LIST ENGNO
     WHERE FPID=10 AND FPVAL='A603'
           AND VPID=260 AND MAXV>120.6
     VIA PATH-6
```

Query 1.8-DMS

```
LIST ENGNO
     WHERE (FPID=10 AND FPVAL='A603')
        OR (FPID>0 AND VPID=260 AND MAXV>120.6)
     VIA PATH-6
```

Note the use of a "dummy" qualifier, FPID>0.

Query 1.9-DMS

```
LIST PARTSN
   WHERE VPID=260 AND MAXV>120.6 AND PARTDESC='HPOTP'
   VIA PATH-5
```

Although DMS-1100 provides enough retrieval power for the SSME historical data base, the complexity of the query language is a major drawback. Additionally, the implementation of a DMS data base would be considerably more complex than the corresponding implementation of a hierarchical or relational data base. There is a CODASYL DML for FORTRAN, but again its complexity is a disadvantage. Overall, DMS-1100 would seem to be an acceptable, but perhaps not ideal, choice for a SSME historical data base.

5. ORACLE Evaluation.

ORACLE is a relational data base management system marketed by Relational Software Incorporated, implemented at MSFC on the VAX 11/780. It has as its query language SQL (or SEQUEL as it was formerly known), a relationally complete language which was developed at IBM. Coupled with SQL in ORACLE is UFI (User Friendly Interface), a sublanguage which allows editing while constructing SQL queries, and HLI (High-level Language Interface) which allows access to ORACLE from within a high-level procedural language.

Query Language. SQL is an English-like version of a more fundamental relational sublanguage called SQUARE (Specifying Queries as Relational Expressions) which is founded on mathematical set-theoretic concepts. Today SQL is easily the most important relational query language and its use is likely to be incorporated into many of the major relational systems developed for some years to come. It includes adequate computational capabilities, including one-command averages, sums, counts, and maximum and minimum values for attributes. Updating is accomplished very easily from within SQL, and the types of nested queries (subqueries) allowed provides considerable query flexibility.

As implemented in ORACLE, SQL procedures may be defined and stored as standard files, maintained by the operating system text editor, which are then executed from within UFI using a call command, START. These procedure files can be written to allow the use of any number of parameters, which are passed by value when START is used. The current version of ORACLE does not contain query language graphical output capability.

Procedural Language Interface. ORACLE's procedural language interface is accomplished through a DML called HLI, which consists of a set of procedures which are called from the host language. Communication with ORACLE takes place via a buffer data area which is established within the user program. SQL queries are passed to ORACLE as parameters in the procedure OSQL. The appropriate OSQL parameter may contain any valid SQL query, data manipulation, data definition, or data control statement. The SQL statement passed may contain "substitution variables" which can in turn be modified by another HLI procedure. Rather than being forced to pass a new SQL statement as another parameter in OSQL, the user program is able to dynamically alter an existing SQL statement and then execute the altered statement. Results of SQL statements can be passed to buffer variables within the user program via a OFETCH call. HLI is not particularly complex, and since SQL statements are utilized for the actual data base retrievals, the result is a DML which is non-navigational, imposes no currency awareness requirements upon the user, and allows program independence from the physical data base structure.

Implementation/Maintenance Complexity. As is typical with relational data bases, implementation and maintenance are both quite simple and straightforward with ORACLE. Since the data is stored in tables which are interconnected relationally by the DBMS, there are fewer details, than with the hierarchical or network models, for the user to be concerned about during implementation and maintenance. That is, such things as access paths, hierarchy chains, etc. are not dealt with explicitly in the relational model. Basically, all that needs to be done is to communicate the relational table structure to the DBMS, and the system takes it from there. Both content and dictionary updating are easily accomplished, and file/index reorganization is transparent to the user.

Query Set 1.1-1.10 in ORACLE. The underlying data structure which seems most natural for the SSME historical data is a simple extension of the category structure given in Fig 1.1 (also used to model the MIRADS and DMS-1100 data base schema). In Figure 5.1, we give the ORACLE tables used in the SQL queries that follow. Note that in the relational model, we remove the necessity for hierarchy/network structures by placing a relation-defining field, TESTNO in each case here, in the appropriate tables.

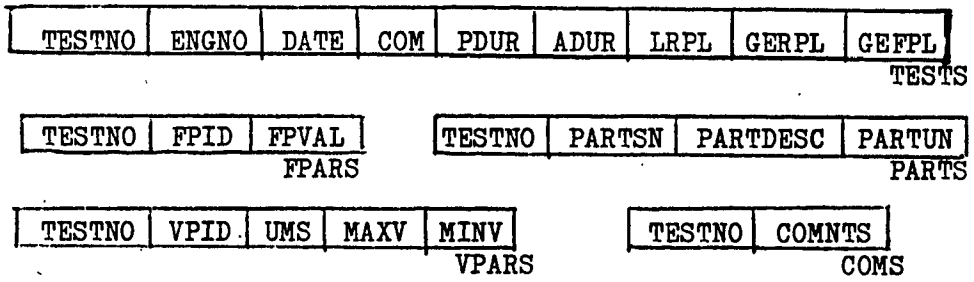

FIGURE 5.1
Relational Tables

Query 1.1-OR (refer to section 1 for query definitions)

```
SELECT TESTNO, ENGNO FROM TESTS
      WHERE ADUR >300
```

Query 1.2-OR

```
SELECT MAXV FROM VPARS
      WHERE ENGNO=2208 AND VPID=260
            AND TESTS.TESTNO=VPARS.TESTNO
```

Notice how corresponding entries from the two tables VPARS and TESTS are "joined", or made available at the same time, by the condition TESTS.TESTNO=VPARS.TESTNO.

Query 1.3-OR

```
SELECT MAXV, FPVAL, PARTSN FROM VPARS,FPARS,PARTS
  WHERE VPID=260 AND FPID=10 AND PARTDESC='HPOTP' AND ENGNO=2208
        AND VPARS.TESTNO=FPARS.TESTNO
        AND FPARS.TESTNO=PARTS.TESTNO
        AND PARTS.TESTNO=TESTS.TESTNO
```

Query 1.4-OR

```
SELECT TESTNO, ENGNO FROM TESTS
      WHERE VPID=260 AND MAXV>120.6
            AND VPARS.TESTNO=TESTS.TESTNO
```

Query 1.5-OR

```
SELECT ENGNO FROM TESTS
      WHERE ( (VPID=260 AND MAXV>120.6)
              OR (VPID=270 AND MAXV>100) )
            AND VPARS.TESTNO=TESTS.TESTNO
```

Query 1.6-OR

```
SELECT ENGNO FROM TESTS WHERE
  VPID=260 AND MAXV>120.6 AND VPARS.TESTNO=TESTS.TESTNO
        AND TESTS.TESTNO
            IN (SELECT TESTNO FROM VPARS
                WHERE VPID=270 AND MAXV>100)
```

Query 1.7-OR

```
SELECT ENGNO FROM TESTS
       WHERE
         (VPID=260 AND MAXV>120.6 AND VPARS.TESTNO=
                                              TESTS.TESTNO)
       AND (FPID=10 AND FPVAL='A603' AND FPARS.TESTNO=
                                              TESTS.TESTNO)
```

Query 1.8-OR Replace the third AND with OR in query 1.7-OR.

Query 1.9-OR

```
SELECT PARTSN FROM PARTS
       WHERE VPID=260 AND MAXV>120.6 AND VPARS.TESTNO=
                                              PARTS.TESTNO
```

Query 1.10-OR

```
SELECT MAXV FROM VPARS
       WHERE VPID=260 AND
           VPARS.TESTNO IN
               (SELECT TESTNO FROM VPARS
                    WHERE VPID=270 AND MAXV>108.6)
```

In summary, ORACLE scores well in all areas of user friendliness, and has a relationally complete query language. One weakness is the lack of graphical output capability in SQL. Additionally, it is possible that the performance speed of ORACLE might be a limiting factor in some environments. But, within reason, this would not be important for the SSME historical data base, and ORACLE would seem well suited for that application.

DATATRIEVE Evaluation.

DATATRIEVE is a Digital Equipment Company data base management system which is implemented on the VAX/780 at MSFC. It includes a relational-like query language and the capability of using that language from within a high-level procedural language.

Query Language. The DATATRIEVE query language is a user-friendly language with many relational features. It is not as powerful or as elegant as SQL, but it does contain enough relational features to allow the user to model his data in relational tables. Updating is done easily from within the query language, and it contains an adequate computational capability. Query language procedures are easily defined, with parameters being passed by responding to system prompts. The FIND command and nested FOR commands allow certain classes of nested queries to be performed. An easily used graphical output capability is included.

Procedural Language Interface. The high-level procedural language interface in DATATRIEVE is somewhat similar to that of ORACLE.

The DML consists of a set of procedures that can be called from an accessing FORTRAN program. Data base manipulation is accomplished by passing query language commands as procedure parameters, and then receiving retrieved information in buffer variables within the user program. As a consequence, the resulting DML allows non-navigational data base access via the query language, with no currency indicator requirements on the user as in DMS-1100. Of course, this use of the query language as the data base accessing tool also allows program independence from the physical data base.

Implementation/Maintenance Complexity. DATATRIEVE data bases are very easy to implement and maintain. Data dictionary facilities are included in the query language. The appropriate domain and record definitions are automatically stored in the VAX Common Data Dictionary by DATATRIEVE. The files in which the actual data is stored are ordinary VAX RMS data files. These can be created and maintained from within DATATRIEVE or completely independently of DATATRIEVE. Content and dictionary updating can be accomplished in a straightforward way from within the query language.

Query Set 1.1-1.10 in DATATRIEVE. In order to write queries 1.1-1.10 in DATATRIEVE, we will use the relational tables given in Figure 5.1 (used for the ORACLE SQL retrievals).

Query 1.1-DTR (refer to section 1 for query definitions)

```
PRINT TESTNO,ENGNO OF TESTS
      WITH ADUR>300
```

Query 1.2-DTR

```
PRINT MAXV OF VPARS CROSS TESTS OVER TESTNO
      WITH ENGNO=2208 AND VPID=260
```

Note that we accomplish a "join" of VPARS and TESTS with a CROSS operation using the field TESTNO as the joining field. This creates the connection between those tables that we got in SQL with TESTS.TESTNO=VPARS.TESTNO .

Query 1.3-DTR

```
PRINT MAXV,FPVAL,PARTSN OF
    FPARS CROSS VPARS OVER TESTNO CROSS PARTS OVER
          TESTNO CROSS TESTS OVER TESTNO
    WITH VPID=260 AND FPID=10 AND PARTDESC='HPOTP' AND
                                          ENGNO=2208
```

Query 1.4-DTR

```
PRINT TESTNO,ENGNO OF TESTS CROSS VPARS OVER TESTNO
      WITH VPID=260 AND MAXV>120.6
```

Query 1.5-DTR

```
PRINT ENGNO OF TESTS CROSS VPARS OVER TESTNO
      WITH (VPID=260 AND MAXV>120.6)
         OR (VPID=270 AND MAXV>100)
```

Query 1.6-DTR

```
FOR A IN TESTS CROSS VPARS OVER TESTNO WITH
                VPID=260 AND MAXV>120.6
   FOR B IN TESTS CROSS VPARS OVER TESTNO WITH
                B.TESTNO=A.TESTNO AND VPID=270
                AND MAXV>100
      PRINT B.ENGNO
```

Query 1.7-DTR

```
PRINT ENGNO OF TESTS CROSS VPARS OVER TESTNO CROSS
                    FPARS OVER TESTNO
      WITH (VPID=260 AND MAXV>120.6)
        AND (FPID=10 AND FPVAL='A603')
```

Query 1.8-DTR Change the second AND to OR in query 1.7-DTR.

Query 1.9-DTR

```
PRINT PARTSN OF VPARS CROSS PARTS OVER TESTNO
      WITH VPID=260 AND MAXV>120.6
```

Query 1.10-DTR

```
FOR A IN VPARS WITH VPID=270 AND MAXV>108.6
    FOR B IN VPARS WITH B.TESTNO=A.TESTNO AND B.VPID=260
    PRINT B.VPID,B.MAXV
```

DATATRIEVE is an easily implemented and maintained system with a moderately powerful user-friendly query language. A nice feature of that query language is its graphical output capability, which is particularly valuable for the SSME historical data application. The author is somewhat skeptical about DATATRIEVE's performance capabilities, but no evidence is available yet to make any definite conclusions in this area. Evaluation of a DATATRIEVE prototype data base should provide the necessary information on this matter.

7. Comparative Summary of MIRADS, DMS-1100, ORACLE, and DATATRIEVE.

Figure 7.1 summarizes much of the evaluation against the criteria of Table 2.1 that was done in sections 3-6. When performance factors are added to the criteria of Table 2.2, we can make a qualitative summary of the four systems as in Figure 7.2.

	MIRADS	DMS-1100	ORACLE	DATATRIEVE
Query Language	User-friendly. Limited power.	Complex to use. Reasonably powerful.	SQL: User-friendly. Relationally complete. Industry standard.	User-friendly. Adequate power. Graphical output capability.
Procedural Language Interface	Of little use. DML limited.	Complex. Navigational.	Moderately complex. Non-navig. Embeds SQL.	Moderately complex. Non-navig. Embeds query language.
Implement-ation/ Maintenance Complexity	Moderately complex.	Very complex.	Not complex. Can be done within SQL.	Not complex. Can be done within query language.

FIGURE 7.1

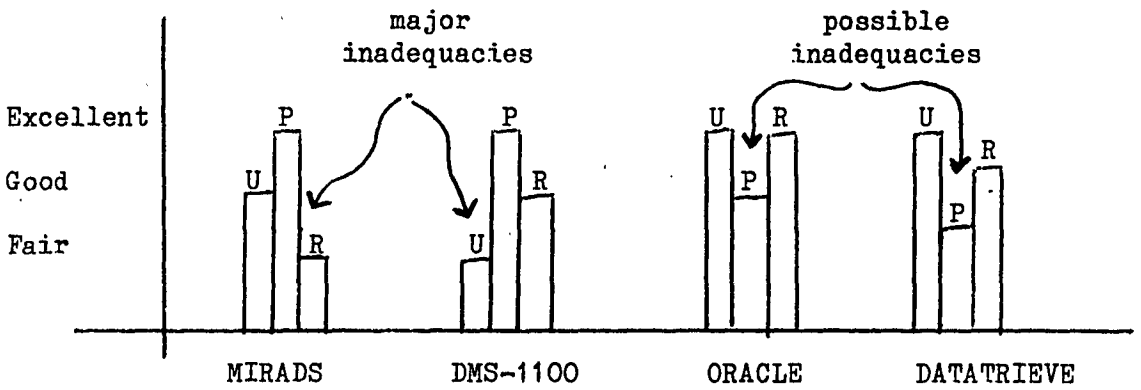

U= user-friendliness
P= performance
R= retrieval power

FIGURE 7.2

As can be seen from Figure 7.2, both MIRADS and DMS-1100 have major deficiencies for the SSME historical data base application: the limited retrieval power of MIRADS and the inherent complexity of DMS-1100. On the other hand, ORACLE and DATATRIEVE are weak only in the area of performance, which is probably not a crucial factor for the SSME historical data base. However, before this factor can be discounted completely, more quantitative performance information is needed.

Conclusions

The basic conclusion of this report is that a data base management system would be a desirable tool for managing SSME historical data. This conclusion is supported by the analysis, in section 1, of both the kind of data involved and the information retrieval requirements against the data. A set of SSME environment-particular evaluation criteria is derived in section 2 (Figure 2.1), and it is recommended that any DBMS considered for this task be evaluated relative to those criteria. Particular emphasis should be placed on the criteria involving query language user-friendliness and power, and maintenance complexity, since performance in those areas is likely to be crucial to the sytem's successful use.

Of the four particular systems evaluated, only two seem reasonably well suited for the SSME historical data base, namely ORACLE and DATATRIEVE (supporting arguments are summarized in section 7). The choice between these two is not obvious from our study. DATATRIEVE's graphical output capability is clearly important for the present application. On the other hand, its query language, while adequate for present information retrieval, is inferior to ORACLE's SQL. As retrieval requirements change, ORACLE would be more likely to gracefully accommodate those changes than would DATATRIEVE.

Since, as was mentioned in the "Objectives" section of this report, a significant new hardware acquisition at MSFC is pending, a reasonable course of action seemed to be to implement a large prototype SSME historical data base using DATATRIEVE, taking advantage of the graphical output capability at present, and providing an opportunity to study the performance capability of DATATRIEVE in a production environment. Then a re-evaluation can take place after the identity of the new hardware is known, and after DATATRIEVE has been evaluated via the prototype, with the objective of perhaps implementing a true relational system with a relationally complete query language, such as ORACLE's SQL. Specific recommendations concerning the construction and use of the DATATRIEVE prototype can be found in a separate document, User/Implementation Guide for THIST, which can be obtained from the author or his NASA counterpart.

References

Bradley, James, File and Data Base Tecniques, Holt, Rhinehart and Winston, New York, 1982.

Boyce, R.F. et. al., "Specifying Queries as Relational Expressions," Comm ACM 18(11), pp621-28, 1975.

Chamberlin, D.D. and R.F. Boyce, "SEQUEL, a Structured English Query Language," Proc. ACM SIGMOD Workshop on Data Description, Access, and Control, pp249-64, 1974.

Date, C.J., Introduction to Data Base Systems, Addison-Wesley, Reading, Mass., 1977.

Kim, W., "Relational Data Base Systems," ACM Computing Surveys, 11(3), pp185-211, 1979.

Reference Manuals:

MIRADS User's Manual
MIRADS Implementation Manual
ORACLE UFI/Terminal User's Guide
ORACLE Applications Designer's Guide
ORACLE Data Base Administrator's Guide
Sperry Univac DMS-1100 Data Administrator's Reference Manual
Sperry Univac DMS-1100 FORTRAN DML Programmer's Reference Manual
Sperry Univac QLP-1100 Conversational Commands User's Reference
VAX-11 DATATRIEVE Reference Manual
VAX-11 DATATRIEVE Guide to Programming and Customizing
VAX-11 DATATRIEVE User's Guide
VAX-11 DATATRIEVE Guide to Using Graphics

D2

1984

NASA/ASEE SUMMER FACULTY RESEARCH FELLOWSHIP PROGRAM

MARSHALL SPACE FLIGHT CENTER
THE UNIVERSITY OF ALABAMA

SRM FILAMENT WOUND CASE RESIN CHARACTERIZATION STUDIES

Prepared by:	Libby W. Chou, Ph. D.
Academic Rank:	Professor
University and Department:	Alabama A & M University Chemistry
NASA/MSFC Division: Branch:	 Non-Metallic Materials Polymers and Composites
MSFC Counterpart:	W. J. Patterson, Ph. D.
Date:	August 10, 1984
Contract No.:	NASA-NGT-01-002-099 The University of Alabama

SRM Filament Wound Case Resin Characterization Studies

By

Libby W. Chou
Professor of Chemistry
Alabama A & M University
Normal, Alabama

ABSTRACT

This study will involve characterization on the amine cured epoxy wet winding resin used in fabrication of the SRM filament wound case. High pressure liquid chromatography will be utilized extensively to study lot-to-lot variation in both resin and curing agent, and to assess the validity of quantitative hplc methodology currently under development by Hercules, Incorporated, for in-process resin/catalyst assays.

ACKNOWLEDGEMENTS

The author wishes to thank many individuals for their assistance, comments, and kindness, especially my NASA Counterpart: Dr. W. J. Patterson; N. Hundley and D. Morris who helped to make the instruments running smoothly; Dr. T. Koenig, a fellow participant of this program, who ran the mass spectra of a sample of the curing agent; and Guy Smith of the Environmental & Energy Studies at UAH for a continuous suply of water used in this study.

List of Tables

List of Figures

INTRODUCTION

To reduce the weight of the solid rocket motor (SRM), composite material is used to replace steel in some segments of the SRM. The composite material consists of graphite fiber wound with amine cured epoxy resins, which are produced by the reaction of epichlorohydrin with 2,2'-bis(p-hydroxyphenol) propane (BPA or bisphenol A), or with 1,4-butanediol as follows:

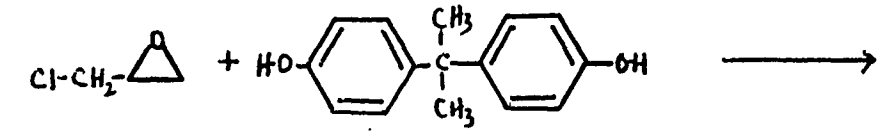

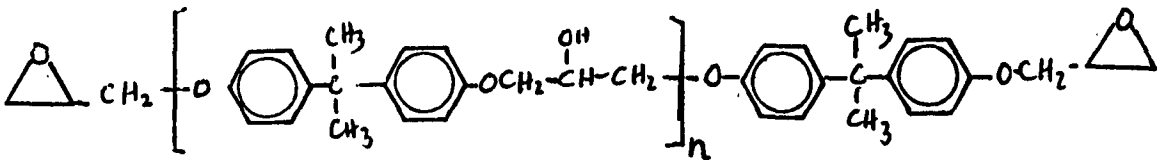

The commercial curing agent used is Tonox 60/40, which is 60% of 4,4'-methylene dianiline (MDA) and 40% of m-phenylene diamine (PDA). High pressure liquid chromatography (HPLC) was used to study the lot-to-lot variation in both the resin and the curing agent and to assess the validity of quantitative HPLC methodology currently under development by Hercules, Incorporated, for in-process resin/catalyst assays.

OBJECTIVES

1. Study the lot-to-lot variation in (A) Tonox 60/40, and (B) Resins.

2. Quantitative study of resin/catalyst mixtures.

3. Quantitative study of Benzoflex (dipropylene dibenzoate) used for cleaning out Tonox in the automated dispensing equipment.

Instrumentation & Results

1A. Tonox. A liquid chromatography instrument by Waters Associates was used. It has a uv detector at 254 nm, which is connected to a Hewlett Packard 3380A Integrator. Two 100 A ultrastyragel columns were used. The mobile phase was THF. The retention times for MDA and PDA were 15.7 and 17.0 min, respectively, at a flow rate of 1.0 ml/min. The areas of absorption due to the two components in each lot of Tonox were checked against various concentrations. Within each lot, the area ratio should remain constant at different concentrations, but it did not. MDA/PDA area ratio increases linearly with decrease concentration (Table 1, and Figure 1). This is true for all five lots, one of which is known to be contaminated with sodium formate. All of them showed the same pattern of four peaks plus a shoulder. The only difference for the contaminated lot is that it solidified easily after the can was opened. The functional ability of Tonox is quite wide regardless of the MDA/PDA ratio. It would cause concern, should additional peaks appear, or should the MDA or PDA peak vanish. From a preliminary mass spectral analysis of Tonox (Figure 2), the peak at 14.6 min is probably due to the coupling of MDA and PDA in the presence of air:

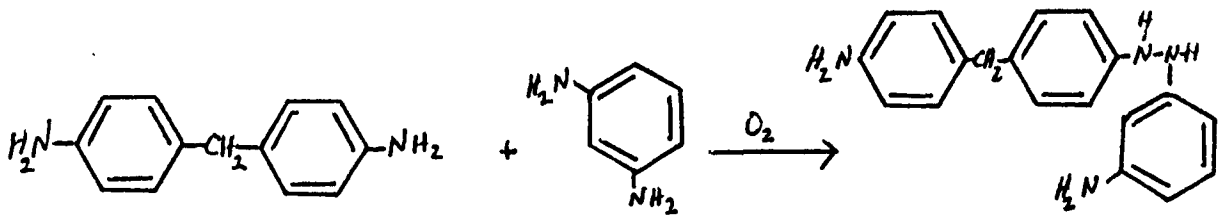

m/e	198	108	304
RT	15.7 min	17.0	14.6

1B. Epoxy Resins. The conditions were the same as above. BPA type resin showed a major absorption at 15.3 min, two minor ones at 13.1, and 14.2 min, and a deflection at 12.2 min. EpiRez, which is the 1,4-butanediol resin, showed no absorption in the uv region. Epon, EpiRez, and three lots of modified resins were analyzed. The percentage of BPA of the different lots were calculated by comparing the total absorption area of BPA in the mixtures to that of the Epon (Table 2, and Figure 3):

$$\%BPA = \frac{A_{mix} \times m_{Epon} \times 100}{A_{Epon} \times m_{mix}}$$

where A_{Epon}, and A_{mix} are the total areas of Epon, and the mix, respectively; and the m's are the masses. An attempt has been made to analyze the 1,4-butanediol resin content by using RI detector. However the absorptions by BPA and EpiRez are too close to be identified in the modified resins (Figure 4). It may be possible to separate them if C_{18} column is used with acetonitrile/water mixture. At this time the RI detector in the hplc instrument equipped with gradient programmer needs servicing.

2. Mixtures of Tonox and Resins. Waters chromatography was connected to a gradient controller, Perkin Elmer LC75 with variable uv detector selected at 214 nm, and Sigma 15 integrator. C_{18} equipped with a guard column was used. Solvent mixture acetonitrile/water (50:50) was chosen at a flow rate of 1.5 ml/min. The method developed by Hercules, Inc., was followed, and results were tabulated (Table 3, Figure 5). The agreement between Tables 2 and 3 is sporadic. The procedure calls for running the working standard until resin peak area agreement is within 1%. However, even as automated as it was, the one-percent agreement on one day may be different from that on the next day (Table 4). This method does provide a qualitative analysis for Tonox, whereas on GPC Tonox and resin have similar retention times. There is one precaution: The pattern for Tonox changes with concentration (Figure 6).

3. Benzoflex. Attempts have been made to detect the trace amount of Benzoflex in the automated resin dispensing system by the method developed by Hercules. Conditions used were same as part 2. It was possible to establish an area count within 5% from injection to injection for a solution that was 0.69% in Benzoflex (Table 5, Figures 7A,B). However, it was not possible to get consistent area count for the concentration suggested in the procedure (0.25%, see Figure 7C). It appears that hplc can detect benzoflex quantitatively at a concentration of .7%, but only qualitatively at lower concentrations.

CONCLUSIONS & RECOMMENDATION

HPLC can be used qualitatively for Tonox, quantitatively for the resin in the resin/Tonox mixes, and semi-quantitatively for Benzoflex contamination. One might be able to analyze the amount of 1,4-butanediol resin by using the reverse phase with acetonitrile/water, when the RI detector functions again.

Table 1

MDA/PDA vs Mass; Five Lots

00100

Mass X(I)	MDA/PDA Y(I)
4.4800	1.5600
3.9600	1.6500
3.6400	1.7000
3.4700	1.7100
3.0500	1.9100
2.9700	1.8100
2.8106	1.7900
2.3500	1.9200
1.9800	1.9000
1.4900	1.9300

020W

X(I)	Y(I)
4.0600	1.6500
3.6800	1.7200
3.4800	1.7800
2.9900	1.8050
2.9250	1.8950
2.9000	1.8900
2.3400	1.9400
2.3000	1.9400
1.1500	1.9900
0.7800	2.0900

022W

X(I)	Y(I)
3.5000	1.7000
2.8000	1.7500
2.4500	1.7300
2.1000	1.8500
1.8500	1.9200
1.1100	1.9400
0.7500	1.9400
0.6750	2.0000
0.6000	2.0700
0.5250	1.9600

0042

Mass X(I)	MDA/PDA Y(I)
4.3040	1.6250
3.7600	1.7200
3.2280	1.8050
2.9440	1.8950
2.6900	1.9350
2.5760	1.9800
2.2080	1.9850
2.1520	2.0500
1.8400	2.0350
1.5410	2.0550
1.4720	2.1000
1.3700	2.0750
1.1980	2.1150
1.0270	2.1250
0.8560	2.1100
0.6850	2.1400
0.5140	2.2500

003V

X(I)	Y(I)
3.4090	1.7550
2.9820	1.8300
2.5560	1.9050
2.1300	1.9600
1.7040	2.0000
1.3140	1.9550
1.2780	2.0100
1.1680	1.9700
1.0220	1.9950
1.0000	2.0150
0.9000	2.0250
0.8760	2.0300
0.8000	2.0300
0.7300	2.0350
0.7000	2.0650
0.6000	2.0650
0.5840	2.1250
0.5000	2.0950
0.4380	2.1350
0.4000	2.1050

Table 2

BPA Content of Modefied Resins

Lot number	Epon 826	RDX 50125 CRD 0040	Hysol Blend	RDX 50125 CRD 0001	EpiRez 5022
Amount (m)	.06040g	.06395g	.05605g	.05395g	.03090g
Resin Abs. Area	219624 221325	173237 173088	166881 164253	148028 148185	0
Average	220475	173163	165567	148107	
Theo. Area 220475 m 0.06040	220475	233433	204596	196930	112793
%BPA (A/th.A)100	100	74.2	80.9	75.2	0

Table 3

BPA Content of Modefied Resins/Tonox Mixtures

Lot number	Epon 826	RDX 50125 CRD 0040	Hysol Blend	RDX 50125 CRD 0001	EpiRez 5022
Amount (m)	.89380g	.91805g	.90070g	.90110g	.90830g
Resin Abs. Area	468.58 468.87 468.66 468.50	359.60 373.88 370.63 377.40	359.7 359.2 357.3	354.6 358.5	0
Average	468.65	370.6	358.73	356.55	
Theo. Area 468.65 m	468.65	481.36	472.27	472.40	494.54
%BPA (A/th.A)100	100	77.0	76.0	75.5	0
Parts Resin (Hercules)	155	119	127.7	117	0

Table 4

BPA Peak Area in Different Runs

Lot number	Epon 826	RDX 50125 CRD 0040	Hysol Blend	RDX 50125 CRD 0001	EpiRez 5022
Amount (m)	.06040g	.06395g	.05605g	.05395g	.03090g
Resin Abs. Area	202079 202381	171031	167444	152548 149482	0

Table 5

Absorption of Benzoflex

Run	1	2	3	4	Average
Total Area	5.1074	5.3059	5.2596	5.2508	5.2309
Other values:	3.4974	9.2793	3.3197	7.0205	
	5.7584	6.3507	5.7296		

Figure 1

MDA/PDA Ratio vs. Mass of Tonox

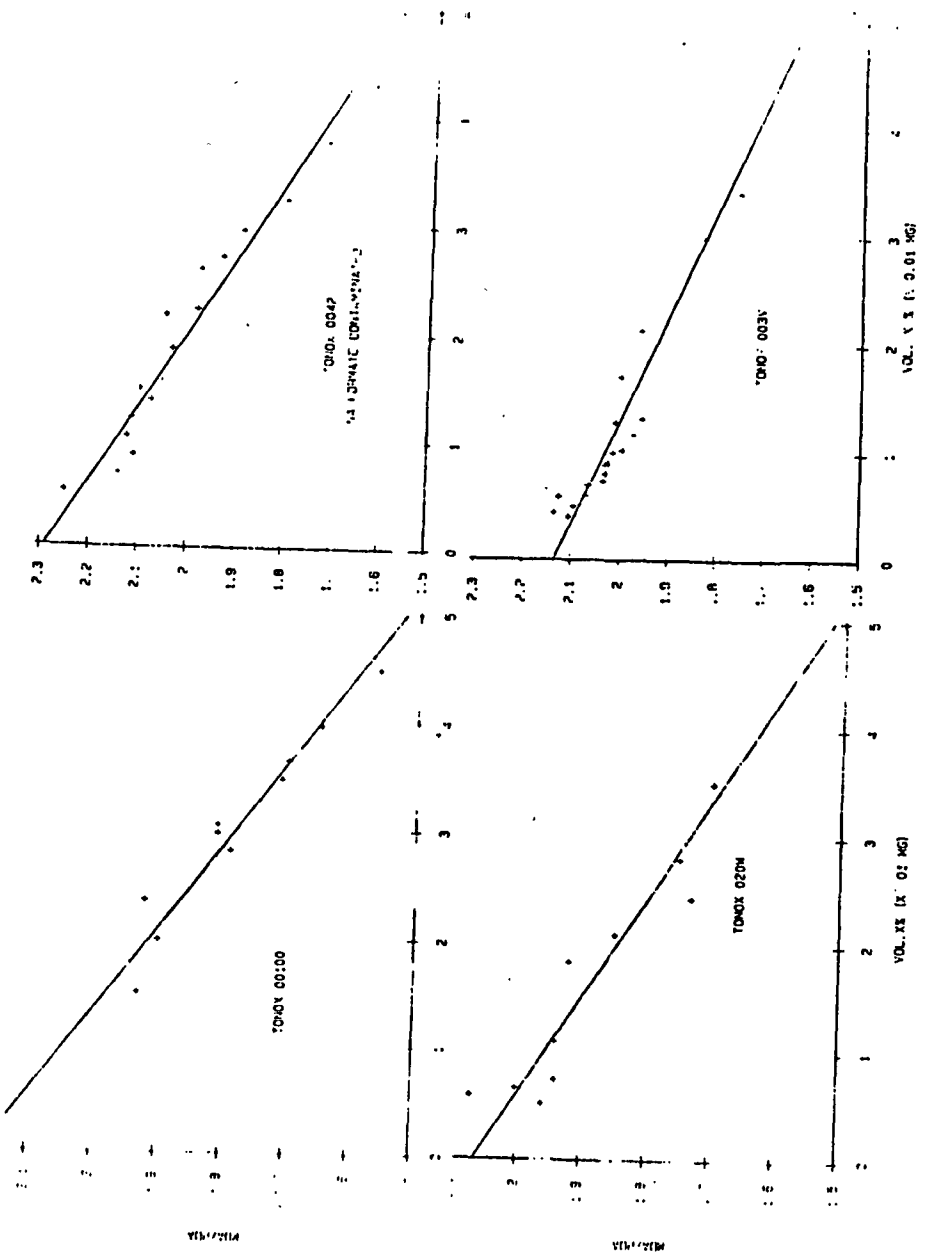

Figure 2: Mass Spectra of Components in Tonox

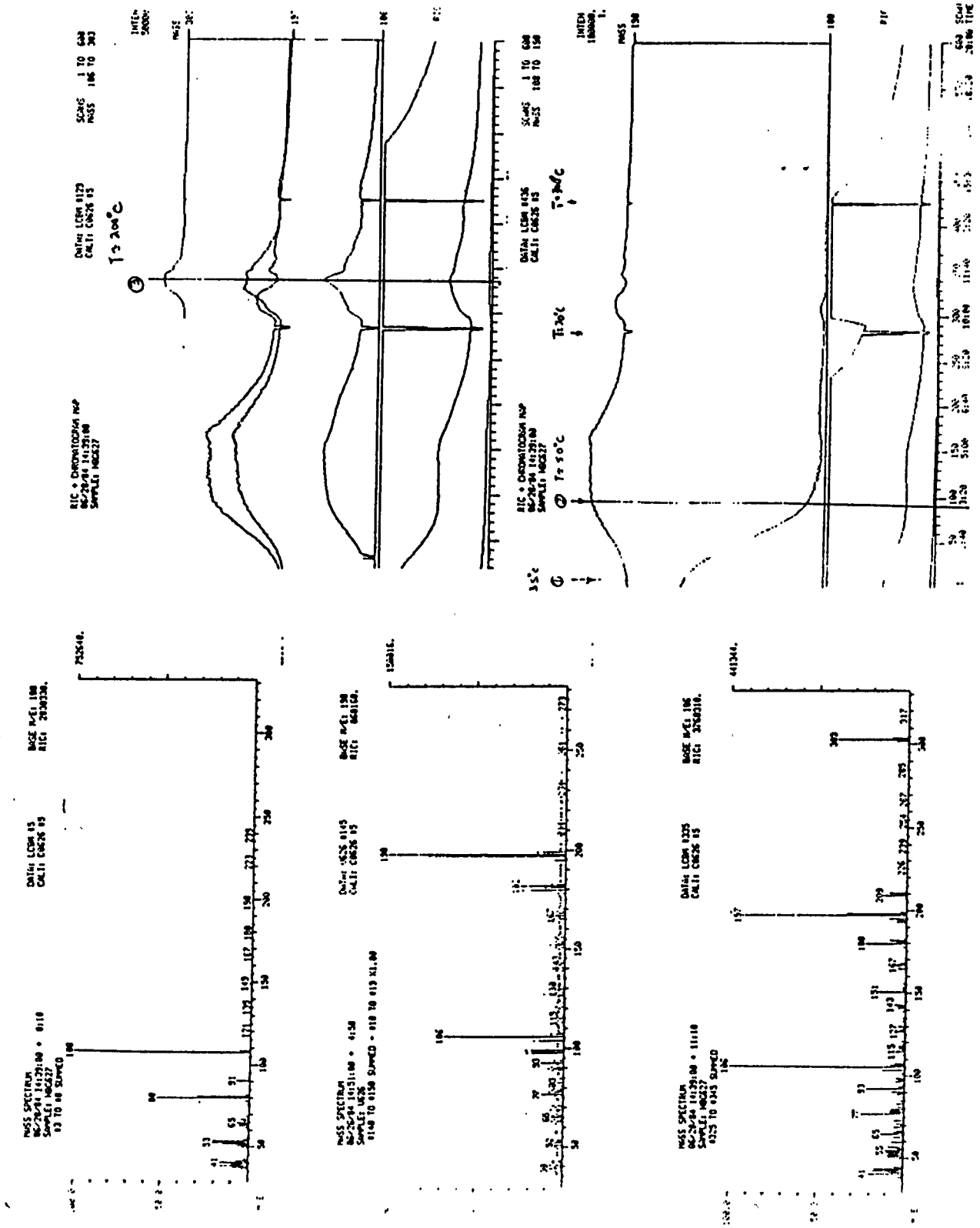

Figure 3

Chromatograms of Resins

Epon

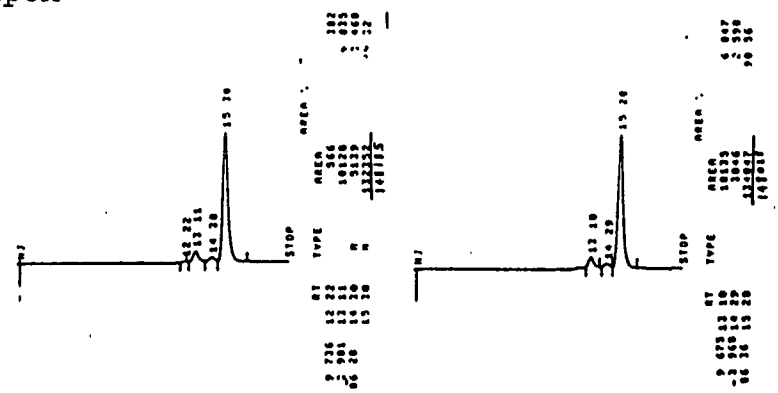

CRD 0040

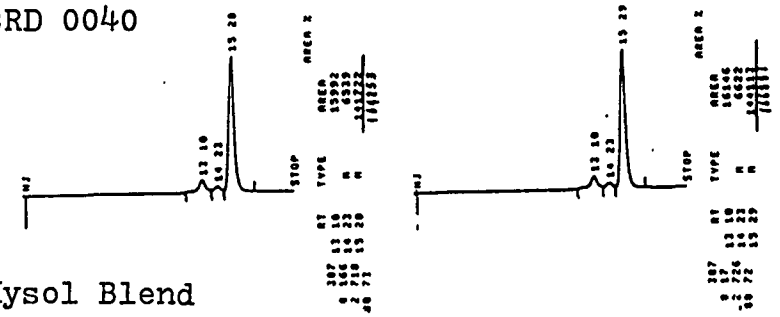

Hysol Blend

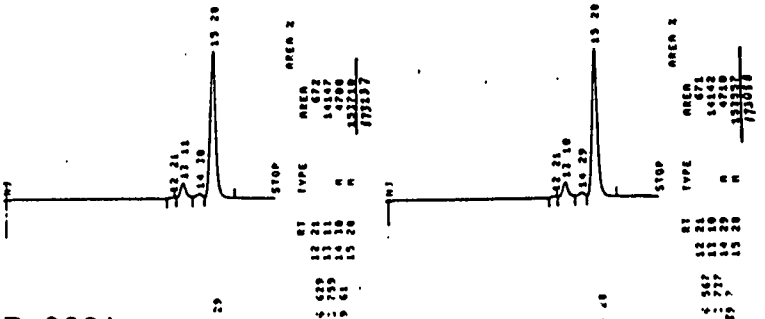

CRD 0001

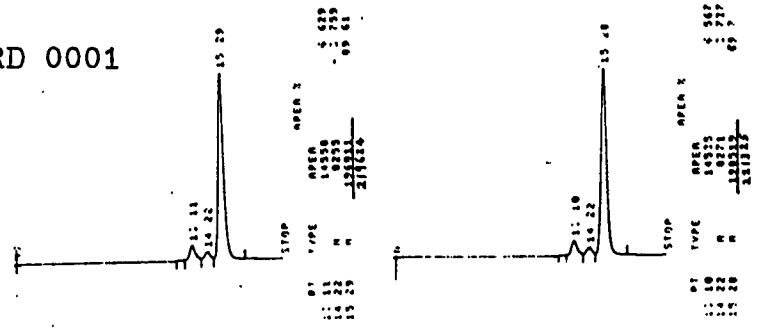

Figure 4

Chromatograms of Resins, RI Detector

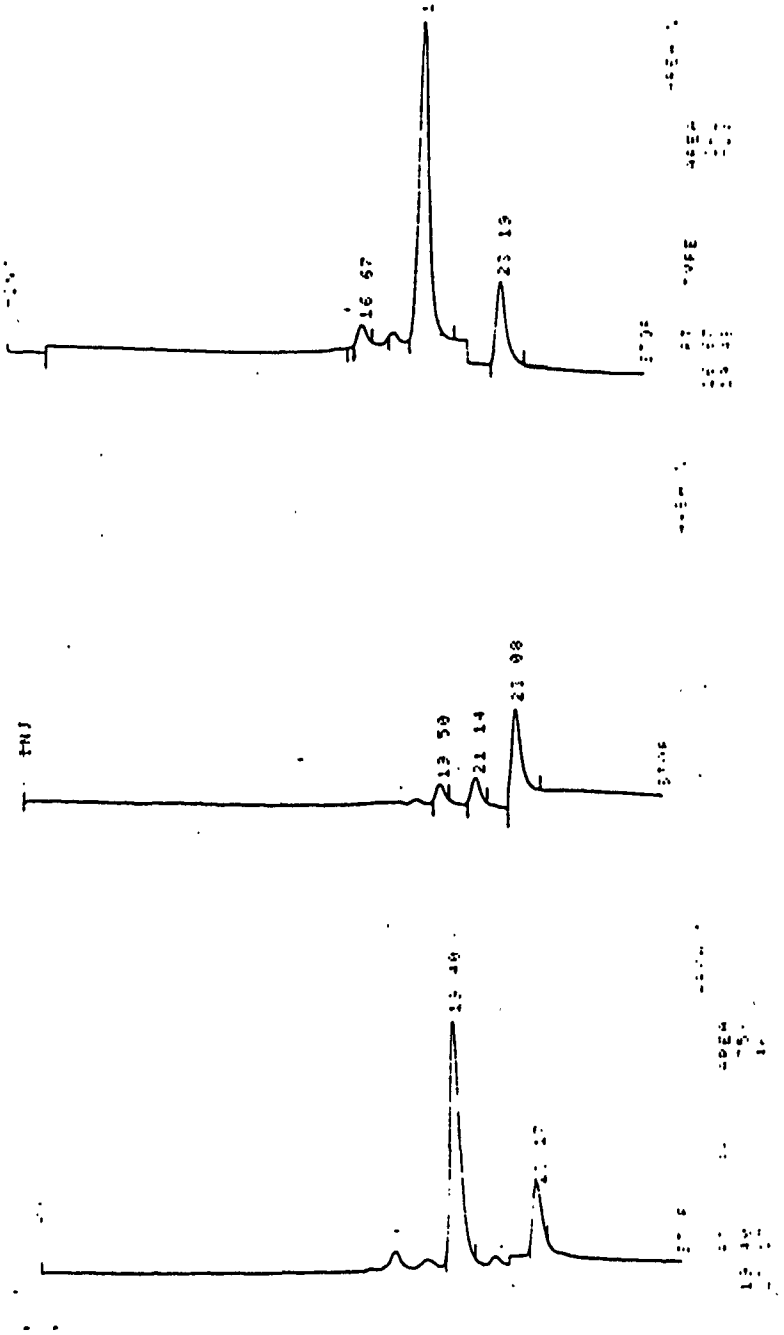

Figure 5

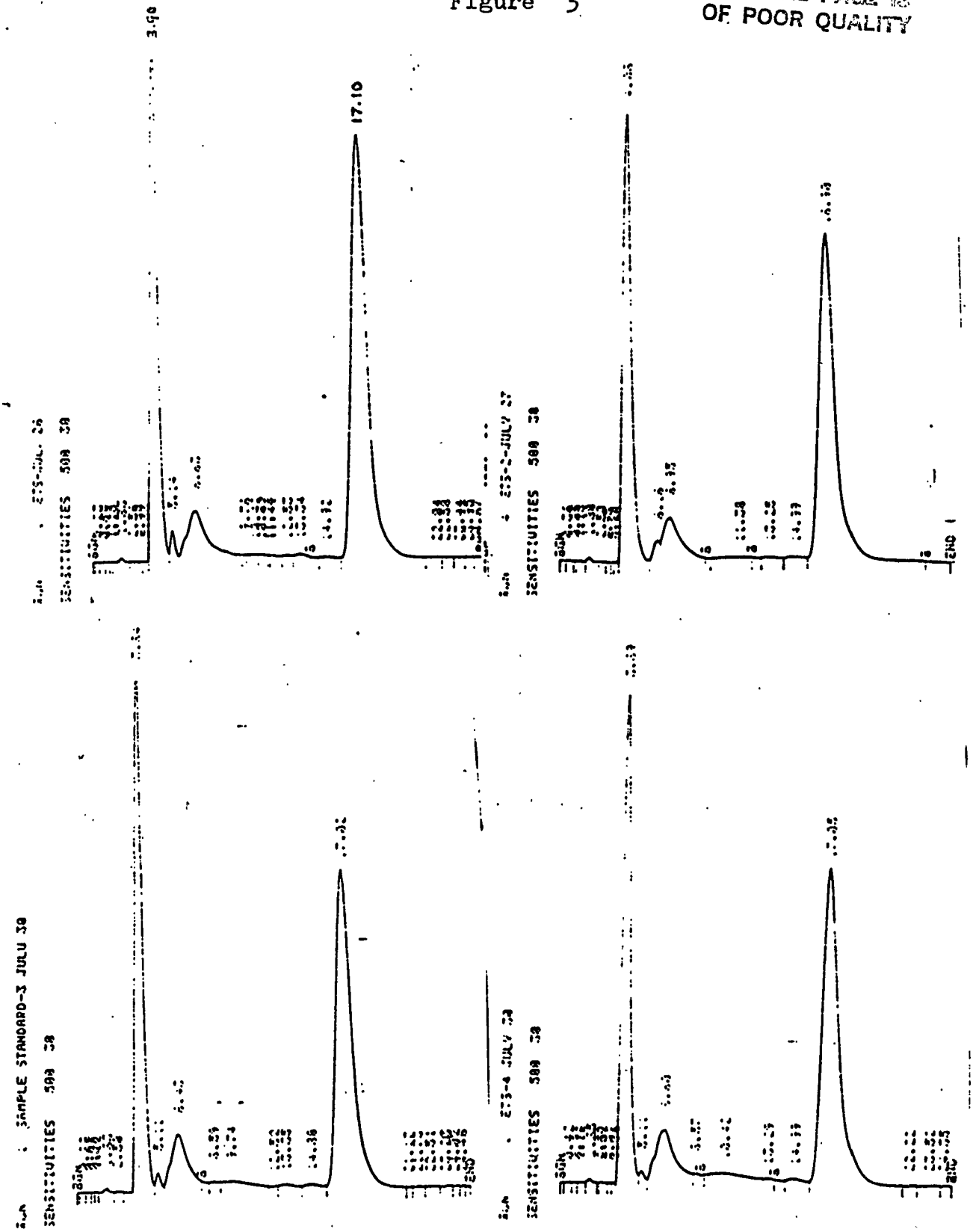

Figure 6

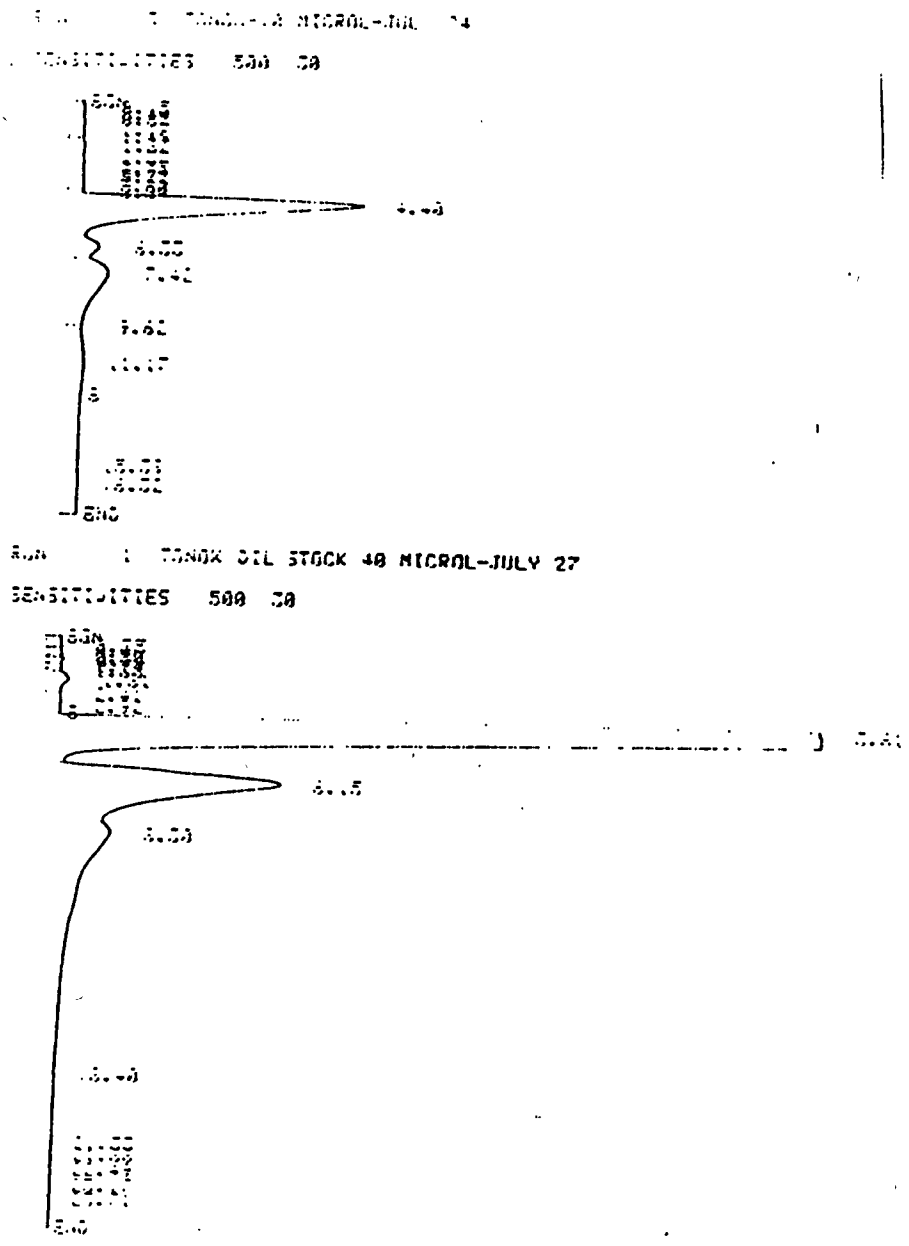

Figure 7A

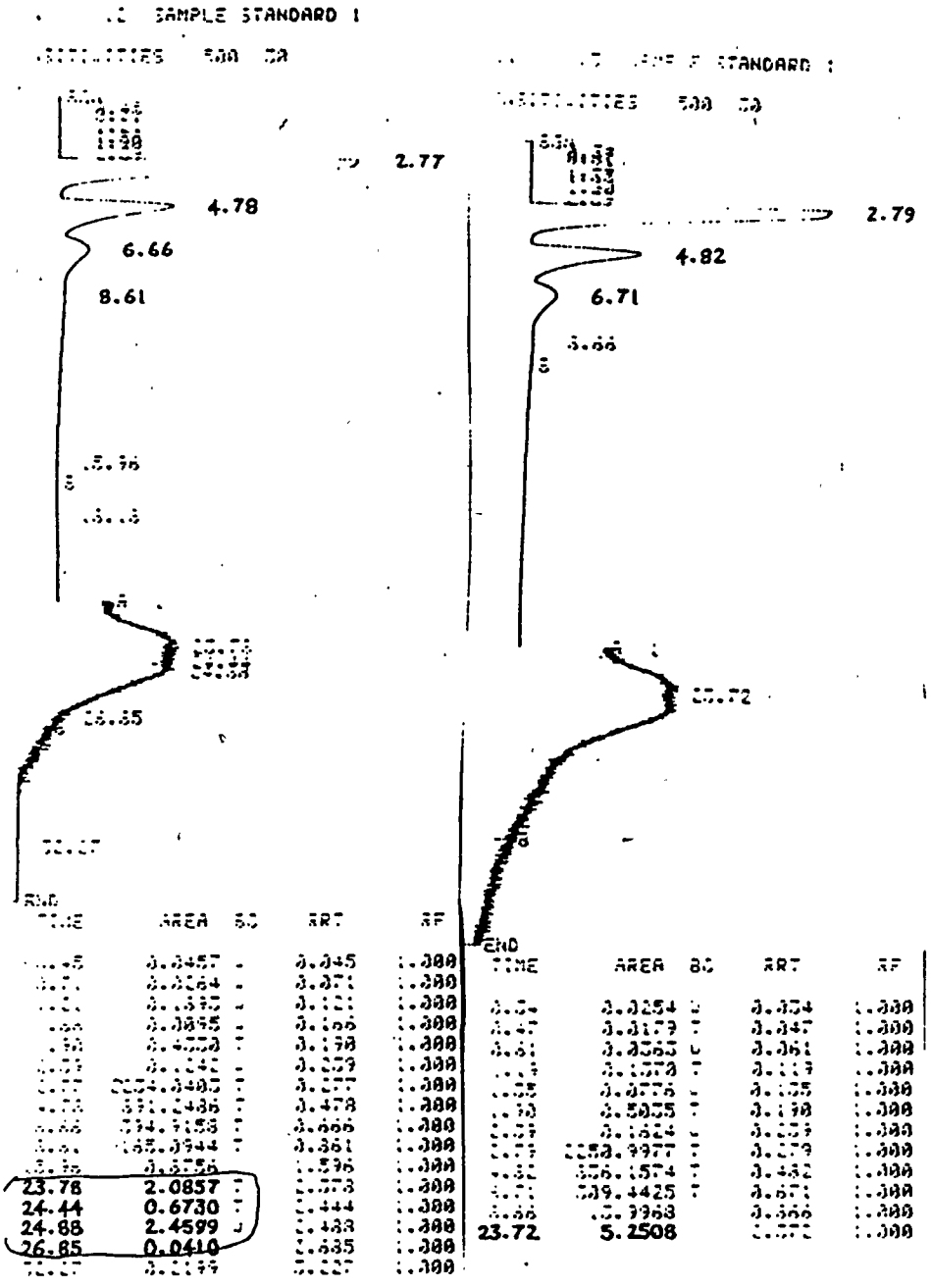

TIME	AREA	BC	ART	AF
23.78	2.0857	T	2.078	1.000
24.44	0.6730	T	2.444	1.000
24.88	2.4599	V	2.488	1.000
26.85	0.0410		2.685	1.000

TIME	AREA	BC	ART	AF
23.72	5.2508		2.372	1.000

Figure 7B

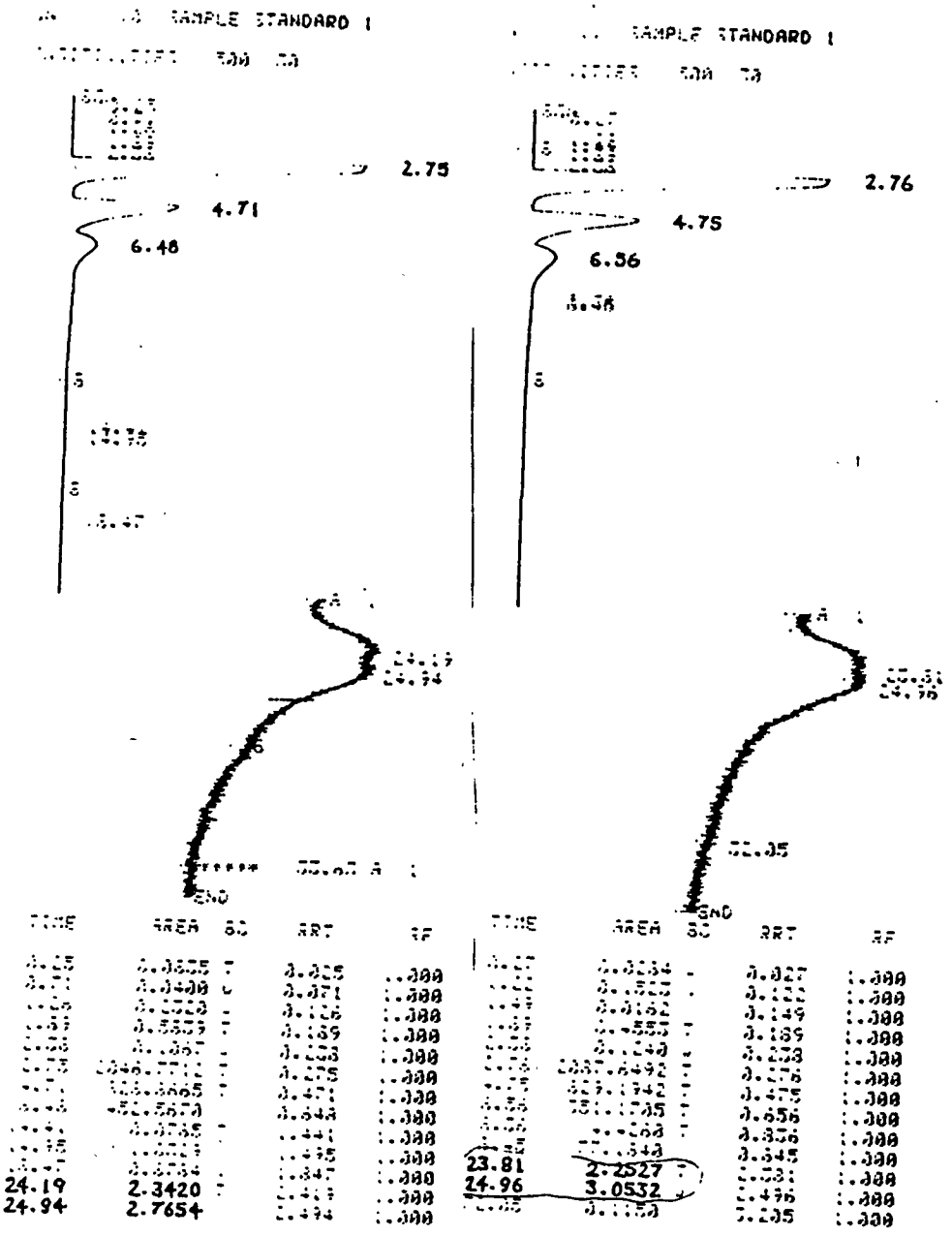

TIME	AREA	BC	ART	RF
24.19	2.3420			
24.94	2.7654			

TIME	AREA	BC	ART	RF
23.81	2.2527			
24.96	3.0532			

ORIGINAL PAGE IS
OF POOR QUALITY

Figure 7C

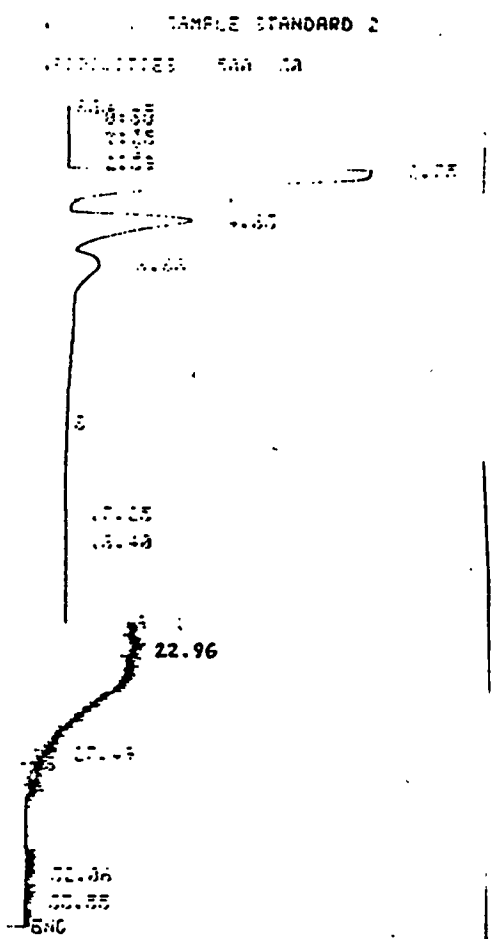

TIME	AREA	BC	ART	RF
22.96	1.7452	-	2.[illegible]	1.000

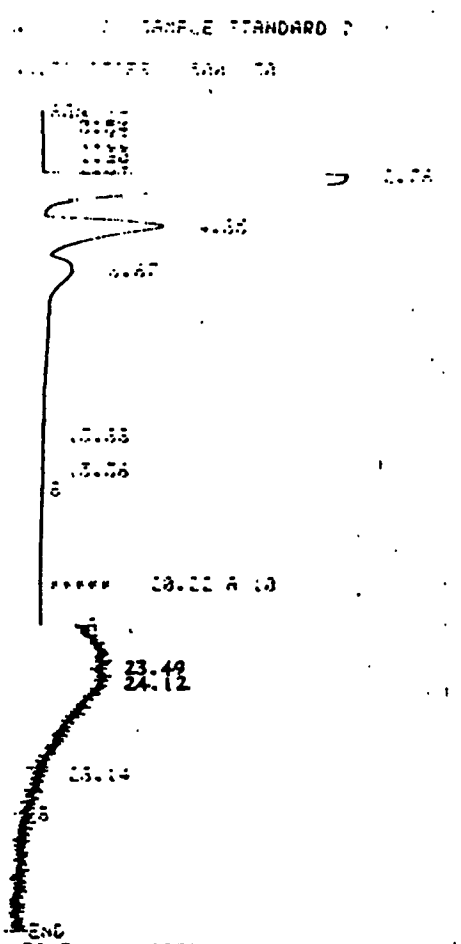

TIME	AREA	BC	ART	RF
23.49	0.8931	T	2.[illegible]	1.000
24.12	1.7516	-	2.[illegible]	1.000

Method 5

Analyzer Control

```
INJ TEMP          25
DET ZONE 1.2      65          25
AUX TEMP          25
FLOW A,B          5     5
INIT OVEN TEMP,TIME             76   999
```

DATA PROC

```
STD MT.SMP WT             0.0000      1.0000   0
FACTOR,SCALE               1    0
TIMES      35.00          0.00   327.67   327.67   327.67   327.67
SENS-DET RANGE            500    30      0.00      2    0    0
UNK,AIR     1.000           0.00
TOL        0.0000         0.050       1.0
REF PK      0.000          0.00      0.00      0.00
STD NAME
```

EVENT CONTROL

```
ATTN-CHART-DELAY              10     5     0.01
```

TIME	DEVICE		FUNCTION	NAME
22.00	ATTN	A	1	ATTN 0

1984

NASA/ASEE SUMMER FACULTY RESEARCH FELLOWSHIP PROGRAM

MARSHALL SPACE FLIGHT CENTER
THE UNIVERSITY OF ALABAMA

INVESTIGATION OF THE EFFECTS OF NaOH DOPANT LEVEL ON THE PHYSICAL AND MECHANICAL PROPERTIES OF CARBON/PHENOLIC COMPOSITE MATERIAL.

Prepared by:	Raymond G. Clinton,Jr.,Ph.D.
Academic Rank:	Instructor
University and Department:	Georgia Institute of Technology School of Mathematics
NASA/MSFC:	
Division:	Nonmetallic Materials
Branch:	Ceramics and Coatings
MSFC Counterparts:	H.M.King, M.L.Semmel, B.E.Goldberg
Date:	August 31, 1984
Contract No:	NASA-NGT-01-002-099 The University of Alabama

Investigation of the Effects of NaOH Dopant Level on the Physical and Mechanical Properties of Carbon/Phenolic Composite Material.

By

Raymond G. Clinton,Jr.
Instructor of Mathematics
Georgia Institute of Technology
Atlanta, Georgia 30332

Marie Louise Semmel
Benjamin E. Goldberg
Marshall Space Flight Center
Nonmetallic Materials Division

ABSTRACT

The near-catastrophic erosion of the STS-8A solid rocket booster nozzle was the instigating factor in the recent, and on-going, intensive investigation of carbon/phenolic composite materials. Much of this effort has been focused on the effect of sodium contamination on the carbon fibers. It is known that sodium acts as a catalyst in the oxidation of the fibers at elevated temperatures. However, the effect of such contamination upon the phenolic resin and matrix-controlled mechanical properties was unknown. To this end, a study was undertaken to determine what changes were caused by variation in sodium content.

Investigations were conducted in three areas: phenolic resin, carbon/phenolic prepreg, and cured laminates. Due to the exploratory nature of the studies, a variety of tests in addition to those normally run in production facilities were considered. The experimental methodologies and results of these experiments are discussed, and recommendations for improving techniques and extending the research program are presented.

1. INTRODUCTION

Quality control, both in the constituent materials and throughout the fabrication process, is the critical factor in the production of reliable composite parts. To be assured of the reliability of the product, it is necessary to (1) have a thorough understanding of the parameters involved in each processing step, (2) have representative material property allowables, and (3) be able to nondestructively evaluate the integrity of the part.

The importance of the above requirements was underscored by the discovery that sodium contamination of carbon cloth used in the construction of the shuttle carbon/phenolic solid rocket booster nozzles was a contributing factor in the near failure of STS-8A nozzle. Results of initial studies of this anomaly indicated that sodium, known to be a catalyst in the oxidation of carbon fibers at elevated temperatures, (1-4) accelerated material erosion. However, the effect of sodium contamination on resin properties was not addressed. The research described in the following pages was undertaken to assess this effect and to examine test techniques for the qualification of carbon/phenolic materials.

Investigations were conducted to determine resin, prepreg, and cured laminate properties at specific dopant levels. The prepreg series included analyses of resin flow; resin, cloth, and carbon filler contents; volatile constituent identification and standard volatiles content; sodium content, and gel permeation chromatography. Tests conducted on the phenolic resin included gel time, differential scanning calorimetry, thermomechanical analysis, thermogravimetric analysis, gas chromatography, gel permeation chromatography, infrared spectrophotometry and viscosity. The cured laminates were subjected to a variety of NDE methods before being machined into specimens. The mechanical properties characterized were those which depended to varying degrees on matrix properties: short beam shear, compression, and flexure.

2. PHENOLIC RESIN STUDY

The phenolic resin analyzed in this part of the investigation was Borden's SC-1008. This system is presently being qualified under military specification MIL-R-9299C for the production of nozzles for the solid rocket boosters. At the outset, it will be necessary to briefly discuss basic resin chemistry, but only to the extent to which it impacts the study. For additional information, there are numerous texts written on the subject of phenolic polymerization which deal with the process in much greater detail. (5,6)

There are two kinds of phenolic resins, one stage and two stage. Ironside 91LD (used in the prepreg) and the SC-1008 are both one stage resins. A simplified reaction for the production of a phenolic resin is shown in Figure 1. Phenol reacts with formaldehyde under neutral or slightly basic conditions to yield two major products, ortho-methylol phenol and para-methylol phenol. Ortho substitution is kinetically preferred and thus there will be a greater relative percentage of this product. As noted, the para-substituted product will react faster, thus

reducing gel times. One other feature of interest is the chromophore formed by the pendant hydroxyl group and the benzene ring. A color change will result when the hydrogen in the hydroxyl group is replaced, for example, by sodium. Such a change was noted in several trial laminates constructed from resin impregnated white bleeder paper. The matrix darkened with increased sodium content.

An elementary polymerization reaction is also shown in Figure 1. The hydroxyl groups lost in the cross-linking process form water which is the dominant constituent of volatiles given off during curing. In reality, the condensation polymerization is of much greater complexity than that shown here.

The key point is the effect of sodium hydroxide doping on these reactions. In the first reaction, Na^+ will attack the OH^- group yielding sodium phenolate. It is consistent with theory (6) that this is a more active compound and may lead to a higher incidence of para-substitution. Also sodium hydroxide will degrade resin oligomers; i.e., break down the small to medium length chains into even smaller chains. (7) The addition of sodium may promote the formation of ether linkages during polymerization (Williamson ether synthesis) (6). This linkage is weak and may start to degrade at elevated temperatures.

Finally, it is worth noting that compounds often used in the processing of two stage phenolic systems were identified in the SC-1008 and the 91LD resins. The presence of hexamethylenetetramine, which is used as an activator in the polymerization of two stage resins, was indicated by ammonia efflux noted during get time tests. It has been suggested that hexa was introduced to control the pH (7). Furancarboxaldehyde is added to two stage resins to control the flow rate, as these resins are often used as molding compounds. It was identified, using the gas chromatograph-mass spectrometer technique described in section 3.4.2, as a constituent of the 91LD phenolic. The role of the additive in the single stage resin is unknown at this time.

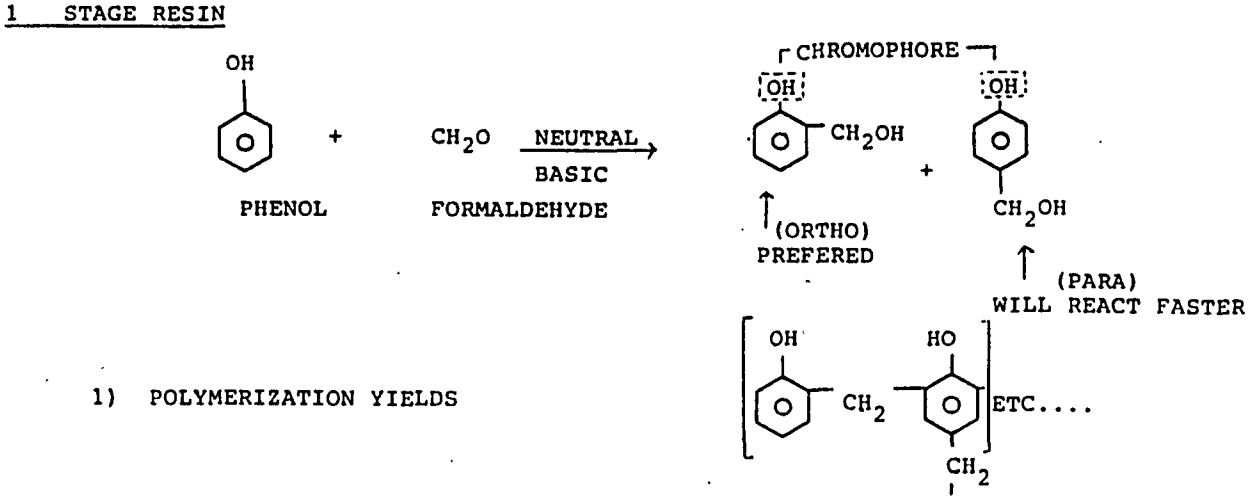

Figure 1. Simplified Reactions for Phenolic Resin Production and Polymerization

2.1 Gel Time

The effect of sodium hydroxide doping on resin gel time was determined using a Fisher-Johns Melting Point Apparatus. All tests were conducted at a constant 350° F. Two critical parameters which must be controlled to obtain repeatable results are drop size and surface area exposed to elevated temperature. Drop size was kept constant at 0.167 grams by using a micro pipette. Due to changes in viscosity with sodium content (discussed in section 2.3) it was necessary to evenly spread the drop to maintain an initially uniform surface area.

The variation in gel time with sodium content is shown graphically in Figure 2. On the semi-log scale, the relationship between the two parameters is a linear one. The fact that gel times are reduced with increasing sodium level agrees well with the hypotheses concerning the effect of NaOH addition proposed in the prior section.

2.2 Differential Scanning Calorimetry

Samples of NaOH doped resin (approximately 0.2 grams) contained in volatile pans were tested in a nitrogen atmosphere under a pressure of 225 psi. using a Dupont 910 Differential Scanning Calorimeter. The chamber was initially purged with nitrogen, and the temperature rise rate was set at 2°C/minute.

The DSC traces are presented in Figure 3. It is apparent that increasing the sodium content lowers the polymerization onset temperature and increases the reaction rate. These results are consistent with the behavior observed during gel time tests and may possibly be attributed to a higher incidence of para-substitution caused by sodium addition. However, further work is necessary to substantiate this hypothesis. Note also that the exotherm increases with sodium level.

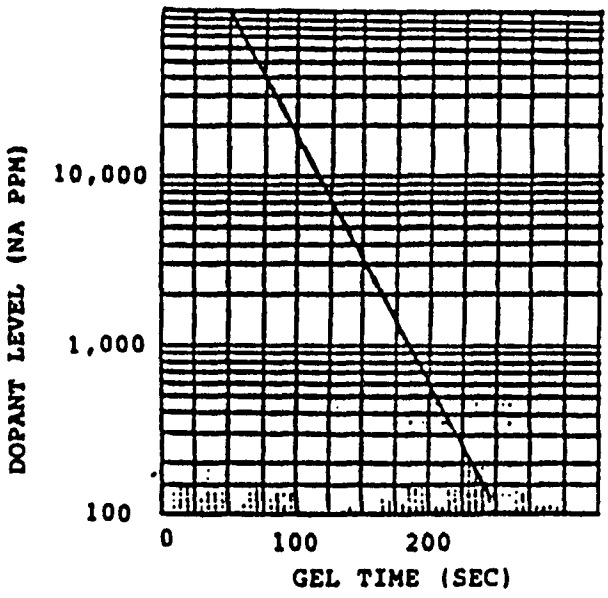

Figure 2. SC-1008 Phenolic Resin Gel Time as a Function of Sodium Content

2.3 Viscosity

Resin viscosity as a function of sodium content was measured at room temperature using a Brookfield Model LVDT Digital Viscometer. To obtain prescribed sodium levels, equal volumes of several concentrations of aqueous sodium hydroxide were added to pure resin. The viscosity of each sample was compared to that of a baseline solution which consisted of pure resin mixed with a volume of deionized water equal to that of the sodium hydroxide solutions. The viscosities of the aqueous NaOH solutions were also measured. The baseline for these measurements was pure deionized water.

The percent changes in viscosity with respect to baseline values are presented in Table 1. It is evident that the increase in viscosity at the 1000 ppm and 2000 ppm levels was due primarily to a chemical change in the resin as there was no measurable difference in the viscosities of the aqueous sodium hydroxide solutions. At a concentration of 5000 ppm, a transition had begun in which the dominant influence on the viscosity shifted from being chemical in nature to simply a "thickening" effect as evidenced by the increase in the viscosity of the aqueous NaOH solution. As the sodium level was increased, this effect became obvious.

2.4 Gel Permeation Chromatography

Gel permeation chromatography (GPC) is the separation by molecular size of molecules in solution. (8) Since the effective size of the polymer molecule is closely related to the molecular weight of the polymer, molecular weight distributions may also be obtained. This technique was utilized to both compare the two resin systems and to evaluate sodium effects and resin advancement.

A Waters High Performance Liquid Chromatograph with Sigma data station was used with Waters Ultra Gel Permeation columns having pore sizes of 1000 Å, 500 Å, and 100 Å. Further, a flow rate of 1 ml/minute was chosen and sample size was standardized at 40 microliters.

Three solutions, 0.5% by weight, SC-1008 resin to tetrahydrofuran (THF) were examined. The first solution was pure SC-1008 phenolic resin. The second was pure SC-1008 resin which had been exposed to ambient conditions for 15 days prior to solution preparation. The third solution was SC-1008 doped with 5000 ppm sodium.

By comparing the results of the latter two solutions with those of the pure resin solution, the following conclusions were drawn:

1. Resin exposed to ambient conditions for 15 days had a higher number of higher molecular weight constituents, indicative of resin advancement, and

2. Sodium hydroxide doped samples had lost some high molecular weight constituents and gained some low molecular weight constituents. This shift in the molecular weight distribution can be attributed to the breaking down of the oligomers. This degradation is caused by sodium addition, as stated previously.

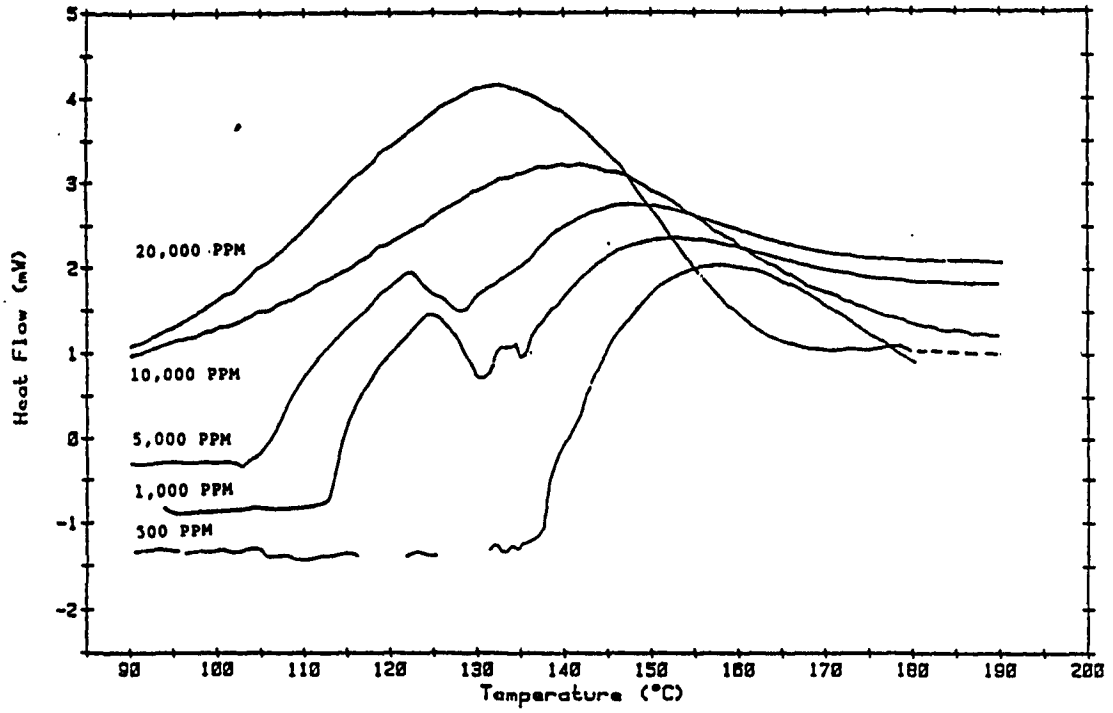

Figure 3. Differential Scanning Calorimetry Traces of Sodium Hydroxide Doped SC-1008 Phenolic Resin.

TABLE I

Viscosity Analysis

DOPANT LEVEL (Na ppm) SC-1008 + H_2O	% CHANGE RESIN Baseline	% CHANGE NaOH + H_2O Baseline
1000	9.4	0
2000	16.0	0
5000	18.9	10
10000	75.5	75
20000	132.0	175.0

2.5 Infrared Spectrophotometry

Samples of pure, and sodium hydroxide doped SC-1008 phenolic resin were studied using a Perkin-Elmer Model 137 Sodium Chloride Spectrophotometer. This analysis was conducted to determine if differences existed among the molecular structures of the pure and doped resin solutions. Several unidentified and unexpected peaks were observed, and reserach on the sources of these peaks is continuing. However, with the present instrumentation, it is not possible to obtain the information necessary for a proper analysis. Equipment of greater sophistication is required.

3. PREPREG ANALYSIS

The carbon/phenolic prepreg material used in this investigation was U.S. Polymeric FM 5055. The phenolic resin was Ironside 91LD, which was qualified under military Specification MIL-R-9299C. The carbon cloth, qualified under Thiokol Corporation Specification STW4-3184, was a rayon-based, eight harness satin fabric. Limits on the thread count were set at 45-55 yarns per inch in both the warp and fill directions, yielding a fabric weight range of 7.5 - 9.5 ounces per square yard. The third constituent was a carbonaceous filler, specifically P33, having a minimum carbon assay of 99%.

Before discussing the test methods and results, it is appropriate to describe the procedure used for NaOH doping of the prepreg. Four concentrations of a deionized water-sodium hydroxide solution were prepared and sprayed uniformly on one side of the test plies using a commercial air brush. The concentrations were calculated to add approximately 500, 1000, 1500, and 3000 ppm of sodium to the as-received material which served as the sodium content baseline. The amount of solutions sprayed on each ply did not vary amoung dopant levels. A control group (designated "water wash") which was sprayed with an equivalent amount of deionized water was also included.

Immediately after having been sprayed, materials were placed in a vacuum chamber at room temperature for one hour to remove excess moisture. It was determined that this period of time was sufficient to return the material to its weight before spraying, plus, of course, the added sodium. At this point, the doped prepreg material was ready for testing or fabricating into laminates.

Standard prepreg qualification tests required by Thiokol specification STW5-2649E were conducted. Additionally, several other tests not normally run in a production environment were incorporated, which did provide useful information. Methods for these additional tests will be explained, and standard test methods will be described in cases where it is felt that improvements can be made or potential problems exist.

3.1 Sodium Content

The prepreg content in parts per million (ppm) was determined using a Perkin-Elmer Model 5000 Atomic Absorbance Spectrophotometer. Samples weighing approximately 2 grams were placed in an oven for 16-18 hours at 1112°F to burn off the organics, thereby leaving sodium and other inorganic metals. This material was then put into solution with 5 milliliters of 12.1 N hydrochloric acid and 5 milliliters of deionized water used to rinse all matter from the crucible. The solution was diluted by a factor of 100 to 1 with deionized water before measurements were made.

The variation in the sodium level along the length of the as received prepreg can be seen in Table 2. Substantial differences in the level of sodium contamination are apparent, even in samples taken from roughly the same area, as evidenced by the values at 26 feet. These changes in concentration certainly contributed to the variation of sodium content in doped samples. Average values for each dopant level are also shown in Table 2.

3.2 Prepreg Resin, Cloth, and Filler Contents

The contents of the primary constituents of the carbon/phenolic prepreg were measured both to qualify the material with respect to Thiokol certification and to ensure that the sodium doping procedure did not alter these quantities. The following method was used to determine the percentages, by weight, of the three main constituents of the prepreg.

A room temperature sample, approximately 2 grams, was initially weighed, and then stirred in 450 milliliters of THF (tetrahydrofuran) at 95° F for 30 minutes. The solution was filtered and the fabric and separated fibers removed from the filter. This material was repeatedly washed with THF and the filtrant collected until the washing solution remained clear. Fabric and fibers, and the filter paper were then dried under vacuum at 113° F. The weight of filler was determined from the difference between initial and final filter weights. Resin weight was calculated by subtracting the cloth and filler weights from the devolatilized initial sample weight, (see section 3.4 for volatile content). The percentage was determined by dividing the weight of each constituent by the devolatilized sample weight.

Measurements were made on as received material and on samples considered to be extremes from this state, water wash and 3000 ppm added. Results of the analysis are presented in Table 3. The slight deviations of the 3000 and WW values from the as received state were within experimental error. It was concluded that the sodium doping procedure had a negligible effect on the resin, cloth, and filler content of the material.

TABLE 2

Sodium Contents of Prepreg Samples

As Received		Doped Material	
Location (ft)	Average Na (ppm)	Sample Designation	Average Na(ppm)
1	463	Waterwash	502
26	497	500	1214
26	890	1000	1358
44	385	1500	1792
75	524	3000	2708
100	462		
121	806		

TABLE 3

Resin, Cloth, and Filler Contents of Prepreg Material

	Thiokol-Supplied Batch Properties (%)	As Received (%)	3000 ppm Added (%)	Waterwash (%)
Resin Content	32.8	31.7	31.2	32.6
Cloth Content	52.8	53.8	55.9	54.9
Filler Content	14.4	14.4	12.9	12.5
Volatile Content	4.2	5.2	5.0	5.3

3.3 Resin Flow

The standard resin flow test as specified by Thiokol involves cutting four 4" x 4" squares of prepreg across the fabric width, stacking the squares to form a four-ply laminate, and recording the weight of the stack. All plies are to be bias cut to avoid fiber loss. The specimen, sandwiched between release plies, is placed in a heated press (325° F) and 150 ± 10 psig is applied immediately. After 10 minutes, the specimen is removed; resin flash is scraped away; and the specimen is weighed. The percent resin flow is calculated from the difference between the initial and final weights.

The prepreg material supplied by Thiokol was five inches wide, thus prohibiting use of a four inch square specimen cut on a 45° bias. The choice was either to piece together a four inch specimen or run a smaller three and one-half inch square bias cut specimen. Initially, there was concern that a nonlinear relationship might exist between specimen size and percent resin flow, so tests were conducted on three inch and three and one-half inch square specimens. Resin flow averaged 23.87% and 24.27% respectively. Obviously two points cannot settle a question of nonlinearity. However, since the ranges of the data sets completely overlapped and test results from pieced specimens (4", 3.5", and 3" square) were much too variable, it was decided to conduct flow tests using 3.5" square bias cut specimens.

The results of the tests are presented in Figure 4. The actual sodium contents listed are representative values based on chemical analysis described in section 3.1. The dark circles surrounding the white square are reduced reproductions of actual flow specimens. Resin flow areas are darkened, and the white square is the area from which the four-ply specimen was removed. From Figure 4, it is apparent that the flow decreases with increasing sodium content. The trend is fully supported by the experimental data, in which a nearly inverse proportionality is evident between percent resin flow and sodium content.

This behavior corroborates the results of the resin study. In the discussion of basic resin chemistry, one proposed effect of sodium addition was the tendency for a higher incidence of para-methylol phenol, which reacts more quickly and thus reduces gel time. The hypothesis was supported experimentally by the results of gel time and differential scanning calorimetry tests. The impact of increased sodium on resin flow is an obvious reduction due to faster gel.

As a final comment on the test procedure, it must be noted that the time during which the specimen is exposed to elevated temperature before the application of pressure is a critical factor. At 325° F the resin cures rapidly, and delays in pressure application will significantly influence the data. The time differential should be monitored and reported with the flow data. For all test results reported herein, this time was 19 ± 2 seconds.

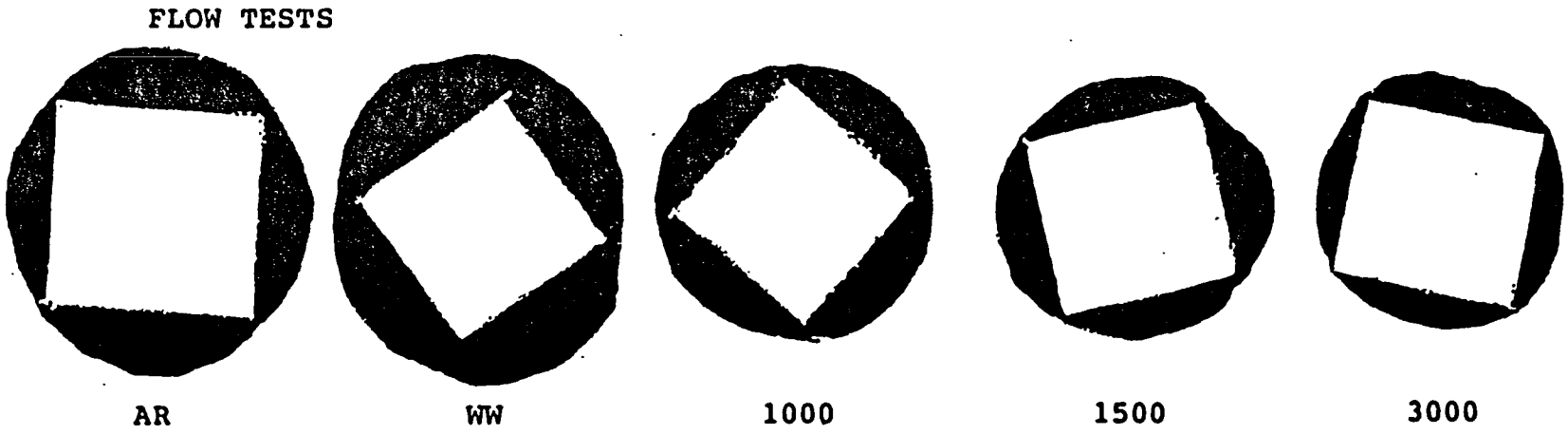

Sample Designation	Representative Sodium Level (ppm)	Resin Flow (%)
Water wash	500	26.27
As Received	600	26.68
500 PPM Doped	1200	23.10
1000 PPM Doped	1400	22.64
1500 PPM Doped	1800	20.89
3000 PPM Doped	2700	17.57

Figure 4. Visual and Quantitative Results of Prepreg Resin Flow Tests

3.4 Volatiles Analysis

3.4.1 Standard Test

The standard test for volatile content is straightforward. The weight loss of a sample of prepreg fabric (4" x 4") is measured after exposure to 323° F for 10 minutes in a recirculating oven. This value, when divided by the initial weight, yields the percent volatiles content.

Due to the excess water introduced into the material by the doping procedure, it was necessary to place the specimens under vacuum for one hour at room temperature to remove the moisture before testing. As received specimens were also vacuumed for consistency. Tests conducted on doped samples were limited to extreme states, WW and 3000, to ascertain whether differences existed and tests at intermediate levels were warranted.

Results are presented in Table 4. Although values from tests of the 3000 ppm added samples were slightly below those obtained from either of the other groups, the differences among the three groups were considered to be insignificant.

Also displayed in Table 4 are results from specimens tested without exposure to vacuum. The as received and the water wash samples were exposed to ambient laboratory atmosphere for 24 hours before testing. It is evident upon comparison with the above data that the one hour exposure to vacuum did not affect the volatile content of these two groups.

However, a significant difference in the volatile content of the sodium doped samples after exposure to ambient laboratory atmosphere can be seen. After one hour, an increase is noted, which could arguably be due to residual moisture from doping. However, there is little doubt that the change observed in the 24 hour value is due to accelerated moisture absorption caused by the presence of sodium.

3.4.2 Identification of Volatiles

It was stated in the previous section that high levels of sodium (3000 series) had no effect on the amount of volatiles released when the samples were vacuumed before testing. But there was concern that the volatile constituents might be altered by the level of sodium contamination. Therefore, the following precedure was developed to investigate this hypothesis.

Prepreg specimens of identical weight were placed in sealed canisters held at 120° F for 16 hours. Samples of gases extracted from the canisters were analyzed using a Perkin-Elmer Sigma 300 Capillary Chromatograph with Sigma 15 data station to obtain quantitative data on the volatiles. Next, samples were extracted for analysis on a Finnigan Model 4000 Automated Gas Chromatograph Mass Spectrometer System, which separates compoundsin the GC and then, through computer analysis of mass spectra, determines the compounds present.

An initial series of tests was conducted on AR, WW, and 3000 prepreg material at 150° F to identify the low boiling point effluents. The major constituents were ethanol, isopropanol, and methyl isobutyl ketone, and the minor constituents were ethyl acetate, 2-furancarboxaldehyde, and methyl ethyl ketone. No dopant effects on either the amounts or the relative amounts of these components were noted.

An additional series of tests using a Hewlett-Packard 5710A Gas Chromatograph was conducted at 203°F to determine the amount of phenol present in the volatiles. The quantity of phenol released was strongly influenced by sodium content. The phenol measured in the volatiles of the 3000 ppm specimens was approximately 5 times that observed in the analysis of the water wash samples and 8 times that measured from the as-received samples.

TABLE 4

Volatiles Content - Standard Test

	Group Designation	Volatiles Content (%)	
1 hr. Vacuum	As Received	5.23	
	Water Wash	5.28	
	3000	5.01	
No Vacuum	As Received (24 hours)*	5.22	
	Water Wash (24 hours)*		
	3000 (1 hour)*	5.47	--- Moisture
	3000 (24 hours)*	7.33	Absorption

*Note: Times listed in No Vacuum set denote length of exposure to ambient conditions before testing.

3.5 Gel Permeation Chromatography

The instrumentation and experimental conditions used to study the prepreg (91LD phenolic resin) were identical to those described in section 2.4. Resin was extracted with THF from a quantity of prepreg which had been calculated to yield a 0.5% solution of resin (by weight) and THF. Three solutions were prepared. The first was taken from a sample of as received material. The second was taken from a water wash sample, and the final solution was from a doped piece of material which had a sodium concentration approximately 3000 ppm greater than the as received prepreg.

Data from the prepreg analyses were compared within the group and also with that obtained from the SC-1008 study. The following are results of those comparisons:

1. The two resin systems appeared to be basically the same; however, a peak was evident in the prepreg (91LD) which was not present in the SC-1008. At this time, the source of the peak has not been identified.

2. The above peak is smaller in water wash and 3000 ppm traces than in those from the as received material.

3. The 3000 ppm samples appear to have lost some high molecular weight constituents and gained some low molecular weight constituents.

The third result is similar in nature to that observed in the sodium doped SC-1008 samples and provides additional experimental evidence of the degrading effect of sodium on these resins.

4. CURED LAMINATE ANALYSIS

Eighteen carbon-phenolic panels were fabricated for test specimens to investigate the effect of sodium concentration on matrix-influenced mechanical properties. The mechanical tests conducted were compression (warp), flexure (warp), and short beam shear. One panel was produced for each property at each of the six targeted sodium levels: as received (AR), waterwash (WW), 500 ppm added, 1000 ppm added, 1500 ppm added, and 3000 ppm added. Sodium was introduced in the prepreg material in the manner described in section 3. The compression and flexure panels were each constructed from four plies of material, and the short beam shear panels were comprised of nine plies.

All panels were cured in a heated press. A hydroclave cure cycle recommended by Thiokol, Wasatch Division, was adapted for use with the press. The steps are listed below.

1. Debulk under full vacuum for 30 minutes prior to cure

2. Increase pressure to 225 psig at room temperature

3. Raise temperature to 180 ±10°F; hold for 90-120 minutes

4. When temperature reaches 170°F, increase pressure to 1025 psig at an average rate not to exceed 20 psi per minute

5. Raise temperature to 220 ±10°F; hold for 60-90 minutes

6. Raise temperature to 310 ± 10°F at a rate not to exceed 1°F/minute

7. Hold at 310°F for a minimum of 5 hours

8. Decrease pressure to 200-250 psig at a rate not to exceed 50 psi/minute while holding at 310°F

9. Cool to 160°F at an average rate of 0.5°F/minute, maximum

10. Continue to cool for an additional 90 minutes, minimum, to room temperature before dropping pressure and vacuum.

Thermocouples were inserted in the edges of the laminates to monitor part temperature and thus to ensure the proper rise rate.

4.1 Laminate Quality Assurance

4.1.1 Nondestructive Evaluation

Several nondestructive evaluation techniques including computer aided tomography (CAT-Scan), radiography, through transmission ultrasound, alcohol wipe, and ultrasonic C-scan were employed to assess the integrity of the panels. The utilization of these methods was not targeted specifically to sodium dopant level analysis. Instead, these series of tests were designed to determine which of the techniques were suitable for evaluation of panels of this material and of these thicknesses. The effectiveness of the methods is summarized briefly in the following paragraphs.

CAT-scan analysis was generally not useful for these thin carbon-phenolic materials. Some visually identifiable surface defects were observed in the scans, and several of these did correlate with assumed low density areas located by alcohol wipe. However, other "suspect" regions identified by one of the methods were not substantiated by the remaining two. Bulk densities were also determined with CAT-scan in five different locations, and the average increased with increasing sodium content. This trend was not present in the actual measured values. However, it must be noted that the CAT-scan values were obtained from a small (.060" wide) slice of the panel.

X-ray analysis provided very little information. Only one defect, a surface bubble, was detected. The samples were too thin for this technique to be successful.

Through transmission ultrasonic measurements were made on each panel at four equally spaced locations along the centerline. Unlike the previously described methods, the effort in this series of tests was directed toward

correlation of signal characteristics with sodium dopant level. Velocity and attenuation data were evaluated; however, no trends were evident. One surface defect was analyzed, and a frequency shift in the wave form was observed. This anticipated result indicated that a 100% scan would be useful in the detection of flaws.

The ultrasonic C-scan inspection proved to be the most useful of the techniques studied. Density variations were readily apparent in the scans, which were run using a Sperry Reflectoscope Model S80. Representative C-scan results for a compression and a flexure panel are shown in Figure 5. Areas which appear white in the figure are regions of high attenuation. High scattering is responsible for much of the apparent density variations around the edges, and the four circles in each panel near the corners are the fixture posts. Overall, the scans indicated a high degree of uniformity in the panels' central portions from which all specimens were taken.

4.1.2 Sodium Content and Resin Content

After the nondestructive evaluations were completed, the panels were machined into the various specimen configurations. Initially, a 1-inch-wide trim area was removed from the perimeter of the laminates. Samples from the trim, adjacent to the specimen area were analyzed to determine sodium content and resin content of each panel. The sodium analysis was performed in the manner described in section 3.1, and the results are shown in Table 5.

The percent resin contents were determined according to the following procedure:

1. Clean material samples and weigh to nearest 0.001 g.

2. Place specimens in Vycor test tube and connect to a flask with cold finger condenser and a vacuum source attached.

3. Evacuate the system to 10 ±5 mm of mercury absolute.

4. When pressure stabilizes, place one Fisher burner under the samples in the end of the tube. Adjust the flame to cover the sample completely.

5. Pass an additional Fisher burner along the bottom of tube to drive out gases and prevent residue condensation in tube.

6. Continue pyrolysis for approximately 30 minutes or until pressure gauge reading returns to value prior to pyrolysis, whichever is longer.

7. When pyrolysis is complete, cool to room temperature while maintaining vacuum.

8. Turn off vacuum and slowly let air into the test tube until equilibrium is reached. Remove and weigh the specimen to nearest 0.001 g.

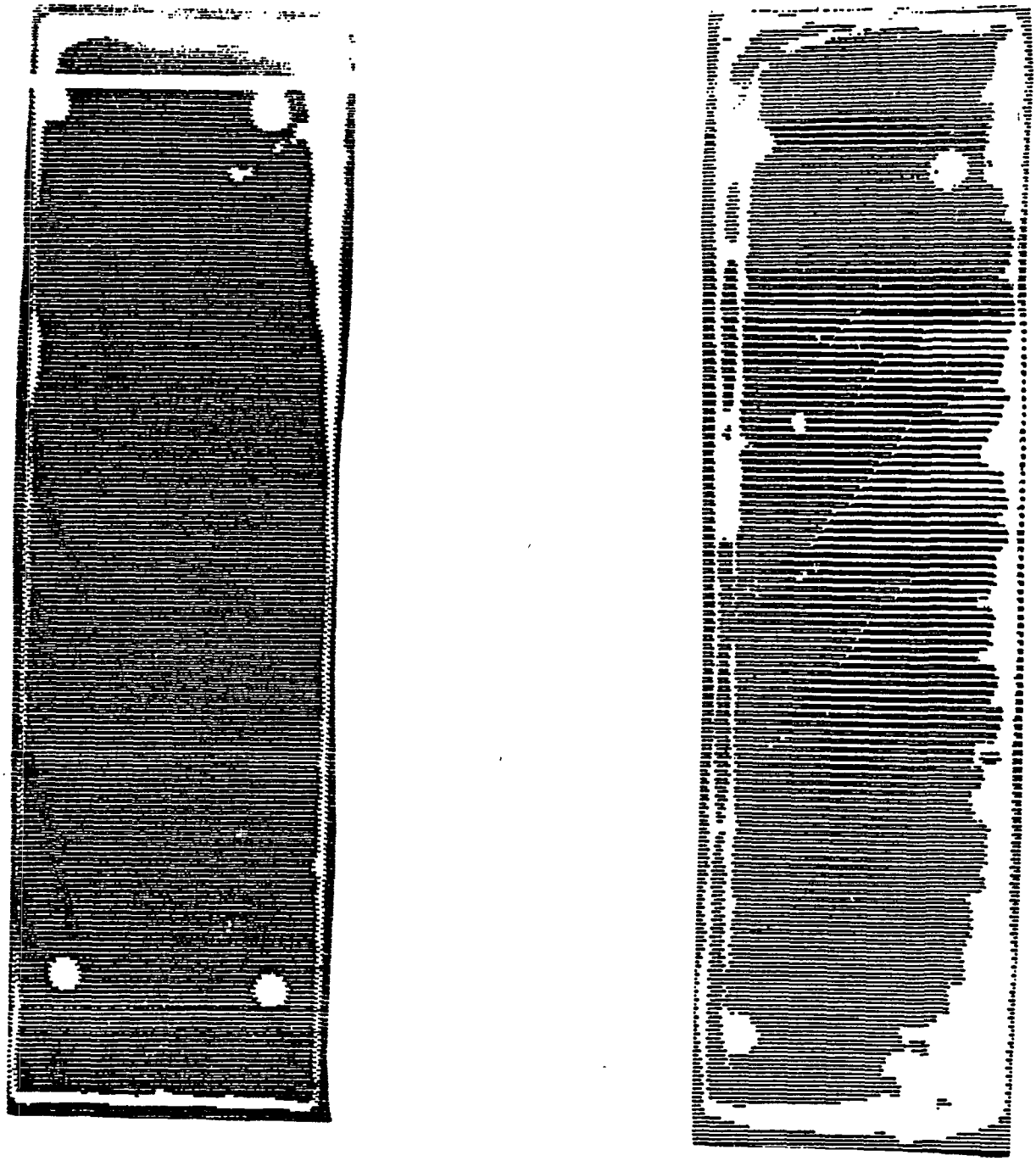

Figure 5. Representative Ultrasonic C-scans of Thin (0.060") Carbon/Phenolic Test Panels.

9. Calculate dry resin content using equations below

Resin content (%) = (1.00 - final weight/initial weight)(100)(K)

where K is an empirical constant, for this material which equals 2.008.

The resin content for each specimen panel is shown in Table 6.

Table 5. Average Sodium Content (ppm) of Test Panels

Panel Designation \ Target Sodium Level	AR	WW	500	1000	1500	3000
SBS	610	765	996	1461	2286	3726
COM	642	697	1197	1710	2028	3531
FLX	640	516	1302	1967	2797	4090

Table 6. Average Percent Resin Content of Test Panels

Panel Designation \ Target Sodium Level	AR	WW	500	1000	1500	3000
SBS	33.1	34.0	33.8	35.4	36.1	33.6
COM	38.3	33.7	39.1	39.5	37.3	37.2
FLX	36.4	34.1	37.7	35.9	37.9	41.0

4.1.3 Microscopy

Two types of microscopy were employed in the investigation: optical and scanning electron. Optical microscopy was used primarily qualitatively. Each specimen was examined to assess void content, to inspect irregularities in surface layers, and to detect abnormalities in ply spacing and orientation. The void content was observed to be low, but no measurements were made to quantify this value. No imperfections in the ply spacing were observed in the sample population. However, in addition to the small "bubble" mentioned previously, two types of surface defects were detected and examined. One type consisted of irregular patterns in the matrix surface layer caused by distortion of the release ply. The second were small indentations extending into the top ply. This flaw was due to either a trapped yarn from the fiberglass overbleed ply or wrinkling of the release ply. All shear and

flexure test specimens were required to be defect-free. Surface-type flaws were permitted in tab regions of compression specimens provided they were an ample distance from the gauge section.

The fracture surfaces of several samples were examined under a scanning electron microscope. Regions were studied to determine whether differences existed in the fiber-matrix adhesion (due to sodium doping) and to compare the chemical analysis of selected areas obtained via the energy dispersive X-ray (EDX) technique.

A preliminary indication from this effort is that no apparent differences exist in the interfacial bonding respective to sodium content. Chemical analysis work is also continuing at present, and no definite results are available. However, an example of the information provided by the EDX technique is presented in Figure 6. It is evident that the composition of the particulate on the surface (appears white) shown as the solid trace, does not differ substantially from that of the matrix, represented by the dotted line. The particulate may well be bits of fragmented matrix material. It should be noted that the aluminum and silicon peaks are artifacts of the system. Additional details and results of this analysis will be presented in a subsequent final report.

4.1.4 Thermogravimetric Analysis

Thermogravimetric (TGA) tests were conducted on carbon broadgoods and carbon/phenolic laminates representing various levels of sodium contamination. A Dupont 951 Thermogravimetric Analyzer was used for the study. An isothermal heat treatment at 512 °C for 30 minutes under a nitrogen atmosphere was found to be sufficient to separate sodium contents greater than 500 ppm (sensitivity to approximately 500 ppm).

Samples of carbon fabric were doped to obtain the desired sodium levels using a procedure similar to that described in section 3. The results from tests on these samples are presented in Figure 7. The increase in weight loss with sodium content is apparent, and is attributed to the fact that sodium catalyzes the oxidation of carbon fibers at elevated temperatures.

During evaluation of carbon/phenolic laminates, a dramatic increase in weight loss was noted when samples were tested with normal (50 mL/minute) airflow as compared to results from similar tests conducted with no air flow. This behavior is illustrated by the traces from 1000 ppm added specimens which are shown in Figure 8. The exact cause of this phenomenon is not known at the present time, but the responses are reproducible and investigation is continuing. Since TGA is used as a quality assurance test, the air flow through the test chamber should be monitored and reported with the results to enable meaningful comparison of data.

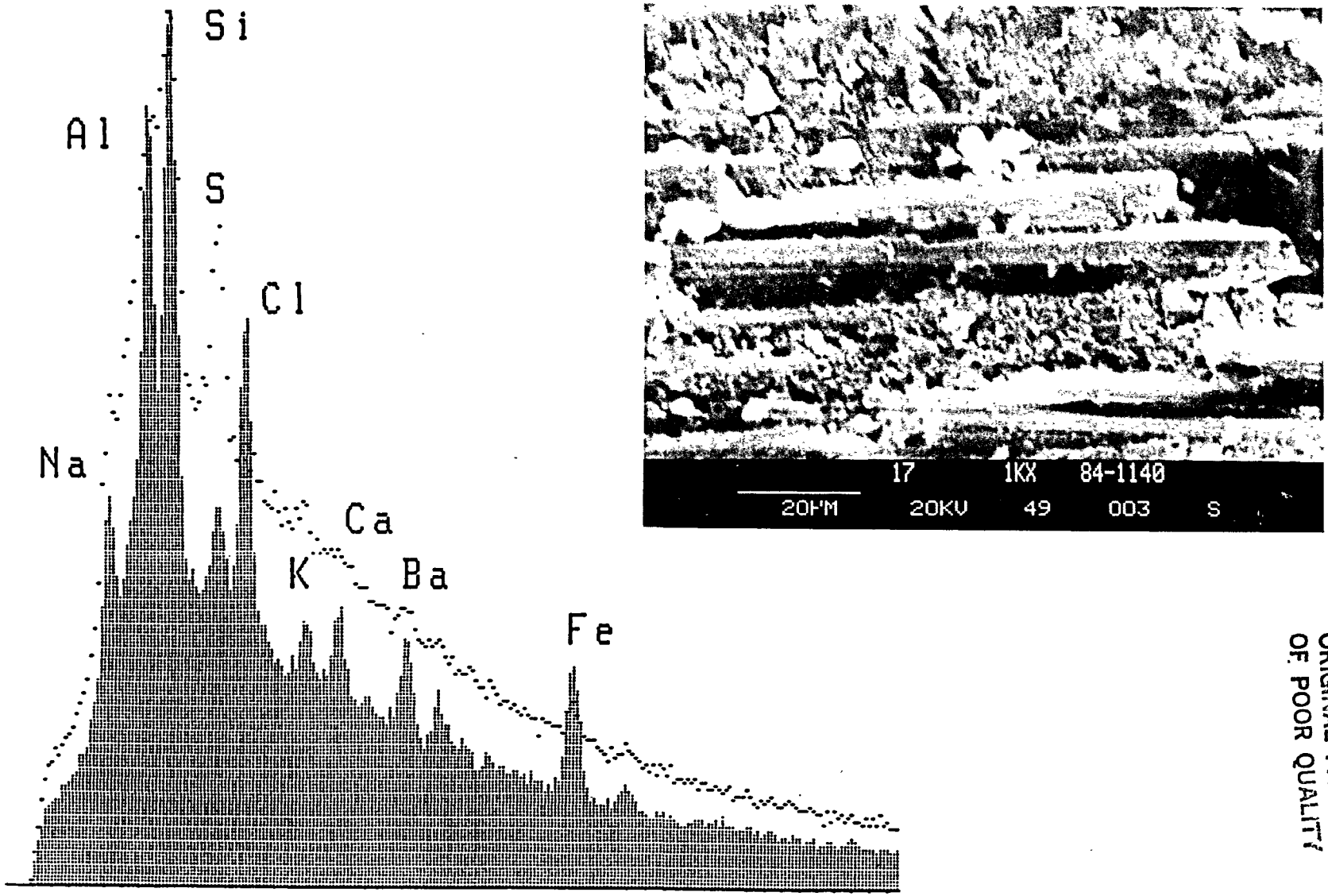

Figure 6. Scanning Electron Micrograph and Chemical (EDAX) Analysis of White Particulate and Matrix of Carbon/Phenolic Material.

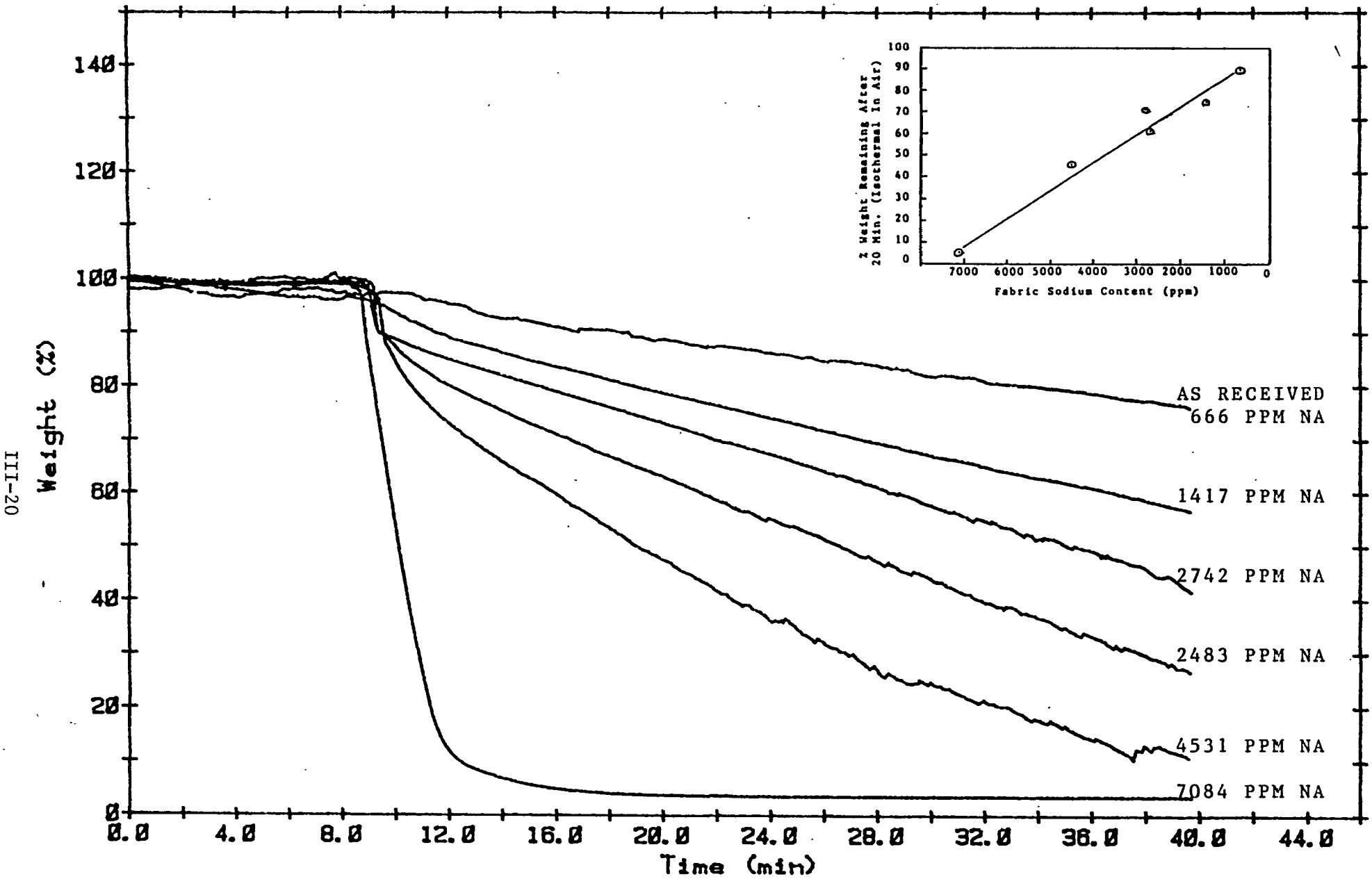

Figure 7. Results of Thermogravimetric Analysis of Sodium Hydroxide Doped Carbon Cloth.

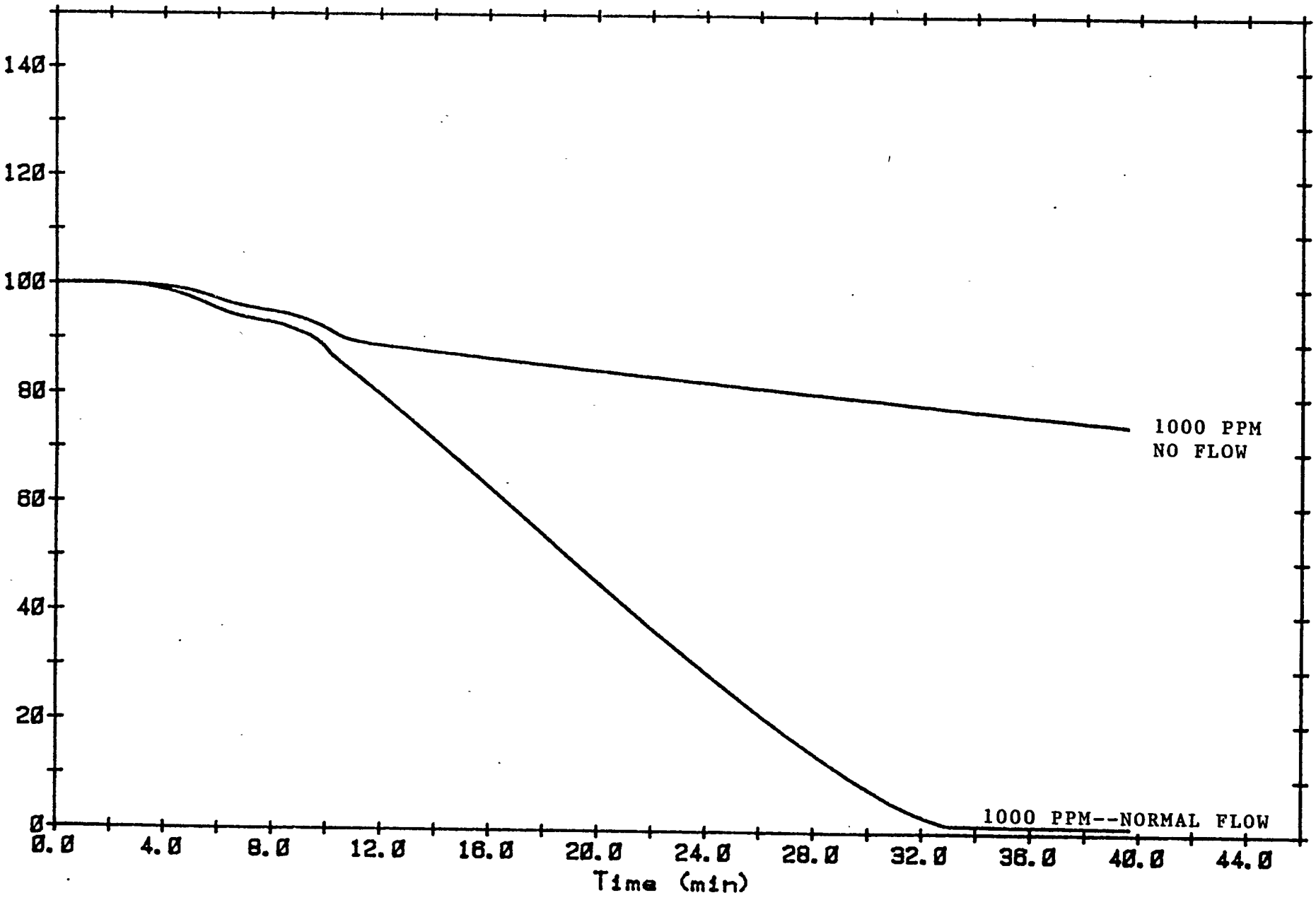

Figure 8. Influence of Air Flowrates on Results of Thermogravimetric Analysis of Sodium Hydroxide Doped Carbon/Phenolic Laminate.

4.2 Mechanical Property Tests

4.2.1 Compression Tests

Compressive strength and modulus values in the warp direction were obtained following ASTM D3410-75, Test for Compressive Properties of Oriented Fiber Composites. The standard requires use of the so-called "Celanese" test fixture, and features a specimen design which has an unsupported gauge length of 0.5 inch. Specimens were constructed from four plies of prepreg which yielded an average gauge section thickness of 0.052 inch.

Tabs were constructed from four plies of the as received carbon-phenolic material and a 0.25-inch, 6° taper was milled into each piece. The tabs were bonded to specimens with AF-191, a supported epoxy bonding film produced by 3M. Bonding was accomplished using a heated press according to the cure cycle recommended by the vendor, with the exception that maximum temperature was 300 °F.

Two-section strain gauges (longitudinal and transverse) were fixed to one side of each specimen and a single gauge was bonded on the opposite side to monitor buckling. Strain and load values were recorded automatically by an Acurex Autodata Ten/50 and a hard copy of the data produced. Tests were conducted in a Baldwin-Emery SR-4 testing machine at a constant crosshead speed of 0.05 inches per minute. Six specimens per sodium dopant level were tested.

Results of the compression tests are presented in Table 7. The strength was not a function of sodium content. However, there was an apparent reduction in modulus values with increasing sodium content. The 500 group was a noted exception to this trend. At present, tests of pure and doped resin are in progress which may provide additional information leading to a better understanding of the observed behavior.

4.2.2 Short Beam Shear Tests

The short beam shear method was used for determination of apparent interlaminar shear strengths. Although not a popular technique for evaluating carbon-phenolic materials, some interesting results were obtained. Problems arise in the use of this method when specimens fail in a complex mode involving both shear and flexural type failures. According to Peters[9] the data from complex failure mode tests should not be used even as a conservative estimate of shear strength. With regard to this argument, it must be emphasized that the significant results of these tests are not limited to comparisons of strengths; failure analysis must be considered.

Specimens were constructed from nine plies of prepreg material, and were machined to provide a square cross-section. Test conditions and specimen geometry as prescribed in ASTM D 2344-76 were followed. The span to thickness and length to thickness ratios were 5:1 and 7:1, respectively, required for carbon yarn reinforcement. The test fixture had an adjustable span to accommodate slight variations in thickness. An Instron model 1125 testing machine was used for these tests, which were conducted at a constant crosshead speed of 0.05 inch per minute. The minimum number of specimens tested for each dopant level was ten.

For a clear understanding of the shear tests results, both strength values and failure analysis observations have been included in Table 8. A comparison of the stress values above suggests that the interlaminar shear strength increased with sodium content. The departure of the 1000 group from the apparent trend cannot be explained at present. Additional research is necessary to further substantiate the response pattern and to determine if this particular group's behavior is simply anomalous. However, in view of the failure analysis, the reporting of the average of the 1500 and 3000 groups as a shear strength is arguable.[9] Although it is not the purpose of this article to rigorously defend the choice, certain evidence merits consideration. Specimens of these two groups which failed in shear exhibited a higher strength, on average, than those of the lower sodium groups. Further, the high sodium shear failure stresses were interspersed with those produced by flexural and combined failure modes. Therefore, the reported values appear to be reasonable, if somewhat conservative, representations of the shear strength.

It is evident from the results of these tests that the presence of sodium in such levels has toughened or "plasticized" the matrix to enable the material to withstand higher shear loads. The performance has reached a transitional region where failure can occur by either shear, flexure, or a combination of both. The physical phenomena responsible for the observed behavior have not been documented, but the resin test series mentioned in the prior section is expected to provide information necessary to determine the causes.

4.2.3 Flexure Tests

The flexural strength and modulus values in the warp direction were determined according to the procedures stated in ASTM D790-81. Two different load application methods, three-point and four-point bending, are presented in the standard; the three-point procedure was followed. According to Zweben, et al,[10] in their examination of the standard, the specified procedures provide reliable strength data, but the modulus values could be misleading. A suggested correction to this problem was to employ a high span-to-depth ratio. The span on the test fixture was limited to a minimum of two inches. Specimen geometry was designed subject to the restriction to yield a support span-to-depth ratio of 32 to 1. However, the average thickness of the four-ply specimens was 0.057 inch, thus increasing the ratio to 35 to 1. The cross-head rate of 0.104 inch per minute was adjusted to account for slight variations in thickness. Two different rates, averaging 0.140 and 0.096 inch per minute, were used for the AR, WW, and 1000 groups. All groups consisted of six specimens. The higher rate was calculated by interpolation of conditions for 40 to 1 span-to-depth ratio which was realistic for the thinner specimens in these groups.

The differences observed in the strength and modulus values of the AR specimens tested at the two rates were negligible. The effect of the variation was more evident in the WW and 1000 groups. Both strength and modulus values were greater at the higher rate. The amount of the increase was on the order of 10% for all properties except the WW strength which increased by approximately 15%. It is not known at present whether the

Table 7. Results of Compression Tests

Sample	Strength (psi)	Modulus (Msi)	Poisson's Ratio
WW	33836	3.99	.19
AR	36638	3.94	.20
500	34640	4.38	.18
1000	36017	3.67	.22
1500	37069	3.42	.18
3000	33037	2.94	.19

Table 8. Results of Short Beam Shear Tests

		Failure Mode		
Sample	Shear Strength (ksi)	Shear	Flexure	Combination
WW	4.3	11	1	
AR	4.2	8	1	1
500	4.6	10		
1000	4.0	11		
1500	4.8	3	5	2
3000	5.0	2	5	3

Table 9. Results of Flexure Tests

Sample	Flexural Strength (ksi)	Flexural Modulus (Msi)
WW	37.8	2.50
AR	52.3	2.93
500	36.8	2.79
1000	48.7	3.25
1500	46.9	2.87
3000	40.6	2.76

disparities are due to loading rate effects or simply interpanel variability. Additional tests are required for verification.

Results of the flexure tests, failure strength and tangent modulus are presented in Table 9. Average properties for the three groups discussed above were reported. No correlation of modulus values with sodium content is evident. But, there appears to be a relationship between flexural strength and sodium level. As the concentration increases, the failure stress decreases. The WW and 500 groups obviously do not adhere to the pattern. However, from unreported test results of an off-nominal produced WW panel, there is reason to believe that failure stress could be on the order of the AR group. Further testing is required for a clear understanding of the effect of sodium contamination.

4.3 Failure Analysis

4.3.1 Short Beam Shear

The majority of the significant information obtained from the microscopic evaluation of the failed specimens has been discussed in section 4.2.2. Shear failures indicated by cracks parallel to the 0° fibers in the interfacial/interlaminar regions are shown in Figure 9. The cracks appear as white traces on the surface of the specimen.

Another failure mode observed in the specimens but not mentioned previously is a tensile rupture. Evidence of this type of failure can be seen in Figure 10. While many of the visible cracks are along the 0°/90° fiber interface, indicative of shear failure, there are several which run at approximately 45°. These cracks through the 90° fiber bundles are due to a resolving of the shear stresses into a tensile mode.[11] Fractures of this nature were observed in every group.

A flexural failure of a short beam shear specimen is shown in Figure 11. The failure zone is located at the bottom center of the photograph with the cracks visible as dark lines. Although not clearly reproduced in the picture, the lower two 0° fiber layers fractured due to tensile stress. Some shear and tensile rupture failures are evident, but damage is local to the primary flexural area, suggesting that these cracks may well have occurred subsequent to the initial fracture. As stated previously, the dominent failure mechanism in the majority of the higher sodium content samples was tensile flexure.

An additional type of fracture mode, termed combination, was observed frequently in the higher sodium level specimens. Two mechanisms, shear and tensile flexure, were active in the failure process. Unlike the mode visible in Figure 11, the shear cracks were removed and distinct from the flexural region. In Figure 12, tensile flexure is evident in the white area on the bottom right. Shear cracks are visible as faint white traces left of center of the specimen. From the evidence observed, it appears that these mechanisms acted independently of one another.

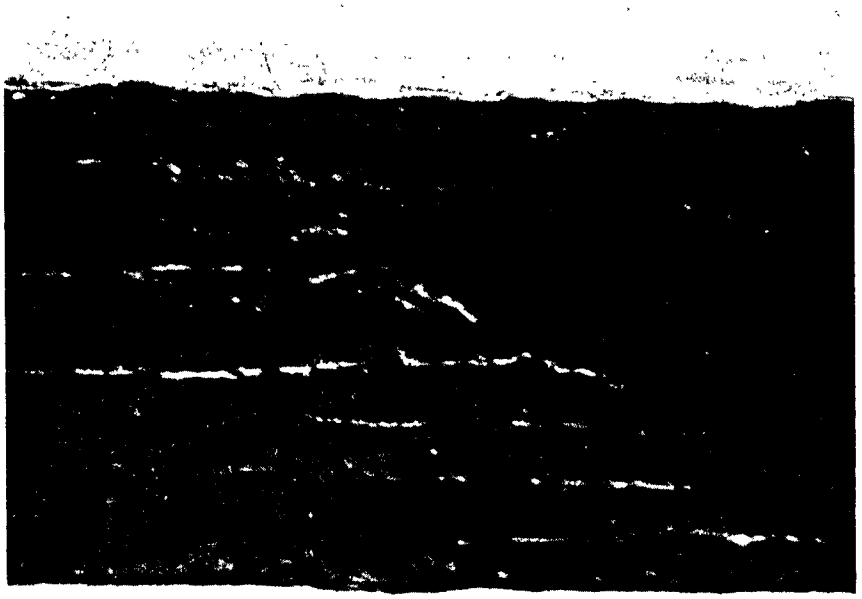

Figure 9. Typical Microstructure of Shear Failure Mode in Short Beam Shear Specimen.

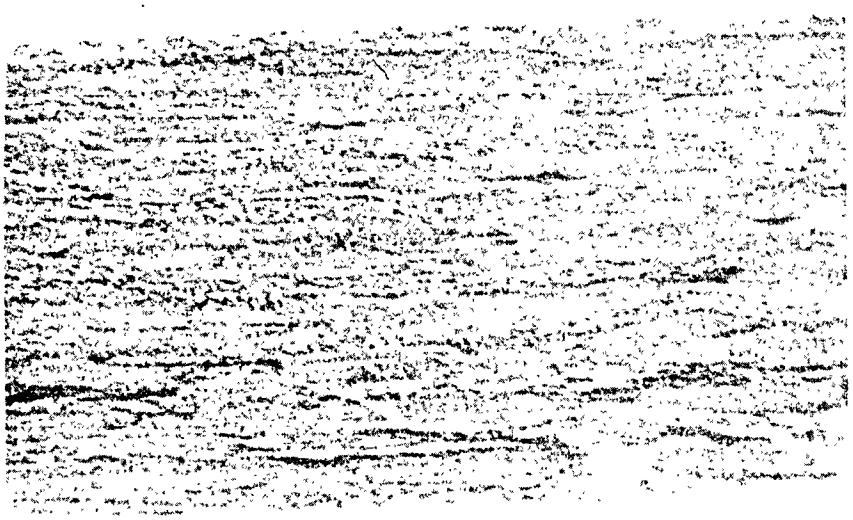

Figure 10. Typical Microstructure of Shear and Tensile Rupture Failure Modes in Short Beam Shear Specimen. Note Cracks at 45° Indicative of Tensile Rupture.

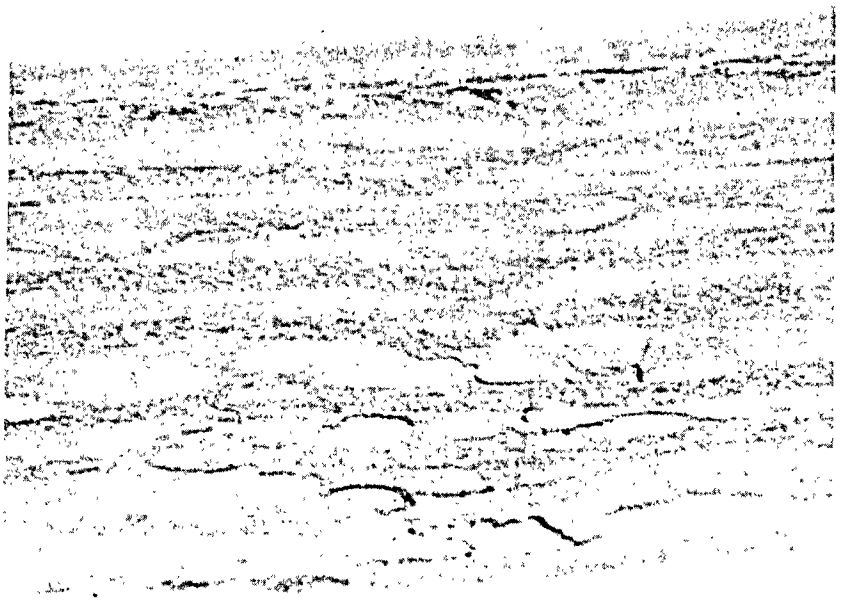

Figure 11. Typical Microstructure of Flexural Failure in Short Beam Shear Specimen

Figure 12. Typical Microstructure of Combined Flexural and Shear Failure Modes in Short Beam Shear Specimen. Note Flexure at Lower Right and Shear at Left Center.

In section 4.2.2, the conclusion was drawn that there was a transition sodium level below which failures were almost exclusively shear or a shear-produced tensile rupture, and above which flexure and combination failures dominated. Associated with the transition was an apparent increase in shear strength. The cause of this behavior was proposed to be a toughening of the matrix brought about by sodium addition. Miller and Winger [11] have observed a similar behavior in short beam shear tests wherein the transition of failure modes is determined by temperature. They have attributed the behavior to a decrease in the modulus on the matrix (softening) when progressing from lower to higher temperatures. The lower modulus material promotes the apparent shear fracture mode. A decrease in strength values with increasing temperature across the transition region was also observed. Data from resin tests now in progress will be necessary to confirm the transition mechanism in this study.

4.3.2 Flexure

The failure analysis of the flexure specimens supports the hypothesis proposed in section 4.2.3 that a relationship exists between flexural performance and sodium content. There appears to be a change in failure mechanisms as evidenced by fracture surface characteristics which is similar to that observed in the shear tests, although the transition is somewhat less distinct.

Three of the AR samples and one of the WW samples broke into two pieces indicative of brittle fracture. The characteristics of the failure surface displayed in Figure 13 were representative of the remaining AR and WW samples. The lower two plies* were completely shattered in a tensile flexure mode. Extensive damage was evident in ply 2 and cracks often were visible in the 0° fibers of the top ply. Note that damage was reasonably local to the flexural failure zone, i.e., there was an absence of translaminar and interlaminar cracks extending more than approximately two thicknesses away. The above discribed features are typical of what was termed brittle failure.

A failed specimen from the 500 group is shown in Figure 14. Several of the surface features evident in the photomicrograph are similar to those discribed above, but there are noteworthy differences. Again, the lower two plies were shattered in tensile flexure, and damage was local to the flexural failure zone. But, in contrast to the AR and WW groups, damage in ply 2 was not as severe, and cracking in ply 1 was either minor or unobservable at this magnification(20X). These failures are still of the brittle type.

Considering only the extent of failure of the 0° fibers, the performance of the 1000 group was similar to that of the 500 group. However, a change in the failure mechanisms involved was evident. Most significant was the development of large interlaminar cracks between the lower plies. A representative fracture of this type is shown in Figure 15. Concomitant with the interlaminar shear/tensile flexure fracture mode was the extension of cracking beyond the primary failure area. Such behavior represented a departure from the exclusively brittle fracture previously observed to a more "plastic" type, matrix-influenced mode.

* Plies are numbered from the upper surface 1-4.

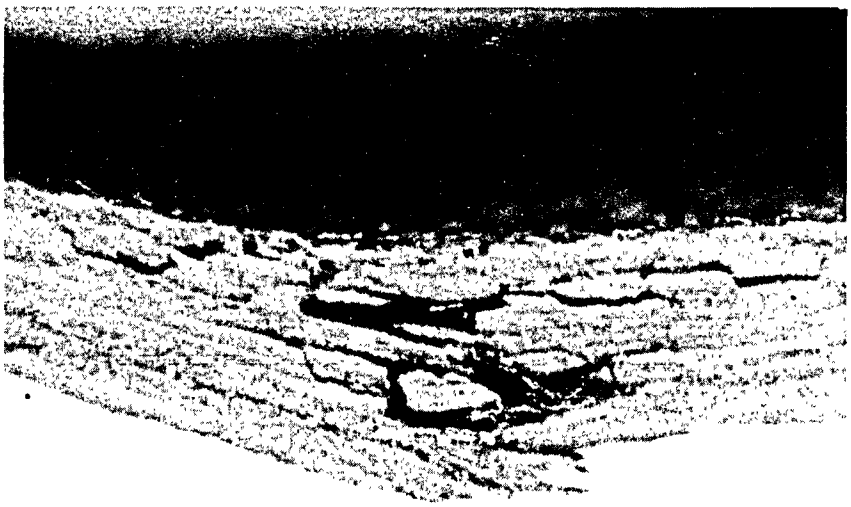

Figure 13. Typical Microstructure of Brittle Failure in AR and WW Flexure Specimens.

Figure 14. Typical Microstructure of Brittle Fracture in 500 Flexure Specimen.

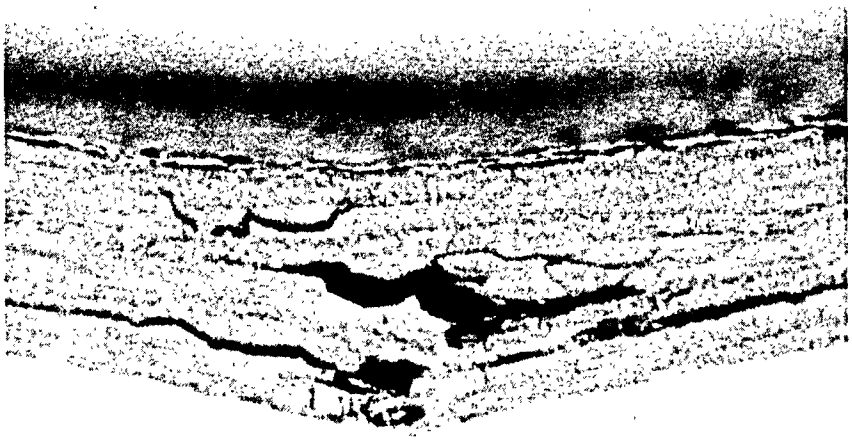

Figure 15. Typical Microstructure of 1000 Group Flexure Specimen. Note Increased Interlaminar Cracking in Lower Plies.

Figure 16. Typical Microstructure of Failed 1500 and 3000 Flexure Specimens. Note Large Interlaminar Crack Between Lower Plies and Absence of Damage in Upper Plies.

At sodium levels of the 1500 and 3000 groups, there were significant changes in the failure characteristics. A representative fracture surface, taken from the 1500 group, is shown in Figure 16. The bottom ply failed in tensile flexure and a large delamination developed between plies 3 and 4. In the majority of the tests, no damage was observed in plies 1 and 2, and in many of these, the third ply survived with little or no damage. The appearance of the specimens suggests that the failure mode has become strongly matrix-influenced at these levels of sodium contamination.

The operative failure mechanisms appear to be functions of sodium content similar to the behavior observed in the shear tests. The transition region is near the 1500 ppm added level. But, at present, the phenomena responsible for this performance are not known. Tests of the matrix material alone may provide additional information necessary for a clearer interpretation of these results.

5. CONCLUSIONS

The investigation described in the previous pages was undertaken to assess the effects of sodium contamination level on the physical properties of phenolic resin and the matrix-influenced mechanical properties of carbon-phenolic composite laminates. Proposed effects of sodium hydroxide addition to the resin, which were consistent with basic resin chemistry, were (1) an increase in the relative percentage of para-substitution, a faster reacting product, and (2) degradation of the resin oligomers.

These hypotheses were supported with experimental evidence from gel permeation chromatography tests. A decrease in high molecular weight constituents and an increase in low molecular weight constituents were noted, indicating resin degradation upon sodium hydroxide addition. Further, an increase in reaction kinetics producing a decrease in gel time and a lowering of polymerization onset temperature were observed at increasing dopant levels. Greater sodium contamination also led to an increase in moisture absorption by the prepreg under ambient conditions and an increase in the phenol efflux measured during volatiles tests.

Properties of cured laminates were also shown to be dependent upon sodium level. An increase in sodium content apparently led to a decrease in compressive modulus and flexural strength and an increase in shear strength. Operative failure mechanisms were related to dopant level, and transitions were observed in the cases of shear and flexural modes. Results from thermogravametric analysis indicated that higher levels of sodium may also lead to matrix degradation at lower temperatures.

Finally, it was stated at the outset that prior studies had been focused on sodium effects on carbon fibers. Clearly, sodium contamination also has a significant influence on resin and matrix-related properties which should not be overlooked. The results presented have provided an indication of the severity of this problem. Further work is warranted to clarify many points brought out in the investigation and to more firmly establish the relationship between sodium content and material performance.

6. RECOMMENDATIONS

The following recommendations were made based on the findings of the study.

1. Determine relationship between laminate moisture absorption and dopant level
2. Perform elevated temperature mechanical property tests
3. Evaluate the performance of very low sodium content material
4. Assess aging effects
5. Report time at temperature before pressure application in flow tests
6. Monitor volatile efflux and identify constituents
7. Investigate resin modulus as a function of dopant level
8. Include fracture analysis with mechanical property results
9. Initiate interface/bonding studies
10. Institute GPC, FTIR, GC/MS, DSC, and TGA quality control tests.

ACKNOWLEDGEMENTS

The authors would like to express their appreciation to J. Perkins for his assistance in the development of the volatiles identification method, and to J. Coston for the SEM and EDAX work. The authors are also sincerely grateful to B. Holden and G. Waggoner, B. Stevenson and J. Oakley without whose help the compression tests could not have been conducted.

REFERENCES

1. Walker, P.L., Chemistry and Physics of Carbon, vol. 4, Marcel Dekker Inc., New York, 1968, pp. 287-324.

2. Walker, P.L. and Thrower, P.A., Chemistry and Physics of Carbon, vol. 8, Marcel Dekker Inc., New York, 1973, pp. 212-216.

3. McMahon, P.E., "Oxidative Resistance of Carbon Fibers and Their Composites," Advanced Composite Materials - Environmental Effects ASTM STP 658, J.R. Vinson, Ed., American Society for Testing and Materials, 1978, pp. 254-266.

4. Gibbs, H.H., Wendt, R.C., and Wilson, F.C., "Carbon Fiber Structure and Stability Studies," Polymer Engineering and Science, vol. 19 No. 5, April, 1979, pp. 342-349.

5. Gould, D.F., Phenolic Resins, Reinhold Publishing Co., New York, 1959.

6. Reusch, W.H., An Introduction to Organic Chemistry, Holden-Day Inc, San Francisco, 1977.

7. Lynn, R.O., private communication, Materials and Processes Lab., Marshall Space Flight Center, August, 1984.

8. "Effects of Resin on the Formation of Defects in Carbon-Carbon" Final Report for period August 1981 - March 1984, AFWAL-TR-84-4058, Materials Lab, Wright Patterson AFB, June, 1984.

9. Peters, P.M.W., "The Interlaminar Shear Strength of Unidirectional Boron Aluminum Composite," Journal of Composite Materials, Vol, 12, Jan. 1978, p. 53.

10. Zweben, C., Smith, W.S., and Wardle, M. W., "Test Methods for Fiber Tensile Strength, Composite Flexural Modulus, and Properties of Fabric Reinforced Laminates," Composite Materials: Testing and Design (Fifth Conference) ASTM STP 674, S.W. Tsai, Ed., American Society for Testing and Materials, 1979, p. 228.

11. Miller, A.G., and Wingert, A.L., "Fracture Surface Characterization of Commercial Graphite/Epoxy Systems," Nondestructive Evaluation and Flaw Criticality for Composite Materials, ASTM STP 696, R.B. Pipes, Ed., American Society for Testing and Materials, 1979, pp. 223-273.

D4

1984
NASA/ASEE SUMMER FACULTY RESEARCH FELLOWSHIP PROGRAM

MARSHALL SPACE FLIGHT CENTER
THE UNIVERSITY OF ALABAMA

SILICON CARBIDE-SILICON NITRIDE FIBERS: PREPARATION AND CHARACTERIZATION OF POLYCARBOSILAZANE PRECURSORS

Prepared by:	David J. Crouse, Ph.D.
Academic Rank:	Assistant Professor
University and Department:	Tennessee Technological University Department of Chemistry
NASA/MSFC:	
Laboratory:	Materials and Processes
Division:	Non-Metallic Materials
Branch:	Polymers and Composites
NASA/Counterpart:	Benjamin G. Penn, Ph.D.
Date:	August 24, 1984
Contract No.:	NASA-NGT-01-002-099 (The University of Alabama)

SILICON CARBIDE - SILICON NITRIDE FIBERS PREPARATION AND CHARACTERIZATION OF POLYCARBOSILAZANE PRECURSORS

By

David J. Crouse
Assistant Professor of Chemistry
Tennessee Technological University
Cookeville, Tennessee

ABSTRACT

Silicon carbide-silicon nitride fibers have shown potential as replacements for graphite in composite materials where high electrical resistance and thermal stability are required. The objective of this study is to examine the effect of modifications of the chemical structure of the monomers on the properties of the polymeric precursor and ceramic fibers.

A group of silaneamines, $R'-Si(NH-R)_3$, taken from the series where R' is methyl or phenyl and R is n-propyl, n-butyl, phenyl or allyl, are converted to polycarbosilazanes by heating in excess of 500°C. Resins obtained from this polymerization are characterized by NMR and IR spectroscopy and GPC. Each resin is tested for fiber-forming properties. Resin samples and fibers are hydrolytically cured.

Thermogravimetric analyses are conducted on the cured resins to compare the relative thermal stability and examine the pyrolysis process. Cured fibers are tested for tensile strength.

LIST OF TABLES

LIST OF FIGURES

INTRODUCTION

Fiber-reinforced resin-matrix composites are now used extensively in aerospace applications from aircraft structural materials to rocket motor nozzles. The Technological demand for higher performance and decreased weight in aircraft and missile parts is one impetus to research and development in the area of advanced reinforcement in the area of advanced reinforcement fibers. Fibers made from boron, carbon or silicon carbide exhibit the high mechanical strength, high elastic modulus and low density necessary for these applications. Carbon or graphite fibers are the predominant high strength, high modulus reinforcing agent currently used in high performance composites. In general, performance has been more than adequate, often exhibiting impressive strength, stability, stiffness and fracture toughness.

Despite the advantages of carbon fibers, there exist areas where improvement can be made by the development of alternate fibers for composite materials. Carbon fibers are subject to oxidative degradation in air at temperatures above 400°C giving off a volatile oxide.[1] Carbon fibers also show high electrical conductivity. This has led to some concern over product safety during manufacture, application and disposal.[2] The hazards would primarily be posed by fibers accidently released into the atmosphere where they may interfere with or damage unprotected electrical equipment causing resistive loading, short circuits or arcing.3 Carbon fibers sometimes show poor adhesion with thermoplastic or metal matrices, leading to debonding of the fibers from the matrix at low stress. Many of the most desirable applications of composite materials are in high temperature areas such as gas turbine blades, plasma devices and rocket motors. Current carbon fibers show insufficient temperature stability for applications of this type.

The above limitations necessitate the search for new materials with potential as carbon fiber replacements. Silicon carbide-silicon nitride (SiC - Si_3N_4) fibers have been suggested as a potential candidate.[4] Fibers of this type are currently under development in the Materials and Processes Laboratory of the Marshall Space Flight Center. Such fibers are oxidation resistant at high temperatures and posses other properties similar to carbon fibers.[5] Silicon carbide-silicon nitride fibers prepared at MSFC show a tensile modulus of approximately 29 x 10^6 psi.

At this stage of development, this compares favorably with that of graphite fibers with an average value of 55 x 10^6 psi. The electrical resistivity value of these fibers is measured at 7 x 10^8 ohm-cm. This lies in the semiconductor range but approaches the value of a true insulator ($\geq 10^{12}$).

The material currently under investigation at MSFC is similar to that prepared by Verbeek. A monomer is prepared by the reaction of methyl trichlorosilane with methyl amine (Eq. 1).

$$CH_3SiCl_3 + 6\ CH_3NH_2 \longrightarrow CH_3Si\text{-}(NHCH_3)_3 + 3\ CH_3NH_3^+\ Cl^-$$

EQUATION 1

This monomer, tris (N-methylamino) methylsilane (TMMS), is subsequently polymerized by heating to temperatures in excess of 500°C. Although the structure of this polycarbosilazane is not totally characterized, it is believed to be analogous to other polysilazanes[6] (Eq. 2). The polycarbosilazane resin prepared in this manner is a transparent yellowish-brown brittle material soluble in conventional organic solvents. It reacts with moisture in the air an melts at or near 220°C. Fibers are either hand drawn or spun from a resin melt. The fibers are then cured by placing in an enviroment of 95% relative humidity and 100°C. Fibers obtained from this process no longer melt and are noncombustible. The cured fibers are finally pyrolyzed at 1500°C in an inert atmosphere to the inorganic silicon carbide-silicon nitride.

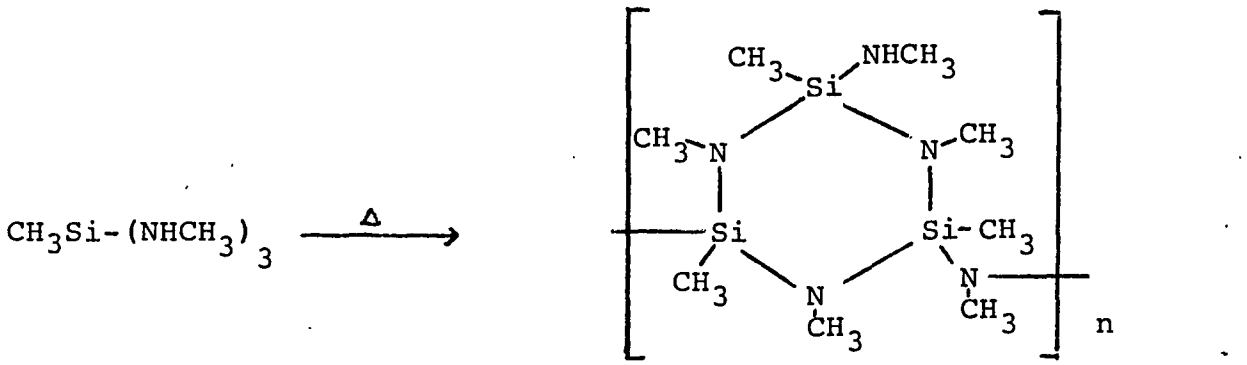

EQUATION 2

Although fibers formed from TMMS have shown great potential as graphite substitutes, further development is required. During pyrolysis, mass is lost due to elimination of volatile by-products. Excessive mass loss is undersirable as it can result in fiber defects and high shrinkage.[7] Structural modification of the monomer may lead to polycarbosilazanes exhibiting lower pyrolytic mass loss and shrinkage. A series of modified monomers has been prepared for evaluation (Table I).[8]

The objective of this project is to prepare modified polycarbosilazane resins for evaluation as silicon carbide-silicon nitride precursors. Each of the previously prepared monomers is to be polymerized. The resultant resins are to be pulled into fibers and cured hydrolytically. The hydrolyzed fibers will be tested for mechanical strength and thermal stability. Some fibers will be pyrolyzed following hydrolysis and will also be tested for strength, stability and electrical properties.

EXPERIMENTAL

Synthesis of Tris(Alkyl Amino) Silane Momers

A detailed description of the equipment and technique used to prepare the monomer is presented elsewhere.[4,8] Briefly the procedure is described below.

Tris (alkylamino)silanes were prepared by the dropwise addition of methyl or phenyl trichlorosilane to a solution of the alkyl amine in toluene or petroleum ether at low temperature under a dry nitrogen atmosphere. After addition was complete, the solution was refluxed for one hour. The mixture was then filtered to remove salt produced during the reaction. The product was purified by distillation at reduced pressure.

Monomers were chracterized by boiling point and IR and NMR spectroscopy. This data is also contained in previous reports.

Preparation of Polycarbosilazane Resins

The general method of polymerization uses the apparatus shown in Figure 1, which is basically a total reflux distillation system. Quantities of the tris (alkylamino)silane monomer were placed in the apparatus under anhydrous conditions. The temperature of both the distillation pot and column furnance were raised until the majority of the monomer was passing over the glass Raschig rings at a temperature of 520°C. Polymerization times ranged from 1.5 to 4.5 hours.

After completion of the polymerization, the resin was dissolved in chloroform and transfered to a weighing pan. The solvent and unreacted monomer were evaporated off under a stream of dry nitrogen. The polycarbosilazane resin produced was usually a yellow to brown, brittle, transparent product soluble in coventional organic solvents.

Polycarbosilazanes were characterized by melting point and IR and NMR spectroscopy. Molecular weights were determined by gel permeation chromatography (GPC).

C-3

Preparation of Fibers

Precursor fibers for silicon carbide-silicon nitride preparation were hand drawn from the polycarbosilazane resin melt under a stream of dry nitrogen.[9] The surface of the melt was touched with a glass rod and stretched to obtain fibrous material.

After drawing, precursor fibers were conditioned in an enviromental chamber at 100°C and 95% relative humidity until made unmeltable. Some of the conditioned fibers were placed under tension in ceramic holders and heated in a furnace under nitrogen from room temperature to 1200°C in 5 hours followed by heating from 1200°C to 1500°C during one hour.

Pysical and Chemical Properties Determination

Infrared (IR) spectra were determined using a Perkin-Elmer 137 Sodium Chloride Spectrophotometer. The polycarbosilazane was sampled in solution using chloroform solvent.

Nuclear Magnetic Resonance (NMR) spectra were determined with a Varian Associates EM 360L system. Resin samples were dissolved in deuterochloroform as solvent and tetramethylsilane as an internal reference.

Gel permeation chromatography (GPC) was used to determine the weight average molecular weight ($\bar{M}_w$).[10] A Waters Model 244 GPC with a 440 UV detector (254 nm fixed wavelength) was used with tetrahydrofuran as the solvent. The GPC runs were carried out at room temperature using four columns (500 Å, 100 Å, 100 Å, 1000 Å). The flow rate was 1 ml/min. The molecular weight was determined using a universal calibration curve.[11] Intrinsic viscosities for use in calculating the $\bar{M}_w$ were determined with a Ulbelohde viscometer in THF solution at 30°C.

Thermogravimetric analyses were carried out using a DuPont 951 Thermogravimetric Analyzer and 1090 Thermal Analyzer. The weight loss of the hydrolyzed resins was measured from 25°C to 1000°C in both nitrogen and air, at a rate of 10°C/min.

The tensile strength of the fibers was determined using an Instron 1100 series system with a 10-20 gram range load cell. The gauge length was 0.75 inch and the crosshead speed was 0.05 in/min.

RESULTS AND DISCUSSION

Polymerization of Aminosilane Monomers

Results from the polymerization of the TMPS monomer were inconsistent. Resin yields and melting points varied depending on reaction time and temperature. Yields of polycarbosilazane ranged from 15-78% of the monomer used. Repeated polymerizations gave resins with melting points from 45-170°C. There was no correlation between the percent yield and the melting point of the resin obtained.

With respect to the preparation of suitable fibers, the melting point is of major importance. Resins which melt lower prove to be easy to draw into fibers. However, the hydrolytic cure of the resin takes much longer if the initial temperature must be far below 100°C. The higher melting resins, while allowing hydrolysis to be carried out at 100°C, were more difficult to draw into fibers. The fiber drawing was performed under a stream of dry nitrogen to prevent hydrolysis of the resin. At the temperature necessary to soften the higher melting resins, the material rapidly became unusable due to hydrolysis or crosslinking. Fibers were drawn using a small sample of resin which was discarded when it became unworkable.

Attempted polymerizations of the TPMS and TAMS monomers never yielded a resin suitable for fiber formation. Reaction times as long as 4 hours were used but the product was always a fluid.

Characterization of TMPS Resin

The infrared (IR) spectrum for the TMPS resin (Figure 2) showed absorptions for NH (3600 cm^{-1}), CH (2900 cm^{-1}), aromatic CH (3010 cm^{-1}) and SiC_6H_5 (1140, 1190 and 1410 cm^{-1}). The nuclear magnetic resonance (NMR) spectrum (Figure 3) showed a series of peaks at δ 1.57-3.53 ppm ($N-CH_3$) and δ 6.23-8.57 (SiC_6H_5). The weight average molecular weight was determined to be 1910 by gel permeation chromatography (Figure 4).

Fiber Formation, Curing and Pyrolysis

Fibers of up to 6 feet in length were drawn from the melted TMPS resin. If a high melting resin batch was used, the fibers were humidity conditioned at 100°C as specified. Since some of the resin batches melted below this temperature, the hydrolysis of these fibers was initiated at 40°C. As the fibers hydrolyzed, the temperature was increased gradually. This process required several days to obtain unmeltable fibers. When either batch of fibers above was subjected to pyrolysis conditions, only slivers remained which were too small for further testing.

Mechanical Properties of Hydrolyzed TMPS Fibers

The tensile strengths of hydrolyzed TMMS fibers prepared by Penn, et.al. are presented in Table 2 for comparison to that obtained from TMPS fibers (Table 3). Comparing fibers of similar diameter (1.74 vs. 1.5 mil), the TMPS fibers with a tensile strength of 21 ksi appear to be superior to the TMMS fibers at only 4.0 ksi. The TMPS fibers do not show the regular increase in tensile strength with decreasing diameter that is exhibited by the TMMS fibers. This is in part due to the few samples of TMPS fibers available for testing.

Thermogravimetric Analysis of Hydrolyzed Resins

Samples of hydrolyzed resins were subjected to thermogravimetric analysis from ambient to 1000°C under nitrogen. The TMMS resin prepared by Penn, et.al. was found to lose 25% of its mass between 500 -700°C (Figure 5). Previous work[4] had shown a 38% mass loss upon pyrolysis. Obviously additional mass is lost above 1000°C, but the major portion is lost in the lower temperature range. Under similar conditions, the TMPS resin prepared in this study lost 36% of its mass in the range 400-700°C (Figure 6). Based on this data and experience in attempted pyrolysis, the TMPS resin appears to display greater mass loss and shrinkage than does the TMMS resin. This is exactly the opposite of the desired property.

Both resins were also examined in air. Here again the TMMS resin was superior, losing 27% of its mass between 300-600°C (Figure 7). When tested similarly, the TMPS resin lost 53% of its mass in the range 300-700°C (Figure 8). This process involves oxidation and as such is not really indicative of occurrences during pyrolysis.

CONCLUSIONS AND RECOMMENDATIONS

Overall this study has not produced a material superior to the existing silicon carbide-silicon nitride fibers currently under investigation. Of the three new monomers tested (TMPS, TAMS, TPMS) only one (TMPS) produced a resin suitable for fiber formation. The conditions for polymerization vary soewhat from one monomer to another. Time was not sufficient to determine the optimum conditions in each case. It is still possible that the TAMS and TPMS monomers may yield suitable polymers moreover, since silaneamines may undergo amine interchange,[12] polymerization of monomers with heavy amine groups may occur more readily if the amine is removed from the system as it is produced. The TMPS fibers produced were more difficult to hydrolyze than the corresponding TMMS material. This, in turn, lead to difficulty in pyrolysis such that no ceramic fibers were available for testing.

Hydrolyzed TMPS fibers proved to have superior tensile strength versus the TMMS fibers. This advantage was somewhat offset by the results of thermal analysis. One goal of this study was to find a material which would show less pyrolytic mass loss. The TMPS resin was shown to be inferior to TMMS in this respect. This may be due in part to the increased carbon/silicon ratio in the TMPS material. This ratio is certain to be responsible for the increased degradation in air. These preliminary findings may be interpreted to mean that the monomers with larger alkyl groups will alter the properties of the precursor contrary to that desired. However, insufficient information is present at this time to draw any such conclusion.

Only one of the six monomers prepared in the previous study[8] has been even partially evaluated. Therefore considerable work is left to be done before rigid conclusions can be drawn. Indications are that fiber properties will change significantly with minor structural modifications in the monomer, but only when alarge number of pur polymers is available will these properties be fine tuned. This honing of fiber properties will most likely occur using copolymers or blends of several polycarbosilazanes.

REFERENCES

1. Jenkins, G. M. and Kawamura, K., "Polymeric Carbons-Carbon Fibre, Glass and Char", Cambridge University Press, 1976.

2. Cagliostro, D. E., Textile Research Journal 632, Oct. 1980.

3. Springer, G. S., Mashtizadeh, S. A. and Keller, R. B., J. Composite Materials 13, 225 (1979).

4. Penn, B. G.; Ledbetter, F. E. III; Clemons, J. M. and Daniels, J. G.; J. App. Polym. Sci. 27, 3751 (1982).

5. Verbeek, W., Ger. Offen. 2, 218, 960 (1973).

6. Kruger C. R. and Rochow, E. G., J. Polym. Sci. A 2, 3179 (1964).

7. Fitzer, E., Angew. Chem. Int. Ed. Engl. 19, 375 (1980).

8. Crouse, D. J., Report of NASA/ASEE Summer Faculty Research Fellowship Program, Contract No. NASA/NGT 01-008-021, XI (1983).

9. The author wishes to thank J. Clemons and F. Ledbetter for assistance in the drawing and mechanical testing of fibers.

10. The author wishes to thank N. Hundley for doing the GPC runs and B. Penn for the viscosity measurements and molecular weight calculations.

11. Grubisic, Z.; Rempp, P. and Benoit, H.; J. Polym. Sci. Polym. Lett. Ed. 5, 753 (1967).

12. Eaborn, C., "Organosilicon Compounds", Academic Press Inc., New York, 1960.

TABLE I

SILANEAMINE MONOMERS
$R\text{-}Si\ (NH\text{-}R')_3$

	R	R'
tris (N-methylamino)phenylsilane (TMPS)	C_6H_5	CH_3-
tris (anilino)methylsilane (TAMS)	CH_3-	C_6H_5
tris (N-propylamino)methylsilane (TPMS)	CH_3-	n-C_3H_7-
tris (N-butylamino)methylsilane (TBMS)	CH_3-	n-C_4H_9-
tris (allylamino)methylsilane	CH_3-	CH_2=CH-CH_2-

TABLE II

TENSILE STRENGTHS OF PREPYROLYZED TMMS FIBERS

Fiber Diameter (mil)	Tensile Strength (ksi)
0.52	13.8
1.74	4.0
4.97	1.8

TABLE III

TENSILE STRENGTHS OF PREPYROLYZED TMPS FIBERS

Fiber Diameter (mil)	Tensile Strength (ksi)
1.5	21.2
2.2	20.4
2.7	23.5

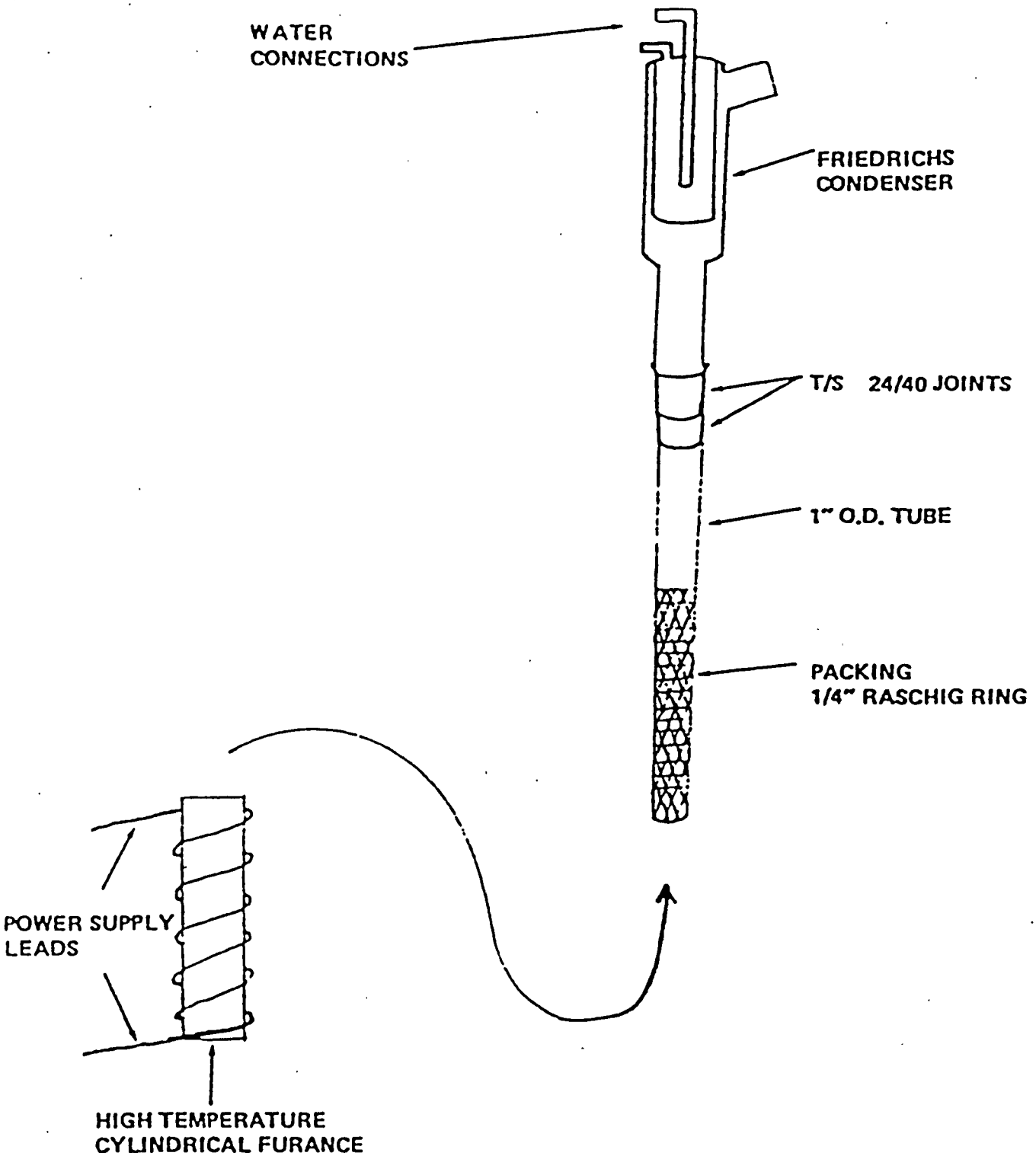

FIGURE 1. HIGH TEMPERATURE POLYMERIZATION SYSTEM

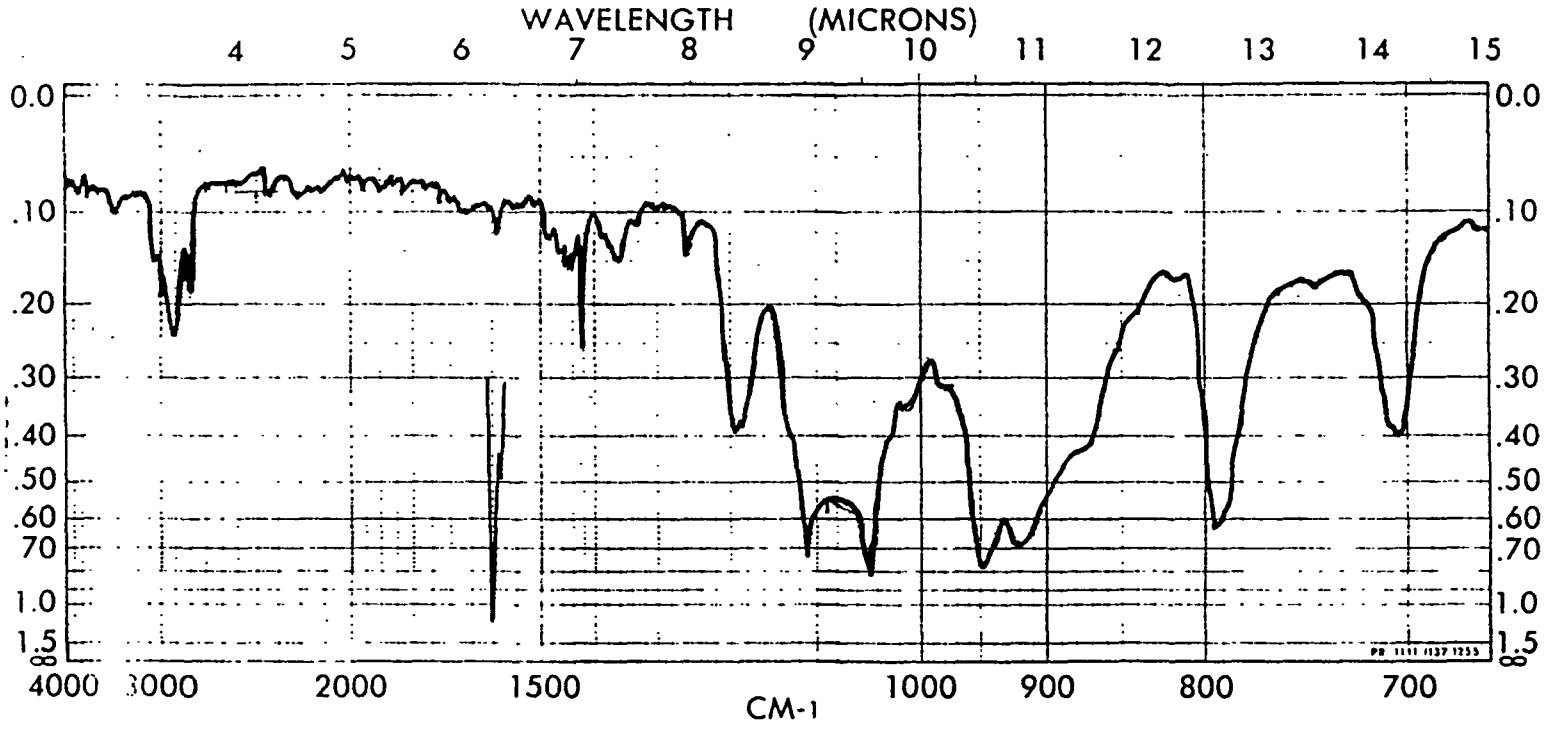

FIGURE 2. IR SPECTRUM OF TMPS RESIN

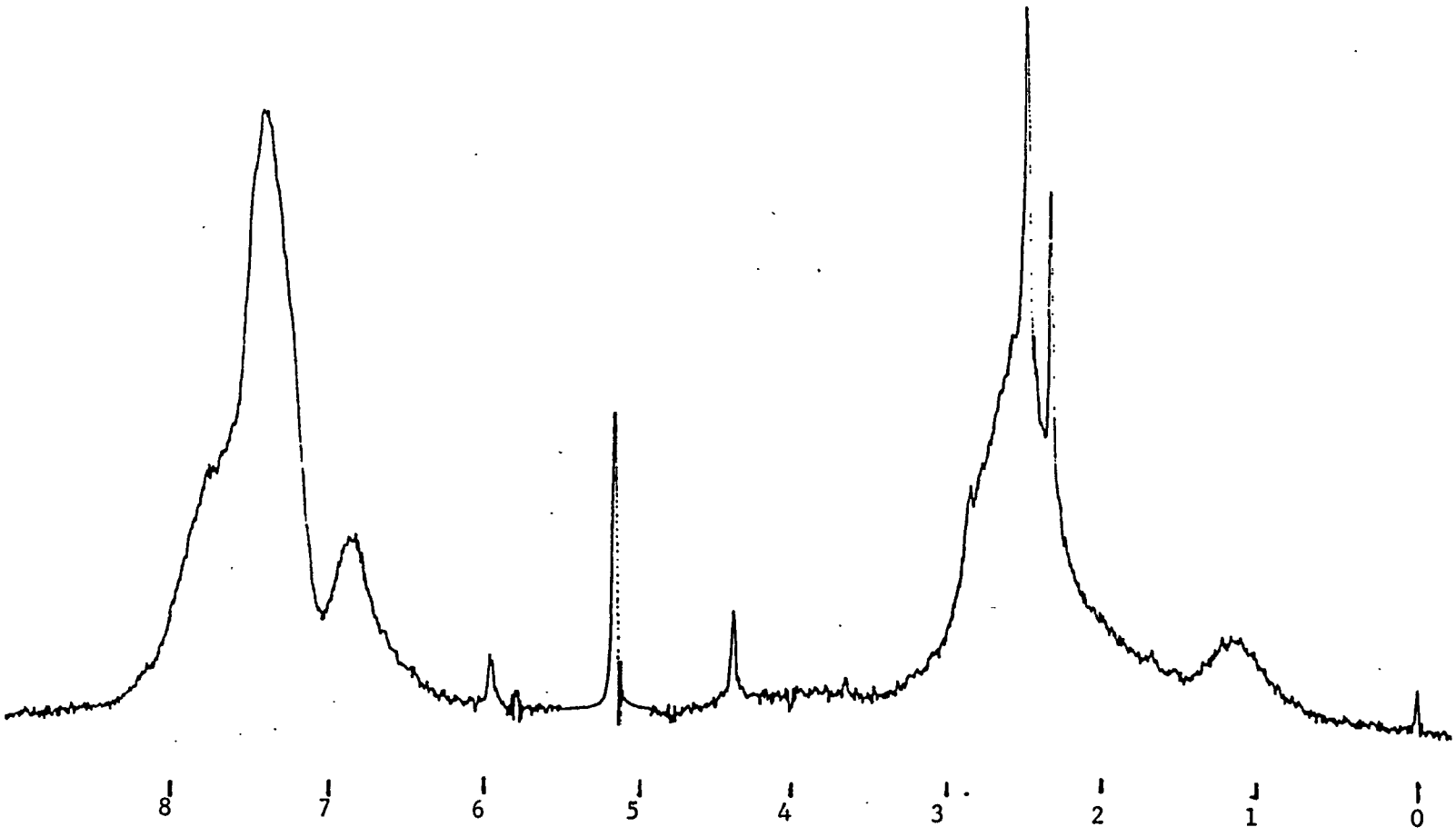

FIGURE 3. NMR SPECTRUM OF TMPS RESIN

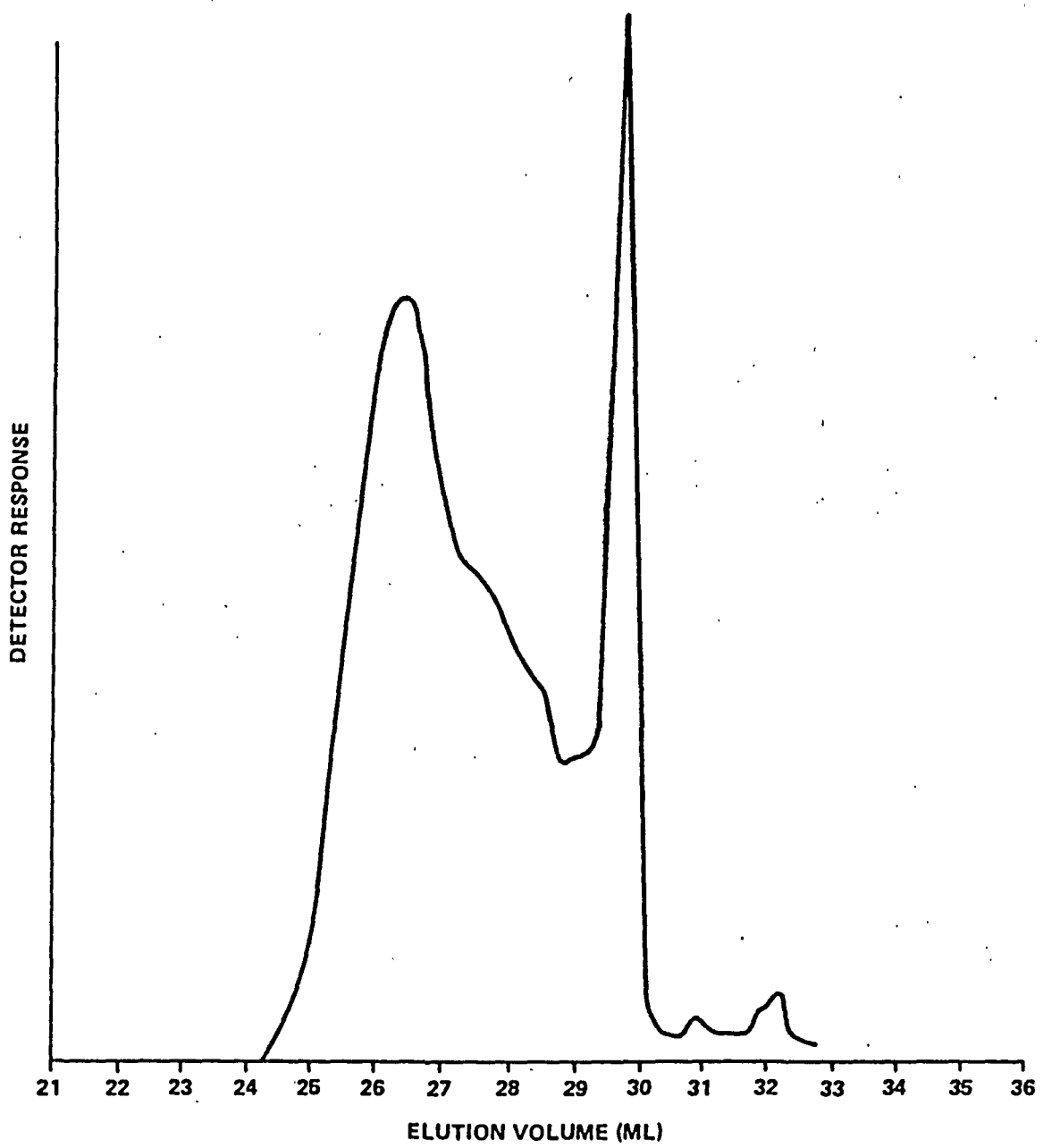

FIGURE 4. GEL PERMEATION CHROMATOGRAPHY OF TMPS RESIN

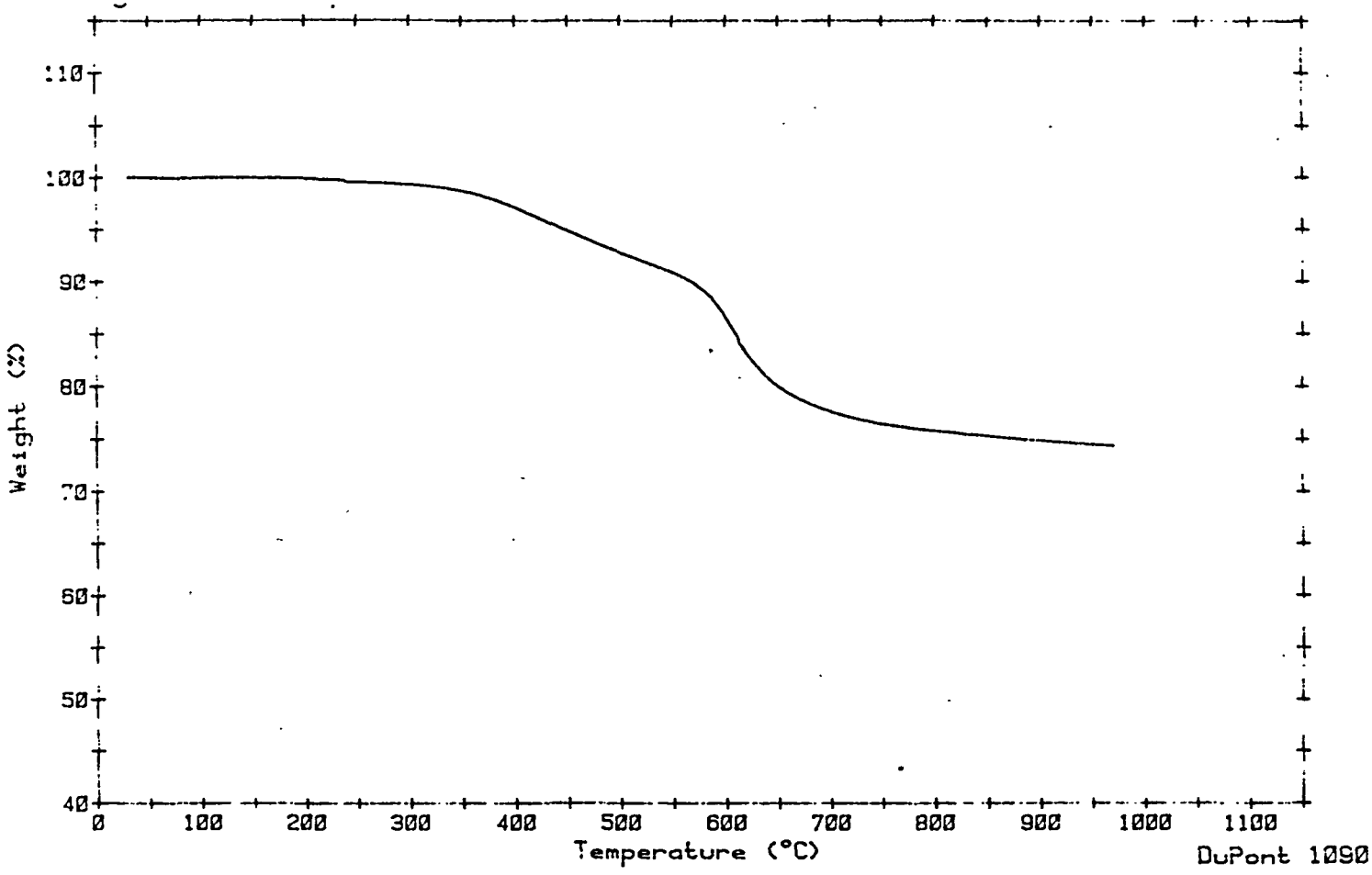

FIGURE 5. TGA OF HYDROLYZED TMMS RESIN IN N_2

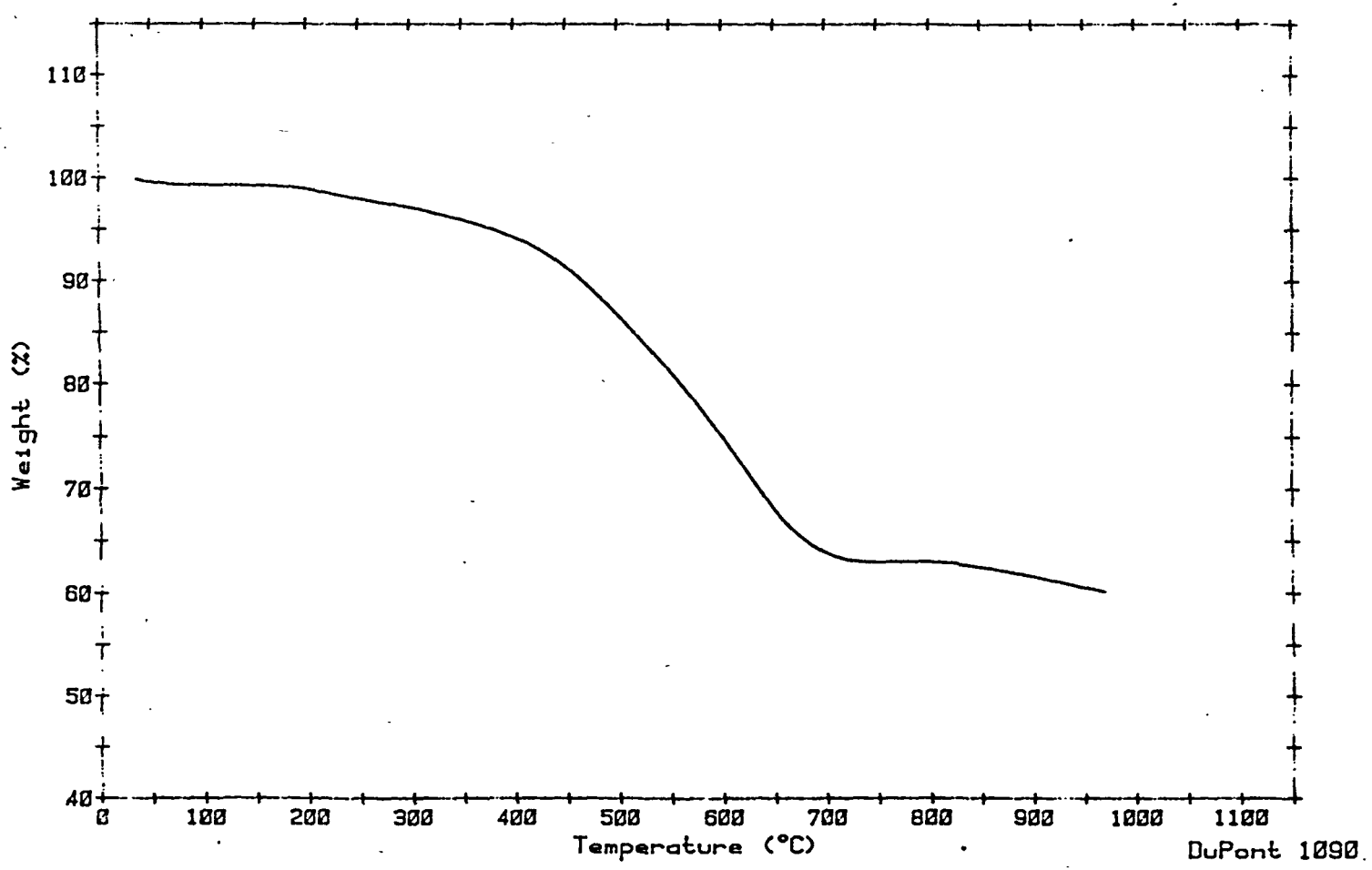

FIGURE 6. TGA OF HYDROLYZED TMPS RESIN IN N_2

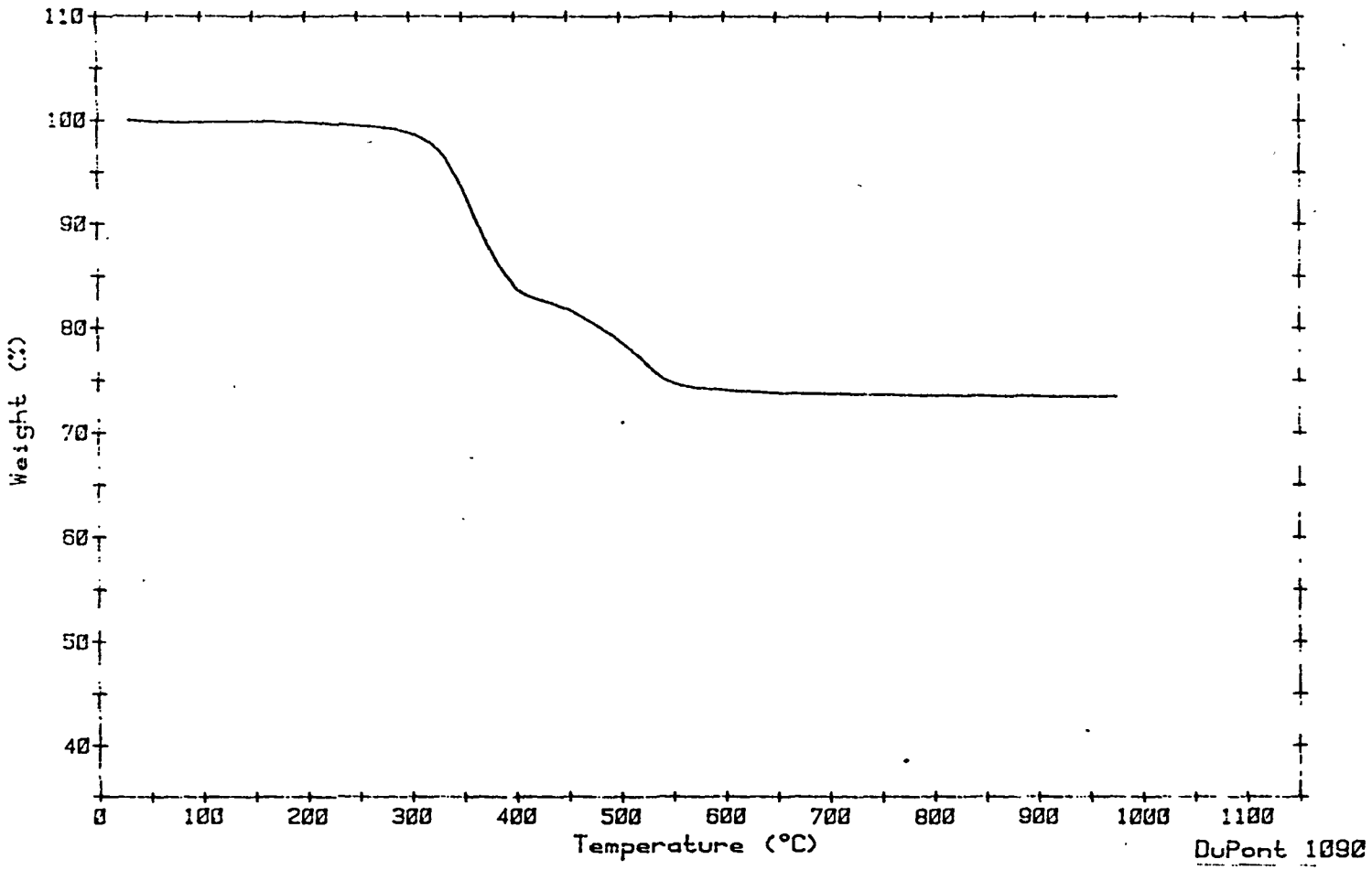

FIGURE 7. TGA OF HYDROLYZED TMMS RESIN IN AIR

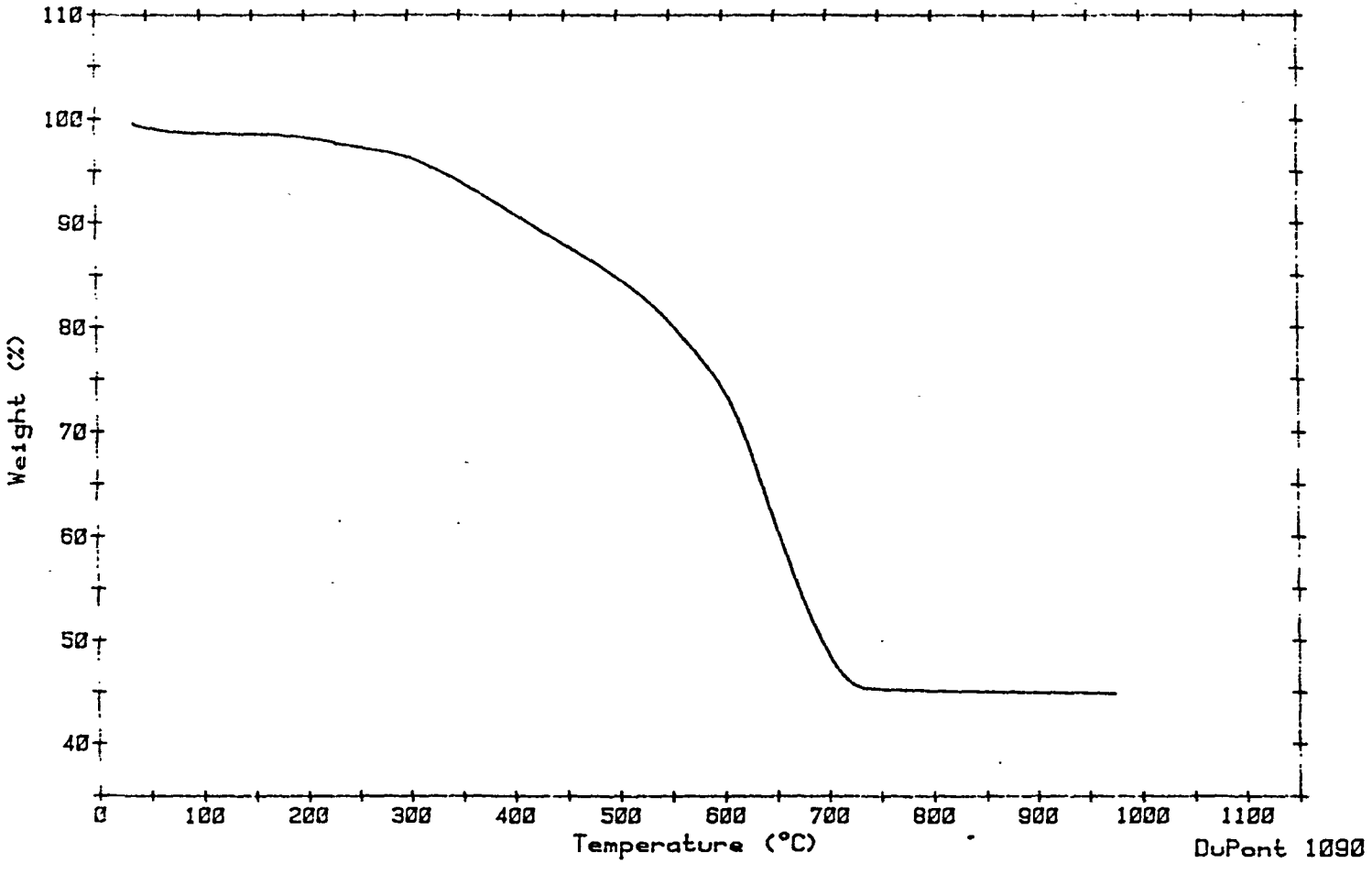

FIGURE 8. TGA OF HYDROLYZED TMPS RESIN IN AIR

1984

NASA/ASEE SUMMER FACULTY RESEARCH FELLOWSHIP PROGRAM

MARSHALL SPACE FLIGHT CENTER
THE UNIVERSITY OF ALABAMA

STUDY OF THE POTENTIAL USEFULNESS OF SUPERFINE HOLOGRAPHIC X-RAY GRATINGS IN AXAF AND ASTROPHYSICS IN GENERAL

Prepared by:	Paul L. Csonka, Ph.D.
Academic Rank:	Professor
University and Department:	University of Oregon Institute of Theoretical Science
NASA/MSFC:	
Laboratory:	Space Science Laboratory
Division:	Astrophysics
Branch:	High Energy Physics
NASA Counterpart:	Martin C. Weisskopf
Date:	August 24, 1984
Contract No.:	NASA-NGT-01-002-099 (The University of Alabama)

STUDY OF THE POTENTIAL USEFULNESS OF SUPERFINE HOLOGRAPHIC X-RAY GRATINGS IN AXAF AND ASTROPHYSICS IN GENERAL

Paul L. Csonka
Professor of Physics
Institute of Theoretical Science
University of Oregon
Eugene, Oregon 97403

Abstract

Present day high energy electron storage rings and insertion devices (wigglers and undulators) provide the necessary technology to manufacture superfine (line density $\gtrsim 10^5$/mm) holographic X-ray gratings. The objective of this investigation is to determine the usefulness in future astrophysical research of such gratings, as a function of the grating size and line density. A model design is given for an instrument which would fit within the (presently specified) constraints of the planned Advanced X-ray Astrophysics Facility (AXAF).

1. SUPERFINE GRATING (ELEMENT) PRODUCTION

1. Background

Presently available gratings usually have of the order of up to $3 \cdot 10^3$ lines per millimeter. Superfine gratings, on the other hand, would have line densities $\gtrsim 10^5$ lines per millimeter. So far, no such gratings have been manufactured. However, the technology is now in hand to produce such gratings.

A method of superfine grating production has recently been suggested[1]. According to that suggestion, first a stationary interference pattern is to be generated between two branches of a sufficiently collimated, monochromatic and spatially restricted X-ray beam, generated in the form of synchrotron radiation by a high energy electron storage ring. Second, the interference pattern is imprinted on a recording medium, such as a polymer (e.g. PMMA) or an amorphous resist. Third, the recorded image is transferred onto a metal (such as gold) which will then form the grating. This method of production would not only enable one to reach the desired line densities, but would also ensure that the distance between neighboring lines would be stable across the entire grating surface.

Superfine gratings so produced could be realized as reflection gratings, or transmission gratings. The transmission gratings can be "free-standing" with an appropriate grid structure supporting the grating proper.

The line densities, grating dimensions and quality which can be produced by this method depend on the intensity, angular divergence and spectrum of the synchrotron radiation generated by the high energy storage ring considered; the stability of the generating electron beam, as well as the stability of the recording instrument relative to the

ring, and the stability of the various parts within the recording instrument; the grain size and sensitivity of the recording medium; and details of the procedure which transfers the pattern from the recording medium onto the grating metal.

2. Recording Optics

To generate the interference pattern, the recording X-ray beam has to satisfy certain requirements on monochromaticity, collinearity and beam cross section[1].

Monochromaticity:

Let λ be the wavelength of the recording X-ray beam. Assume that λ is restricted to lie within the region $\lambda_o \pm \frac{1}{2} \Delta\lambda$. Denote by $\Delta\ell$ the maximum pathlength difference which occurs between the two branches of the recording X-ray beam while imprinting the interference pattern of interest. In this notation, the requirement of monochromaticity can be written as

$$\frac{\Delta\lambda}{\lambda} \lesssim \tfrac{1}{2} f_1 \frac{\lambda_o}{\Delta\ell} , \qquad (1)$$

where f_1 is an arbitrary constant (to be satisfied below) satisfying $0 \leq f_1 \leq 1$.

Collinearity:

Denoting by $\Delta\theta$ the (full) angular divergence of the beam, one needs

$$\Delta\theta \lesssim f_2^{\frac{1}{2}} \left(\frac{\lambda_o}{\Delta\ell}\right)^{\frac{1}{2}} , \qquad (2)$$

where, again, $0 \leq f_2 \leq 1$ is an arbitrary constant.

Photon beam cross section:

For rectangular cross section, denoting by D_{sx} and D_{sy} the beam diameter at the beam source along the two transverse axes x and y respectively, and writing D_x and D_y for the corresponding beam diameters at the interference

pattern, the beam has to satisfy

$$L \gtrsim (\Delta_x^2 + \Delta_y^2)\, f_3 \frac{F}{\lambda_o} , \tag{3}$$

with $$\Delta_i^2 = \begin{cases} (\tfrac{1}{2} D_{si} + \tfrac{1}{2} D_i)^2, & \text{if } D_{si} \geq D_i, \quad (i = x,y) \\ 2\, D_{si} D_i, & \text{if } D_{si} < D_i, \quad (i = x,y) \end{cases}$$

where L is the greatest length of the beam from it source to the interference apparatus, F is a function of beam cross section which assumes the value unity when the cross section is rectangular, and $0 \leq f_3 \leq 1$ is a constant, for which

$$f = \left[f_1^2 + f_2^2 + f_3^2 \right]^{\frac{1}{2}} < 1 \tag{4}$$

must hold.

To ensure conditions (1) - (4), one can channel the synchrotron radiation through a monochromator, and collimate the beam as well as restrict its diameters by the use of an appropriate sequence of slits.

3. Intensity, Brightness

Many presently operating high energy storage rings were built as high energy physics research tools. In such rings the produced synchrotron radiation is a byproduct, rather than a design goal. The intensity and brightness of the radiation has, therfore, not been maximized, and can generally be increased in several ways:

1. Reduce the coupling, κ, between horizontal and vertical beam oscillations for the circulating electron beam ($\kappa \lesssim 0.1$, 0.05 can be achieved).

2. Go to single beam mode operation, in which one of the two (colliding) beams is absent. That improves the emittance of the remaining beam.

3. Retune the magnetic fields which guide the beams to minimize emittance in single beam mode operation (rather than maximizing luminosity for colliding beam mode operation).

4. Generate photons from a low beta section of the ring. Those sections were originally designed as interaction regions where two beams collide. There the electron beam cross section is smaller, which improves the photon beam emittance. (The electron beam angular divergence, on the other hand, is higher there, but that has little effect on the photon beam, since the photon angular divergence is dominated by relativistic kinematic effects.)

5. Increase the circulating electron beam intensity (at least for short times, to avoid overheating of storage ring components), either by increasing the number of circulating electron bunches, or by increasing the number of electrons in each bunch.

6. Place insertion devices (wigglers or undulators)[2] into the storage ring. These devices can increase the brightness of the emitted S.R. in a chosen wavelength region by a factor 10^2 - 10^3.

7. Microbunch the circulating electron beam. This will result in a several orders of magnitude increase of the radiation intensity up to at least the soft X-ray region.[3,4]

8. Use the S.R. from the storage ring to pump a soft X-ray laser.[5,6] The radiation from the laser would have a brightness improved by orders of magnitude in the wavelength region of the coherent photons produced. Furthermore, these photons would be monochromatic to a high extent as produced, and could be used directly for imprinting the desired interference pattern.

In the following (see below) we will estimate the size of gratings which can be manufactured by the proposed method. In those estimates

two cases will be considered: First, typical high energy storage ring parameters will be used, without assuming any of the improvements just listed. Second, we will assume that an insertion device is located in the ring which will improve the brightness by (only) a factor of 10^2. In both cases, therefore, our estimates will be rather conservative.

4. Recording of the Interference Pattern

Ground vibrations, and their frequency and time distribution have been studied at various storage rings.[7] The stability of the electron beam differs from ring to ring, feedback beam regulators have been installed in several laboratories. By such means unwanted beam oscillations are being reduced. The use of optical tables with appropriate cushions allows the imprinting of the desired interference pattern.

The most widely used resist is PMMA. Grain size limits its resolution to of the order of 200 $\mathring{A}$. Amorphous resists[8], on the other hand, have resolution $\lesssim$ 10 $\mathring{A}$, but have lower sensitivity and thus require higher intensity S.R. beams. Studies of the behavior of various resist materials in S.R. beams have been reported, e.g. in reference.[9]

In order that a grating used in normal incidence be useful, the bars which form the grating must be high enough. On the other hand, when the density of lines on the grating is increased, the width of each bar is reduced, so that keeping the height of the bars constant, the "aspect ratio" of the bars (i.e. their height to width ratio) is increased. Present day technology permits the fabrication of gratings with aspect ratios up to about 15 or 30. Therefore, one limitation on the use of superfine gratings will come from this restriction. To see

more clearly what this condition implies, we consider gratings made of gold, when the line density is $\frac{1}{2}\cdot 10^5$ lines/mm, or $1\cdot 10^5$ lines/mm. One finds that for efficient gratings the aspect ratios are as listed in Table I. It is clear from the table that superfine gratings of the conventional construction will be restricted to X-ray photon energies $\lesssim$ 1 keV. On the other hand, one can contemplate the possibility of manufacturing gratings of a new type, namely gratings in which the spaces between the bars are filled with some "filler" material of low index of refraction. One expects that it will be possible these new types of gratings with arbitrarily high aspect ratios. In this manner the restriction on aspect ratios can be circumvented altogether.

5. Grating (element) Size

In this section the dimensions of grating elements will be calculated. A specific interference geometry will be assumed (one which is also convenient for general holographic X-ray studies). In this geometry, the S.R. beam is split into two branches of equal intensity, each is incident on a plane mirror at 45^o and then reaches the recording plane surface at 45^o from opposite sides of the surface normal.[1] The exposure time, T, required to produce a sufficiently good quality superfine grating whose sides are $\sqrt{2}\ D_x$ and D_y long, can be calculated from the formula:

$$T = \left[n_\gamma D_x D_y M \frac{A^{(o)}_{xyt}}{N^{(o)}\lambda_o^2} \right] \frac{D_x}{\lambda_o} \cdot \frac{8\sqrt{2}\ F^2}{f_1 f_3^2} \cdot \frac{B^2}{b_x b_y} , \qquad (5)$$

where $b_i = D_i/D_{is}$; $i = x,y$

$$a_i = \begin{cases} (1+b_i)^2/4b_i & ; \text{ if } b_i \geq 1 \\ 1 & ; \text{ if } b_i < 1 \end{cases}$$

$d = D_{ys}/D_{xs}$

$B = \frac{1}{2}\,(a_x b_x/d + a_y b_y d)$

n_γ is the number of photons required per square centimeter of recording surface to imprint a sufficiently high quality grating.

$A^{(o)}_{xyt} = d_{sx} D_x D_{sy} D_y L^{-2} \frac{\Delta\lambda}{\lambda_o} T$ is the six dimensional phase space into which photons are emitted by the synchrotron radiation port used, during time T.

$N^{(o)}$ is the total number of photons emitted by the source into the six dimensional phase space volume $A^{(o)}_{xyt}$.

M is a factor which takes into account absorption by the mirror(s) and monochromator.

F is a factor which corrects for non-rectangular beam cross section.

Fig. 1 shows the necessary exposure time as a function of b_x and b_y, in the case when $n_\gamma = 5 \cdot 10^{14} cm^{-2}$, M=F=1, and the other parameters are as listed in Table II. Keeping in mind that the assumptions made in calculating the curves in Fig. 1 were rather conservative, one concludes that during exposure times of the order of several days one expects to be able to manufacture superfine grating elements with diameters up to of the order of a millimeter. At line density $N = 10^5$ lines/mm that corresponds to a diltractive element with potential $\lambda/\Delta\lambda = 10^5$.

2. GRATING AGGREGATES

The production of grating elements was discussed in section 2. Such grating elements have the property that the distance between neighboring bars is accurate everywhere across the grating element; and therefore,the potential resolution which can be produced by the element is proportional to the number of bars contained within it.

By using lithographic techniques, an arbitrary number of essentially identical copies can be made from any grating element. These copies can then be laid out next to each other, to cover an arbitrarily large area. That can be done in two ways:

1. Neighboring elements are positioned so that the lines on both are parallel to each other, and the distance between the last line of one element and the first line of the next element is identical to the interline distance near the common edge of both gratings. If this were done, new larger grating elements could be produced. The potential energy resolution attainable by then would be proportional to the total number of lines across the entire face of the new resultant element. To position elements in this manner, with adequate accuracy, is at,or beyond the boundary of what is technologically feasible today. Therefore, this option will not be further considered here.

2. One can cover large areas with identiaal copies of a single grating element, each oriented so that the lines on all of them are parallel to each other. No attempt is made to maintain the interline distances across the element boundaries. In this manner large surfaces can be covered, and here we will refer to such devices as "grating aggregates". The potential energy resolution achievable by a grating aggregate is no larger than that which can be reached by a single one of its component elements, but its total light gathering area is,

of course, higher. In this section we will consider the fabrication of grating aggregates.

Assuming that elements of 1mm x 1mm size can be manufactured, one would have to make 10^4 copies of it to cover a 10 cm x 10 cm area, or 10^6 copies to cover a $1m^2$ area (comparable to the AXAF telescope effective area). The required numbers of copies are high enough to warrant a study of alternative strategies to achieve the desired goal. Figure 2 illustrates the problem. In this example, a total number of M=18 elements are needed to cover an area. That can be done, for example by making 18 copies of the original (Fig. 2a), or, alternatively, one can proceed as follows: First, make three copies of the original, then make two copies of these three together, and, finally, three copies of these two. In the first case, 18 lithographic exposures are required, in the second case only 3+2+3=8. When M is larger, one expects significant savings by choosing the correct reproduction strategy.

In general, one can make n_1 copies of the original element, then make n_2 copies of the n_1 copies laid out next to each other, then make n_3 of these, and so on. If the area of the original grating element is A_o, while the area of the desired grating aggregate is A_{tot}, then clearly

$$n_1 \cdot n_2 \cdot n_3 \ldots n_m \cdot A_o = A_{tot} \tag{6}$$

The number of lithographic exposures required to achieve this is

$$n_{tot} = n_1 + n_2 + \ldots + n_m \tag{7}$$

Our aim here is to find that set of n_1, n_2, ... for which n_{tot} is minimum under the condition that Eq. (6) hold.

Using the method of lagrange multipliers, one find that

$$n_1 = n_2 = \ldots = n_m \quad . \tag{8}$$

Putting this into Eq. (6), using the notation n_1=n, gives

$$n^m = \frac{A_{tot}}{A_o} \quad , \qquad m = (\ell n \frac{A_{tot}}{A_o}) \; / \; \ell n \; n \; ,$$

and Eq. (7) becomes

$$(\ell n \frac{A_{tot}}{A_o}) \frac{n}{\ell n \, n} = n_{tot} \; .$$

The extremum of n_{tot} with respect to variations of n lies at

$$n = e = 2.718... \qquad . \tag{9}$$

This exact mathematical solution is not an integer, but it suggests that for the physical case the best strategy will be to choose n_1, n_2, ..., n_m = 2 or 3.

Before performing a search, however, one has to note that certain secondary considerations can affect the answer. For example, one can use the original in any step instead of one of its own replicas (See Fig. 2c). That will further reduce the required lithographic exposures (for the example considered in Fig. 2, to n_{tot}=6). In such a case, in general one has instead of Eq. (7)

$$(n_1-1) + (n_2-1) + ... + (n_m-1) = n_{tot} - m = n_{tot}^{(1)} \tag{10}$$

The optimal solution is again $n_1 = n_2 = ... = n_m = n$, but now n satisfies

$$\ell n \; n = 1 - \frac{1}{n} \quad ,$$

so that n lies between 1 and 2.

Further factors which need to be considered are whether lithographing large sizes is more desirable than lithographing several smaller sizes, etc. In any case, it is clear that n_i will be close to 2 or 3, thus, to produce a grating aggregate of 10 cm x 10 cm out of grating elements of

size 1 mm x 1 mm, one will need about 20 lithography exposures, and to produce one with 1 m x 1 m size, about 27 exposures will be needed (instead of the 10^4 and 10^6 mentioned earlier). These are reasonable numbers, so that one can conclude that aggregates of up to about 1 m x 1 m size can be made, and may be assumed to be available for instrument design purposes.

The problems of how to stabilize the aggregate after it has been produced, how to protect it against shock and vibrations, particularly during launch of a space vehicle, will not be discussed here.

3. INSTRUMENT CONSTRUCTION

Figure 3 shows a model design for an instrument which utilizes a superfine grating aggregate. It has the following features:

1. It fits within the constraints of the planned Advanced X-Ray Astrophysics Facility (AXAF), as they are specified at the time of this writing. In particular it can be placed inside the instrument carousel.

2. It has a slit to decrease background and allow segregating regions of the field of view.

3. The grating aggregate is used in normal incidence.

4. The instrument accepts the entire beam produced by the AXAF telescope (total viewing angle at focus is $\theta^o = 5.73^0$).

It is assumed that:

The collecting mirror focal length F = 10m (as in AXAF).

The collecting mirror angular resolution ε = 1 arc sec = $4.85.10^{-6}$ radians (as in AXAF).

The grating line density $\frac{N}{D} = \rho_\ell = 10^5$ lines/mm.

The diameter, d, (perpendicularly to the grating lines) of a grating element is $(\lambda/\Delta\lambda\rho_\ell)$. For $\lambda/\Delta\lambda = 2.10^4$, then, one requires only d = 0.2 mm.

Detector element diameter > 20 μm (except for the design in the last line of Table III).

The wavelength resolution of the instrument is given by the formula

$$\frac{\lambda}{\Delta\lambda} = \frac{N}{D} \frac{\sin \psi_{max}}{\varepsilon \text{ (in radians)}} \frac{L_o}{F} \qquad (11)$$

Two design variations will be considered

A. No additional reflections are used,

B. One additional reflection is used to make the beam converge faster at the focal spot, and thus reduce the effective mirror focal length F. The mirrors producing the additional reflection would be used at grazing incidence, thus no significant reduction in efficiency is expected. The additional mirrors are not shown in Figure 3. They may located to the left of the slit in that figure. Reducing in this manner F by a factor of 3, the D and $\lambda/\Delta\lambda$ will both be increased by the same factor of 3. The results are summarized in Table III.

The grating may be curved, or have the line spacing vary across it, or both[10,11]. If the grating has the shape of a ribbon, curved in one direction only, it is expected that it can be well approximated by a few (< 5) grating aggregate sections, each with possibly a different line spacing, but the same line spacing maintained over each section.

The energy resolution can be further increased by further increasing L_o. If enough space is available, that should present no problem, and then $\lambda/\Delta\lambda = 10^5$ could be approached. In AXAF, however, space within the carousel is limited, and further increase of L_o would require that either the detector element size be decreased or that the X-ray beam be additionally reflected once or more. Grazing incidence reflection in the soft X-ray range would result in little deterioration of efficiency, but only small angles of deflection could be achieved in each reflection. Multilayered mirrors can achieve 20%, and probably even > 60% reflectivity for normal incidence in the wavelength region of interest to us. Such mirrors used in normal incidence require smaller diameters, and tolerances on configuring are reduced. In this case, however, the reflected λ would have to match the layer structure in the

mirror, which would limit one to a wavelength band of $\lambda \pm 0.1\ \lambda$ for each such mirror. For these matched wavelengths, the X-ray beam could be reflected straight back toward the collecting telescope mirror, and reflected once more by a multilayer mirror placed on the axis of the telescope (where at present no instrument is planned, and space appears to be available), thus allowing L_o up to about 2000 cm. For these λ values, then, one would achieve $\lambda/\Delta\lambda \approx 10^5$.

An alternative method to increase L_o consists of placing the grating in front of the focus. In this case no slit would be employed.

If the collecting telescope angular resolution is assumed to be 0.5 arc sec instead of 1 arc sec, all $\lambda/\Delta\lambda$ would be doubled.

Acknowledgments

I wish to thank Krishna Apparao, Wesley Darbro, Ronald E. Elsner, Bryan Ramsey, and especially Martin C. Weisskopf of MSFC, and Michael C. Hettrick of the University of California Space Sciences Laboratory, for interesting discussions and comments.

References

1. Paul L. Csonka, "Holographic X-ray Gratings Generated by Synchrotron Radiation", J. Appl. Phys. 52, 2692 (1981).

2. G. Brown, K. Halbach, J. Harris, and H. Winick, Nuclear Instruments and Methods, 208, 65 (1983).

3. Paul L. Csonka, in "Wiggler Magnets", ed. H. Winick and J. Knight, SSRL Report 77/05 (1977);; and SSRL Report 79/04 (1970); and Particle Accelerators, 8, 225 (1978), and 11, 45 (1980).

4. Avi Gover, Paul L. Csonka, and D. Deacon, in Proceedings of the New Rings Workshop, Stanford SSRL Report 83/02 (1983).

5. Paul L. Csonka, "Suggested Methods for coherent X-ray production by combined X-ray and low energy photon pumping", University of Oregon preprint No. N.T. 055/74 (1974); Phys. Rev. 13A, 405 (1976).

6. Paul L. Csonka, SSRL Report No. 77/03 (1977).

7. G. E. Fischer, SLAC Note AATF/80/18 (March 1980).

8. A. Yoshivara, S. Hirota, O. Ochi, A. Takeda, Y. Mizushima, J. Appl. Phys. 20, 181 (1981).

9. R. Tatchyn, I. Lindau, V. G. Su, R. Gutcheck, J. Muray, and Paul L. Csonka, "X-ray Lithography on Beam Line III-IV (3°) at SSRL," SPIE, 393, 114 (1983).

10. Michael C. Hettrick and Stuart Bowyer, Applied Optics, 22, 3921 (1983).

11. Michael C. Hettrick, "Aberrations of Varied Line-Space Grazing Incidence Gratings in Converging Light Beams" (to be published in Aplied Optics).

Table I

E_γ (ev)	ρ_ℓ (lines/mm)	
	$0.5 \cdot 10^5$	$1 \cdot 10^5$
10^2	4	8
10^3	20	40
10^4	800	1600

Listed are the required aspect ratios for a grating made of gold, and used in normal incidence, as a function of X-ray photon energy, E_γ, and line density ρ_ℓ.

Table II

Source		Target	
σ_x(mm)	1.6	D_x(mm)	$D_{sx}\, b_x$
σ_y(mm)	0.8	D_y(mm)	$D_{sy}\, b_y$
$\Delta\Theta_x$(mrad)	1.7	Photon beam requirements	
$\Delta\Theta_y$(mrad)	1.6	$f_1=f_3$	$2^{-1}2^{-\frac{1}{2}}$
$\frac{N^{(0)}}{A^{(0)}_{xyt}}$($cm^{-2}sec^{-1}rad^{-3}$)	$3.9\cdot10^{22}$	f_2	10^{-2}
D_{sx}(mm)	0.3	$\Delta\lambda/\lambda o \leq$	$5.9\cdot10^{-6}b_x^{-1}$
D_{sy}(mm)	0.3	L(cm)$\geq$	$\left(\frac{D_{sx}}{3\cdot10^{-2}cm}\right)^2 5.1\cdot10^{-}$
L_s(cm)	10^2		

The left half of the table lists the assumed source parameters. The right half contains the target parameters and conditions on the beam as a function of the assumed f_1, f_2, f_3 values. Here $2\sigma_x$ $2\sigma_y$ are the diameters and $\Delta\theta_x$ $\Delta\theta_y$ are the full angular widths of the S.R. beam along the x and y transverse dimensions, respectively, as produced by the ring, and L_s is the distance between the port and the first slit. The $N^{(0)}$ refers to the case S.R. intensity without any insertion device.

Table III

Case	Effective F (cm)	L_o (cm)	L_d (cm)	D (cm)	Detector Element Size (μm)	$\frac{\Delta\lambda}{\lambda}$ at $\lambda = 100$ Å
(A)	10^3	40	120	4	8,000	$\lesssim$ 117
(A)	10^3	120	80	12	24,000	$\lesssim$ 26
(B)	333	40	120	12	24,000	$\lesssim$ 39
(B)	333	120	80	36	72,000	$\lesssim$ 8.7

Parameters for various instrument designs.

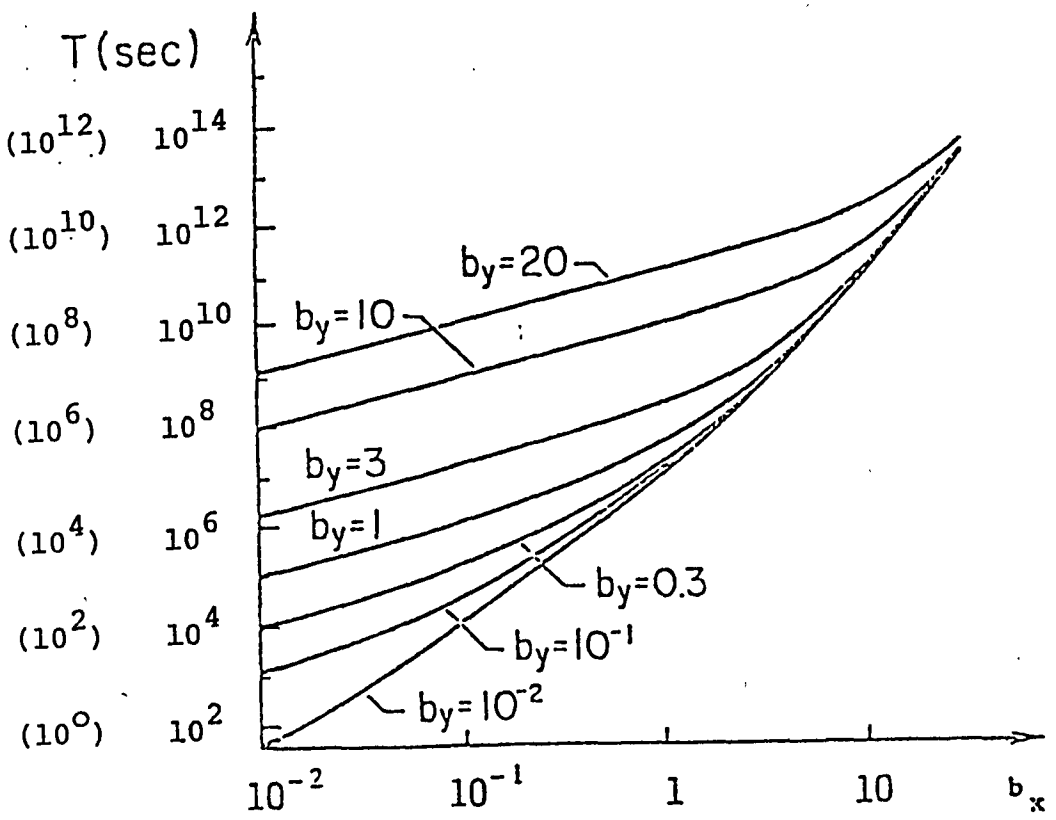

Figure 1. Exposure time, T, as a function of b_x and b_y computed from Eq. (5) for the parameters listed in Table II, assuming M=F=1. Two sets of times are given. The ones in parentheses refer to the case when the storage ring under consideration has an insertion device which increases the S.R. intensity and thus N^0 by a factor 10^2, while the rest of the numbers refer to the case when such a device is absent.

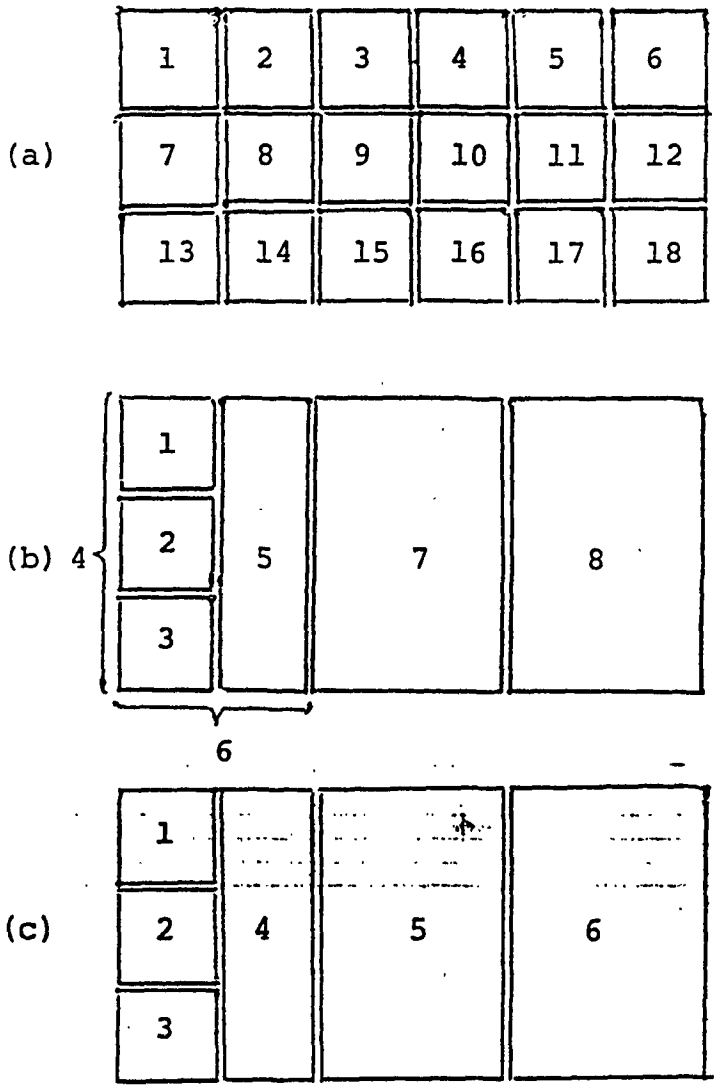

Figure 2

An illustration of various reproduction strategies

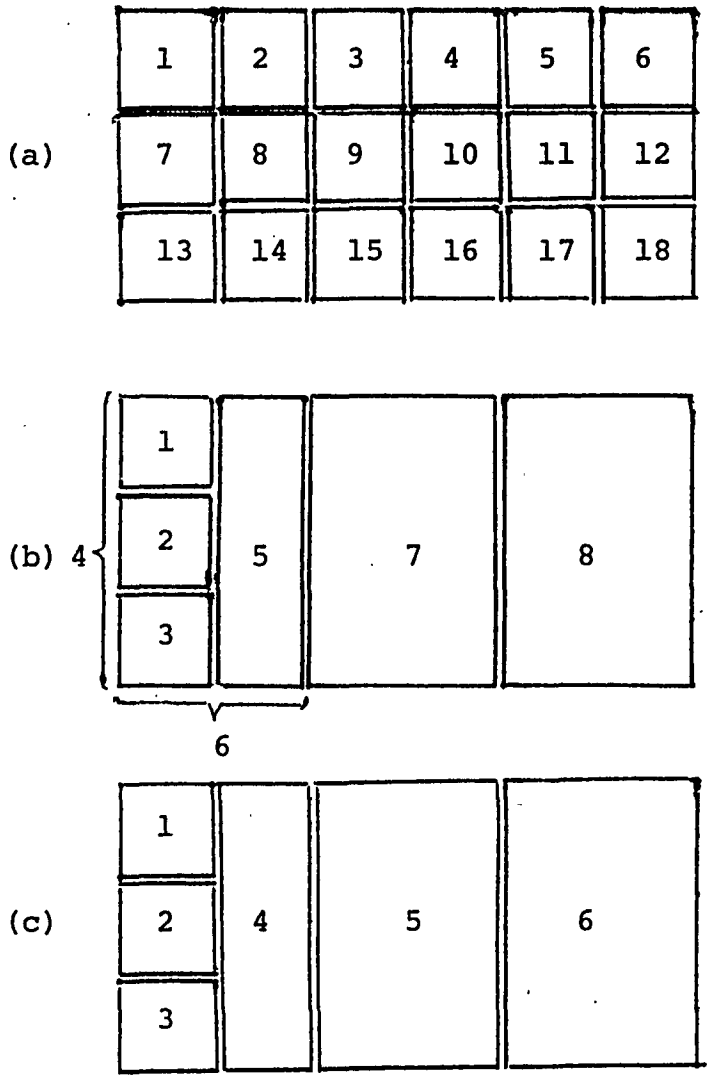

Figure 2

An illustration of various reproduction strategies

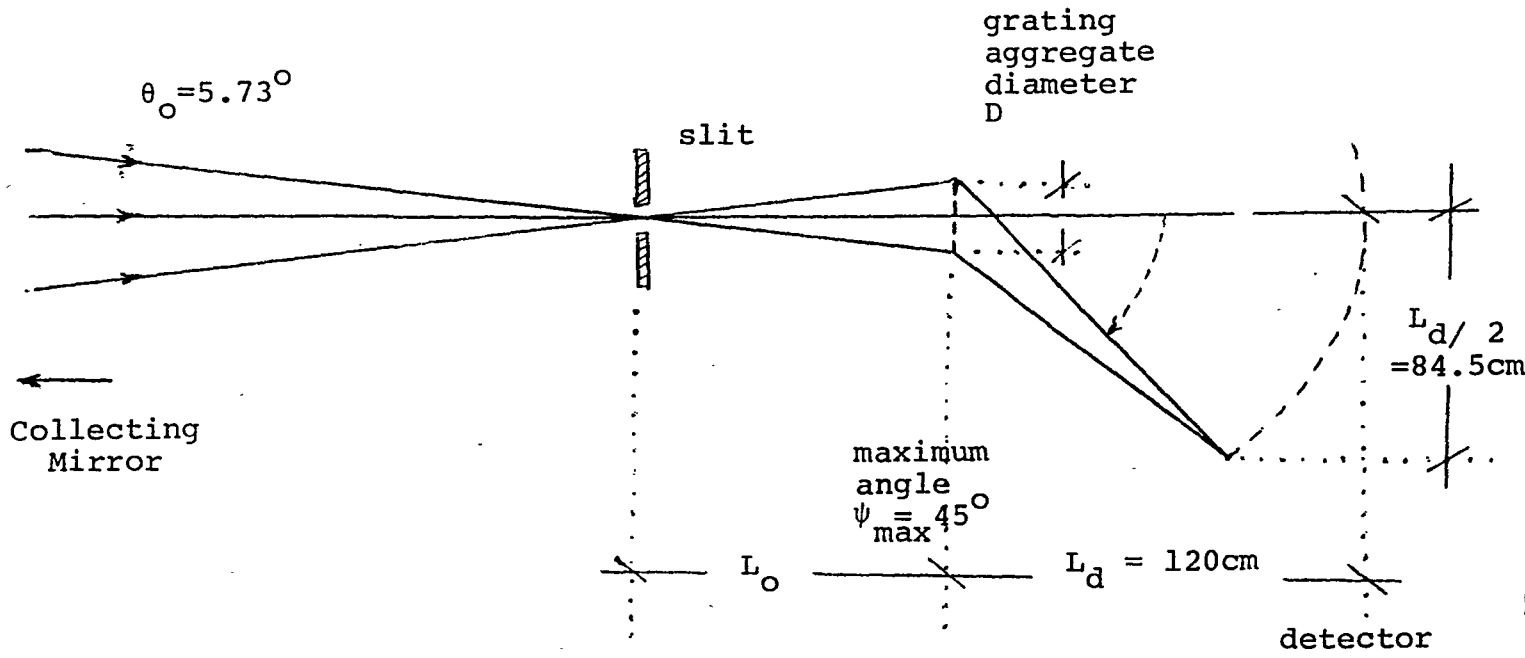

Figure 3

Model design for an instrument using a superfine grating aggregate

1984

NASA/ASEE SUMMER FACULTY RESEARCH FELLOWSHIP PROGRAM

MARSHALL SPACE FLIGHT CENTER
THE UNIVERSITY OF ALABAMA

INVESTIGATION OF FOAM FLOTATION AND PHASE PARTITIONING TECHNIQUES

Prepared by:	Ben L. Currin, Ph. D.
Academic Rank:	Instructor
University and Department:	Calhoun Community College Department of Natural Sciences
NASA/MSFC: (Laboratory) (Division) (Branch)	 Space Science Laboratory Space Processing Separation Processes
MSFC Counterpart:	Robert S. Snyder
Date:	August 3, 1984
Contract No.:	NGT-01-002-099 University of Alabama

INVESTIGATION OF FOAM FLOTATION AND PHASE PARTITIONING TECHNIQUES

By

Ben L. Currin, Ph. D.
Department of Natural Sciences
Calhoun Community College
Decatur, Alabama

ABSTRACT

The present status of foam flotation as a separation process is evaluated and limitations for cells and proteins are determined. Possible applications of foam flotation to separations in microgravity are discussed. Application of the fluid mechanical aspects of foam separation techniques is made to phase partitioning in order to investigate the viscous drag forces that may affect the partitioning of cells in a two phase poly(ethylene glycol) and dextran system.

INTRODUCTION

Separation and purification methods are of great importance both in research and in applied science and technology. Foam separation methods have been utilized for many years in the field of mineral processing and in recent years there have been many new variations of these techniques in which removals of species such as organic compounds and colloidal substances have been achieved. The use of foam flotation methods for separation and purification of proteins and cells is somewhat limited due to the sensitive nature of these substances.

Phase partitioning is a separation technique that has great promise in the area of biological materials. The main advantage of phase partitioning over foam flotation for the separation of cells and proteins is the ability to separate cells and proteins without damaging their fragile structures.

Because these two separation techniques are similiar, it is helpful to apply principles of one technique to the other in order to better understand and improve each method.

OBJECTIVES

I. To evaluate the present status of foam flotation as a separation process on earth.

II. To determine the present achivements and limitations of foam flotation in the separation of cells and proteins.

III. To investigate the fluid mechanical aspects of phase partitioning.

FOAM FLOTATION

Foam flotation is a subdivision of an extensive area of separation methods known as adsorptive bubble separation techniques. These techniques are based on the difference in surface activity of the substances in a solution or suspension. Substances which may be molecular, colloidal, or macroparticulate in size are selectively adsorbed or attached at the surfaces of bubbles rising through the liquid. This allows their separation and concentration in a small volume of collapsed foam. A substance which is not surface active itself can often be made effectively surface active through interaction with a surface active species.

The Gibbs equation (1) describes the adsorption of surface active species from aqueous solution at a gas-liquid interface. For a two component (water - solute) system in which the dividing surface between the gas phase and solution is chosen so that the surface excess of the solvent is zero, the Gibbs equation is given by

$$\Gamma = -\frac{a}{RT}\frac{d\gamma}{da} \qquad (1)$$

where Γ is the surface excess of the solute, a is the activity of the solute, and γ is the surface tension. The ratio Γ/a is a ratio of the amount of solute at the interface to the amount in the bulk solution. Figure 1 shows the effect of adsorption of solute at the interface on the surface tension. At low concentrations there are few surface active molecules or ions present to lower the surface tension. At higher concentrations, the adsorption of the surface active species increases. In this concentration range, separation of surface active species from the solution may be achieved by an adsorptive bubble separation method. At high concentrations, the formation of micelles, aggregrations of long-chained surface active ions into large charged units which are surface inactive, results in poor removals by adsorptive bubble separation techniques. Although the Gibbs equation is based on equilibrium conditions and cannot be applied directly to adsorptive bubble separation techniques, comparison of the Gibbs equation with experimental results for surfactant removal by foaming has shown good agreement (2).

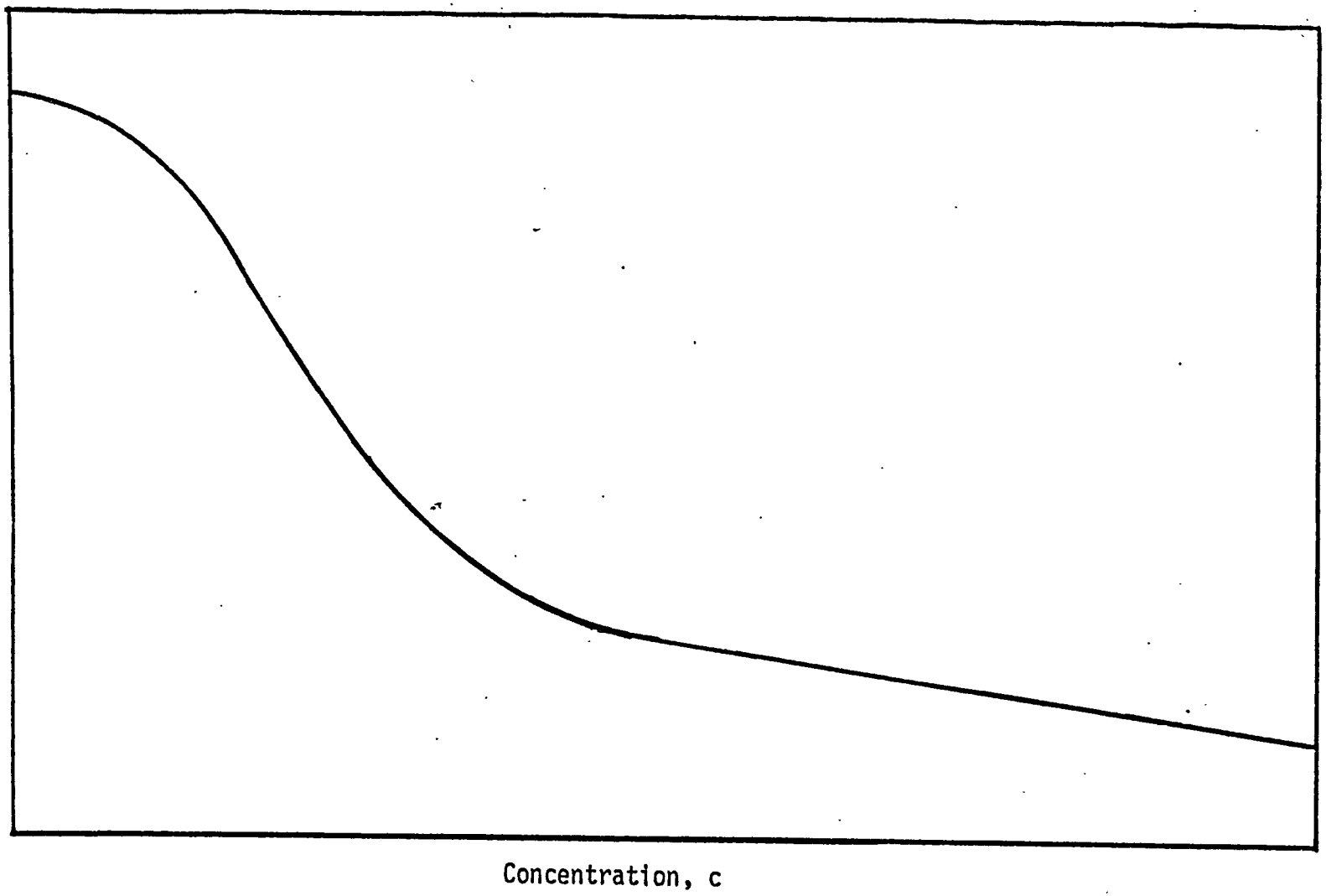

FIGURE 1. Hypothetical Surface Tension - Concentration Curve for a Surface Active Species.

A classification scheme for adsorptive bubble separation methods is shown in Figure 2 (3). The techniques are divided into two groups based on whether or not a foam is generated for removal of material. A description of each method is given by Lemlich (4).

Foam separation involves the passage of air or a gas through the solution containing the species to be removed and a surfactant. The adsorbed components are separated by simply removing the foam and breaking it using various chemical or mechanical methods. The simplest procedure is the use of a batch system shown in Figure 3(a). This method is not feasible for a large-scale process, so the continuous mode of operation, shown in Figure 3(b), is used.

Foam separation methods are dependent upon a number of variables, such as solution pH, ionic strength, surfactant concentration, gas flow rate, and specific adsorption of competing ions.

There has been much activity in the theory and application of foam separation techniques. Comprehensive general reviews of separation by flotation were written by Clarke and Wilson (5) and by Grieves (6) in which theory and models, removal of metals, removal of anions and organic compounds, and applied and large scale studies were reviewed.

The separation and purification of proteins on the basis of surface properties is discussed in the literature. Some examples of this technique include the concentration of protein in starch wash water (7), the separation of urease and catalase (8), the separation of the enzymes pepsin and renin (9), recovery of protein from potato juice waste water (10), and the separation of components of wood and paper pulp (11).

The application of foam flotation techniques to the separation of proteins, enzymes, and cells is somewhat limited due to the possibility of denaturing the species of interest. A protein molecule is a polymer of amino acids containing hydrophilic parts on its surface and hydrophobic parts, most of which are located in the interior of the molecule. When a protein is exposed to an air-water interface, the stresses may cause alterations in its structure. Although the denatured protein is unable to carry out its biological function, it may be useful as a source of food. Examples of proteins that are denatured upon contact with surfaces are albumin and hexokinase. Examples of enzyme proteins that are not denatured when in contact with surfaces are tripeptide synthetase, lactic acid dehydrogenase, catalase, amylase, cellulase, d-amino acid oxidase, aryl pyruvate keto-enol, and automerase (12).

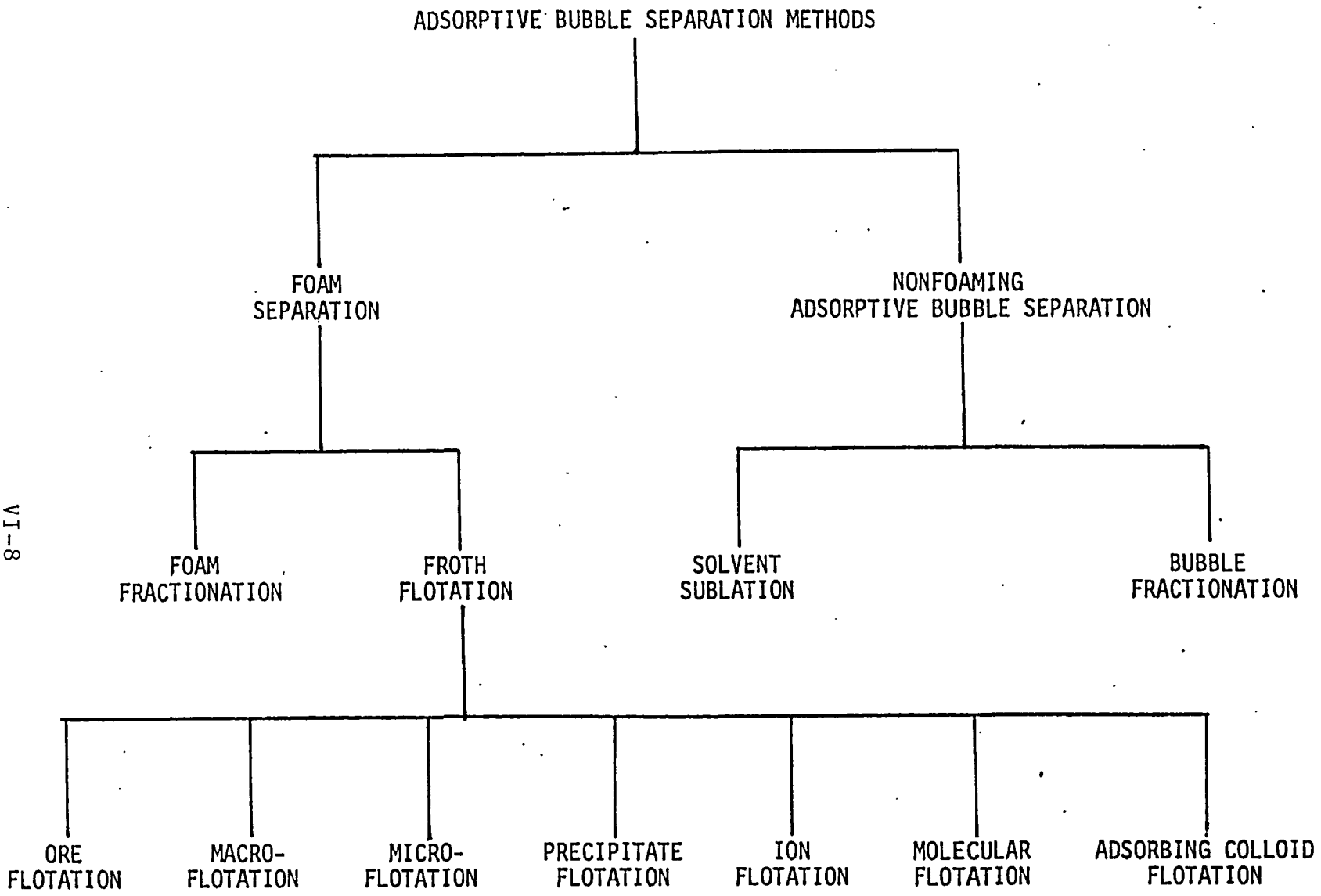

FIGURE 2. Classification of Adsorptive Bubble Separation Techniques

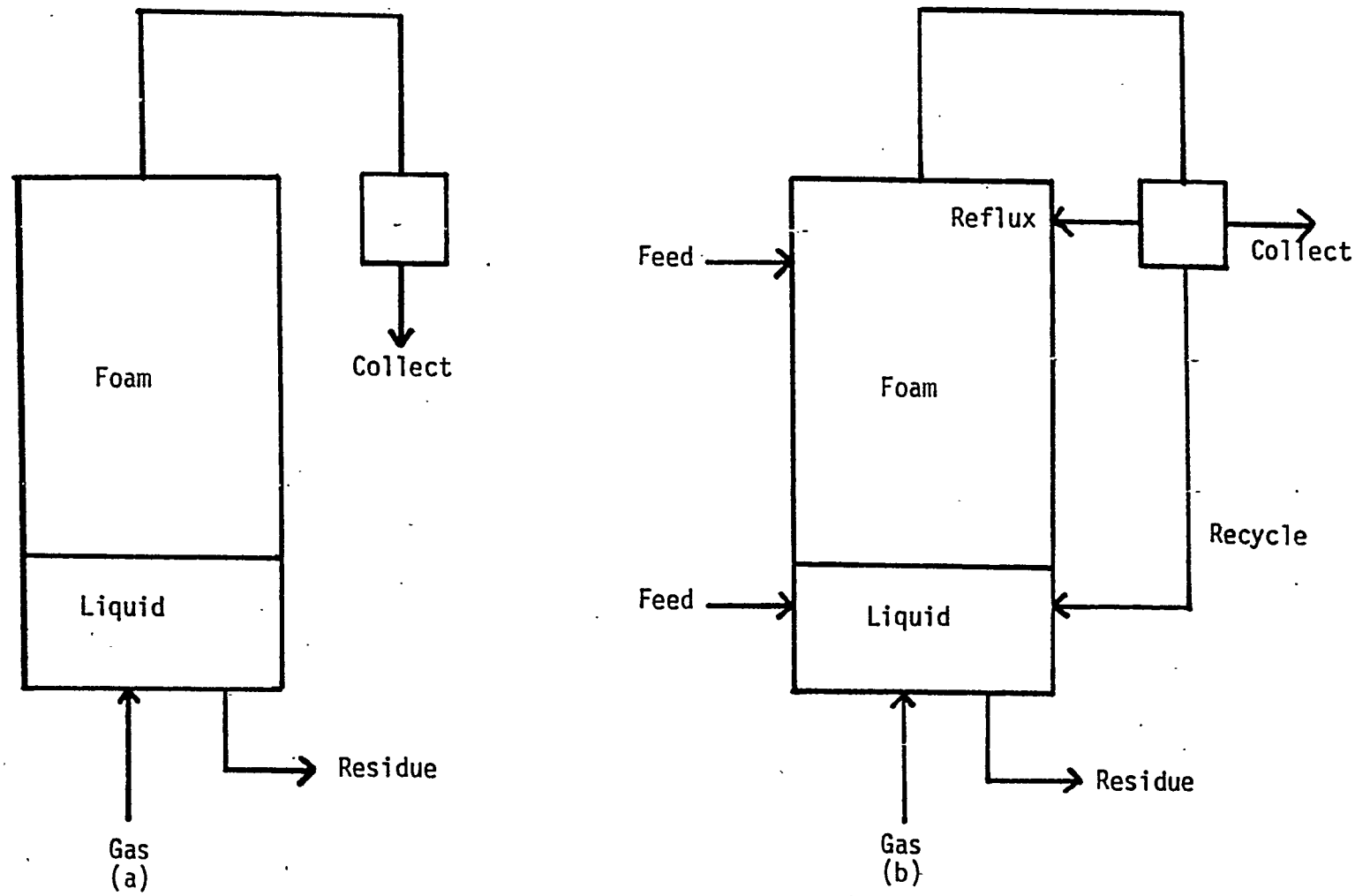

FIGURE 3. Modes of Foam Column Operation

PHASE PARTITIONING

The development of separation and purification methods for proteins, nucleic acids, and whole cells is of extreme importance to fields such as cell biology, pathology, and biochemistry. A frequently encountered problem in biotechnological experiments is the isolation of the species of interest from complex mixtures of degradative enzymes, proteins, nucleic acids, and cellular debris. The intolerance of the products to any but the mildest solvent or thermal environments severely limits the range of conventional engineering that can be used (13).

There has been increasing interest in the application of liquid-liquid distribution techniques using special aqueous phase systems prepared by mixing aqueous solutions of two incompatable polymers prepared in concentrations such that phase separation occurs and each phase is enriched in one of the two polymers. If biological materials, such as cells, are added to a system of this type, an unequal distribution of the material between the phases is observed. The basis for separation by a two-phase system is the selective distribution of substances between the phases. For soluble substances, distribution takes place between the two bulk phases, but when suspended particles are present, the interface may adsorb relatively large amounts of material. Therefore, in the separation of cell particles there are three "phases" to consider; the upper, the -inter, and the lower phase (14).

A two phase system is formed when aqueous solutions of the polymers dextran and poly(ethylene glycol) are mixed above certain concentrations. The upper, less dense phase is enriched in poly(ethylene glycol) and the lower, denser phase is enriched in dextran. By addition of certain salts, the system can be made compatable with cells. When cells are added to such a system, they will partition between one or both phases and the interface. To achieve equilibrium in a reasonable amount of time, the phase system containing the particles is shaken so that contact between the phases and the cells may be increased.

It is possible to experimentally control the chemical and physical properties of the phases in order to determine the distribution pattern of the substance of interest. The most important factors that determine partition in these

systems are the surface properties of the cells. Added salts can create a Donnan potential which can interact with the cell surface potential. Also, various affinity ligands may be attached to one of the polymers to increase the degree to which it adsorbs to the cell surface.

A quantitative representation of cell partition is

$$K = \text{constant} \times \exp(\Delta G/fkT) \qquad (2)$$

where K is the partition coefficient (ratio of the number of cells in one phase to number of cells at the interface), ΔG is the free energy of the cell in one phase relative to that at the interface, k is Boltzmann's constant, T is the absolute temperature, and f is a factor that represents a randomizing energy.

It has been shown that if thermal energies were the only factors that caused distribution of cells in these systems, all cells would be adsorbed at the interface (15). Experimental results imply that an unknown randomizing energy causes cells to be removed from the interface (i. e. $f \geq 20$). Two possible sources of this unknown energy are fluid shear stresses during phase separation and the addition of kinetic energy to the cells when the system is shaken. In order to increase the efficiency, sensitivity, and resolution of phase partitioning, a better understanding of the nature of this randomizing energy is necessary.

CONCLUSIONS AND RECOMMENDATIONS

Under conditions of low gravity, it should be possible to investigate the behavior of foams in order to determine ways to improve the techniques of foam flotation and to carry out separations that are difficult to achieve on Earth. The buoyancy force of a gas bubble in a fluid is the driving force behind foam separation methods. Since this buoyancy force is proportional to the acceleration of gravity, experiments carried out under conditions of microgravity will be characterized by a virtual elimination of buoyancy forces. This should allow gas bubbles to remain in suspension for long periods of time, facilitating the determination of interfacial properties.

Two problems associated with foam separation techniques are uncontrolled rise of bubbles of different sizes and the drainage of wet foams. If a bubble is too large, its rapid rise through a liquid may result in the stripping of adsorbed particles by viscous forces and in the inability of certain particles to be attached. A wet foam may be stripped of adsorbed particles by drainage of liquid through the interstices of the bubbles. Both problems could be minimized by the absence of the buoyancy force under microgravity conditions. The use of electrophoresis as a controlled driving force for bubble movement in the absence of gravity is feasible.

An understanding of the randomizing energy that results in the removal of cells from the interface of the two phases during phase partitioning would be helpful in optimizing the effectiveness of this method. Some fluid mechanical aspects of foam flotation may be utilized in estimating the various forces that affect phase partitioning. During the separation of the phases, cells are attached to the interface between droplets of one phase and the other phase. This is somewhat similiar to the attachment of particles to an air-water interface on a rising bubble. Using the approach of Clarke and Wilson (16), the free energy change during the attachment of a cell to the interface between two phases may be approximated by

$$\Delta G = -\gamma_{i2} \pi r^2 (1 - \cos \theta)^2 \qquad (3)$$

where γ_{i2} is the interfacial tension, r is the cell radius, and θ is the contact angle between the cell and the two phases.

The viscous forces on a cell attached to a droplet can be approximated by

$$F_v = 3\pi a^2 \eta \, v/r \qquad (4)$$

where a is the cell radius, η is the viscosity of the liquid through which the droplet is rising and r is the radius of the droplet.

A chamber has been designed to investigate the effects of the above factors on the attachment and detachment of cells to phase droplets and is shown in Figure 4. The chamber consists of a piece of square glass tubing with an inner width of 3 mm. A small, circular, glass capillary tube (0.300 mm I. D. and 0.550 mm O. D.) is attached through the wall of the square tube so that its tip is in the center. The circular capillary is connected to a syringe to allow formation of droplets at its tip. A microscope may be used to observe the chamber. A solution of dextran is pumped through the square tube so that laminar flow is occuring and a small droplet of poly(ethylene glycol) solution is suspended from the circular capillary. Cells may be present in either solution. The flow of one phase past a droplet of the other phase will simulate buoyancy and by adjustment of flow rate, the effect of viscous forces can be observed.

Some recommended experiments are:

1. Observe the effect of flow rate on cell attachment and detachment. An increased flow rate will result in higher viscous forces.
2. Observe the effect of solution concentration. This factor will cause changes in interfacial tension and in viscosity.
3. Observe the effect of temperature. This will cause changes in viscosity.
4. Observe the effect of droplet size and of cell size.

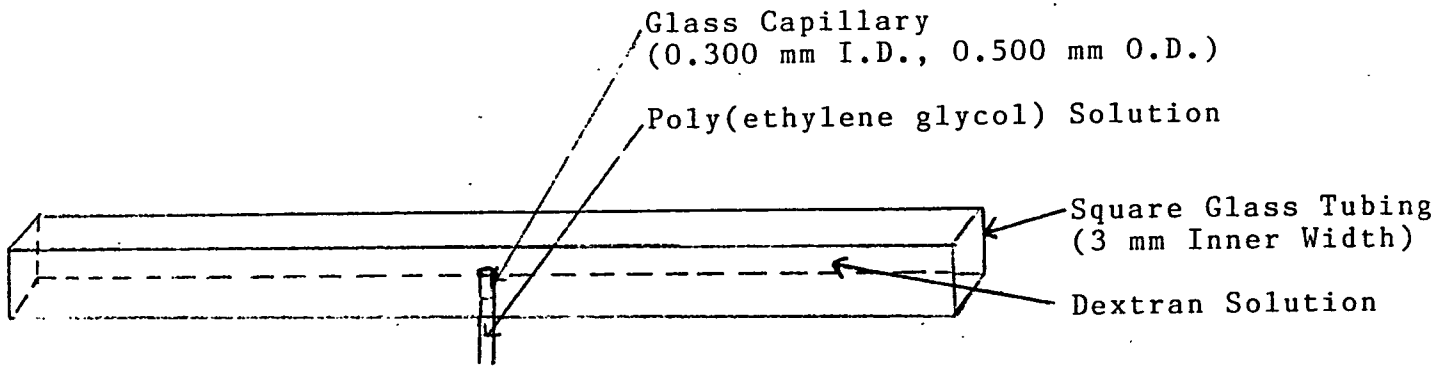

Figure 4. Chamber for investigation of Phase Partitioning

REFERENCES

1. A. W. Adamson, "Physical Chemistry of Surfaces,",3rd Ed., Wiley-Interscience, 1976, Chapter 2.

2. I. H. Newson, J. Appl. Chem., 16: 43 (1966).

3. B. L. Karger, R. B. Grieves, R. Lemlich, A. J. Rubin, and F. Sebba, Separ. Sci., 2: 401 (1967).

4. R. Lemlich, Ed., "Adsorptive Bubble Separation Techniques," Academic Press, New York, 1972.

5. A. N. Clarke and D. J. Wilson, Separ. Purif. Methods, 7: 55 (1978).

6. R. B. Grieves, in "Treatise on Analytical Chemistry," 2nd Ed., P. J. Elving, Ed., John Wiley & Son, New York, 1982, Part I., Vol. 5, p. 371.

7. W. Ostwold and A. Siehr, Kolloid-Z., 79: 11 (1937).

8. M. London , M. Cohen, and P. B. Hudson, Biochim. Biophys. Acta, 13: 111 (1954).

9. G. Andrews and F. Schutz, Biochem J., 39: 11 (1945).

10. D. C. Weijenberg, J. J. Mulder, A. A. H. Drinkenberg, and S. Stemerding, Ind. Eng. Chem. Process Des. Dev., 17: 209 (1978).

11. T. Lindstroem and G. Glad-Nordmark, J. Colloid Interface Sci., 94: 404 (1983).

12. In Reference 4, p. 159.

13. D. E. Brooks, Biotechnology, 1: 668 (1983).

14. P.-A. Albertsson, "Partition of Cell Particles and Macromolecules," 2nd Ed., Wiley-Interscience, New York, 1971.

15. D. E. Brooks, J. M. Van Alstine, J. M. Sharp, and S. Bamberger, submitted to Biophysical Journal.

16. A. N. Clarke and D. J. Wilson, "Foam Flotation, Theory and Applications," Marcell Dekker, Inc., New York, 1982.

1984

NASA/ASEE SUMMER FACULTY RESEARCH FELLOWSHIP PROGRAM

MARSHALL SPACE FLIGHT CENTER
THE UNIVERSITY OF ALABAMA

MODELS OF THE UPPER ATMOSPHERE

Prepared by:	T. Michael Davis, Ph.D.
Academic Rank:	Associate Professor
University and Department:	North Georgia College Department of Physics
NASA/MSFC:	
Laboratory:	Systems Dynamics
Division:	Atmospheric Sciences
Branch:	Atmospheric Physics
NASA Counterpart:	Robert E. Smith
Date:	August 15, 1984
Contract No.:	NASA-NGT-01-002-099 (The University of Alabama)

ACKNOWLEDGEMENTS

It is a pleasure to acknowledge the help and patience of Dr. Dale Johnson; our association this summer has been fruitful. It is my sincere desire to continue this working relationship with him.

I deeply appreciate the confidence of Dr. Robert Smith and Dr. Mike Freeman in my ability to perform at the standards of such an outstanding research program. Working at Marshall Space Flight Center and in Dr. Smith's division in particular has been a very exciting and enlightening experience.

MODELS OF THE UPPER ATMOSPHERE

by

T. Michael Davis
Associate Professor of Physics
North Georgia College
Dahlonega, Georgia

ABSTRACT

Several computer models of the thermosphere are currently being used at Marshall Space Flight Center. J70MM, the Jacchia 1970 model with matrix and matrix mean output, and J703X, the Jacchia 1970, 1971, and 1977 models, are of primary interest. The subroutines in these programs were studied in detail, and several mistakes were found and corrected. One subroutine was modified substantially.

Slowey has proposed that a weighted average of the three-hour geomagnetic index be used in the models rather than a single index value. The densities (for a given date and time) generated by the J703X program (all three models), using both a single value of the index and weighted averages for three different lag times, are tabulated and discussed.

Most of the equations used in the models are the results of empirical curve fits. An attempt was made to generate a theoretical prediction of the thermospheric temperature profile based on a simple physical model of atmospheric heat conduction in a spherically-symmetric shell. Although this theory was developed by others in the early 1960's, an inaccurate model of the variation of thermal conductivity, k, of gases with temperature was used. The "exponential heating" theory and the temperature dependence of k are discussed.

LIST OF FIGURES

LIST OF TABLES

INTRODUCTION

The thermosphere extends from an altitude of approximately 90 kilometers to hundreds of kilometers. The temperature in this region rises from about 200 K to, generally, well over 1000 K, and the density falls from around 10^{-9} g/cm^3 to 10^{-16} g/cm^3, depending on solar, geomagnetic, and other conditions.

The Space Shuttle orbits the earth in the thermosphere. It is highly desirable, therefore, for one to be able to predict accurately the conditions - temperature, densities of gaseous components, total density - in the upper atmosphere. For this purpose many models of the upper atmosphere have been developed. Researchers at Marshall Space Flight Center have preferred the use of Jacchia's models (Jacchia, 1970; 1971; 1977), which they have had adapted to the computer.

OBJECTIVES

The objectives of this study were to:

1) determine whether there were any mistakes in the MSFC computer programs and correct any that were found,

2) improve the computer models,

3) make trial runs of the J703X model,

4) study the feasibility of using a weighted average geomagnetic index in the calculations rather than a single (at the time of calculation) value, and

5) investigate atmospheric heating theory to, if possible, suggest enhancements.

MODIFICATIONS OF THE JACCHIA COMPUTER MODELS

Two FORTRAN programs on the Atmospheric Sciences Division's Hewlett-Packard 1000F computer are of primary importance in this study. J70MM, the Jacchia 1970 model with matrix and matrix mean output, has long been the preferred program, and J703X, the 1970, 1971, and 1977 models, is essentially untried. Many of the subroutines used in J70MM also appear in J703X; therefore, most modifications will apply to both programs.

Some modifications (Davis, 1984) are required by mistakes in the programs; some are suggested by improvements in accuracy and function. These modifications have been incorporated into the models and the programs saved under new names. J84MM is the improved version of J70MM. J3X12, J3X15, and J4X15 are improved versions of J703X. J3X12 is used for low altitude calculations, where the density is about 10^{-12} g/cm^3, and J3X15 is used for high altitude calculations. J4X15 is the same as J3X15 except that only one run of date, time, and altitude is allowed. J3X12, for example, is run on the Hewlett-Packard by typing RU,J3X12::34 after LOGON has been executed.

One note of caution is in order. The "improved" versions of J703X were changed with specific requirements in mind. The result was that program size limitations forced restrictions on what the new programs could do. J3X12, for example, generates only total densities in matrix form (with matrix mean) for only certain latitudes (-90 to +90, increment 10) and longitudes (-180 to +160, increment 20), and these densities can not be over $9.999(10)^{-12}$ g/cm^3. Also, due to the placement of the altitude "DO loop," only one altitude case can be run at a time, even though one is asked to input the number of cases. Up to about four different date/time cases may be run at once, but after that the dimension of some array variables becomes a problem, causing an inaccurate output.

The TME SUBROUTINE, which calculates Julian date and solar hour angle, was altered substantially. The old program (J70MM and J703X), new program (J84MM and J3X12), and Astronomical Almanac (e. g., 1983) values of solar hour angle for six dates are given in Table 1. Note that old program values are typically about one-half degree off. This discrepancy becomes greater as time advances on the date in question, because the coordinates of the sun are assumed constant, causing a variance of almost 2 degrees. The solar coordinates are modeled more precisely in the modified programs as can be seen from the data in Table 1 and Table 2.

Date	Almanac value	New program value	Old program value
Mar 08, 1969	177°.25417	177°.26961 Δ = 0°.015	177°.83066 Δ = 0°.576
Aug 22, 1969	179°.25417	179°.27361 Δ = 0°.019	179°.94659 Δ = 0°.692
Dec 13, 1969	-178°.49583	-178°.4964 Δ = 0°.0006	-177°.98628 Δ = 0°.49
Jan 01, 1983	179°.21667	179°.21264 Δ = 0°.004	179°.64572 Δ = 0°.43
Jul 07, 1983	178°.96667	178°.95345 Δ = 0°.013	179°.63838 Δ = 0°.33
Sep 09, 1983	-179°.40833	-179°.39833 Δ = 0°.010	-178°.80732 Δ = 0°.40

Table 1. Solar hour angles for 0000 UT and 0° longitude.
Δ = |program value| - |Almanac value|.

Table 2 lists the solar coordinates as calculated by the new programs (top row for each date) and the coordinates given in the Almanac (bottom row for each date). Note that the differences between new program and Almanac values never exceed about 1 minute for solar hour angle, 2 minutes for celestial longitude, 36 seconds for declination, and 9 seconds for right ascension.

The length of this report limits discussion of the reasons for the changes in SUBROUTINE TME. A detailed analysis has been written and is available upon request. Figure 1 is a listing of the Applesoft (BASIC) program written to calculate Julian date and solar coordinates. It contains all the modifications of the FORTRAN program.

WEIGHTED AVERAGING OF THE GEOMAGNETIC INDEX

The strength of the earth's magnetic field is not constant. The (primarily solar activity-induced) variations in field strength are constantly monitored, the disturbances being reported as one of several geomagnetic indeces. The most common indeces are K_p and a_p, which are obtained at 3-hour intervals during the 24-hour day. K_p and a_p give essentially the same information, but they differ in that a_p is a linear scale of magnetic disturbance, measured in units of gammas (1 Tesla = 10^9 gammas), and K_p is approximately logarithmic. The K_p scale runs from 0 for "very quiet" to 9 for "very disturbed"; a_p values range from 0 to 400.

The temperature and density of the upper atmosphere rise with the level of magnetic disturbance. There is a lag time between the time of disturbance and the resulting change in density, the duration of lag time being smaller at higher latitudes. Until recently, the standard procedure was to simply use the K_p index which occured 6.7 hours prior to the time at which the density was to be calculated, regardless of latitude. The Jacchia 1977 model incorporates a latitude dependence in the use of K_p.

The possibility that a single value of K_p at a given lag time may not be sufficient to account for residual effects of preceding values of K_p was suggested by Slowey (1984). He proposed the use of a weighted average of the form (with his constant, c, set equal to 1 day^{-1})

Date	Celestial longitude	Declination	Right ascension
Jan 00, 1957	279°17'09"	-23°07'11"	18h40m25s
	279°18'03"	-23°07'02"	18h40m29s
Apr 01, 1957	10°59'42"	04°21'07"	00h40m26s
	11°00'03"	04°21'17"	00h40m27s
Aug 01, 1957	128°27'26"	18°09'11"	08h43m32s
	128°28'08"	18°08'49"	08h43m36s
Dec 01, 1957	248°32'16"	-21°43'58"	16h27m13s
	248°31'32"	-21°43'49"	16h27m12s
Jun 20, 1968	88°44'12"	23°26'14"	05h54m30s
	88°43'07"	23°26'22"	05h54m25s
Apr 10, 1969	19°57'17"	07°48'12"	01h13m42s
	19°56'50"	07°48'01"	01h13m39s
Dec 06, 1969	253°41'59"	-22°26'54"	16h49m17s
	253°41'08"	-22°26'59"	16h49m15s
Feb 15, 1971	325°37'14"	-12°58'56"	21h51m32s
	325°38'59"	-12°58'25"	21h51m39s
May 15, 1971	53°32'46"	18°39'45"	03h24m38s
	53°31'33"	18°39'34"	03h24m34s
Aug 15, 1971	141°30'23"	14°20'13"	09h35m32s
	141°31'15"	14°19'52"	09h35m38s
Nov 15, 1971	231°58'18"	-18°15'46"	15h18m13s
	231°56'52"	-18°15'38"	15h18m10s
May 04, 1974	43°10'25"	15°47'43"	02h42m53s
	43°09'43"	15°48'19"	02h43m02s
Feb 15, 1983	325°42'44"	-12°57'01"	21h51m53s
	325°44'21"	-12°56'42"	21h51m57s
Nov 15, 1983	232°03'50"	-18°17'08"	15h18m36s
	232°03'17"	-18°16'51"	15h18m31s

Table 2. Solar coordinates for 0000 UT.

```
1     DIM ID(12)
2     DATA 31,28,31,30,31,30,31,31,30,31,30,31
3     FOR I = 1 TO 12
4     READ ID(I)
5     NEXT I
10    HOME
20    PI = 3.141592654
30    INPUT "DATE (YYYY(>1800),MM,DD) = ";YY,MM,DD
32    ID(2) = 28
35    GOSUB 1040
40    INPUT "TIME OF DAY (HH,MM) = ";IH,IM
50    INPUT "LONGITUDE (- WEST, + EAST) = ";LNG
60    GMT = 60*IH + IM
70    JC = (J - 2415020.5)/36525
80    GP = 99.69098333 + 36000.76892*JC + 0.00038708*JC^2
      + 0.250684477*GMT
90    GP = GP - (INT(GP/360))*360
100   RP = GP + LNG
110   RP = RP - (INT(RP/360))*360
220   JD = J - 2435839 + GMT/1440
230   LS = 0.0172028*JD + 0.0335*SIN(0.017202*(JD - 3)) - 1.407
240   YR = INT(LS/(2*PI))
250   LS = LS - 2*PI*YR
260   LS = LS*(180/PI)
270   D = INT(LS)
280   X = (LS - D)*60
290   M = INT(X)
300   Z = X - M
310   S = INT(Z*60 + 0.5)
320   XJ = (JD + 20819)/36525
330   EPS = 23.4523 - 0.013*JC
340   EPS = EPS*PI/180
350   LS = LS*PI/180
360   U = SIN(LS)*SIN(EPS)
370   SDA = ATN(U/SQR(-U*U + 1))
380   V = TAN(SDA)/TAN(EPS)
390   RAS = ATN(V/SQR(-V*V + 1))
400   GOSUB 600
410   SDA = SDA*180/PI
420   RAS = RAS*12/PI
430   IF SDA<0 THEN GOSUB 770
440   IF SDA<0 THEN GOTO 500
450   DD = INT(SDA)
460   XD = (SDA - DD)*60
470   MD = INT(XD)
```

Figure 1. Applesoft program used to calculate Julian date and solar coordinates.

```
480   ZD = XD - MD
490   SA = INT(ZD*60 + 0.5)
500   DR = INT(RAS)
510   XR = (RAS - DR)*60
520   MR = INT(XR)
530   ZR = XR - MR
540   SR = INT(ZR*60 + 0.5)
545   PRINT : PRINT "JULIAN DAY = ";J
550   PRINT : PRINT "CEL LONG (D,M,S) = ";D; TAB(24);M; TAB(28);S
560   PRINT : PRINT "SOL DECL (D,M,S) = ";DD;TAB(24);MD;TAB(28);SA
570   PRINT : PRINT "RIGHT AS (H,M,S) = ";DR;TAB(24);MR;TAB(28);SR
572   RAS = RAS*PI/12
575   SHA = (RP*PI/180 - RAS)*180/PI
577   GOSUB 900
580   PRINT : PRINT "SOL HR ANGLE = ";SHA
585   PRINT : PRINT : GOTO 20
590   END
600   RAS = ABS(RAS)
610   TEMP = ABS(LS)
620   IF (TEMP - PI/2)<= 0 THEN GOTO 730
630   IF (TEMP - PI/2)> 0 THEN GOTO 640
640   IF (TEMP - PI)<= 0 THEN GOTO 660
650   IF (TEMP - PI)> 0 THEN GOTO 680
660   RAS = PI - RAS
670   GOTO 730
680   IF (TEMP - 3*PI/2)<= 0 THEN GOTO 700
690   IF (TEMP - 3*PI/2)> 0 THEN GOTO 720
700   RAS = PI + RAS
710   GOTO 730
720   RAS = 2*PI - RAS
730   IF LS < 0 THEN GOTO 750
740   IF LS >= 0 THEN GOTO 760
750   RAS = -RAS
760   RETURN
770   SDA = -SDA
780   DD = INT(SDA)
790   XD = (SDA - DD)*60
800   MD = INT(XD)
810   ZD = XD - MD
820   SA = INT(ZD*60 + 0.5)
830   DD = -DD
840   SDA = -SDA
850   RETURN
900   IF SHA < 0 THEN GOTO 910
905   IF SHA >= 0 THEN GOTO 940
```

Figure 1. (cont'd)

```
910   IF (SHA + 180) < 0 THEN GOTO 920
915   IF (SHA + 180) >= 0 THEN GOTO 970
920   SHA = SHA + 360
930   GOTO 910
940   IF (SHA - 180) <= 0 THEN GOTO 970
945   IF (SHA - 180) > 0 THEN GOTO 950
950   SHA = SHA - 360
960   GOTO 940
970   RETURN
1040  IF (YY - 4*(INT(YY/4))) = 0 THEN ID(2) = 29
1042  IF (YY - 100*(INT(YY/100))) <> 0 THEN GOTO 1050
1045  IF (YY - 400*(INT(YY/400))) <> 0 THEN ID(2) = 28
1050  IF (MM - 1) <> 0 THEN GOTO 1080
1060  ID = DD
1070  GOTO 1140
1080  KE = MM - 1
1090  ID = 0
1100  FOR I = 1 TO KE
1110  ID = ID + ID(I)
1120  NEXT I
1130  ID = ID + DD
1140  DY = ID/365.2422
1150  J = 2378496 + 365*(YY - 1800) + ID
1155  XX = ABS(YY - 1801)
1160  LDD = INT(XX/4)
1165  IF YY >1900 AND YY < 2100 THEN LDD = LDD - 1
1170  J = J + LDD
1180  RETURN
```

Figure 1. (cont'd)

$$K_p'(t_o) = \frac{\sum_{t=t_o-\tau-5}^{t_o-\tau} K_p(t)\exp(-(t_o-\tau-t))}{\sum_{t=t_o-\tau-5}^{t_o-\tau} \exp(-(t_o-\tau-t))}, \qquad (1)$$

where t_o is the time of calculation of density or temperature, τ is the lag time in days, and t is the variable time between $t_o - \tau - 5$ days and $t_o - \tau$ days.

The Applesoft program listed in Figure 2 was used to calculate K_p' for three different times on May 25, 1967, leading up to the large magnetic storm. The program listed in Figure 3 transformed the averaged K_p values to equivalent a_p values, which are required as input to the J703X computer model. The 3-hour K_p values must be typed in the K_p-averaging program as DATA statements 80 through 120. The program then generates K_p' values for three lag times (0, 3, and 6 hours) averaged for times ranging from 5 days, as suggested by Slowey, to 1/8 day. The results for 2230 UT, 1330 UT, and 0130 UT are shown in Figures 4, 5, and 6, respectively.

These times were chosen to correspond to LOGACS data given by DeVries (1971). The accelerometer-measured densities were taken from DeVries' paper, and the 10.7-cm solar radio fluxes for this date were obtained from MSFC sources. It was not clear at what altitudes the accelerometer measurements were made, so the perigee of each orbit (143 km for all orbits considered) was used in the calculation. These data were input to J3X12 and the value of a_p changed until the density generated by mode 3 (the full magnetic coordinate-dependent 1977 Jacchia model) was equal to the density given by DeVries. These values of a_p are indicated by horizontal lines in the figures. Two lines are drawn in Figure 4 because it was not clear from the DeVries data which of two values of density should be used for 2230 UT. It may be that the two measurements were made in the same orbit at different altitudes and latitudes.

The results shown in Figures 4 and 5 suggest a weighted average of less than 1 day with a short lag time. Results in Figure 6, however, indicate no match at all. Clearly, no trend in lag time and averaging time can be deduced from only these three cases in which the nature of the experimental data is not well defined.

Since useful data were not available for comparison, a contrast of models similar to (but not as extensive as) that done by Johnson (1983) was carried out. The data chosen for

```
5     HOME
10    DIM SU(12): DIM KP(43): DIM D(12)
20    SUM = 0
30    FOR I = 1 TO 12
40    DATA 8.4598, 8.3729, 8.1365, 7.494, 5.7475, 5.3796, 4.9627
      4.4904, 3.9551, 3.3486, 2.6613, 1.8825
50    READ SU(I)
60    NEXT I
70    FOR I = 0 TO 42
80    DATA 8.333, 5.333, 1, 2, 1.667, 2.333, 4.333, 3.333
90    DATA 2.333, 1.667, 1.667, 1.333, 1.667, 3.333, 4, 1.667
100   DATA 1, 1.333, 1, 1.667, 0.667, 0, 0.333, 0.333
110   DATA 0.333, 0.667, 1.333, 1, 2.333, 2.333, 3.333, 1
120   DATA 0.667, 1, 0.333, 1, 1, 2.333, 1.333, 1, 0.667, 1, 1.333
130   READ KP(I)
140   NEXT I
150   FOR I = 1 TO 12
160   DATA 5, 4, 3, 2, 1, 7, 6, 5, 4, 3, 2, 1
170   READ D(I)
180   NEXT I
190   FOR J = 1 TO 12
195   IF J > 5 THEN D(J) = D(J)/8
200   FOR K = 0 TO 2
220   FOR I = K TO D(J)*8 + K
240   SUM = KP(I)*EXP(-(I - K)/8) + SUM
245   NEXT I
250   AVG = SUM/SU(J)
255   AVG = 0.001*INT(AVG*1000 + 0.5)
260   IF D(J) < 1 THEN GOTO 290
270   PRINT D(J);"-DAY AVG FROM T MINUS ";K*3;" H = ";AVG
280   GOTO 300
290   PRINT D(J)*8;"/8-DAY AVG FROM T MINUS ";K*3;" H = ";AVG
300   SUM = 0
310   NEXT K
315   PRINT
320   NEXT J
330   END
```

Figure 2. Applesoft program used to calculate the weighted average K_p.

K_p	mode 0	1	2	3
0	0.4574	0.4574	0.4574	0.4574
1	0.5443	0.5183	0.5179	0.5163
2	0.6002	0.5883	0.5875	0.5840
3	0.7157	0.6711	0.6699	0.6642
4	0.8271	0.7741	0.7725	0.7641
5	0.9476	0.9112	0.9092	0.8968
6	1.0939	1.1141	1.1116	1.0921
7	1.3422	1.4604	1.4572	1.4222
8	1.7482	2.1870	2.1843	2.1047
9	3.0399	4.2077	4.2218	3.9851

Table 3. Densities (10^{-15} g/cm^3) for June 20, 1984, 1200 UT.

```
20    DIM AP(29): DIM KP(29)
30    HOME
40    DATA 0, 2, 3, 4, 5, 6, 7, 9, 12, 15, 18, 22, 27, 32, 39,
      48, 56, 67, 80, 94, 111, 132, 154, 179, 207, 236, 300, 400, 0
50    FOR J = 1 TO 29
60    READ AP(J)
70    NEXT J
80    FOR I = 1 TO 28: KP(I) = (I - 1)/3: NEXT I
90    INPUT "KP = ";K
100   FOR I = 1 TO 28
110   IF KP(I) > K THEN GOTO 130
120   NEXT I
130   I = I - 1
140   FRAC = (K - KP(I))*3
150   AP = AP(I) + FRAC*(AP(I + 1) - AP(I))
160   PRINT : PRINT "AP = ";INT(AP + 0.5)
170   PRINT : PRINT : GOTO 90
```

Figure 3. Applesoft program used to transform K_p values to equivalent a_p values.

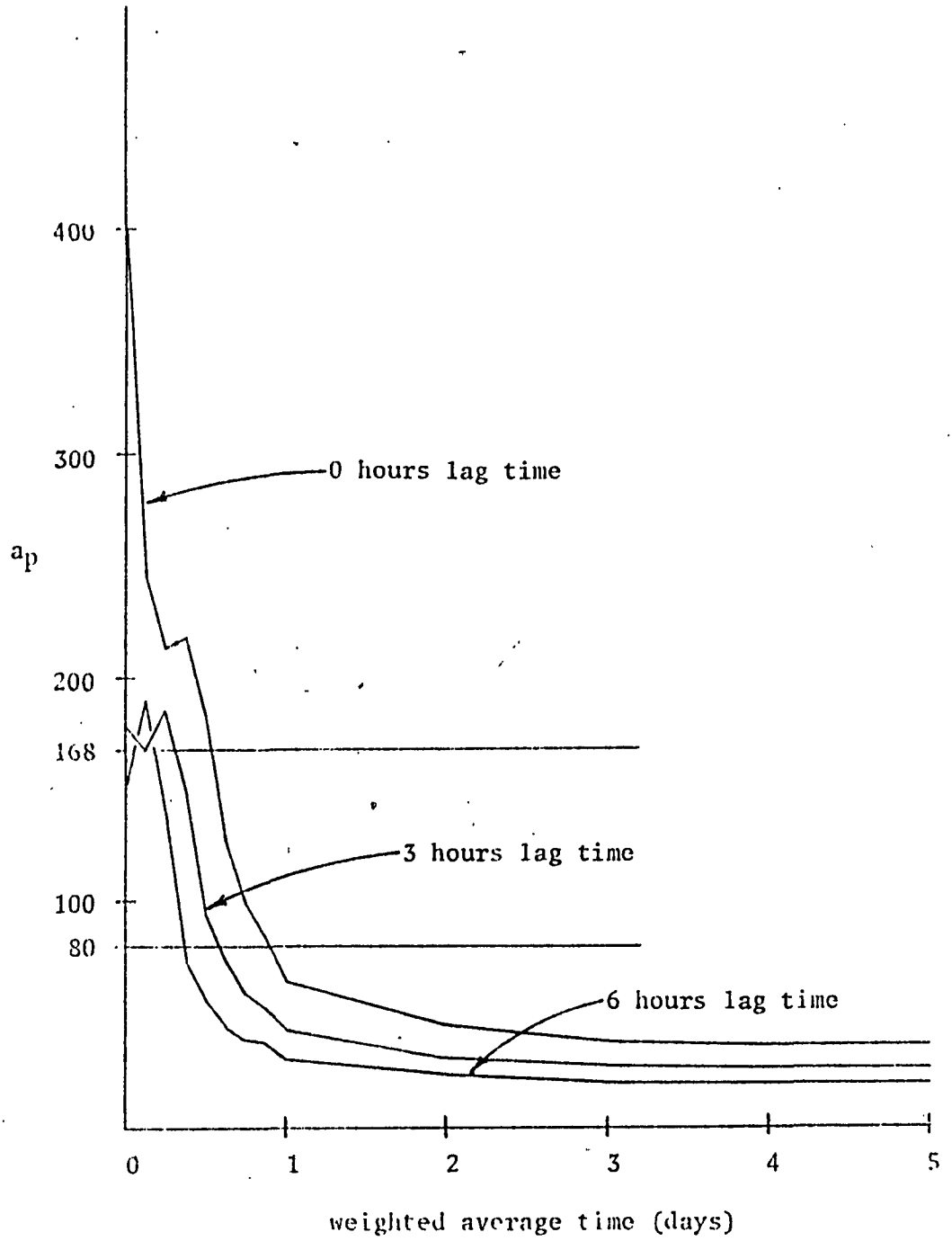

Figure 4. Weighted average values of a_p for 2230 UT, May 25, 1967.

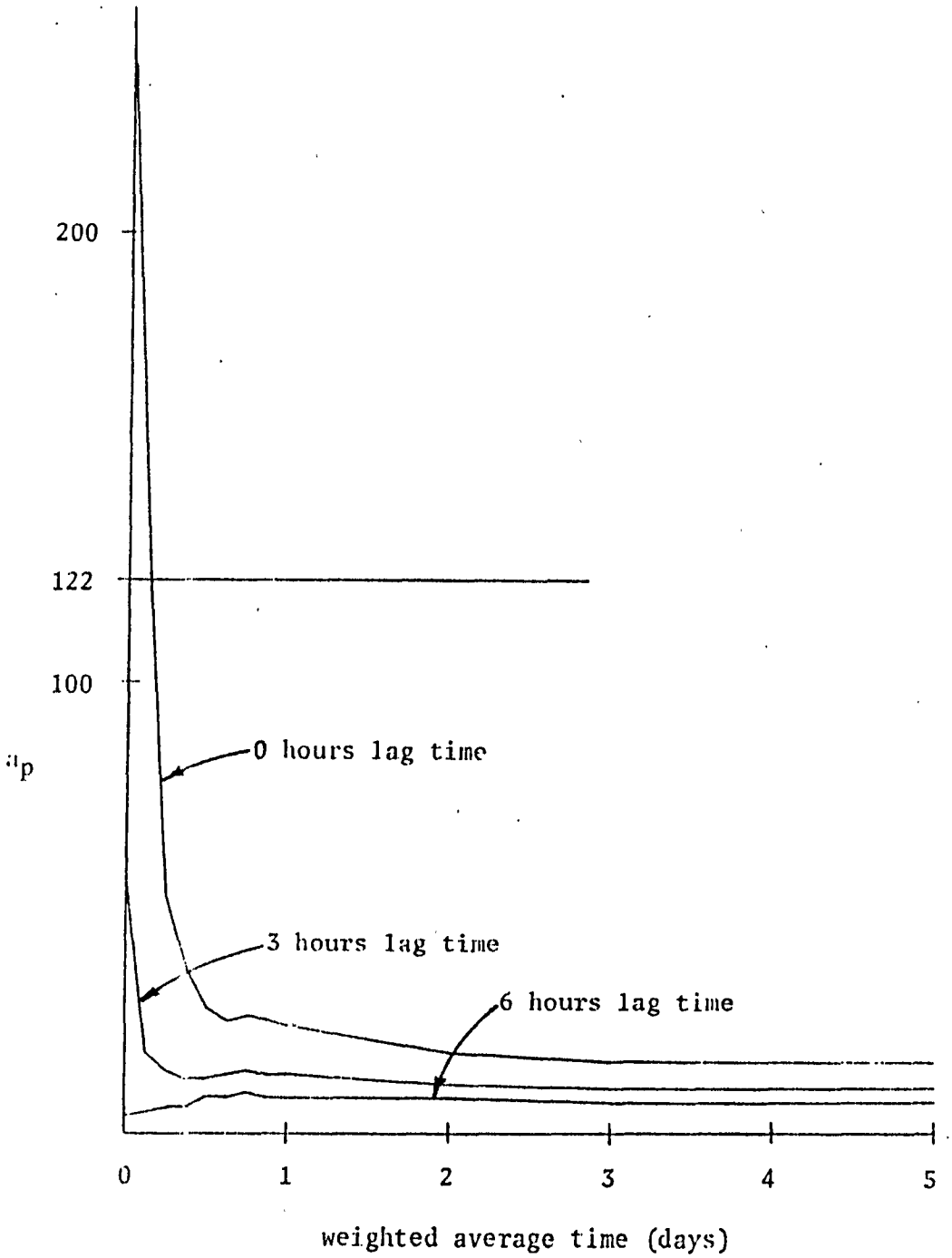

Figure 5. Weighted average values of a_p for 1330 UT, May 25, 1967.

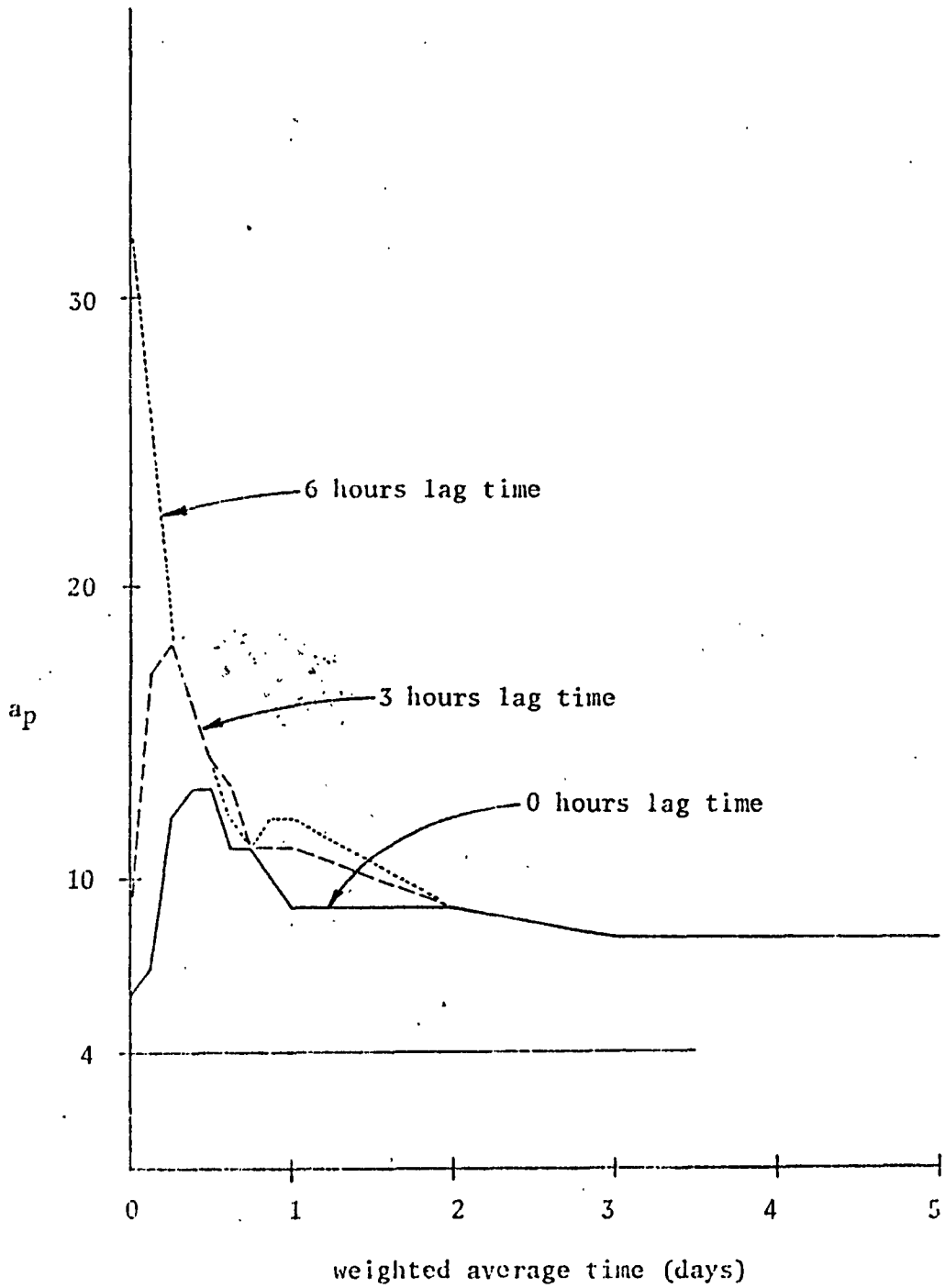

Figure 6. Weighted average values of a_p for 0130 UT, May 25, 1967.

input to J3X15 were: date/time June 20, 1984, 1200 UT, radio flux 150, average radio flux 150, and altitude 500 km. The densities generated by the different modes in J3X15 for different values of K_p are listed in Table 3. Note that at 500 km altitude mode -1 (1971 model) densities are equal to mode 0 (1970 model) densities and, so, are not listed. Modes 1, 2, and 3 are results of different ways of treating the 1977 model. Figure 7 shows how the densities change with an increase in K_p for the different modes. The percent difference is

$$\Delta = \frac{\rho(K_p) - \rho(K_p - 1)}{(\rho(K_p) + \rho(K_p - 1))/2} \times 100 \quad . \tag{2}$$

Figure 8 shows how the densities of modes 1, 2, and 3 compare with those of mode 0, the 1970 model being the one most commonly used at MSFC. The percent difference here is

$$\Delta = \frac{\rho(\text{mode } 0) - \rho(\text{mode } n)}{\rho(\text{mode } 0)} \times 100 \quad , \tag{3}$$

where n is 1, 2, or 3. Note that the differences become quite large for large K_p.

ATMOSPHERIC HEATING THEORY

It can be shown (Iribarne and Cho, 1980) that a simple model in which monochromatic radiation normally incident on an atmosphere consisting of one species of absorbing molecule that exhibits an exponential distribution in height results in heating of the atmosphere that is also exponential in nature. This so-called "Chapman profile" of rate of heating versus altitude can be approximated (Cole, 1962; Harris and Priester, 1963) by

$$Q = Q_o \exp((r - r_o)/h) \qquad r \leq r_o \quad , \tag{4a}$$

$$Q = Q_o \exp((r_o - r)/h) \qquad r \geq r_o \quad , \tag{4b}$$

where Q is the rate of heating in ergs cm^{-3} sec^{-1}, r is the distance from the center of the earth, Q_o and r_o refer to the level of maximum heating, and h is a constant scale distance.

The steady-state heat flow equation for a spherical shell is

$$\frac{d}{dr}\left(4\pi r^2 k \frac{dT}{dr}\right) = 4\pi r^2 Q(r) \quad , \tag{5}$$

where k is the thermal conductivity of the gas making up the atmosphere and T is the temperature. The solution of this equation now depends on what function of the temperature is used for the

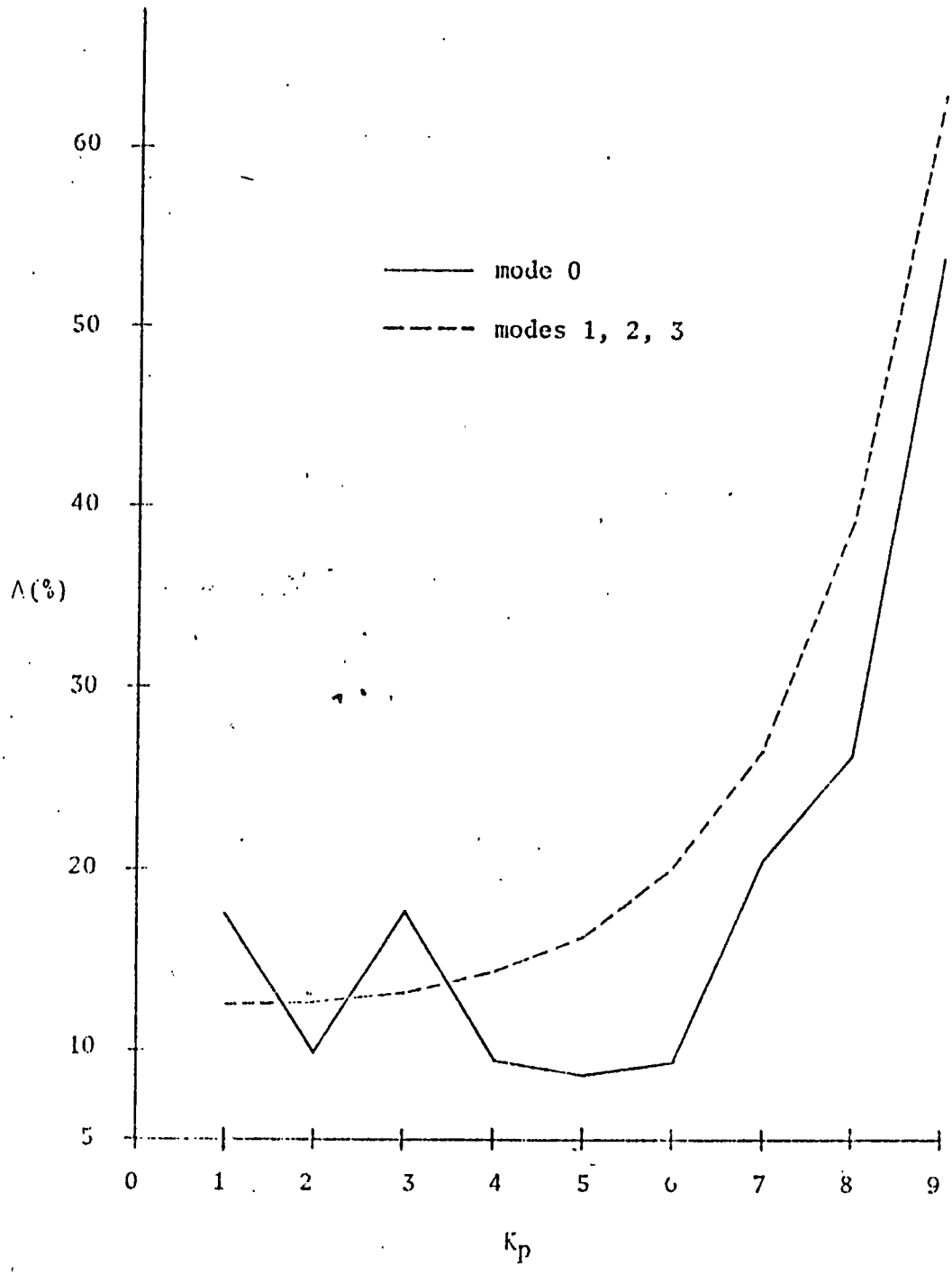

Figure 7. Percent difference between densities for consecutive values of K_p for June 20, 1984, 1200 UT.

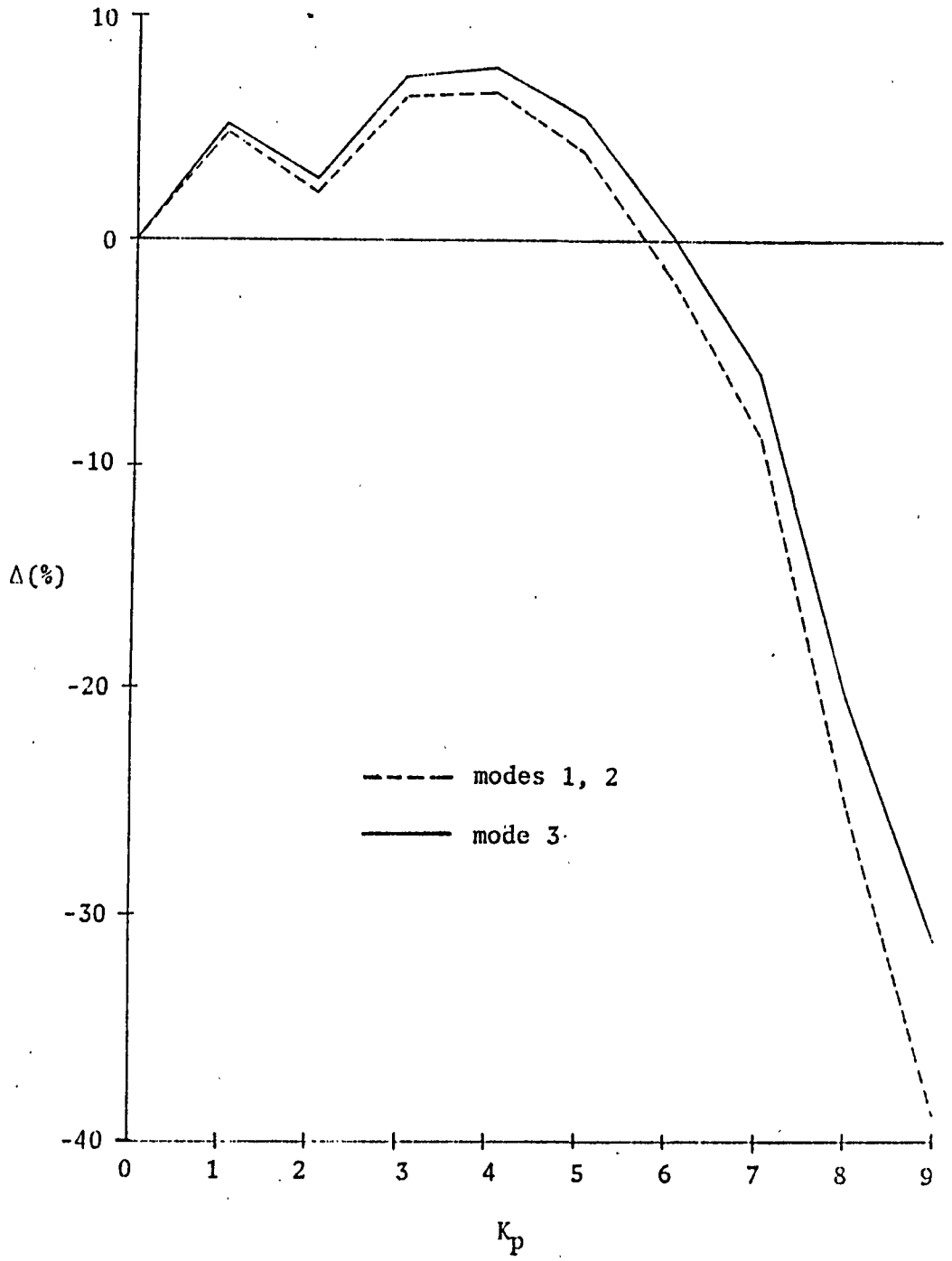

Figure 8. Percent difference between mode 0 densities and modes 1, 2, and 3 densities for June 20, 1984, 1200 UT.

thermal conductivity.

Simple kinetic theory involving collisions of hard spheres gives

$$k = AT^{1/2} \quad , \tag{6}$$

where A is a constant equal to 180 erg cm^{-1} sec^{-1} $K^{-3/2}$ for nitrogen (N_2). The thermal conductivities of air and nitrogen are very nearly equal over a large range of temperatures. A least squares fit to the thermal conductivity experimental data (Weast, 1982) gave

$$k = (21.9 \pm 0.8)T^{(0.824 \pm 0.005)} \quad . \tag{7}$$

Loeb (1961) showed that refinements of the theory result in the power of the temperature being closer to 0.75 than 0.5. Therefore, as a compromise the power was taken as 0.8, and another fit to the data yielded

$$k = (26.1 \pm 1.2)T^{0.8} \quad . \tag{8}$$

Figure 9 shows how equations (6) and (8) compare with the data.

If equations (4a) and (8) are substituted in to (5) and the resulting equation integrated from r_1, T_1, $(dT/dr)_1$ to an arbitrary point r, T, we get

$$T^{1.8} = T_1^{1.8} - 1.8(1/r - 1/r_1)r_1^2T_1^{0.8}(dT/dr)_1$$
$$+ (1.8Q_oh^2/26.1)(\exp((r-r_o)/h) - \exp((r_1-r_o)/h))$$
$$+ (1.8Q_ohr_1^2/26.1)(1/r - 1/r_1)\exp((r_1-r_o)/h),\ r \le r_o. \tag{9}$$

A similar equation is obtained for $r \ge r_o$ with r_2, T_2, $(dT/dr)_2$ as the upper limit to the integration. (Note that the use of $k = AT^{\frac{1}{2}}$ (Cole, 1962) does not produce the results reported by Cole.) The following parameters were chosen to best match the temperature profile used by Jacchia (1977): r_1 = 6447 km, T_1 = 188 K, $(dT/dr)_1 = 0$, r_2 = 6757 km, T_2 = 1000 K, $(dT/dr)_2 = 0$, r_o = 6482 km, $Q_o = 1.49(10)^{-7}$ erg cm^{-3} sec^{-1}, and h = 45 km. The results of this "exponential heating" theoretical calculation and the Jacchia (1977) profile are shown in Figure 10.

It was also found that different exospheric temperatures, T_2 or T_∞, require different values of Q_o and h, as would be expected. The relationship between Q_o and T_∞ is shown in Figure 11. The total flux, Q_oh, ranged from 0.24 erg cm^{-2} sec^{-1} for T_∞ = 500 K to 1.38 erg cm^{-2} sec^{-1} for T_∞ = 2000 K, in good agreement with the values given by Harris and Priester (1963).

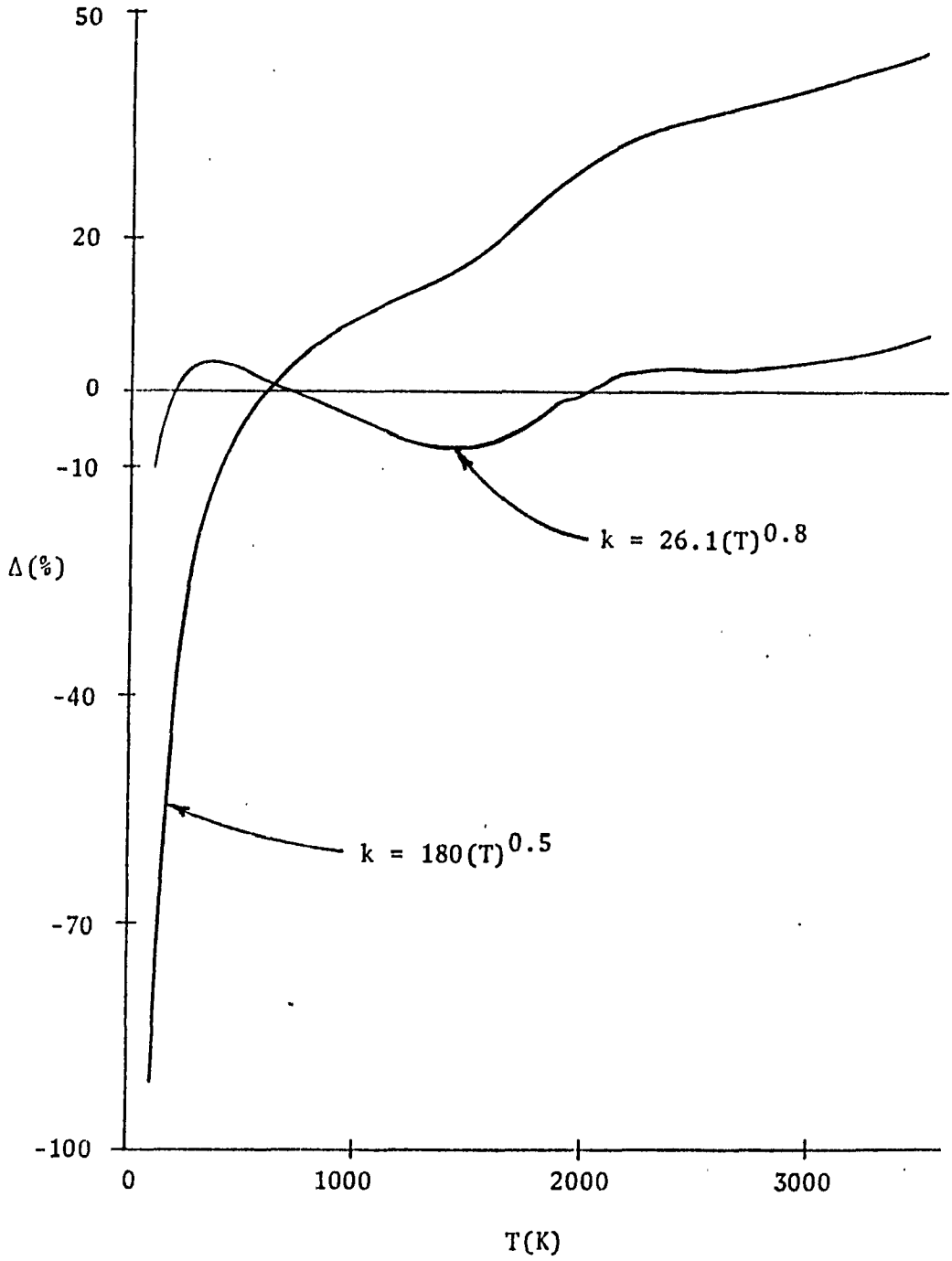

Figure 9. Percent difference between two theories of thermal conductivity and the experimental data. $\Delta = 100(k(\text{data}) - k(\text{theory}))/k(\text{data})$.

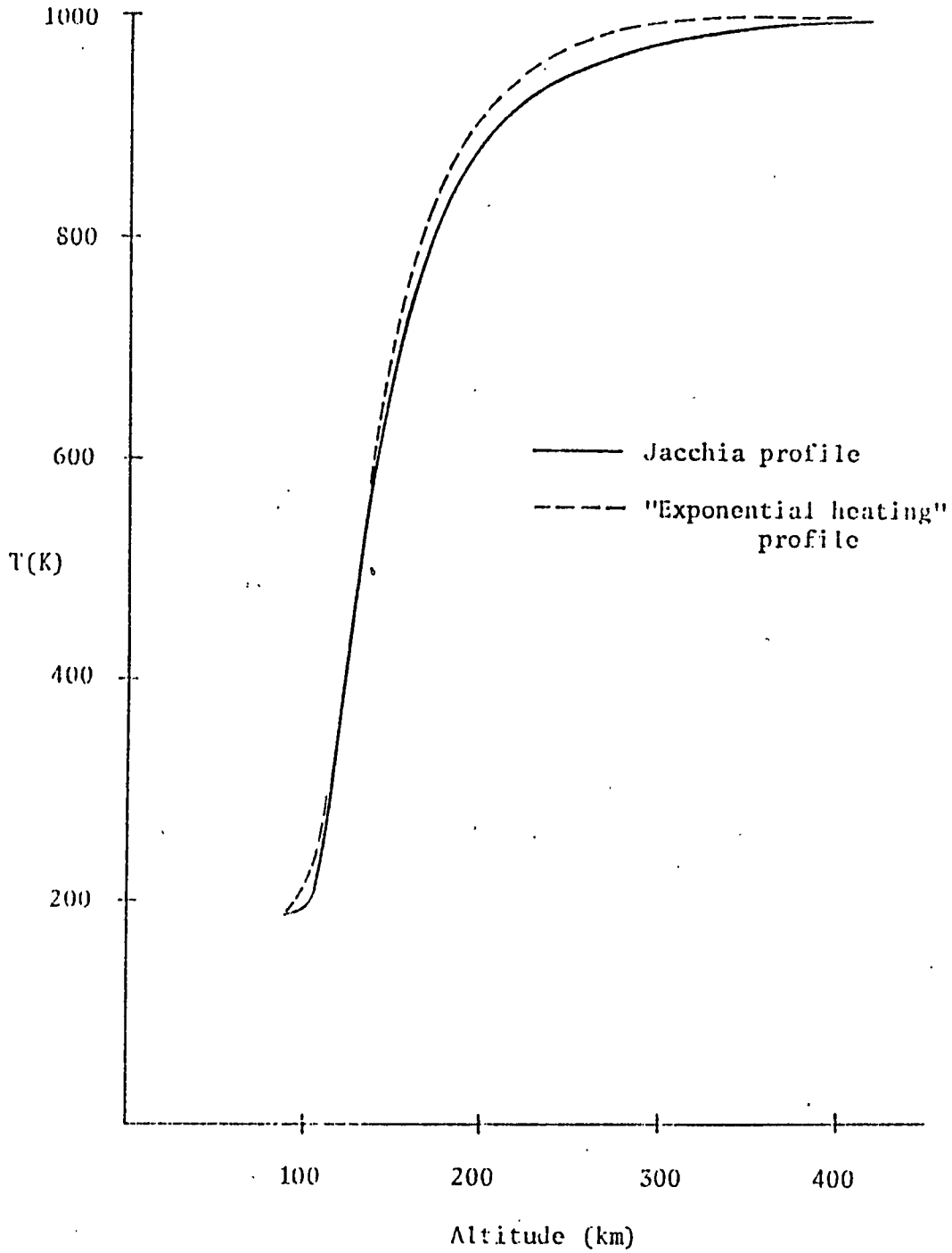

Figure 10. Temperature profiles from Jacchia (1977) and "exponential heating" theory.

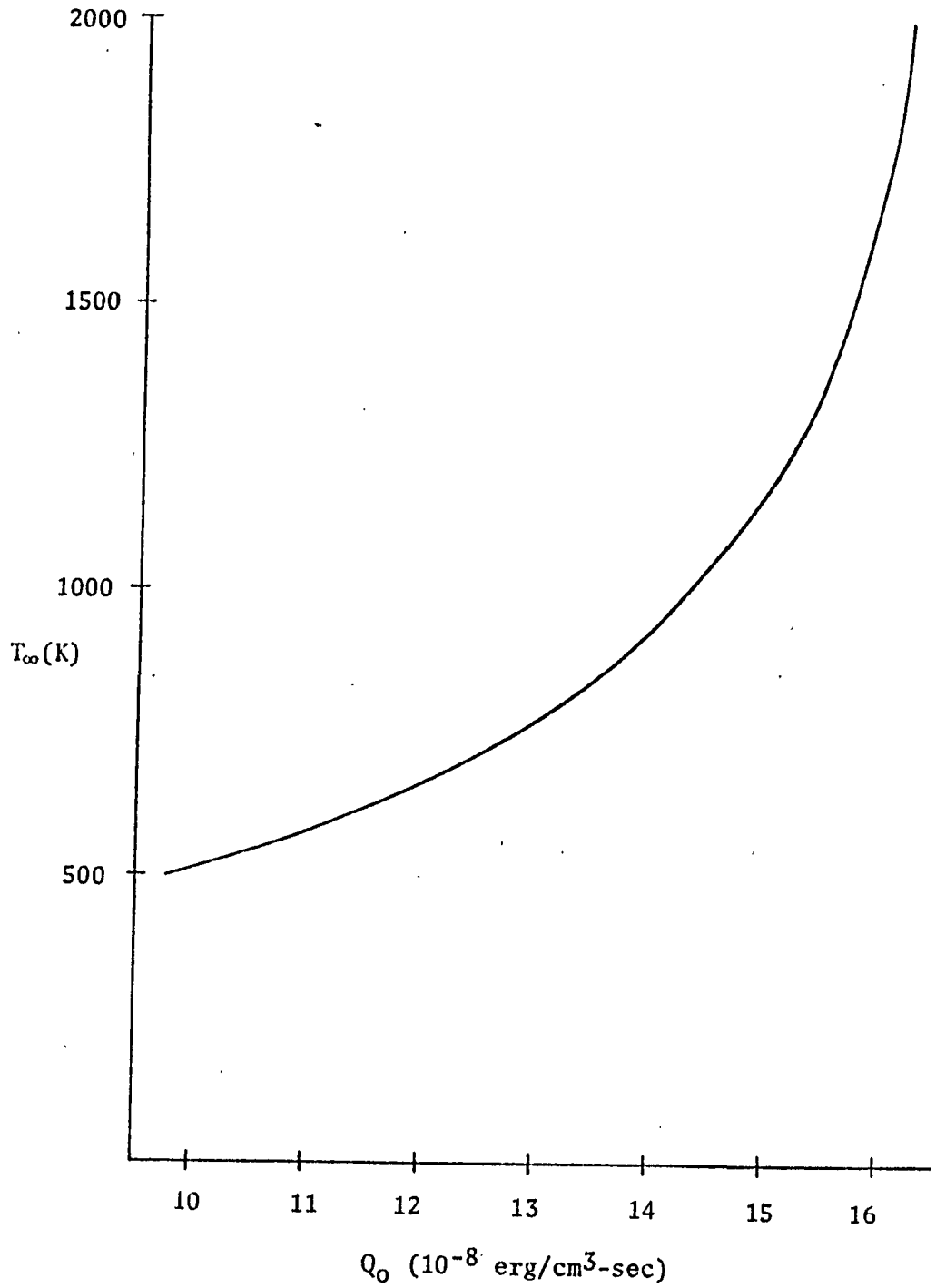

Figure 11. Relationship between exospheric temperature and reference level heating rate.

CONCLUSIONS AND RECOMMENDATIONS

The objectives concerning the computer models were satisfactorily achieved. Objectives 4 and 5 were met to a good degree. Limitations of time and availability of data were crucial.

As a result of this study, the following recommendations are put forth:

1) continue modification of the J703X program to remove the restrictions in the new versions as discussed earlier (for example, ask for input of latitude and longitude ranges, allow for flexibility in output of density values by using E specification rather than F specification in the FORMAT statements, change order of calculations to allow more than one altitude case),

2) obtain as much good density data as possible (with longitude, latitude, and altitude) to complete the study of geomagnetic index averaging,

3) follow up on the question of the temperature dependence of thermal conductivity of gases and how it enters into the Harris and Priester theory, which is a more realistic model than the one used here and by Cole.

REFERENCES

Cole, K. D., "Joule heating of the upper atmosphere," Austr. J. Phys. 15, 223 - 235 (1962).

Davis, T. M., "Modifications of the Jacchia computer models at Marshall Space Flight Center," J. Geophys. Res. (1984), submitted for publication.

DeVries, L. L., "Analysis and interpretation of density data from the low-g accelerometer calibration system (LOGACS)," invited paper at XIV COSPAR meeting (1971).

Harris, I., and W. Priester, "Heating of the upper atmosphere," in Space Research III edited by W. Priester, John Wiley and Sons, Inc., New York (1963), pp. 53 - 75.

Iribarne, J. V., and H. R. Cho, Atmospheric Physics, D. Reidel Publishing Co., Boston (1980), pp. 56 - 58.

Jacchia, L. G., "New static models of the thermosphere and exosphere with empirical temperature profiles," Special Report 313, Smithson. Astrophys. Observ., Cambridge, Mass. (1970).

Jacchia, L. G., "Revised static models of the thermosphere and exosphere with empirical temperature profiles," Special Report 332, Smithson. Astrophys. Observ., Cambridge, Mass. (1971).

Jacchia, L. G., "Thermospheric temperature, density, and composition: New models," Special Report 375, Smithson. Astrophys. Observ., Cambridge, Mass. (1977).

Johnson. D. L., "Sensitivity/comparison study between the Jacchia 1970, 1971, and 1977 upper atmospheric density models," NASA Technical Memorandum 82534 (1983).

Loeb, L. B., The Kinetic Theory of Gases, Dover Publications, Inc., New York (1961), pp. 215 - 252.

Nautical Almanac Office, The Astronomical Almanac, U. S. Government Printing Office, Washington (1983).

Slowey, J. W., "Dynamic model of the earth's upper atmosphere," Final report for contract No. NAS8-34947, Smithson. Astrophys. Observ. (1984).

Weast, R. C. (editor), CRC Handbook of Chemistry and Physics, CRC Press, Inc., Boca Raton, Florida (1982), p. E-3.

D8

1984

NASA/ASEE SUMMER FACULTY RESEARCH FELLOWSHIP PROGRAM

MARSHALL SPACE FLIGHT CENTER

THE UNIVERSITY OF ALABAMA

SINGULAR ASYMPTOTIC EXPANSIONS IN NONLINEAR ROTORDYNAMICS

Prepared by:	William B. Day, Ph.D.
Academic Rank:	Associate Professor
University and Department:	Auburn University
	Department of Computer Science
NASA/MSFC	
Laboratory:	Systems Dynamics
Division:	Control Systems
Branch:	Servomechanisms & Systems Stability
NASA Counterpart:	Luke A. Schutzenhofer, Ph.D.
Date:	August 10, 1984
Contract No.:	NASA-NGT-01-002-099
	(The University of Alabama)

SINGULAR ASYMPTOTIC EXPANSIONS IN NONLINEAR ROTORDYNAMICS

BY

WILLIAM B. DAY, Ph.D.
ASSOCIATE PROFESSOR OF COMPUTER SCIENCE
AUBURN UNIVERISTY, ALABAMA

ABSTRACT

During hot firing ground testing of the Space Shuttle's Main Engine, vibrations of the liquid oxygen pump have occurred at frequencies which cannot be explained by the linear Jeffcott model of the rotor. The model becomes nonlinear after accounting for deadband, side forces, and rubbing. Two phenomena present in the numerical solutions of the differential equations are unexpected periodic orbits of the rotor and "tracking" of the nonlinear frequency. A multiple-scale asymptotic expansion of the differential equations is used to give an analytic explanation of these characteristics.

LIST OF FIGURES

1. Introduction:

Excessive vibrations of the liquid oxygen turbopump in the Space Shuttle's Main Engine have been recorded during hot firing ground testing. Examination of the power spectral density (PSD) plot reveal frequencies which cannot be explained using the linear rotordynamics model of Jeffcott [5]. Consequently, numerous investigations have been undertaken to study such rotors and to provide descriptions of the solution of the two, coupled, second-order differential equations which describe the motion of the rotor's center of mass. Following the early work in rotordynamics by Yomamoto [7], one introduces a nonlinearity to the Jeffcott equations by including the effect of bearing clearance or deadband. In the pump this deadband refers to the load carriers (ball bearings) and physically describes the clearance between the outer race of the bearing and the support housing. Both empirical results by Childs [1,2] and Gupta et al. [4] and numerical solutions using the fourth order Runge-Kutta algorithm by Control Dynamics Company [3] have been helpful in understanding the rotor's motion for the nonlinear problem. This report extends the earlier work by using analytic expressions obtained from singular asymptotic expansions (methods of multiple scales) to quantize the solution.

Section 2 presents the general analysis of a Jeffcott rotor with deadband and sinusoidal forcing. This discussion includes a derivation of the characteristic, nonlinear frequency which is responsible for "tracking", a shift in the subsynchronous frequency as a function of the external force. Then the method of multiple scales provides justification for inclusion or exclusion of the subsynchronous term in the solution expression.

Section 3 displays three examples. The first example illustrates the major theoretical devices of section 2. Example 2 uses data from CDC report [3] where the subsynchronous frequency begins at one-half the forcing frequency. It reiterates the mathematical development of section 2. The last example uses the data of example 1 to produce a frequency-response plot for the nonlinear problem. How this plot differs from the corresponding linear case and what one may expect in the general case are the major points

made in this example. All the examples use the method of Runge-Kutta to obtain numerical solutions.

Section 4 concludes the report with brief descriptions of extension and related problems. These include multiple external forces (e.g. sideforce), rubbing, asymmetric stiffness, and stability analysis.

2. General Theory:

The linear Jeffcott equations which describe the motion of a rotor in the inertial, Cartesian coordinate system are these:

$$(1.)\quad m\ddot{y}=-C_S\dot{y}-K_Sy-Q_Sz+mu\omega^2\cos\omega t$$

$$(2.)\quad m\ddot{z}=-C_S\dot{z}+Q_Sy-K_Sz+mu\omega^2\sin\omega t$$

where

m = mass (kg.)

C_S = seal damping (kg./s.)

K_S = seal stiffness (kg./s.^{2})

Q_S = cross-coupling stiffness of seal (kg./ s.^{2})

u = displacement of the shaft center of mass from the geometric center (m.)

ω = angular velocity of the shaft (rad./s.)

For the model to include bearing forces which hold the rotor in position, one adds the terms

$$-K_B(y-y\delta/\sqrt{y^2+z^2})+\mu K_B(z-z\delta/\sqrt{y^2+z^2})$$

and

$$-\mu K_B(y-y\delta/\sqrt{y^2+z^2})-K_B(z-z\delta/\sqrt{y^2+z^2}),$$

respectively, to the right-hand sides of equations (1.)

and (2.). Here K_B (kg./s.^{2}) is the bearing stiffness, δ (m.) is the clearance or deadband between the housing and the bearing, and μ (nondimensional) is the coefficient of friction between the housing and the bearing. These bearing forces occur only when $\sqrt{y^2+z^2}>\delta$; otherwise, they are zero. Equations (1.)-(2.) then become

(3.) $\ddot{y}+(C_S/m)\dot{y}+(1/m)[K_S+K_B(1-\delta/r)]y+(1/m)[Q_S-\mu K_B(1-\delta/r)]z$

$=u\omega^2\cos\omega t$

(4.) $\ddot{z}+(C_S/m)\dot{z}-(1/m)[Q_S-\mu K_B(1-\delta/r)]y+(1/m)[K_S+K_B(1-\delta/r)]z$

$=u\omega^2\sin\omega t$

when $r=\sqrt{y^2+z^2}>\delta$; otherwise, $K_B=0$.

Equations (3.)-(4.) can be put in nondimensional form using a displacement g and a frequency σ. Thus, using $Y=y/g$, $Z=z/g$, and $\tau=\sigma t$, the dimensionless equations are these:

(5.) $Y''+CY'+[A+k(1-\Delta/R]Y+[B-\mu k(1-\Delta/R)]Z=E\phi^2\cos\phi t$

(6.) $Z''+CZ'-[B-\mu k(1-\Delta/R)]Y+[A+k(1-\Delta/R)]Z=E\phi^2\sin\phi\tau$

where prime denotes differentiation with respect to τ and $C=C_S/m/\sigma$, $A=K_S/m/\sigma^2$, $k=K_B/m/\sigma^2$, $B=Q_S/m/\sigma^2$, $\Delta=\delta/g$, $R=r/g$, $E=u/g$, and $\phi=\omega/\sigma$.

Equations (5.)-(6.) can be reduced to the following single equation by defining $W=Y+iZ$:

(7.) $W''+CW'+\{A+k(1-\Delta/|W|)+i[-B+\mu k(1-\Delta/|W|)]\}W=E\phi^2\exp(i\phi\tau)$

Furthermore, the polar form of equations (5.)-(6.) is

(8.) $R''+CR'+[A+k(1-\Delta/R)-(\Theta')^2]R=E\phi^2\cos(\phi\tau-\Theta)$

(9.) $R\Theta''+(2R'+CR)\Theta'=R[B-\mu k(1-\Delta/R)]+E\phi^2\sin(\phi\tau-\Theta)$

where $R=(Y^2+Z^2)^{1/2}$ and $\Theta=\text{Arctan}\ (Z/Y)$. Since μ is nondimensional and typically small, one may regard it as zero without affecting the qualitative results.

Consider the homogeneous (E=0) equation corresponding to equation (7.). If this equation were also linear ($\Delta=0$),

then exponentially growing or decaying solutions would result for a given set of system parameters. In the special case that $(B/C)^2=A+k$, a sinusoidal solution is obtained with frequency $\beta=B/C$. To see this, consider the characteristic equation for $W=\exp(m\tau)$:

$$m^2+Cm+[A+k-iB]=0$$

$$m=-C/2\pm\{C^2/4-A-k+iB\}^{1/2}$$

$$m=-C-iB/C,\ iB/C.$$

In the nonlinear, homogeneous problem, k is replaced by $k(1-\Delta/R)$; hence, if R is a constant, then there is a wide spectrum for which $(B/C)^2=A+k(1-\Delta/R)$; i.e., if

(10.) $$A<(B/C)^2\leq A+k,$$

then there is a constant value of R (with $R>\Delta$) for which $(B/C)^2=A+k(1-\Delta/R)$. This value of R is denoted by a and the corresponding frequency by $\beta_0=B/C$. This frequency is labeled the characteristic, nonlinear frequency. Thus, whenever inequality (10.) is satisfied, equations (5.)-(6.) with E=0 have steady-state solutions $Y=a\cos(\beta_0\tau)$ and $Z=a\sin(\beta_0\tau)$.

The same results can be found from the polar equations (8.)-(9.) by assuming R and Θ' are constants. Then with E=0 those equations become

$$[A+k(1-\Delta/R)-(\Theta')^2]R=0, \qquad C\Theta'=B.$$

Thus, $\beta_0=\Theta'=B/C$ and $a=R=k\Delta/(A+k-\beta_0^2)$.

Notice that $\beta_0=B/C\leq A+k=\{(K_S+K_B)/m\}^{1/2}/\sigma=\omega_0$, the dimensionless natural frequency of the linear system. Thus, in considering the general nonhomogeneous problem, it is necessary to be aware of these three dimensionless frequencies:

β_0 - the characteristic, nonlinear frequency,

ω_0 - the natural frequency,

ϕ - the driving frequency.

Either β_0 or ω_0 is an appropriate choice for σ, the non-dimensionalizing frequency. Correspondingly, one would select either a (with β_0) or u (with ω_0) as the base displacement g.

One final rearrangement of equation (9.) is made here to emphasis the characteristic, nonlinear frequency:

(11.) $W''+CW'+\kappa W=\varepsilon f(W)+E\phi^2\exp(i\phi\tau)$

where $\kappa=A+k(1-\Delta/a)+i[-B+\mu k(1-\Delta/a)]$ and

$f(W)=k\Delta(1+i\mu)/\varepsilon[1/|W|-1/a]W$.

Asymptotic expansions may now be introduced to solve equation (11.). The singular method of multiple scales, as described by Nayfeh [6], is appropriate for this problem. The method of averaging gives similar results.

Instead of one time scale τ, assume the problem depends on many time scales:

$$T_0=\tau,\ T_1=\varepsilon\tau,\ T_2=\varepsilon^2\tau,\ldots$$

Henceforth, only T_0 and T_1 are used. Let $W(\tau)=W(T_0,T_1)=W_0(T_0,T_1)+\varepsilon W_1(T_0,T_1)+\ldots$ Equation (11.) becomes a partial differential equation since

$$d/d\tau=(\partial/\partial T_0)(dT_0/d\tau)+(\partial/\partial T_1)(dT_1/d\tau)=D_0+\varepsilon D_1$$

and $(d^2/d\tau^2)=(D_0+\varepsilon D_1)^2$.

Thus, one finds

(12.) $(D_0+\varepsilon D_1)^2(W_0+\varepsilon W_1+\ldots)+C(D_0+\varepsilon D_1)(W_0+\varepsilon W_1+\ldots)$

$+\kappa(W_0+\varepsilon W_1+\ldots)=\varepsilon f(W_0+\varepsilon W_1+\ldots)+E\phi^2\exp(i\phi T_0)$.

Equating like powers of ε yields

(13.) $\varepsilon^0: D_0^2W_0+CD_0W_0+\kappa W_0=E\phi^2\exp(i\phi T_0)$.

This is a linear problem with this steady-state solution

$$W_0=M\exp(i\beta_0T_0)+N\exp(i\phi T_0)$$

where $N=E\phi^2/(-\phi^2+iC\phi+\kappa)$ and $M=M(T_1)$. To determine M one must examine the ε-order problem and chose M to eliminate secular terms; see Nayfeh [6]:

$$\varepsilon^1: \; D_0^2W_1+CW_1+\kappa W_1=-2D_0D_1W_0-CD_1W_0+f(W_0).$$

with $L=k\Delta/\varepsilon$, the right-hand side of the last equation becomes

$$-2i\beta_0M'\exp(i\beta_0T_0)-CM'\exp(i\beta_0T_0)$$

$$+L(1/|W_0|-1/a)[M\exp(i\beta_0T_0)+N\exp(i\phi T_0)]$$

where $|W_0|=\{|M|^2+|N|^2+\bar{M}N\exp[i(\phi-\beta_0)T_0]+M\bar{N}\exp[i(\beta_0-\phi)T_0]\}^{1/2}$

To avoid secular terms one requires that the collective coefficient of $\exp(i\beta_0T_0)$ be zero. Although an analytic solution of the differential equation for $M(T_1)$ has not been found, one can qualitatively assess M based on a similar problem (van der Pol's equation) and specific numerical results (presented in the next section).

Since $M(T_1)$ is complex, it may be written as $M(T_1)=\rho(T_1)\exp[i\hat{\beta}(T_1)]$. Thus,

$W_0=\rho(T_1)\exp[i\beta_0T_0+i\hat{\beta}(T_1)]+N\exp(i\phi T_0)$ or, assuming $\hat{\beta}(T_1)$ is analytic near $t=0$, $W_0=\rho(T_1)\exp[i(\beta_0+\varepsilon\beta_1)\tau+\ldots]+N\exp(i\phi\tau)$. Thus the fundamental frequency of the nonlinear problem is not β_0 but $\beta=\beta_0+\varepsilon\beta_1+\ldots$; however, β must reduce to β_0 when $E\phi^2=0$. This frequency shift can account for the phenomenon of "tracking" that has been observed experimentally [2]. Similarly, the frequency $\gamma=\phi-\beta_0$ that appears in the expression for $|W_0|$ should be considered as $\gamma=\phi-\beta$. Then $1/|W_0|$ shows all frequencies $n\gamma$ and $W_0/|W_0|$ shows all frequencies $n\gamma\pm\beta$, for $n=0,1,\ldots$ This suggest that M has a complex Fourier series of the form

$$\sum_{n=-\infty}^{\infty} s_n \exp(in\gamma T_1).$$

Another factor of M must also be included since numerical examples show that $M\equiv 0$ if $E\phi^2$ is greater than some fixed value. This is similar to the behavior of the van der Pol oscillator; see [6]. Thus, one may speculate that M has a

factor of the form $F=1/[1+\exp(-\eta T_1)]$ where $\eta=\eta(E\phi^2)$. This would imply that $F\to 1$ as $\tau\to\infty$ when $\eta\geq 0$ and $F\to 0$ as $\tau\to\infty$ when $\eta<0$. Thus, M looks like

$$1/[1+\exp(-\eta T_1)] \sum_{n=-\infty}^{\infty} s_n \exp(in\gamma T_1).$$

PSD plots of R show frequencies of $n\gamma$ only while plots of Y show frequencies of ϕ and $n\gamma\pm\beta$.

3. Examples:

Example 1. In this example the system constants used are these: $\mu=0$, $m=1$ lb.-s.^{2}/in., $C_s=240$ lb.-s./in., $K_s=0.$, $K_b=1{,}305{,}000$ lb./in., $Q_s=200{,}000$ lb./in., $\delta=.0000285$ in., and $\omega=500$ Hertz $=1000\pi$ rad./s. Thus, $\beta_0=833.33$ rad./s. and $a=.000060915$ in. The system is made nondimensional using a for the g-displacement and β for the σ-frequency. With these choices, the constants of this equation

$$W''+CW'+[k(1-\Delta/|W|)-iB]W=E\phi^2\exp(i\phi\tau)$$

have these values: $C=.288$, $k=1.8792$, $\Delta=.467865$, $B=.288$, and $\phi=6\pi/5$.

Figures 1 and 2 show changes in the solution Y vs. Z as E assumes the values $100n/(1000\pi)^2a$ for $n=0,1,\ldots,7$. The graphs are plotted for $.2<t\leq .5$s. The initial circle (for E=0) opens into an annular region, which becomes larger and thicker as E increases until a (transition) value of E occurs and the coefficient of $\exp(i\beta\tau)$ becomes zero. Thus, $W=N\exp(i\phi\tau)$, a circle of radius $|N|$. As E increases beyond this transition value, the solution remains a circle (figure 2.d) with radius $|N|=|E\phi^2/(-\phi^2+iC\phi+k(1-\Delta/|N|)-iB)|$.

The characteristic, nonlinear frequency β_0 is the angular frequency of the circle when E=0, but this frequency increases as E increases. This tracking phenomenon is displayed in the PSD plots of figures 3 and 4 using the dimensional frequency β. In these figures only the 120-180 Hertz range is shown. At $E=7/10{,}000\pi^2a$, there is no frequency in this range; instead, the circle is tranversed at the forcing frequency, ω.

Figure 5, a typical full PSD plot, is the case $E=4/10{,}000\pi^2 a$. As shown earlier, one expects frequencies of ω and β to appear, as well as harmonics of $n\gamma \pm \beta$ where $\gamma=\omega-\beta$ and $n=1, 2, \ldots$ Thus, with $\beta=150$ Hertz, and $\omega=500$Hertz, one predicts that the PSD plot will exhibit peaks at 150, 200, 500, 550, 850, 900, ... Hertz.

Example 2. In this example, the system constants from CDC[3] are these: $\mu=0$, $m=.20422$ lb.-s.^{2}/in., $C_s=200$ lb.-s./in., $K_s=200{,}000$ lb./in., $K_b=1{,}000{,}000$ lb./in., $\omega=500$ Hertz, $Q_s=C_s\omega/2$ lb./in., and $\delta=.0005$ in. Thus, $\beta=250$ Hertz$=500\pi$rad./s. and $a=.0007183$ in. Figure 6 summarizes changes in Y vs. Z as E varies by $250n/(1000\pi)^2 a$, $n=0,1,\ldots,4$. These graphs are plotted for $.45<t\leq.5$s.

In general, if the time interval is sufficiently large, the plots of annular regions will be completely filled (visually if not mathematically). However, when the ratio of β to γ is p/q for small, positive integers p and q, then the curve actually falls on itself as time evolves and some attractive patterns appear. Figure 6.d is a case where $\beta/\gamma=5/4$, and the picture would look essentially the same whether shown for $.45<t\leq.5$ s. (actual) or for $.45<t\leq50$ s. On the other hand, figure 6.c is more typical and would show a black annulus for $.45<t\leq50$ s.

Example 3. This example uses the same data as example 1, but considers variations in the forcing frequency rather than E; i.e., $E=.7$ and ϕ varies.

For each frequency ϕ one expects to see a plot similar to one of those shown for example 1; thus, at each value of ϕ either a circle or an annulus will describe Y vs. Z. Furthermore, based on continuity considerations, the ϕ-axis will be subdivided into intervals within which each curve is a circle or an annulus.

Example 1 showed that as E increased, the magnitude of the forcing function, $E\phi^2$, increased, and all plots were circles above the transition value of E (and hence $E\phi^2$). A more careful analysis shows that this transition value is based not on the magnitude of the forcing function, but rather on the magnitude of the response at the forcing frequency; i.e., on $E\phi^2/(-\phi^2+iC\phi+\kappa)$. In example 1, ϕ is far

from β_0 and the magnitude of the response is roughly E. But in the present example, one must consider values of ϕ near and far from β_0. For those values near β_0, not only the size of E but also the proximity of ϕ to β_0 will make the magnitude of the response large. Therefore, one may predict that a circle at the forcing frequency will be seen for a plot of Y vs. Z when ϕ is near β, except for very small values of E. Elsewhere, one predicts an annular region unless the value of E is large.

Figures 8 and 9 show the response values Y vs. Z for $.4<t\leq.5$ s. as ϕ assumes the values .33, .385, .66, .99, 1.10, 1.32, 1.43, 1.65, 2.2, and 3.3 with E held at .7. Here the σ-frequency for nondimensionalizing is ω_0. These irregularly-spaced frequencies were chosen for these reasons:

a. .33 and .385 bound the value of transition from annulus to circle;

b. .66, .99, 1.10 are values close to β;

c. 1.32 and 1.43 bound the value of transition from circle to annulus;

d. 1.65 has a nice picture;

e. 2.20 and 3.30 are limiting values of interest

At another value of E, the pictures would be similar although the transition values would be different. The extreme case E=0 is a circle of radius a with frequency β_0, regardless of ϕ's value. This was shown in figure 1.a.

If a three-dimensional plot Y vs. Z vs. $\phi(=\omega/\omega_0)$ were made for fixed E, one would find a frequency-response plot similar to the usual plots in linear theory. In particular, the maximum value of $(Y^2+Z^2)^{1/2}$ occurs near $\phi=1$. This is shown in figure 8.d where the scale is four times as large as the scale of the other plots. The height of the response curves corresponds to the radius of the steady-state response when the plot is a circle or the outer radius when the plot is an annulus. In general, these response curves will be discontinuous at the transition points.

4. Conclusions:

In studying the Jeffcott rotor with deadband and sinusoidal forcing, one must consider these three frequencies: (a) the forcing frequency ω; (b) the natural frequency, ω_0, of the associated linear problem (deadband $=\delta=0$); and (c) the characteristic, nonlinear frequency β_0. The frequency ω depends only on the forcing function; ω_0 depends only on the system parameters; β, with its base value β_0, depends on both the forcing function and the system parameters.

For a given system and a nonzero, external, sinusoidal force, the y-z response is either a circle at the forcing frequency or an annulus composed of the (major) frequencies β and ω as well as the (minor) harmonic frequencies $n(\omega-\beta)\pm\beta$, for positive integers n.

Frequency-response curves for a nonlinear problem and its associated ($\delta=0$) problem are similar, both reaching a maximum near $\omega=\omega_0$. Each point of the nonlinear plot, however, may represent either the radius of a circle or the outer radius of an annulus. There are also jump discontinuities in the response curves at points of transition between circles and annuli.

Two related problems, which show similar results in preliminary analyses, are rotors with sideforces and rotors with rubbing. Since the analysis of section 2 remains valid if $E\phi^2$ is replaced by one coefficient G, one may consider sideforces as sinusoidals of the form $G\exp(i\omega\tau)$ where $\omega=0$. A rubbing problem may be reduced to a problem with a sideforce if one examines the response in the rotating rather than inertial coordinate system. Both of these problems will be considered more carefully in future work.

The principal obstacle remaining in this analysis is that of finding an explicit expression for transition values; i.e., expressing the transition point from an annulus to a circle as a function of the system and forcing parameters.

This analysis does not allow two or more external forces (e.g., mass imbalance and sideforces). These problems appear to introduce no new theory, but do increase the computational

complications since one must consider not only forcing frequencies ω_1, ω_2 ,..., but also harmonic frequencies $\omega_1+\omega_2$, $\omega_1-\omega_2$, etc.

The addition of asymmetric stiffness introduces difficulties that promise intriguing analyses based on preliminary Runge-Kutta solutions. Not only do the circle/annulus plots become elliptic and occur with their axes rotated with respect to the y, z axes, but there may be other shapes and more than one transition point to consider. These problems, however, greatly extend the model's mimicry of an observed rotor's behavior.

Finally, one needs to consider stability questions for these nonlinear problems. Superficially, their stabilities are dictated by the corresponding linear problem's stability, but this has not yet been proven.

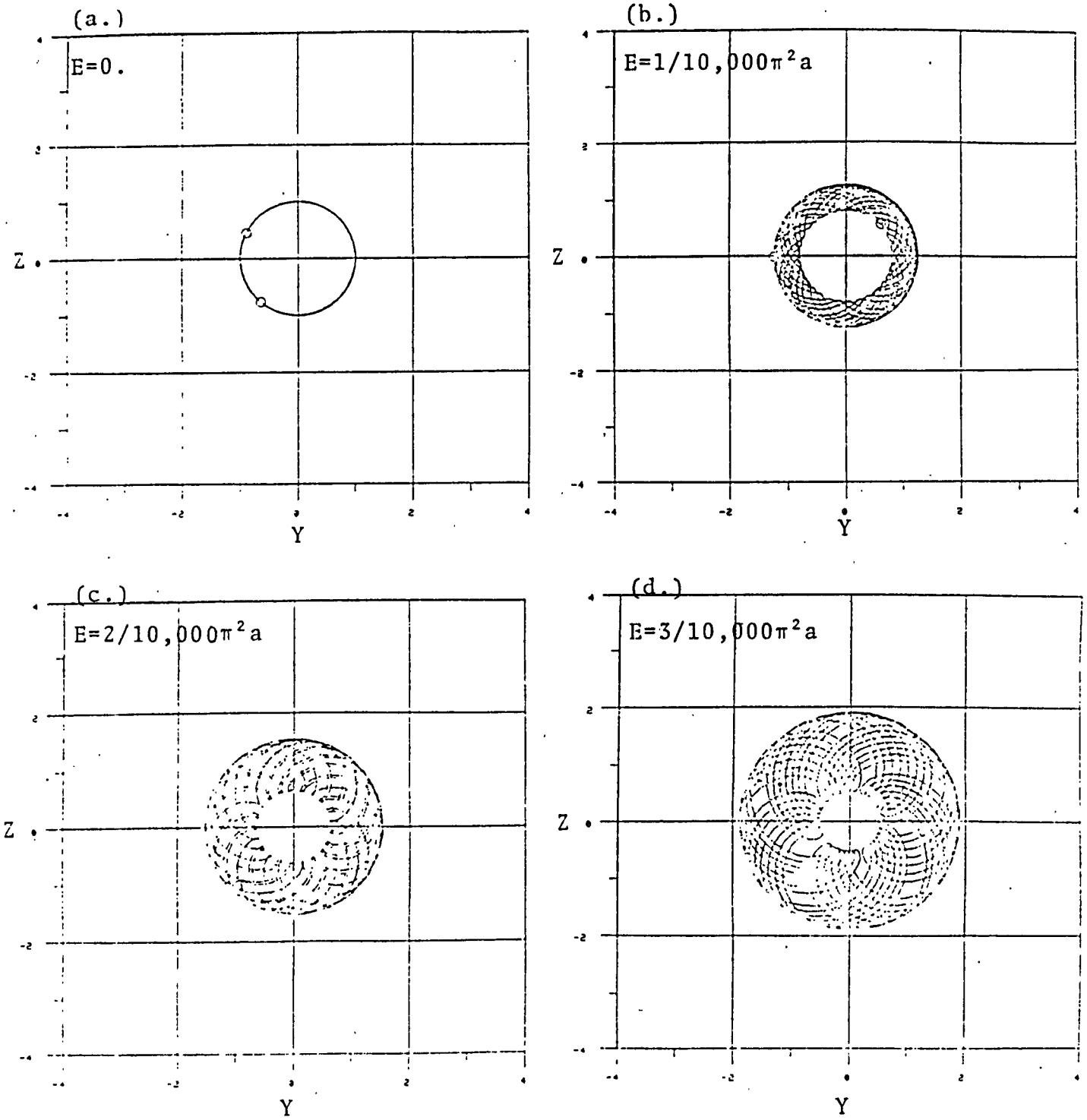

FIGURE 1

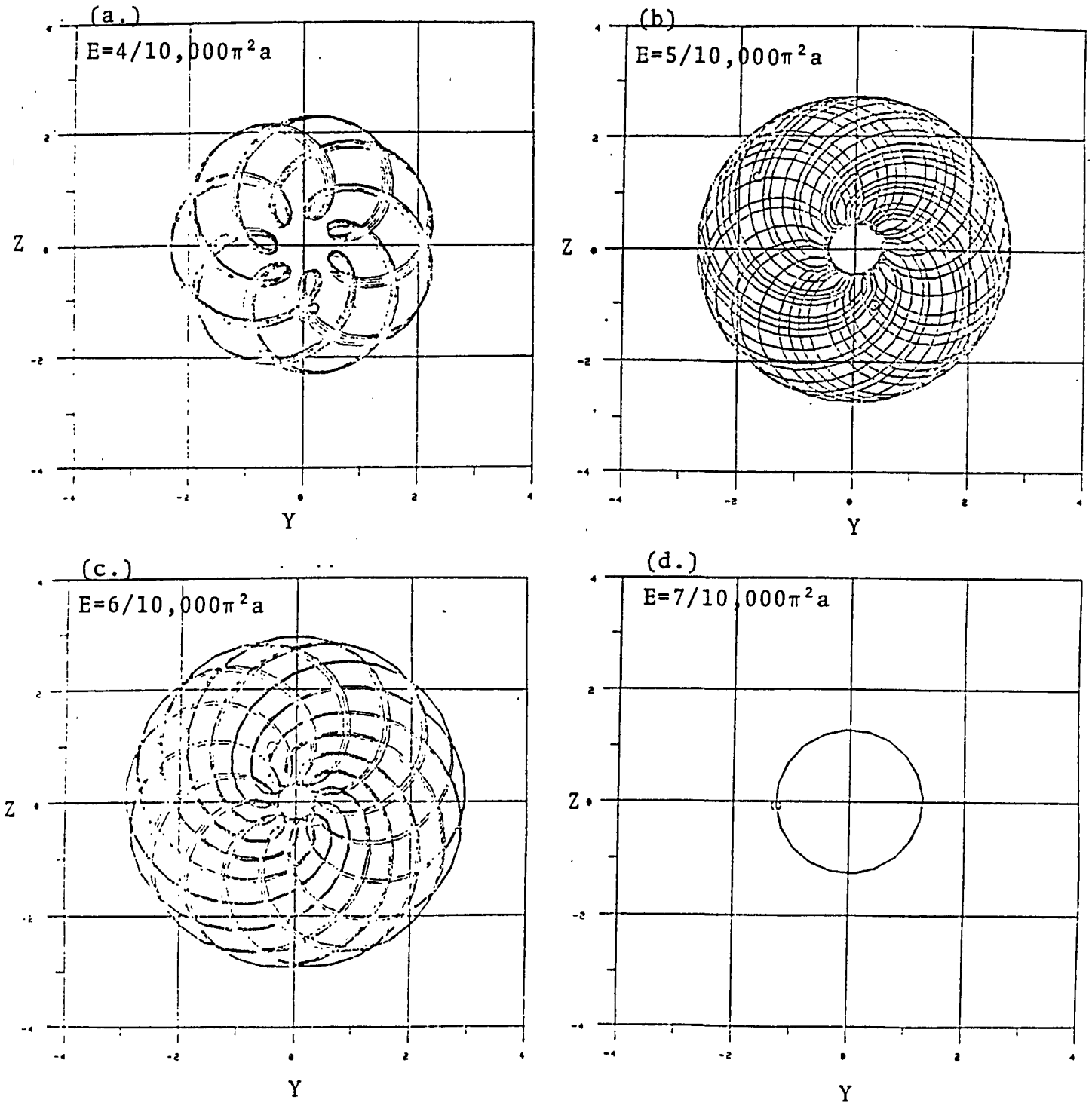

FIGURE 2

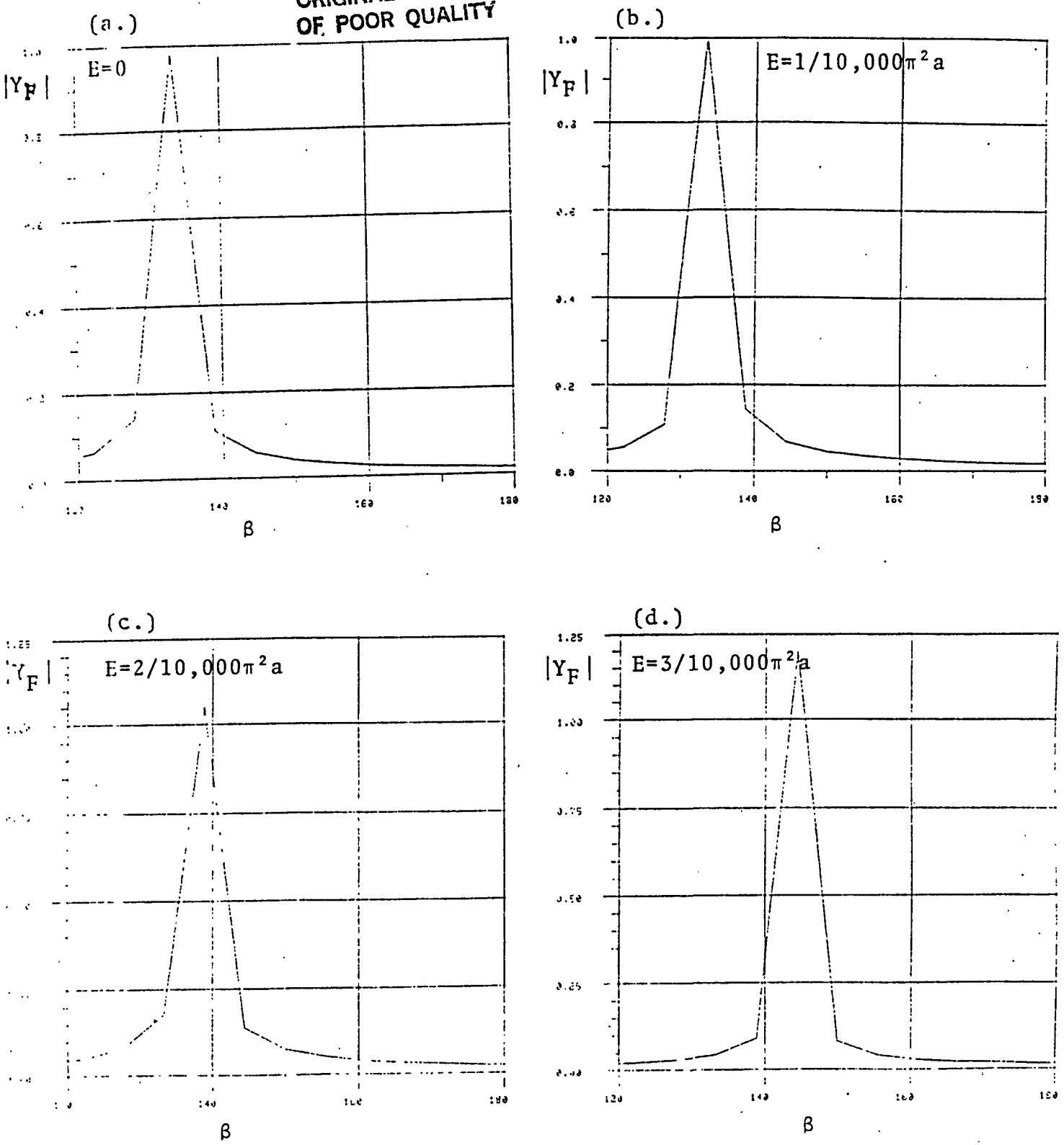

FIGURE 3

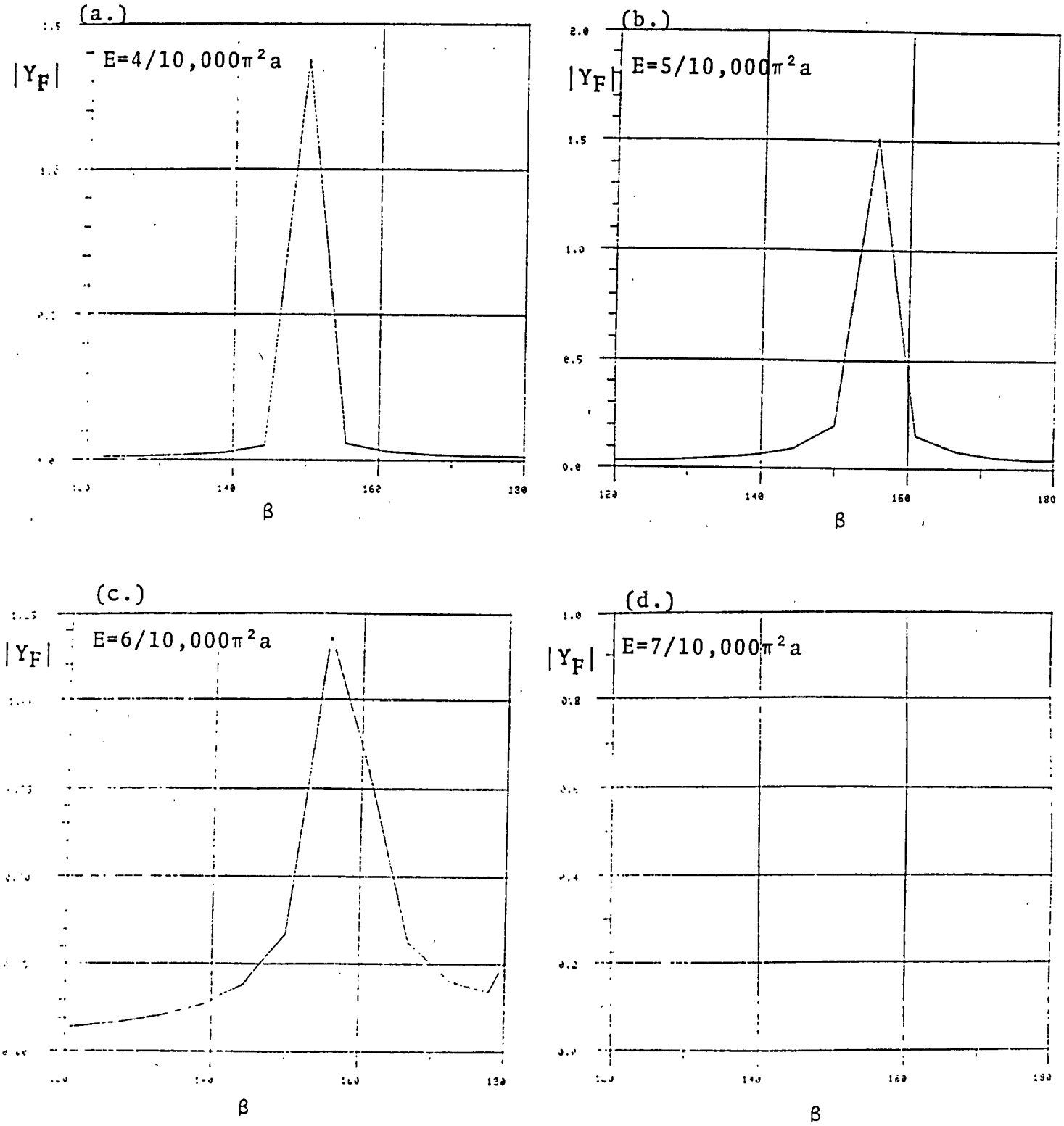

FIGURE 4

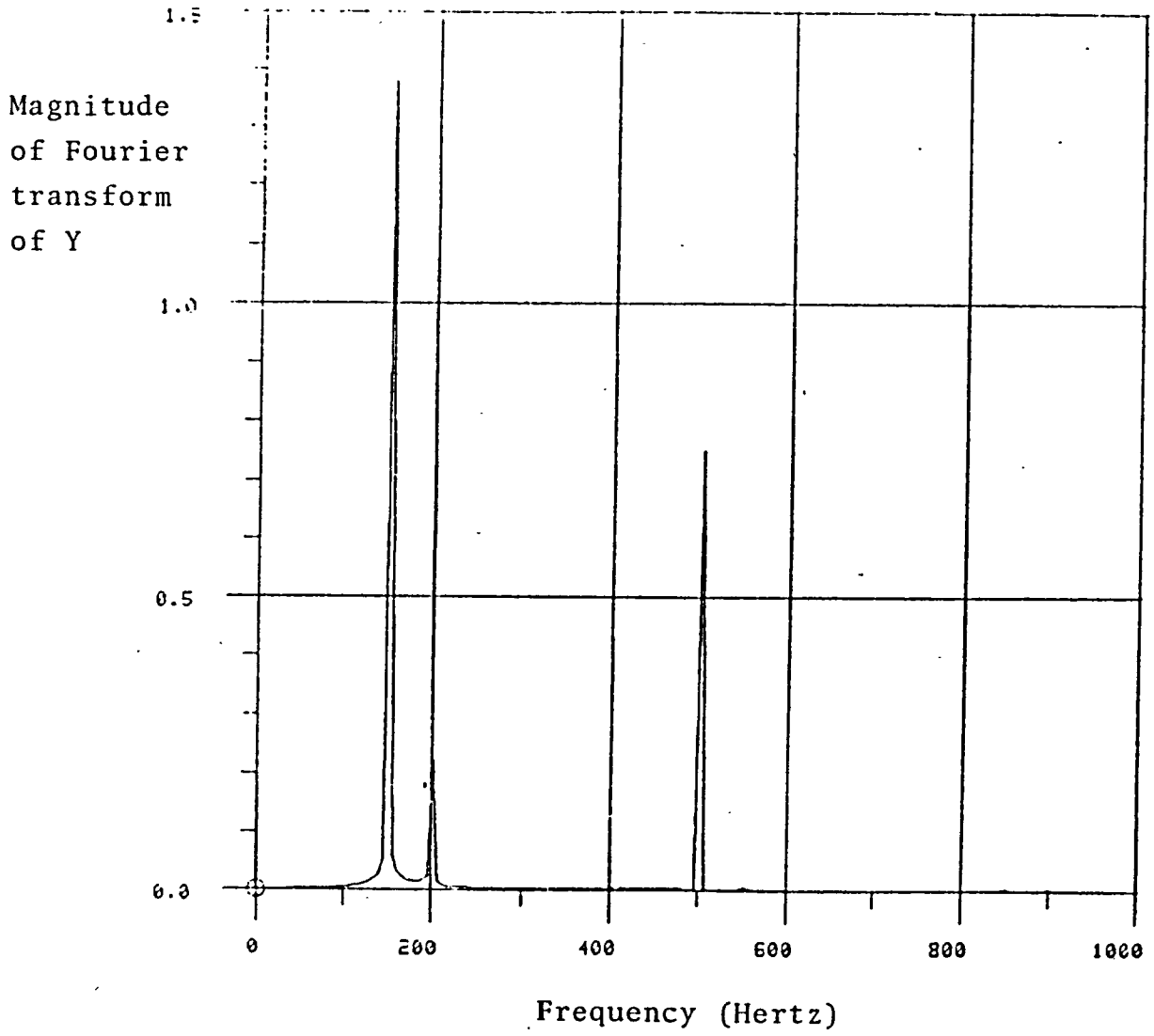

FIGURE 5

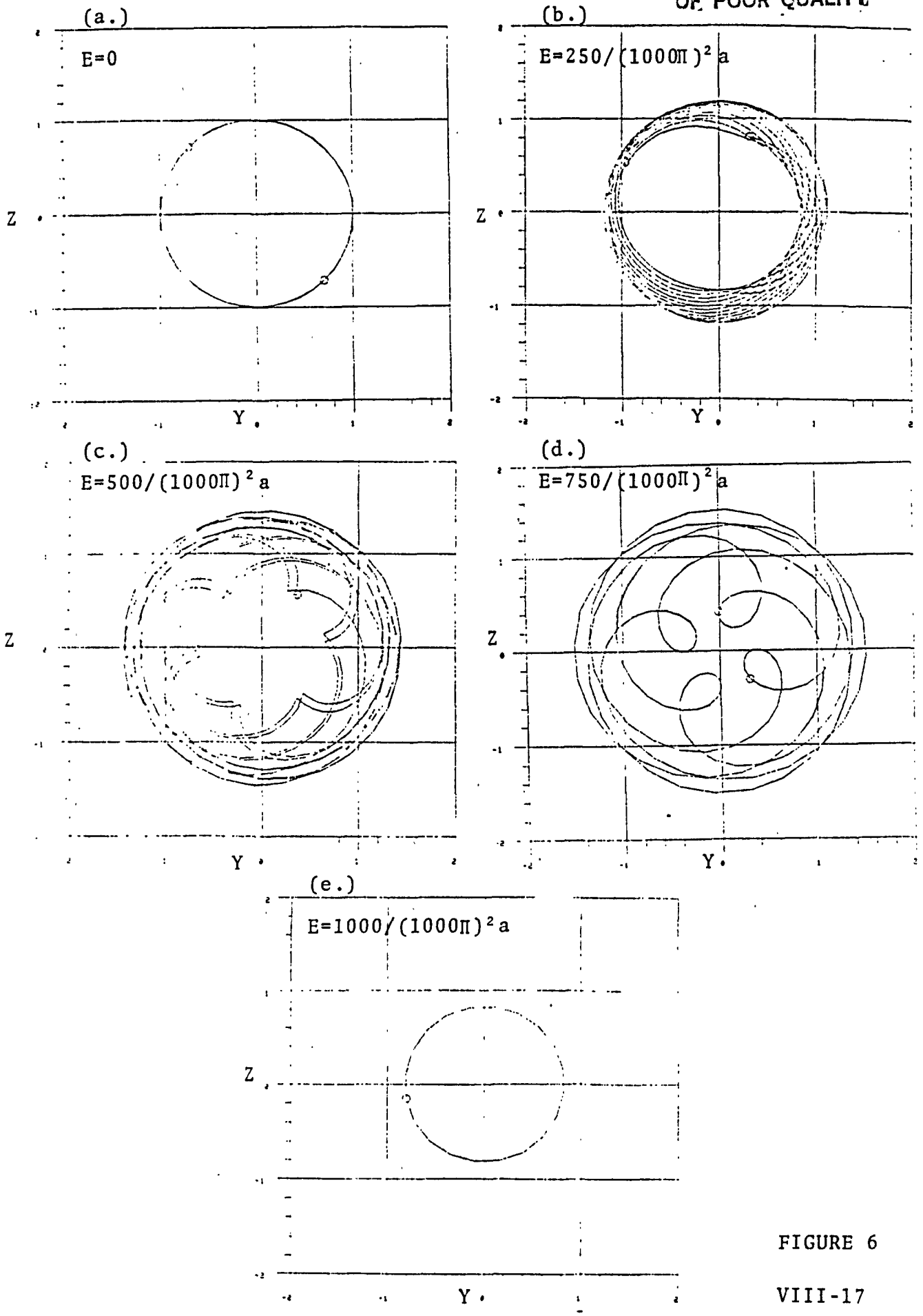

FIGURE 6

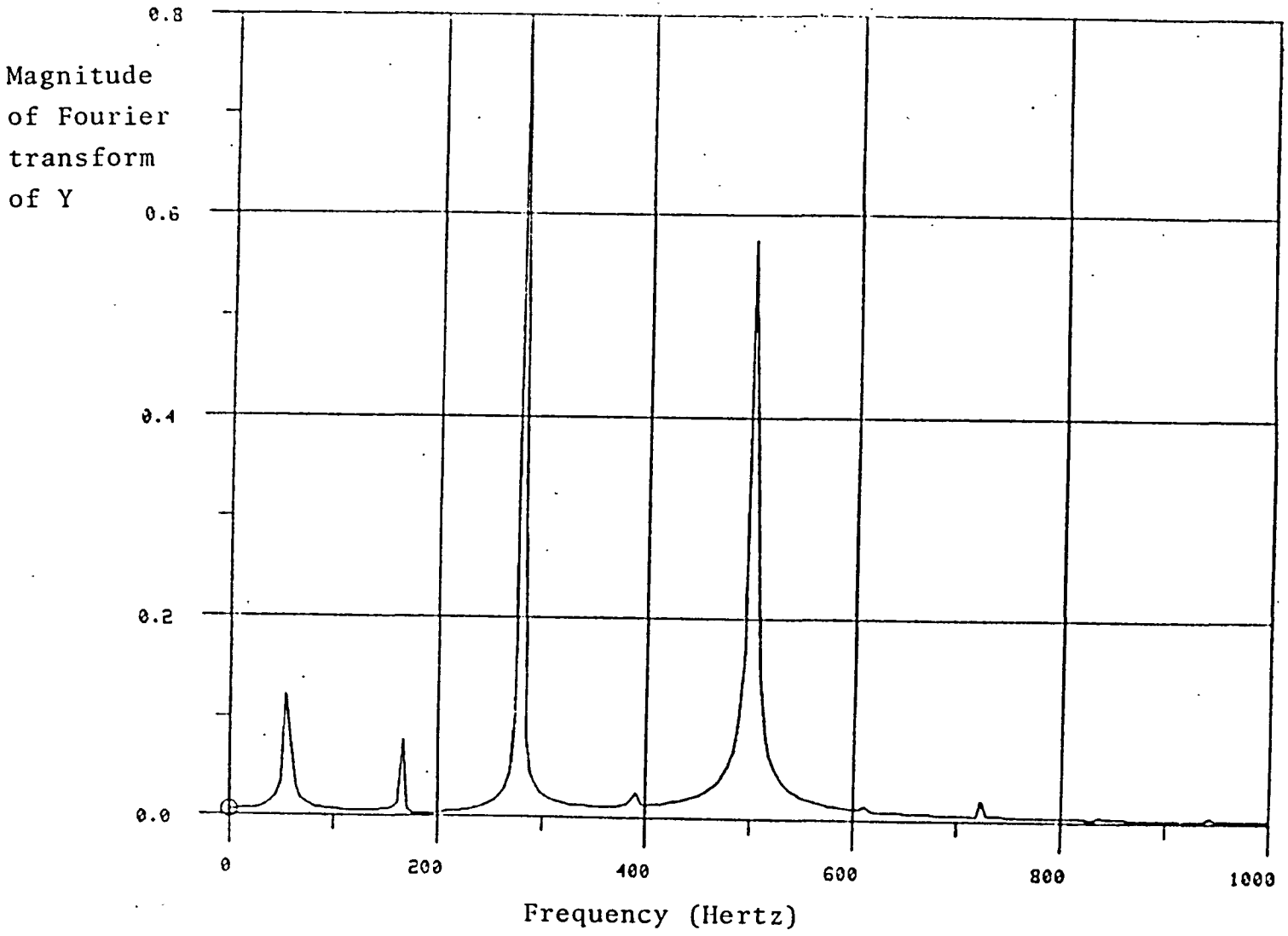
Magnitude of Fourier transform of Y
0.8
0.6
0.4
0.2
0.0
0
200
400
600
800
1000
Frequency (Hertz)

Figure 7

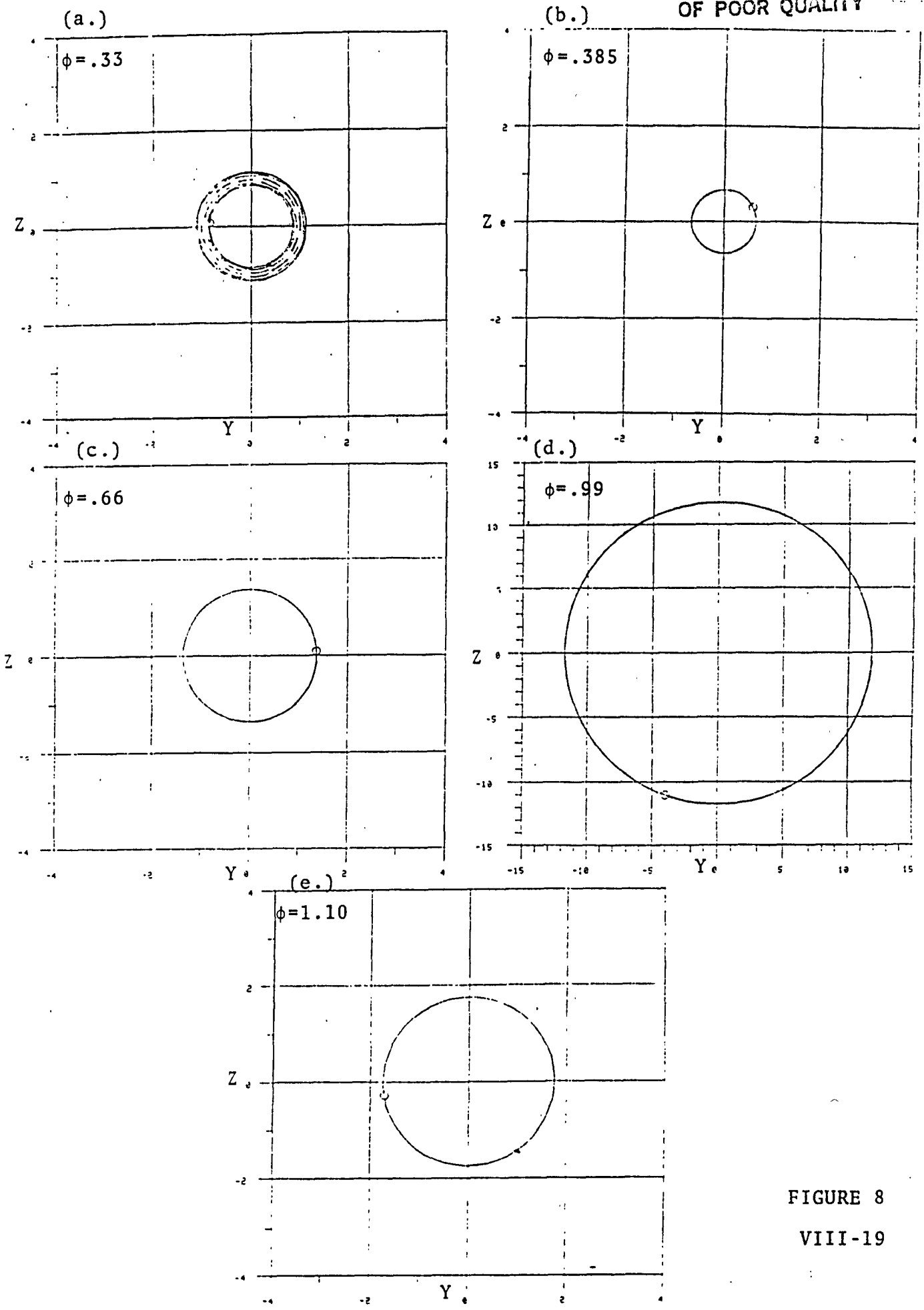

FIGURE 8

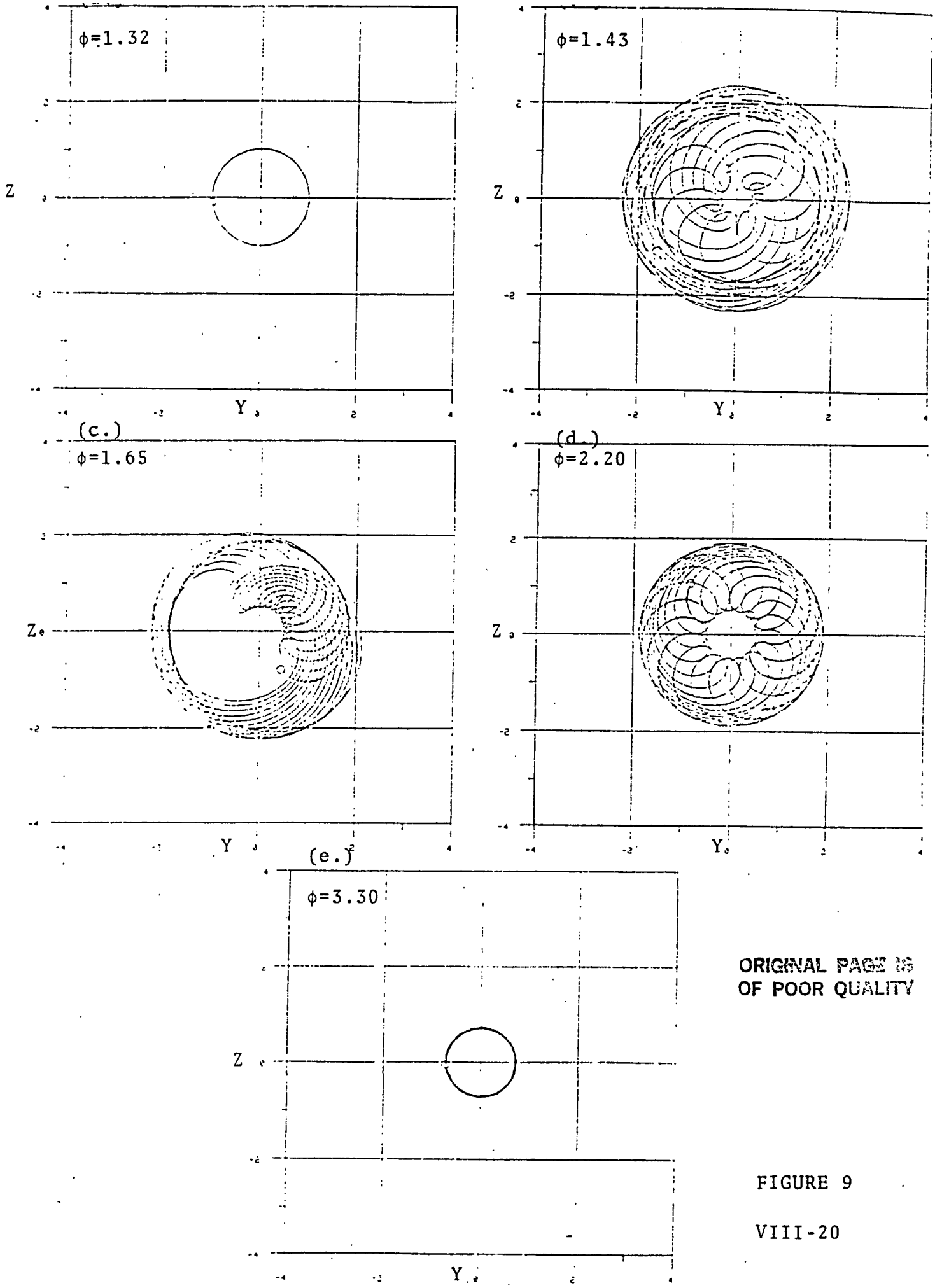

FIGURE 9

5. References:

1. Childs, D. W., "The Space Shuttle Main Engine High-Pressure Fuel Turbopump Rotordynamics Instability Problem", Trans. ASME, Journal of Engineering for Power, Jan. 1978, pp. 48-57.

2. Childs, D. W., "Rotordynamic Characteristics of the HPOTP (High Pressure Oxygen Turbopump) of the SSME (Space Shuttle Main Engine)", NASA MSFC Contract NAS8-34505, Turbomachinery Laboratories Report RD-1-84, 30 January 1984.

3. Control Dynamics Company, "Effects of Bearing Deadbands on Bearing Loads and Rotor Instability", NASA MSFC Contract NAS8-35050, 20 January 1984.

4. Gupta, P. K., Winn, L. W., and Wilcock, D. F., "Vibrational Characteristics of Ball Bearings", Journal of Lubrication Technology, ASME Trans., Vol. 99F, No. 2, 1977, pp. 284-289.

5. Jeffcott, H. H., "The Lateral Vibration of Loaded Shafts in the Neighborhood of a Whirling Speed-The Effect of Want of Balance", Philosophical Magazine, Series 6, Vol. 37, 1919, p. 304.

6. Nayfeh, A. H., Perturbation Methods, J. Wiley & Sons, 1973.

7. Yamamoto, T. T., "On Critical Speeds of a Shaft", Memories of the Faculty of Engineering, Nagoya (Japan) University, Vol. 6, No. 2, 1954.

N85-22219 D9

1984

NASA/ASEE SUMMER FACULTY RESEARCH FELLOWSHIP PROGRAM

MARSHALL SPACE FLIGHT CENTER
THE UNIVERSITY OF ALABAMA

A STUDY OF THE COMPATIBILITY OF AN EXISTING CFD PACKAGE WITH A BROADER CLASS OF MATERIAL CONSTITUTIONS

Prepared By:	Kenneth W. French,Jr. PhD
Academic Rank:	Associate Professor
University and Department:	John Brown University Mechanical Engineering
NASA/ MSFC:	
Laboratory:	Systems Dynamics
Division:	Atmospheric Sciences
Branch:	Fluid Dynamics
NASA Counterpart:	N. C. Costes, PhD
Date:	August 10,1984
Contract NO.:	NASA-NGT-01-002-099 (The University of Alabama)

ACKNOWLEDGEMENTS

My summer experience has been mutually rewarding due especially to the efforts of the following persons. First to my counterpart Nick Costes who went beyond congeniality and went carefully into the interesting anomalies of granular materials via a series of mini-lectures which saved me a great deal of time. Further I want to thank Nick for encouraging a rational approach to the modeling problem. Prof. S. Sture was very gracious in condescending to speak at length to a "fluid-mechanicer". Warren Campbell and Charles Shafer of NASA were very patient in showing me what the PHOENICS code really is. My compliments to Jim Dozier for excellent match-making and finally I would like to express my appreciation to Mike Freeman for his subtle management, clear communications, and attention to the detail that is so essential to success in short-term projects.

A STUDY OF THE COMPATIBILITY OF AN EXISTING CFD PACKAGE WITH A BROADER CLASS OF MATERIAL CONSTITUTIONS

By

Kenneth W. French, Jr.
Associate Professor of Mechanical Engineering
John Brown University
Siloam Springs, Arkansas

ABSTRACT

This study was directed at probing the flexibility of the PHOENICS computational fluid dynamics package. This flexibility was viewed along two general avenues; parallel modeling and analog modeling. In parallel modeling the dependent and independent variables retain their identity within some scaling factors, even though the boundary conditions and especially the constitutive relations do not correspond to any realistic fluid-dynamic situation. The analog view maps stress onto enthalpy, strain onto concentration, etc. so that any "physical insight" built into the code may actually inhibit successful solution.

Modeling commenced with the Davis & Mullenger rational rate-type concept of granular constitution and used PHOENICS to generate a CFD model that should exhibit the physical anomalies of a granular medium and permit reasonable similarity with boundary conditions typical to membrane or porus piston loading. A considerable portion of the study was spent prying into the existing code with a prejudice toward rate-type and disarming any inherent fluid behavoir. This prying resulted in a covey of suggestions for parameter and computation control in modeling.

The final stages of the study were directed at the more specific problem of multi-axis loading of a cylindrical geometry with a concern for the appearance of bulging, cross-slab shear failure modes, etc. Special attention was taken to indicate handling of this set of boundary conditions.

LIST OF FIGURES

CONTENTS

INTRODUCTION

The analogy between particular flows of fluids and loadings of solids have been noted since the first formulation of the differential equation models in mechanics. There was considerable effort in the late 1950' s and early '60' s to reduce the differences then appearing in the various realms of continuum mechanics - most strongly evidenced by the formation of University Departments in Engineering Science. During that era it was popular to reference analogous situations viz Langlois(1964) relates the viscous pipe flow problem he is solving to torsion in a solid elastic cylinder. Professor R.R.Long of Johns Hopkins was even so optimistic as to publish an undergraduate textbook entitled Mechanics of Solids and Fluids; a sure signpost of the anticipated direction of mechanics in 1961. Now in the 80'es there seems to be a renewed interest in the elegant results of rational mechanics.

In the intervening 20 years the Engineering Science phenomenon has all but disappeared and numerical preoccupation with specifics has dimmed the vision of a unified mechanics. However, as with it's stress, mechanics shows its most novel behavior where it is diverging. Evidence of the current divergence in mechanics is easily found in a survey of the journal titles for journals sporting less than a decade of existance. The advancing maturity of numerical analysis has perhaps reopened the door to a prospect of a unified mechanics.

Herein a glance is taken at the prospects of using a tool from one branch of mechanics on a problem distinct to another branch. The tool is PHOENICS(Spalding(1981)), a computational fluid dynamics package commercially available from CHAM,N.A.,Inc; Huntsville AL. The following are pertinent excerpts from the PHOENICS manual;

> "...they should be warned that fluid flow computations proceed in a different manner from those of, for example, the analysis of stress and strain in solid structures. In the latter calculations, non-linearities are often absent, or of minor influence. In fluid-flow computations, they are dominant; and, as s consequence, the user of a fluid-flow code has to be content with rather less automation than the structural code user has become accustomed to."
>
> "...The user of PHOENICS will soon learn to do some things with this computer code which its developers have never done;and, though most of these may be highly successful, some will certainly not be. It is impossible for the developers to have anticipated all the tricks PHOENICS may be asked to perform and to insure that it never stumbles or falls."

OBJECTIVES

This project has been a rather broad based search for the common ground between an existing CFD numerical analyzer,PHOENICS, and the mechanics of granular media. The search sought to commence with the default PHOENICS model and to approach by increments the rate-type constitutive behavior model of discrete media until the conversion became tenuous. Usually that has meant pursuit until terms appear that cannot be induced within the CFD framework. It might be pointed out at this juncture that since the particular CFD code considered is particularly flexible the resulting code can be either a parallel model or an analog model which no longer corresponds with any real fluid flow variables, but is just a similarity of finite domain models and boundary conditions. The first objective was to distinguish these approaches and consider the possibilities of simultaneous uncoupled models and coupled mixtures of these two types.

The second objective of this study was to highlight those flexibilities built into PHOENICS that will allow some extensions toward the realm of granular mechanics. The third objective was to show the potential for a "rational" linkage between the tool and the granular realm starting with a general rate-type formulation. Further it was desireable to view the prospects and dangers for non-parallel uses of the numerical tools in the PHOENICS package. That is the ability to disarm all inherent fluid prejudice while using the numerical mechanisms of the package. Examples are heat conduction in a solid, torsion of a solid cylinder, 1-d consolidation, mantle convection, etc.

The final objective was to consider the special case of a tri-axial test with a "failure" condition built into the model. These studies to culminate in suggestions for building a PHOENICS model and and to anticipate problems that will arise in simulating the boundary conditions.

THE STRUCTURE AND FLEXIBILITY OF PHOENICS

The ability of the PHOENICS code to model in a general continuum mechanics sense can be partitioned into four realms:

Option	Location
Ancillary Variable Solution	SAT: group 8-12
Variable Exchange Coefficients	GRD: chapter 13
Definable Boundary & Grid	SAT: group 2-7&14
Selectable Iteration Scheme	SAT: group 26-31.

Selections are made via multiple-state flags placed in the SATLIT coding. The specification of simple behavoir (constant,linear or parabolic) is also completed in SATLIT. More complex constitutions are flagged over to FORTRAN coded models built by the user in the GROUND subroutine. This latter option would of course be necessary with non-newtonian fluids or granular solids.Figure 1 shows a user oriented view of the control space graph. The arrowheads indicate the points at which the user interacts with SATLIT-groups and GROUND-chapters.

PHOENICS is a numerical paradigm of Newton's Second Law, the conservation of energy and the conservation of mass by phase and chemical specie. These principles are modeled on a common "transport" framework. Further the PHOENICS system permits and interacts with user defined FORTRAN models which fit into that same framework. However, the package does not run any conservation for a variable unless it has been turned-on; SOLVAR.

The twenty-five dependent variables in PHOENICS might be categorized:

FLOW:	P1	PP	U1	U2	V1	V2	W1	W2	
FLOW ASSOCIATED:	KE	EP							turbulence
ANCILLARY:	R1	R2	RS						phase volume fractions
	H1	H2	H3						enthalpies
	C1	C2	C3	C4					concentrations
RADIATION:	SOLVAR - 21,22,23								
UNSPECIFIED:	SOLVAR - 24,25								

Density can also be a GRD defined dependent variable, but its transport is discussed below. These variables are related by the transport equations for the ith phase and the jth quantity, ϕ_{ij}:

$$\frac{\partial}{\partial t}(\rho\beta R\phi_j)_i + \underline{\nabla}\cdot(\rho\beta R\underline{V}\phi_j)_i = \underline{\nabla}\cdot(\beta R\Gamma\underline{\nabla}\phi_j)_i + R_i S_{ij}$$

In which ρ is mass density, β is porosity (or blockage), R is the phase volume fraction and Γ is the exchange coefficient.

*-- β is an array entered in SAT
*-- ρ, Γ, S are parameters with builtin SAT versions and flags for extension in GRD
*-- R, ϕ, V are variables

An alternate version of the transport equation is:

$$\frac{\partial}{\partial t}(X\phi) + \underline{\nabla}\cdot(X(\underline{V}\phi - \frac{\Gamma}{\rho}\nabla\phi)) = RS$$

The grouping; $X = \rho\beta R$; will be called the transport density; and appears in all terms if Γ/ρ is used in the diffusion term and is perhaps the most crucial in seeking a relationship with strain or dilitation (trace of strain) and in making the distinction between rate of deformation and rate of strain. If is taken as a constant;

$$X_{,t} + \nabla\cdot(X\underline{V}) = \frac{XS}{\rho\beta\phi_c} = XS'$$

or if $Y = \ln X$ and $\underline{\nabla}\cdot\underline{V} = 0$,

$$Y_{,t} + \underline{V}\cdot\underline{\nabla}Y = S'$$

Another view of the general transport relation which shows conservation of mass in the conventional manner, since $\mathrm{tr}\,\mathbb{D} = \frac{1}{\rho}\frac{D\rho}{Dt}$ is

$$\rho\frac{D\phi}{Dt} = \frac{1}{R\beta}\underline{\nabla}\cdot(X\frac{\Gamma}{\rho}\underline{\nabla}\phi) + \frac{S}{\beta} + \frac{\phi X}{R\beta}\mathrm{tr}\,D$$

The most rudimentary version of the transport equation is that of a steady state, zero velocity, source-free, diffusion of enthalpy or concentration with constant Γ/ρ, for which;

$$\nabla^2\phi = 0$$

However, while the general vector versions of model formulation are straight forward, the prejudices of PHOENICS strongly affect the model building especially for a non-flow problem.

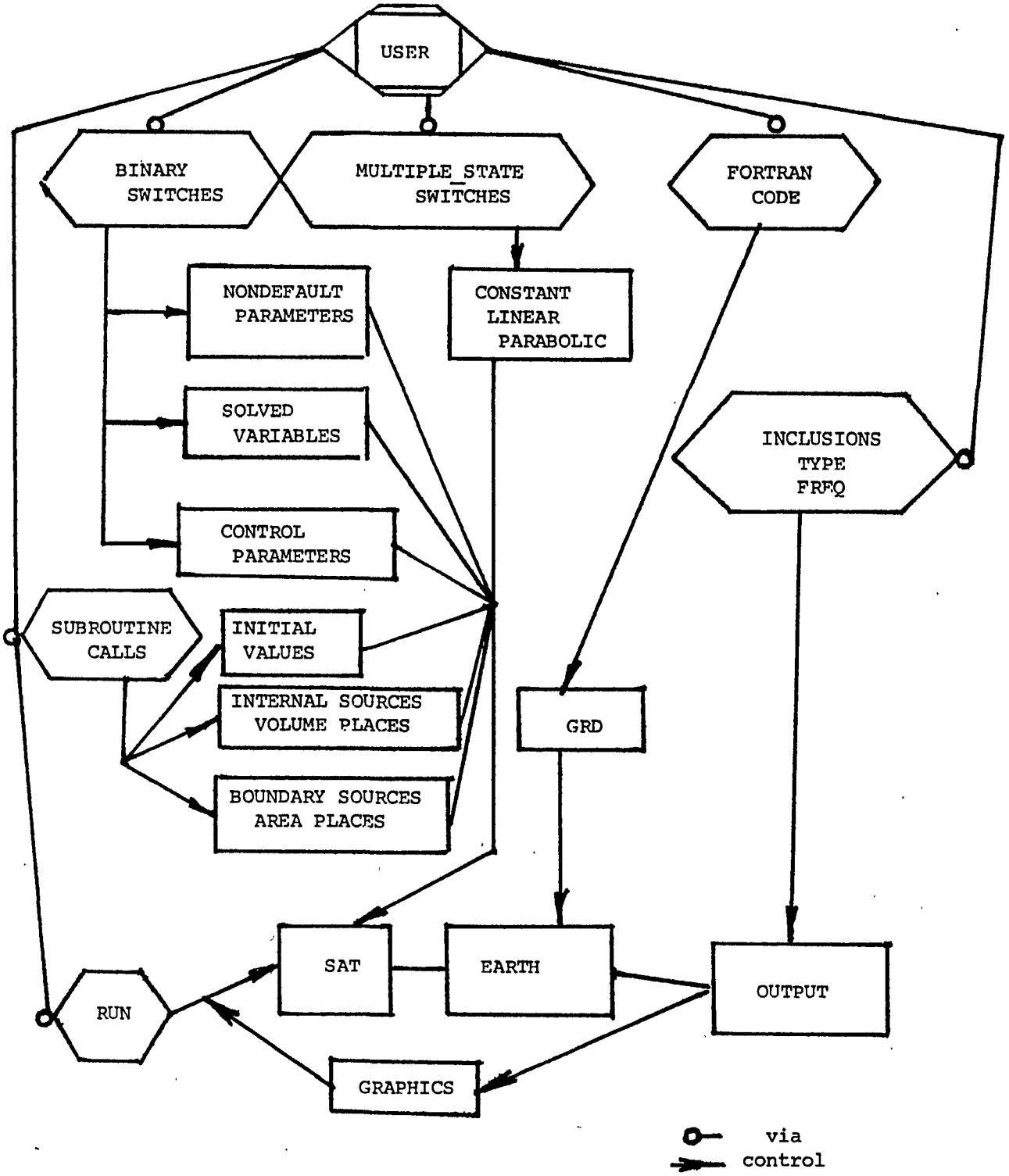

CONTROL STATE GRAPH

FIGURE 1

That is the coordinate system must be aligned with the flow of stress,strain, strain rate, etc. In PHOENICS cartesian notation the X & Y coordinates are interchangeable "in-slab" variables, the Z coordinate is the "slab-pointer" and has several, flagged, computational path and iteration counters. In polar cylindrical notation, X represents the tangential direction on a circular slab. For this reason it is much easier to solve a pure transient diffusion problem;

$$\phi_{,t} = \left(\frac{\Gamma}{\rho}\right) \nabla^2 \phi$$

in X-Y than in X-Z or Y-Z coordinates.

The hierarchy of a slabwise solution is shown in Figure 2 (Gunton '83: 4.5-5). Note that LITC,last interation on concentration, is the inner-most controllable loop counter. The variables KE & EP were labeled "flow-associated" above because they are inherently linked with the momentum exchange coefficients; and have built in sources.

$$\Gamma_{MOM,i} = \left(\mu_{LAM} + c\rho k^2/\varepsilon\right)_i/\text{SIGMA(i)}$$

i-	3	4	5	6	7	8
	U1	U2	V1	V2	W1	W2

DEFAULT:	SIGMA(i)	=	1.0	i odd
		=	1.0E10	i even

ρ, Γ, & S are each fully definable in terms of the geometry,time, and four slab-fulls of the other 24 independent variables. The slabs are the current slab and its immediate time prededent, as well as the adjacent LOW (in Z)slab and the adjacent HIGH slab.Other slab data can be accessed with the READIZ subroutine if long range effects or long memories must be included.

PHOENICS

SLAB-WISE SOLUTION

FIGURE: 2

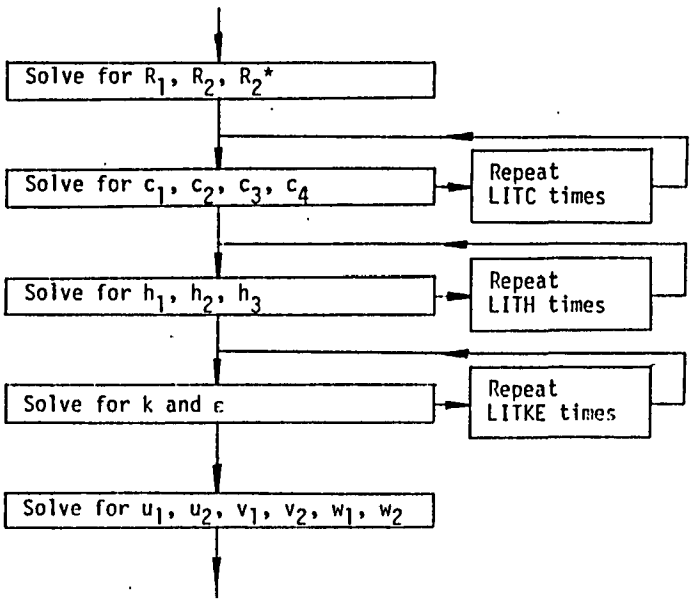

COMMON GROUND AND EXPLOITATION

Modeling granular is considered along two general avenues; parallel modeling and analog modeling, see Figure 3. Parallel modeling is taken to mean that the independent and dependent variables retain their identity to within some scaling factors, even though the boundary conditions and especially the constitutive relations do not correspond to any real physical fluid-dynamic situation. This latter failure is inconsequential unless it triggers some safeguard in the PHOENICS code which makes completion of the numerical procedure impossible. The alternative avenue is an analog view of the problem, which maps granular loading variables onto PHOENICS variables with totally different meaning or no preset meaning (eg: stress onto enthalpy, strain onto concentration, strain rate onto VAR(25)). While the allowable range of constitutions is much broader with analog modeling, so is the danger of mis-interpreting the result or of inducing an error with the numerical procedure. The physical insight built into the code may actually inhibit successful solution. Of course mixed parallel-analog modeling may ultimately prove to be necessary to handle the difficult constitutions of granular mechanics.

First to consider the prospects of pure parallel modeling; in parallel modeling, "velocity is velocity" and so on... the momentum equation is;

$$\nabla \cdot \underline{\sigma} = \rho \frac{D\underline{v}}{Dt} - \underline{B} = \underline{A}$$

the LHS is the commonality term in continuum mechanics; the RHS is frequently set to zero in solid mechanics and granular mechanics as a quasi-static approximation. In the general PHOENICS transport equation given in the last section, with the transported quantity being momentum per mass, the parallel correspondence with the divergence of the stress tensor would be:

$$\nabla \cdot \underline{\sigma} \quad \Leftrightarrow \quad \nabla \cdot (\Gamma \frac{\Gamma}{\rho} \nabla \phi) + R S_T$$

GRANULAR MODEL PHEONICS

$$\nabla \cdot \underline{\sigma}^* - \nabla P \quad \Leftrightarrow \quad \nabla \cdot (\Gamma \frac{\Gamma}{\rho} \nabla \phi) + R S_T$$

The source term being only a portion of the full PHOENICS source term since the body forces and the boundary effects are also embedded into the momentum transport equation in the source term;

$$S = S_{BF} + S_{BOUNDARY} + S_T$$

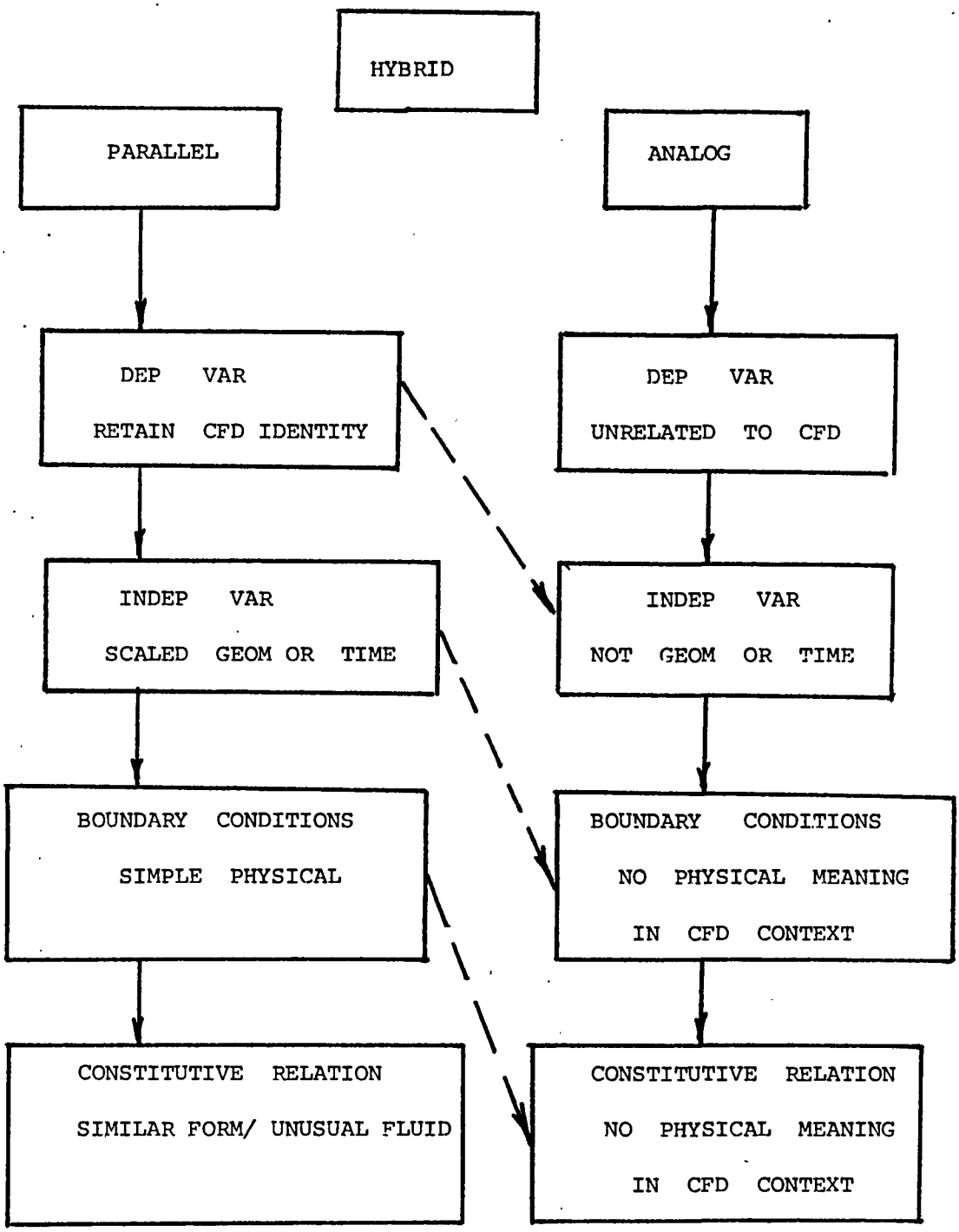

MODELING SCHEMES

FIGURE 3

The immediate prospect is to use; $S_\tau = 0$

and; $\sigma = \chi \frac{\Gamma}{\rho} \nabla\phi$

a form which could be implemented as an analog model in the transport relation for c or H, but not here with parallel correspondence and transport quantity, PHI = U,V,W; since Phoenics uses builtin interactions in the momentum equations. One of the builtins is for turbulent transport and appears in the exchange coefficient;

$$\frac{\Gamma_{MOM}}{\rho} = \left(\gamma_{LAM} + c\frac{\rho k^2}{\rho\varepsilon} \right)_i / \text{SIGMA(I)}$$

the other is a source term to represent negative gradient of pressure. Where γ is the kinematic viscosity and k(KE) and ε (EP) are the two PHOENICS turbulence parameters, which separately obey the transport relation. Using the transport density from the last section, and noting that PHOENICS is very sensitive to conservation of mass;

$$\frac{\Gamma}{\rho} \nabla\chi \cdot \nabla\phi + \chi \nabla\frac{\Gamma}{\rho} \cdot \nabla\phi + \chi \frac{\Gamma}{\rho} \nabla^2\phi$$

$$\underline{V} \cdot \nabla\chi = \chi(S^\tau - \nabla \cdot \underline{V}) - \chi_{,t}$$

which represent PHOENICS in full flight.

The pressure and pressure perturbation mindset in CFD is perhaps the greatest obstacle to making a direct rational transition to other branches of mechanics. In PHOENICS the pressure perturbation is the "outermost" of the dependent variables. The classical relation between stress and deformation rate in terms of the Lame' constants is:

$$\sigma = -p\mathbb{I} + \lambda \operatorname{tr}\mathbb{D}\,\mathbb{I} + 2\mu\,\mathbb{D}$$

and the pressure is then:

$$p = -\tfrac{1}{3}\operatorname{tr}\sigma + (\lambda + \tfrac{2}{3}\mu)\operatorname{tr}\mathbb{D}$$

and takes on its "standard" value if ; $\lambda = -\frac{2}{3}\mu$

or if; $\operatorname{tr}\mathbb{D} = 0$

and is separable from the rest of the divergence of the stress in the momentum equation. However since a granular medium must be modeled as a "rate-type" material a considerable problem arises in the uncoupling and building the source term. The classical constitutive relation for an elastic material is;

$$\sigma = \lambda \operatorname{tr}\mathbb{E}\,\mathbb{I} + 2\mu\mathbb{E}$$

and for a Rate-Type material;

$$\overset{\circ}{\sigma} = -\dot{p}\mathbb{I} + \overset{\circ}{\sigma_*}$$

$$\triangleq \dot{\sigma} - W\sigma + \sigma W$$

$$= f_n(\sigma, \mathbb{D}, \rho)$$

in which the following are understood to indicate;

σ	Cauchy stress tensor
$\overset{\circ}{()}$	substantial derivative
$\mathbb{D}$	rate of deformation tensor
$\mathbb{W}$	spin tensor
$\mathbb{E}$	infinitesimal strain matrix
λ, μ	functions of thermodynamic state

$$\nabla \underline{V} = \mathbb{D} + \mathbb{W}$$

The overlying circle indicates a Jaumann derivative, the overlying dot indicates a total derivative, the trailing asterik indicates a deviatoric quantity, $tr\, \sigma^* \mathbb{D}^*$ is the deviatoric stress power, and $\underline{V}$ is the velocity vector.

Since Jaumann and deviatoric are not commonplace to fluid dynamics they will be discussed in the general context of coordinate system differences between PHOENICS and granular mechanics. In granular mechanics it is convenient to use three offsets; "effective"(from pore-pressure), "incremental" (from local averaged), and "deviatoric" (from $\frac{1}{3} tr\, \sigma$). It is fortuitous that a rate model linearly relating stress rate and strain rate can be reduced to one relating incremental stress and incremental strain. This reduction is very convenient to those with a history of incremental models, but not particularly for those with a history of stress-strain rate models. Deviatoric quantities are offset by pressure and fractional rate of change of specific volume (dilitation rate) which is zero for an isochoric process;

$$tr\, \sigma = 3p \quad \{src\} \quad : \quad tr\, \mathbb{D} = tr\, \nabla \underline{V} = \nabla \cdot \underline{V} = -\frac{\dot{\rho}}{\rho}$$

The Jaumann derivative is included to insure objectivity; that is invariance under coordinate transformation -Eringen(1962)pp110. It is of course desirable to pose constituitive models that are objective. Stress and deformation rate tensors being inherently objective can be used in building constituitive relations. However if a material demands a time dependency there is a difficulty as the stress rate and spin tensor are not objective. It is possible to formulate an objective function from combinations of stress rate and spin; these functions are termed "stress fluxes" and are neither unique nor equal. On this basis the "hypo-elastic" constitutions are written as:

$$\text{STRESS FLUX} = F_{tensor}\ (\text{STRESS, DEFORMATION RATE})$$

and the "Rate-Type" relations as;

$$\text{STRESS FLUX} = G_{tensor}\ (\text{STRESS, DEFORMATION RATE, DENSITY})$$

The three traditional stress fluxes are;

JAUMANN: $\overset{\circ}{\sigma} = \frac{D\sigma}{Dt} - W\sigma + \sigma W$

OLDROYD: $\hat{\sigma} = \frac{D\sigma}{Dt} - \underline{\nabla V}\,\sigma + \sigma\,\underline{\nabla V}$

TRUESDELL: $\check{\sigma} = \frac{D\sigma}{Dt} - W\sigma + \sigma W + \sigma\,\underline{\nabla}\cdot\underline{V}$

In a series of publications, Davis & Mullenger(78,79,81,84a,84b) drew on the first of the stress fluxes above in describing soil as a Rate-Type material. Then introducing a number of reductions and special pressure dependencies into the coefficients they instill real soil behavoir (critical state, yield surfaces, etc.) into the model. They also show a concern paralleling that for an inclusive constituitive model, which is to establish a simple failure prediction tool within the same constituitive framework. The failure (79,81,84b) appears as the null points of a determinate which relates two invariant based vectors.

Departing from Davis & Mullenger(1978) at equations (43-44) and moving toward PHOENICS thought gives;

$$\dot{p} = -\varkappa p \dot{v} - \frac{2b\mu p}{M^2}\left[1 - \left(\frac{\gamma}{\gamma_c}\right)^{\gamma}\right] \mathrm{tr}\,\sigma^{*}\mathbb{D}^{*}$$

$$\overset{\circ}{\sigma^{*}} = 2\mu\left[\mathbb{D}^{*} + \left(b\left(\frac{\gamma}{\gamma_c}\right)^{\gamma}\frac{\mathrm{tr}\,\sigma^{*}\mathbb{D}^{*}}{M^2}\right)\sigma^{*}\right]$$

and ignoring the prospect that

$\gamma = \gamma(p)$ & $\varkappa \sim p^{-\lambda}$ →

$$-\nabla p = \nabla\left(\frac{\dot{p}}{\varkappa \dot{v} + \frac{2b\mu}{M^2}\left[1 - \left(\frac{\gamma}{\gamma_c}\right)^{\gamma}\right]\mathrm{tr}\,\sigma^{*}\mathbb{D}^{*}}\right)$$

PHOENICS - momentum flux source term

$$\nabla\cdot\sigma^{*} = \nabla\cdot\left(\frac{\overset{\circ}{\sigma^{*}} - 2\mu\mathbb{D}^{*}}{2\mu b\left(\frac{\gamma}{\gamma_c}\right)^{\gamma}\frac{1}{M^2}\mathrm{tr}\,\sigma^{*}\mathbb{D}^{*}}\right)$$

and so the exchange coefficient becomes (for momentum flux):

$$\Gamma_{MOM\,i} = \left(\frac{\overset{\circ}{\sigma^{*}} - 2\mu\mathbb{D}^{*}}{2\mu b\left(\frac{\gamma}{\gamma_c}\right)^{\gamma}\frac{1}{M^2}\mathrm{tr}\,\sigma^{*}\mathbb{D}^{*}}\right) \Big/ \nabla V_i$$

& $M^2 = \sigma^{*}\sigma^{*} = f(p)$ YIELD FUNCTION

PHOENICS has a builtin provision for compressibility that should be useful for instilling critical state soil behavoir in a model. It is coded as D1DP & D2DP and computes the fractional change of specific volume with pressure; so that in terms of the isothermal and constant pressure compressibilities;

$$D1DP = \frac{1}{v}\frac{dv}{dP} = \frac{1}{v}\left(\frac{\partial v}{\partial P}\right)_T + \frac{1}{v}\left(\frac{\partial v}{\partial T}\right)_P \frac{dT}{dP}$$

Then the critical state specific volume-pressure relation can be given as:

$$v_{c_0} - v_c = \frac{1}{\kappa_L} \ln\left(\frac{P}{P_0}\right)$$

```
D1DP = 1/(P*LN(P/P0) )
```

D2DP is for the second phase, which if decoupled, could be run independently of the active load response. Equation (35) from Davis & Mullenger (1978) becomes;

$$D1DP = \frac{\dot{\rho}}{\dot{P}\rho} \quad \cdots\cdots \dot{(\,)} = \frac{D(\,)}{Dt}$$

$$= \frac{1}{\mathcal{K} v P} - \frac{2\mu}{\mathcal{K} M^2 v P}\left[1 - \frac{v}{v_c}\gamma\right] \mathrm{tr}\,\boldsymbol{\sigma}^* \mathbf{D}^*$$

It is also of interest to note that; $\rho = 1/v \ \ldots$

$$D1DP = -\frac{\nabla \cdot \mathbf{V}}{\dot{P}}$$

And if one reconsiders the pressure grouping above;

```
P = K1*RHO1/D1DP*(1/ ( 1+( K*F(RHO1)/ RHO1dot) * tr σ*D*)
```

with;

```
F(RHO1) = RHO1**2 * ( 1 - (RHOC/RHO1)**γ)
```

and the sign of K is dependent on the realm of deviatoric stress power; $\mathrm{tr}\,\boldsymbol{\sigma}^* \mathbf{D}^*$, while gamma, γ, is in general a function of pressure. For the case of negligible deviatoric stress power;

$$P = \frac{1}{\mathcal{K}}\frac{\dot{P}}{\dot{v}} \rightarrow \frac{1}{\mathcal{K}}\frac{\partial P}{\partial v} = \frac{1}{\mathcal{K}}\frac{dP}{dv} \cdots P = P(v)$$

which is verified as Davis & Mullenger's equation (30).

There is of course another strategy; one more amenable to "PHOENICS thought". That is to leave the grad p momentum source term alone, and build an equation of state in the form of density specified as a function of pressure, pressure rate, density rate, and so on. The full relation as given above will not yield however to an analytic manipulation of this sort, and so the strategy would have to be implemented numerically. That is a root solver would have to be built into GROUND to proceed from pressures, and unsundry rates to the current value of density.

An analog or a hybrid approach to the granular problem might take a very different appearance. For example the following could be computed by PHOENICS with null velocity and pressure fields (ie not turned on) to inhibit coupling and using an enthalpy or a concentration (H1,H3,C4,solvar(25),...) instead of the actual physical variables.

$\nabla^2 T = 0$	Torsion in a solid rod
....stress	(Langlois)
$a\nabla^2 u = u_{,t}$	Terzaghi's consolidation problem;fluid in porus
.....pore pressure	solid (Holtz&Kovacs)
$\nabla^2 S_x + \nabla^2 S_y + \nabla^2(aET) = 0$	Thermoelasticity in Plane Stress
.....stress, temperature	(Ugural & Fenster)
$\nabla^2(\nabla^2\phi) = 0$	Stress/Strain Potential or Bifurcation
.....stress*length	(Biot)

The inclusion of stress flux in the constituitive model makes a special suggestion for the momentum equation: that is to take its substantial derivative.

$$\frac{D}{Dt} \quad (\quad \text{momentum} \quad \text{equation} \quad)$$

$$\nabla\cdot\dot{\sigma} = \frac{D}{Dt}\left(\rho\frac{DV}{Dt} - \underline{B}\right)$$

$$\nabla\cdot\left(\overset{\circ}{\sigma} - W\sigma + \sigma W\right) = \cdots$$

$$\& \quad \nabla\cdot W = 0 \quad \& \quad \nabla\cdot\sigma = RHS_{MOM}$$

This matter was taken up by Biot(1965) in his Appendix, "Equilibrium Equations with Rate Variables". Biot followed the tradition of solid mechanics in leaving $\rho\frac{DV}{Dt}$ identically zero, although components of

grad velocity are included in the stress flux and probably would have also appeared in the constituitive equation (as rate of deformation) if he had posed one. The RHS of the momentum equation would however require considerable thought and reduction for special cases because of the tedious nature of;

$$\left(\frac{\partial}{\partial t} + \underline{V}\cdot\nabla\right)\left(\frac{\partial}{\partial t} + \underline{V}\cdot\nabla\right)\underline{V}$$

In the absence of $\underline{B}$ perhaps the RHS c-ould be reduced to the terms;

$$\rho(\underline{\nabla}\cdot\underline{V})(V\cdot\nabla V)$$

$$\rho u\left(\frac{du}{dx}\right)^2 \ldots\ldots\ldots \text{1-D}$$

CONCLUSIONS & RECOMMENDATIONS

The primary modeling problems anticipated for the full specification of a granular medium in a PHOENICS environ are listed below. They are coincident with the recommendations for extensions of this work.

a] To determine when and where tr **D** can be set equal to zero: interesting granular problems will have nonzero tr $\mathbb{D}$.

b] To compare the treatment of pressure and its perturbation in PHOENICS (PH) and the coupling between pressure and pressure rate in the granular model (GM).

c] To use incremental strain (GM) as opposed to deformation rate (PH)& Rate-Type.

d] To convert stress space coordinate results to Eulerian physical coordinates (PH).

e] To include catastrophic changes of modeled behavoir (GM) on reaching failure yield, critical state or loading parity, and the parallel computations which must be run(like tr $\boldsymbol{\sigma}^{*}\mathbb{D}^{*}$, tr Π;etc.) and monitored for these bifurcations.

f] To require objectivity that constituitive models may be posed in terms of stress flux (PH).

g] To establish compatibility with an encroaching solid boundary; total effective load equal the sum of the outputs of the boundary momentum sources.....and the mass occupying the displaced volume; $\int \underline{x}\dot{\underline{\delta}}\cdot d\underline{A}$ must be redistributed in a fashion (eg over a few cycles) that will not cause a false excessive local density.

h] To exploit the porosity greater than unity allowance (PH) so that the membrane boundary (triaxial loading) is permitted to bulge in addition the momentum sources representing this boundary should be set proportional to peripheral length. Further angular symmetry should be imposed to give a preference to circular (minimum periphery) cross-section; this condition should be automatic if a full thermodynamic specification is made.

i] To consider term-wise the enthalpy transport relation with stress power included (PH) in order to determine which terms dominate which applied load realms and to calculate a field of tr $\boldsymbol{\sigma}^{*}\boldsymbol{D}^{*}$ values for e] above.

j] To include the Davis & Mullenger simple and comprehensive failure criteria;

$$\det G = 0.$$

k] To embark on a loading model of the triaxial type and with a simple material; ideal gas, (PH).

l] To find a search strategy for locating shear bands and a discriminator for pseudo-bands that may appear due to the discretization...antialiasing so to speak.

m] To build the exchange coefficients separately from k] and find a simple physical case to test for their correct calculation.

REFERENCES

1. Biot, M.A.; Mechanics of Incremental Deformation J. Wiley, 1965.

2. Davis, R.O. & G. Mullenger;Int. J. for Numerical and Analytical Methods in Geomechanics; J. Wiley

   1978 v.2 pp 255 "A Rate-Type Constituitive Model for soil with a Critical State".

   1979 v3 pp 279 "Derived Failure Criteria for a Granular Media".

   1981 v5 pp 155 "A Unified Yield Criterion for Cohesionless Granular Material".

   1984av8 n2 with R.F. Scott pp 125 "Rapid Expansion in a RATE-Type Soil".

   1984b pp144 " Rapid Shearing in a Rate-Type Soil".

3. Eringen, A.C.;Nonlinear Theories of Continuous Media; McGraw-Hill, 1962.

   The Mechanics of Continua; J Wiley; 1967.

   Continuum Physics; Academic Press; 1976.

4. Fung, Y.G.; The Foundations of Solid Mechanics; Prentice-Hall, 1965.

5. Gunton, M.C., H.I. Rosten, D.B. Spalding, & D.G. Tatchell; PHOENICS - An Instruction Manual;CHAM;London; 1983.

6. Hill, R. & J.W. Hutchinson; "Bifurcation Phenomena in the Plane Tension Test"; J. Mech. PHYS SOLIDS; v 23; 239; 1975

7. Spalding, D.B.; "A General Purpose Computer Program for Mulit-Dimensional One and Two Phase Flow"; Mathematics and Computers in Simulation; North Holland Press;v 23; 1981.

8. Truesdell, C.; Continuum Mechanics I - The Foundations of Elasticity and Fluid Dynamics;Gordon& Breach; NY; 1966

1984

NASA/ASEE SUMMER FACULTY RESEARCH FELLOWSHIP PROGRAM

MARSHALL SPACE FLIGHT CENTER
THE UNIVERSITY OF ALABAMA

CHARACTERIZATION OF MATERIAL SURFACES EXPOSED TO ATOMIC OXYGEN ON SPACE SHUTTLE MISSIONS

Prepared by:	Albert T. Fromhold, Ph.D.
Academic Rank:	Professor
University and Department:	Auburn University Department of Physics
NASA/MSFC:	
Laboratory:	Materials and Processes
Division:	Engineering Physics
Branch:	Physical Sciences
MSFC Counterpart:	Ann F. Whitaker
Date:	August 10, 1984
Contract No.:	NASA-NGT-01-002-099 (The University of Alabama)

ACKNOWLEDGEMENTS

The author wishes to thank Dr. L. M. Freeman, Dr. James B. Dozier, and Mr. Leroy Osborn for their efforts in conducting the NASA Summer Faculty Fellowship Program. He appreciates the technical cooperation of Ms. Ann F. Whitaker and Ms. Sally A. Little. The efforts of Dr. Kasra Daneshvar, Dr. Bruce Tatarchuk, Dr. Dave Worley, and Mr. Hideya Kishi in carrying out the various measurements are gratefully acknowledged.

D10

CHARACTERIZATION OF MATERIAL SURFACES EXPOSED TO ATOMIC OXYGEN ON SPACE SHUTTLE MISSIONS

BY

Albert T. Fromhold
Professor of Physics
Auburn University
Auburn University, AL 36849

ABSTRACT

Material samples prepared for exposure to ambient atomic oxygen encountered during space shuttle flights in low earth orbit were characterized by the experimental techniques of ELLIPSOMETRY, ESCA, PIXE, and RBS. The first group of samples, which were exposed during the STS-8 mission, exhibited some very interesting results. The second group of samples, which are to be exposed during the upcoming STS-17 mission, have been especially prepared to yield quantitative information on the optical changes, oxygen solution, and surface layer formation on metal films of silver, gold, nickel, chromium, aluminum, platinum, and palladium evaporated onto optically-polished silicon wafers.

INTRODUCTION

With increasing sophistication of the space program, the need has increased for more detailed knowledge of the effects of the ambient space environment on the physical and mechanical properties of materials used for building instrumentation and fabricating structures which will operate effectively in orbit. Specifically the space telescope requires solar cell interconnects which must not fail over time periods of the order of years. Presently, silver is being utilized for these components since it has good electrical characteristics and is easily welded. It has been found, however, that severe tarnishing and marked degradation of the surface electrical properties occurs when silver is exposed to the low pressure atomic oxygen atmosphere surrounding the space shuttle. The focus of our work last summer[1] was to offer recommendations on the selection of metal samples to be exposed to atomic oxygen on the STS-8 flight. Literature data were reviewed concerning the oxidation properties of a variety of metals, and techniques for characterizing the parent metals and the surface oxides were described. The focus of our work this summer is to prepare silver specimens and various metals having potential for protective overcoatings to be exposed on the STS-17 mission which will occur later this year. A number of metal samples (viz., Ag, Au, Ni, Cr, Al, Pt, Pd) are being prepared for this test series. These samples will be examined both before and after flight with surface analysis techniques to quantify surface degradation and to characterize any oxide overlayers which form. Specifically, ellipsometry, Rutherford backscattering, proton-induced x-ray emission, and ESCA measurements are utilized.

OBJECTIVES

The objectives of my project this summer were two-fold:

(a) To carry out (in conjunction with Auburn University personnel) the characterization of the effects of the interaction of atomic oxygen with material specimens prepared last summer[1] and exposed during the STS-8 mission.

(b) To cooperate with MSFC personnel in the preparation and characterization of a group of material specimens to be exposed during the upcoming STS-17 mission.

SURFACE ANALYSIS TECHNIQUES UTILIZED

Five experimental techniques were employed to study the interaction of atomic oxygen with materials exposed during the STS-8 mission, namely, ESCA, PIXE, RBS, IR, and ELLIPSOMETRY. A brief description of each of these techniques and the results obtainable by each is given below.

ESCA -- The acronym ESCA stands for "Electron Spectroscopy for Chemical Analysis." Another acronym used for this technique is XPS, which stands for X-Ray photoelectron spectroscopy. (The appropriate acronym apparently depends upon whether one affiliates with chemists or with physicists.) In either case, the technique consists of the analysis of the kinetic energies of ejected electrons from the material being studied. The electrons are ejected from the cores of the atoms of the target material by incident soft x-rays of well-defined energy. A calculation of the core electron binding energy from these results is then possible. Since the binding energy reflects the oxidation state of the material, which in turn depends sensitively on the local chemical environment, much pertinent information can be thereby deduced. The technique is limited to materials which are stable to x-ray bombardment. One problem arising for dielectric samples is that of surface charging which leads to a shift in the absolute positions of the peaks. The technique is a surface technique in that it is limited to the upper 100 A or so of the sample, the depth from which ejected electrons can emerge.

PIXE -- The acronym PIXE stands for proton-induced X-ray emission. Typically an accelerator is used to produce an incident proton beam well-defined in energy, and this beam causes the emission of X-rays characteristic of the elements making up the target material. This is an excellent technique for studying the elemental composition of complex materials such as the paint specimens flown on the STS-8 mission.

RBS -- The acronym RBS stands for Rutherford back-scattering. In this technique, a helium ion beam having energy in the range of 0.1 to 5 MeV is scattered from the target material. The energy of the scattered helium contains salient information about the depth profile of the surface layer and the atomic concentration. Typically surface regions 100 to 6000 A in depth can be studied by this method.

IR -- Infrared (IR) techniques are well-known in spectroscopy. This technique was employed to study the surface of the organic specimens flown on the STS-8 mission to see if any changes could be detected in the surface bonding due to interaction of the material with atomic oxygen.

ELLIPSOMETRY -- Polarized light spectroscopy is termed ellipsometry because it involves the production and analysis of elliptically polarized light and the changes which take place in this light when it is reflected from the surface of a material specimen. It is an extremely sensitive technique which can detect changes in surface layer thickness, on the average, which are only a fraction of a monolayer. For example, a metal sample can be monitored continuously in a non-destructive manner under exposure to oxygen, starting from the freshly-cleaned condition of the parent metal and extending to the point of formation of thick surface oxides. The continuous changes produced in the ellipticity of the light can be used to calculate the surface oxide layer thickness as a function of time in order to deduce the kinetics of growth of the layer. The technique is also excellent for comparison of flight and control samples of various materials, such as the paint specimens studied on STS-8, in order to deduce the overall changes in the surface refractive index and absorption coefficient due to the interaction of the material with atomic oxygen.

EXPERIMENTAL RESULTS FOR STS-8 SPECIMENS

A variety of material specimens were studied from the STS-8 mission. These can be categorized into three groups -- metals, organics, and paints. The results obtained for specific materials in each of these groups are described below.

Metals -- Silver, copper, nickel, magnesium, lead, tungsten, and molybdenum were exposed on the STS-8 mission. The greatest effects, by far, were observed for silver, where the surface layers were visibly colored a dark grey or dark brown, and moreover were mechanically and perhaps chemically unstable, as evidenced by a flaking and peeling of the layers from the surface. This spalling of the layer made analysis difficult, since loss of this material often resulted in observations of the underlying surface only. For example, ESCA showed two oxygen peaks, but both peaks were present in the control sample as well as in the flight sample. RBS data indicated oxygen penetration in the flight sample to depths of at least 2000 A, but the concentration was definitely less than 10 (and probably less than 1) atomic percent. It is believed that no measurement was obtained of the flaky surface layer itself by RBS (or by ESCA). Ellipsometry showed large changes in the refractive index and in the absorption coefficient produced in the flight sample by exposure. The refractive index increased and the absorption coefficient decreased, both indicating a change in the surface from the metallic to dielectric or semiconducting behavior. Specific numerical results and plots of the data can be found in the monthly reports of contract NAS8-35914, and so will not be duplicated here, but suffice it to say that the refractive index was observed to increase by as much as a factor of 10 and the absorption coefficient was observed to decrease by as much as a factor of 2. Resistance measurements carried out by NASA personnel showed great changes in the electrical conductivity of thin silver films exposed on this mission. The observed increase in resistivity is in accord with our ellipsometry data on the surface optical constants of silver. Auger electron spectroscopy (AES) measure-

ments have been carried out at MSFC by Dalins with the negative result that no evidence was found for an oxygen content in the silver which could be directly associated with exposure to space environment. Independent AES measurements by Misra (MCR-84-551, Contract NAS8-30300 by Martin Marietta) indicated the presence of Ag and O in a silver interconnect specimen, with a shift in peaks indicating some kind of compound formation like silver oxide. However, these measurements indicated only 18 atomic percent oxygen (within large experimental error), which would be consistent with a compound such as Ag_4O. Although the suboxide Cu_4O has been reported in the literature for copper exposed to molecular oxygen, no such oxide has so far been observed by direct diffraction measurements for silver, to this author's knowledge. It is not certain whether the surface layer flaking so commonly observed for silver upon exposure to atomic oxygen is a bulk lattice effect or whether it is some type of a grain boundary effect. That is, it is conceivable that atomic oxygen penetrates the grain boundaries of the polycrystalline silver, thus forming a compound such as silver oxide which is chemically unstable or mechanically deleterious, with a consequent flaking of the surface layers of the silver specimen. Another possibility is that the atomic oxygen interaction converts the crystalline silver at the surface into some sort of an amorphous layer which has attendant degraded optical, electrical, and mechanical properties. An experiment to determine whether the interaction is a bulk lattice effect or a grain boundary effect is suggested later in this report.

In sharp contrast to silver, the metals lead, tungsten, and molybdenum showed little effect of the interaction with atomic oxygen, at least to within the experimental uncertainties of the study. The samples employed in this study were not the most sophisticated with respect to sample preparation, so the error limits in the results are quite large relative to what is possible using optical quality samples such as those described subsequently in this report which are being readied for the STS-17 mission. RBS data on the molybdenum sample did indicate, however, atomic oxygen penetration in the flight sample to a depth of approximately 600 A. It is interesting to contrast this with tungsten, where no evidence of oxygen penetration was found in the RBS measurements.

Moderate changes were observed for the samples of copper, nickel, and magnesium which were exposed during the STS-8 mission. Visible differences could be seen between masked and unmasked portions of one of the copper samples, but surprisingly, the optical constants of these two areas were not found to be drastically different. RBS measurements indicated oxygen penetration in one of the flight samples which was directly exposed to the flux of atomic oxygen, to a depth of 1100 A or so, but as in the case of silver, the atomic percent was quite low, being of the order of or less than 10%. It is interesting that the above-mentioned copper sample which had both masked and unmasked portions received only indirect exposure to atomic oxygen, in contrast to direct exposure, and in this sample the exposed portion was found by RBS measurements to have much less penetration by atomic oxygen than the 1100 A or so found for the directly exposed copper sample. In the case of nickel, some changes in the optical constants were found for the flight samples, but no evidence of a surface oxide was found in the RBS measurements. In the case of magnesium, both RBS and ellipsometry measurements indicated differences between the exposed and unexposed areas of the sample. The RBS spectrum, in particular, showed effects of a surface layer of oxide, and perhaps also dissolved oxygen within the material.

One additional metal sample was examined in detail because of its importance for space telescope optics. This sample consisted of aluminum evaporated onto quartz, with a protective overlayer of MgF_2. The RBS spectrum for this sample indicated clearly the layered configuration, and PIXE verified the presence of Mg as well as Al on the surface. Ellipsometry indicated that essentially no effects were brought about in the flight sample relative to the control sample. The precision of these measurements was extremely good, due to the excellent optical quality of the samples.

Organics -- Kapton H, Kapton F, tedlar, and mylar were the organic samples which were examined. PIXE data indicated the presence of fluorine in Kapton F, with the concentration being reduced in the flight sample relative to the control sample. White tedlar was found by PIXE to contain the elements F, Na, Si, and V, with concentration reductions occurring in the

flight sample relative to the control. The percent of elemental loss during flight was found to decrease with increasing atomic weight of the element. Infrared data indicated no significant changes in the surface bonding of kapton in the flight sample relative to the control, although there were minor differences in the spectra.

Paints -- Chemglaze Z-302, Nextel 401-C10, and A-276 white paint were examined in this study. PIXE data revealed that Z-302 contained P, S, K, and Ca; Nextel 401-C10 contained P, S, K, and Cr; and A-276 contained Na, Mg, S, and Ti. The ratio of the amounts of each of these constituents in the flight sample relative to the control sample were also deduced from the PIXE data. Ellipsometry showed that the flight samples exhibited a systematic increase in the refractive index relative to the control sample for each of the specimens. Changes were also observed in the absorption coefficient, but the results were particular to the paint in question. The greatest difference was observed for the white paint Chemglaze A-276, for which the absorption coefficient increased by more than a factor of 5 due to atomic oxygen exposure.

STS-17 SPECIMENS

The experimental results described in the preceding section were for samples which were exposed during the STS-8 mission. A group of higher quality samples has been prepared by Bob DeHaye of NASA for the upcoming STS-17 mission in order to obtain more detailed physical data. Optically polished silicon wafers were selected as substrate material for evaporated metal layers of Ag, Au, Ni, Cr, Al, Pt, and Pd. We are examining these samples by RBS and ellipsometry before flight in order to obtain a good baseline for interpreting the effects of exposure to atomic oxygen during flight. In each case, a control sample will be examined at the same point in time (both before and after flight) as the flight sample is examined.

CONCLUSIONS AND RECOMMENDATIONS

The conclusions of this study are that most materials are affected, to a greater or lesser extent, by the interaction with atomic oxygen present in low earth orbit. The most pronounced effects were observed for silver, whereas the least observable effects (for the lower temperature range in effect for the exposure) occurred for molybdenum.

To enable the separation of the effects of exposure to atomic oxygen into bulk lattice and grain boundary effects, it is recommended that a group of three single crystals of silver having the principal crystal orientations [(111), (110), (100)] be carefully prepared, packaged under ultra-high vacuum conditions of cleanliness (probably in an ambient inert gas), exposed to atomic oxygen under closely monitored conditions during shuttle flight, and repackaged to maintain ultra-clean conditions during and following re-entry. These samples should then be analyzed utilizing the best and most modern surface analysis techniques to understand the fundamental interaction of the ambient low-orbit atmosphere with Ag. The use of single crystals devoid of grain boundaries would enable one to delineate whether the deleterious effects of the exposure were due to a bulk lattice interaction mechanism or due, on the other hand, to some type of grain boundary diffusion process. It would be of great fundamental interest to ascertain whether the same type of flaking of the surface layer takes place upon exposure of single crystal silver as has been observed for the polycrystalline silver specimens which were exposed on the STS-8 mission.

REFERENCES

1. Fromhold, Albert T., "Atomic Oxygen Effects on Materials", Ch. XIV in Research Reports - 1983 NASA/ASEE Summer Faculty Fellowship Program (NASA CR-170942).

1984

NASA/ASEE SUMMER FACULTY RESEARCH FELLOWSHIP PROGRAM

MARSHALL SPACE FLIGHT CENTER
THE UNIVERSITY OF ALABAMA

AN INVESTIGATION OF SPACE SHUTTLE MAIN ENGINE SHUTDOWN CHUGGING INSTABILITY

Prepared by:	Paul E. George, II
Academic Rank:	Asst. Professor
University and Department:	The University of Tennessee, Knoxville Mechanical and Aerospace Engineering
NASA/MSFC:	
Laboratory:	Structures and Propulsion
Division:	Propulsion
Branch:	Turbomachinery and Combustion Devices
MSFC Counterpart:	Dr. T. Dwayne McCay
Date:	August 31, 1984
Contract No.:	NASA-NGT-01-002-099 (The University of Alabama)

ACKNOWLEDGMENTS

The assistance of Carol Dexter in compiling SSME information and answering my many questions is gratefully acknowledged. Brenda Anderson and Dale Blount taught me how to use the HP computer and provided valuable assistance in implementing the chugging model. Bob Grimes assisted with the high frequency data. Thanks are due also to the many data room personnel who provided graphical data.

Special mention and thanks to Jim Pearson who was both friend and mentor. His patience in explaining SSME operation was critical to developing a working understanding of the engines in a short time. Particular thanks to Dr. Dwayne McCay, my NASA counterpart, for providing an interesting problem and guidance for its solution and to Dr. Mike Freeman the NASA/ASEE summer faculty program coordinator.

The financial support of the National Aeronautics and Space Administration (NASA) and the American Society for Engineering Education (ASEE) is gratefully acknowledged.

AN INVESTIGATION OF SPACE SHUTTLE MAIN ENGINE SHUTDOWN CHUGGING INSTABILITY

by

Paul E. George, II
Mechanical and Aerospace Engineering
The University of Tennessee, Knoxville

ABSTRACT

The Space Shuttle Main Engines experience a low frequency pressure pulsation in both the fuel and oxidizer preburners during shutdown. The pressure pulsations (chugging) occur during the helium purge of oxidizer from the preburner manifolds. Possible causes and triggering mechanisms are considered as details of the chugging process are presented and discussed. A simple chugging model capable of predicting pressure excursion amplitudes and frequencies is proposed and preliminary results presented.

AN INVESTIGATION OF SPACE SHUTTLE MAIN ENGINE SHUTDOWN CHUGGING INSTABILITY

INTRODUCTION

The Space Transportation System, better known as the Space Shuttle, is propelled into earth orbit by two solid rocket boosters and three main engines. The Space Shuttle Main Engines (SSME) utilize liquid hydrogen and liquid oxygen as propellants. The engines have successfully completed 12 flights and several hundred test stand firings. There have, however, been some problems with the engines both in flight and on the test stand. This report addresses one problem, namely a low frequency instability which occurs when the engines are shutdown. The work reported here is a part of a continuing effort to develop analysis techniques for determining the stability characteristics of liquid fuel rocket engines.

To provide an appropriate background for the discussions in this report, the main engines are described briefly below. A short discussion of instability applicable to any liquid propellant rocket follows. With the appropriate background developed, the details of the shutdown instability are presented followed by a discussion of the results of a data review and modeling effort.

SSME DESCRIPTION

The Space Shuttle Main Engines supply a nominal thrust of 470,000 lbf at rated power level and may be operated up to 512,000 lbf for brief periods. Two preburners are used on each engine to preheat the hydrogen and supply power for the fuel and oxidizer pumps. Most of the hydrogen enters the main combustion chamber via the preburners while most of the oxygen enters directly from the pumps into the main combustor oxidizer manifold.

Figure 1 is a propellant flow schematic of the SSME showing the major equipment. Cryogenic liquid hydrogen enters the engine from the external tank via a low pressure pump which supplies sufficient head to prevent cavitation of the high pressure fuel pump. Power for the low pressure fuel pump is provided by a hydrogen feed from the high pressure fuel line. Hydrogen from the three stage high pressure fuel pump cools the nozzle, main combustion chamber and preburners prior to entering the low pressure pump or preburners. The majority of the fuel flows through the preburners where it is partially combusted prior to the main combustion chamber.

The oxygen follows a similar path except that oxygen is not used for chamber cooling and most of the oxygen is supplied directly to the main combustion chamber. Because the oxygen is primarily supplied to the main combustion chamber, the pressure at the outlet of the single stage pump is less than 5000 psia. A portion of the oxygen is supplied to the preburner pump which is attached to the same shaft as the high pressure oxidizer pump. The preburner pump supplies oxygen at approximately 8000 psia to the fuel and oxidizer preburners.

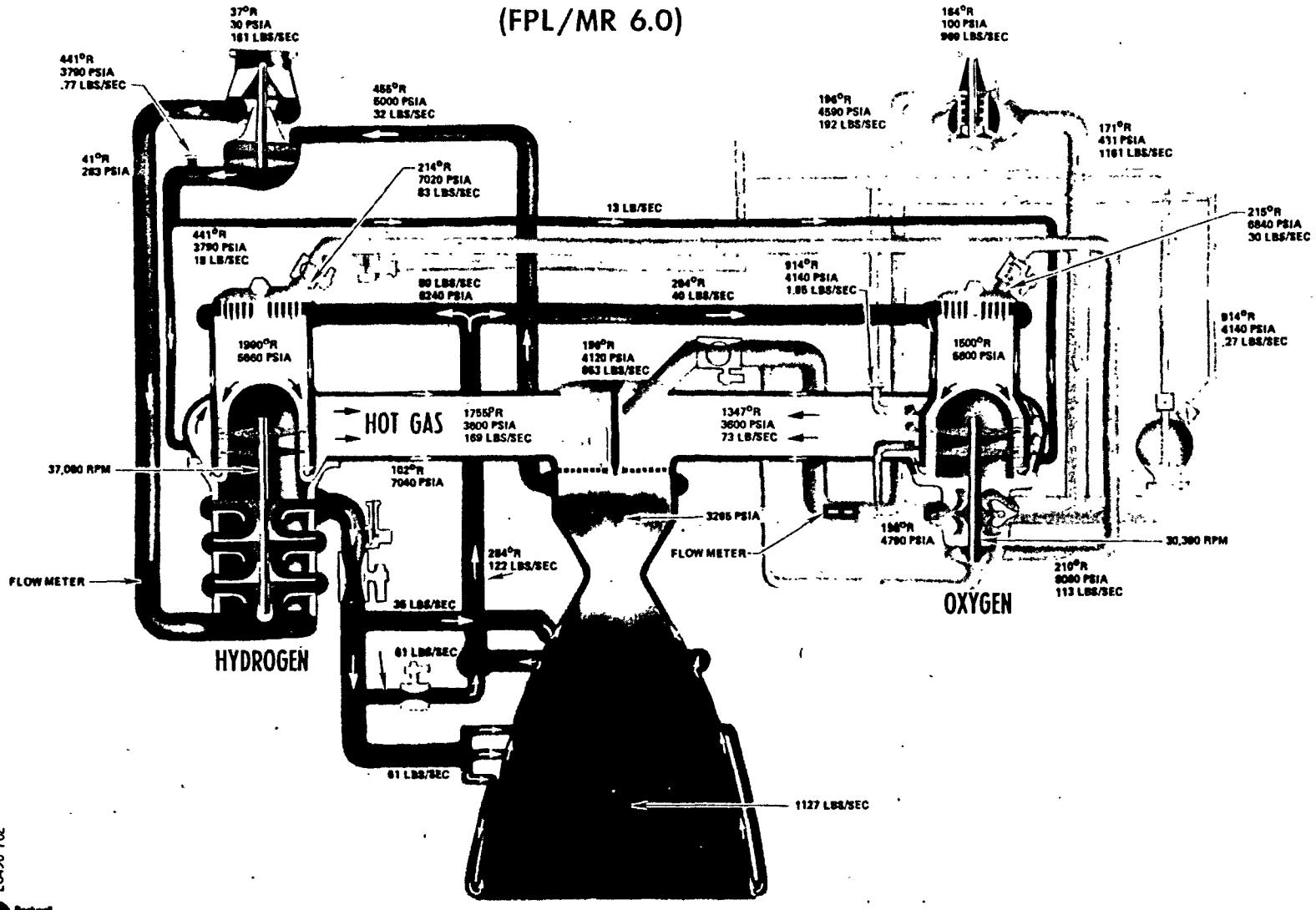

Figure 1. SSME Propellant Flow Schematic

During operation the main fuel valve and the main oxidizer valve are full open. Engine throttling is accomplished by throttling the oxidizer flow to the two preburners to reduce fuel and oxidizer flow. The preburners operate at a mixture ratio near 1.0 lbm oxidizer per lbm fuel (equivalence ratio = 8.0). The main combustion chamber operates with a mixture ratio of 6.0 lbm/lbm (equivalence ratio = 1.333). Figure 1 gives flow rates for the full power level (FPL) of 512,000 lbf thrust. The engine may be operated at a minimum power level (MPL) of 360,000 lbf or any power level between these extremes. The region of interest in this report is operation of the engine during shutdown. Figure 2 gives the shutdown valve sequence. Note that the oxidizer preburner oxidizer valve (OPOV) closes first followed by the fuel preburner oxidizer valve (FPOV). The main fuel valve (MFV) closes last. This sequence insures that an oxidizing condition will not exist in any hot region at any time. The shutdown instability occurs after FPOV closure but before MFV closure.

ROCKET INSTABILITY

Although low frequency pressure excursions in the preburners are the principal focus of this report, a brief general discussion of rocket engine instability will be presented here. Instability refers to a condition which leads to uncontrolled pressure excursions in the rocket combustion chamber. In the extreme case these excursions may destroy or severly damage the rocket engine; at the least they represent a loss of performance. Instability is classified according to the frequency range of the pressure excursions and the principal mechanism causing the instability. Low, intermediate and high frequency excursions are called chug, buzz, and scream, respectively. Low frequency instability (chug) involves a coupling between the combustion pressure and the feed system pressure. Both the feed and combustion chamber pressures are considered to be spacially uniform. High frequency instability (scream) is a coupling between the combustion process and pressure waves crossing the combustion chamber. Intermediate frequency instability (buzz) involves standing pressure waves in the feed system.

Chug

Chugging is characterized by a coupling between the combustion energy release and the propellant feed process. Frequencies are generally of the order of 50 to 200 Hz with the mechanism being dominated by the variations in feed to the chamber caused by chamber pressure variations. An increase of pressure in the chamber naturally decreases the flow, while a decrease in the chamber pressure increases flow. A pressure excursion may result from any disturbance, but will usually die out quickly unless energy is supplied by combustion. Constructive coupling between energy release and pressure oscillations in the feed system requires a time delay between injection and combustion. Because of mixing and chemical kinetic limitations, the delay always exists but may not necessarily be of the correct length to drive the instability.

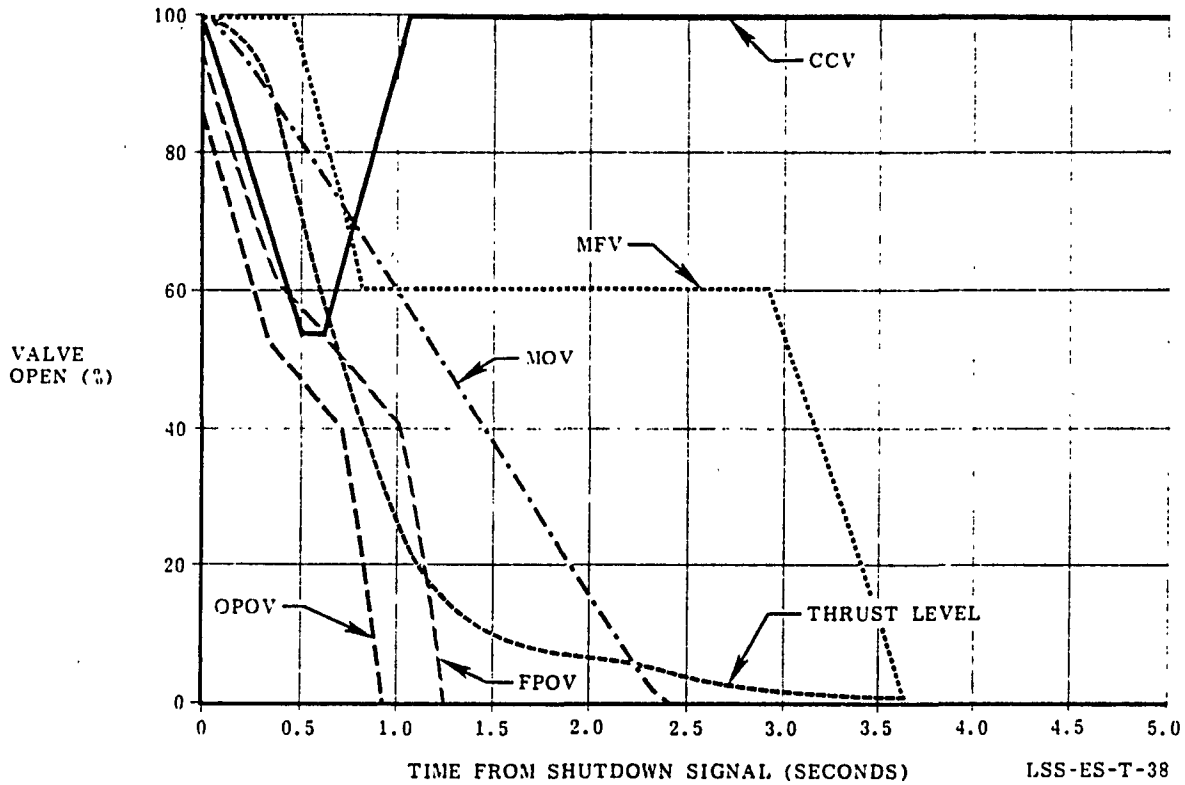

Figure 2. Typical SSME Shutdown Valve Sequence

Chugging is particularly sensitive to "softness" in the feed system which allows pulsating flows. Standing waves in the feed system and in the combustion chamber are not important. Chugging is controlled by eliminating feed system softness and by high injector pressure drops. High injector pressure drops serve to reduce the degree of change associated with a given pressure excursion level, and the high drop also represents substantial frictional loss which is manifested as damping during chug. The frictional loss is undesirable for normal operation, and high pressure drop cannot be obtained for all operating conditions, particularly startup and shutdown.

Previous analyses applied to the chugging problem have sought to identify those conditions that were conducive to an undamped or driven condition, which could potentially produce excessive pressures in the combustion chamber. Crocco and Cheng (1956) and Harrje and Reardon (1972) present lumped parameter models for chugging. The equation for conservation of mass is written and appropriate assumptions are made to represent the burning and injection rates as functions of pressure. This yields an ordinary differential equation for pressure as a function of time. An exponential solution is assumed which yields a complex characteristic equation wich is solved for the real (exponential growth or decay) and imaginary (oscillation frequency) roots. Chugging is indicated for any condition with a positive real part of the root. This type of modeling provides insight into the probability of instability, but provides no information on the limits to excursion amplitude caused by nonlinearities.

Buzz

Buzz is similar to chugging in that the feed system is an important part of the problem. In this case, however, the acoustic properties of the feed system are more important than the "softness." Standing waves are set up in the feed system that provide a pulsating flow through the injector. Energy losses in the injector are compensated by the energy release of combustion. As with chug, a system without combustion time delay would be stable.

Buzz is usually controlled by high pressure drop through the injector and by placing an acoustic cavity at the quarter wave point of the fuel line to absorb pressure fluctuations. Although pressure waves in the feed system are important, combustion chamber pressure waves are not usually considered to be significant.

Models of buzz are similar to the chugging models in that lumped parameter methods are usually used. Harrje and Reardon (1972) present buzz analysis techniques.

Scream

Scream refers to high frequency instability associated with the presence of standing waves in the combustion chamber. In this case,

the feed system does not influence the instability, and the analysis can be restricted to the main chamber. Even though the analysis only considers the main chamber, the problem is difficult since it is truly three-dimensional. Modeling consists of determining resonant frequencies for longitudinal, radial, and tangential acoustic modes and coupling this determination with a combustion model that suggests which conditions are conducive to a constructive time delay. Harrje and Reardon present models for scream. As for chug and buzz, current models simply predict whether or not the system is predisposed to instability, but provide no information on likely triggering and suppression mechanisms or an estimate of the limiting amplitude.

PROBLEM DESCRIPTION

The Space Shuttle Main Engines are stable for steady-state operation above minimum power level. On shutdown, however, the engines consistently experience a low frequency pulsation of pressure in both the fuel and oxidizer preburner combustion chambers. The amplitude, frequency and duration of the chug appears to depend on power level at cutoff and helium purge conditions. One aspect of this investigation was to determine if there was an identifiable triggering mechanism for the chug, and if chug could be eliminated. The second objective was to develop an analysis capability for predicting the occurrence and severity of chugging.

Since the chug occurs during shutdown, loss of performance is of no concern. Peak pressures during chug never exceed 1000 psia in a chamber that was designed for pressures in excess of 6000 psia; thus, chamber failure is not a concern. Because of these facts, the chugging had received little attention. Developments which linked the chug to the failure of the augmented spark igniter oxidizer line (Dexter and McCay, 1984) renewed interest in controlling the problem. Oxidizer preburner chugging has also been suggested as having a deleterious effect on turbopump bearings. There have been no catastrophic failures associated with preburner chugging.

The chug occurs only on shutdown during the helium purge of the preburner oxidizer manifolds. Figure 3 is a schematic of the fuel preburner manifold and purge system. Following shutdown, helium flows into the oxidizer manifold and clears the residual oxygen behind the preburner oxidizer valve into the preburner combustion chamber. The augmented spark igniter oxidizer line is also cleared by the helium purge. Following completion of the oxidizer purges, the fuel flow is stopped. Since chugging occurs on shutdown, the shutdown sequence is reviewed below.

Shutdown of the engines is preceded by a ramp down to a predetermined cutoff power level. For ground tests, this is usually greater than 90% thrust; for flight, cutoff usually occurs at about 65% of rated thrust. Figure 2 presents the valve closing sequence for the time

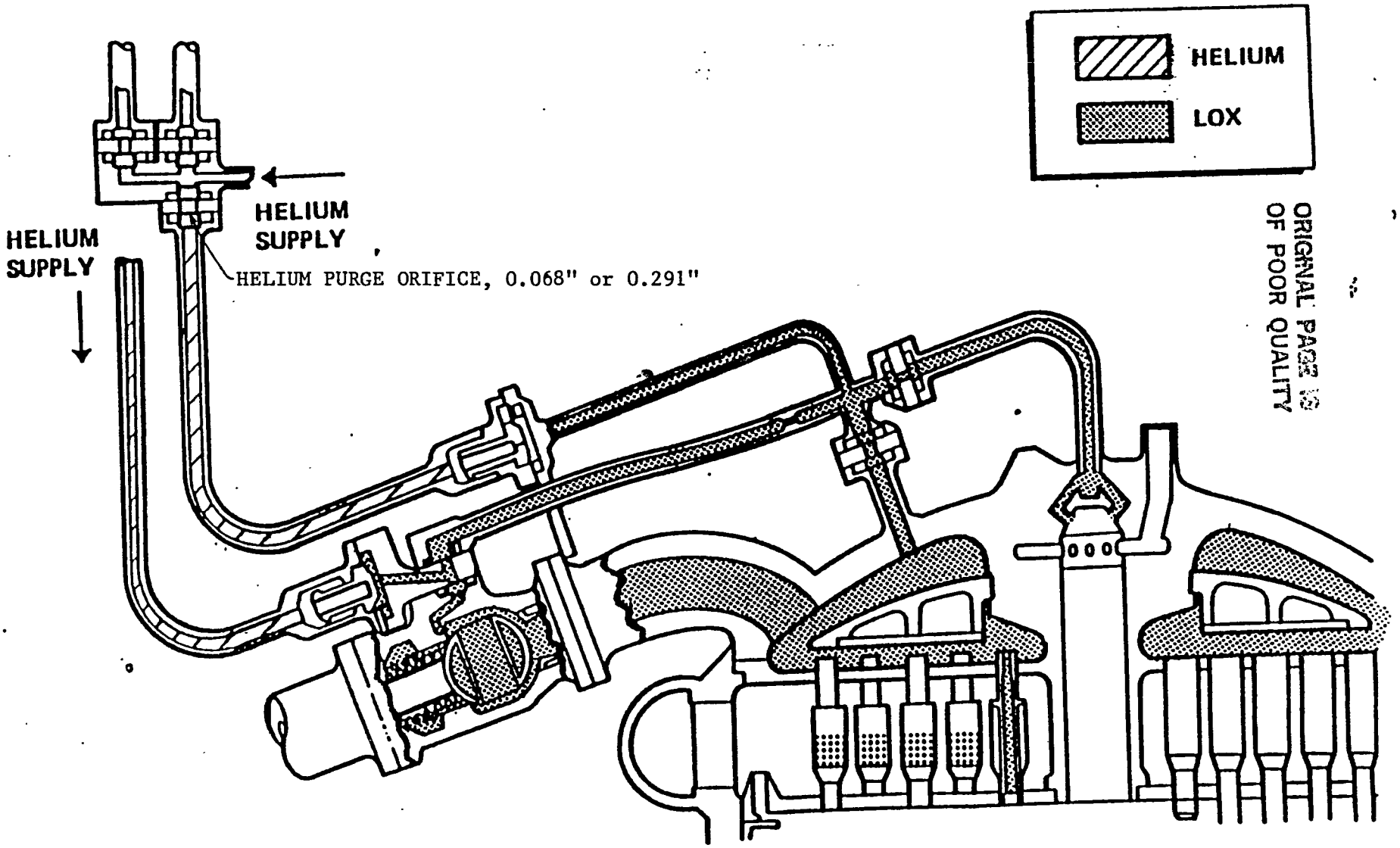

Figure 3. Fuel Preburner Manifold and Purge System Schematic

following cutoff command. Table 1 presents the effective closing times for the various valves. The valves are ball valves and, therefore, the main flow path closes well before the valve reaches a zero position indication. The valve seals are cam-operated and do not seat until the valve is almost closed. Table 1 also gives the valve characteristics for the four valves that influence the preburner system.

Figure 4 outlines typical shutdown performance. Notice that chugging begins after the FPOV, OPOV and MOV have closed. Chugging characteristics change, depending on the size of the helium orifice in the fuel preburner purge line. Chugging consistently ends between 3.0 and 3.1 seconds for both the fuel and oxidizer preburners. The chug "pause" mentioned in Figure 4 refers to a reduction in amplitude of the chug at about 2.5 seconds after cutoff. Additional details of the problem will be presented later.

APPROACH

Prior to analyzing this particular problem, the literature was reviewed to provide background for the study and to identify any useful analysis techniques. On the basis of this study, it was determined that chugging probably depended primarily on the oxidizer system since the helium purge provides the necessary softness. Other possibilities identified were:

a. Sympathetic coupling between the preburners through the fuel or hot gas injection system.
b. Oscillations induced by oscillating pressure or flow in the helium system.
c. Oscillations induced by oscillating fuel pressure.
d. Oscillations induced by pump rotor dynamics or speed variation.
e. A mechanism involving the main combustion chamber pressure feedback to the preburners through the hot gas injection system.

Two paths were used to study the problem. Data from static firings were analyzed, and a simple model incorporating the major features of the chug was developed. The primary purposes of the test data review were to determine the conditions in the preburners at the time of chugging and to identify triggering mechanisms for the chug. The data review was also expected to eliminate some of the possible mechanisms for the pressure oscillations, as well as provide guidance to the modeling effort. The model departed from previous analysis techniques in that the amplitude of the oscillations, as well as the frequency, were of interest. The model should not only assist in identifying possible solutions to this particular problem, but should be helpful in future design studies. The data review is presented first since the results of this effort guided the modeling approach.

Table 1. Valve Shutdown Characteristics

SHUTDOWN CONTROLLED BY PROGRAMMED CLOSING OF:

VALVE	TIME COMPLETELY CLOSED
OPOV	~1.5 SEC
FPOV	~2.2 SEC
MOV	~2.7 SEC
MFV	> 5 SEC

MAIN FLOW PATH CLOSED FOR PREBURNER VALVES AT 45% POSITION:
SEALS CLOSED ~ 8% POSITION

MOV: MAIN FLOW PATH CLOSED ~ 31%
SEALS CLOSE ~15%

MFV: MAIN FLOW PATH CLOSED ~ 31%
SEALS CLOSED ~ 5%

OPOV & FPOV ARE CLOSED BEFORE CHUG STARTS

MOV SEALS CLOSE BEFORE CHUG STARTS

MFV CLOSES AFTER PURGE AND CHUGGING ARE COMPLETE

CONCLUSION: CHUGGING IS

A. NOT DIRECTLY RELATED TO OR TRIGGERED BY VALVE CLOSING
B. ASSOCIATED WITH THE OXIDIZER PURGE PROCESS

TYPICAL SHUTDOWN PERFORMANCE

TIME AFTER CUTOFF	
1.4 SEC	OPOV SEALS CLOSE. OPB CHAMBER PRESSURE DROPS SMOOTHLY FROM 800 PSIA TO 500 PSIA.
1.8 SEC	HELIUM CHECK VALVES OPEN PUSHING OXIDIZER FROM OPB MANIFOLD INTO CHAMBER. CHAMBER PRESSURE RISES TO 750 PSIA AND STABILIZES. HELIUM FLOW SUBSIDES AFTER INITIAL SPIKE.
2.2 SEC	FPOV SEALS CLOSE. HELIUM FLOW IMMEDIATELY RISES. MOV SEALS CLOSE (AFTER FPOV SEALS).
2.3 SEC	HELIUM FLOW STABILIZES AS DO FPB AND OPB CHAMBER PRESSURES FOR SMALL ORIFICE TESTS. HELIUM FLOW CONTINUES TO INCREASE FOR LARGE ORIFICE.
2.3 - 2.5 SEC	CHUGGING BEGINS IN FPB: LARGE AMPLITUDE FOR LARGE ORIFICE, SMALL AMPLITUDE FOR SMALL ORIFICE. LOW LEVEL CHUGGING MAY ALSO BEGIN IN OPB.
2.5 SEC	LARGE AMPLITUDE CHUG BEGINS FOR SMALL ORIFICE FPB AND ALL TESTS. CHUG "PAUSE" OCCURS FOR LARGE ORIFICE FPB.
3 SEC.	CHUGGING ENDS

Figure 4. Typical Shutdown Performance

TEST DATA REVIEW

The eight tests chosen for detailed study are summarized in Table 2. Since a cursory review of the available preburner data had shown that the chug was sensitive to the size of the orifice in the helium purge line, four tests were chosen with small purge orifices and four with large orifice. Of the four small orifice tests, two exhibited pops (sharp spikes in pressure or acceleration usually associated with detonations) during the chug. Two large orifice tests were chosen that did not exhibit substantial chugging. No tests with small orifices exhibited low-level chugging. An attempt was made to choose all tests with a cutoff power of 90%; however, only one 90% test had low-amplitude fuel preburner chug and test 750-237 was picked as the second low-chug test. Test 750-237 cut off from 100% power. All tests were chosen from A3 test stand, engine 2308 to minimize the effects of engine variations. The number of tests that could be reviewed was limited by the time required to obtain analog data from high frequency tapes made during the tests.

Table 3 presents the analog data that were studied for each test. Additional digital data were also reviewed. Although the digital data sample rate is insufficient to trap chugging oscillations, these data were useful in establishing mean properties during chugging. Table 3 also shows six measurements considered to be crucial to the study that were not available. No fuel-system or oxidizer-system high frequency analog data were available for the tests chosen except the balance cavity pressures for the fuel and oxidizer pumps. In spite of the paucity of analog data, it was possible to eliminate all of the suggested chugging mechanisms except chugging coupled to the oxidizer/helium purge system. The triggering and suppression mechanisms were not identified.

Chug Identification

High frequency analog data is recorded as an FM signal onto magnetic tape for each test. The frequency response of the instruments (primarily pressure transducers and accelerometers) is usually from DC to about 20,000 Hz. Pump speed and flow meter data are also recorded. In analyzing a chug, the data were filtered to exclude frequencies less than 50 Hz and greater than 200 Hz. This choice was based on counted frequencies from the unfiltered tape. A subsequent review of the data suggests that a more appropriate window would be $70 < f < 500$ Hz. The high frequency recommendation is based on finding frequencies near the 200 Hz limit and concern over filter rolloff. The low frequency limit is intended to delete 60 Hz noise, which was a problem for some tests. No frequencies of significance less than 90 Hz were observed. It may also be useful in the future to delete the upper frequency cutoff, since pops are excluded by an upper bound on frequency.

In order to isolate a chug, the filtered analog data were scanned visually for an amplitude surge representing the chug. When a chug was noticed, the data were electronically plotted as pressure (or acceleration, etc.) versus time. The frequency could then be determined by

Table 2.

TEST REVIEW SUMMARY

ENGINE NO.	TEST NO.	TEST DURATION	CUT OFF CONDITIONS			FPB HELIUM ORIFICE	POP DURING CHUG	POPS AFTER CHUG	COMMENTS
			POWER (%)	FPOV (%)	OPOV (%)				
2308	750-197	320	90	77	60	0.068	YES	YES	
2308	750-198	320	90	77	60	0.068	NO	YES	
2308	750-205	320	90	77	60	0.068	NO	YES	
2308	750-209	320	90	79	62	0.068	YES	YES	
2308	750-224	50	90	77	63	0.291	NO	YES	
2308	750-234	100	90	78	62	0.291	NO	YES	
2308	750-237	300	100	80	70	0.291	NO	?	LOW AMPLITUDE CHUG
2308	750-239	300	90	77	62	0.291	NO	?	NO CHUG

Table 3.

DETAILED TEST REVIEW

B. HIGH FREQUENCY DATA FOR EACH TEST WERE STUDIED FOR

1. FPB-PC
2. OPB-PC
3. MCC-PC (AVAILABLE ON FIRST 4 TESTS ONLY)
4. MCC-HG. IN. PR (AVAILABLE ON LAST 4 TESTS ONLY)
5. HPOP BAL CAV. PR] ONLY AVAILABLE HIGH FREQUENCY
6. HPFP " " "] FUEL & OXIDIZER SUPPLY DATA
7. FPB LONG. ACCEL
8. FPB RAD. ACCEL
9. HPFP SPEED
10. ENGINE HELIUM FLOW

CRITICAL DATA NOT AVAILABLE

1. OPB OX MANIFOLD PRESSURE
2. " FUEL " "
3. FPB OX MANIFOLD PRESSURE
4. " FUEL " "
5. OPB CHAMBER EXIT TEMPERATURE
6. FPB " " "

counting peaks over a selected time segment, or counting the total number of cycles in the chug and dividing by the chug duration. Both methods were used. It was also possible to do an electronic frequency analysis and produce a power spectral density (PSD) plot. These plots provide a measure of the power represented by a given frequency. Generally, the counted frequencies and the peak frequency from the PSD were in reasonable agreement.

Typical Chug Plots

Characteristic shapes were noted for the preburner chugs under various conditions. Figures 5 through 9 are typical chug plots. All plots cover a 1-second time period beginning x seconds after cutoff; x is the last number in the upper title (3.3 for the first plot). Figure 5 shows the typical chug shape for the fuel preburner on a small orifice test (750-205). The chug begins at approximately 2.6 seconds after cutoff and extends to almost 3.1 second past cutoff. The amplitude for this plot seems to be clipped by the upper and lower bounds but is believed to be about 420 psid peak to peak. It is perhaps important to note that these plots were made with equipment and software designed for accelerometer data, and hence the format of the plots is not optimal. The principal interest in Figure 5 is the shape of the plot. Notice that a low-level chug appears to precede the main chug. The main chug blossoms rapidly, requiring only 5 cycles to reach maximum amplitude. The amplitude then decays smoothly. Frequencies in the prechug area were typically higher than for the main chug and less consistent. During the time of the chug, the digital data indicated a mean pressure that was falling slightly but centered around 400 psia. This datum is reported as read with the note that for most chugs, the chamber pressure was near 650 psia.

Figure 6 shows the OPB trace for test 750-205. Again notice the high frequency, low amplitude prechug. In this case, the prechug frequency is near 200 Hz and the amplitude may have been affected by filter rolloff. The chug develops as a series of clusters suggesting a beat behavior. As for the fuel preburner, the chug ends just before 3.1 seconds. The mean pressure here is 600 psia. The maximum peak above the mean is about 190 psid, which gives an absolute peak pressure at 790 psia. This is higher than the helium purge pressure and may potentially push fuel or combustion products back into the oxidizer manifold or the ASI oxidizer line. This characteristic is common to all tests and is believed to be at least partially responsible for the ASI line detonations on the fuel preburner. (Dexter and McCay, 1984).

Figure 7 is the FPB chamber pressure for a large orifice test (750-234). Notice the radically changed shape of the chug. Now the chug begins near 2.3 seconds and grows slowly, requiring about 25 cycles to reach maximum amplitude. The frequency is noticeably greater at the start of the chug than in the middle. At about 2.5 seconds the amplitude goes through a minimum before rising slowly again and then decaying smoothly. It is the opinion of the author that the initial prechug

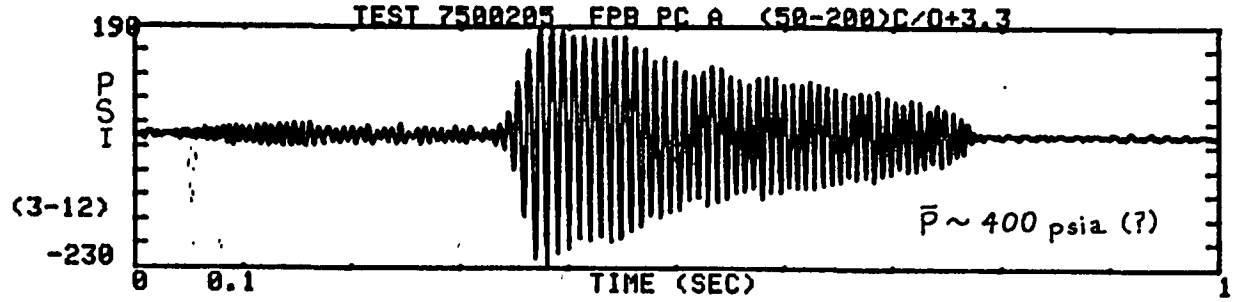

Figure 5. Fuel Preburner Chug Trace for Test 750-205

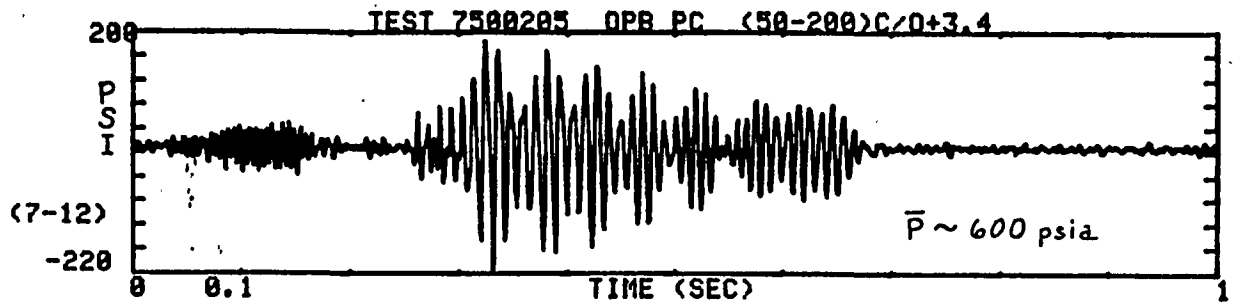

Figure 6. Oxidizer Preburner Chug Trace for Test 750-205

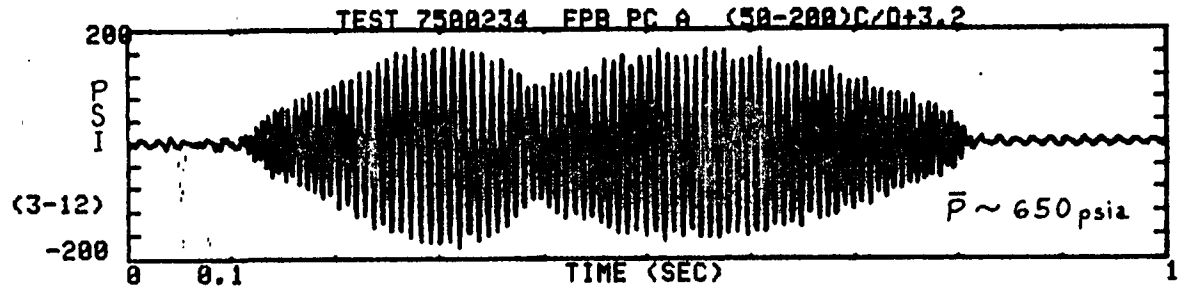

Figure 7. Fuel Preburner Chug Trace for Test 750-234

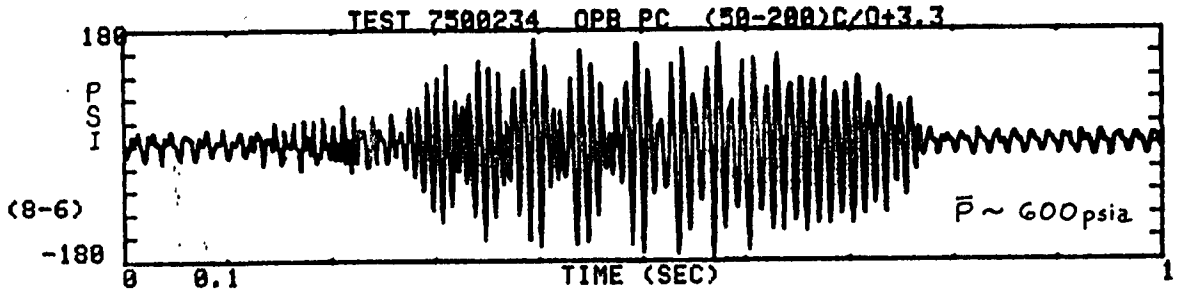

Figure 8. Oxidizer Preburner Chug Trace for Test 750-234

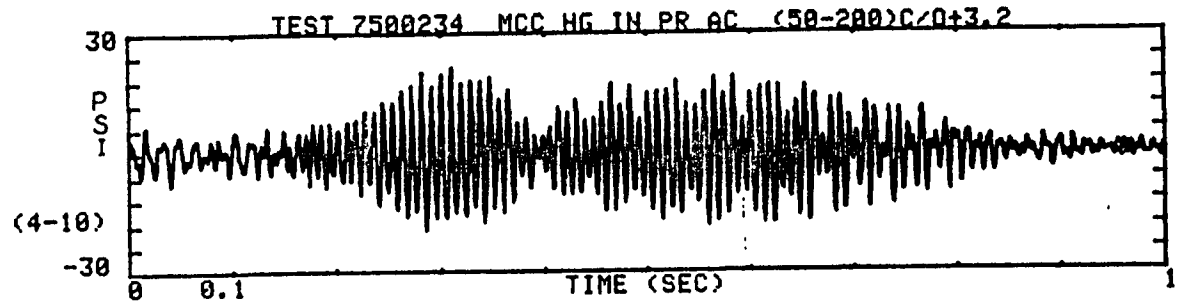

Figure 9. MCC Hot Gas Injection Pressure Chug Trace for Test 750-234

noticed in Figure 5 has been amplified by the increased helium flow. The chugging process must be nonlinear since the frequency decreases with amplitude and is less than the frequency of the prechug.

Figure 8 is the OPB chamber pressure for test 750-234. Notice that there is not an obvious prechug in this case, although it may be obscured by the 60 Hz noise. The main chug begins earlier than before but still shows the characteristic beat behavior until near the end of the chug. As before, the chug terminates near 3.1 seconds.

Hot gas injection pressure for test 750-234 is plotted in Figure 9. The amplitude is now less than 50 psid. The shape is characteristic of the FPB in that two distinct blossoms are observed. The latter section shows a slight beat behavior suggesting the influence of the OPB. The pressure measurement is taken on the FPB side of the hot gas manifold, so the stronger influence of the FPB is to be expected.

Table 4 is a summary of the data collected from the analog data for the fuel preburner. The chugs for the first four tests have fairly consistent start and stop times, frequencies and amplitudes. The mean duration is about 0.4 seconds. The three tests with a large orifice which exhibited chug have a noticeably earlier starting time and a longer duration. The amplitude is reduced slightly. Notice that the obviously anomalous amplitude from test 237 has been deleted from the average. It is difficult to reach any firm conclusions from the sparse data presented here. Carol Dexter (1984) provided the plots of Figures 10 and 11 based on a different compilation of FPB data. These figures support the longer duration, lower amplitude conclusions drawn above.

The results for the OPB are summarized in Table 5. The same general conclusions of decreased amplitude and increased duration linked to earlier start time are valid here. Test 750-237 data are again out of line with other data. This is probably due to the different cutoff power levels.

Two additional columns are shown in Tables 4 and 5. These are chug start time minus helium surge time and chug start time minus the time when the OPOV is fully closed. These represent an attempt to delete the effects of different valve positions at cutoff on chug start times. This collapses the start time data slightly, but provides very little new information except that the chug is not tied directly to the start of helium purge or the closing of the OPOV since the same changes in start time are noted here as for the times measured from cutoff.

Perhaps one of the more intriguing observations of this study is that there is an effect of the increased helium purge orifice on the OPB. The larger orifice was installed in the FPB purge line only. Predictions of helium flow show that the flow to the FBP should increase by 24% with the large orifice, while OPB flow should decrease about 4%. There should be a net increase of 18% in total helium flow. This corresponds well with the increase in measured total helium flow and

Table 4.

OXIDIZER PREBURNER TEST REVIEW SUMMARY

TEST NO.	CHUG START	CHUG END	CHUG DURATION	CHUG PAUSE	COUNTED FREQUENCY (TOTAL)	COUNTED FREQUENCY (CENTER)	MAX. AMPLITUDE (PEAK–PEAK)	CHUG START –He. SURGE	CHUG START –OPOV CLOSED
197	N. A.	N. A.	.42	**	105	108	492	?	?
199	2.70	3.070	.370	**	105	92.5	460	.89	1.170
205	2.640	3.090	.450	**	97.8	100	407	0.86	1.110
209	2.675	3.120	.445	N. O. *	98.9	95	470	0.90	1.145
224	2.52	3.025	.505	N. O. *	105.0	100.0	320	0.77	1.02
234	2.495	3.090	.595	N. O.	102.5	101.3	338	0.72	.995
237	2.41	3.025	.615	N. O.	121.9	128.3	48	.66	.90
					MAY BE NOISE				
239	2.41	3.105	.695	2.57	1ST 195 2ND 99.1	195 95	270	.697	.93
MEAN	2.55	3.075	.512		104.4		350.6	.785	
MEAN 1	2.67	3.093	.421		101.7		457.2	.883	
MEAN 2	2.459	3.061	.602		107.12 (102.2) †		244 (309) †	.712	

**LOW AMPL. CHUG PROCEEDS THIS CHUG

*SUSPECT LOW AMPLITUDE CHUG PRECEEDS THIS CHUG

† WITHOUT TEST 237

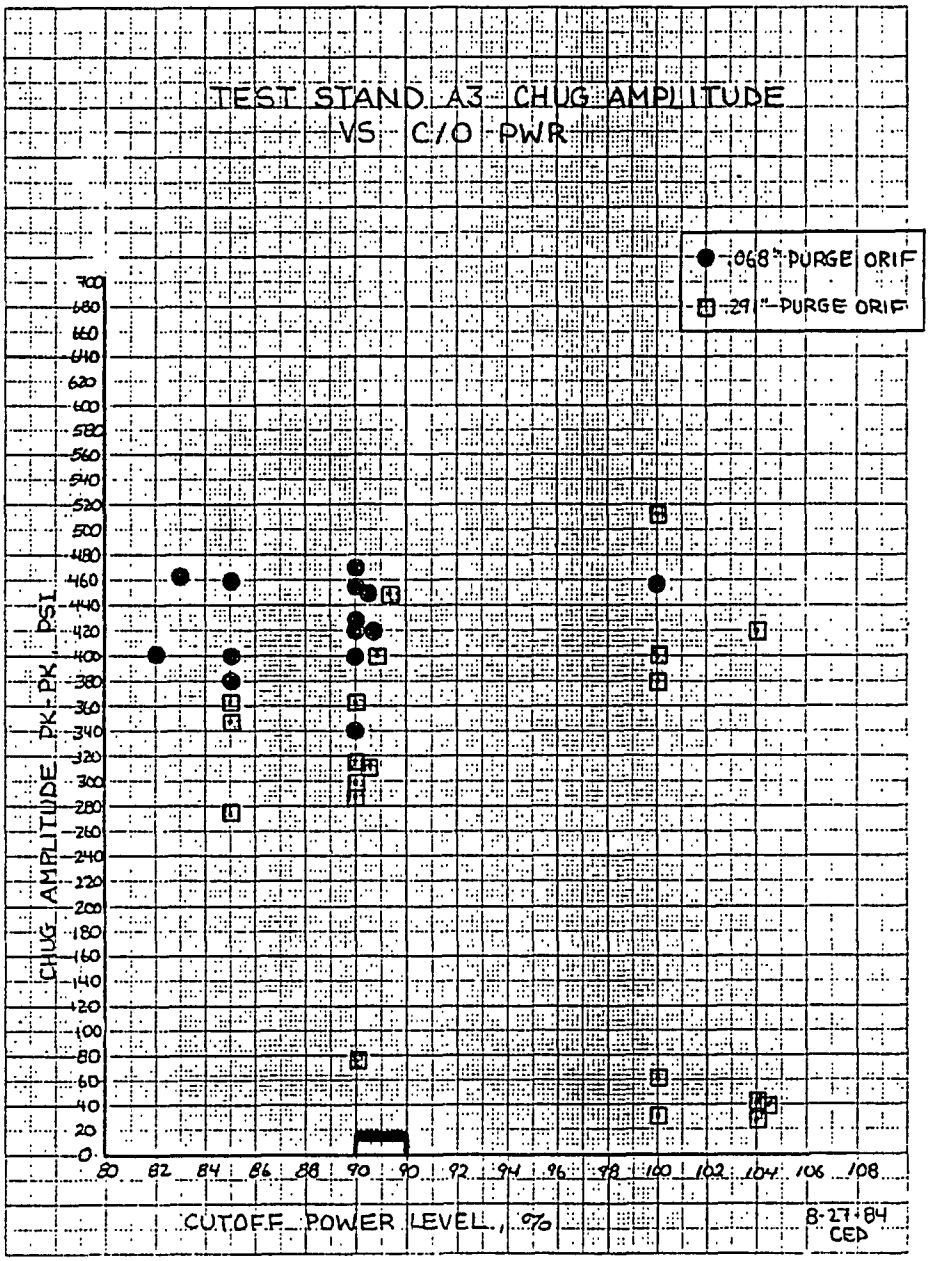

Figure 10. Fuel Preburner Chug Duration vs. Cutoff Power level

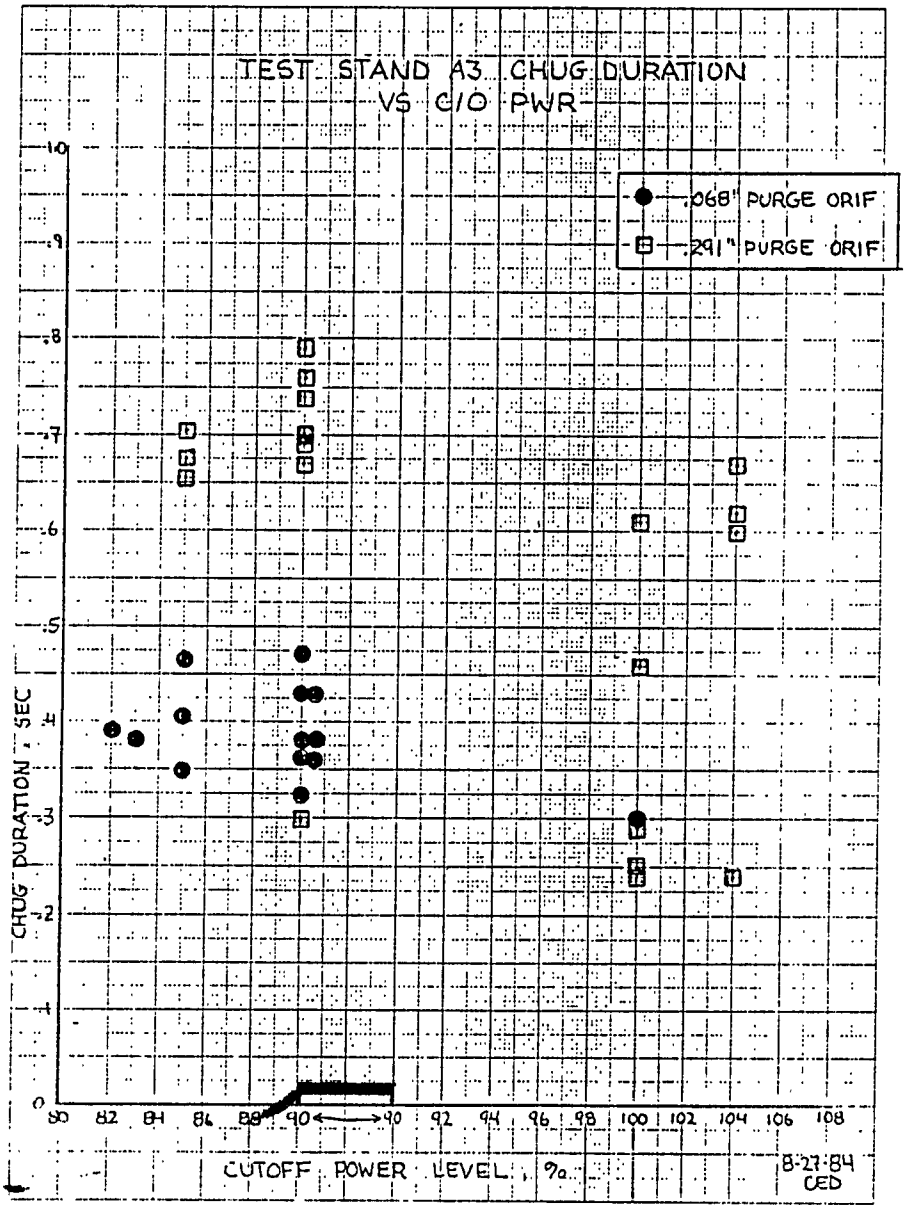

Figure 11. Fuel Preburner Chug Amplitude vs. Cutoff Power Level

Table 5.

FUEL PREBURNER TEST REVIEW SUMMARY

TEST NO.	CHUG START	CHUG END	CHUG DURATION	CHUG "PAUSE"	COUNTED FREQUENCY (TOTAL)	COUNTED FREQ. (CENTER)	MAX. AMPLITUDE (PEAK–PEAK)	CHUG START –Ho. SURGE	CHUG START –OPOV CLOSED
197	2.645	2.985	.340	†	117	115	432	.401	1.095
198	2.690	3.070	.363	†	122	118	418	.500	1.160
205	2.630	3.075	.445	*	120.2	117.5	450	.505	1.100
209	2.655	3.090	.435	*	119.5	110	420	.405	1.125
224	2.205	2.945	.740	2.505	125.7	118.3	360	.08	.705
234	2.30	3.02	.72	2.59	116	117	335	0.11	.80
237	2.425	3.04	.615	N. O.	159	136.6	33	.137	.915
239	N. O.	N. O.	N. O.	N. O.	–	–	–	–	–
MEAN	2.507	3.032	.523		125.6		400.8	.305	
MEAN 1	2.655	3.056	.396		119.7		430.0	.463	
MEAN 2	2.310	3.002	.692	2.55	133.6		342.5	.109	

LEGEND

† = INCOMPLETE DATA – NO PRE–CHUG OBSERVED, BUT MAY EXIST

* = LOW AMPLITUDE CHUG PRECEEDS THIS CHUG

N.O. = NOT OBSERVED

suggests that the orifice should have little or no effect on the OPB. Since the OPB chug is affected, increased purge flow alone must not be responsible for the difference.

Accelerometer, helium flow, and pump speed data have not been discussed since chugs were never observed. Chug-like blossoms were observed on the main combustion chamber pressure, but these appeared at random throughout the test, were low amplitude, and correlated poorly with the other known chugs. They are assumed to be noise. The pump balance cavities did show low amplitude pressure fluctuations with PSD peaks near the characteristic frequencies of their respective preburners. These fluctuations were continuously present; their relation to the chugs is unknown. Table 6 summarizes the major conclusions of the test data review, and Table 7 summarizes the implications of the data review for modeling the chugging process.

CHUG MODELING

The amplitude of the chug pressure excursion was considered to be important to the secondary effects exhibited by the shutdown chugging. The characteristic frequency was also important to understanding the causes and possible control mechanisms for the chug. The characteristic frequencies could be addressed by existing models, but the prediction of amplitudes requires a new approach. In the short time available, a complete and comprehensive model was not anticipated; rather, the approach was to utilize an existing model to determine characteristic frequencies and begin development of a model that would allow transient conditions and chug amplitudes to be predicted.

A version of AUTOCOM (Reichel et al., 1973), a combustor design code developed by Aerophysics Research Corporation for NASA, was available. This code, an extensive combustor optimization code, includes analysis of chugging using the Crocco and Cheng model. Since the program was not reliably operational, the first task was to understand the code and run some test cases. Efforts in this area were hampered by what appear to be undocumented local modifications to the code. For example, one of the primary input name lists includes over 50 parameters that do not appear in the users manual. The program is further complicated by extensive use of equivalence statements, which makes the parameter passing process between subroutines opaque. The code includes two subroutines that the users manual states specifically were deleted at NASA's request, suggesting that this version, even before modification, may not have been the final code. All this criticism leads to an admission of failure; AUTOCOM was not successfully applied to the preburner chugging problem. The program is probably capable of analyzing preburner chugging, but the number of manhours required to unravel the problems appears to be excessive. AUTOCOM should be abandoned in favor of less ambitious, more recent, and better documented programs that are available. Fewer manhours would be required to reprogram the specific parts of AUTOCOM that are useful than to revise and document AUTOCOM.

Table 6.

TEST REVIEW CONCLUSIONS

1. CHUGGING FREQUENCY FOR FPB > OPB THEREFORE; CHUGGING IS NOT SYMPATHETIC

2. START/STOP TIMES SIMILAR SUGGESTING SIMILAR TRIGGER/ SUPPRESSION MECHANISM

3. END OF CHUGGING NOT ASSOCIATED WITH COMPLETION OF OXIDIZER PURGE SINCE INCREASED HELIUM FLOW DOES NOT HASTEN END OF CHUG

4. OPB CHUG IS AFFECTED BY LARGER ORIFICE IN FPB LINE. PREDICTIONS OF HELIUM FLOW WERE

   FPB - 24% INCREASE FROM 761 TO 942 SCFM

   FPB - 4% DECREASE FROM 194 TO 186 SCFM

   NET - 18% INCREASE FROM 956 TO 1128 SCFM

   ACTUAL DATA SHOWS 15% INCREASE FROM 31.2 TO 35.9 ACFM

   HENCE: INCREASED PURGE FLOW IS NOT PER SE RESPONSIBLE FOR VARIATIONS IN CHUGGING BEHAVIOR

5. OPB CHUG SHOWS A CLEAR TREND TO LONGER DURATION AND LOWER AMPLITUDE WITH INCREASED ENGINE OPERATING TIME (TEST NO.) SUGGESTING THAT FATIGUE, WEAR OR FOREIGN MATERIAL ACCUMULATION MAY BE PARTLY RESPONSIBLE FOR CHUGGING VARIATIONS.

6. CHUGGING DURATION AND AMPLITUDE CHANGES AND ELIMINATION OF CHUGGING IN TWO CASES SUGGEST THAT CHUGGING CAN BE CONTROLLED BY RELATIVELY MINOR REDESIGN.

7. CHUGGING OCCURS DURING A RELATIVELY HIGH FUEL FLOW, THEREFORE FUEL STARVATION IS NOT LIKELY TO INHIBIT CHUGGING.

Table 7.

TEST REVIEW IMPLICATIONS FOR MODELING

1. LACK OF SYMPATHETIC OSCILLATION BETWEEN PREBURNERS SUGGESTS
    - EACH MAY BE MODELED SEPARATELY
    - PRESSURE FLUCTUATIONS IN THE FUEL SYSTEM ARE PROBABLY UNIMPORTANT.
    - PRESSURE FLUCTUATIONS DOWNSTREAM OF THE TURBINE ARE PROBABLY UNIMPORTANT TO CHUGGING CHARACTERISTICS.
2. SIMILARITY OF BEHAVIOR SUGGESTS A SINGLE MODEL COULD BE APPLIED TO BOTH PREBURNERS WITH AN APPROPRIATE CHANGE OF CONSTANTS.

One important consideration that came from reviewing the previous models for instability was that assumptions are frequently intertwined so tightly with the solution algorithm that modifications are difficult or impossible to make. On the other hand, AUTOCOM is an example of a program which, in trying to do everything, actually accomplishes nothing. To circumvent the problem, the new model was conceived as a chugging-only model with solutions being built up from very simple cases to more realistic versions. This would allow a new user to solve, say, a simple spring-mass-damper problem initially to build confidence in the code and understand the proper input. As the user's sophistication improved, more difficult tasks could be performed. The approach is an anathema to sophisticated programmers (which most engineers are not) and requires more time and storage than "production" programs. In the current era of super computers, there is no reason, other than snobbery or perhaps proprietary smoke-screening, to write programs that are opaque to the user. Sloppy and inefficient programming is not suggested, but clarity and simplicity are.

Model Description

Program TSTCHUG was designed to demonstrate the important features of chugging as it applied to the SSME during shutdown. That is, the oxidizer system still contains liquid oxygen but a helium purge is underway. The oxidizer manifold is isolated from the remainder of the oxygen system by the preburner oxidizer valve. The helium provides a pneumatic spring behind the relatively incompressible LOX while the combustion chamber provides a time-dependent pneumatic spring in front of the oxidizer "piston."

Figure 12 is a schematic of the model. Flow conditions are not considered in this initial model, and the oxidizer piston mass is assumed to remain constant. Future modifications can incorporate flow, changes in mass, and realistic combustion by replacing constants in the governing equation by functions as needed. In addition to the pneumatic springs, a linear spring is also programmed to allow the new user to solve a familiar problem. The governing equation is

$$M\frac{d^2x}{dt^2} = -Kx + \frac{C_1}{(L_1 + x)} - \frac{C_2 T}{T_0(L_2 - x)} - F_1\frac{dx}{dt} - F_2\left|\frac{dx}{dt}\right|\left(\frac{dx}{dt}\right)$$

where x is the position of the piston, M the oxidizer mass, K, C_1 and C_2 the linear and pneumatic spring constants, F_1 and F_2 the friction coefficients, and T the right-hand chamber temperature. As currently programmed, K, C_1, C_2, F_1 and F_2 are constants. T, the temperature of the right-hand chamber, is programmed to increase with the x position following a time delay. This is equivalent to burning the oxidizer τ seconds after it enters the chamber (τ is the time delay). This aspect of the program has not been adequately checked out; the results presented below use only a simple isothermal compression.

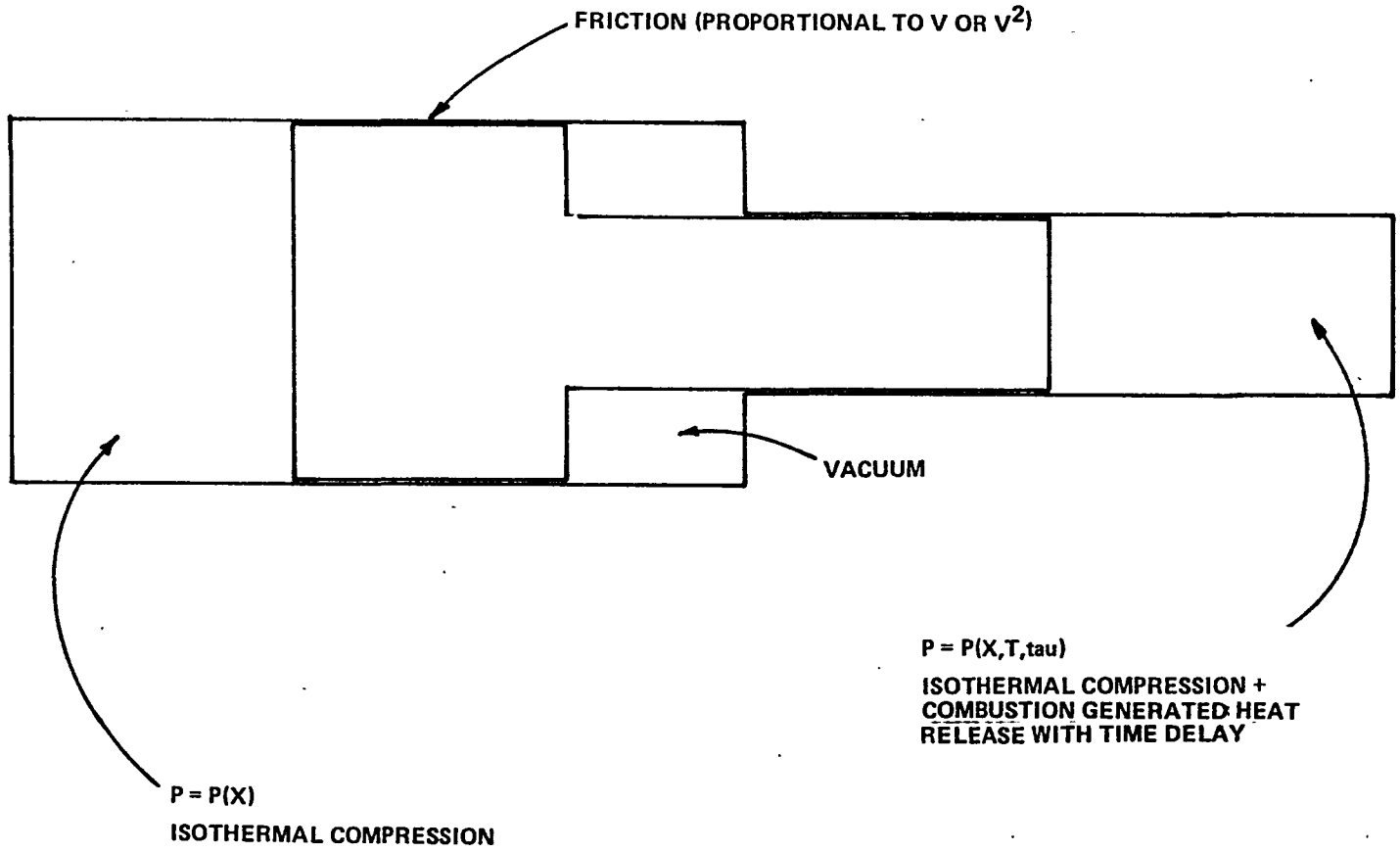

Figure 12. Model Schematic.

The governing equation was initially programmed using a single-step, first-order algorithm. This algorithm proved to be fast and satisfactory for the linear spring without damping, although time steps of 1×10^{-6} times the oscillation period were required. The method failed for cases with damping, particularly second-order damping, due to numerical inaccuracy and apparent instability. The program was rewritten to use a fourth-order Runge-Kutta single-step algorithm. This proved satisfactory for all cases tested so long as the time step was less than 1×10^{-3} times the period. Accuracy is improved by reducing step size at the expense of additional computational time. TSTCHUG was programmed in FORTRAN 77 and implemented on an HP-1000 computer. 2.5×10^{6} time steps requires about 20 minutes to complete. Since less than 100 cycles are needed to analyze a chug, most cases require substantially less time (100 cycles @ 1000 steps/cycle = 1×10^{5} steps = 1 minute).

Even for the Runge-Kutta algorithm, undamped neutrally stable cases were observed to grow in amplitude. This apparent instability is actually numerical inaccuracy, but the effect is the same, increasing amplitude. With small step sizes as suggested above, the amplitude grows in the fifth significant figure during each cycle (not each time step). The slight increases in amplitude introduced numerically should not usually be confused with the dramatic increases in amplitude which are of interest for chugging. Utilizing a multi-step method such as the Adams-Moulton fourth-order algorithm could improve accuracy and speed while at the same time providing a check on the numerical accuracy. This has not been programmed, but should be considered.

Model Application and Results

To apply the simple model, it is necessary to define the various constants in the governing equation. Of primary concern were the volumes and lengths of the chambers and the mass of the oxidizer. The characteristic frequency was found to be sensitive to all these parameters. Table 8 shows the computational procedure for each of the constants and the final value used. The volume of the helium-filled ullage increases as the oxygen mass decreases; therefore, a special series of tests was conducted with mass as a linear function of volume of the left chamber as shown in Figure 13. The chamber was assumed to be a cylinder; therefore, the length increased linearly with the volume. Because there was no driving force, all these cases exhibited decreasing amplitude. The frequency was the primary interest, however. Frequencies of 300 to 500 Hz were predicted. Figure 14 shows the frequencies predicted by the model for seven conditions during a purge. The frequencies are seen to reach a minimum near the midpoint of the purge and then increase as the purge completes. There were some tests where the end frequencies were greater than the middle frequencies, but this was not consistently observed. The shift of frequencies suggests that a triggering event would not be necessary if an oscillating disturbance were continually present: the chug would begin when the natural frequency passed through the disturbance frequency. If the trigger frequency

Table 8.

MODEL PARAMETER SELECTION

$C_1 = P_1V_1 = (5.2\times10^6\ \text{Pa})(1.64\times10^{-3}\ \text{m}^3) = 8.5\times10^3$ (maximum)

$C_2 = P_2V_2 = (3.8\times10^6\ \text{Pa})(1.0\times10^{-2}\ \text{m}^3) = 3.8\times10^4$

$L_1 = 0.25$ (maximum)

$L_2 = 0.24$

$F_1 = 0$

$$F_2 = \frac{(dp)(A)}{V^2} = \frac{(1.09\times10^7\ \text{Pa})(1.06\times10^{-3}\ \text{m}^2)}{(1.48\times10^3\ \text{m}^2/\text{sec}^2)} = 7.7$$

To compensate for no combustion, $F_2' = F_2/10 = 0.8$

M = (density)(volume) = 1.64 kg (maximum)

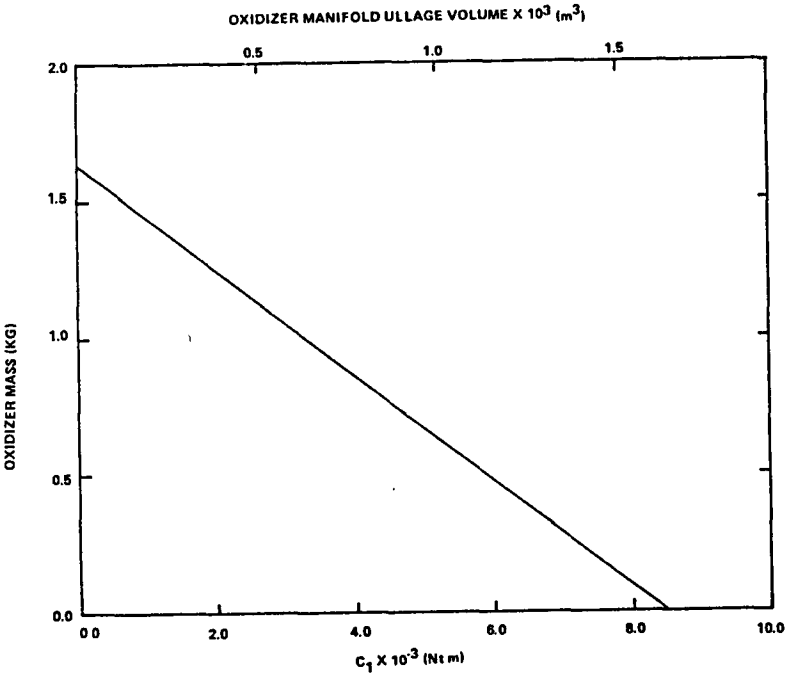

Figure 13. Oxidizer mass versus ullage volume or C_1.

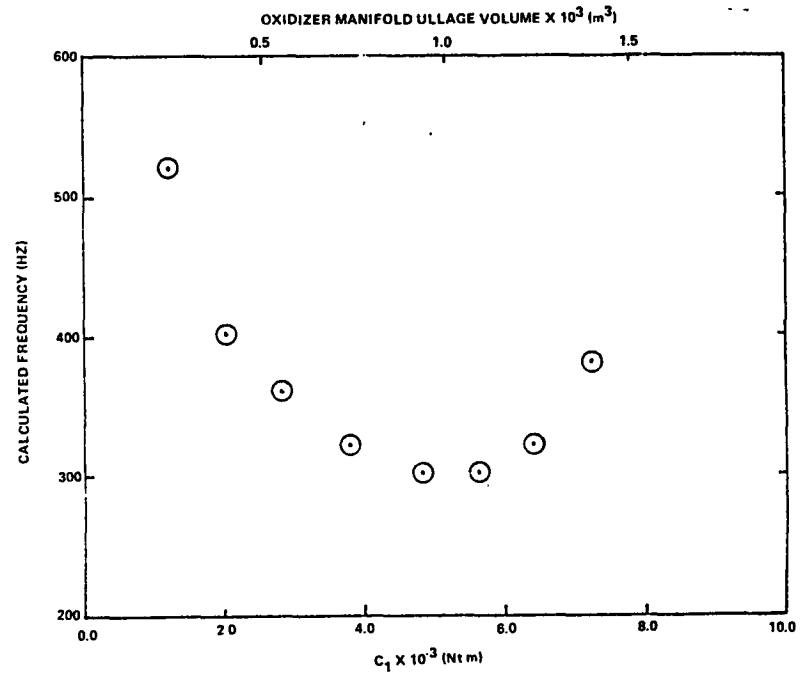

Figure 14. Predicted frequency for varying oxidizer ullage conditions.

were near the minimum frequency, this could explain the relatively constant frequencies observed. Furthermore the chug would not necessarily be combustion-driven. These predictions do not eliminate the possibity of single triggering event nor do they provide any insight on the augmentation of the pre-chug by increased helium purge flow.

The model is currently too primitive to provide much insight into the problem as evidenced by the high predicted frequencies. Part of this problem is in choosing the parameters to use for the model, part due to the absence of flow, and part due to the absence of combustion. This model does, however, have the capability of expansion to include flow and combustion, and a more careful assessment of volumes and appropriate lengths can and should be undertaken. The model has demonstrated that a numerical computation of amplitudes and frequencies is possible and potentially useful in understanding and correcting chugging problems.

CONCLUSIONS AND RECOMMENDATIONS

Table 9 summarizes the conclusions of this work. Briefly, the data suggest that chugging is not sympathetic between the two preburners, nor is triggering of one by the other indicated. The most likely cause seems to be a specific event that triggers the chugging, although the possibility that conditions change during the shutdown from stable to unstable has not been eliminated. Helium-flow surges, pump-speed surges and main combustion chamber feedback have been eliminated. Attempts to identify the triggering mechanism were not successful. Areas investigated included fuel and oxidizer valve closings, helium check valve opening, helium pressure surges, fuel pressure surges and hot gas injector pressure surges. None of these events correlated with the chugging. Chugging also changed following enlargement of the FPB helium purge orifice. The prechug increased in amplitude and blended with the main chug. The amplitude was decreased for both the fuel and oxidizer preburners at the same time that the duration was lengthened. Chugging was also found to be a function of cutoff power level and, to a lesser extent, test duration. Although the triggering mechanism was not isolated, the absence of chugs on some tests and the low amplitude of chugs on others suggests that chugging can be controlled, if not eliminated.

Additional data are needed to confirm the trends observed in the few tests reviewed. High frequency data are needed for fuel and oxidizer

Table 9.

CONCLUSIONS

FROM TEST REVIEW

1. OPB & FPB SIMILAR BUT NOT SYMPATHETIC
2. CHUGGING CHARACTERISTICS HAVE CHANGED AND MAY BE CONTROLLABLE
3. UNRESOLVED
    1. TRIGGERING MECHANISM
    2. TERMINATING MECHANISM

FROM MODEL

1. INITIAL RESULTS ENCOURAGING
2. NUMERICAL DIFFICULTIES MINIMAL WITH PROPER METHODS

manifold pressures on both preburners. These data may be difficult to obtain, but particularly the fuel pressure should be observed. Although the difference in frequencies suggests that the fuel system is not involved, it cannot be completely eliminated until fuel pressures near the preburner manifolds are observed. Temperature data at the exhaust of the preburners could help to determine if oscillating combustion is responsible for the chug or if some other mechanism is dominant.

Although no failures have occurred on the oxidizer preburner, data on chug start and stop times, frequencies and amplitudes should be gathered on a routine basis to develop the same backlog of experience that is available on the fuel preburner. Routine collection of this data will require a change in the method of data processing. All data presented in this report were processed by a technician working primarily for a pump dynamics analysis group as a favor to the author. The equipment for processing these data exists in the SSME data room but is currently inoperative. The Norland equipment should be repaired and data room personnel trained to operate it. Data from each test stand can then be automatically acquired without engineering intervention and will be available when needed. Routine use of the equipment will improve data formatting and may interest other engineers in using the capabilities.

The modeling effort should be continued and supported by a review of other programs that may be available commercially or through other NASA agencies. It appears that the emphasis of other analysis techniques has been on determining whether or not a system may chug. For this work, the system is known to chug; the analysis is intended to isolate causes, anticipate problems and suggest control mechanisms. Stability analysis programs will be useful in identifying the effect of varying propellant temperature and chamber pressure on the probability of chugging, but cannot predict the magnitude. One area of concern is that chugging seems to be more severe on high altitude shutdown than for ground testing. It is imperative then to develop a model with nonlinear behavior which can analyze this condition. The simple model presented above has shown that it is numerically possible to do such computations; the challenge now is to incorporate appropriate extensions to the model that allow accurate predictions of the chug frequency and amplitude. This development should proceed as rapidly as possible to provide an analysis tool for future generations of SSME and to determine if a simple design change or variation of operating procedure could eliminate the chugging. It will also provide guidance on the severity of any possible secondary effects, such as pushing combustion products and fuel into the oxidizer manifold.

This study has laid the ground work for a continuing study of SSME shutdown chugging. Several possible causes have been eliminated, and the changes associated with enlarged helium purge orifices examined. The model, although primitive at this time, will assist in understanding the chugging on these and future engines as it is developed from a test code to an analysis tool.

LIST OF REFERENCES

Crocco, L. and Cheng, S. (1956): Theory of Combustion Instability in Liquid Propellant Rocket Motors, Butterworths Scientific Publications, London, C.B.

Dexter, C. E. (1984), EP23, Marshall Space Flight Center, Huntsville, AL, Personal Communication.

Dexter, C. E. and McCay, T. D. (1984): "Space Shuttle Main Engine fuel preburner augmented spark ignitor shutdown detonations," NASA Technical Memorandum, Unpublished.

Harrje, D. T. and Reardon, F. H. (Eds.) (1972): Liquid Propellant Rocket Combustion Instability, NASA SP-194, National Aeronautics and Space Administration, Washington, D.C.

Reichel, R. H., Hague, D. S., Jones, R. T., and Glatt, C. R. (1973): Program Users Manual for Optimizing the Design of a Liquid or Gaseous Propellant Rocket with the Automated Combustor Design Code Autocom, NASA CR-2293, NASA, Washington, D.C.

D12

NASA/ASEE SUMMER FACULTY RESEARCH FELLOWSHIP PROGRAM

MARSHALL SPACE FLIGHT CENTER
THE UNIVERSITY OF ALABAMA

RELIABILITY OF STRUCTURAL BRITTLE MATERIALS

Prepared by:	William B. Hall, Ph.D.
Academic Rank:	Professor
University and Department:	Mississippi State University Department of Chemical Engineering
NASA/MSFC:	
Division:	Non-Metallic
Branch:	Ceramics & Coatings
MSFC Counterpart:	Ron L. Nichols
Date:	August 17, 1984
Contract No:	NASA-NGT-01-002-099 The University of Alabama

ACKNOWLEDGMENTS

The authur wishes to acknowledge the invaluable assistance of J. Daniels and F. Ledbetter in the generation of the computer program and modulus of rupture data.

RELIABILITY OF STRUCTURAL BRITTLE MATERIALS

BY

William B. Hall
Professor, Chemical Enigneering
Mississippi State University
ASEE-NASA Fellow

Ron L. Nichols
Ceramics Unit, EH34
Marchall Space Flight Center
ASEE-NASA Counterpart

ABSTRACT

Traditionally, the use of brittle materials has been avoided in demanding structural applications because of their unreliability. They have been used however, due to other desirable properties, in non-structural applicatitons or where the mechanical load is minimal. It is not surprising that there is limited knowledge or experience in design approaches for these brittle materials applications, an effort to develop an acceptable design approach is past due.

The most common method utilized today for the design approach of brittle materials is the probabilistic, which takes into consideration the flaw and stress distribution within the brittle material. It does not take into consideration the fracture mechanics effect of strength degradation while aging under a mechanical load. This project will combine the two methods, probabilistic and fracture mechanics, into a more reliable design method for brittle materials.

INTRODUCTION

Space related materials in the immediate future will be required to operate for longer periods of time, withstand more cycles of use and be usable at higher operating temperatures. Ceramic materials are prime candidates for some applications, however, ceramic materials are inherently brittle.

The major distinction between the mechanical strength characteristics of ductile and brittle materials is the unusually high degree of variability exhibited by the brittle materials.

The large scatter in strength data is due to the size of the specimen, the volume and area under stress, and flaw size and distribution in the ceramic materials.

Basically, the possible design approach utilizing brittle materials may be put into five areas:

1. Empirical
2. Deterministic
3. Probabilistic
4. Fracture Mechanics
5. Combination(s) of the above

The first two design approaches are impractical due to the large safety factors required. Probabilistic approach does take into account the flaw distributuion and stress distributiton. The normal method evalutating flaw and stress distribution. The normal method evaluating flaw and stress distribution effect on failure of ceramics is the utilization of the Weibull approach. However, the Weibull approach uses essentially instantaneous strength values, while fracture mechanics reveals that strength of brittle materials decreases with aging under a mechanical load.

Strength results for nominally identical ductile metal specimens will seldom vary more than 5% and a design strength value can be idealistically specified. Similar specimens of a brittle material however may have strength values with variation of 100% or more. It should be emphasized that this variation is not due to bad quality control, it is an inherent characteristic of a material that cannot deform plustically. Because of this variation, the average strength value is not an adequate basis for design specifications. The design engineer must think in terms of probability rather than virtual certainty. This presents a major problem in the utilization of brittle (ceramic) materials in the aerospace and space technologies, the fields which have the greatest potential of needs for the other superior properties of ceramic materials.

The current popular means of looking at probability is by the Weibull approach[1]. It is based on the weakest link theory, which assumes that a given volume of a ceramic under a uniform stress will fail at the most severe flaw. The two parameter form of the Weibull distribution function as applied to stress and probablitiy of failure is:[6]

$$P_f(\sigma) = 1 - \exp - \; -VK\sigma^m$$

where P_f is the probability of failure, is the maximum stress V = volume of the body, K = a normalizing constant, and m = the Weibull modulus which is a measure of the variability of the failure stress. The larger the value of m, the lower the scatter. Note that the above form applies to subsurface, or volume, flaws, while for surface flaws the surface subjected to the tensile stress, S, rather than the volume, V, must be considered. It is assumed that the flaw distribution is at random through the volume or surface under consideration.

It is generally assumed that if N tests are conducted and the observed fracture stress $\sigma_1, \sigma_2 \cdots \sigma_n$ are numbered in ascending order that

$$P_f(\sigma_m) = \frac{m}{N+1} \quad \text{or} \quad P_f(\sigma_m) = \frac{m-.5}{N+1}$$

Then, re-writing the first equation in the form of

$$\ln \ln (1-P_f)^{-1} = \ln VK + m \ln \sigma$$

we can plot $\ln \ln (1-P_f)^{-1}$ against $\ln \sigma$. The slope of the resultant line is m, the Weibull modulus, and VK can be determined for the intercept.

Using uniform tension equivalent or effective size rather than the actual volume or surface area, the P- relationship for an experimentally observed system may be extrapolated to any other system. The methods to do so have been discussed in the literature. Simply,

$$P_1 = 1 - (1-P_2)^{V_1/V_2}$$

where P_1 and V_1 refer to the desired configuration and P_2 and V_2 refer to the known configuration. For surface flaws, S rather than V must be considered. As a corollary to the above equation, the relation between stresses for a given probability of two members having different effective sizes is

$$\sigma_1 = \sigma_2 \left(\frac{V_2}{V_1}\right)^{\frac{1}{m}}$$

If the tested specimen has significatly smaller effective size than the size of the component, then a large number of specimens will be necessary to define the P-σ relation covering the failure stress range of interest. However, if the effective size of the specimen is approximately equal to or even larger that the component, relatively few data points are required. Linear regression analysis is used to determine the slope, or Weibull modulus, M. Rearranging $P_f(\ ) = 1 - \exp - -VK\ m$ and taking the natural logarithm,

$$\ln (1-P_f)^{-1} = VK\sigma^m$$

Thus for a given material of Weibull modulus, m,

$$\frac{\sigma_1}{\sigma_2} = \left[\frac{\ln(1-P_{f_1})^{-1}}{\ln(1-P_{f_2})^{-1}}\right]^{\frac{1}{m}}$$

Then taking σ_2 to be the mean strength, P_{f2} is, by definition, .5, we can find the probability of failure associated with any other stress level using the equation

$$\sigma_{allowable} = \sigma_{mean}\left[\frac{\ln(1-P_f)^{-1}}{\ln 2}\right]^{\frac{1}{m}}$$

However, the Weibull modulus is determined by the instantaneous breaking of a brittle material while fracture mechanics shows that the strength of a brittle material is a function of loading rate and time. Brittle materials have excellent strength when one restricts the testing to compressive loading. However, when testing the same materials in tension the strength values decrease in order of magnitude with a huge increase in the variance of the data. The most popular method of testing these materials in tension is the three point bond test, giving a breaking stress or modulus of rupture. The breaking stresses of brittle ceramics vary from 1,000 psi to 300,000 psi. This difference in strength is related to flaws in the brittle material, usually surface flaws. For example, commercial flint glass rods typically have modulus of rupture values in the range of 20,000 psi, while these same rods, when etched properly in dilute hydrofluoric acid, can have strengths in the range of 300,000 psi. Griffith was first to publish on this subject, and hed developed a failure criterion based on an energy inventory at the tip of a crack. He stated that a crack will propagate in a material provided[1]

$$\frac{\partial E}{\partial c}\left[-\frac{\pi\sigma^2c^2}{E}(1-\nu^2)+4c\alpha\right]$$

where c = crack length, σ = applied stress, E = Young's modulus, ν = Poisson's ratio, and α = energy per unit area of surface created by fracture propagation. When the above equation is solved for σ, the Griffith stress is obtained:

$$\sigma \geq \sqrt{\frac{2\alpha E}{\pi c(1-\nu^2)}} \equiv \sigma^*$$

The applied stress σ must equal or exceed the Griffith stress σ^* for the crack to propagate and rupture occur.

Glass and ceramics are noted for their inertness to most corrosive atmospheres, but they are susceptible to stress corrosion caused by water in the environment.[5] This phenomenon is known as stress corrosion static fatigue, or delayed failure. Griffith did not take this property into consideration in his determination of σ^*, the Griffith stress, in equation 2, above. It is currently believed that static fatigue results from the growth of small surface cracks until the crack length, c in equation 2, causes the stress σ to exceed σ^*, at which point catastrophic failure occurs.

The susceptibility of ceramics and glass materials to stress corrosion was first observed by Grenet[5] who observed time dependent failure and strength values that were dependent upon loading rate. One method for studying stress corrosion is to measure the velocity of macroscopic cracks as

a function of selected variables such as load and environment. These experimental determinations are generally called fracture mechanics studies. Fracture mechanaics is important in characterizing subcritical crack growth because the crack tip stresses that cause crack growth are directly proportional to the stress intensity factor.[6]

The angular (θ) and spatial (r) distribution of normal stresses at the tip of a crack, σ_n, for plane strain crack displacements can be given by:[7]

$$\sigma_n = \frac{K_I f(\theta)}{\sqrt{2\pi r}}$$

where K_I referred to the stress intensity factor. A simple dimensional analysis of a body containing a crack of length 2ℓ subjected to an applied stress, σ_e, indicates that the stress intensification at the crack must be related to σ_e and ℓ by:[7]

$$K_I = \sigma_e Y \sqrt{\ell}$$

where Y is a dimensionless constant which must depend on the variables of shape and size of specimens and the crack shape. Brittle materials will then rupture when the stress at the crack tip exceeds the bond strength. There is a stress intensity factor corresponding to this condition and this should be a material parameter.[7] Measurments of K_I for fast fracture verifies this material parameter, and it is known as K_{IC}, the critical stress intensity factor.

Two theories on delayed fracture have been published, that of Charles and Hillig along with that of Hasselman.[4] Charles and Hillig state that delayed fracture is due to a stress enhanced chemical reaction, with the parameters being stress intensity factor, environment of crack tip (moisture content), and the character of the material itself. Wiederhorn's and other's (8-10) stress corrosion studies have done much to confirm the Charles-Hillig theory. Hasselman states that the microcracks grow by the stess enhanced, thermally activated formation of vacancies at the crack tip. This theory agrees with data taken on a typical industrial glass.

Project Goal

The most common method utilized today for the design approach of brittle materials is the probabilistic, which takes into consideration the flaw and stress distribution within the brittle material. It does not take into consideration the fracture mechanics effect of strength degradation while aging under a mechanical load. This project will attempt to combine the two methods, probabilistic and fracture mechanics, into a more reliable design method for brittle materials.

Experimental Procedure

The base line data will be obtained from two sets of commercial glass rods. One set will have the normal surface finish while the other set will have a polished surface. These two sets will differentiate between fractures occuring from surface flaws (normal commercial finish) and volume flaws

(polished surface). The initial Weibull modulus will be determined from modulus of rupture data utilizing a four point bend test. The Weibull modulus will be redetermined after glass rod samples have aged under a mechanical load for periods of 3, 6, 12 and 18 months. Fifty specimens will be the number of specimens per test set to insure a statistically valid determination.

Test Results To Date:

A computer program was written to determine the Weibull modulus from MOR data generated from the four point test. This program was written for the personal computer available in the M & P Laboratory, which was a HP-85 computer. The program is given in Table 1. Four sets of 50 specimens each were broken to evaluate the computer program and MOR-Weibull modulus fit. The four sets of specimens were 28 received 6mm glass rods, 26 recieved 10mm glass rods, the 6mm rods grit blasted and the 6mm rods flame polished. The data for these speicmens are given in Figures 1, 2, 3, and 6, along with the linear regression curve for the data. The curves for the grit blasted and flame polished specimens had a "knee" in the curves. This discontinuity normally means a change in fracture source, i.e. surface to volume. This data is broken up into two sets, the values below the knee, and the values above the knee. The two sets of data from both curves were reploted, and these curves are shown on Figures 4, 5, 7, and 8. The Weibull modules M, and the average MOR is shown on each curve. It can be noted that the Weibull modulus measure variability of the data, as there is no relationship between high-low strengths and high-low Weibull modulus. However, the data does fit the curves in an excellent manner and therefore, the goals of this project should be obtainable with the outlined test procedures.

Conclusions:

1. Modulus of rupture data obtained from four point bend test do fit the Weibull distribution theory.

2. A computer program was written that determines and plots the Weibull data along with a linear regression curve.

3. Initial data was obtained from four sets of glass rods and Weibull modulus and curve obtained.

4. Long range goals of this project should be obtainable within outlined test procedures.

REFERENCES

1. W. Weibull, "A Statistical Distribution Function of Wide Applicability", J. App. Mech., 18, September, 1951.

2. M. Cohen, Internal Letter MPR-79-0227, Rockwell International, March, 1979.

3. D. W. Richerson, Modern Ceramic Engineering, Dekker, 1982.

4. S. D. Brown, "Fracture Mechanics of Cer-Vit C-101 Glass Ceramic" Final Report, ASEE-NASA Summer Faculty Fellowship Program, MSFC, 1973.

5. S. M. Weiderhorn and L. H. Bolz, "Stress Corrosion and Static Fatigue of Glass," J. Am Ceram. Soc., 53 543 (1970).

6. S. M. Wiederhorn, "Subcritical Crack Growth in Ceramics," pp 613-646, in Fracture Mechanics of Ceramics, R. C. Bredt, D. P. H. Hassleman, and F. F. Lange, eds., Plenum Press, New York, 1973.

7. A. G. Evans, "Fracture Mechanics Determination," pp 17-37, in Fracture Mechanics of Ceramics, R. C. Bredt, D. P. H. Hassleman, and F. F. Lange, eds., Plenum Press, New York, 1973.

8. S. M. Wiederhorn, "Fracture of Ceramics," Mechanical and Thermal Properties of Ceramics, J. B. Wachtmon, ed., Nat. Bur. Stand. (U.S.) Spec. Publ. No. 303, pp 217-41, 1969.

9. S. M. Weiderhorn, A. G. Evans, and D. E. Roberts, "A Fracture Mechanics Study of the Skylab Windows," 829-841, in Fracture Mechanics of Ceramics, R. C. Bredt, D. P. H. Hassleman, and F. F. Lange, eds., Plenum Press, New York, 1973.

10. E. B. Shand, "Strength of Glass -- The Griffith Method Revised," J. Am. Ceram. Soc. 48, 43 (1965).

Table 1. Computer Program for HP-85 To Determine Weibull Modulus


```
10 LIMIT 0,250,0,250
30 LOCATE 15,95,15,75
40 DIM S(50),M(50),P(50),M1(50)
   ,P1(50)
50 P=0 @ D1=0
60 X1=0 @ X2=0 @ Y2=0
70 X=0 @ Y=0 @ Z=0
80 DISP "INPUT NUMBER OF DATA P
   TS"
90 INPUT N
100 DISP "INPUT DIAMETER OF RODS
    IN INCHES"
110 INPUT D
120 DISP "DOES DATA FILE ALREADY
    EXISTS?"
130 INPUT A$
140 REM CREATE DATA FILE
150 IF A$="Y" THEN 290
160 DISP "WHAT FILE NAME DO YOU
   WANT?"
170 INPUT F$
180 CREATE F$,4
190 ASSIGN# 1 TO F$
200 REM STORE DATA IN FILE
210 FOR I=1 TO N
220 DISP "INPUT LOAD IN POUNDS"
230 INPUT P
240 PRINT# 1 ; P
250 NEXT I
260 ASSIGN# 1 TO *
270 GOTO 310
280 REM OPEN DATA FILES
290 DISP "WHAT IS FILE NAME?"
300 INPUT F$
310 ASSIGN# 1 TO F$
320 READ# 1 ; S(1)
330 REM RANK AND ORDER ARRAYS
340 FOR I=2 TO N
350 READ# 1 ; S(I)
360 I1=I-1
370 FOR J=1 TO I1
380 L1=I+1-J
390 L2=I-J
400 IF S(L1)>=S(L2) THEN 460
410 Q=S(L1)
420 R=S(L2)
430 S(L1)=R
440 S(L2)=Q
450 NEXT J
460 NEXT I
470 ASSIGN# 1 TO *
480 PRINT "ARRAY DATA FOR FILE "
   ;F$
490 FOR I=1 TO N
500 PRINT S(I)
510 NEXT I
520 REM SET UP GRAPHS
530 SCALE 8,12,-5,2
540 LAXES -.5,1,8,-5.2,1
550 REM LABEL GRAPH
560 SETGU
570 LORG 1
580 MOVE 40,5
590 LABEL "LN M.O.P."
600 DEG @ LDIR 90
610 MOVE 5,40
620 LABEL "LNLN P.O.F "
630 REM CALCULATE AND PLOT POINT
   S
640 FOR I=1 TO N
650 M(I)=S(I)*64/(3*PI*D^3)
660 P(I)=1/(1-I/(N+1))
670 M1(I)=LOG(M(I))
680 P1(I)=LOG(LOG(P(I)))
690 SETUU
700 PENUP
710 PLOT M1(I),P1(I)
720 SETGU
730 PENUP
740 RPLOT -.025,-.025
750 IPLOT 0,.1
760 IPLOT .1,0
770 IPLOT 0,-.1
780 IPLOT -.1,0
790 PENUP
800 REM PUTS SQUARE AROUND DATA
   POINT
810 RPLOT -.2,-.2
820 IPLOT 0,.5
830 IPLOT .5,0
840 IPLOT 0,-.5
850 IPLOT -.5,0
860 NEXT I
870 REM CALCULATE WEIBULL MODULU
   S, MEAN, STD DEV
880 FOR I=1 TO N
890 X1=X1+M(I)
900 X=X+M1(I)
910 Y=Y+P1(I)
920 Z=Z+M1(I)*P1(I)
930 X2=X2+M1(I)^2
940 Y2=Y2+P1(I)^2
950 NEXT I
960 B=(Z-X*Y/N)/(X2-X^2/N)
970 A=Y/N-B*X/N
980 R2=(Z-X*Y/N)^2/((X2-X^2/N)*(
   Y2-Y^2/N))
990 X1=X1/N
1000 D1=SQR((X2-N*X)^2)/(N-1)
1010 REM DRAW IN LINE OF "BEST F
   IT" WEIBULL MODULUS
1020 T1=(-5-A)/B
1030 T2=(2-A)/B
1040 SETUU
1050 MOVE T1,-5
1060 DRAW T2,2
1070 PRINT "THE COEFFICIENT OF D
   ETERMINATION IS ";R2
1080 PRINT "THE WEIBULL MODULUS
   IS ";B
1090 PRINT "MEAN MOR IS";X1
1100 END
```

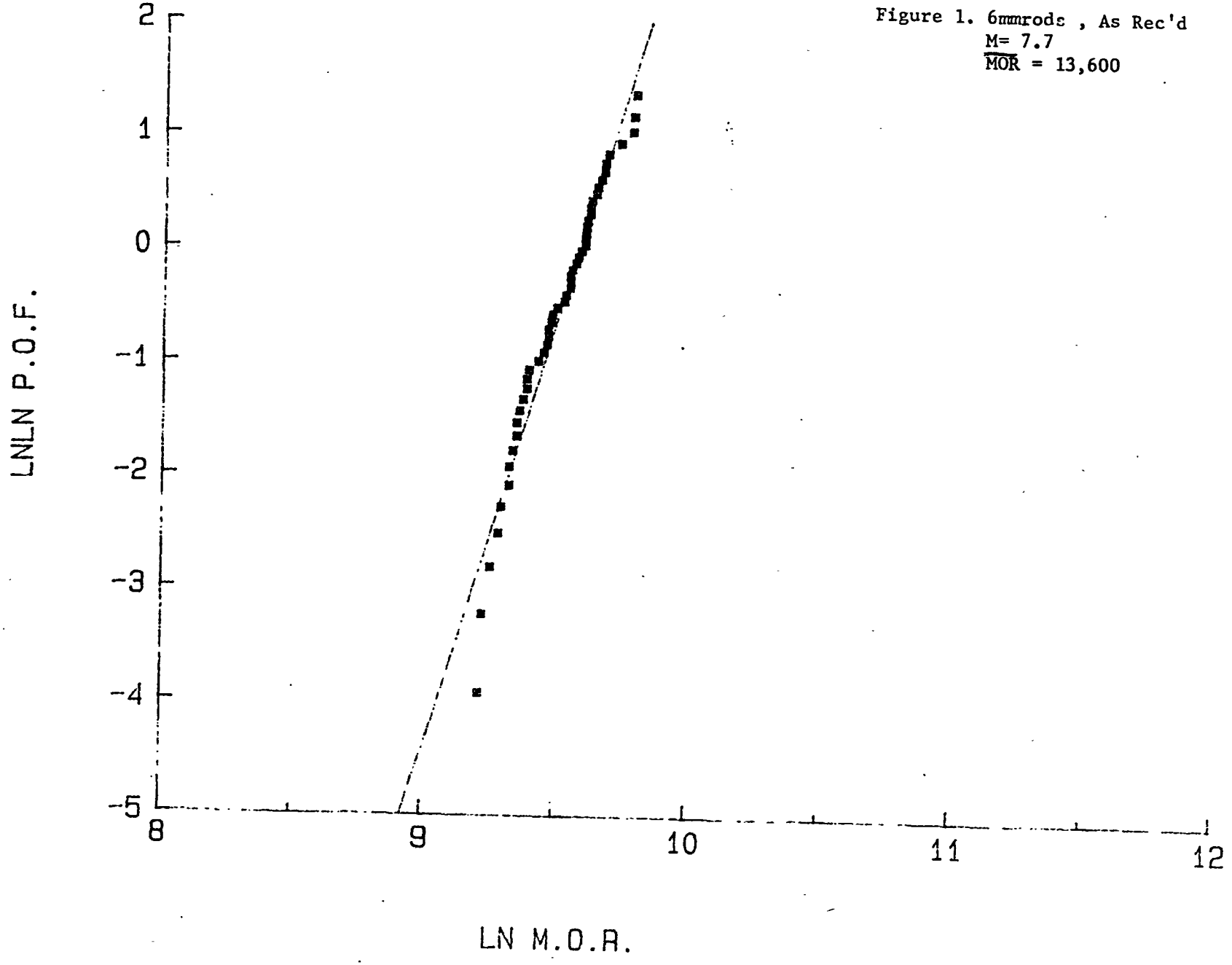

Figure 1. 6mmrods , As Rec'd
M= 7.7
$\overline{MOR}$ = 13,600

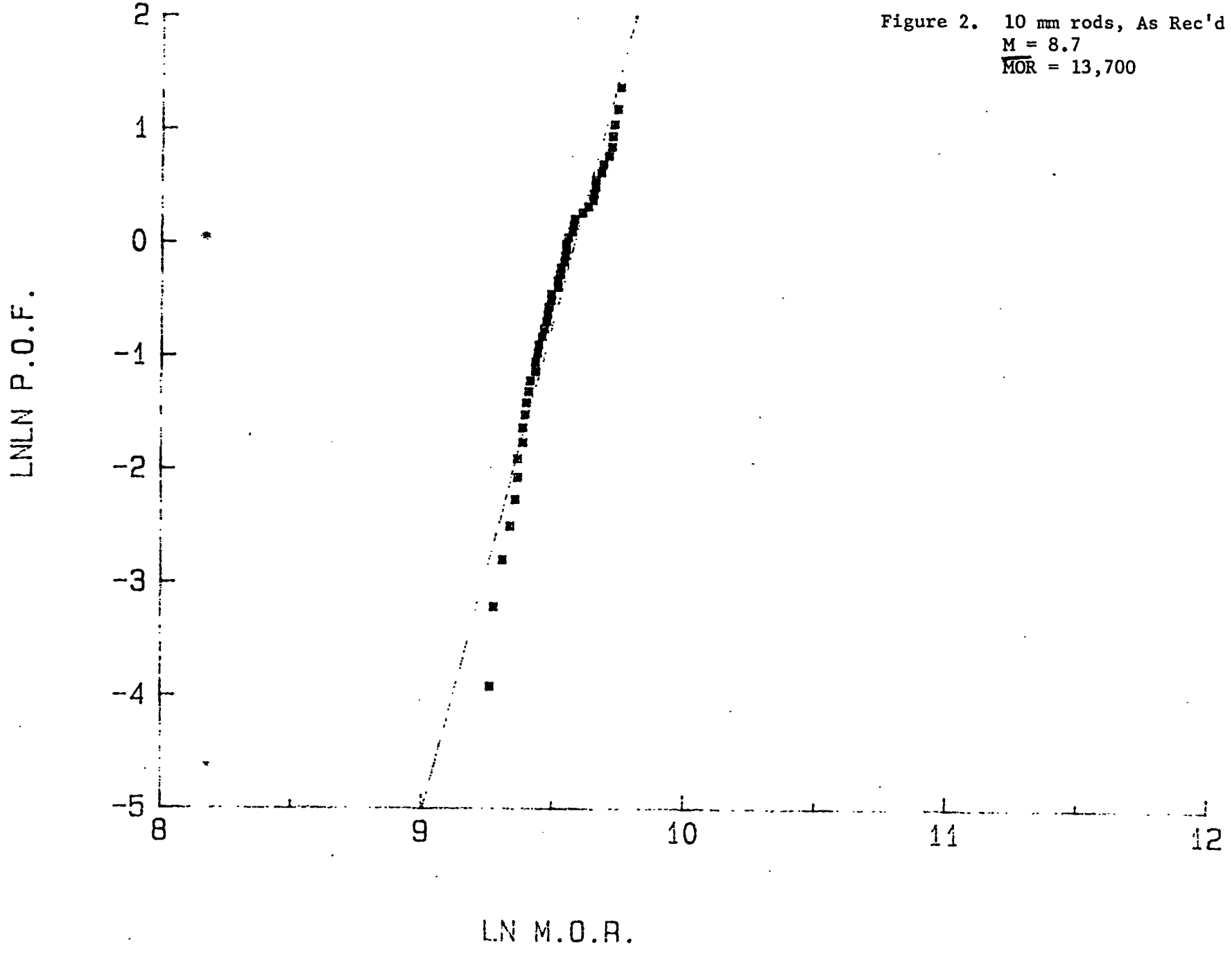

Figure 2. 10 mm rods, As Rec'd
M = 8.7
$\overline{MOR}$ = 13,700

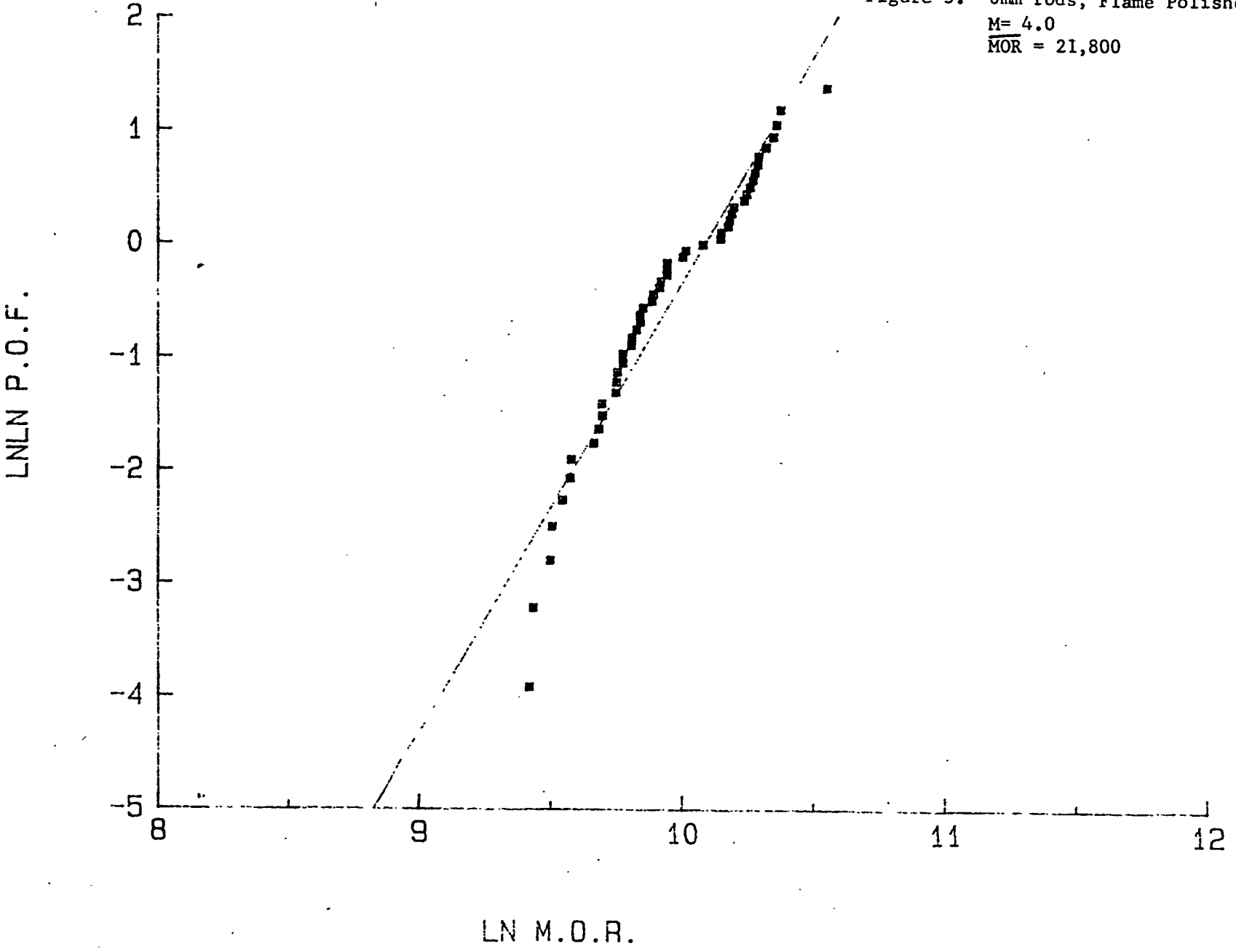

Figure 3. 6mm rods, Flame Polished
M= 4.0
$\overline{MOR}$ = 21,800

Figure 4. 6mm rods, Flame Polished, Lower
$\underline{M} = 7.0$
$\overline{MOR} = 17,200$

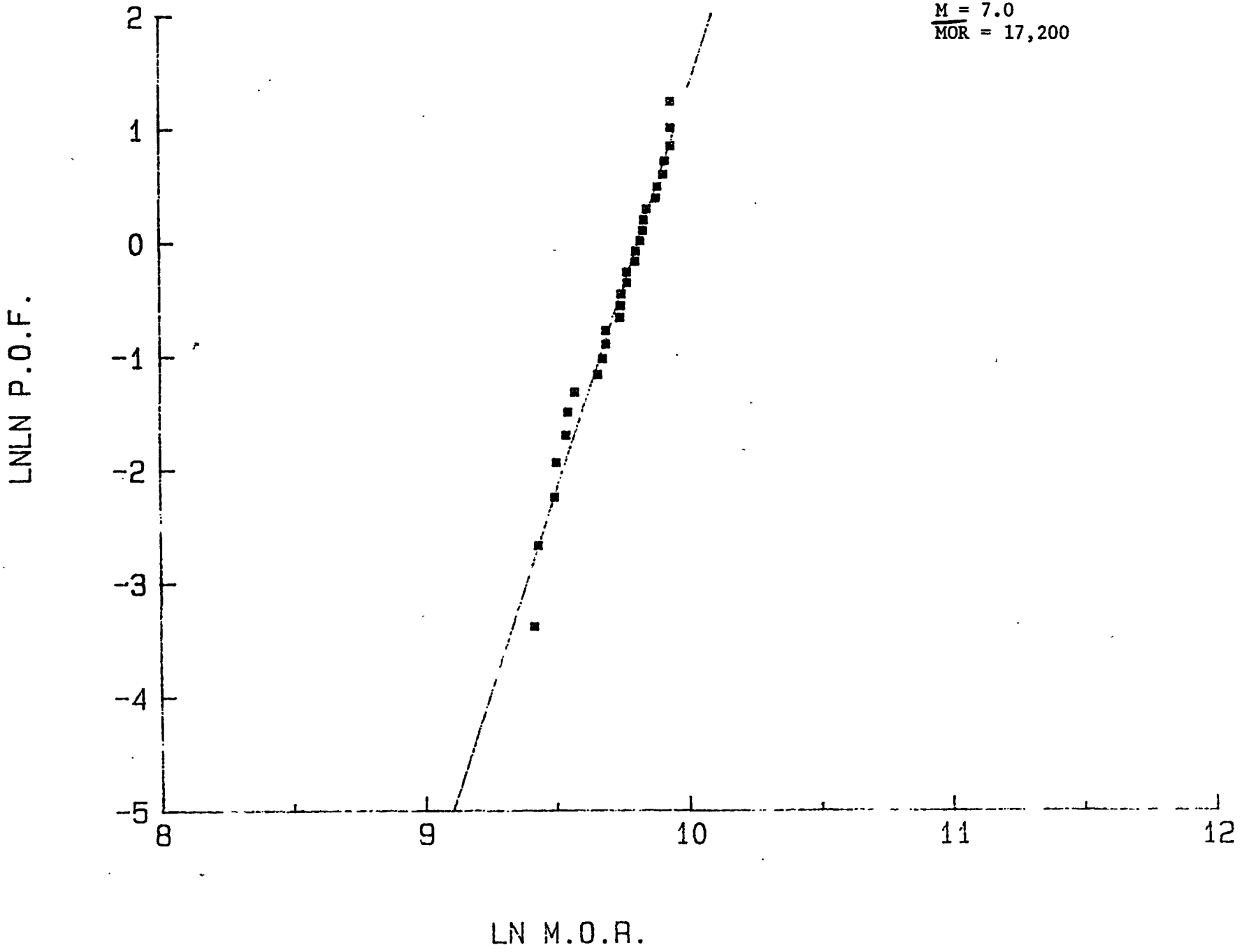

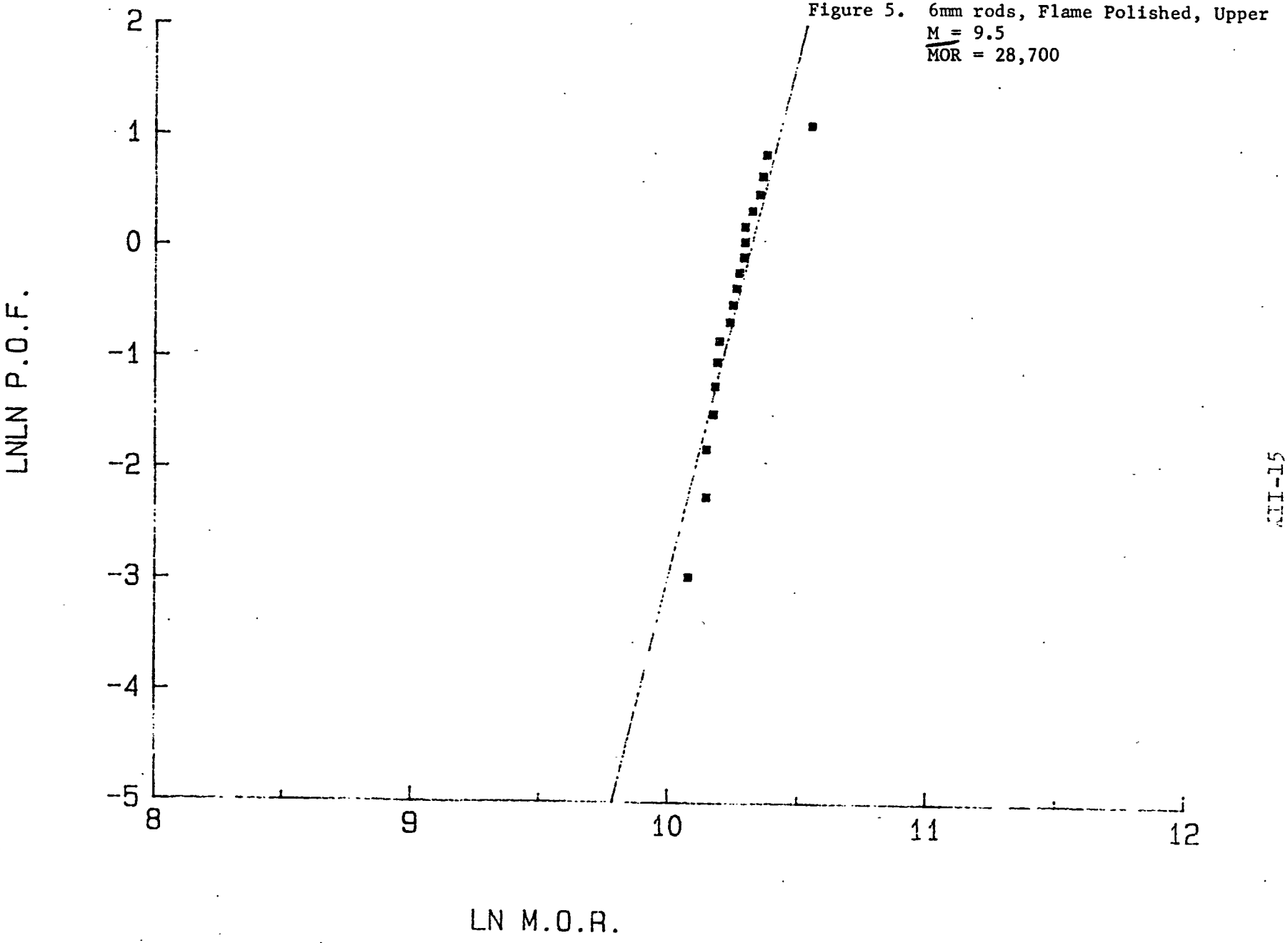

Figure 5. 6mm rods, Flame Polished, Upper
$\bar{M}$ = 9.5
MOR = 28,700

Figure 6. 6mm rods, Grit Blasted
M = 8.0
$\overline{MOR}$ = 6,180

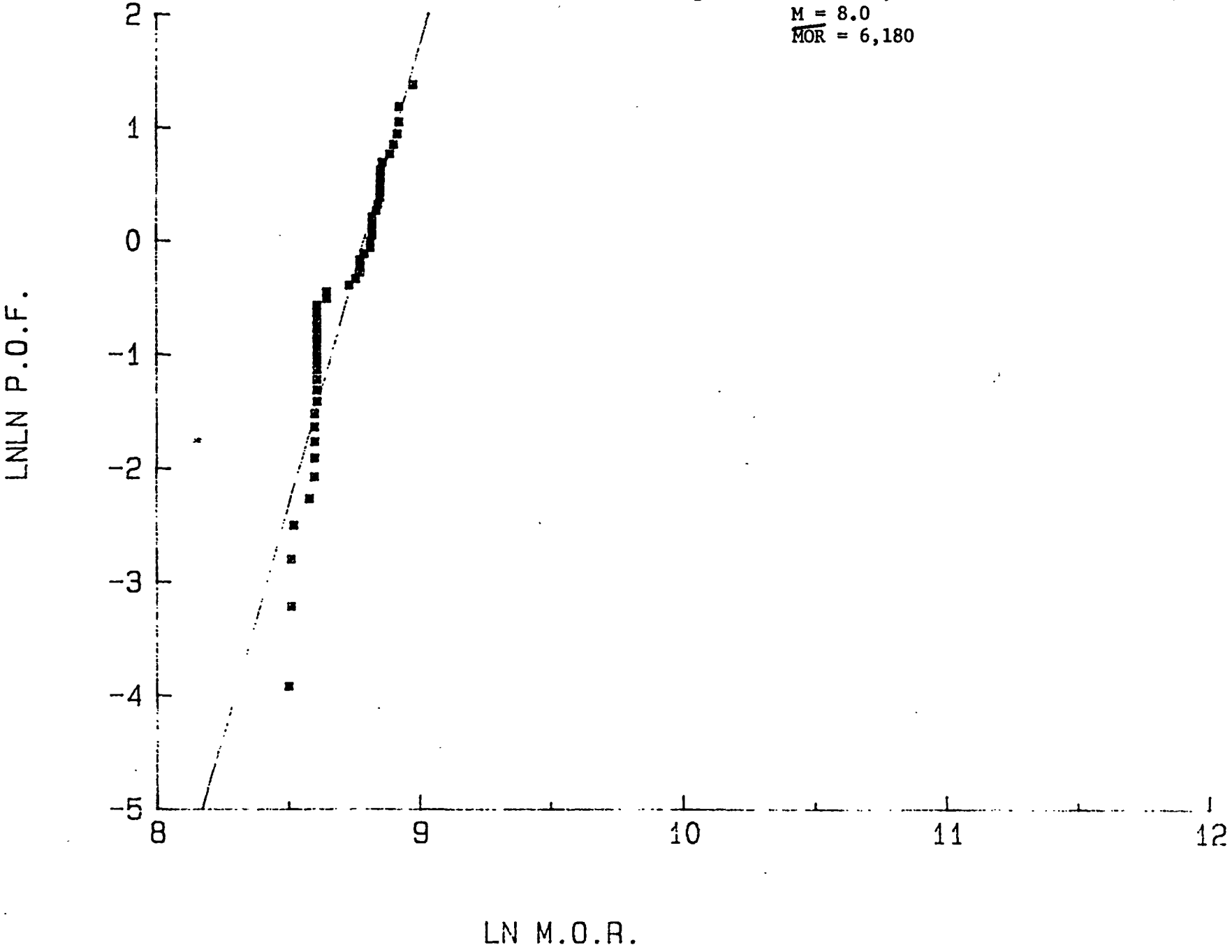

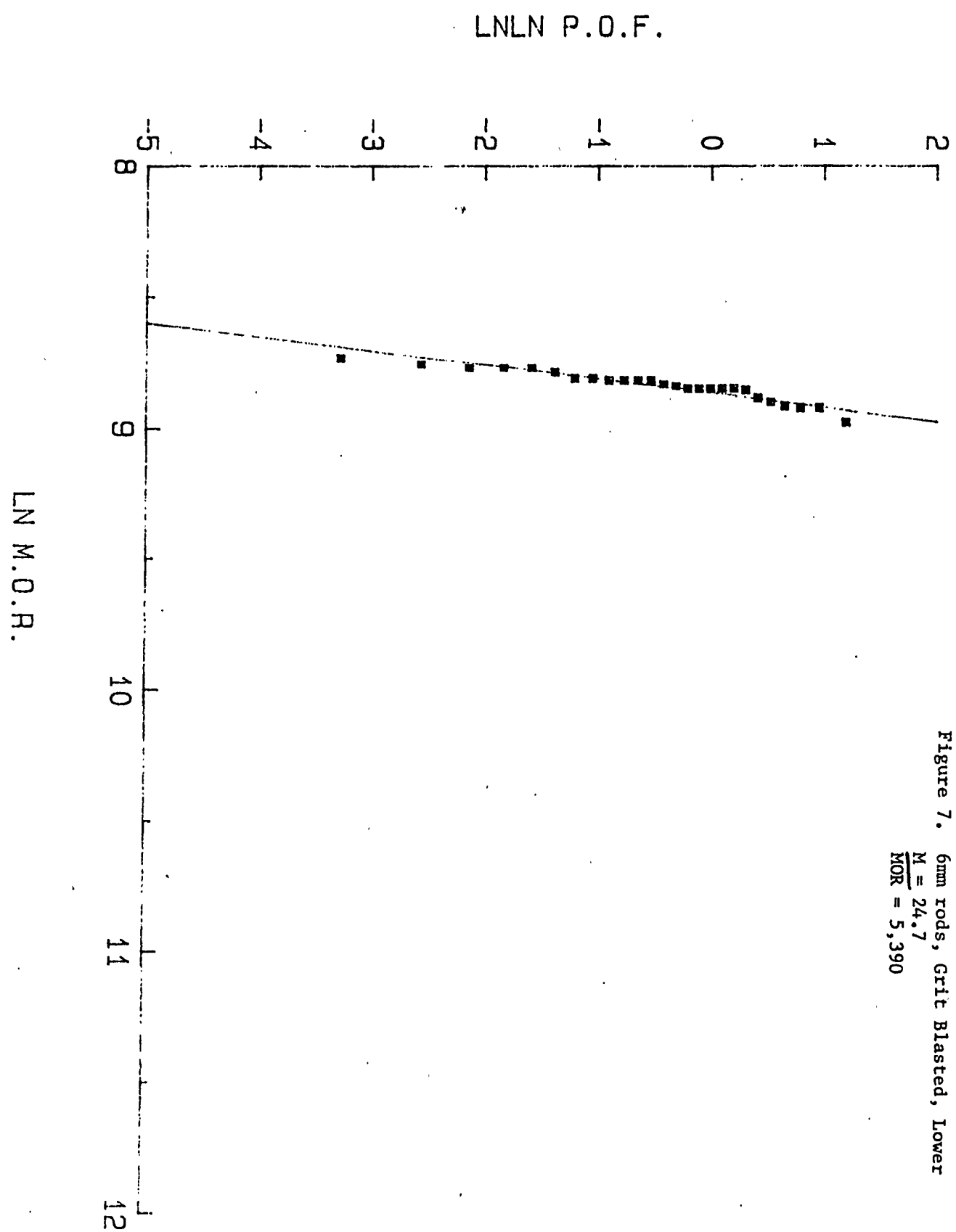

Figure 7. 6mm rods, Grit Blasted, Lower
$\overline{M} = 24.7$
$\overline{MOR} = 5,390$

Figure 8. 6mm rods, Grit Blasted, Upper
$\underline{M}$ = 18.6
MOR = 6,910

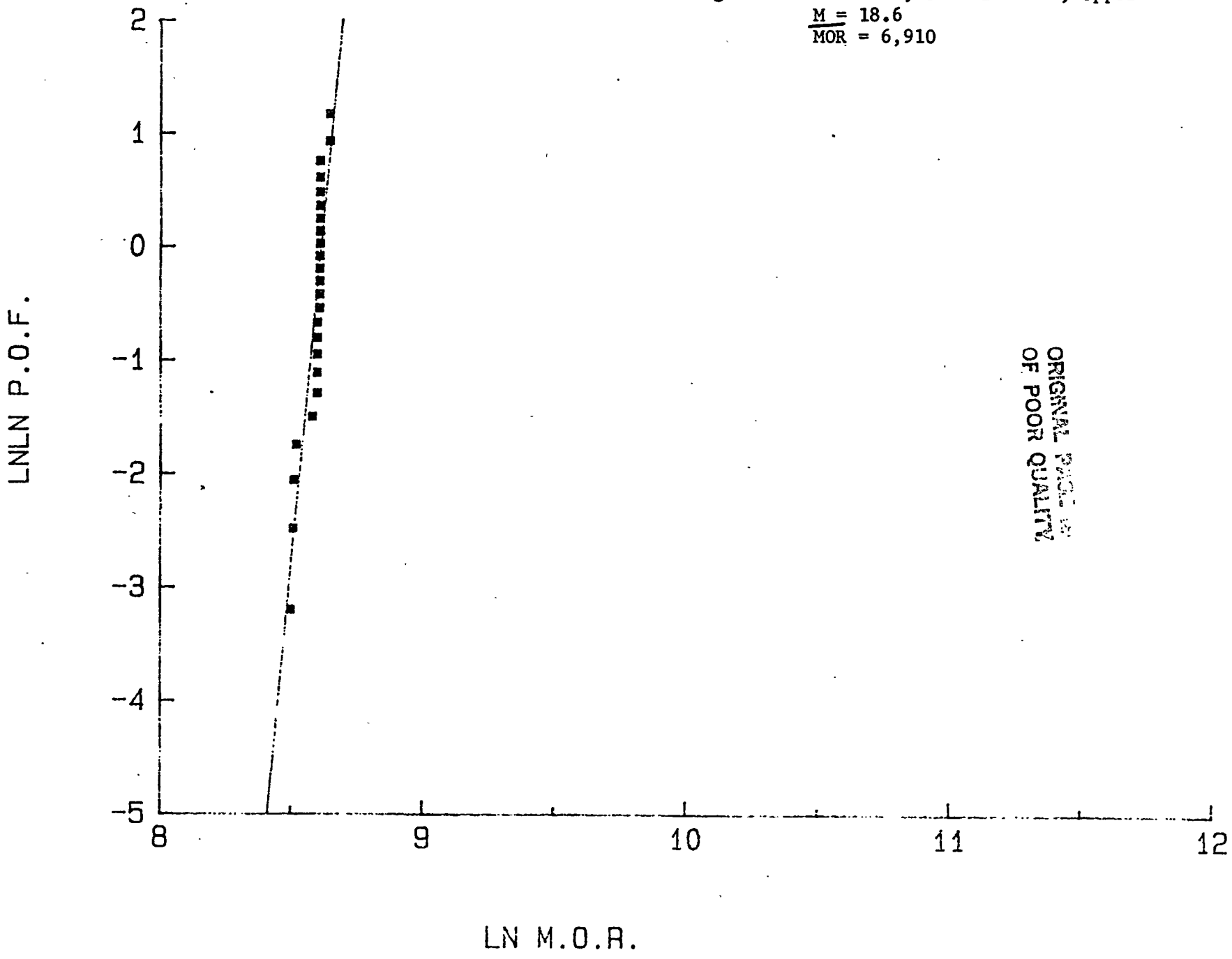

D13

1984 NASA/ASEE
SUMMER FACULTY RESEARCH FELLOWSHIP PROGRAM

MARSHALL SPACE FLIGHT CENTER
THE UNIVERSITY OF ALABAMA

HYDRODYNAMIC STABILITY PROBLEM FORMULATED BY NUMERICAL SOLUTIONS OF THE NAVIER-STOKES EQUATIONS

Prepared By:	J. M. Hyun
Academic Rank:	Associate Professor
University and Department:	Clarkson University Department of Mechanical Engineering
NASA/MSFC:	
Laboratory:	Systems Dynamics Laboratory
Division:	Atmospheric Science
Branch:	Fluid Mechanics
NASA Counterpart:	Charles Schafer
Date:	July 18, 1984
Contract No.:	NASA NGT-01-002-099 (The University of Alabama)

ACKNOWLEDGEMENTS

Sincere appreciation goes to Charles Schafer, my counterpart at MSFC, who made the arrangements for the fellowship. I also greatly appreciate the friendship and hospitality of Warren Campbell.

HYDRODYNAMIC STABILITY PROBLEM FORMULATED BY NUMERICAL SOLUTIONS OF THE NAVIER-STOKES EQUATIONS

J. M. Hyun
Clarkson University
Potsdam, New York

Abstract

The problem of hydrodynamic stability and the transition from laminar to turbulent flows are reformulated by seeking numerical solutions of the full, unapproximated Navier-Stokes equations. This method differs significantly from the well-known Orr-Sommerfeld equation approach. The oncoming laminar flow is disturbed by forced, time-dependent perturbations. The magnitudes of these perturbations are arbitrary. Then, the ensuing spatial and temporal development of the imposed perturbations on the basic flow is calculated by direct numerical solutions of the time-dependent Navier-Stokes equations. One of the main advantages of this method is its ability to simulate nonlinear processes. The detailed numerical procedure advocated by Ref. 1 is critically reviewed. As a specific application of this technique to SSME (Space Shuttle Main Engine) flow configurations, computer programs have been written for the two-dimensional flow over a backward-facing step. This numerical code will be tested for operational use as part of a continued research collaboration effort with the NASA/MSFC counterparts.

Reference
1. H. Fasel, 1976, Fluid Mech., 78, 355-383.

HYDRODYNAMIC STABILITY PROBLEM FORMULATED BY NUMERICAL SOLUTIONS OF THE NAVIER-STOKES EQUATIONS

J. M. Hyun
Department of Mechanical Engineering
Clarkson University
Potsdam, New York 13676

1. Introduction

The theoretical approach to hydrodynamic stability and transition from laminar to turbulent flows has been principally built upon the stability theory of small disturbances. The total flow field, consisting of the basic laminar flow and the imposed perturbations, satisfies the governing Navier-Stokes equations. Invoking the smallness of the perturbations, one can linearize the equations resulting in the well-known Orr-Sommerfeld equations. This procedure usually seeks the flow conditions leading to the time-wise amplifying (or decaying) perturbations, thus identifying the unstable (or stable) regime in a suitably arranged parameter space. The Orr-Sommerfeld equation approach has been firmly established; several of its mathematical solutions for simple geometries have been shown to be consistent with the available experimental data (Ref. 1).

It is important to recognize that the Orr-Sommerfeld equations are limited to the linearized analysis of small-amplitude disturbances. Therefore, the onset of instability can be predicted by using the linear stability theory. However, the ensuing development of flow into finite-amplitude disturbances can not be understood by

this theory. Another major restriction for the application of the Orr-Sommerfeld equations is that the basic flow has to be parallel.

In an effort to overcome the aforementioned difficulties of the Orr-Sommerfeld equation approach, a numerical method has been proposed recently to investigate the hydrodynamic stability and the associated perturbation-amplication processes (Ref. 2). The method calls for direct numerical solutions to the unapproximated Navier-Stokes equations governing the total flow field. The oncoming laminar flow is disturbed by forced time-dependent perturbations. Then, in a finite domain downstream of the point of the introduction of the forced perturbations, the spatial and temporal evolution of the total flow is calculated by numerically solving the time-dependent Navier-Stokes equations. The amplitudes of the imposed perturbations are arbitrary; this enables us to simulate the nonlinear processes. In addition, the basic flow is not required to be parallel.

The idea is quite straightforward and not new. This kind of direct numerical simulations was not feasible in the past due to the inadequacy of the computers to handle the vast amount of numerical computations. With the advent of modern computers and the refined numerical analysis schemes, this procedure becomes better suited for complex flow configurations.

In this report, the method advocated by Ref. 2 is critically reviewed. Possible extensions to flows with significant heat

transfer will be considered. As a specific application, numerical codes have been written for the two-dimensional flow over a backward-facing step, a flow configuration of interest to SSME (Space Shuttle Main Engine) flow analyses.

2. The numerical model

The Navier-Stokes equations are written in terms of the vorticity ω and the velocity components (u, v) in dimensionless form:

$$\frac{\partial \omega}{\partial t} + u\frac{\partial \omega}{\partial x} + v\frac{\partial \omega}{\partial y} = \frac{1}{Re}\left(\frac{\partial^2 \omega}{\partial x^2} + \frac{\partial^2 \omega}{\partial y^2}\right), \tag{1}$$

$$\frac{\partial^2 u}{\partial x^2} + \frac{\partial^2 u}{\partial y^2} = \frac{\partial \omega}{\partial y}, \tag{2}$$

$$\frac{\partial^2 v}{\partial x^2} + \frac{\partial^2 v}{\partial y^2} = -\frac{\partial \omega}{\partial x}, \tag{3}$$

$$\frac{\partial T}{\partial t} + u\frac{\partial T}{\partial x} + v\frac{\partial T}{\partial y} = \frac{1}{Pr \cdot Re}\left(\frac{\partial^2 T}{\partial x^2} + \frac{\partial^2 T}{\partial y^2}\right). \tag{4}$$

In the above, the nondimensionalization has been made by using H, u_∞, T_∞ as the characteristic length, velocity, and temperature, respectively. The Reynolds number is $Re \equiv u_\infty H/\nu$.

The first task is to compute the undisturbed basic flow over the step (see Fig. 1). This can be accomplished by solving (1)-(3) in the calculation domain with $\partial\omega/\partial t$ eliminated. The calculation domain is chosen such that the depth is at least

three times the boundary layer thickness and the length four times the wavelength of the disturbance. Along the upstream boundary, the oncoming flow is taken to be the Blasius profile. On the boundary wall along the solid surface, no-slip boundary consitions are imposed. On the upper boundary, the free stream values are assumed. One of the delicate point is the specification of the boundary conditions at the downstream boundary. Ref. 2 suggests that the second derivatives of the flow variables with respect to X vanish at the downstream boundary.

After the basic flow has been determined, one computes the time-dependent vorticity and velocity field as solutions of the unsteady Navier-Stokes equations. At the inflow boundary, sinusoidally-varying perturbations of arbitrary amplitudes are forced upon the basic flow field. Thus, the total flow field at the inflow boundary is represented as

$$u(0, y, t) = U_B(y) + a\, U_A'(y) \cos(\beta t),$$

$$v(0, y, t) = V_B(y) + a\, V_A'(y) \cos(\beta t + \pi/2),$$

$$\omega(0, y, t) = \Omega_B(y) + a\, \omega_A'(y) \cos(\beta t).$$

where u, v, ω are the total fields, U_B, V_B, Ω_B are the basic flow profiles, and U_A', V_A', ω_A' are the perturbation fields. The amplitude a of the perturbations is in principle, arbitrary. The frequency of the sinusoidal perturbations is given by β.

In order to facilitate the computations, the profiles u_A', v_A', ω_A' are assumed to be given by the solutions of the linear stability analyses for the boundary layer flow over a flat plate (Ref. 3). The difficult job of specifying a consistent set of boundary conditions, especially at the downstream outflow boundary, remains to be examined further. As an initial step, the boundary conditions recommended by Ref. 2 could be used.

3. Discussion of the model

The boundary conditions used in Ref. 2 for the boundary layer flow over a flat plate were shown to produce accurate results for that problem. It is not clear a priori that the same set of boundary conditions would give equally valid results for different flow situations. The potential problem areas are, among others, the upper boundary, the downstream outflow boundary, and the convex corner on the step. Several different numerical techniques for the convex corner should be evaluated (Ref. 4).

As long as the buoyancy effect is smaller than the effect due to forced convection, the temperature equation is decoupled. In this case, therefore, (4) can be solved separately after the velocity field has been determined. This numerical model can be easily modified to accommodate the effect of natural convection.

Since the present method requires accurate numerical solutions to strongly time-varying Navier-Stokes equations, proper numerical schemes are of paramount importance. A fully implicit finite-difference scheme will be used. Finite-differencing

of several illustrative terms is shown below:

$$\left.\frac{\partial \phi}{\partial t}\right|_{i,j}^{n} = \frac{3\phi_{i,j}^{n} - 4\phi_{i,j}^{n-1} + \phi_{i,j}^{n-2}}{2\Delta t} + O(\Delta t^2),$$

$$\left.\frac{\partial \phi}{\partial x}\right|_{i,j}^{n} = \frac{\phi_{i+1,j}^{n} - \phi_{i-1,j}^{n}}{2\,\Delta x} + O(\Delta x^2),$$

$$\left.\frac{\partial^2 \phi}{\partial x^2}\right|_{i,j}^{n} = \frac{\phi_{i+1,j}^{n} - 2\phi_{i,j}^{n} + \phi_{i-1,j}^{n}}{\Delta x^2} + O(\Delta x^2),$$

where i, j, n denote the indices for x, y and time, respectively. The boundary conditions will be discretized using second-order accurate, one-sided difference approximations.

Actual solution schemes for the finite-difference algebraic equations will be based on the line-by-line Thomas algorithm. Iterations will continue along a vertical grid line, while the global sweep moves in the horizontal direction. Based on previous experience of the present author, a strong under-relaxation will be needed for convergence. Even with a strong under-relaxation, it is not clear whether this proposed numerical model would yield satisfactory convergence for large values of the Reynolds number. It is expected that exhaustive numerical experiments will be required for stable numerical computations.

4. Future work

A FORTRAN code has been written for the specific problem of the laminar flow over a backward-facing step. The code has been loaded into the Clarkson University's IBM 4341 Computer. A

thorough debugging and code refinement will follow. It is planned that the code will be used to examine the two-dimensional Poiseuille flow over a backward-facing step as a sequel to the present problem.

References

1. Schlichting, H. 1966 Boundary Layer Theory. McGraw-Hill.
2. Fasel, H. 1980 In "Computational Fluid Dynamics". Hemisphere Publ. Corp.
3. Jordinson, R. 1970 J. Fluid Mech. 43, p. 801.
4. Roache, P. 1972 Computational Fluid Dynamics. Hermosa Publ.

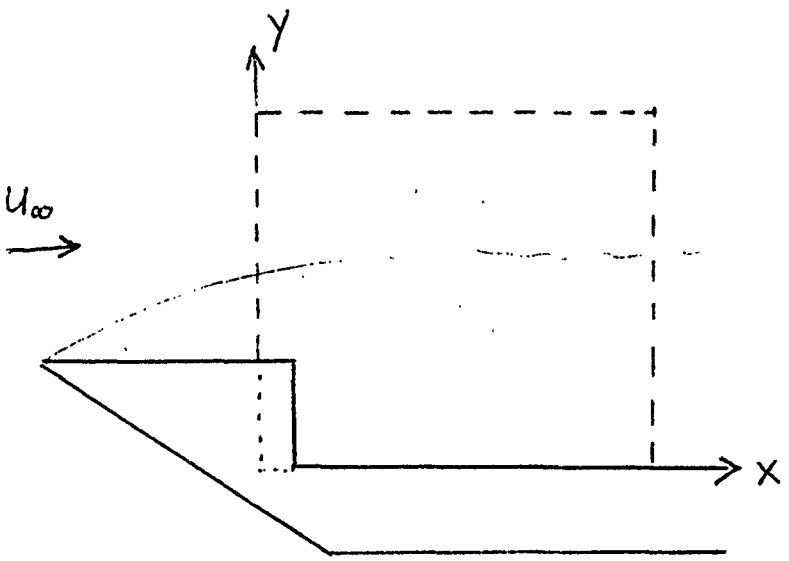

Fig. 1. Flow geometry

1984

NASA/ASEE SUMMER FACULTY RESEARCH FELLOWSHIP PROGRAM

MARSHALL SPACE FLIGHT CENTER
THE UNIVERSITY OF ALABAMA

THE STRENGTH AND CHARACTERISTICS OF VPPA WELDED 2219-T87 ALUMINUM ALLOY

Prepared by:	Wartan A. Jemian, Ph.D.
Academic Rank:	Professor
University and Department:	Auburn University Mechanical Engineering and Materials Engineering
NASA/MSFC:	
Laboratory:	Materials and Processes
Division:	Process Engineering
Branch:	Metals Processes
NASA Counterpart:	W. A. Wilson
Date:	August 24, 1984
Contract No.:	NASA-NGT-01-002-099 (The University of Alabama)

ACKNOWLEDGEMENTS

The author thanks Mr. W. A. Wilson for providing this opportunity and for help in many ways. His generous encouragement and support are deeply appreciated. This project has been one of those "hoped for" research situations where the observations and experimental results lead directly to a definite conclusion. In this instance, the size of the interdendritic particles accounted for a variation in weld strength.

Mr. Carl Wood was most helpful in providing assistance in many useful ways. His friendship will always be remembered. Vanita Brown made the word processor available and useful, sharing the use of her office so that this report could be finished on time. Messrs. E. Bayless, Bobby Rowe, Dr. A. C. Nunes and Miss L. Johnston were most helpful in providing information and in discussions. J. Sexton and Jeff Norris welded the panels, cut and prepared the test samples, willingly putting up with a number of special requests. W. DeWeese prepared and photographed the sections for metallurgical analysis and G. De Ramus performed the mechanical testing. Mr. Poorman, who is recently retired, and Dr. C. Lovoy also provided helpful insights and Dr. J. W. Montano assisted in analyses and in locating records of past, related work. Finally, J. Coston and D. Nicholas must be thanked for the hours spent searching, with the SEM, for "the largest" particles on fracture surfaces.

THE STRENGTH AND CHARACTERISTICS OF VPPA WELDED 2219-T87 ALUMINUM ALLOY

BY

Wartan A. Jemian, Ph. D.
Professor, Mechanical Engineering and Materials Engineering
Auburn University
Auburn, Alabama

24 August 1984

ABSTRACT

The purpose of this research is to study the variable polarity plasma arc (VPPA) welding process and to identify those factors that control the structure and properties of VPPA welded aluminum alloy 2219-T87. The importance of joint preparation, alignment of parts and welding process variables are already established. Internal weld defects have been eliminated. However, a variation of properties was found to be due to the size variation of interdendritic particles in the fusion zone. These particles contribute to the void formation process, which controls the ultimate tensile strength of the welded alloy. A variation of 150 microns in particle size correlated with a 10 ksi variation of ultimate tensile strength. It was found that all fracture surfaces were of the dimple rupture type, with fracture initiating within the fusion zone.

It was also found that weld strength is improved if welding is done in alignment with the plate rolling direction. The application of water cooled blocks along the weld track produced a small increase in weld strength and toughness. The results of this research are used to assess the relative importance of a number of materials variables.

Introduction

Alloy 2219 was introduced in 1954 (1) to meet the need for a high strength, heat treatable aluminum alloy with retention of structural integrity up to 600 ^{o}F. It withstands higher service temperatures than any other aluminum alloy and retains excellent mechanical characteristics to -423 ^{o}F (20 ^{o}K) in both the welded and unwelded conditions (2). The static mechanical properties of alloy 2219 over this range of temperatures are shown in Figure 1. Nominal room temperature weld test values are also shown. It has a high weldability with 2319 filler metal (7,12). Nominal compositions of these alloys are listed in table 1. It is the principal structural alloy of the space shuttle external tank.

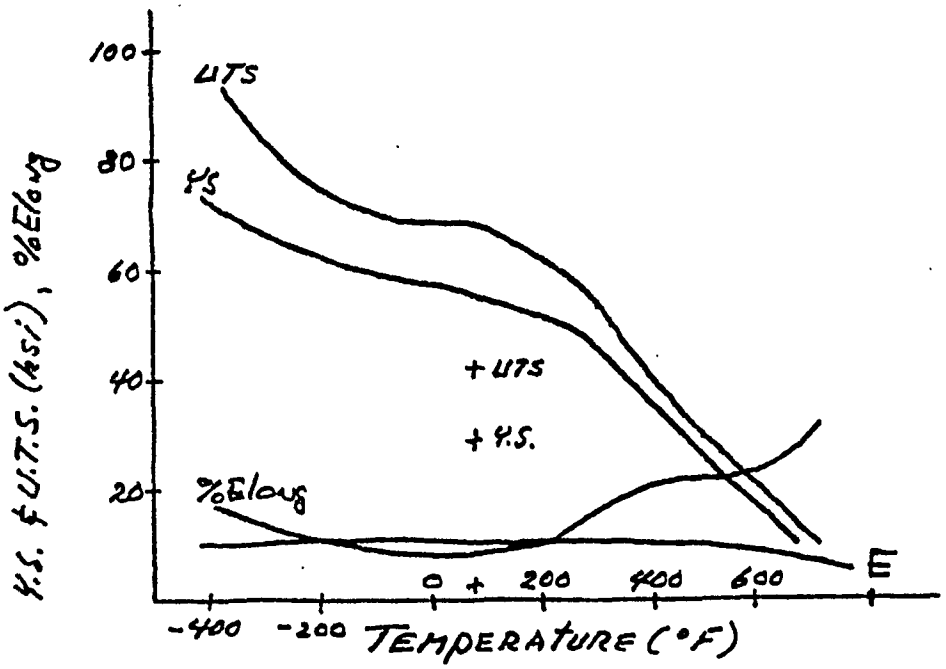

Figure 1. The variation of ultimate tensile strength (UTS), yield strength (YS), percent elongation (%Elong) and Youngs modulus (E) with temperature for alloy 2219-T87 and typical room temperature values for weld test samples (2319 filler wire) (2).

Variable polarity plasma arc (VPPA) welding is a modification of arc welding with special advantages for aluminum alloys. The process features alternating polarity with adjustable arc current, voltage and time in each portion of the cycle. The primary advantage is in the cleaning action of the reverse polarity portion of the cycle (4 msec duration) which removes the oxide layer by bombardment with heavy argon ions, which are a major component of the plasma. In the forward polarity cycle (19 msec) the alloy is heated by impingement of hot electrons, which are another component of the plasma (12). Other advantages, which make VPPA welding useful for many alloy systems, are plasma constraint, which reduces sensitivity to working distance between torch and weld metal and the "keyhole" mode of welding. By controlling beam current and gas flow rate, plasma pressure can be increased to form a stable keyhole which moves with the weld. This keyhole is total penetration through the metal during welding and is filled as the keyhole moves on. Electron beam and laser welding are also keyhole processes. The liquid layer in the keyhole is so thin that gasses released during freezing are swept away rather than being entrapped as porosity in the final joint.

The VPPA process offers many advantages and is now replacing the tungsten inert gas (TIG) welding process that was used initially. To date, in over 24,000 inches of VPPA welds on the space shuttle external tank there has been no internal defect requiring manual preparation and welding (7). Repairing this type of defect represents a major cost in TIG welding.

Process conversion is conducted with great care to ensure that gain in production efficiency is not at the price of weld quality. A rigorous program of TIG/VPPA weld comparisons and study of sensitivity to VPPA process variables is underway. The importance of joint preparation, part alignment and welding process variables are well established and internal welding defects appear to have been totally eliminated. There is, however, a need to identify and explain a residual variation of properties. Possible causes that were considered for investigation include the following factors:

a. geometry
b. chemistry
c. metallurgical structure
d. welding control

Factors within each category were identified and examined

in relation to probable importance and a program of analysis and experimental evaluation was initiated. A portion of this investigation involved review of weld test results from ongoing tests at Marshall Space Flight Center (MSFC) and Michoud Assembly Facility/Martin Marietta Company (MAF/MMC). Other experimental procedures were planned and performed specifically for this study.

The purpose of this research is to study the VPPA process as it applies to the structural weldability of aluminum alloy 2219-T87. Structural weldability is a measure of the level of strength that can be achieved through welding in a system (material and process). Weldability, by the usual meaning, is the capacity to be welded without cracking.

Two specific goals are to identify, on the basis of welding physical metallurgy, the highest strength attainable in welding this alloy system, and to evaluate or estimate the consequences on weld properties associated with the variation of processing controls.

Table 1
Nominal Compositions of Alloys (2,6)

Chemical Element	Alloy 2219	Alloy 2319	Alloy M-934
Silicon	0.20 max	0.20 max	2.05
Iron	0.30 max	0.30 max	0.15
Copper	6.3	6.3	6.7
Manganese	0.3	0.3	0.73
Magnesium	0.02 max	0.02 max	1.51
Zinc	0.10 max	0.10 max	-
Titanium	0.06	0.15	0.06
Vanadium	0.10	0.10	0.01
Zirconium	0.18	0.18	0.17
Beryllium	none	0.0008 max	-
Others, each	0.05 max	0.05 max	
total	0.15 max	0.15 max	
Aluminum	remainder	remainder	remainder

1. Composition.

Copper is the principal alloying element in 2219 and other 2000 series aluminum alloys. The binary phase diagram (Figure 2) shows an eutectic transformation at 548 ^{o}C with solid solution, eutectic and intermetallic compound ($CuAl_2$) compositions of 5.7, 33.2 and 52.5% Cu (by weight) at that temperature (3). Phase solubility limits decrease at lower temperatures. At room temperature the solid solution is the matrix and minor amounts of a number of secondary phases are located at grain boundaries and within the grains. This faithfully represents the parent metal and most of the heat affected zone (HAZ).

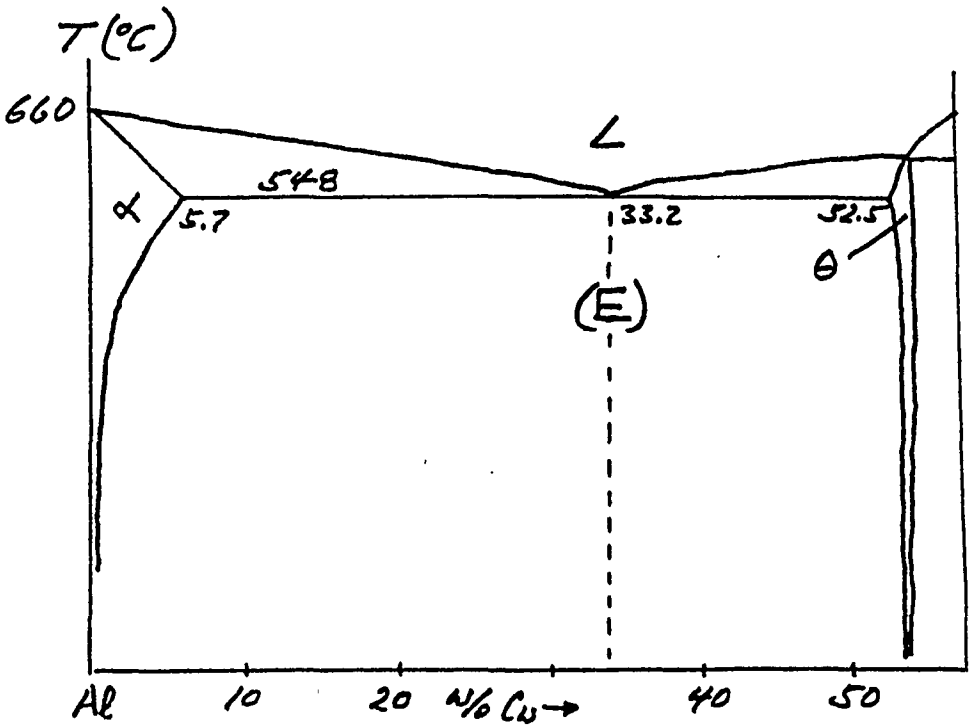

Figure 2. Aluminum rich portion of the Al-Cu binary equilibrium phase diagram. (10)

2. Structure.

Heat treatment to the T87 condition is a two step

procedure. The alloy is first solution annealed at 995 °F and then quenched in water to room temperature. In this condition the alloy is supersaturated with respect to copper. The elevated temperature soak saturates the solid solution with respect to the available alloying elements since solid solubility generally decreases monotonically with temperature and the quench is fast enough to cool the alloy before the copper precipitates out of solution as the intermetallic compound phase. Mechanically, the alloy is soft in this condition and has good ductility. However, it is unstable and tends to form the intermetallic compound at ambient temperature. 2024 aluminum alloy does this spontaneously at room temperature within about 48 hours. Alloy 2219 is designated T37 when it has been solution treated and cold worked 8%. It is designated T87 following a 24 hour aging treatment at 325 °F to achieve the desired condition (2). The changes that take place in the alloy during the ageing treatment are primarily the development of a finely divided, submicroscopic precipitate of the intermetallic compound phase. The increase in toughness of the alloy is attributed to the influence of the large number of submicroscopic hard intermetallic compound particles distributed throughout the grains of the alloy (4). The optimum particle is a 0.01 micron thick ellipsoidal platelet with a diameter of 0.03 microns. These particles interfere with the motions of dislocations. It is more difficult for the dislocations to glide, which raises alloy strength, but movement is still possible, thus retaining ductility. Further heating of the alloy, whether in the heat treating furnace or in the HAZ during welding, causes the submicroscopic particles to grow in size, decreasing in number and lose their strengthening effect.

3. Strength.

The mechanical characteristics of alloy 2219 are due to a number of contributing factors. Young's modulus and other elastic properties are constants for all metallurgical conditions. Strength is structure-sensitive and is controlled by chemistry, microstructure, and dislocation content. The grain size of a wrought alloy, such as 2219-T87 parent metal has a strong influence on strength. Yield strength is inversely proportional to the square root of the average grain diameter. This relation does not apply to the grains in the fusion zone, which have a different subgrain structure. The secondary dendritic branch spacing, which is a feature within fusion zone grains, is the applicable parameter (8). Hardness and yield strength are inversely proportional to the square root of this spacing.

Alloying elements are incorporated in two ways. Copper combines with aluminum to form the intermetallic compound, $CuAl_2$, which precipitates along grain boundaries and to a lesser degree within the grains. Other alloying elements in the formulation, especially manganese, form other second phase particles that can be seen in the microstructure. A portion of the 6.3% copper in the system is incorporated within the aluminum rich solid solution, which is the principal constituent of the microstructure. The chemical elements in solid solution modify strength and other structure-sensitive properties. The resulting solid solution strengthening is a component of the total alloy strength. The actual dissolved amount of any chemical species is a function of temperature and is, therefore subject to control through heat treatment.

Since yield strength is a measure of the stress required to move dislocations, any condition that impedes dislocation movement results in an increase in strength. Solid solution strengthening, decreases in grain size and secondary dendrite spacing, described above, have this effect. Any embedded particles, such as those large enough to be seen in the microstructure, also disrupt the continuity of slip planes and have this same effect. Second phase particles also have a stabilizing effect on the microstructure, in that they prevent grain growth (8,9). The submicroscopic, coherent particles that are produced by heat treatment in the age hardening process are much more effective in their dislocation blocking action. The development of this system of "hidden" particles throughtout each grain doubles the strength. The contributions to the strength of the age hardened alloy can be approximated in the following way:

a.	base strength (aluminum)	25%
b.	solid solution content	10%
c.	grain size control	10%
d.	dislocation content	10%
e.	age hardening	45%

The base strength represents the proportion of the total strength that is associated with typical, polycrystalline aluminum (with the addition of those second phase particles that are scattered throughout the grains). The other factors indicate their relative contribution to the strength of alloy 2219-T87.

The ultimate strength of the alloy either corresponds to the breaking strength or marks the onset of necking in a tensile test. Necking is a form of plastic instability

that occurs in tensile testing a ductile alloy. It is due to the production of vacancies and their accumulation into voids which counteract strain hardening. Vacancies and voids are produced within the metal during testing, and are not a part of the original microstructure (9). Since both plastic deformation and void production involve dislocation movement, there is a correlation between yield and ultimate strengths. The size of any hard particle (intermetallic compound or eutectic colony) in the microstructure plays a dominant role in the ultimate strength of the alloy because these particles act as vacancy and void sources. The larger the particles, the more effective void production, and the lower the ductility.

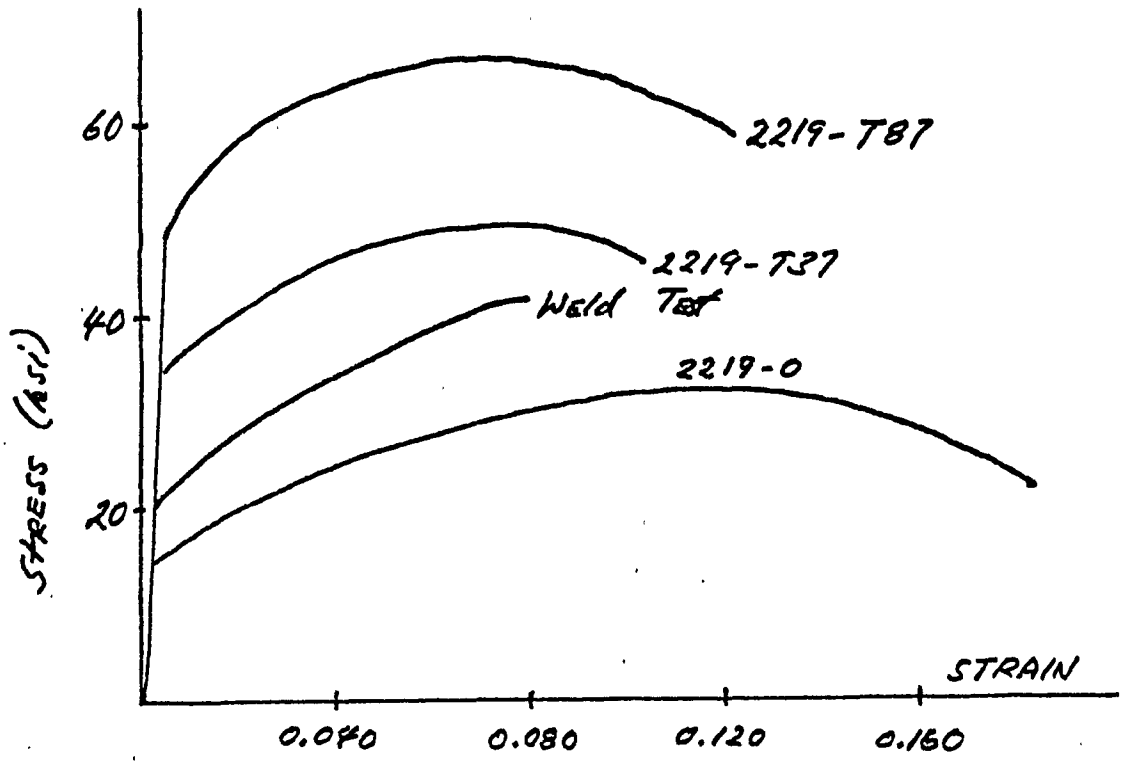

Figure 3. Stress strain curves for alloy 2219 in the fully annealed (2219-O), solution treated and 8% cold worked (2219-T37) and age hardened (2219-T87) conditions. The stress strain curve for a typical transverse weld test is included for comparison. (1,10)

The nominal values of yield and tensile strengths for the 2219-T87 engineering alloy are 56,000 psi and 67,000

psi, respectively. Various processing controls, based on the factors described above, can be used to either raise or lower these values. The upper limit in UTS attainable in aluminum base alloys appears to be 110,000 psi (alloy 7075-T6).

4. Weld Structure.

The fusion zone microstructure is produced by the eutectic transformation. The first solid to form on cooling is in the form of dendritic grains of solid solution, which was formed at temperatures above the eutectic. Since the solid solution composition is less than that of the average liquid in the weld puddle, the liquid is enriched by those alloying elements not frozen out. Enrichment occurs to a great enough degree that the eutectic constituent is formed between the dendritic branches. Based on the copper content of alloy 2219 the eutectic constituent is 2.2% by weight of the alloy.

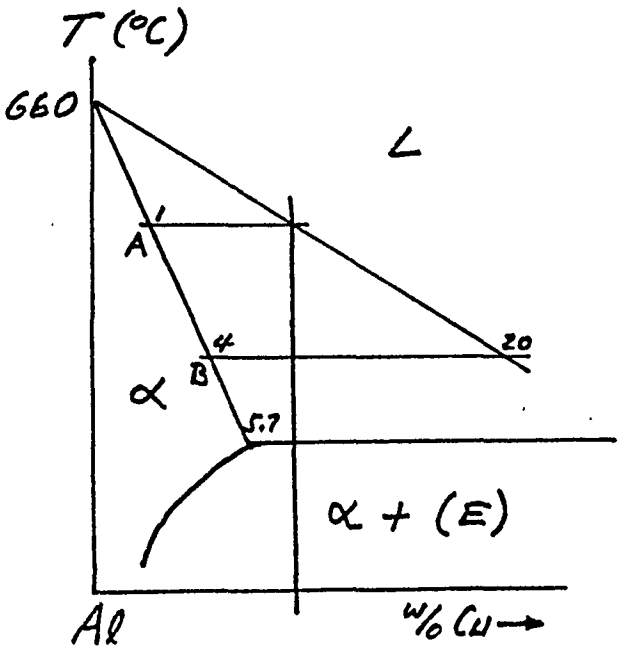

Figure 4. Phase diagram showing fusion zone compositions at start of solidification.

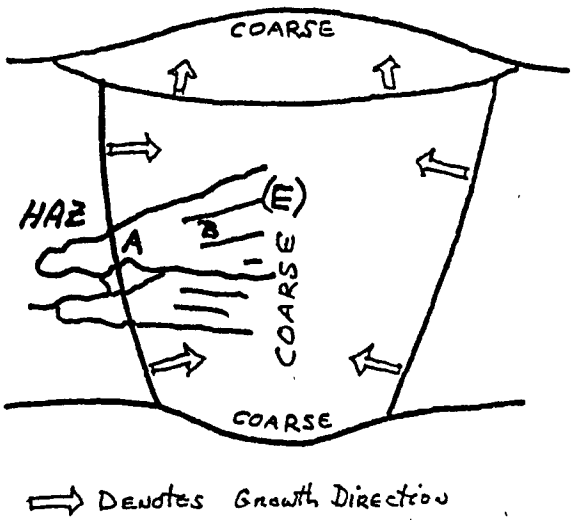

Figure 5. Fusion zone microstructure and growth direction.

The structure of the weld is best understood in reference to the aluminum-copper phase diagram. The composition of the liquid in the weld pool is based on the

average alloy composition (which will be used in this discussion), some dilution by filler metal and further modifications by segregation effects. The first solid to form is a dendritic solid solution of 1% Cu that forms at 623 C. Figure 4 is a portion of Figure 2 in which the average alloy composition and the composition of the first solid to form are shown. As solidification progresses the solidifying dendrites do not utilize all of the available copper, therefore the composition of the remaining liquid steadily increases. This is indicated by the lower isotherm marking equilibrium between a solid of 4% Cu and a liquid of 20% Cu. Chemical segregation effects actually cause the liquid composition to have a higher composition at the solidifying surface.

Finally the last liquid to freeze contains all of this excess copper. The copper-enriched solid is an eutectic mixture with an average composition of 33.2% copper, by weight. The eutectic is a lamellar mixture of solid solution and $CuAl_2$ intermetallic compound. Dendrites grow in alignment with the principal direction of heat transfer, which is into the adjacent parent metal. In the cover pass, which is not a keyhole weld, cooling is into the unmelted portion of the first weld pass. The sequence of structual transitions is similar in many respects to the transitions from the parent metal HAZ into the keyhole fusion zone.

There is a HAZ in both the parent metal and the preceding fusion zone in a multipass weld. Immediately adjacent to the fusion zone, where the alloy was melted totally, is a region where partial melting occurred due to normal chemical segregation within the original grains of the parent metal. Adjacent to this are zones where the alloy was subjected to various elevated temperatures for various periods of time. In alloy 2219, second phase particles are not dissolved to any appreciable extent below the eutectic melting temperature, therefore there is no pronounced region of grain growth. However, the typical microstructure indicates that the condition of the alloy has been changed, primarily with respect to overaging of the heat treated structure and modifications of the alloying element solution conditions.

Mechanical characteristics and properties are related to the chemical and structural condition of the alloy in the way described above. The individual contributions of chemical and structural factors to strength can be approximated in the following way:

a.	alloy composition	30%
b.	metallurgical condition	30%
c.	weld geometry	10%
d.	dendritic spacing	10%
e.	hard particle size	20%

The individual contributions are evaluated in relation to their effect on plastic extension in the tensile test as well as their strengthening effect. For example, an increase in hard particle size does not have a noticeable effect on yield strength or hardness, but increases the void production process, effectively reducing ductility. A ductility of 10% Elong is typical for the welded alloy. Beil and Hahn relate a variation of approximately 10% in UTS to weld geometry (11).

Changes in the microstructure affect properties in the HAZ but the dominant change is in the much lower levels of mechanical properties in the fusion zone. Strength tends towards the values of the fully annealed alloy (yield and tensile strengths of 11,000 and 25,000 psi, respectively and a ductility of 18% Elong). The cooling rate is usually adequate to provide a degree of supersaturation in the fusion zone so that a partial recovery of strength by spontaneous age hardening occurs. This accounts for the measured yield and tensile strength levels of 21,500 and 41,000 psi in weld test samples.

Beil and Hahn (11) have conducted a comprehensive study of the metallurgical condition of this welded system. They identify a number of factors contributing to loss of strength. They place special emphasis on the segregation and accumulation of copper and on the role of microporosity. Their presentation provides a great deal of information and many valuable insights.

5. Filler Metal.

Filler metal composition is chosen to retain properties, match appearance and prevent the formation of corrosion couples. Alloying elements are added through the filler wire to compensate for elements lost through evaporation and to strengthen and refine the microstructure. Poorman and Lovoy (6) studied the effect of different alloying elements on weld strength of 2219-T87. They selected filler metal wires to provide varying amounts of titanium and beryllium and to vary the copper:magnesium ratio. They found the results to be encouraging with respect to potential improvement of weld mechanical properties, but recognized that more testing is

required to make a change in production methods. The need now exists to perform a similar investigation with the VPPA process.

6. Summary

The effect of welding on properties is related to the redistribution of alloying elements in the fusion zone, the modification of microstructure in the HAZ, the production of a completely new microstructure in the fusion zone and a pattern of residual stresses. The dendritic spacing and the size of the interdendritic constituent are the most significant aspects of the new fusion zone microstructure. This constituent is produced under the slowest cooling conditions in both the keyhole and cover pass weld puddle. The size of this constituent is largest at the last part of the structure to freeze, where cooling is the slowest. Since cooling rate is the dominant factor affecting particle size, the intermetallic compound and eutectic particles are large. The differences in yield strength between the parent and weld metals are due, primarily, to metallurgical condition with respect to age hardening. Other factors are secondary. Tensile strength differences, however, are due to the differences in particle size. The largest particles in the wrought alloy microstructure are smaller, by at least an order of magnitude, than those in the weld fusion zone.

Theory of Mechanical Characteristics

The weld tensile sample is normally clamped in the tensile machine by flat, serrated wedge grips, compressing the sample ends (parent metal) in the welding direction. In this orientation, the least bending moment is applied to the sample during the test. The loading configuration involves the in-line separation of laterally constrained grips. Nunes analyzes this test configuration on the basis of a soft interlayer model (13). Bending moments are concentrated in the sample at the grip ends and at the edges of the crown and root reinforcement. Elastic stresses are soon driven to the yield at these points with the result of local cold work and other structural damage to the sample. Cold work where the base metal is gripped is of no serious consequence to test results, but concentrated, early deformation at the other points influences the magnitude of the test results as well as the features of the fracture surface. The magnitude and direction of peaking (angular distortion across the weld) influences the crack starting position.

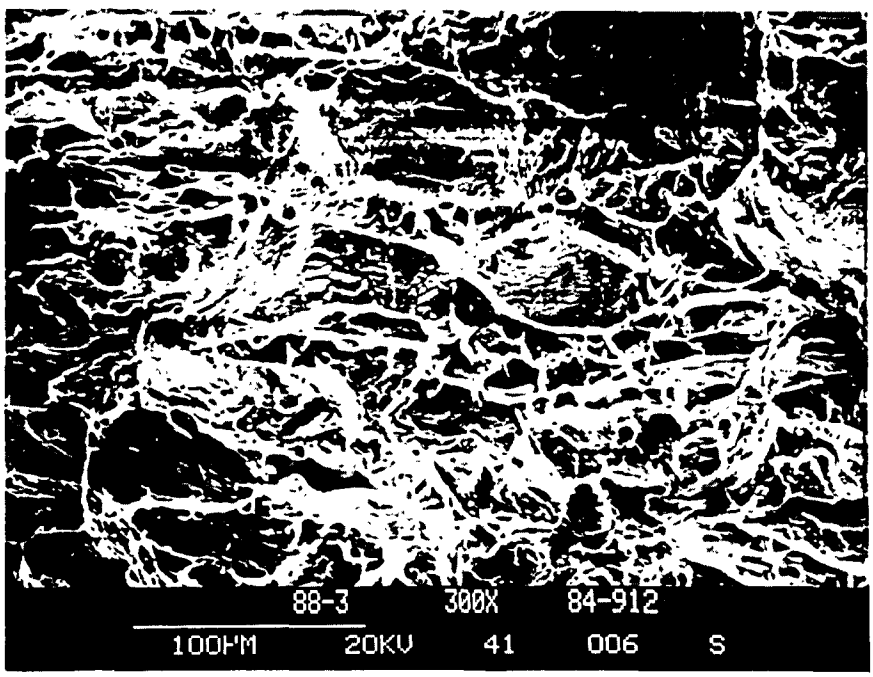

Figure 5. Normal dimple rupture. Average cell diameter, 23.3 microns; maximum cell diameter, 80.8 microns; and particle diameter, 55.6 microns.

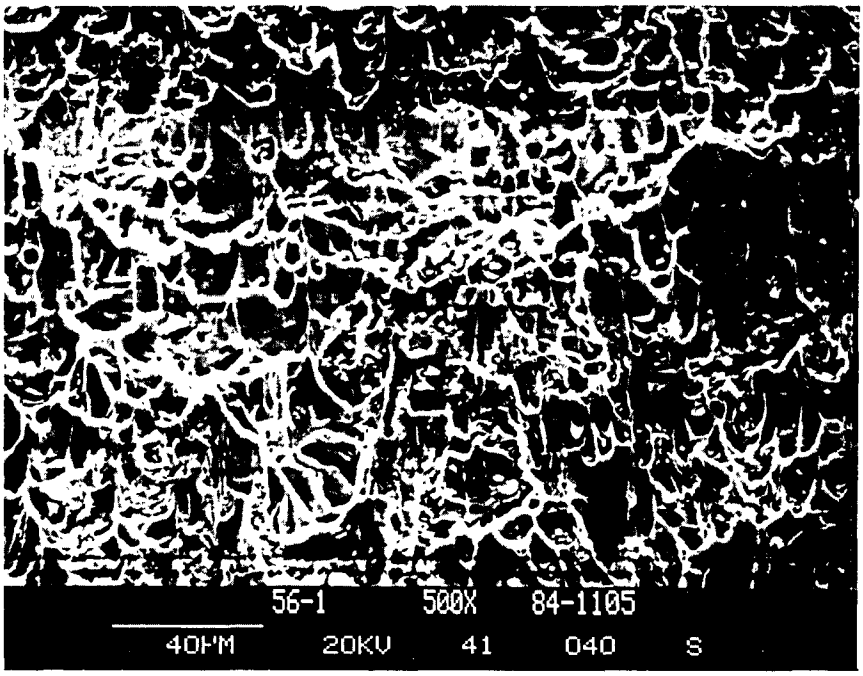

Figure 6. Shear mode dimple rupture.

For the usual case where only small amounts of sample compliance are required, the test continues through the typical stages of general plastic flow in the weld nugget and adjoining regions and finally into appropriate fracture processes. The dominant fracture process in welded 2219-T87/2319 is dimple rupture. Dimple rupture is illustrated in Figures 5 and 6. In Figure 5 dimple rupture occurred under conditions of tensile extension. The dimple rupture in Figure 6 occurred in shear. The dimples are open ended in one direction indicating that the sample was deforming in this manner as the dimples developed. In none of the welds has any other matrix fracture surface feature been observed.

Void production is a process that occurs in two stages at positions throughout each grain of the deformed metal. The first stage is the nucleation of stable voids of a critical size by the interaction of dislocations with hard, second phase particles, grain boundaries or slip bands. The second stage, which leads to dimple rupture, involves

the exaggerated stretching of matrix metal due to unimpeded dislocation glide out of the clean metal surface. This glide involves dislocation multiplication but no dislocation buildup and therefore continues until the metal is thinned to the point of total separation. The entire fracture surface is then covered by a network of cell walls, stretched by this process.

Each cell contains a point of nucleation and possibly a trace of the structural feature involved in void nucleation. Cell size directly depends on hard particle size. There is a characteristic second phase, or eutectic constituent particle size for each welding process depending on alloy system, welding power and speed, chemical segregation in the puddle and factors connected with the ambient and consumables.

The only evidence of brittle failure is within a few hard particles themselves. These particles are usually separated from the matrix, which is a dendritic solid solution. In a number of cases the particle appears to be directly exposed, but in most there is a small layer of solid solution over the surface. Since the void nucleation process involves interactions with dislocations, the process is more likely to occur with the larger particles that intercept a greater number of slip planes. Larger particles allow void production to become critical at lower levels of plastic deformation. Therefore, the tensile strength of the sample is reduced by large, hard particles. Conversely, tensile strength is improved by reducing the size of second phase particles.

Void production is not directly related to alloy yield strength, except in relation to dislocation movements. Yield strength is a measure of the initial motions of dislocations in the sample. The UTS depends on void production. Ductility is directly controlled by the dominant fracture process.

Experimental Procedures

The initial assignment to this research activity was by means of the following tasks:

1. determine the effect of the relation of rolling direction to welding direction,
2. determine the relation of parent metal to weldment strength,
3. compare the grain structures of samples welded at MSFC and MAF/MMC,
4. and determine the effect of impurities in the filler wire.

In considering these tasks and reviewing a number of test samples from an active weld qualification test program conducted by staff of both MSFC and MAF/MMC, a number of specific goals were identified to provide results for each of the tasks and to contribute to a coherent report on the structural weldability of aluminum alloy 2219-T87 by the VPPA process. These goals are listed and described in the following paragraphs.

Goal 1. (Tasks 1 and 2) A program of comparison welding of panels with rolling direction aligned in the welding direction and others aligned across the welding direction provide for the first two tasks. After assembly (tack welding), but before welding, test strips were cut transverse to the intended welding direction and machined into "dog bone" tensile test bars with 3/4 inch guage width. After welding each panel, weld test bars were cut, numbered and finish machined for tensile testing. These were machined to the standard 1 inch finished width. The samples provided enough information to compare the effect of weld/rolling direction alignment with base metal characteristics.

Goal 2. (Task 3) This activity was conducted by studying available samples from the recent 0.800 inch weld test qualification program. A total of 121 samples were available. Of these 78 had acceptable test results and 43 did not qualify as acceptable. It must be pointed out that all test results were within a narrow range. All welds had a good appearance and none contained any internal defects. Of the 78 acceptable samples, 54 were prepared with a J-groove configuration and 9 were shaved for testing.

Goal 3. (Task 4) The study of the effect of impurities in the filler wire was based, primarily, on

welding panels using M-934 filler wire. This filler alloy provides elements that modify the characteristics of the weld metal and was found to impart better mechanical properties over most of the temperature range of interest than other fillers as evaluated in TIG welding in a study reported on by Poorman and Lovoy (6).

Goal 4. Preliminary results of the examination of weld qualification test fracture surfaces indicated the presence of large particles in the region of fracture initiation. A program to control the maximum particle size in the weld, by controlling cooling rate, was planned to study this effect. Cooling rate in the weld was increased by the use of water cooled copper blocks which were attached to the plate surface along the upper half of the weld track. Plate thickness was 0.500 inches in this series of welds.

Goal 5. Understanding the exact conditions for the formation of the microstructure in the fusion zone is fundamental to the interpretation of test results and weld characteristics. A study was initiated to experimentally evaluate features of the microstructure by sectional metallographic examination, using quantitative procedures to every possible degree, and by direct examination of the solidifying surface in the keyhole.

Experimental procedures involved VPPA welding square butt joints of 2219-T87 aluminum alloy plates in the vertical up orientation. Filler wires were aluminum alloy 2319.

Standard static tensile test procedures were followed to determine yield strength, tensile strength and percent elongation. %Elong is calculated on the basis of a gauge length of 2 inches. Fracture surfaces were inspected visually for the source of fracture and for other details of the fracture surface. Scanning electron microscopy (SEM) was used to identify and measure fracture surface features. The measurements were made on photographs. The energy dispersive x-ray analysis attachment to the SEM was used for microchemical analysis to confirm the identity of features. Metallographic analyses were performed using standard methods and Keller's etch.

Results and Discussion

1. Goals Results.

Goal 1. Four samples of parent metal were cut from each weld test panel parallel to the weld test samples. Therefore, there are 12 tests of the parent metal in the rolling direction and twelve tests across the rolling direction. Test results are summarized in Table 1. Each line lists the average values of test results from four test bars of the indicated panel. The average and standard deviation are calculated for the 12 samples from the three average values listed immediately above.

Table 2
Parent Metal Mechanical Properties

Panel Number	Y.S. (psi)	U.T.S. (psi)	%ELONG (%)	ORIENTATION
1072	54,914	67,077	16.7	Cross
1079	54,896	67,171	16.3	"
1080	56,859	69,027	15.2	"
Ave.	55,556	67,758	16.1	"
S. Dev.	1,128	1,010	0.78	
1081	56,272	68,957	13.6	Parallel
1082	55,186	68,161	14.5	"
1083	55,985	69,007	13.1	"
Ave.	55,814	68,708	13.7	"
S. Dev.	563	475	0.71	

These results show a small difference between ultimate tensile strength measured with the rolling direction and across the rolling direction. As expected, tensile loading parallel to the rolling direction yields the higher strength and lower ductility. This difference is due to the difference in effective grain boundary spacing available for slip. The measured increase of UTS above the reference yield is 7.4%, which is accounted for by a grain shape aspect ratio of 1.33, which corresponds with measurements.

Weld test results are listed in the following table.

Table 3
Weld Test Results

Panel Number	Y.S. (psi)	U.T.S. (psi)	%ELONG (%)	Orientation
1072	21,685	38,695	7.4	Parallel
1079	20,012	37,882	8.0	"
1080	20,444	36,371	6.5	"
Ave.	20,714	37,649	7.3	"
S. Dev.	868	1,179	0.75	
1081	20,748	36,609	6.6	Cross
1082	19,057	37,846	7.4	"
1083	20,749	35,754	6.6	"
Ave.	20,185	36,736	6.9	"
S. Dev.	977	1,051	0.46	
1094	19,099	37,072	6.4	Parallel
1095	19,250	37,987	7.1	"
1096	18,889	39,282	8.5	"
Ave.	19,079	38,114	7.3	"
S. Dev.	181	1,110	1.07	
1098	18,715	36,509	5.9	Cross
1099	18,939	37,375	6.9	"
1100	19,103	36,404	6.6	"
Ave.	18,919	36,763	6.5	"
S. Dev.	195	533	0.51	

These results show that the mechanical properties are better if the weld is made parallel to the parent metal rolling direction. This corresponds to current practice. It is unfortunate that the weld test results do not meet specifications of 38 ksi average UTS and minimum sample test of 35 ksi, excepting one set. Never-the-less, for purposes of comparison these test results favor the present practice with respect to orientation of weld direction.

Fracture surface examination shows the same pattern of fracture surfaces reported on under the Goal 2 results.

Parent metal test bar fracture surfaces have a cup and cone profile. Fracture initiated at the center of each sample in a dimple rupture mode and progressed onto shear separation faces, oriented approximately 45 degrees to the loading direction. The fracture mode on these shear faces is also dimple rupture.

Goal 2. A detailed examination of the fracture surfaces of the 121, 0.800 inches thick weld qualification test samples revealed a number of fracture paths. However, it is clear that in all cases, fracture initiated within the fusion zone. The point or region of crack initiation was indicated by several features, which include:

1. A series of fracture path ridges emanating from the fracture source.

2. The longest transverse fracture surface edge, indicating separation with the least plastic deformation (plastic deformation and lateral contraction increase steadily with crosshead movement until separation occurs, thus the amount of deformation provides a record of test time).

3. The position between the two fracture surfaces with the greatest residual separation (this feature also indicates relative time of separation by the principle of progressive permanent deformation).

SEM examination of the fracture surfaces revealed that all surfaces were of the dimple rupture type. Large eutectic or intermetallic compound particles were retained, embedded within dimples on the fracture surface in the region of crack initiation. Most of the larger particles appear to have been fractured and a smaller number appear to have simply been separated from the matrix close to the interphase boundary. Figure 7 shows several eutectic particles. Several cracks are visible. Hartbower et. al. (16) and Heiple and Carpenter (17) report on the cracking of particles during tensile testing, using acoustic-emission techniques. Butcher and Allen (15) have modeled the conditions that lead to fracture or separation of a hard particle in a ductile matrix. Microchemical analysis (Figure 8) in the SEM using the EDAX attachment clearly shows that these large particles contain more copper than the general alloy.

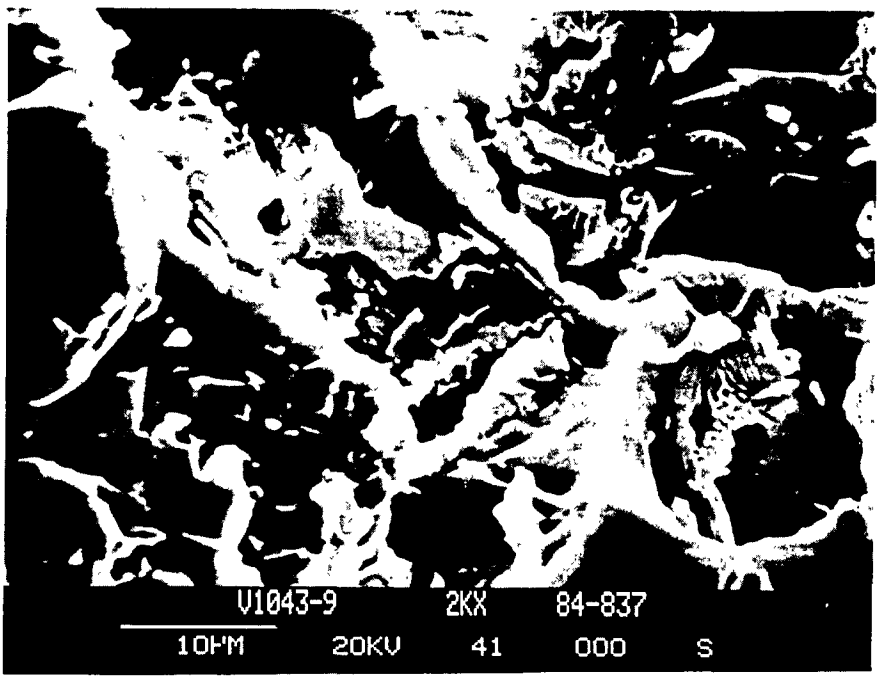

Figure 7. Dimple rupture fracture surface with large eutectic colony particle retained in the large dimple.

SEM analysis was conducted on one sample from each of the groups available. It was not possible to conduct a thorough analysis of each sample. One of the two fracture surfaces was cut from the remaining test bar and bonded to a specimen stage with graphite lacquer, which is electrically conductive. The initial examination procedure involved scanning the entire fracture surface, searching for the region containing the largest particles. Photographs were taken at several candidate locations for later comparison and measurement. The procedure was soon modified by outlining the fracture start region on the

fracture surface, with a soft pencil. The region of crack initiation was identified as described above. This procedure reduced the time required for the analysis and provides a record of the region. A photograph was then made of the spot that contains the largest particle within the marked region.

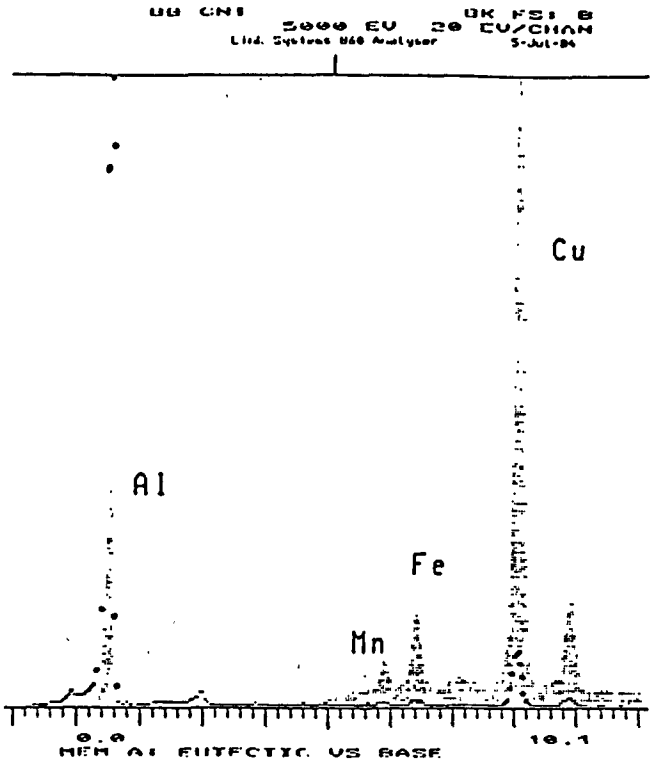

Figure 8. Microchemical analysis of a large particle (a) and the general background of the sample (b).

All subsequent measurements were made from the prints. These measurements included the length of the magnification calibration bar, a count of dimple wall intersections on a randomly placed test line, largest transverse rupture cell diameter and largest transverse interdendritic particle diameter. Processing this data led to measurements of the average cell diameter and maximum cell and particle diameters, in microns. Of the 22 samples evaluated, the test results from two were discarded as being anomalous. The measured particle sizes were out of the range of values for the other samples. Figure 9 is a plot of UTS

versus maximum particle size and figure 10 displays plots of UTS versus the average cell and particle diameters.

The lines drawn through the data points are computed lines. In Figure 9 the line represents all twenty data points shown. In Figure 10, the line represents only the

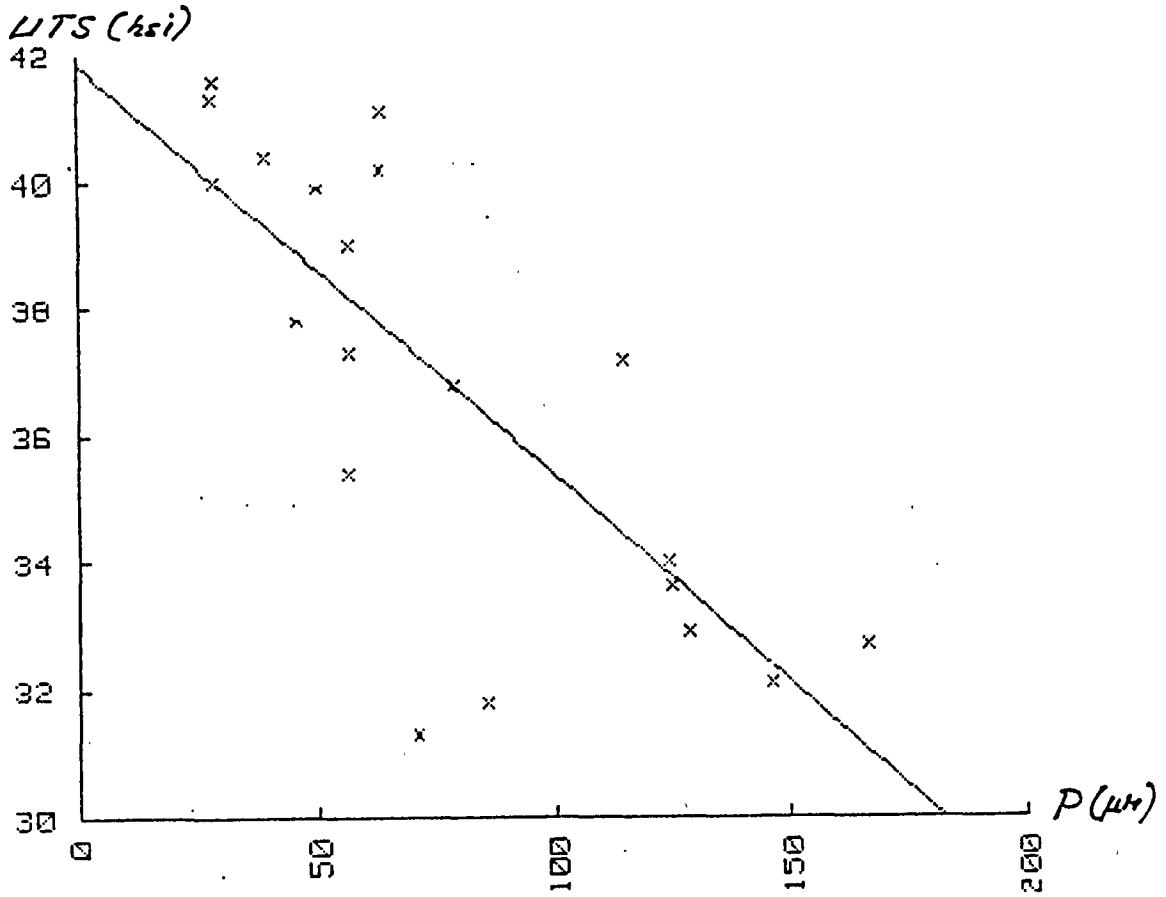

Figure 9. UTS versus largest interdendritic particle size for 0.800 inch VPPA weld test bars of 2219-T87 aluminum plate welded with 2319 filler wire.

20 largest size values. These are the maximum cell diameter values. The other 20 points are the average cell diameters.

Figure 10 indicates the possibility of a trend between tensile strength and largest rupture cell diameter, but the scatter overshadows any such trend. There is no apparent trend between UTS and average cell size. The average,

background dimple rupture cell is related to the average, interdendritic particle size, which is closely related to the secondary dendritic branch spacing.

Goal 3. The effect of impurities on VPPA welding is similar to impurity effects on the TIG process. The investigation of this effect was limited to one demonstration involving the intentional contamination of the weld metal with traces of oil prior to welding. The resulting weld showed an irregularity of form that is very

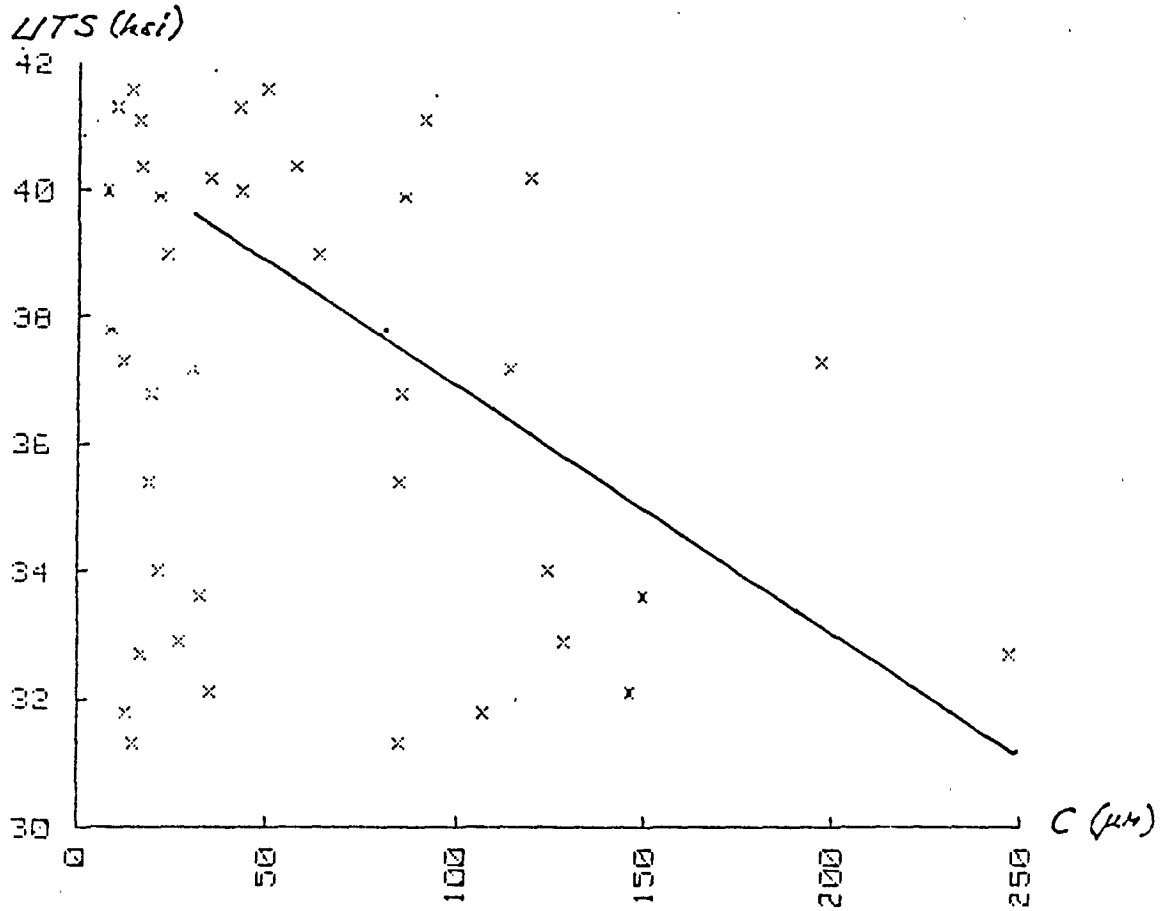

Figure 10. UTS versus largest and average dimple rupture cell diameter on samples represented in Figure 9.

similar to that reported in TIG welding and attributed to the surface activity of the contaminant. This strongly suggests that the keyhole liquid supports currents that are subject to such factors. Additionally, the resulting weld metal included a series of fusion boundary cracks and

porosity in the fusion zone.

The effect of alloy M-934 filler wire on weld test results is shown in the following table, which includes comparable test results reported on in the Goal 1 report. The values listed for 2319 filler metal are copied from Table 3. In both cases, welding was parallel to the rolling direction. The test results compare two groups of 19 samples welded with M-934 filler with two groups of 36 samples welded with the standard 2319 filler wire.

Table 4
Filler Wire Weld Test Comparison

Filler Metal	Y.S. (psi)	U.T.S. (psi)	%ELONG (%)
M-934-1	22,655	37,446	5.8
S. Dev.	591	996	0.38
2319	20,714	37,649	7.3
S. Dev.	868	1,179	0.75
M-934-2	22,014	39,406	6.0
S. Dev.	400	1,631	0.73
2319	19,079	38,114	7.3
S. Dev.	181	1,110	1.07

The results show a higher yield strength countered by a lower ductility. The UTS is slightly lower, but not significantly. This filler alloy does not appear to improve the microstructure. The difference in yield strength is attributed to the solid solution strengthening effects due to the differences in alloy composition. The increase in UTS in the second group welded with M-934 filler wire is not considered to be significant.

Goal 4. The mechanical test results for four panels are listed below. In this table, the welds made in the cooled region are presented first. On the data sheets the samples are designated 1a, 2a, 3a and 4a. The samples that were welded away from the cooling blocks, numbered 5b, 6b,

7b and 8b on the data sheets, are listed as the last four groups.

Cooling produces a significant increase in both yield and tensile strengths at the same level of ductility. In panels 1087 and 1088 the cover pass did not adequately cover the fusion zone of the root pass, but the relationship of the two passes was proper in panels 1089 and 1090. A second distinction is that the cooling blocks were set closer to the weld center line in the second two panels and a 5 ampere adjustment in the plasma current was

Table 5
Cooling Effect Weld Test Results

Panel number	Y.S. (psi)	U.T.S. (psi)	%ELONG (%)	Condition
1087	22,110	39,971	5.5	Cooled
S. Dev.	151	264	0.0	
1088	21,876	41,008	5.9	"
S. Dev.	235	613	0.25	
1089	21,877	41,024	6.0	"
S. Dev.	344	343	0.0	
1090	24,607	39,621	5.6	"
S. Dev.	465	1,376	0.48	
Ave.	22,617	40,406	5.8	"
S. Dev.	1,331	719	0.24	
1087	21,304	38,754	5.5	Uncooled
S. Dev.	449	512	0.0	
1088	21,495	40,179	6.0	"
S. Dev.	235	277	0.0	
1089	21,251	38,777	5.8	"
S. Dev.	457	595	0.29	
1090	20,636	39,283	5.5	"
S. Dev.	190	445	0.0	
Ave.	21,172	39,248	5.7	"
S. Dev.	372	667	0.24	

made when the weld passed into this region in panel 1089 only. The cooling block spacings were 3.0 and 2.0 inches across the weld in the first two and second two panels, respectively.

Goal 5. The temperature and pressure of the plasma liquify an ellipsoidal plug of alloy through the plate. The conical profile of this plug is revealed by the final shape of the weld in cross section. The dominant components of fluid flow are downwards by gravity and forward under plasma pressure. This flow of liquid naturally forms a reinforcement at the root and a groove at the torch side, if not built up by filler metal additions. Excessive plasma pressure results in cutting.

Solidification begins at the widest part of the cone as the source of heat moves on. This solidification is in equilibrium with alloy of almost average composition and at a very low growth rate within the boundary layer of liquid. The liquid, immediately adjacent to the solid is

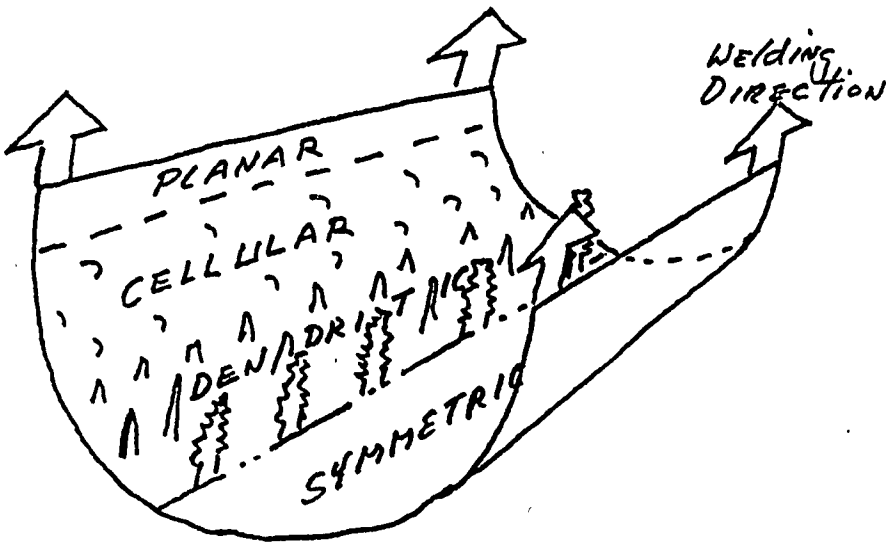

Figure 11. Map of the keyhole solidification surface (schematic).

essentially static due to frictional effects. The new solid is typically a product of epitaxial, planar growth. Grain structures of the HAZ are continued into the fusion

zone. Since the liquid originates, primarily, out of the plate itself., with only a small fraction remixed, and solidifies as it flows, the first portion to solidify is dilute, thus enriching the liquid that flows on.

While liquid freezes at the sides, as described above, solidification also occurs at all surface positions further back around the keyhole. The weld metal composition varies continuously, and is enriched by most alloying elements. Figure 11 is a perspective representation of the surface on which solidification occurs. Alloy composition varies continuously from the line of start to the line of finish. The actual temperature also varies. The surface structure also changes from smooth (planar growth), to cellular (with slight projections) to cellular dendritic (extended projections) and to branched dendritic. At all positions, solidification occurs within the boundary layer that is effectively not moving, so that chemical equilibrium is approximated. The composition of the planar surface is less than that of the branched dendritic surface. Equilibrium is local so that enrichment extends beyond that expected in ingot solidification.

2. Discussion.

The strength of a welded panel depends on a number of coupled factors. The composition of the base metal and modifications by the filler metal govern the dimensions of structural features in the weld metal. Both composition and structural size (as represented by secondary dendrite branch spacing) directly affect alloy strength. For a given composition, spacing is controlled by cooling rate, which is in turn governed by energy input into the weld and other welding parameters and any preheat. The application of the cooling blocks illustrated this effect since there was an increase in strength and toughness.

A variety of factors were considered and studied. The controlled study of alignment between the welding direction and rolling direction of the plates showed that the present practice, is the better of the two. This result is contrary to the effect of rolling direction on base metal strength. In that case, the greater number of grains in the sample cross section increases both the yield and tensile strengths. In the welded sample, the HAZ grains do not reflect the differences in grain dimension with orientation, probably due to recrystallization effects, so that this size effect does not affect fusion metal microstructure and properties in the same way. The pattern

and direction of residual stresses from the base metal cold work also participate in these relations.

The development of the microstructure of the weld metal is a governing factor. This process involves a number of factors within the liquid in the keyhole. Nunes describes the weld pool (not keyhole) using a mathematical model and describes circulation (14). Plasma temperature, dimensions and pressure are important, but the formation of the final microstructure takes place under the liquid in the keyhole, away from direct contact with the plasma. Growth of the metal begins at the side of the keyhole and continues to develop at different positions, finally along the center line. In vertical up VPPA welding the final microstructure reveals this pattern of growth and shows that liquid flow contains a dominant downward component on each side of the keyhole. One might anticipate a vortex component, but there is little or no evidence for it. There is probably an axial (relative to the keyhole) component forced by momentum transferred from the plasma. This axial component may produce a pattern of circulation, but no direct evidence has been found.

The test procedure is important to the measurement of properties. For valid comparisons, test bars must have the same nominal dimensions. They must also be gripped in the same manner, with the same constraints. The reason for both requirements is the dependence on the moment distribution and stress field in the test bar. The orientation of these fields in the vicinity of the reinforcement is critical. Test performance depends on the interaction of the applied stress field with the shape/property field of the weld test sample. During the progress of testing, different portions of the sample respond differently to the stresses, but each part of the sample responds in the sequence of elastic deformation; joined by plastic deformation; joined by void production and accumulation; resulting in separation. Separation begins in that part of the sample that was the first to pass through the deformation stages.

There is an elastic response to each component of the stress field. In a face centered cubic alloy, such as 2219-T87, there are many available slip systems within each grain to support plastic deformation. Plastic deformation, which occurs only in response to shear stress components, favors action on planes inclined to the tensile direction. However, the dimple rupture process, is in response to longitudinal tensile stress components. Dimple rupture is the common fracture process that produces the starting

crack in a typical "cup and cone" tensile test. This crack starter responds to the initial longitudinal stress in the test bar. The effect of the lateral constraint and triaxial stress state is relatively minor. Once the center crack has formed, the stress state changes from one of dominant longitudinal tension to a shear stress condition. The shear surfaces on the side walls of the cup and cone are also dimple rupture surfaces. However, the dimples are open ended, pointing in the shear direction. This description applies to tensile test specimens from many alloy systems including 2219-T87. Most of the fracture surfaces of the weld test specimens that have been studied in this research are cup and cone fractures. The others are also of the dimple rupture mode. In every case fracture began in the fusion zone and progressed through the fusion zone. The differences observed between the shapes reflect variations on the above pattern. In one extreme variation, the fracture surface extends completely through the weld on a near 45 degree diagonal surface. In this case, even the crack starting region, which involved void formation under the action of longitudinal stresses, is on an inclined, stepped surface, in approximate alignment with the shear surfaces. Dimple rupture is the only mechanism over the entire surface.

It was found that the interdendritic particle size correlated with UTS in one series of samples. A variation of 150 microns in particle size correlates with a 10 ksi variation in UTS. In a second series, the variation of UTS was so restricted the correlation was not clearly displayed. However, there is general agreement among metallurgists that particle size is the dominant variable in the void production process. This applies equally to particle crack nucleation as well as to nucleation by dislocation interactions. Particle cracking appears to be the important process for crack nucleation in welded 2219-T87 aluminum plate.

3. Conclusions

It was very apparent that this welded system is ductile, in that all fracture surfaces were totally of the dimple rupture mode. Fracture initiated in the fusion zone and generally followed a pattern of "cup and cone" separation. In a small fraction of the samples, fracture crossed the weld on a relatively planar surface.

The UTS correlates with the largest dimple rupture cell size and the largest interdendritic particle size. The range of variation is approximately 20% of the UTS.

Specifically, a variation of 150 microns particle size was found to correlate with 10 ksi UTS.

It was found that base metal cooling increases both strength and toughness.

Welding parallel to the rolling direction, which is the current practice, is recommended.

Bibliography

1. John Sessler and Volker Weiss, Materials Data Handbook, Aluminum Alloy 2219, Department of Chemical Engineering and Metallurgy, Syracuse University, Contract NAS8-11345, (1966), NASA/MSFC, Sponsor.

2. Ray M. Hart, Alcoa Green Letter: Alcoa Aluminum Alloys 2219 and 2419, Aluminum Company of America, (1983).

3. L. F. Mondolfo, "Aluminum-Copper System," Aluminum Alloys, Structure and Properties, (1976), 253-278.

4. H. K. Hardy, "The Ageing Characteristics of Some Ternary Aluminium-Copper-Magnesium Alloys with Copper:Magnesium Weight Ratios of 7:1 and 2.2:1," J. Inst. Metals, 83, (1954-55), 17-34.

5. C. R. Heiple and S. H. Carpenter, "Changes in Acoustic-Emission Peaks in Precipitation Strengthened Alloys with Heat Treatment," J. Acoustic Sciences, 1, No. 4, (1983), 251-262.

6. R. M. Poorman and C. V. Lovoy, "Improved TIG Weld Joint Strength in Aluminum Alloy 2219-T87 by Filler Metal Substitution," NASA Technical Memorandum NASA TM X-64659, (1972).

7. Personal communication, W. A. Wilson, MSFC.

8. M. C. Flemings, Solidification Processing, (1974), McGraw-Hill, p. 146 ff.

9. K. Easterling, Introduction to the Physical Metallurgy of Welding, (1983), Butterworths, p. 70 ff.

10. "Aluminum Alloy 2219, Plate and Sheet," Federal Specification Sheet, QQ-A-250/30A, (November 19, 1982).

11. R. J. Beil and G. T. Hahn, "The Influence of Weld Process Variables on Crack Initiation and Growth In 2219-T87 Aluminum TIG and VPPA Weldments," Final Report to Martin Marietta Corporation, Contract No. AS 3-756222, (30 September 1983).

12. A. C. Nunes, Jr., E. O. Bayless, Jr., C. S. Jones III, P. M. Munafo, A. P. Biddle, and W. A. Wilson, "The Variable Polarity Plasma Arc Welding Process: Its Application To The Space Shuttle External Tank," to be published.

13. A. C. Nunes, Jr., H. L. Novak, and M. C. McIlwain, "Weld Geometry Strength Effect In 2219-T87 Aluminum," NASA Technical Memorandum NASA TM-82404, (March 1981).

14. A. C. Nunes, Jr., "An Extended Rosenthal Weld Model," Welding Journal, 62, (June, 1963), 165-s - 170-s.

15. B. R. Butcher and P. L. Allen, "Tensile Flow and Fracture at Large Inclusions," Metals Science, (October, 1977), 462-469.

16. C. E. Hartbower, W. G. Reuter, C. F. Morris and P. P. Crimmins, "Correlation of Stress-Wave-Emission Characteristics With Fracture in Aluminum Alloys," NASA Contractor Report NASA CR-2072, (July, 1972).

17. C. R. Heiple and S. H. Carpenter, "Changes in Acoustic-Emission Peaks in Precipitation Strengthened Alloys With Heat Treatment," Journal of Acoustic Science, 1, (October, 1982), 251-262.

D15

1984

NASA/ASEE SUMMER FACULTY RESEARCH FELLOWSHIP PROGRAM

MARSHALL SPACE FLIGHT CENTER
THE UNIVERSITY OF ALABAMA

NON-CONTACTING ELECTROMAGNETIC DE-SPIN SYSTEM FOR EARTH ORBITING SATELLITES

Prepared by:	Prasad K. Kadaba, Ph. D.
Academic Rank:	Professor
University and Department:	University of Kentucky Department of Electrical Engineering
NASA/MSFC:	Advanced Systems Office
MSFC Counterpart:	G. von Tiesenhausen
Date:	17 August 1984
Contract No.:	NGT 01-002-099 The University of Alabama

NON-CONTACTING ELECTROMAGNETIC DE-SPIN SYSTEM FOR EARTH ORBITING SATELLITES

BY

Prasad K. Kadaba
Professor of Electrical Engineering
University of Kentucky
Lexington, Kentucky 40506

ABSTRACT

This investigation is an extension of last year's study relating to electromagnetic satellite de-spin system for orbiting satellites [1]. Exact closed-form solutions for the interacting magnetic flux have been formulated both for the case of the current loop and the bar magnet. The magnet system has been extended to the case of a U-shaped magnet. Magnet design details are outlined. Computer simulation of the interacting flux density profile has been attempted. Data for the de-spin times has been extended to higher rpms.

ACKNOWLEDGEMENTS

The author wishes to acknowledge with thanks the valuable assistance of Mr. Georg von Tiesenhausen during his stay at the Marshall Space Flight Center. He wishes to thank Mr. Howard Lanier for the computer calculations.

INTRODUCTION

The theoretical study undertaken during the summer of 1983 indicated that the non-contacting electromagnetic satellite de-spin system based on the induction of counter-acting eddy-currents in the satellite is practical and requires only moderate amounts of power. The results indicated that it would be possible to reduce satellite spin to a very low value within a reasonable time.

In the study undertaken this year, closed-form solutions for the interacting magnetic flux have been formulated without introducing any approximations. This has been done both for the case of the current loop and the bar magnet. The analysis of the magnet system has been extended to the case of a U-shaped magnet. The weights of the current coil and the magnet assembly have been calculated. Finally, computer simulation of the interacting flux density profile has been attempted.

OBJECTIVES

The objectives of this study are to extend last year's effort in investigating the electromagnetic satellite de-spin system for orbiting satellites. The specific objectives are: (1) Exact closed-form solutions for the interacting magnetic flux; (2) design considerations for a useable U-shaped magnet; (3) computer simulation of the interacting flux density profile; (4) extension of the data to higher rpms; and (5) estimate of the weights of the current loop and magnet assemblies.

DETAILS OF THE STUDY

i) Satellite Motion Characteristics:

Consider a cylindrical, symmetric satellite as shown in Figure 1, which is both spinning and tumbling in space. When these angular rates are passive, i.e., there are no external torques acting on the satellite initially, the total angular momentum vector H of the satellite is fixed in direction in inertial space. The body continues to spin about its longitudinal axis and to precess about the angular momentum vector at a constant angle θ. In the absence of any external torques, the angle θ and the spin and precession rates remain constant for a symmetrical satellite. Figure 1 also shows the coordinate system used for the satellite moving under the influence of passivating torques. The XYZ coordinate system is the moving coordinate frame in the orbit, with X-axis directed outwards along the radius vector; Y-axis being perpendicular to the orbit plane and the Z-axis lying in the orbit plane to complete the right handed system. The xyz system is the body fixed coordinate system rotating with the satellite. The z-axis is the longitudinal axis of the satellite along the axis of symmetry. The x-axis and the y-axis are any two axes, located perpendicular to the z-axis and passing through an origin at the center of mass. Their exact location is immaterial because of symmetry. The location of the body axes referenced to the moving frame is described with the help of the three Eulerian angles (ϕ,θ,ψ).

The equations of motion of the satellite, moving under the influence of the applied torques, can be derived from the total kinetic energy T_s of the satellite via a Lagrangian formulation. The total kinetic energy T_s of a symmetric tumbling body is:

$$T_s = \frac{1}{2}\left[I_{x_s}\,\omega_x^{\,2} + I_{y_s}\,\omega_y^{\,2} + I_{z_s}\,\omega_z^{\,2}\right] \tag{1}$$

From the geometry of the Figure, it is seen that

$$\omega_z = \dot{\phi} + \dot{\psi}\cos\theta \tag{2}$$

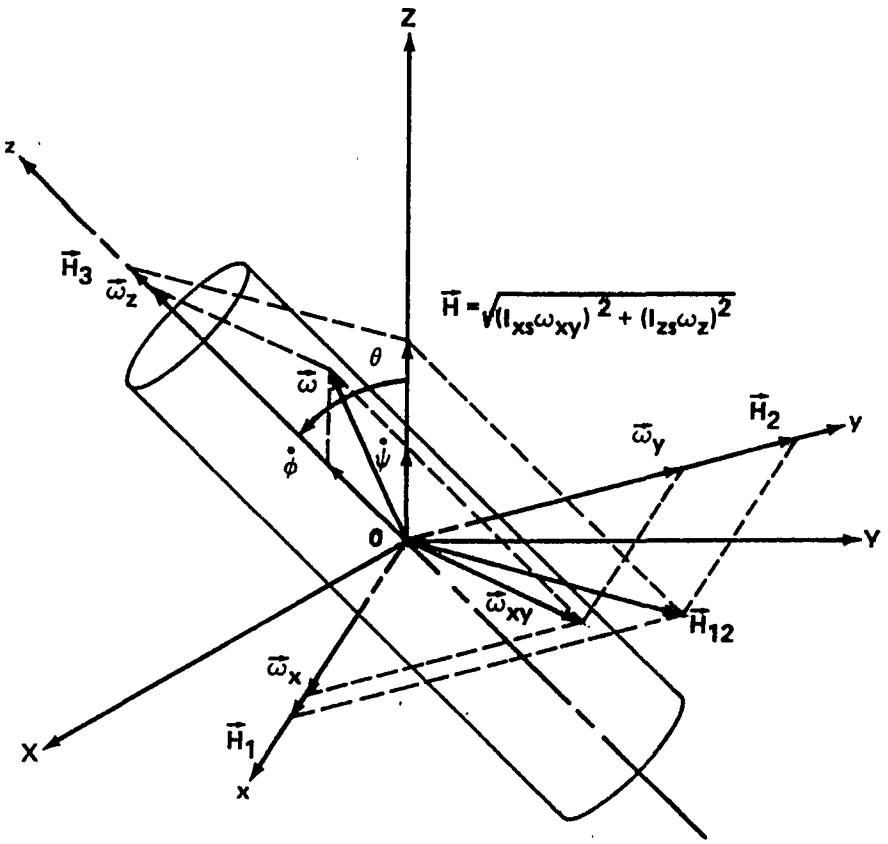

Fig. 1: Satellite axes system.

$$\omega_{xy}^2 = (\omega_x^2 + \omega_y^2) = \dot{\psi}^2 \sin^2\theta + \dot{\theta}^2 \tag{3}$$

and

$$I_{x_s} = I_{y_s} \tag{4}$$

$$T_s = \frac{1}{2} I_{x_s} [\dot{\psi} \sin\theta]^2 + \frac{1}{2} I_{x_s} \dot{\theta}^2 + \frac{1}{2} I_{z_s} [\dot{\phi} + \dot{\psi} \cos\theta]^2 \tag{5}$$

Now, the Euler-Lagrange equations of motion for a rigid body are [2]:

$$\frac{d}{dt} \frac{\partial L}{\partial q_r} - \frac{\partial L}{\partial q_r} = T_r \tag{6}$$

where the Lagrangian $L = (T - U)$, and T_r = generalized force in the direction of the rth generalized coordinate. If we are interested in only relative motion of the satellite with respect to the moving frame, we can neglect the potential energy U of the satellite. In view of this, differentiating the expression for the kinetic energy of the satellite with respect to the three generalized coordinates, i.e., the three Eulerian angles, will yield the equations of motion of the satellite as follows:

ψ direction:

$$(I_{x_s} \sin^2\theta + I_{z_s} \cos^2\theta)\, \ddot{\psi} + 2(I_{x_s} - I_{z_s})(\sin\theta \cos\theta)\, \dot{\theta}\, \dot{\psi} + I_{z_s} (\ddot{\phi} \cos\theta - \dot{\theta} \sin\theta\, \dot{\theta}) = T_1 \tag{7}$$

θ direction:

$$I_{x_s} \ddot{\theta} + (I_{z_s} - I_{x_s})\, \dot{\psi}^2 \sin\theta \cos\theta + I_{z_s} \dot{\phi}\, \dot{\psi} \sin\theta = T_2 \tag{8}$$

ϕ direction:

$$I_{z_s} (\ddot{\phi} + \ddot{\psi} \cos\theta - \dot{\psi}\, \dot{\theta} \sin\theta) = T_3 \tag{9}$$

These equations can be solved exactly with the help of elliptic functions if $T = 0$ or in the case of $T \neq 0$ on the digital computer using second-order Runge-Kutta method of integration.

ii) Expressions for the Interacting Magnetic Flux Density (Exact Solutions):

Current-loop Analysis: With reference to Figure 2 and last year's report, the flux components in cylindrical coordinates are: [c.f. equations (5) and (6) in Reference 1]

$$B_\rho = \frac{\mu_o IN}{2\pi} \frac{z}{\rho[(a+\rho)^2 + z^2]^{1/2}} \left[-K + \frac{(a^2 + \rho^2 + z^2)}{[(a-\rho)^2 + z^2]} E \right]$$

$$B_z = \frac{\mu_o IN}{2\pi} \frac{1}{[(a+\rho)^2 + z^2]^{1/2}} \left[K + \frac{(a^2 - \rho^2 - z^2)}{[(a-\rho)^2 + z^2]} E \right] \qquad (10)$$

$$B_\phi = 0$$

where N is the number of turns in the current loop and a is the radius of the loop. K and E are complete elliptic integrals of the first and second kind, respectively. Converting the above field expressions to rectangular coordinates, we have:

$$B_x = \frac{\mu_o IN}{2\pi} \frac{xz}{\sqrt{x^2+y^2}\,[(a+\sqrt{x^2+y^2})^2+z^2]^{1/2}} \left[-K + \frac{(a^2+x^2+y^2+z^2)\,E}{[(a-\sqrt{x^2+y^2})^2+z^2]} \right]$$

$$B_y = \frac{\mu_o IN}{2\pi} \frac{yz}{\sqrt{x^2+y^2}\,[(a+\sqrt{x^2+y^2})^2+z^2]^{1/2}} \left[-K + \frac{(a^2+x^2+y^2+z^2)\,E}{[(a-\sqrt{x^2+y^2})^2+z^2]} \right] \qquad (11)$$

$$B_z = \frac{\mu_o IN}{2\pi} \frac{1}{[(a+\sqrt{x^2+y^2})^2+z^2]^{1/2}} \left[K + \frac{(a^2-x^2-y^2-z^2)\,E}{[(a-\sqrt{x^2+y^2})^2+z^2]} \right]$$

The flux linkage $d\psi$ when, dx, in the skin of the cylinder rotates through an angle $d\alpha$ is given by:

$$d\psi = (\overline{B} \cdot \overline{1})\, A_s\, dx\, d\alpha$$

where the unit vector $\overline{1} = (\cos\alpha)\overline{a}_y + (\sin\alpha)\overline{a}_z$ and A_s = radial distance to dx from the rotational axis of the cylinder. We have then:

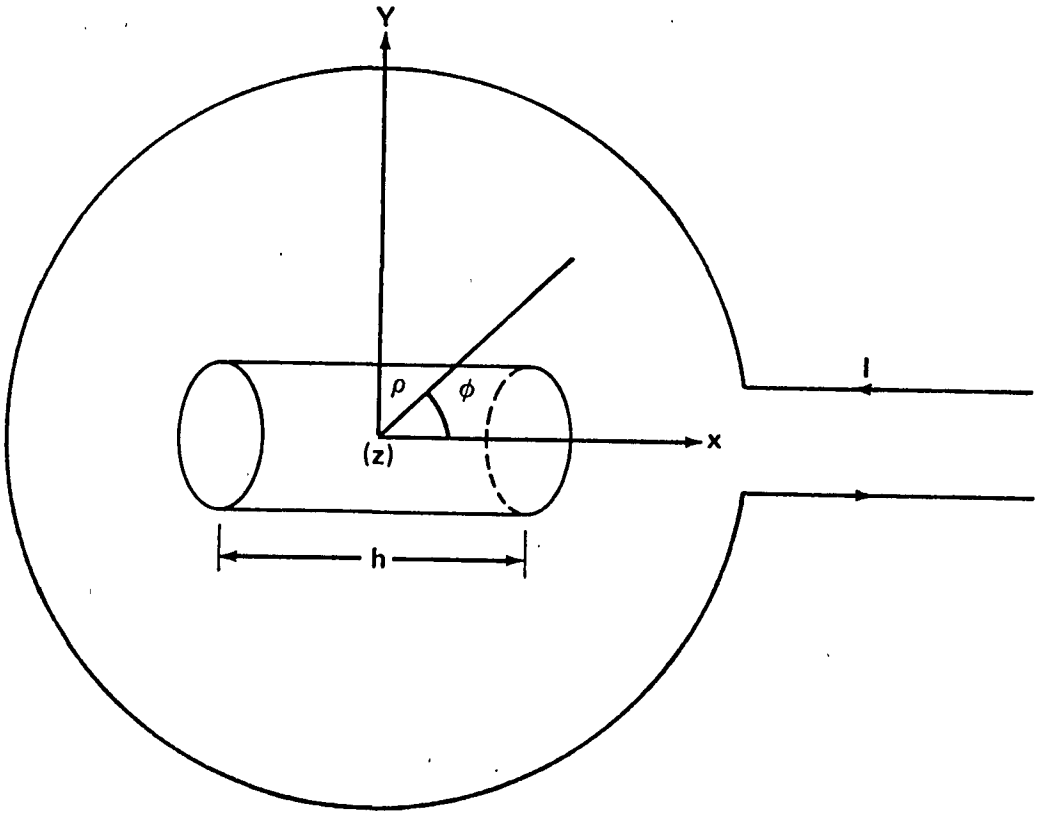

Fig. 2: Configuration of the satellite positioned symmetrically with respect to the current loop; rotation axis of the cylinder is in the plane of the current loop.

$$d\psi = A_s B_y \cos\alpha \, d\alpha \, dx + A_s B_z \sin\alpha \, d\alpha \, dx \tag{12}$$

$z = A_s \sin\alpha$; $d\alpha = \dfrac{dz}{\sqrt{(A_s^2 - z^2)}}$ and equation (12) becomes

$$d\psi = B_y \, dz \, dx + \frac{B_z \, z \, dz \, dx}{\sqrt{(A_s^2 - z^2)}} \tag{13}$$

The motional e.m.f., ε, generated is given by:

$$\varepsilon = 2 \int_{z=0}^{z=A_s \sin\alpha_1} \int_{x=0}^{h/2} \left[B_y + \frac{z \, B_z}{\sqrt{(A_s^2 - z^2)}} \right] dx \, dz \tag{14}$$

where $\alpha_1 = \dfrac{2\pi \text{ RPM}}{60}$. It should be noted that y in the expression for B_y and B_z as given in equation (11) should be replaced by $y = \sqrt{A_s^2 - z^2}$ before the integration with respect to x and z is performed. The eddy current power input to the satellite is given by:

$$P_s = \int_{r=A_{Si}}^{r=(A_{Si} + t/2)} \frac{\varepsilon^2 \, \pi \, r dr}{2 \, \rho_{Ae} \, h} \tag{15}$$

In the integrand of equation (15), A_s in the expression for ε obtained from equation (14) should be changed to the variable, r, before the P_s integral is evaluated.

Magnet System Analysis Allowing for Rotation of the Magnet Around the x-axis:

As shown in the sketch with the magnet oriented at an angle χ with respect to the z-axis, the magnetic flux density $\bar{B}$ at point P(x,y,z) is given by (Reference 1):

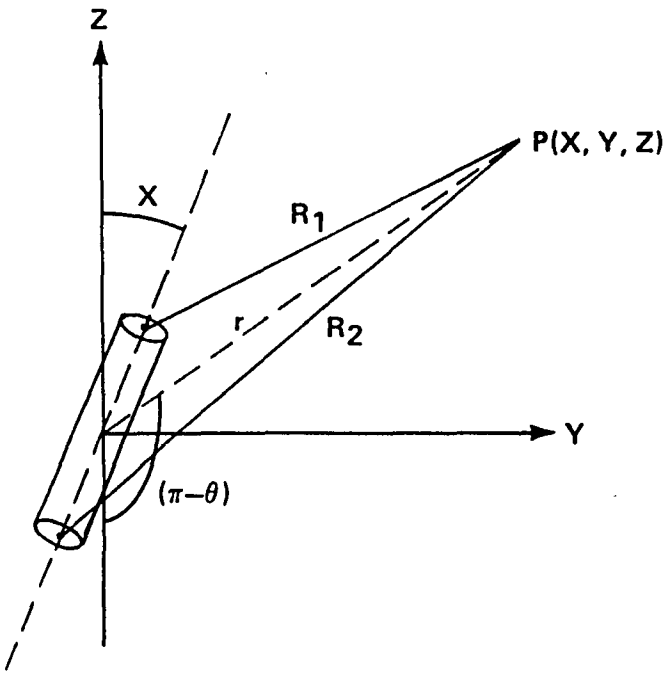

$$\bar{B} = \frac{\mu_o M a^2}{4} \left(- \frac{\bar{a}_{R_2}}{R_2^2} + \frac{\bar{a}_{R_1}}{R_1^2} \right) \tag{16}$$

where M is the magnetization of the bar magnet in Amperes/Meter, a, its radius and $\bar{a}_{R_1}$, $\bar{a}_{R_2}$ are unit vectors along R_1 and R_2 pointing towards the field point P. Changing to rectangular coordinates, the expression for $\bar{B}$ in equation (16) becomes:

$$\bar{B} = \frac{\mu_o M a^2}{4} \left[\frac{\{\bar{a}_x x + \bar{a}_y (y - \frac{d}{2}\sin\chi) + \bar{a}_z (z - \frac{d}{2}\cos\chi)\}}{\{x^2 + (y - \frac{d}{2}\sin\chi)^2 + (z - \frac{d}{2}\cos\chi)^2\}^{3/2}} \right.$$

$$\left. - \frac{\{a_x x + \bar{a}_y (y + \frac{d}{2}\sin\chi) + \bar{a}_z (z + \frac{d}{2}\cos\chi)\}}{\{x^2 + (y + \frac{d}{2}\sin\chi)^2 + (z + \frac{d}{2}\cos\chi)^2\}^{3/2}} \right] \tag{17}$$

Flux linkage in time (dt) by the rotating cylinder is given by:

$$\bar{B}\cdot d\bar{S} = B_x dS_x + B_z dS_z \qquad (18)$$

where

$$dS_z = -(dxdy)$$

and

$$dS_x = \frac{x\ dxdy}{\sqrt{(A_s^2 - x^2)}} \quad .$$

B_x and B_z are the x and z components of the vector $\bar{B}$ in equation (17). Figure 3 shows the axes of coordinates as well as the relative positions of the bar magnet and the cylinder.

The motional e.m.f. ε is given by:

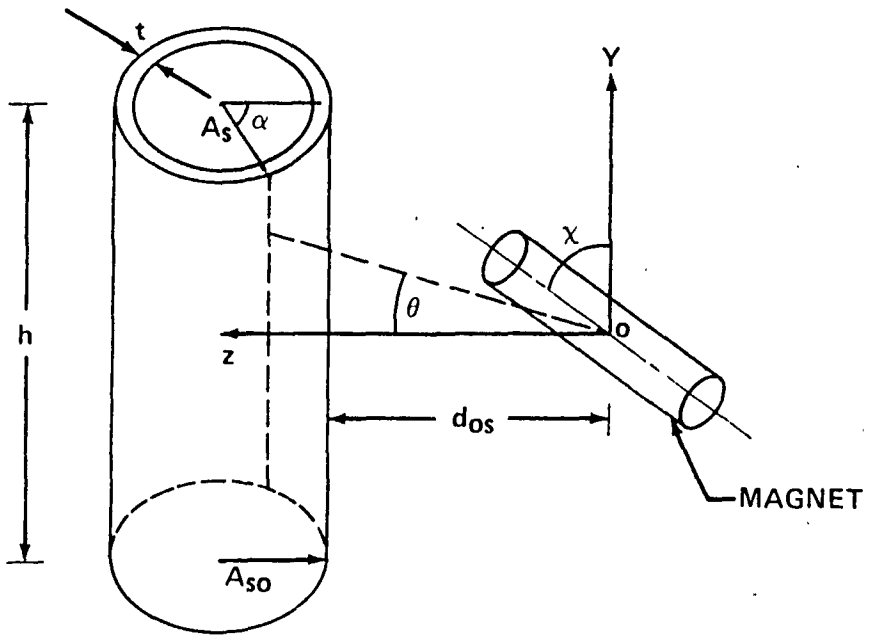

Fig. 3: Configuration for the magnet system; origin of coordinates is at the center of the magnet with the axes as shown. Length of the magnet = D meters; radius of the magnet = A meters.

$$\varepsilon = 2 \int_{y=0}^{y=h/2} \int_{x=0}^{x=A_s \sin\alpha_1} \left[\frac{B_x \, x}{\sqrt{(A_s^2 - x^2)}} - B_z \right] dx dy \qquad (19)$$

where

$$\alpha_1 = \frac{2\pi \ RPM}{60} \ .$$

In the integrand in equation (19), z in the expressions for B_x and B_z should be replaced by:

$$z = [K - \sqrt{(A_s^2 - x^2)}] \text{ with } K = (A_{0S} + d_{0S})$$

where A_{0S} is the outer radius of the cylinder and d_{0S} is defined in Figure 3. The eddy current power input P_s is given by:

$$P_s = \int_{r=A_{Si}}^{r=A_{Si}+T/2)} \frac{\varepsilon^2 \, \pi r dr}{2 \, \rho_{Al} \, h} \qquad (20)$$

where as before A_s in the integral evaluated for ε in equation (19) is replaced by the variable r.

iii) Design Considerations:

(a) Weight of the current loop: The results of last year showed that 9000 A-T is a suitable value to yield a reasonable de-spin time. The power available on the Shuttle for the application on hand is about 6 K.W. Based on this, for a 10 meter diameter coil at room temperature the total weight is around 450 Kgms. Using thinner AWG-8 wire capable of carrying 45 amps, the weight of the coil can be brought down to 100 Kgms. But because of the increased resistance, the power required will be around 29 K.W. At liquid nitrogen temperature, as pointed out in last year's report, the overall diameter of the insulated coil conductor is around 2 inches. This leads to an overall weight of the current loop of around 200 lbs. But if the weight of the 160 liter dewar filled with liquid N_2 required to operate the coil is included, the total weight of the set-up would be around 800 lbs or 364 Kgms. So by comparing this weight with the room temperature weight of 450 Kgms, there does not seem to be a decided advantage in going to liquid N_2. It is true that the power required to energize the current loop at liquid N_2 would be only

1.1 KW; but this advantage is offset by the need for additional equipment to operate the low temperature system.

(b) Weight of the U-shaped electromagnet: As shown in the sketch in Figure 4 an electromagnet (U-shaped) in principle could be designed to provide the necessary interacting magnetic flux. The calculations shown below are for a pole-face diameter of 1.5 m with an airgap of 4 m and a flux density across the gap of 5 gauss. The cross-section of the yoke is chosen as 22 cm^2. Using the above values, the flux density B_m in the yoke works out to 4.545 kilogauss. Using 34% Co-Fe as the magnet material the corresponding magnetic field intensity H_m is 2.7 oersted. The resulting permeability value μ_r is 1683. The length of the yoke L_m, is given by $L_m = \frac{\mu_r B_g L_g}{B_m}$ where L_g is the length of the air gap. Using the above numerical values the total weight of the magnet works out to 365 Kgms. This compares favorably with the weight of the room temperature current loop configuration. The ampere turns (NI) required to drive the flux across the gap is given by [3]:

$$NI = \frac{B_m}{\mu_o}\left[\frac{(L_m - L_g)}{\mu_r} + L_g \frac{S_y}{S_p}\right]$$

where S_y is the area of cross-section of the yoke, S_p is the area of the pole-face and μ_o is permeability of free space.

Using the above numerical values, NI = 2535 A-T. Using AWG-8 wire and I = 45 amps, N = 56 turns. The power required I^2R = 60 watts. Other details of the design of the electromagnet are given in reference [4].

(c) To summarize, for the U-shaped electromagnet:

Weight of the magnet = 365 Kgms

Power required = 60 watts

Material: 34% Co-Fe

Gap flux = 5 gauss

Dimensions: As shown in Figure 4.

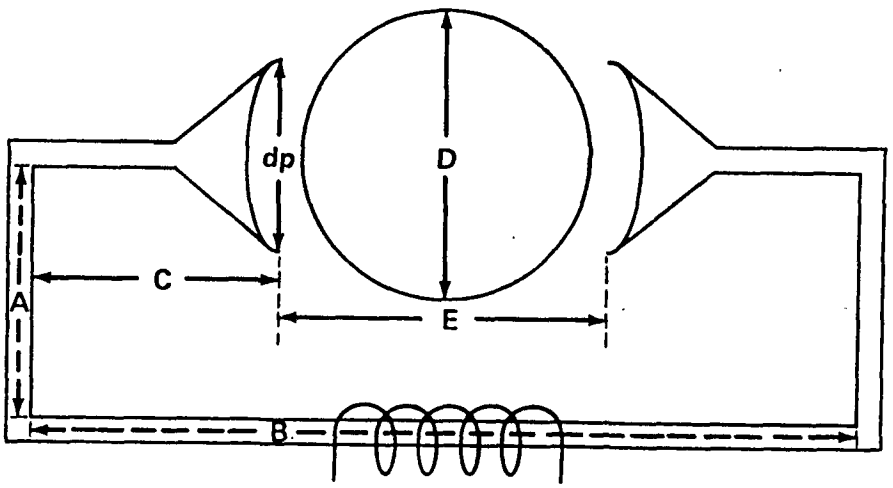

Fig. 4: Sketch of the electromagnet with flared pole faces; typical dimensions in meters: A = 1.55; B = 4.5; C = 0.25; D = 3; E = 4; dp = 1.5.

iv) Results and Analysis

Last year, both in the case of the current loop and the bar magnet — (only magnet type studied) — the various parameters which affect the de-spin time were parametrically analyzed using different ampere-turns and radii for the current loop and using two different magnetization values for the magnet. In the case of the magnet, the position of the magnet was varied relative to the spinning satellite, the closest distance being about 2 feet from the cylinder (satellite). This year's effort has been concentrated on the results for a single ampere-turn coil and a single position of the bar magnet — about 2 ft from the satellite. In addition, the bar magnet was rotated about the x-axis from χ=0 to 90°. The magnet system was also extended for a different configuration, namely, a U-shaped electromagnet.

During the first 2½ weeks of the 5-week assignment, the author concentrated his efforts in finding the reason why in the case of the magnet system, the de-spin time increases as the initial rpm of the spinning satellite increases. This is contrary to what one would expect. To investigate this anamoly, different satellite dimensions and rpms higher than 10 rpm were investigated. In addition computer simulation of the interacting flux plot was obtained for the case of the bar magnet. The de-spin times in all cases consistently increased as the rpm increased. This was not only true for the case of the bar magnet but also for the case of the U-shaped electromagnet, the additional system studied this year. Detailed results are outlined below. One interesting result of this investigation is shown in Table I which compares data for two satellites which differ only in the skin thickness for the case of the bar magnet configuration. The results indicate remarkably close correlation of the de-spin times from 1 to 10 rpm.

Table I: Comparison of the de-spin times in minutes versus rpm for the two satellites which differ only in the skin thickness.

Magnet parameters: $M = 7.96 \times 10^5$ A/M; A = 0.087 M; D = 2.5 M; D_{os} = 1.85 M. Satellite Dimensions: h = 2.5 M; inside diameter = 2.9 M; skin thickness = T

RPM:	1	2	4	6	8	10
Satellite I (T = 0.05)	2.0	2.85	6.4	13.5	26.2	49
Satellite II (T = 0.01)	2.1	2.9	6.4	13.3	26.0	48

It is very probable that the reason why the de-spin time increases as the rpm increases is because the kinetic energy of the satellite increases as the square of the rpm and thus increases much faster compared to the increase in P_s, the eddy-current power input into the

satellite. This explanation is definitely the case in the case of the current loop configuration where the de-spin time increases beyond 20 rpm.

Figure 5 shows the eddy current power input P_s, and de-spin time T, versus RPM for the current loop configuration. The specifications for the current loop are: NI = 9,000 A-T and radius A = 5 M. The satellite dimensions are: height (h) = 2.5 M, diameter (D) = 3 M, skin thickness (T) = 0.05 M. Figures 6 and 7 show the same parameters, namely, P_s and T versus RPM for the case of the bar magnet and U-shaped electromagnet, respectively. The satellite dimensions are the same as indicated above. For the bar magnet, M = 7.96×10^5 A/M, Radius A = 0.087 M; Length D = 2.5 M and the center of the magnet is 1.85 M from the cylinder surface. For the U-shaped electromagnet, the gap flux is 5 gauss; diameter of the pole face is 1.5 M and the gap length is 4 M.

For the current-loop configuration results shown in Figure 5, it was interesting to note that the de-spin time increases with increase in RPM after about 20 RPM, where, as indicated in last year's report, the de-spin time decreases as the RPM increases. The results of last year were only up to 10 RPM. For both the magnet configurations as shown in Figures 6 and 7, the de-spin times increase with increase in RPM right from 1 RPM although for the case of the U-shaped magnet, the de-spin time seems to level off beyond 80 RPM. For the bar magnet configuration as shown in Figure 6 the de-spin time increases rapidly beyond 30 RPM.

The de-spin time at 80 RPM for the bar magnet configuration is 156 minutes whereas for the U-shaped magnet system it is 80 minutes. These results suggest that the bar magnet is less efficient for higher RPMS compared to the U-shaped magnet. At RPMS below 40, de-spin times are lower for the bar magnet compared to the U-shaped magnet. A comparison of the results in Figures 6 and 7 also indicates that the eddy-current power input, P_s, for the U-shaped magnet is relatively higher compared to the bar magnet especially for higher RPMS. This is to be expected as the U-shaped configuration with the pole faces encircling the satellite would be more efficient than the bar magnet in producing higher flux densities on the skin of the satellite.

Figure 8 is a comparison of the P_s values for the U-shaped magnet whose dimensions are given in Figure 4 and the 9000 A-T current loop whose diameter is reduced to 8 meters. There seems to be good correlation between the two systems, the value at 80 rpm being almost the same.

It was thought interesting to see what effect the orientation of the bar magnet would have on the eddy current input. Results were obtained for orientation around the x-axis (Figure 4). It was found that P_s reaches a maximum around $\chi = 15°$ and then drops off. For $\chi = 90°$, P_s has the least value.

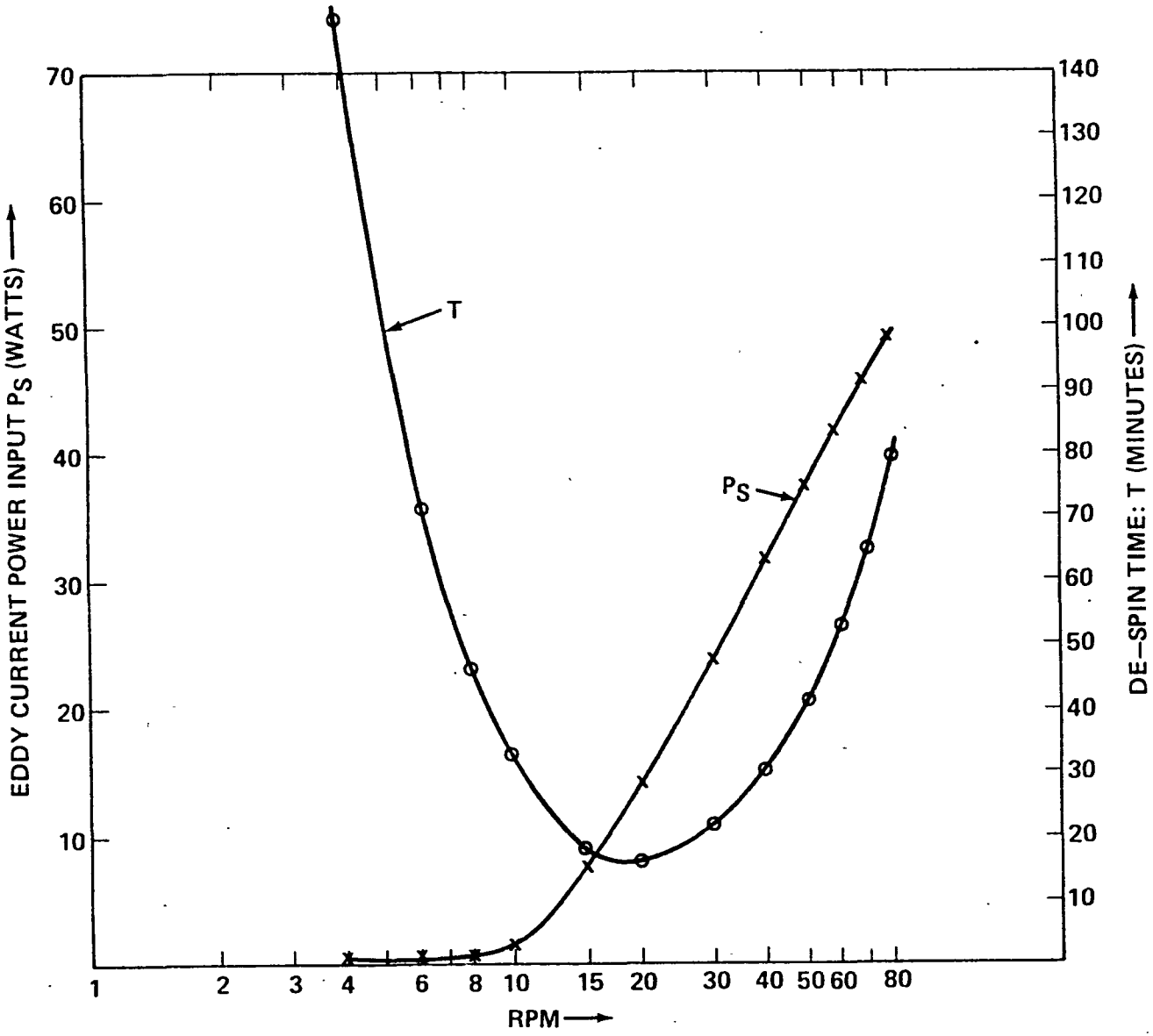

Fig. 5: Eddy current power input, P_S, and de-spin time T, versus RPM for the current loop configuration. NI = 9,000 Ampere-Turns. Loop diameter = 10 M. Satellite dimensions: Height = 2.5 M, Diameter = 3 M, Wall Thickness = 5 cms.

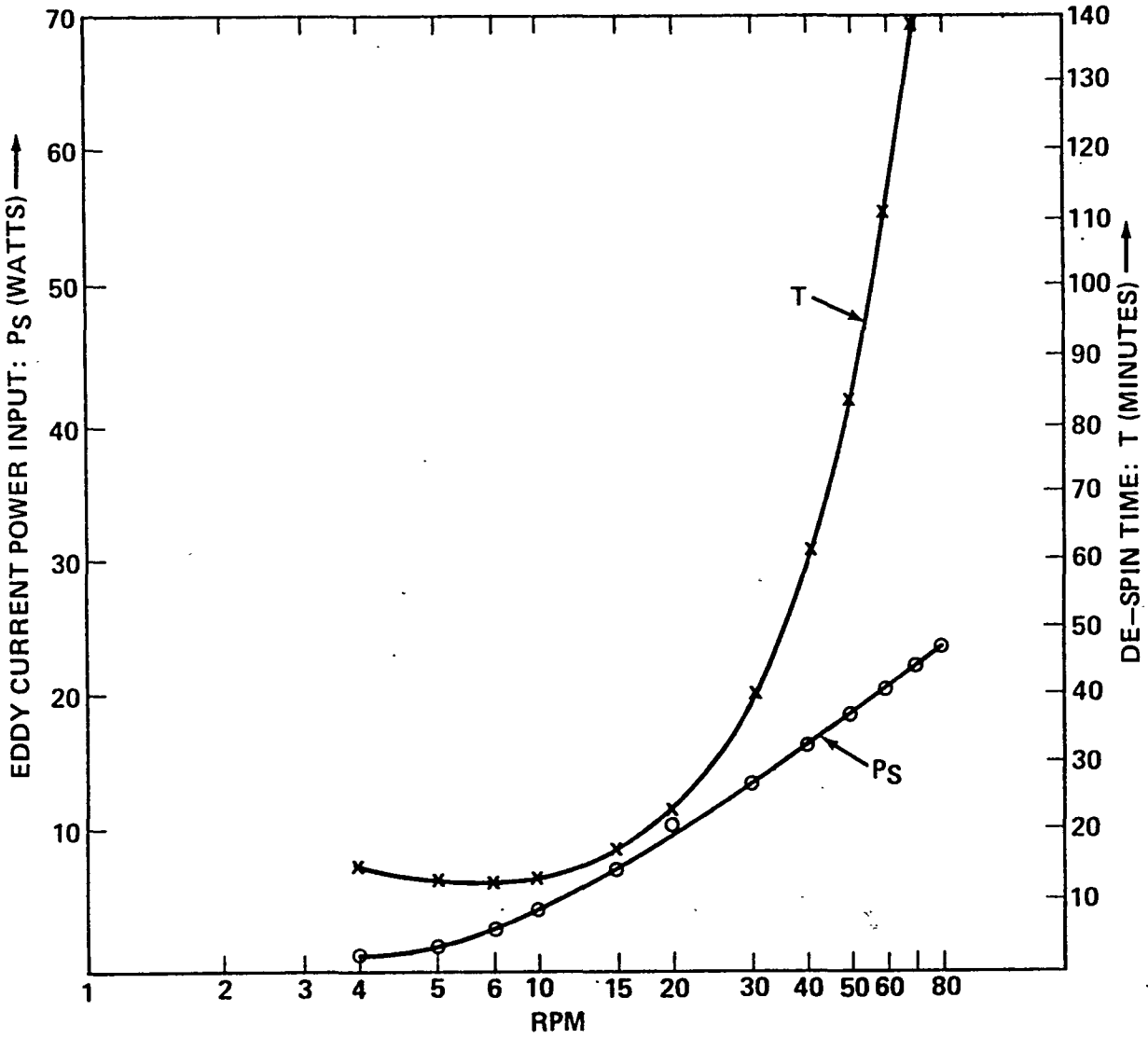

Fig. 6: Eddy current power input P_S and de-spin time T versus RPM for the bar magnet configuration. Magnet dimensions: Length = 2.5 M; Diam. = 0.087 M; Magnetization (M) = 7.96 x 10^5 A/M. Center of the magnet = 1.85 Meters from the cylindrical surface. Satellite dimensions: same as in Figure 5.

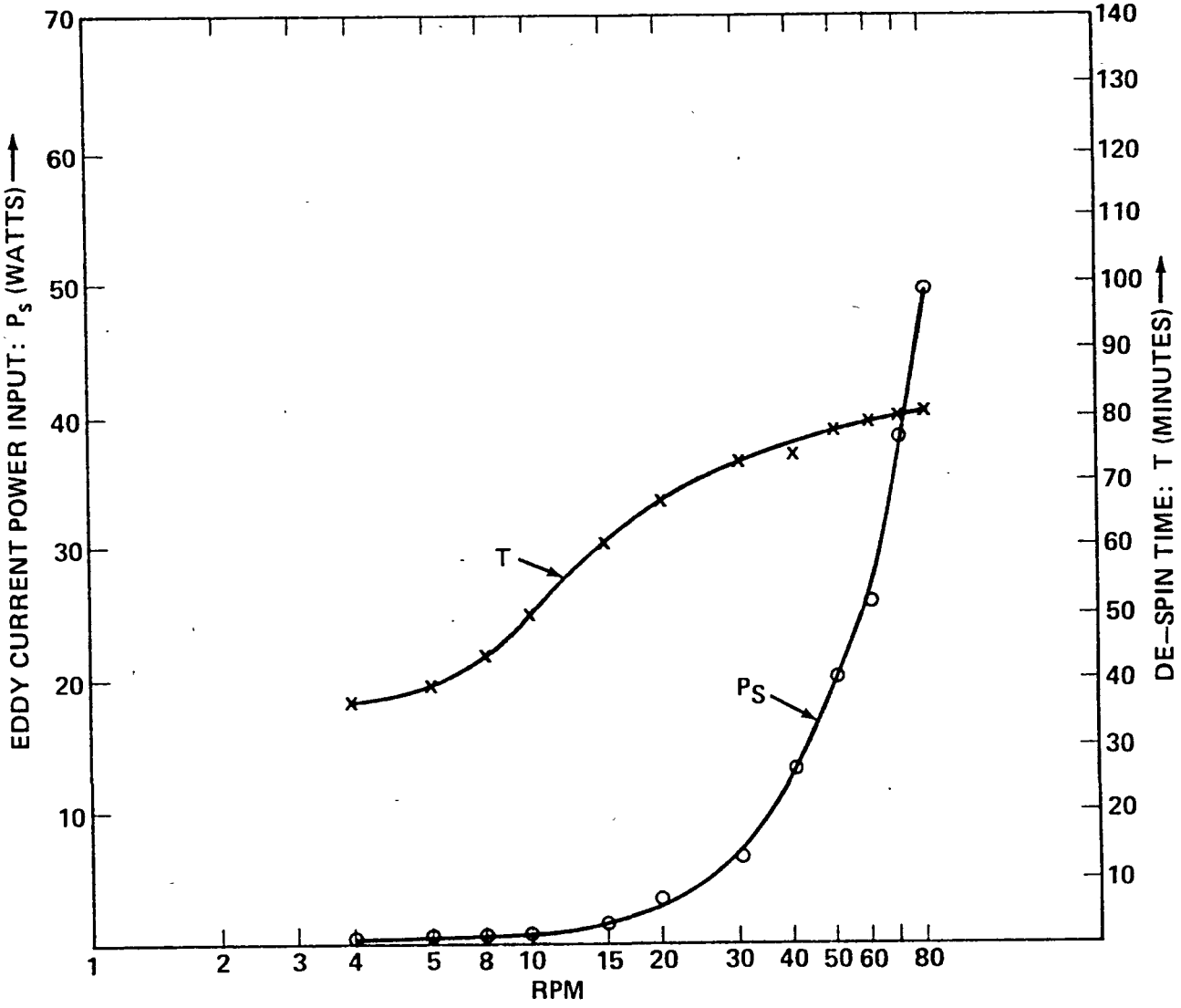

Fig. 7: Eddy current power input P_S and de-spin time T, versus RPM for the U-shaped electromagnet configuration. Flux density in the air gap = 5 gauss; diameter of the pole face = 1.5 M. Satellite dimensions: same as in Figure 5.

A review of the weight considerations for the current loop and U-shaped magnet outlined in Section (iii) suggests that both designs are equally preferred. Both yield reasonable values of de-spin times. Conceptually, perhaps, the coil configuration would be easier to implement than the magnet configuration.

Figures 9 and 10 are the computer plots of vector flux densities for the case of the bar magnet. In Figure 9 the center of the magnet is 1.85 M from the satellite and in Figure 10, the center is 2.85 M from the satellite. The origin of coordinates shown in the flux plots is at the cylindrical surface on one side — that is 1.85 M from the magnet center in Figure 9 and is 2.85 M from the magnet center in Figure 10. An arrow drawn from the origin to any point on the curves is the vector direction of the flux density. The density of the computer plot curves is a measure of the magnitude of the flux density. As is seen in Figure 10 the flux density is reduced and also more evened out as the magnet moves away from the satellite. The Fortran computer program to plot the flux is also enclosed.

Finally, the exact flux density calculations given earlier in the report in Section (ii) yields results about 20% better than the approximate methods used for the calculations last year. The possibility of satellites spinning as high as 80 RPM do exist as, for example, the application technology satellite ATS-5 referred to in Reference [5]. The idea of carrying a large permanent magnet inside the Shuttle may not be feasible in the practical sense. The air gap needs to be short circuited while carrying the device into space. Then the problem of removing the "keeper" and creating the large air gap is not realizable in the practical sense.*

CONCLUSIONS AND RECOMMENDATIONS

i) The seeming anamoly found in last year's study, namely, increase in de-spin time with increase in the initial rpm of the satellite for the bar magnet configuration was investigated in detail. The parameters that were varied were the thickness of the cylinder wall, satellite dimensions, rpms higher than 10. The de-spin times showed a consistent increase as the rpm increases not only for the bar magnet but also for the U-shaped electromagnet encircling the satellite. In addition, even for the current loop configuration the de-spin times increased above 20 rpm. No definite conclusions could be drawn from the computer plots of the interacting flux. It was concluded that the main reason was that the kinetic energy of the spinning satellite increases as the square of the rpm whereas the corresponding eddy current power input to the satellite does not increase that rapidly.

ii) Exact solutions for the flux density calculations yielded about 20% improvement in the results.

*Private communication with Mr. Don Kusterbuck at PERMAG Corporation, 6730 Jones Mill Ct., Norcross, GA 30092.

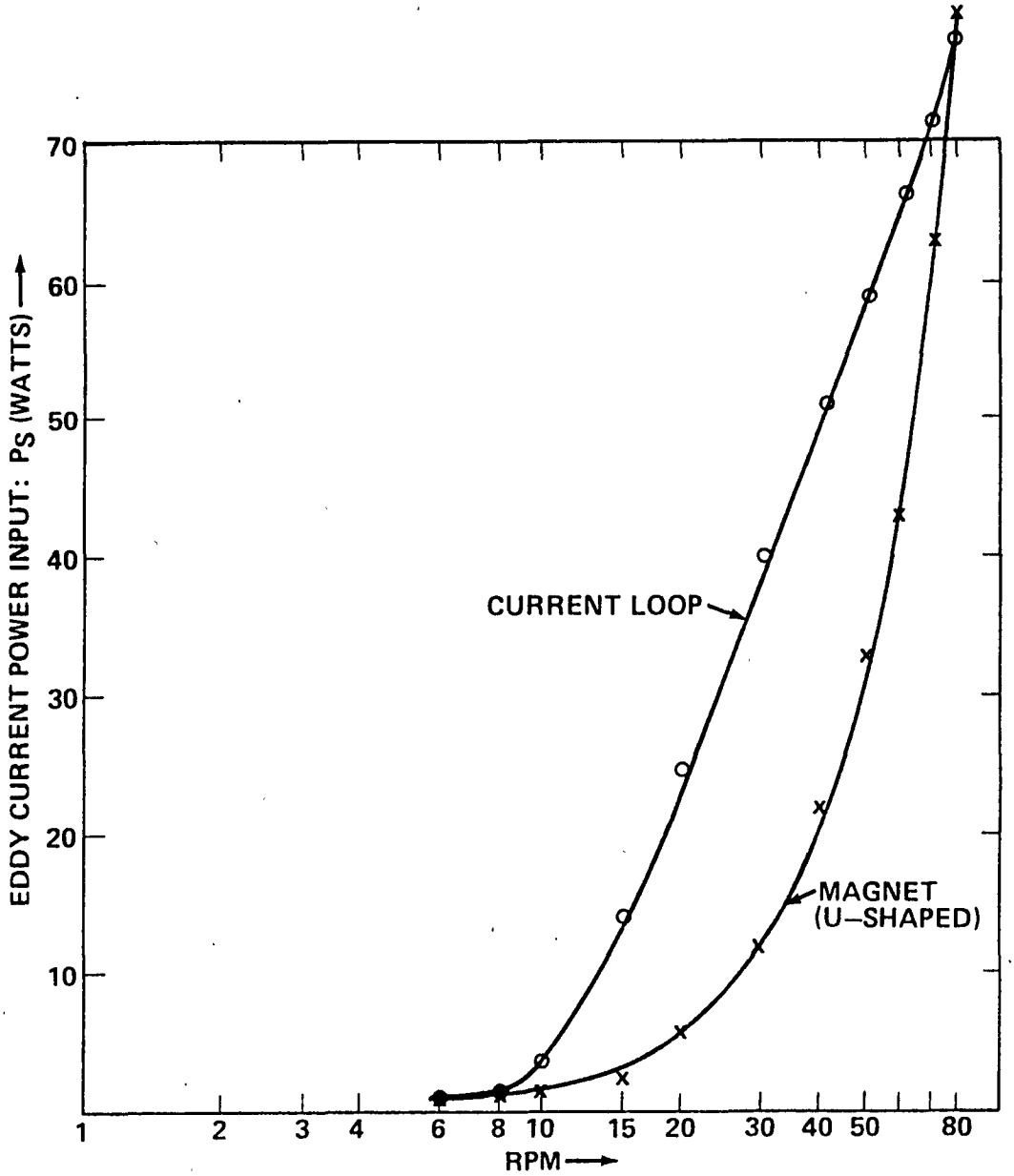

Fig. 8: Eddy current power input versus rpm for current loop and U-shaped magnet; current loop: NI = 9000 A-T; Diameter = 8 M; Magnet: air gap = 4 M; diameter of pole face = 2.5 M. Flux density across air gap = 5 gauss. Satellite dimensions: height = 2.5 M; diameter = 3M, wall thickness = 5 cms.

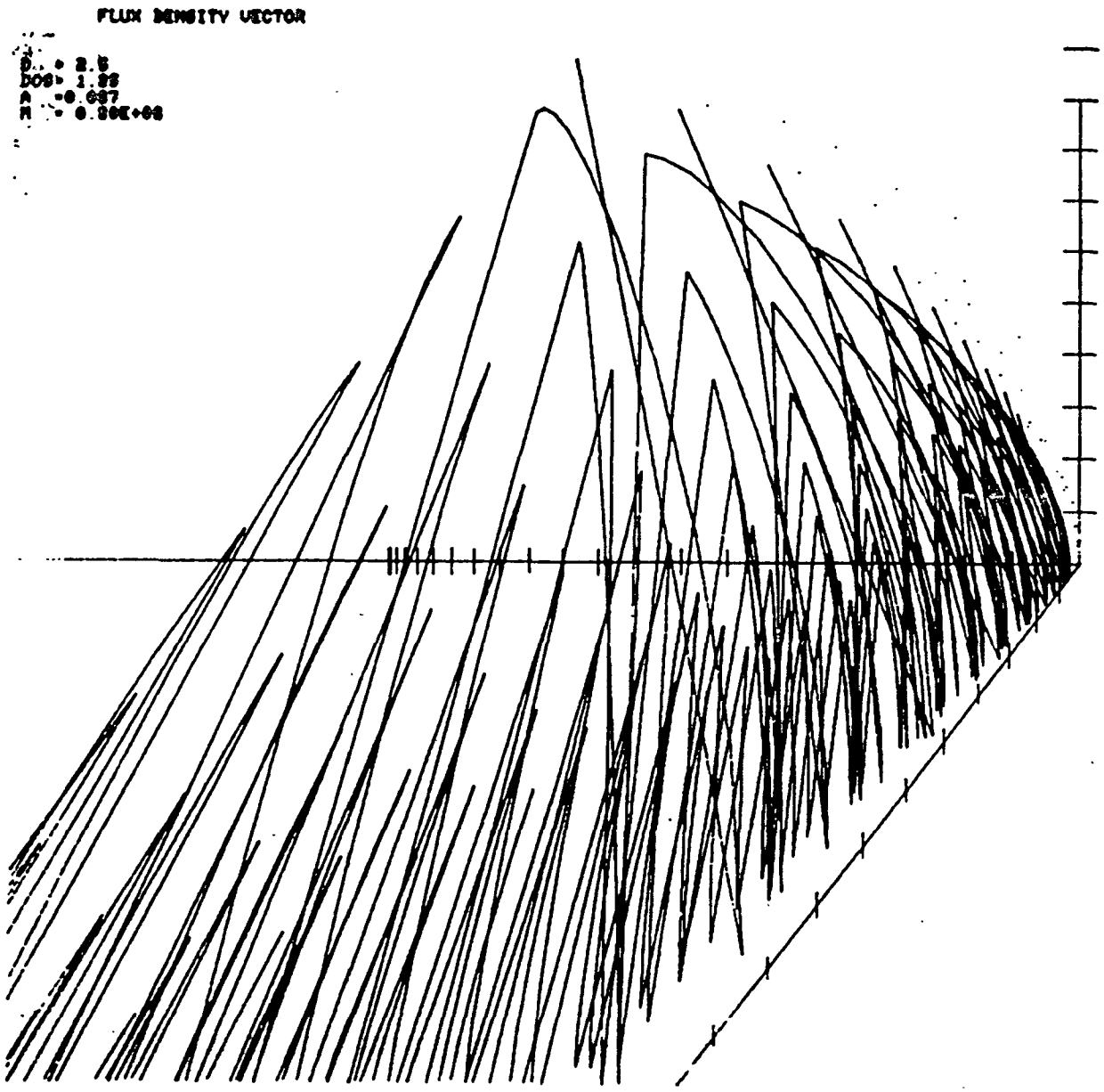

Fig. 9: Computer plot of the interacting flux density for the bar magnet configuration. Magnet parameters: M = 8 x 10^5 A/M, radius A = 0.087 M, length D = 2.5 M, D_{OS} = 1.85 M.

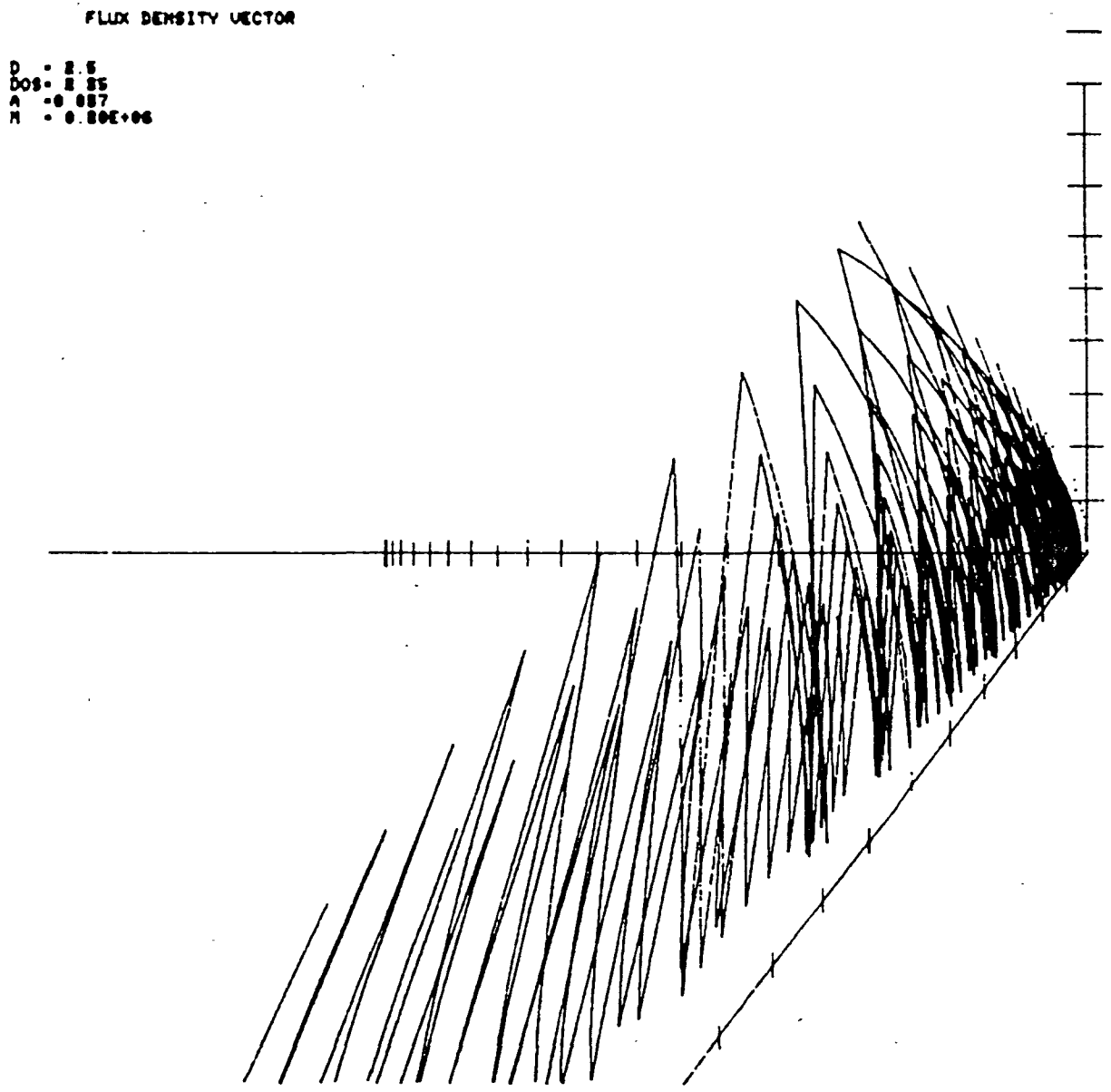

Fig. 10: Computer plot of the interacting flux density for the bar magnet configuration. Magnet parameters: same as in Figure 9; D_{OS} = 2.85 M.

FORTRAN PROGRAM SUBROUTINE FOR FLUX DENSITY PLOT

```
      SUBROUTINE PLOTDAT
      CALL WWINDO(0.,40.,0.,40.)
      CALL SWINDO(0,980,0,750)
      PI=3.14159265
      S30=SIN(PI/6.)
      C30=COS(PI/6.)
      D=2.5
      CMU=1.25664E-06
      CM=7.96E+05
      A=.087
      CON1=(CMU*CM*A**2)/4.
      DOS0=1.85
      DELTX=.1
      DELTZ=.01
      SCALE=1.E+05
      DDOS=1.
      DELZ=.3
      DELX=.15
      DELY=.15
      N=0
1     N=N+1
      DOS=1.85+FLOAT(N-1)*DDOS
      IF(DOS.GT.3.)GO TO 5
      CALL NEWPAG
      PRINT *,'          FLUX DENSITY VECTOR'
      WRITE(6,995)D,DOS,A,CM
995   FORMAT(//2X,'D   =',F4.1/2X,'DOS=',F5.2/2X,'A   =',F5.
     *3/2X,'M   =',E9.2)
      CALL MOVEA(0.,20.)
      CALL DRAWA(31.,20.)
      CALL MOVEA(31.,38.)
      CALL DRAWA(31.,20.)
      CALL DRAWA(19.453,0.)
      Y=0.
      Z=0.
      DO 990 I=1,10
      X=2*I
      XP=.5*X*(1.+.055*X)
      YPLOT=20.+Y-XP*C30
      XPLOT=31.-XP*S30
      CALL MOVEA(XPLOT,YPLOT-.5)
      CALL DRAWA(XPLOT,YPLOT+.5)
990   CONTINUE
      X=0.
      Z=0.
      DO 991 I=1,10
      Y=2*I
      XPLOT=31.
      YPLOT=20.+Y
      CALL MOVEA(XPLOT-.5,YPLOT)
      CALL DRAWA(XPLOT+.5,YPLOT)
991   CONTINUE
      X=0.
      Y=0.
      DO 992 I=1,20
      Z=2*I
      Z1=.5*Z*(1.-.025*(Z-40.))
      XPLOT=31.-Z1
      YPLOT=20.
      CALL MOVEA(XPLOT,YPLOT-.5)
      CALL DRAWA(XPLOT,YPLOT+.5)
992   CONTINUE
      DO 2 I=1,10
      QY=I-1
      Y=QY*DELY
      DO 3 J=1,10
      QX=J-1
      X=QX*DELX
      DO 4 K=1,10
      QZ=K-1
      Z=DOS+DELZ*QZ
      U1=X*X+Y*Y
      U2=Z-D/2.
      U3=Z+D/2.
      VAL1=SQRT(U1+U2*U2)
      VAL2=SQRT(U1+U3*U3)
      XMULT=1./VAL1-1./VAL2
      X1=CON1*X*XMULT*SCALE
      Y1=CON1*Y*XMULT*SCALE
      Z1=CON1*(U2/VAL1-U3/VAL2)*SCALE
      Z1=ABS(Z1)
      XP=.5*X1*(1.+.5*X1)
      YPLOT=Y1+20.-XP*C30
      ZP=.5*Z1*(1.-.025*(Z1-40.))
      XPLOT=31.-ZP-XP*S30
      IF(J.EQ.1)CALL MOVEA(XPLOT,YPLOT)
      CALL DRAWA(XPLOT,YPLOT)
C     PRINT *,X1,Y1,Z1
4     CONTINUE
3     CONTINUE
      CALL HDCOPY
      CALL NEWPAG
2     CONTINUE
      GO TO 1
5     RETURN
      END
```

iii) The weights of the room temperature current loop coil and the U-shaped electromagnet are comparable and both designs are equally preferred. Both yield comparable values of de-spin times. It was concluded that there was no particular advantage in going to liquid nitrogen cooled coils. The extra equipment and more elaborate design would offset the lower power consumption (about 1 KW) of the low temperature coil.

iv) The results obtained for different orientations of the bar magnet had some effect, P_s increasing to a maximum for $\chi = 15°$ and then dropping off.

v) The results indicated that the bar magnet configuration is less efficient than the U-shaped electromagnet configuration.

vi) Permanent magnet system was not desirable because of the difficulty involved in obtaining a wide air gap in space.

The recommendations are:

i) A cost effective 1 to 50 scaled down model of the proposed de-spin system should be constructed and tested as a first step particularly with the current loop configuration.

ii) If the results in step (i) above are found satisfactory, a full scale model could be developed.

iii) The detailed design and cost of the electromagnet should be pursued with some commercial sources such as the PERMAG Corporation.

REFERENCES

1. Kadaba, Prasad K., "A Feasibility Study of Electromagnetic De-spin System for Earth Orbiting Satellites," NASA/ASEE Summer faculty final report, 1983, pp. XVIII-1 to 32.

2. Greenwood, D. T., Principles of Dynamics, Prentice-Hall, Inc., New Jersey, 1965, Chapter 8.

3. Nussbaum, Allen, E. M. Theory for Engineers and Scientists, Prentice Hall, Inc., Englewood Cliffs, New Jersey, 1965, Chapter 5.

4. Kroon, D. J., Electromagnets, Boston Technical Publishers, Cambridge, Mass., 1968.

5. Lenox, Herbert M., "Capture of Uncontrolled Satellites - A Flight Demonstration," Marshall Space Flight Center, Alabama.

1984

NASA/ASEE SUMMER FACULTY RESEARCH FELLOWSHIP PROGRAM

MARSHALL SPACE FLIGHT CENTER
THE UNIVERSITY OF ALABAMA

CONSIDERATIONS FOR UPGRADING MODIFICATIONS TO THE MARSHALL SPACE FLIGHT CENTER'S X-RAY CALIBRATION FACILITY

Prepared By:	J. H. Kitterman, Ph.D.
Academic Rank:	Assistant Professor
University and Department:	South Dakota State University Department of Physics
NASA/MSFC:	
Laboratory:	Test
Division:	Systems and Components Test
Branch:	Environmental Test
MSFC Counterpart:	J. C. Reily, Jr.
Date:	August 3, 1984
Contract No.:	NASA-NGT-01-002-099 (The University of Alabama)

ACKNOWLEDGEMENTS

My thanks and appreciation go to the NASA/ASEE Summer Faculty Fellowship Program for providing me the opportunity to participate. I also wish to extend my thanks and appreciation to W. E. Dickson for hospitality and concern beyond that expected. This acknowledgement would not be complete without my expression of gratitude for the sensitivity and concern of Program Director, L. M. Freeman. Special thanks go to my NASA Counterpart, J. C. Reily, for his friendly discussion of matters regarding this work, and for the personal hospitality he has shown. A special thanks go to Mrs. Pat Blackmon for typing this report.

CONSIDERATIONS FOR UPGRADING MODIFICATIONS TO THE MARSHALL SPACE FLIGHT CENTER'S X-RAY CALIBRATION FACILITY

BY

J. H. Kitterman
Assistant Professor of Physics
South Dakota State University
Brookings, South Dakota

ABSTRACT

The Marshall Space Flight Center's X-Ray Calibration Facility was constructed for pre-flight calibration of the HEAO-B X-Ray Telescope (1978-1981). Calibration requirements for a newly proposed x-ray telescope, AXAF (scheduled for flight early 1990's), go beyond the capabilities of the facility at present. This investigation is concerned with and discusses several of these new requirements, among them: (1) the production of a pure unpolarized x-ray beam, (2) minimizing the target/tube change over time, and (3) how to configure the x-ray source chamber to effectively accommodate both polarized and unpolarized x-ray sources.

NOMENCLATURE

Symbols	Definition
ν	Photon frequency
ν_o	Maximum photon frequency possible for a given electron accelerating voltage
λ	Photon wavelength
ϵ_o, μ_o	Fundamental constants in electromagnetic theory
θ	Angle between electron's velocity vector and field point
a	Acceleration (deceleration) of electron
B	Magnetic (induction) field
c	Speed of light in a vacuum
e	Electron charge
E	Photon energy or electric field
Ec	Ionization shell energy of atom
I	X-ray intensity
K	Designation of x-ray emission associated with K-shell ionization
p	Polarization
P	Radiative power of electron
r	Distance from electron to field point
S	Poynting vector
t	Time
u	Speed of electron
U	Over voltage
V	Electric potential
Z	Atomic number of an element

INTRODUCTION

Preflight calibration (1978) of the HEAO-2 (High Energy Astronomical Observatory), or Einstein Observatory, was performed at the Marshall Space Flight Center's X-Ray Calibration Facility.[1] The essential features of the MSFC facility which are of concern to this paper are shown in Figures 1 and 2. A new stellar x-ray observatory, AXAF (Advanced X-Ray Astrophysical Facility), is scheduled for Shuttle launch in the early 1990's. A discussion of the performance requirements and design considerations, with comparison to same for HEAO-2, can be found in article by Zombeck.[2]

For our purposes the essential features of the calibration facility for HEAO-2 were to provide sources and detection capability for specific (characteristic) x-ray energies from 0.185 keV to 5 keV (the upper cut-off of HEAO-2 mirrors).[2] For AXAF, the energy requirements are 0.1 keV to 10 keV. From the standpoint of x-ray astronomy [2,3] the inclusion x-ray energies in the 5 - 10 keV range is quite important, as highly ionized iron or iron fluorescence radiation ($\sim$7 keV) is a dominant feature in the x-ray spectra of super nova remnants, binary x-ray sources, etc. From the standpoint of the calibration facility this energy range is straight forward. On the other hand, at the low energy range (0.1 keV to 0.5 keV) both HEAO-2 and AXAF have good capability, but for the calibration facility the production these soft x-rays will require quite exacting performance.

Finally, the AXAF observatory has put additional requirements on the calibration facility: (1) pure (100%) polarized sources, (2) pure (100%) unpolarized sources and the requested associated requirements, (3) the ability to rotate the direction of polarization of the polarized source 90°, and (4) the ability to rotate the unpolarized source 90° to check any asymmetry in the unpolarized beam. These requirements related to polarization are a result of the inclusion of a Bragg reflecting polarimeter as part of the AXAF instrumentation. The production of polarized x-ray sources has been discussed by Croft[4] as part of the 1983 NASA/ASEE Summer Faculty Fellowship Program.

The thrust of this report is directed mainly toward the production of unpolarized x-rays. In addition, discussion is included concerning the physical configuration of both polarized and unpolarized x-ray sources for the calibration facility.

X-RAY PRODUCTION: THE CONTINUOUS SPECTRA AND POLARIZATION EFFECTS

When an energetic electron beam strikes a material target, many diverse phenomena can occur.[5] For our purposes we are only concerned with x-ray emission. A typical spectral distribution is shown in Figure 3. The spectrum is characterized by line spectra (K, L, M, etc.) due to ejection of inner shell electrons from target atoms, and the subsequent emission of characteristic spectra as the target atoms relax. The most prominent feature of the continuous spectra is a definite cutoff of intensity at an upper frequency, or short wave length limit (λ_{swl}).

Using $E = h\nu$ (photon energy)

$E = eV$ (electron energy)

and $c = \nu\lambda$

Combining above, $\lambda_{swl} = \frac{12.40}{V}$, with

V in kV, λ_{swl} in $\mathring{A}$

Now the continuous spectrum radiation is also called "bremsstrahlung" ("braking radiation"), a clear indication of the classical attribution of the source of the continuous spectrum to decelerating electrons. As is well known, an accelerating (or decelerating) charge radiates. It is interesting to note that the existence of a sharp upper limit to frequency is a quantum concept. This sharp upper limit is only one of the difficulties encountered by classical attempts to account for the continuous x-ray spectrum.[6]

The characteristic spectral lines are intrinsically unpolarized.[7] Early workers in the x-ray field[6] found the following for the continuous spectra (mostly on thin targets): a high degree of polarization for the overall spectrum e.g. $\sim$ 50 o/o, and percent polarization varying with frequency, being the highest for frequencies near the cutoff limit. Now it has been found that the degree of polarization also has an angular dependence (a nice treatment in Dyson). Figure 4 shows the polarization for various values of V/Z^2 at 90° to the incident electron beam, where the polarization is defined as

$$p = \frac{I_{\parallel} - I_{\perp}}{I_{\parallel} + I_{\perp}} .$$

$I_{\parallel}$, $I_{\perp}$ refer respectively to the intensities of radiation polarized with the electric vector parallel and perpendicular to the plane of emission. Complete polarization with the electric vector parallel to the emission plane corresponds to p = 1. (The plane of emission is defined as the

plane containing the direction of the incident electrons and the direction of observation of the emitted photons.) Some clarification, and simplification, of the above will follow below when the radiation field for a single electron is treated.

The situation for the calibration facility is now clear. Underlying each characteristic line is a (variably) polarized portion of the continuous spectrum. Because the continuous radiation, for a given characteristic line energy, differs only from the characteristic energy in the state of polarization, the polarized continuous spectra cannot be separated. The variation in polarization (at 90° to the electron beam) of Figure 4 should give an approximate estimate of the variation in polarization for the present facility source, where the facility x-ray beam is selected at essentially 90° to the electron beam. The qualification "approximate" is because Figure 4 is for thin targets (a thin target is one in which a substantial fraction of impinging electrons pass through the target); for thick (i.e., electron opaque) targets the polarization should be reduced due to increased electron scattering.[7]

A rather complete discussion of theories of the continuous spectra can be found in the literature.[6,7] The theory can be rather complex, and it is not the intention to reproduce it here to any appreciable extent except so as to gain an understanding of certain aspects of the continuous spectrum, viz. polarization.

In order to examine the continuous radiation, we need to consider the interactions of an electron passing through matter. In these interactions with the target atoms we can have elastic[5] (electron energy unchanged) or inelastic (electron loses energy) collisions. Assuming the electron's initial motion is rectilinear, it is clear that collisions can give rise to a deviation in trajectory. We will not be concerned here with a detailed examination of these trajectories, but take note of the fact that they allow electrons with components of acceleration transverse to the assumed essentially rectilinear electron trajectories.

As a beginning let us follow the treatment of Thomson,[6] and simply assume the electron is brought to rest by a uniform acceleration opposite the direction of motion. Consider an electron moving with velocity u in the positive x direction, and uniform deceleration a. Classical electromagnetic theory [8,9] gives the electric and magnetic radiation fields at a time t and distance r, as follows:

$$\vec{E} = \frac{\dot{e}(\vec{a} \times \vec{r}) \times \vec{r}}{4\pi\epsilon_o c^2 r^3}$$

$$\vec{B} = \frac{e(\vec{a} \times \vec{r})}{4\pi\epsilon_o c^3 r^2}$$

where a is the acceleration at the retarded time t - r/c and we assume the speed of the electron is small compared to speed of light. We can obtain the power emission (per steradian) from the Poynting vector, $\vec{S}$,

$$P(\theta) = r^2 \, |\vec{S}| \quad ,$$

where $\vec{S} = \frac{\vec{E} \times \vec{B}}{\mu_o}$

We obtain

$$P = \frac{e^2 a^2 \sin^2 \theta}{16 \pi^2 \epsilon_o c^3}$$

The radiation pattern, P vs θ, is shown in Figure 5 in both cross-sectional and three dimensional perspective. Certain features are prominent: (1) the radiation pattern has cylinderical symmetry about the direction of acceleration, (2) the intensity goes to zero both in forward and backward direction, (3) the maximum intensity is at right angles to the electron path, and (4) the beam is polarized with its electric vector in the plane of a and r. When u/c is no longer small, a relativistic treatment is needed, as the angular distribution of intensity becomes noticeably tipped forward. The angular distribution for a thin aluminum target is shown in Figure 6. At the high energy limit the pattern is surprisingly similar to a single radiating electron, except that the intensity does not go to zero in the forward and backward directions, even for very thin films whose thickness is a very small percent of the electron's range.[7]

As we have seen, only for an infinitesimally thin sample could we expect the deceleration of electrons in a target to be in line with the incident beam. For real targets, electrons experience trajectory changes (scattering) which give rise to components of acceleration perpendicular to the plane of emission. Assuming isotropic scattering we have a

requirement of symmetry that the x-ray beam in the forward, $\theta = 0$ (or backward), direction be completely unpolarized.[10] This is simply a requirement of assuming that there is no preferential direction for electron scattering deceleration components perpendicular to the primary beam direction.

Hence, we see that the most straight forward means to achieve a completely unpolarized x-ray beam, i.e., $\theta = 0$ or 180°, will require non-standard x-ray generator geometry. Commercial x-ray tubes are produced meeting the requirements of either condition, and will be discussed in the following section. We have encountered an additional potential method of producing an unpolarized beam for standard x-ray tube geometry based upon Figure 4. From Figure 4 $p = 0$ for $V/V_0 \simeq 0.1$. A more recent estimate[11] indicates $p = o$ ($\theta = 90°$) for $V/V_0 \simeq 0.15$. Utilization of this method to produce unpolarized x-rays would require an over voltage of, U, of $1/0.15 \simeq 7$ where the over voltage $U = E/Ec$, with Ec being the shell ionization energy and E is the electron beam energy. By means of an example, consider Figure 4 to be accurate. For an over voltage of 5, $V/V_0 \simeq 0.2$, we have 20% polarization of the continuous spectrum. However, based upon a semi-quantitative estimate from an aluminum target in the HEAO-B report of Reily,[1] the background continuous spectrum has only $1\frac{1}{2}$% of the integrated intensity of the Kα peak (the characteristic spectra is, we recall, unpolarized). Hence, while the polarized portion of the continuum is ~20%, we have percent polarization for the beam as a whole of ~0.3 for the AL Kα line.

This technique of changing the polarization of the x-ray continuum by adjusting the over voltage would prove useful if a rotating crystal polarimeter as will be used for AXAF were made available prior to main AXAF package calibration effort. Unfortunately, that is probably not a likely possibility. The technique does have obvious limitations: the Cu Kα line would require an electron beam energy of ~80 keV (Ec Cu Kα ~8 keV).

X-RAY GENERATORS: UNPOLARIZED

The AXAF requirement for sources of 100% unpolarized x-rays strongly suggests that the present generator must be replaced. The search began with an aim toward locating a modest cost commercial x-ray tube with a replaceable target feature. This latter feature is probably the most attractive capability of the present system; without it the x-ray tube must be changed when the x-ray energy requirement changes. So the task at hand was: (1) who manufactures

tubes capable of producing unpolarized x-rays and (2) can the target (anode) be (easily) replaced? A further objective was to locate firms willing to custom design an x-ray tube, in the eventuality such an option need be considered.

Vendor sources were located primarily from perusal of the 1984 Thomas Register and Dunn and Bradsheet Directory. Direct vendors of x-ray tubes contacted are listed in Table I. Table II is a listing of manufacturers of electron gun evaporators. Electron gun evaporators were considered[12] even though their designed use is for target evaporation. In the interest of utility, rather than formality, the discussion to follow will name the individual (or individuals) contacted or relevant to the subject. Also, because a great deal of the subject matter to follow is based upon notes taken during telephone exchanges, it must be recognized that misinterpretations or actual mistakes may be included. Only those vendors/contacts are discussed for which it is felt useful information worth pursuing was obtained. Titles of individuals are mostly not included as they were generally not known.

Machlett Laboratories, Inc.
George Mahn
(203) 348-7511

The writer was initially made aware of Machlett Laboratories through initial discussions with J. C. Reily. Machlett produces an x-ray tube with toroidal cathode geometry, Figure 7. The symmetry arising from the gun geometry satisfies our prior condition for producing an unpolarized beam. Machlett, however, was apparently not interested in considering a replaceable anode,[12] and this was confirmed by G. Mahn. The tube under discussion, OEG75 or 76, was designed to operate at 3kW, and for an accelerating potential of 20-75 kV. The question of whether the tube could operate at 1-2 kV with sufficient emission, a few milliamps, was questionable. Mahn, who is the designer of this tube, ventured the emission was more likely in the microamp range at 1 kV. He was quick to point out they had never had a request like this, but he indicated that he would try to have some data taken, and if the results were worth reporting, he would notify J. C. Reily. An additional comment was that he had no confident prediction on x-ray spot size for the 1-2 kV range. The nominal spot size of the tube is 1-1.5 cm o.d. for designed operating voltage.

Kevex
Brian Skillicorn
(408) 438-5940

Kevex manufactures a transmission target tube in which the x-ray beam is taken out in-line with the electron beam, Model K-5020. The tube is designed to operate down to 1 kV and still deliver 2 ma emission.

Kevex (Continued)

The tube is rated at 100 watts at 50 kV. The targets are produced by vacuum coating a 0.002"-0.010" thick Be wafer. Such a tube, while satisfying the necessary symmetry requirements for producing an unpolarized continuum, is entirely unsatisfactory for soft x-rays because of excessive absorption. A replaceable anode is also out of the question, as special cathode material is used which would be poisoned upon contact with oxygen. A further impediment to the use of this type tube is heat conduction from the target. Heat removal is solely by conduction through the Be backing foil - nominally 0.010" for 100 watt (50 kV) operation. Kevex is willing to custom design a tube. A possibility would be to produce a windowless tube based upon a tube they designed for x-ray lithography. The tube utilizes an annular cathode and a conical anode; however, they envisioned a replaceable flat anode as no problem. The x-rays would be taken out of the tube "backwards," through the annular cathode (similar to Machlett's tube design). This possibility may be worth further discussion.

Amperex Electronics Corporation
Richard Gumbrecht (Sales Manager)
(516) 931-6200

In 6 to 9 months they will have a low power (150 watts, 1-50kV) end window tube on the market. The tube will be oil filled and sealed, and hence not amenable to target replacement. Amperex will consider designing special purpose x-ray tubes. I was referred to their technical expert, Jerome Pichert, but he was on vacation and not available for discussion until August.

Siemens (E. S. Industries)
Robert Meyers
(609) 983-3616

Siemens produces a full line of x-ray equipment. This includes an end window toroidal geometry tube which is said to be a replacement for Machlett tubes. Siemens products are manufactured in Germany, and any possibility of custom adaptation seems rather remote. Targets in Siemens end window tubes are not replaceable.

VG (Vacuum Generators) (Kurt Lesker Company)
Mike Flinko
(412) 655-9500

Vacuum Generators is a British firm manufacturing a variety of vacuum products. The product under consideration here is an electron gun evaporator designed for target evaporation. Reduced power operation qualifies the system as an x-ray generator. This particular design utilizes electro-

VG (Vacuum Generators) (Continued)

static focusing and toroidal gun geometry and is said[13] to provide a smaller spot size than similar electron guns utilizing magnetic focusing. The target is adaptable to replacement,[13] which is an attractive feature. The upper limit on the gun high voltage is 10 kV. This is a limiting feature for x-ray production; for Cu Kα at Ec = 8 keV, the over voltage is only 1.2, and therefore this system would not be efficient for production of Cu Kα radiation. Nevertheless, this system does seem worthy of further investigation, particularly as the basis of a modified custom x-ray generator.

X-RAY SOURCE CONFIGURATION

It must be recognized that without a firm decision on specific source geometries for polarized and unpolarized x-ray sources the discussion presented here constitutes no more than speculative thinking. The following two requirements[14] for the x-ray sources constitute a serious impediment to simplifying the source configuration:

(1) The unpolarized x-ray source should be amenable to a 90° rotation. This requirement is to verify any asymmetry in the unpolarized beam.

(2) The polarized source must allow a 90° rotation of the direction of polarization in order to calibrate the AXAF polarimeter.

Inasmuch as the time for changeover from one test condition to another is at a premium, it is clear that these additional requirements add a further burden to the source configuration. Each test condition change requires valving off the source chamber and going to atmospheric pressure. After the test conditions are changed the source chamber must be reevacuated. For HEAO-B calibration these test condition changeovers (targets/filters) were accomplished rather easily in about 30 minutes,[12] as targets were replaceable by easily removing the electron gun assembly.

One possible configuration could be as shown in Figure 8a. The configuration shown cannot obviously allow concurrent operation of both sources, but is intended for discussion purposes for possible actual operation. The same type x-ray source (unpolarized) could be used in either position. When a tube is used for producing polarized x-rays, section A is removed to an auxiliary port, and a crystal mounting fixture is attached to the flange at location 2 (Figure 8b).

X-RAY SOURCE CONFIGURATION (Continued)

For a change requiring rotation of the direction of polarization, vacuum cycling of the source chamber is necessary. There are several ways to conceptually effect the 90° rotation: (1) the complete section B could be manually rotated, a seeming unwieldly operation, (2) an auxiliary flanged port (not shown), Fl2, at 90° to Fl would allow the source tube to be moved to the new 90° position. This would have to be accompanied by a proper 90° rotation of the crystal holding end cap. The original tube flange port Fl would have to be capped off, and (3) the configuration of (2) also allows for having two identical source tubes in position at Fl and Fl2. The only rotation required is for the crystal holding end cap.

When the system is to be set up for unpolarized x-rays, the crystal holding end cap at location 2 is removed and the x-ray source A is attached at location 2. Rotation of the source by 90° necessitates the source chamber being cycled at atmospheric pressure.

An important, but unmentioned, problem is that x-ray tubes not in use (here assuming a replaceable target is not feasible) are at atmospheric pressure. Unless the tubes not in use are somehow sealed (as suggested by Kevex representative), a test change will require the substitute tube to be given considerable additional pumping time due to desorption of water and other gases. The ability to keep x-ray tubes not in current use under protective environment deserves strong consideration. One "brute force" possibility is extra flanged ports on the source tube, so that except for test changeovers other tubes "in-line" for test will be under vacuum. Another, suggested by Kevex, is that each x-ray tube has a valve in place of a window and a vacuum connection. With this, albeit probably costly, configuration a given tube will never see atmospheric conditions, except briefly to change targets (if possible), which can be done under dry nitrogen cover.

C - 5

CONCLUSIONS AND SUGGESTIONS

It is recognized that none of the configuration arrangements discussed are conducive to rapid test condition changeover. From the vantage point of the writer there are no easy answers, only elimination of least acceptable alternatives. Several possibilities for unpolarized x-ray sources have been discussed and merit further consideration. None seems worthy of a wholehearted endorsement. One obvious possibility deserves consideration: employ an expert consultant in x-ray technology. Then perhaps what appears to the writer as a very difficult (bordering on intractable) technological problem will become "merely" moderately difficult.

TABLE I

VENDOR'S CONTACTED - X-RAY SOURCE

1. Siemens (E. S. Industries, Marlton, New Jersey)
2. Seifert X-Ray Corporation, Fairview Village, Pennsylvania
3. Dunlee (Affil. with Picker), Bellwood, New Jersey
4. XID, Clifton, New Jersey
5. Philips (Ridge, Inc., Rep., Decatur, Alabama)
6. Picker International, Cleveland, Ohio
7. Agfa - Gevaert, Inc., Teterboro, New Jersey
8. AEG - Telefunken Corporation, Somerville, New Jersey
9. Kevex, Scott Valley, California
10. Amperex Electronic Corporation, Hicksville, New York
11. Eimac (Div. of Varian), Salt Lake City, Utah
12. Diano Corporation, Woburn, Massachusetts
13. EGG - Ortec, Oakridge, Tennessee
14. Machlett Laboratories, Stamford, Connecticut

TABLE II

VENDORS - ELECTRON GUN EVAPORATORS*

1. VG (Vacuum Generators) (Kurt Lesker Company, Pittsburgh, Pennsylvania)
2. Mill Lane Eng. Company, Burlington, Massachusetts
3. Balzers, Hudson, New Hampshire
4. Kimball Physics, Inc., Wilton, New Hampshire
5. Energy Beams, Inc., Bloomingdale, New Jersey
6. Denton Vacuum, Inc., Cherry Hill, New Jersey
7. Partagas, Inc., Cherry Hill, New Jersey

*from 1984 Thomas Register

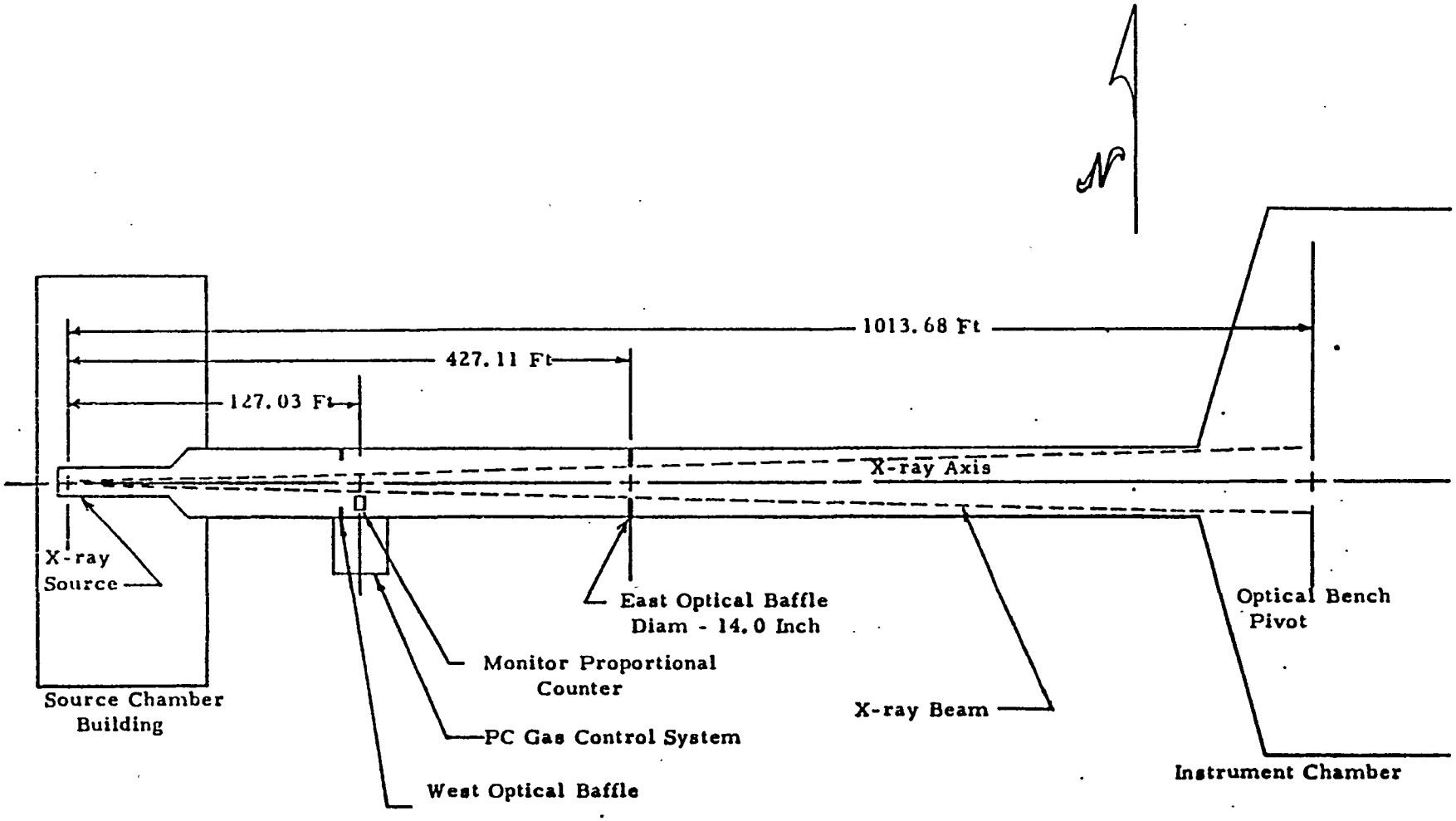

FIGURE 1. X-RAY CALIBRATION SYSTEM LAYOUT

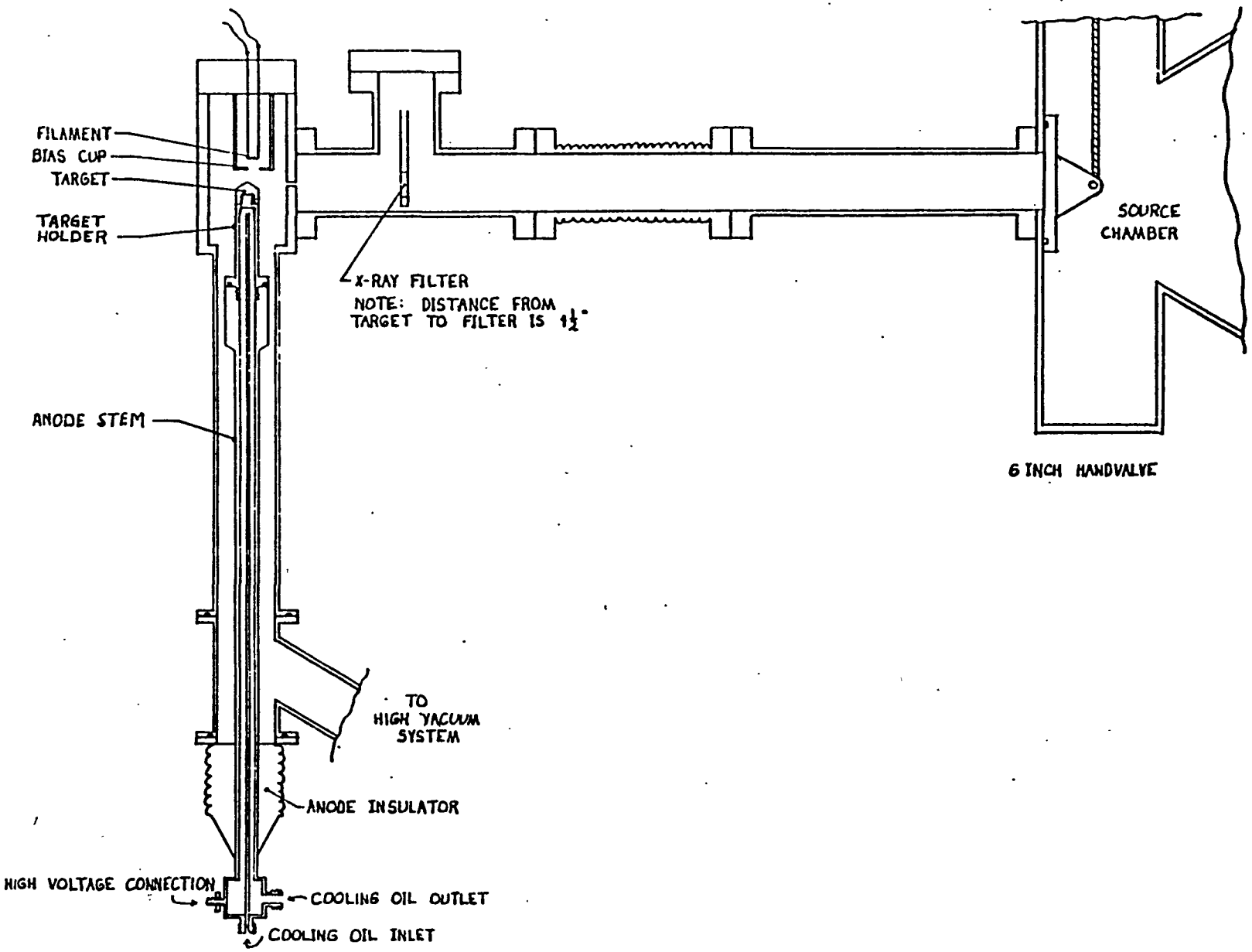

FIGURE 2. SCHEMATIC DIAGRAM - X-RAY TUBE ASSEMBLY

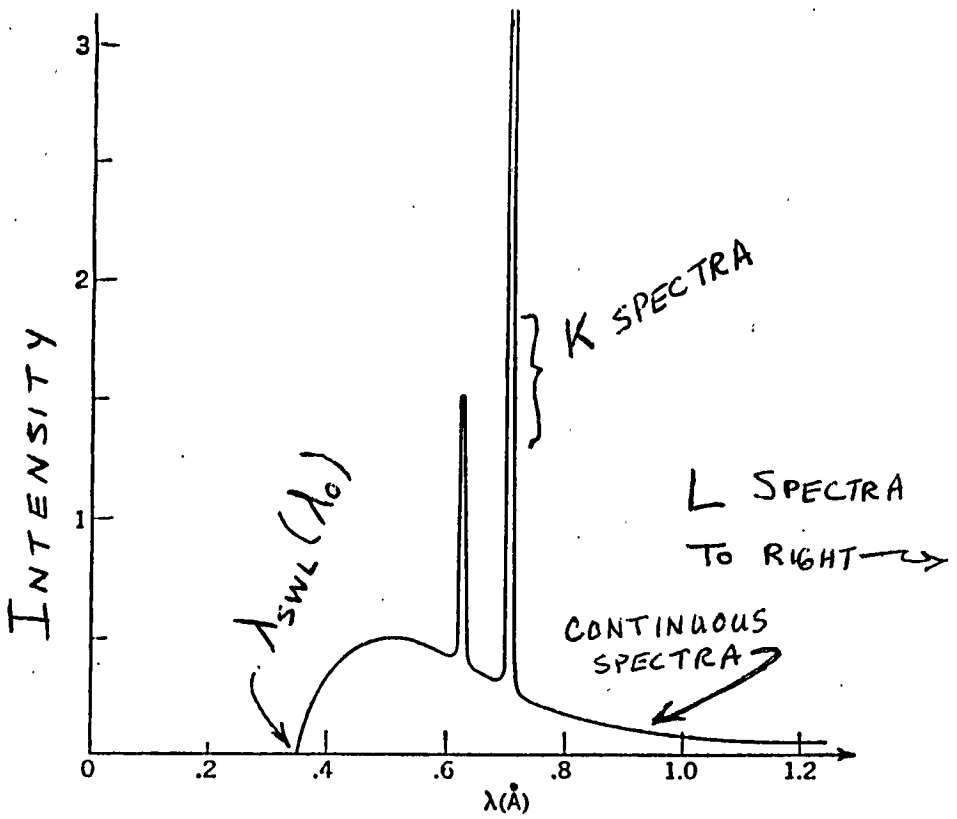

FIGURE 3.
INTENSITY VS. WAVE LENGTH FOR X-RAY TUBE EMISSION

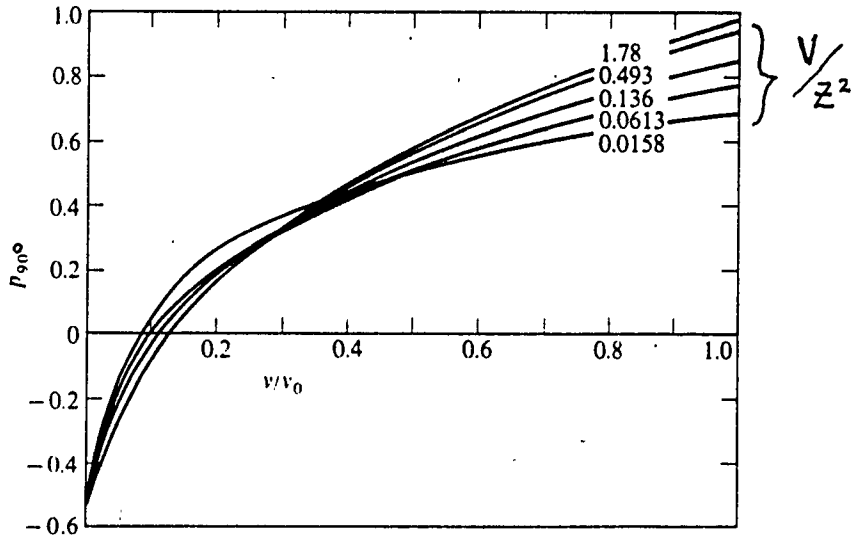

FIGURE 4.
POLARIZATION FOR VARIOUS VALUES OF V/Z^2 AT 90° TO INCIDENT ELECTRON BEAM (DYSON)

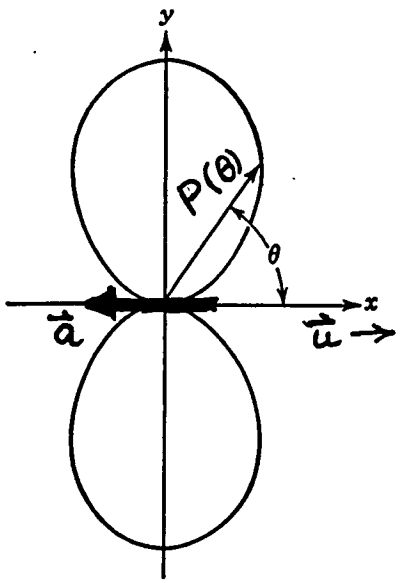

(a) Planar Slice through Axis of Symmetry (X-Axis)

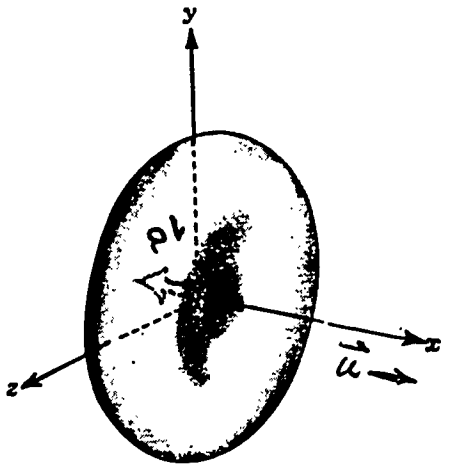

(b) 3 Dimensional Sketch

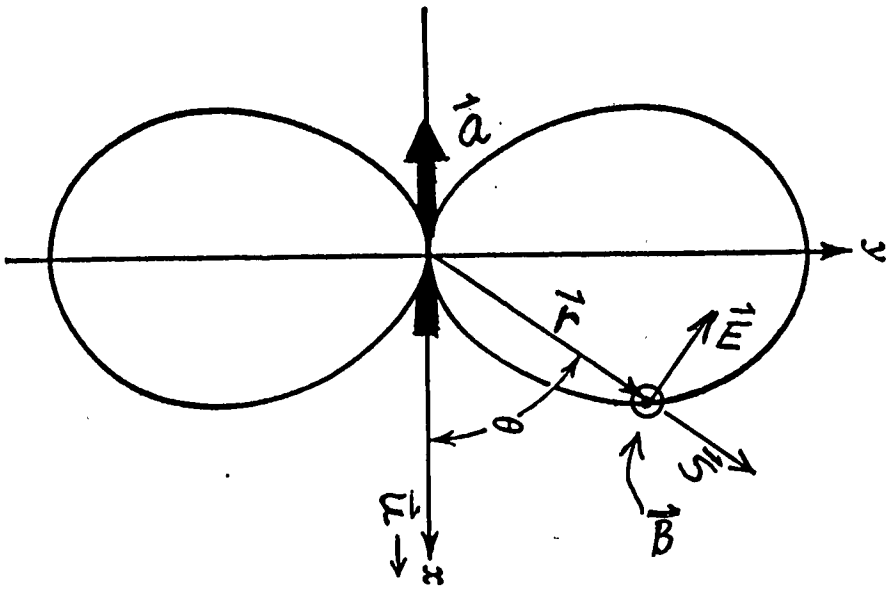

(c) Superposition of E, B, S. The electron acceleration, a, is oppositely directed to velocity, u ($u \ll c$).

FIGURE 5
RADIATION PATTERN FOR DECELERATING ELECTRON

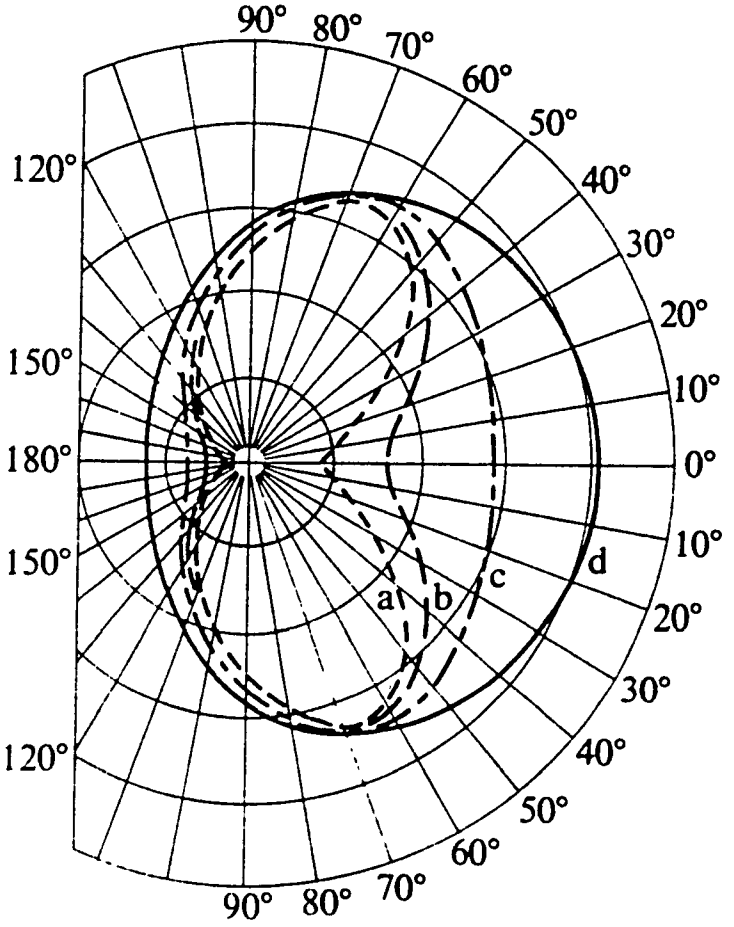

FIGURE 6.
Angular distribution of intensity for several energies in the spectrum (thin AL target, 34kV) (a) $V/V_o = 1$ (b) $V/V_o = 0.7$ (c) $V/V_o = 0.4$ (d) $V/V_o = 0.26$ (Dyson).

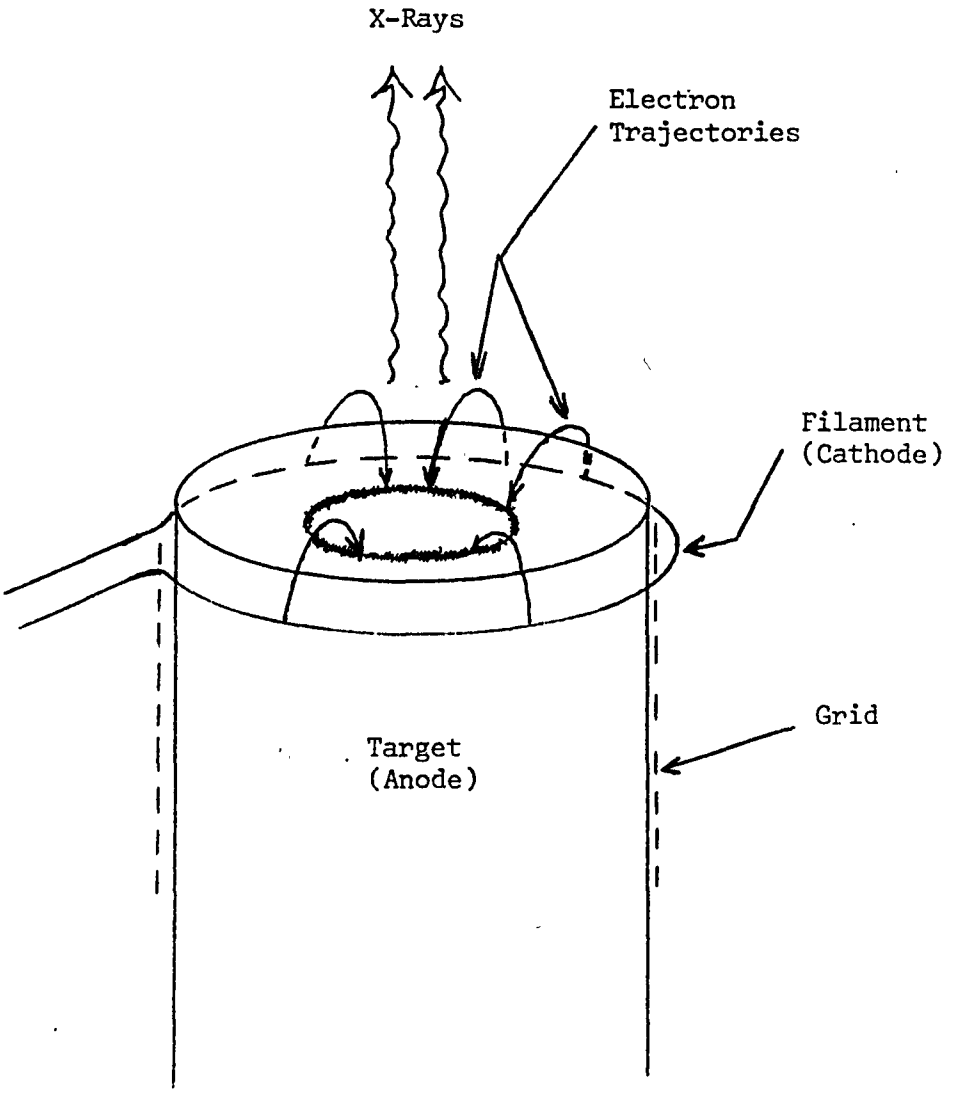

FIGURE 7

The basic features of a toroidal cathode geometry x-ray source (e.g., Machlett Laboratories). Electrons follow curved trajectories due to the controlling grid potential. X-rays produced at the annular electron impact region are taken out "backwards" along the axis of symmetry of the impinging electrons.

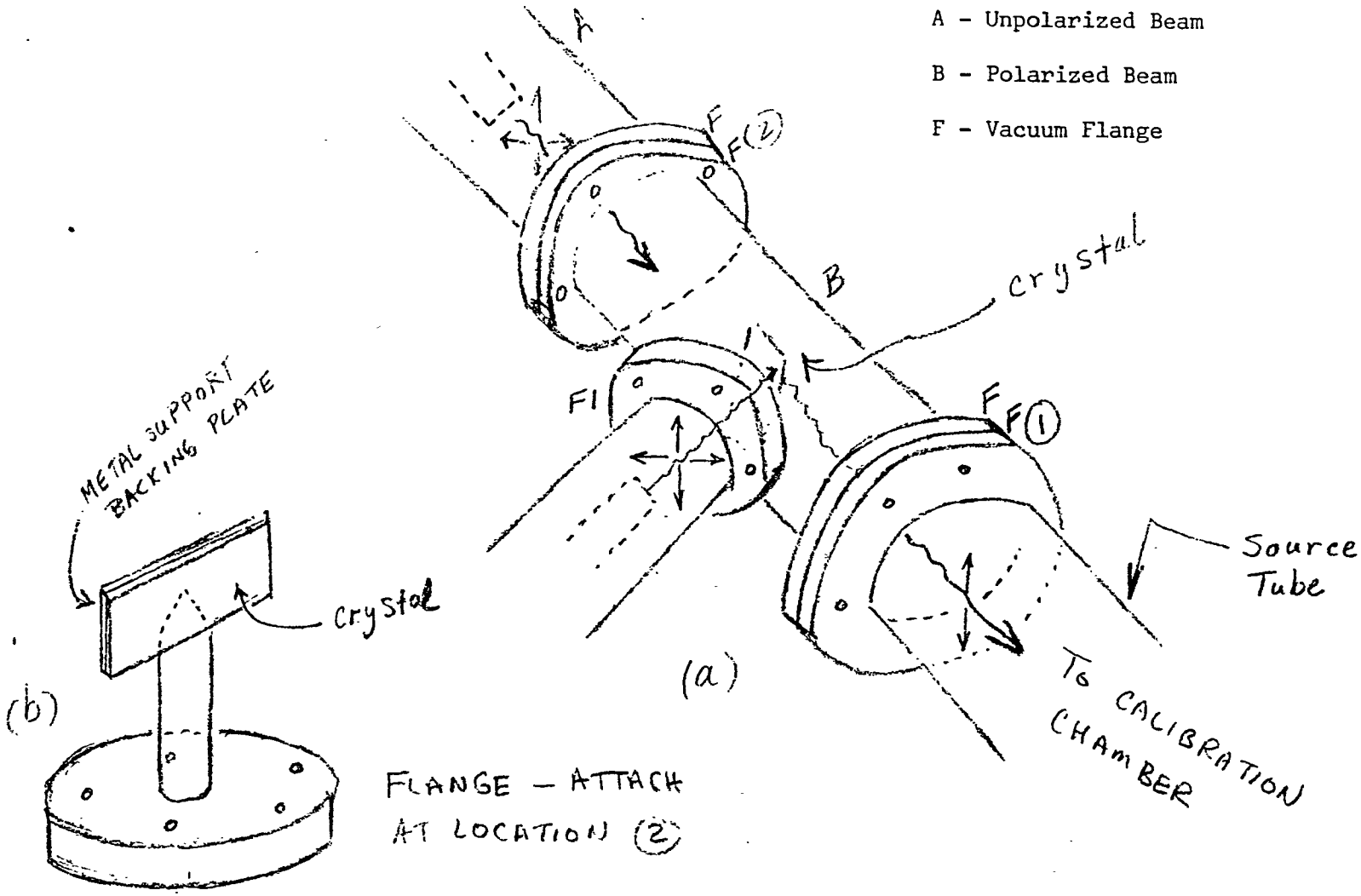

FIGURE 8.
(a) SOURCE LAYOUT
(b) CRYSTAL MOUNTING FIXTURE

In reality sketch (a) is not accurate as polarizing crystal can only be in place when section A removed.

REFERENCES

1. Reily, J. C.: Test Report X-Ray System Operation HEAO-B Telescope Calibration, NASA ET44-HEAO-411 Addendum, April 1978.

2. Zombeck, M. V., S.P.I.E., 184, 50 (1979).

3. Weisskopf, M. C., Presentation on AXAF to NASA/ASEE Summer Fellows, 1984.

4. Croft, W. L., NASA/ASEE Summer Faculty Research Fellowship Program, Contract No. NGT-01-008-021, The University of Alabama in Huntsville, August 1983.

5. Goldstein, J. I., et al, Scanning Electron Microscopy and X-Ray Microanalysis, Plenum Press, New York, 1981.

6. Compton, A. H. and Allison, S. K., X-Rays in Theory and Experiment, D. Van Nostrand Company, Inc., 2nd Edition, 1935.

7. Dyson, N. A., X-Rays in Atomic and Nuclear Physics, Longman Group Ltd., 1973.

8. Leighton, R. B., Principles of Modern Physics, McGraw Hill, 1959.

9. Panofsky, W. K. H. and Phillips, Melba, Classical Electricity and Magnetism, Addison Wesley, 1962.

10. Dyson, N. A., X-Rays in Atomic and Nuclear Physics, 48, Longman Group Ltd., 1973.

11. Dyson, N. A., X-Rays in Atomic and Nuclear Physics, 51, Longman Group Ltd., 1973.

12. Personal Communication, J. C. Reily.

13. Personal Communication, Dr. E. Spiller (IBM)/J. C. Reily.

14. Personal Communication, M. Weisskopf.

1984

NASA/ASEE SUMMER FACULTY

RESEARCH FELLOWSHIP

PROGRAM

MARSHALL SPACE FLIGHT CENTER

THE UNIVERSITY OF ALABAMA

ANALYSES VIA AUTOMATED MASS SPECTROMETRY (MS/DS)

Prepared by: T. Koenig

Academic Rank: Professor

University and Department: University of Oregon
Department of Chemistry

NASA/MSFC:

Division: Non-Metallic Materials

Branch: Analytical and Physical Chemistry Branch

MSFC Counterpart: J. R. Nunnelley

Date: August 4, 1984

Contract No.: NASA-NGT-01-002-099
The University of Alabama

ANALYSES VIA AUTOMATED MASS SPECTROMETRY (MS/DS)

by

T. KOENIG
Professor of Chemistry
University of Oregon
Eugene, Oregon 97403

ABSTRACT

The objective of this project was to establish the basis for new or improved uses of the Finnigan 4000 quadrupole mass spectrometer (MS) with its associated INCOS data system (DS). The first phase of the project involved an evaluative activity in which specific problems with miscalibration and gas chromatographic column conditioning were identified. This phase also revealed one solution to the problem of detection of substances not visible in the gas chromatography detection mode. A second phase of the project was to seek useful applications of the direct inlet systems. This mode of sample introduction has not been previously utilized on the existing equipment and was successfully applied to the analysis of the components of TONOX 60/40 and in the thermal degradation products of some polymeric materials. Suggestions are made for improving and expanding the use of the MS/DS system in materials development and testing.

I. Introduction and Objective

The objective of this summer project was to provide suggestions for new or improved uses of the Finnigan 4000/INCOS mass spectrometer-data system (MS/DS). Considering the rapid expansion in the applications of analytical mass spectrometry over the past 10 years[1], this is a relatively simple task. The major factor in the growth of the power of modern mass spectral methods is the development of computer controlled systems. These allow the chemical analyst to process the very large amounts of spectral information which mass spectrometers are capable of producing. The Finnigan-INCOS system is one of the best (MS/DS) packages available although the version existing at MSFC (1978) is growing obsolete compared with current descendants. The essentials of the system are shown in Figure 1.

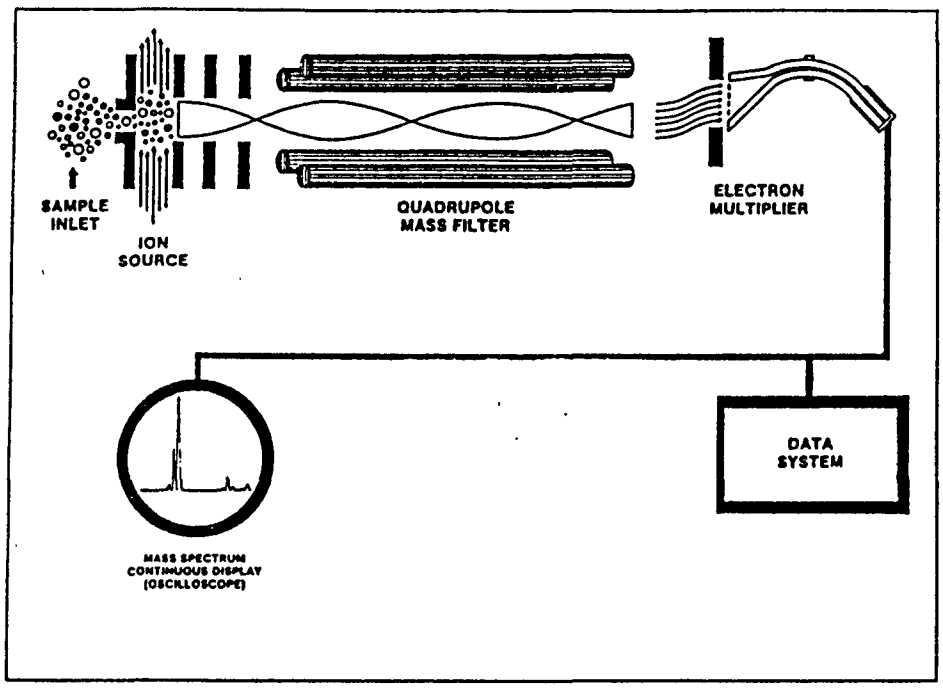

Figure 1. Graphic illustration of a Quadrupole Mass Spectrometer.

The mass filter is a quadrupole swept by the RF and DC voltages of the quadrupole rods. The mass range is 1000 daltons (10% valley resolution) and the system can detect 0.1 nanograms of methyl stearate using electron bombardment (70 ev) as the ionizing source.

The INCOS software package and NOVA 3 computer allow spectral acquisition under computer control. The data rates are reasonable high (10^5/sec) allowing a 1000 dalton spectral range to be read and stored

every 1-2 seconds. The software system has a large set of data handling procedures, most of which have more than 10 subcommands. The DS can read and store up to 10^4 spectra of up to 10^3 mass windows each and the analyst is faced with the problem of choosing the correct procedure, among the ca 10^3 possibilities, that will reveal the pertinent analytical results. Figure 2 shows an oversimplified illustration of the MAP display.

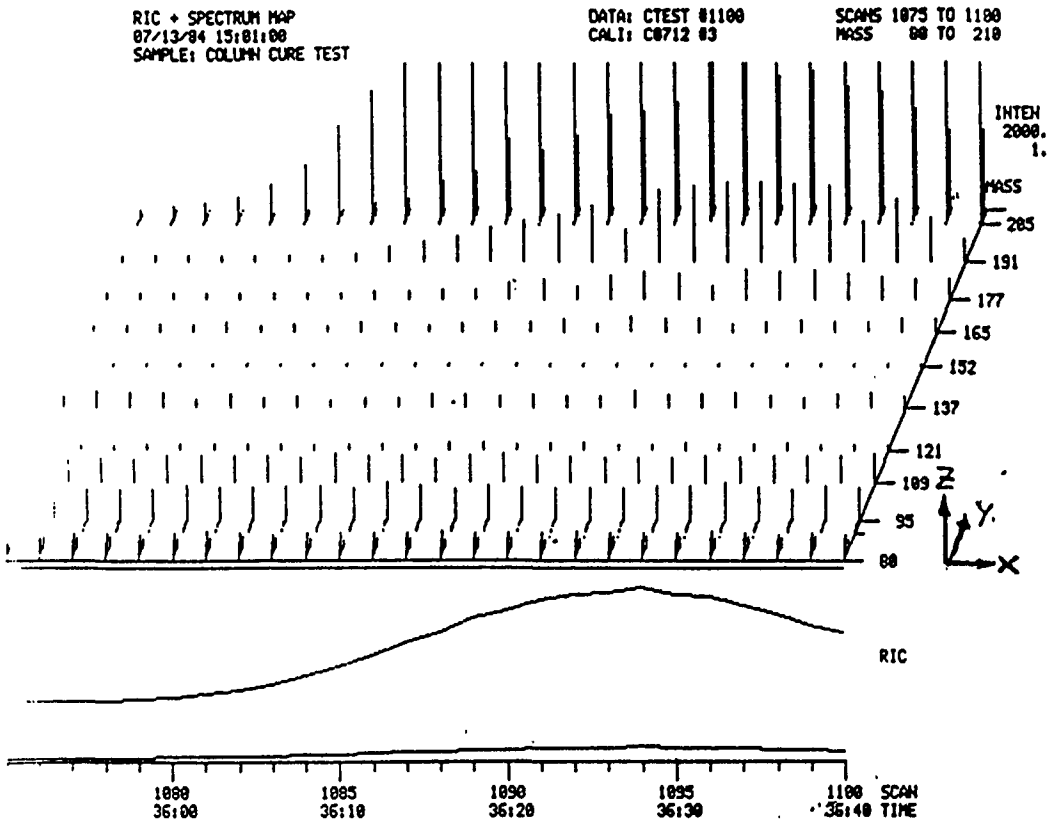

Figure 2. MAP Display of Selected Ion Currents in a 25 Scan Segment.

The lower portion of a MAP display shows the total ion current (RIC) versus scan number. The upper portion is a three dimensional display of ion current (Z-axis) at each mass (Y-axis) during each scan (X-axis). The duration of each scan was 1.95 seconds in this case. The RIC of Figure 2 shows an increase in total ion current from scan 1080 up, peaking near 1094. The individual ion current display shows that the high mass region (M/Z 177-210) is responsible for the RIC increase, the low mass region (M/Z 80-152) being a constant background.

At the present time, use of the MS/DS System at MSFC appears to be restricted to the qualitative analysis substances that vaporize from anything in the inhabited compartments of manned space vehicles.

Current procedures use the MS/DS System to analyze the effluent streams of a packed gas chromatography column (GC/MS/DS). One of the most important features of the INCOS data system is its' library containing the mass spectra of 25,000 known substances. This library can be searched in comparison with an unknown, allowing rapid identification of components detected in data files from the gas chromatographic separation.

This report contains results and recommendations relating to the main existing use of the MS/DS System, analysis of substances found to offgas[a] from materials making up the inhabited compartments of space vehicles. It secondarily contains some crude results on analysis of precursors and thermal degradation products of polymeric materials. The latter utilized the direct inlet sampling mode in place of the GC mode. Suggestions are made for upgrading the role of MS/DS techniques in the overall activities at MSFC.

a) The term "offgas" is used throughout. This terminology maintains integrity with the language of the procedural definitions of reference 3.

II. Offgas Analysis

The principal use of the MS/DS facility at MSFC is in the identification of substances found to offgas from materials or components which could contribute to the atmosphere in the inhabited compartments of space vehicles. The protocol for testing is described in detail in reference 3. Commonly found offgassed substances have been classified in groups (j) according to type of compound. Each substance (ij) as also been given a maximum allowable concentration (MACij). Low values for MACij are of the order of 0.01 parts per million (ppm). The criteria for acceptability of a tested component or material are given by equations (1), (2) and (3) where i refers to a particular substance and j to its' group. Cij is the measured concentration of the substance and MACij is its' maximum allowable concentration.

(1) $Cij/MACij \leq 1.$

(2) $\sum_i (Cij/MACij) = Tj \leq 1.$ (all j)

(3) $\sum_j Tj \leq 1.$ (The sum over j excludes some groups.)

These criteria take into account individual (ij), group collective (j) and possibly synergistic effects of observed combinations off gassed substances. An additional and very important consideration is that a substance, which is evident in an offgas test and which cannot be identified, must be assigned the lowest MAC value. The positive identification of all offgassed substances is therefore of some consequence since a low MAC value for an unidentified offgas component could cause rejection of the tested component or material. This would necessitate a search for a substitute which could, in turn, lead to a costly delay. Efficient positive identification of all offgassed components prevents such situations unless they are really mandated by the certain presence of a substance of low MAC value.

The present project was initiated by an examination of procedure in the offgas product analysis. The procedure is basically the placement of the space vehicle component or material in a closed compartment at specified temperature for a specified time. Small gas aliquots are removed and subjected to GC analysis with a capillary column and flame ionization detection. If the identities of all the components are securely known, then relative response factors can yield concentrations (Cij's) in the sample. The high sensitivity of the flame ionization detector makes small concentrations easily quantifiable. However, the flame ionization GC method is not very reliable for identification.

The MS/DS is much better as an identification tool. However, even when operating under the ideal conditions, the Finnigan 4000 has a

detectability limit (for a known substance) of 100 picograms which translates to about 1cm^3 of gas sample containing at least 0.01 ppm offgassed substance. There are other factors in the calculation of the Cij's to be used with (1)-(3) but the 100 picogram to 0.01 ppm/cm^3 conversion establishes the point that large gas samples are necessary. Presently, samples of 10-30 cm^3 are concentrated in adsorption tubes, desorbed and separated using a packed GC column. The identification of unknowns would be facilitated if the original gas sample size were increased to 100 cm^3. This could be done rather easily using a gas burette in place of the syringes presently employed.

A. Calibration Effects

Figure 3 shows an example of the MAP display of a small portion of GC/MS/DS data obtained from an offgas sample (FESTEST).

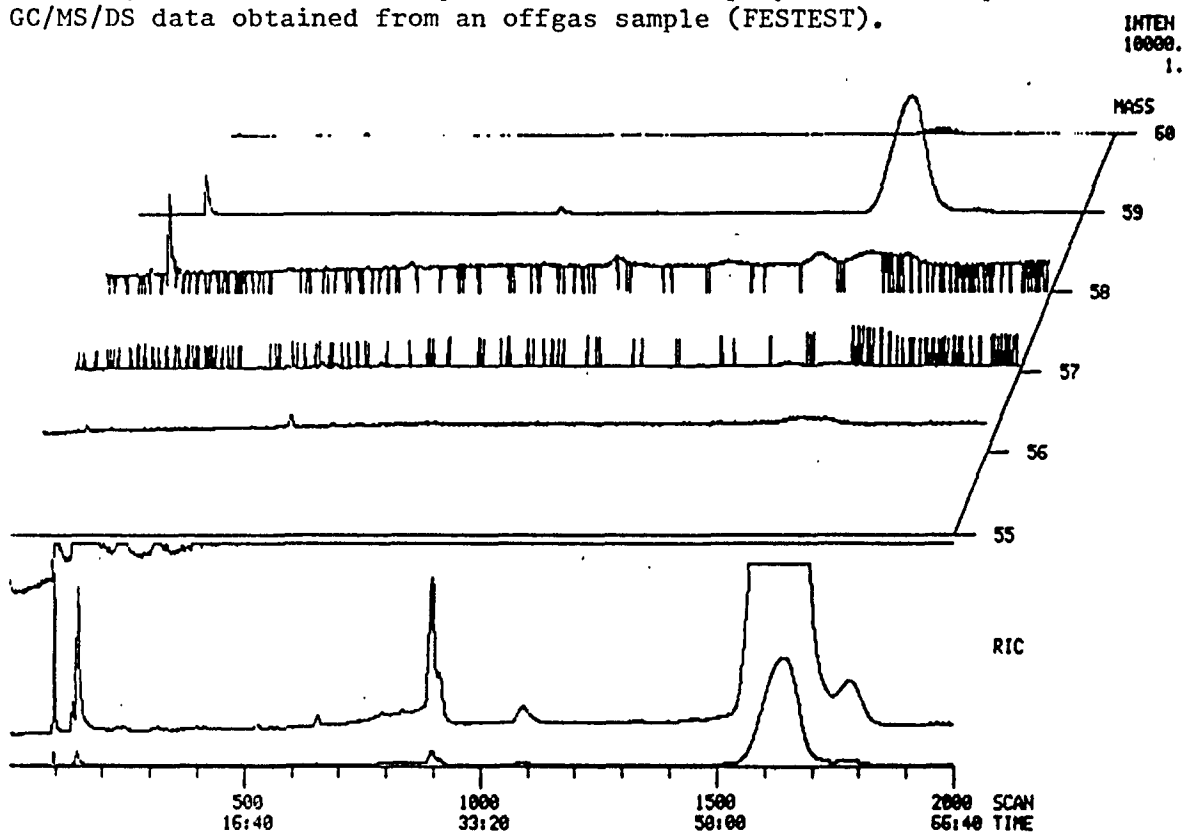

Figure 3. Selective noise, M/Z 57/58 Calibration Error.

The lower curves are the chromatographic response using total ion current (RIC). The upper curves are the individual chromatograms for ions of mass 55-60. The selective and complementary nature of the noise in the 57/58 curves is indicative of computer misreading the ion intensity channels near M/Z 57.5. This ultimately proved to be the correct interpretation. Retuning the quadrupole through lense adjustments largely eliminated the selective noise patterns such as those shown in Figure 3.

The algorithm which allows the computer to assign the intensity patterns as mass unit increments assumes a linear scan function. The correctness of this assumption is determined using the observed spectrum of a calibration gas (perfluoro tributylamine, "FT3"). The CALI and FIT procedures of the INCOS system compare this spectrum to stored values. The computer reading or assignment of the mass responsible for a bit of ion current is made in reference to such a calibration file. Marginal tuning of the quadrupole will show up in marginal statistics in the calibration procedures[4] and finally in selective noise patterns such as shown in the 57/58 masses of Figure 3.

An even more important effect of the use of a marginal calibration file is illustrated in Figure 4. These spectra refer to the first major offgas component of the FESTEST sample (Figure 3, scans 147-160).

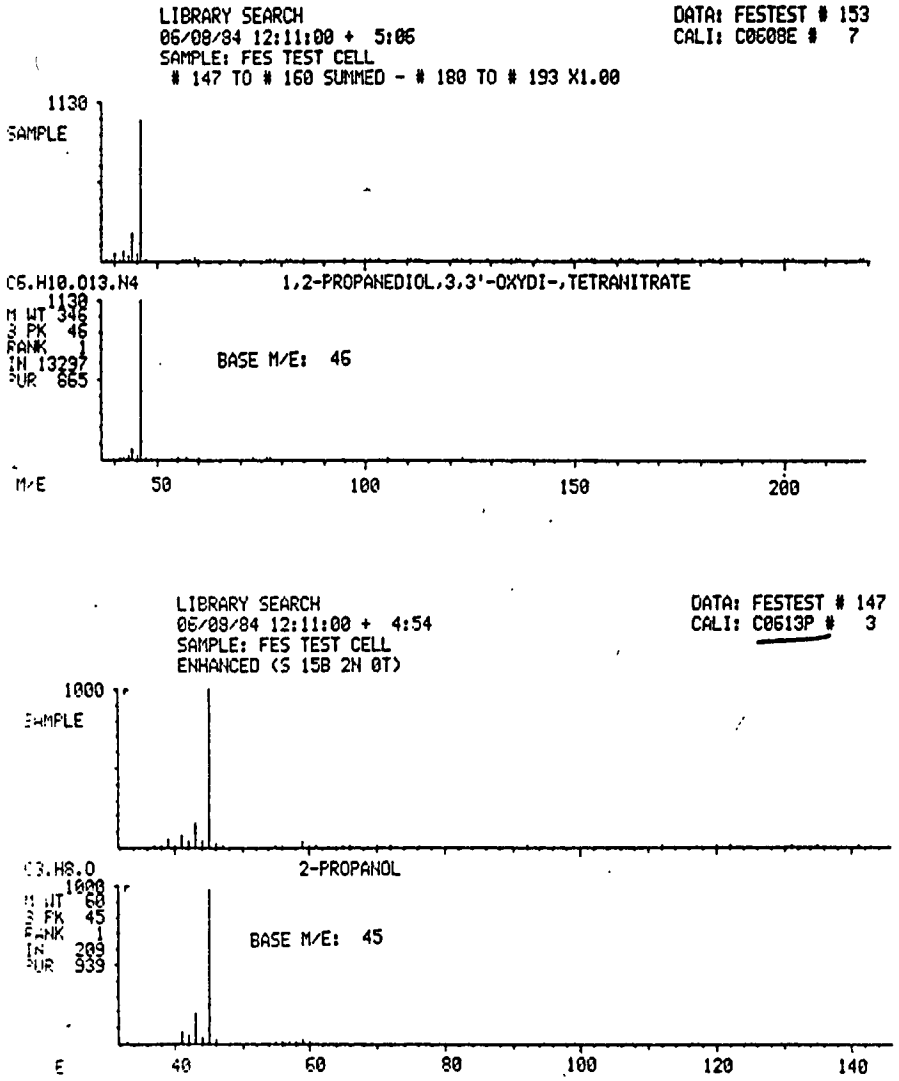

Figure 4. Spectra and SEARCH Results for Scans 147-160 of FESTEST.

The spectrum at the top is the average, after background correction, for the first major offgas component using the incorrect calibration. This spectrum shows the base peak of the offgas component as M/Z 46 and the library search indicated the component to be 3,3'-oxydi-(1,2-propanediol) tetranitrate (second of the upper pair of spectra).

The lower pair of spectra are from the identical data set but using the improved calibration file which eliminated the selective noise at M/Z 57-58 in Figure 3. The averaged spectrum associated with the same component (scans 147-160) shows a base peak at M/Z 45 instead of 46. The identification of the major offgas component is i-propanol (second of the lower set of spectra).

It was finally determined that the marginal tuning and calibration caused constant computer misreads of masses 40-46 in addition to intermittent misreads such as shown at M/Z 57-58 in Figure 3. Such constant misreads are much less obvious. The effect can be the complete misidentification of an offgas component as is illustrated in Figure 4. Several of the other components of the FESTEST data set were initially misidentified due to the marginal calibration procedure.

There are other effects of improper tuning of the quadrupole relating to peak shape. A poor peak shape can cause disk overflow due to computer reading many extraneous fractional mass peaks which are artifacts of the condition of the mass filter. It is clear that careful attention to the tuning of the quadrupole and the calibration/fit procedures is mandatory for reliable compound identification.

B. Column Conditioning

Figure 5 shows the MAP displays which allow the identification of the two major peaks in the FESTEST data set as hexamethylcyclotrisiloxane (M/Z 207, scan 900) and octamethylcyclotetrasiloxane (M/Z 281,207, scan 1600).

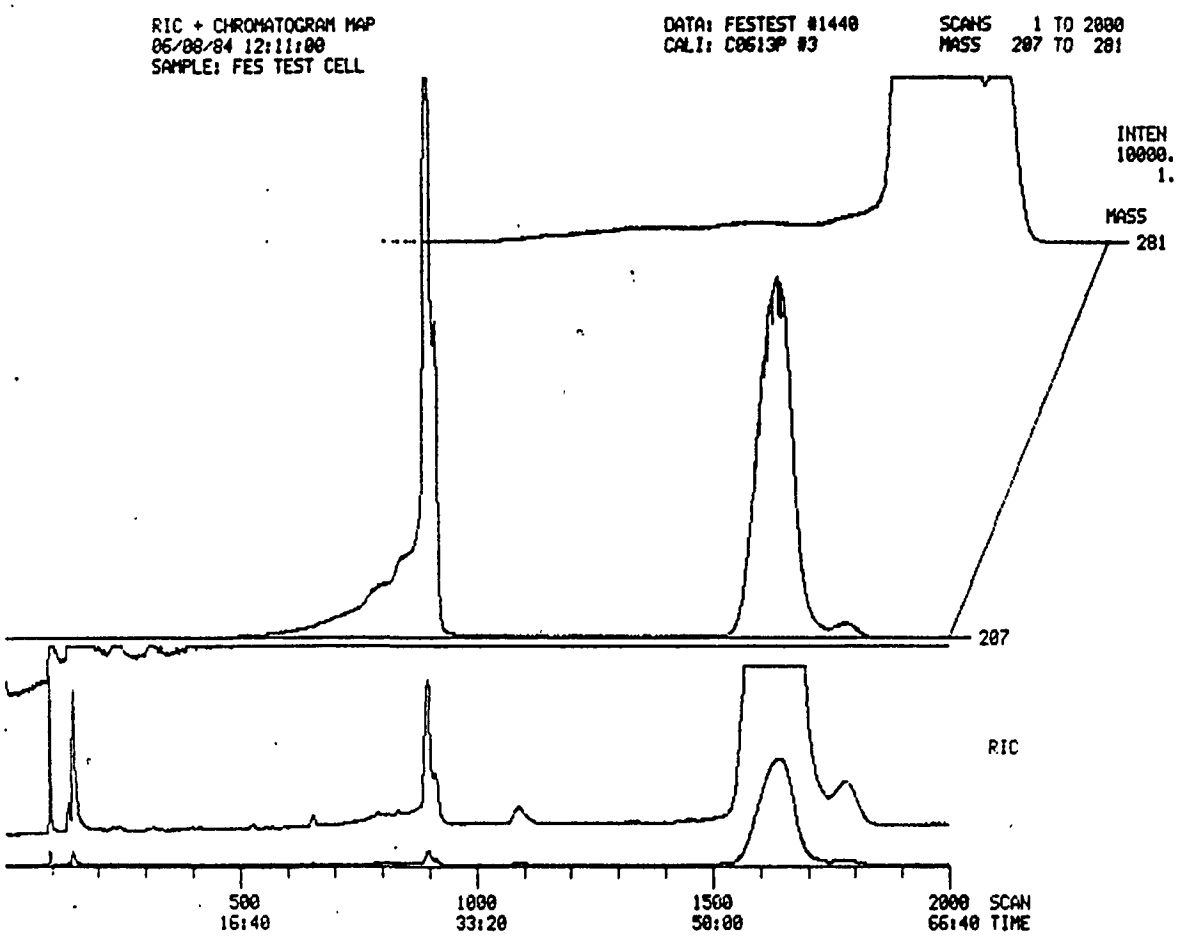

Figure 5. RIC, M/Z 207, M/Z 281
Chromatograms FESTEST Data

The width and shape of these chromatograms is suggestive of column bleeding.[5] The identification as cyclosiloxanes is also indicative of polysilicone material degradation. Examination of the stored data files from offgas tests revealed that broad peaks due to these same cyclosiloxanes were present in every case.

The obvious simple step of preconditioning the column confirmed the column bleed hypothesis. Figure 6 shows the RIC, 207 and 281 chromatograms for the GC system immediately after conditioning the column at 175°C for 1 hour.

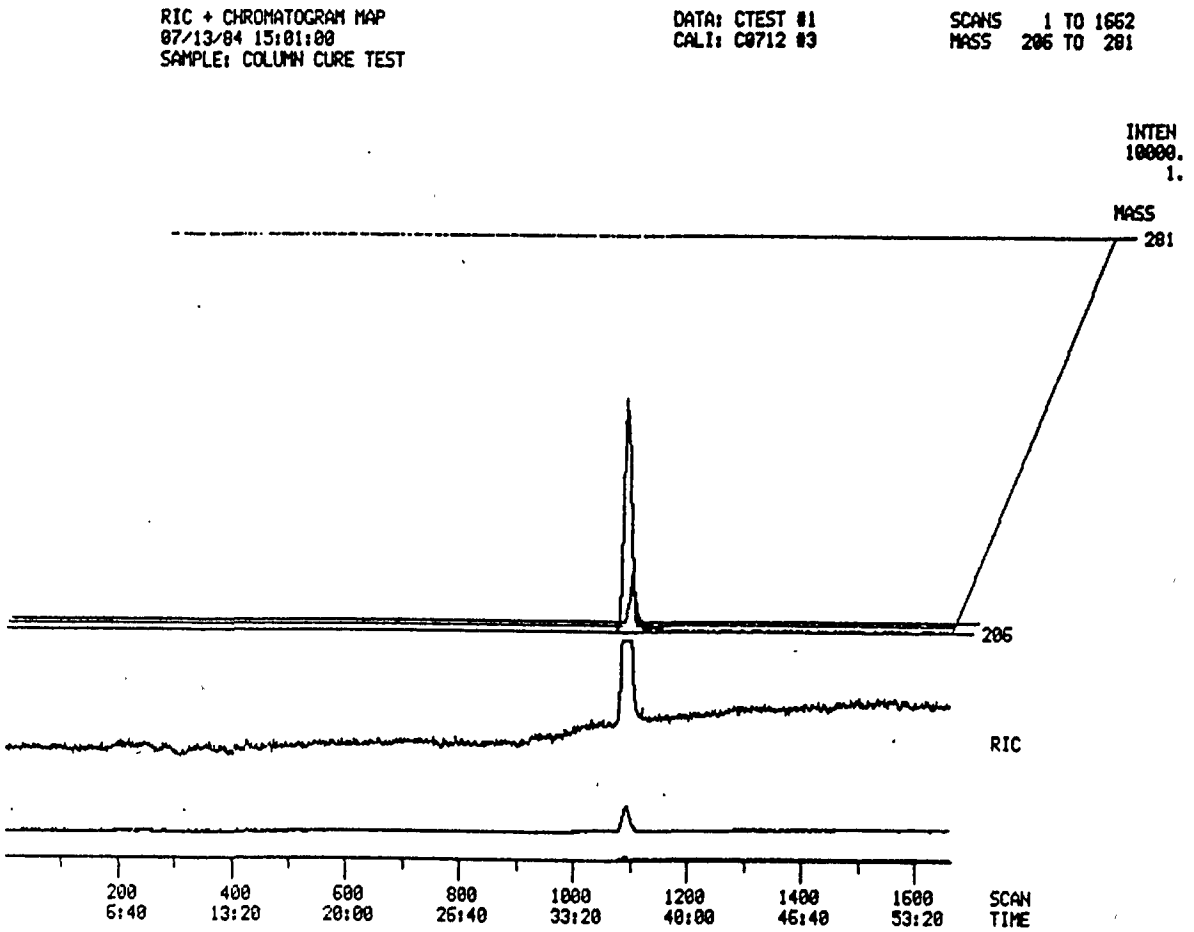

Figure 6. RIC, M/Z 207, M/Z 281 Chromatograms
After Column Conditioning (1 hr., 175°C)

The tetrasiloxane is completely removed by this procedure and the trisiloxane (M/Z 207) is reduced to less than 1% of its' usual presence. It seems clear that inclusion of a column conditioning step in the offgas test sequence would be well worth the effort.

Several tests of this idea revealed that the conditioning step should be done as close in time to the separation sequence as possible. The rise time of the M/Z 207 contaminant appears to be of the order of hours thus limiting the temporal effectiveness of the preconditioning step.

C. Hidden Components

One of the effects of a large amount of contamination from the chromatography system is to hide RIC peaks for the substances of interest which are in much lower concentrations. Figure 7 shows this to be the case in the FESTEST offgas data set.

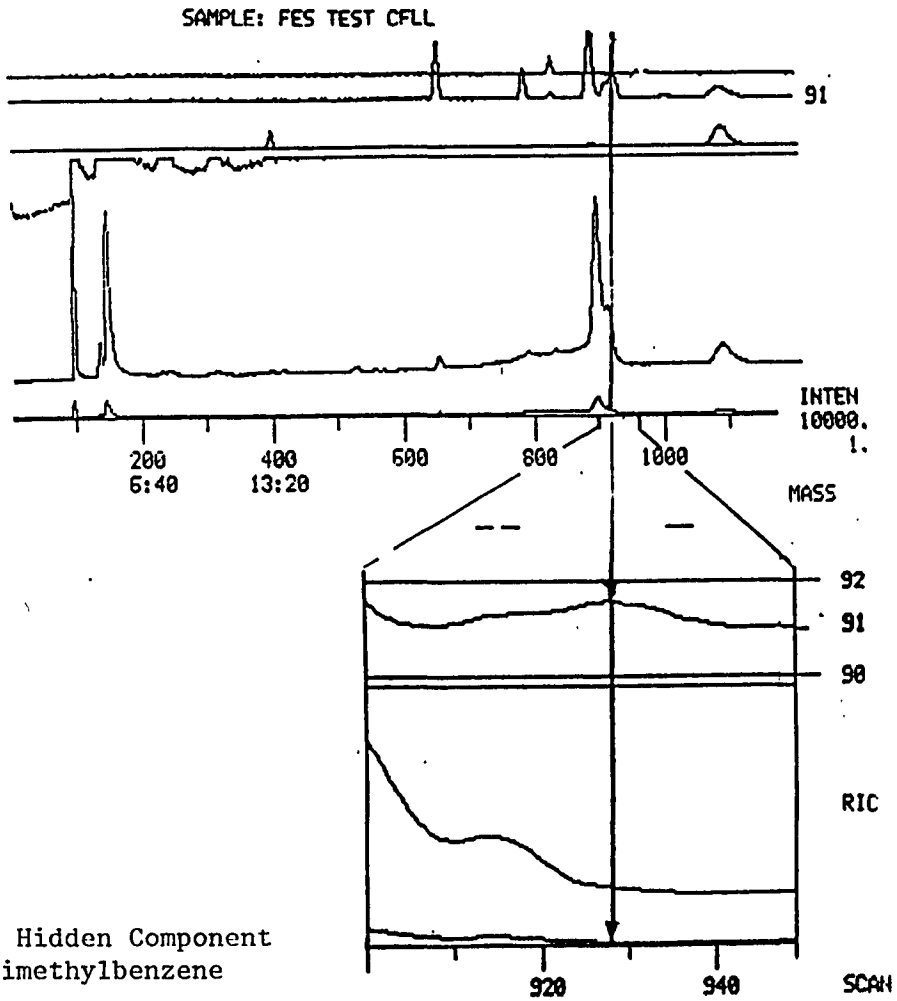

Figure 7. Hidden Component M/Z 91 Dimethylbenzene

The top portion of Figure 7 shows the RIC and several ionic chromatograms. The M/Z 91 chromatogram has a maximum at scan 928 which is not coincident with any hint of a peak in the RIC trace. The lower portion of Figure 7 is an expanded view of the scan 900 to scan 950

section. The maximum in the M/Z 91 trace is clear evidence of an offgas component which is hidden by the trisiloxane in the RIC trace. This component was identified as dimethylbenzene by the SEARCH procedure. The presence of this component was confirmed by the capillary GC analysis where column bleed is not a problem.

The results, summarized on Figure 7, show how powerful the MS/DS system can be in locating components of the sample stream even when they are nearly coincidental and present in vastly differing amounts. These data also show how the reduction or elimination of contaminants, such as those derived from the chromatography system in the FESTEST run, would greatly facilitate the identification of offgas components.

III. Direct Inlet Sampling

MS/DS techniques have a number of applications relevant to the interests of MSFC. In fact it is somewhat surprising that mass spectrometry presently plays such a small role here. One particularly obvious area is in the characterization of thermal properties and processes in the formation of polymeric materials.[6] The existing Finnigan 4000 mass spectrometer is equipped with a direct inlet sample introduction system which can be useful for solid samples. This capability has not been utilized at MSFC and its' application amounts to an extension of mass spectral analysis here.

Since the direct inlet system had not been previously used, it was natural to expect that the vacuum chamber for introduction of the sample to the high vacuum source region might be contaminated. This proved to be the case. It is important for future users to pump this chamber for several days in order to remove the contaminants that backstream from the roughing pump and that seriously contaminate all samples introduced through this means. Once the direct inlet chamber is pumped clean, it is important that the rough pump cycle time be kept to a minimum (less than 30 seconds, the time required for the pressure to reach 0.01 torr).

A second operational factor which had to be determined was the temperature-time characteristics of the direct inlet probe. This probe can be resistively heated up to 350°C at variable rates, the fastest being at an initial rate of about 100°C/minute. The direct inlet probe is in thermal contact with the source region which is maintained at 300°C or above. Thus, even without external heating, the sample heats at a slow rate reaching a steady state temperature of 140-150°C in 3-4 hours. This conductive heating-time relationship determines the lowest available sample temperature in the absence of an external coolant. The temperature rise can be approximately reproduced by equation (4).

$$(4)\quad T(_t)\ ^{o}C = T_o + (150-T_o)\left(-\frac{kt}{1+kt}\right),$$

where $T(_t)$ is the temperature at time t, T_o is the initial temperature (t=0), k is 0.06 min^{-1} and t is the time in minutes.

A. Epoxy Resin Curing Agent

One example of an expanded use of the MS/DS facility, using the direct inlet sample probe, was an analysis of the curing agent (TONOX 60/40)[7] of the resin used in the fabrication of the graphite filament wound case of the solid rocket motor. Quality control of each of the products going into this composite material case is one step that would help prevent a costly failure. Mass spectrometry has many possible applications in such analyses.

The reported content of the curing agent is a 60/40 mixture of

4,4'-diaminodiphenylmethane ("methylenedianiline") and m-phenylenediamine ("m-phenylenedianiline"). Figure 8 shows the mass spectral thermograms from a 50 microgram sample of this curing agent using the direct inlet device. The sample was heated according to equation (4) for the first 9 minutes (to 70°).

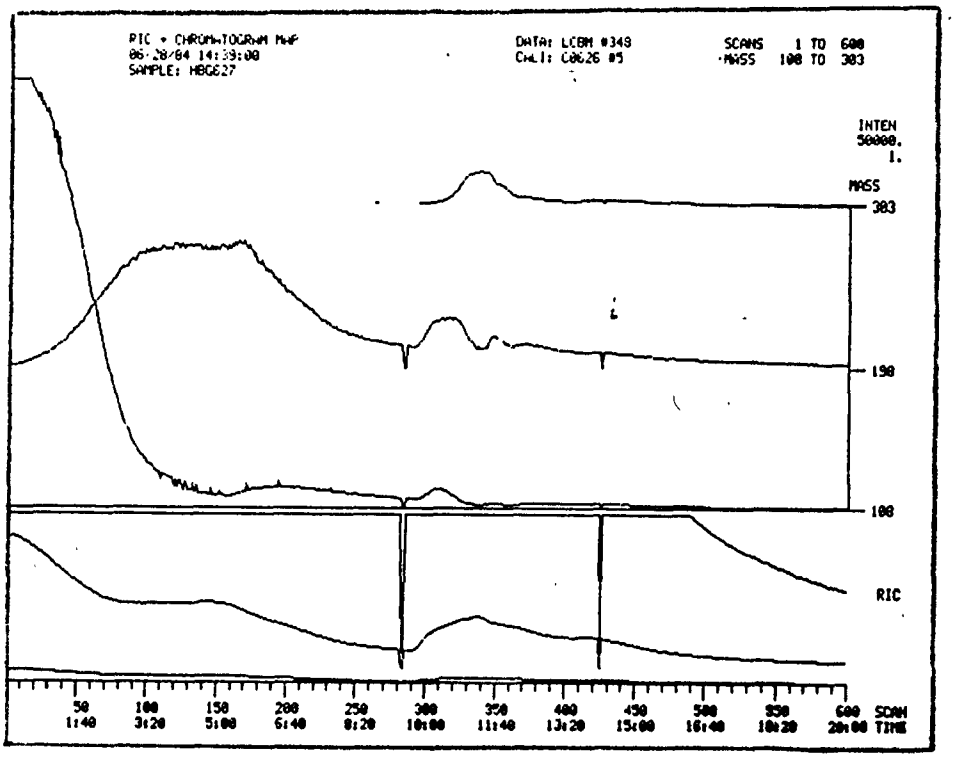

Figure 8. Direct Inlet Analysis of TONOX 60/40
M-Phenylene Dianiline M/Z 108;
Methylene Dianiline M/Z 198;
Oxidation Product M/Z 303

The spikes mark the beginning and end of resistive heating to 300°C. The M/Z 108 curve responds to the volatilization of the lighter (molecular weight 108) component, m-phenylenediamine or its isomers. The M/Z 198 curve responds to the volatilization of the heavier (4-4'-diamino) diphenylmethane. Scans 1-50 are essentially phenylene diamines alone while scans 120-150 correspond to diaminodiphenylmethanes essentially free of the more volatile main component. The library SEARCH showed acceptable identification of these substances.

The M/Z 303 trace shows that higher molecular weight impurities are present which volatilize on heating after the main components have evaporated. The fragments in the 300° spectra show intense 107 and 197

ions in addition to the 303 peaks. These spectra are suggestive of an oxidative dimenzation giving rise to the higher molecular weight substances (like equation (5)).

(5) $R\text{-}NH_2 + R'NH_2 + 1/2\ O_2$ ----½ R-NH-NH-R'(MW 304) + H_2O

A more complete determination of the contents of varying batches of TONOX 60/40 would be possible with a combination of GC and direct inlet analyses.

B. PARALENE

PARALENE[8] is the trade name of a polymeric film marketed by Union Carbide Corp. It was chosen as a second example, which could demonstrate extended application of the MS/DS facility, because it is of mutual interest to MSFC and research at the University of Oregon. This product has been tested and qualified for uses such as coatings on electronic boards by the Ceramics and Coatings group at MSFC. New precursors to this material, allowing generation of the critical intermediate (p-xylylene) at lower temperatures, have been synthesized at Oregon.[9]

Figure 9 shows the thermogravimetric analysis[10] of samples of such polymers. The infrared spectra of these film samples were essentially identical to the literature spectrum. The PAR1 curve was from a polymer

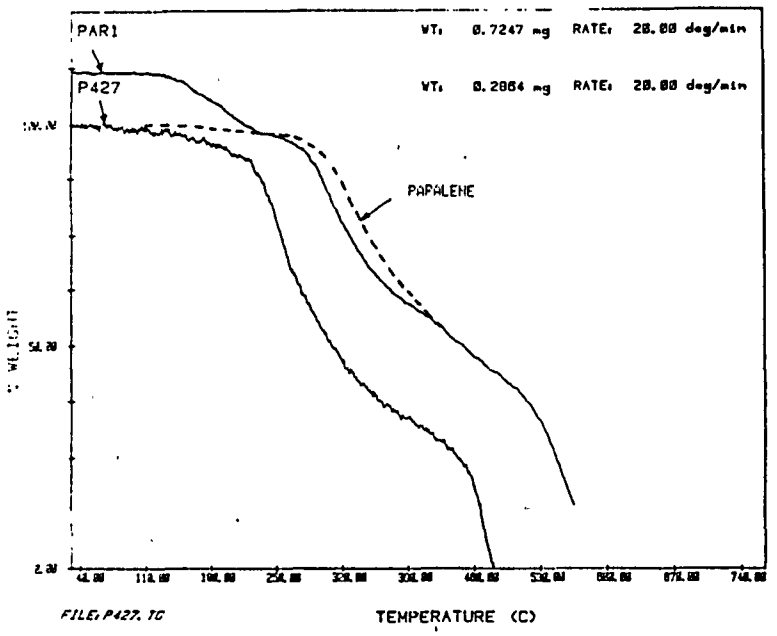

Figure 9. Thermogravimetric Analysis of Paralenes in Air. PAR1-Polymer from 2,2-paracyclophane pyrolysis (670°C).[9] P427-Polymer from p-xylylene-bis-manganese pentacarbonyl[9], PARALENE, data of reference 11.

sample prepared by pyrolysis of 2,2-paracyclophane at 670°C. The low temperature weight loss between 110°C and 250°C for the PAR1 sample (Figure 9) is inconsistent with literature data which is shown as the dashed curve labelled PARALENE. This low temperature loss suggests about 12 percent of a volatile or extremely labile impurity.

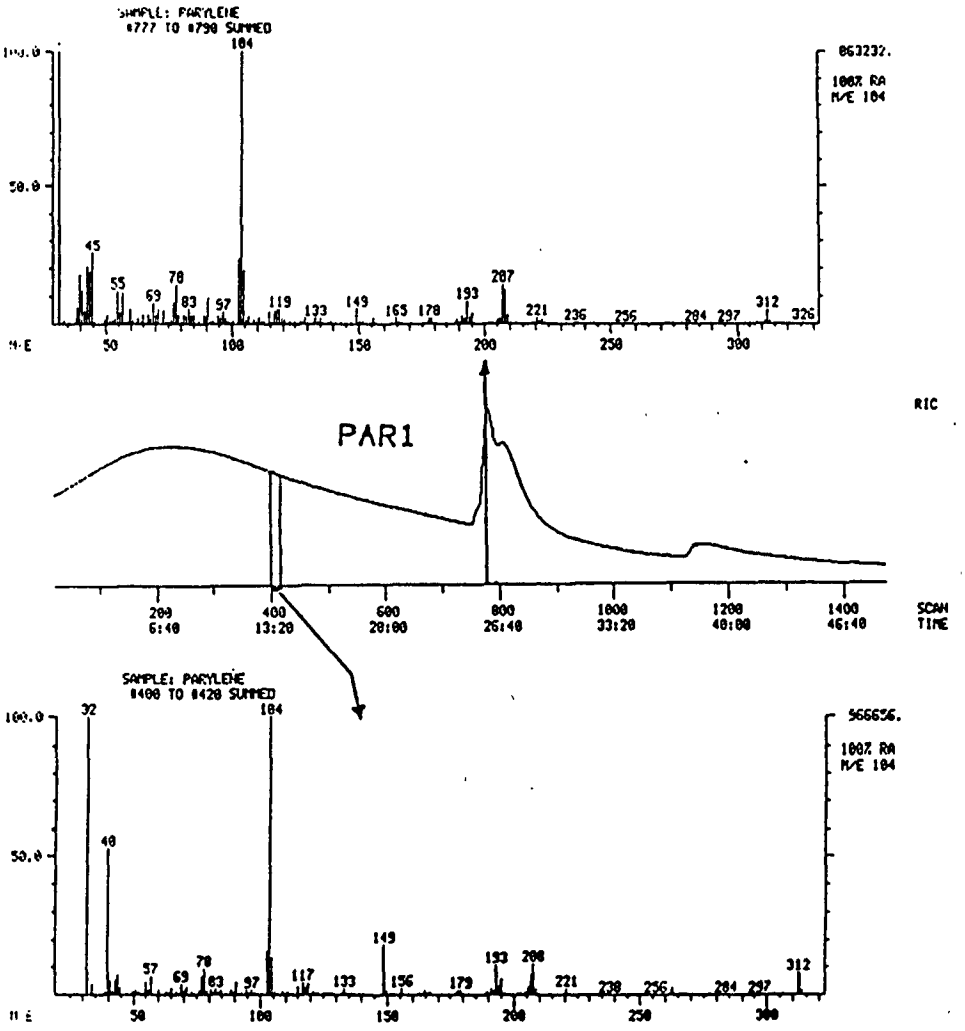

Figure 10. Direct Inlet Mass Spectral Analysis of PAR1.

Figure 10 shows the result of MS/DS analysis of the PAR1 sample using the direct inlet system. The broad peak in the total ion current (RIC, middle) curve occurred during conductive heating (equation (4), 45° to 140°, 0 to 24 minutes, scans 1-720). The sharp peak in the RIC curve near scan 800 occured as the sample was resistively heated to 270°C. The spectra at the top and bottom of Figure 10 are from scans 777-790 and 400-420 respectively. The two spectral averages are almost the same and can be ascribed to the low temperature weight loss component of the PAR1 curve of Figure 9. The prominence of the 104, 208 and 312 masses are indicative of cyclic dimers trimers and possibly

tetramers which would vaporize in the 100°-200°C temperature region and lead to the observed weight loss.

Referring again to Figure 9, the weight loss curve for the sample labelled P427, which was prepared from a bis-manganesepentacarbonyl at 300°C, is displaced to lower temperatures compared to the literature data on the PARALENE curve. This suggests thermal degradation should occur around 300°C. Figure 11 shows two spectral averages from the P427 material taken for a total ion current (RIC) peak at 70°C (top spectrum) and at 350°C (bottom spectrum). The top spectrum indicates the sample contains some of the product of reductive dimerization of the monomer to give 4,4'-dimethyl-1,2-diphenylethane (M/Z 210,105) as a volatile side product. The 350°C spectrum is consistent with the TGA behavior[11] (Figure 9) of this sample since it can be assigned the reported thermal degradation products of PARALENE at unusualy low terperatures.

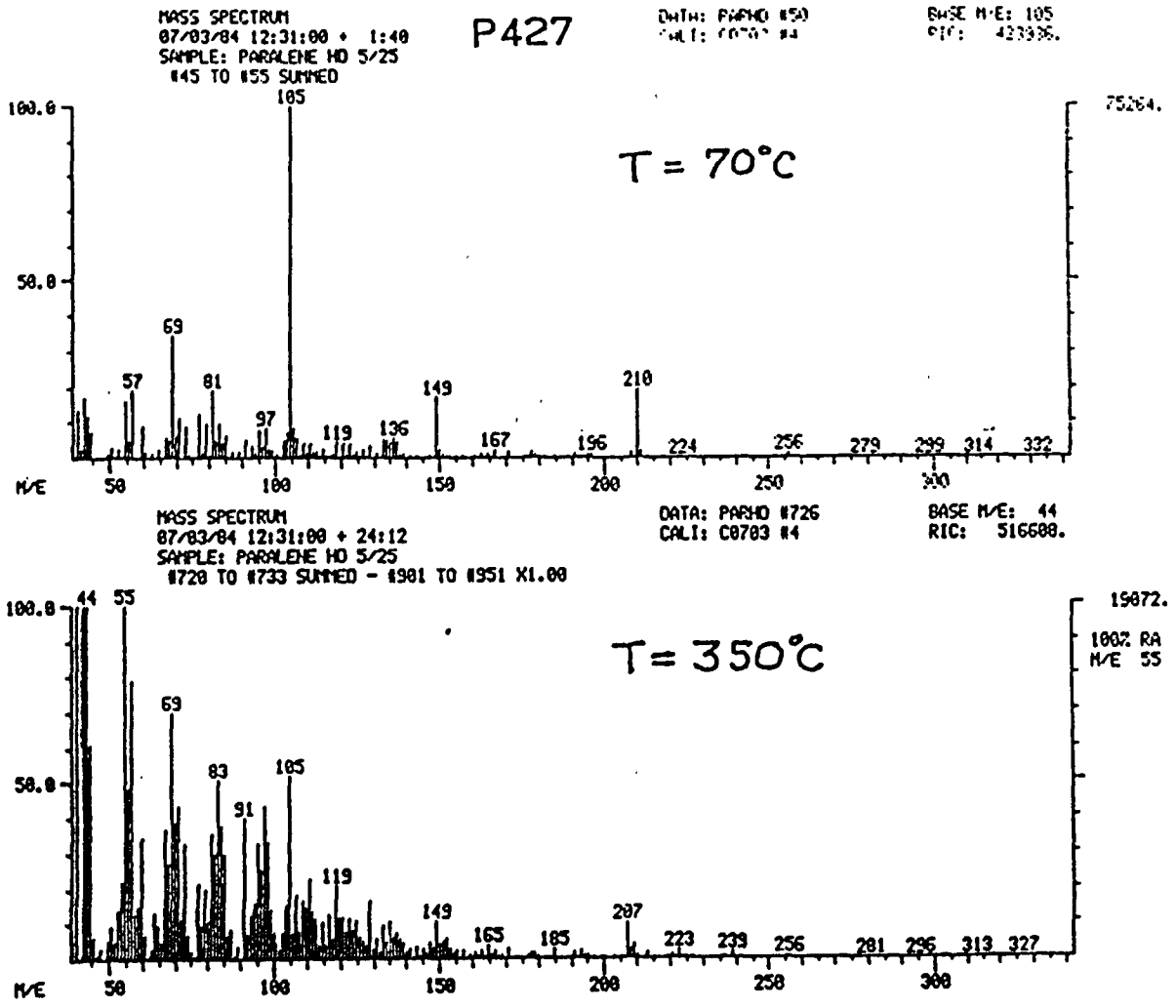

Figure 11. Direct Inlet Mass Spectra of P427.

Both of the spectra of Figure 11 are very different from those of Figure 10 whereas the infrared spectra of the materials were quite similar. These very crude results suggest that the MS/DS -- direct inlet system could be used to develop analyses of a variety of polymer products and processes which are part of the economical production of spaceworthy systems.

IV. Conclusions and Recommendations

The main concern of MSFC with regard to the MS/DS facility is in the identification of materials detected in the offgas procedure. The present work reveals that this identification process can be seriously in error if careful attention is not given to the performance characteristics of the mass analyzer. The operator of the MS/DS system must be able to determine that the peak shapes and positions are acceptably close to those expected in the ICOS calibration-fitting algorithms. The operator must also make sure that the deviation statistics of these data system procedures are within acceptable limits. The computer system cannot overcome severe malfunctions in the mass filter.

The present work demonstrates that the existing offgas procedure is complicated by contamination from the chromatography system. Even with such contamination, offgas substances which are not obviously visible in the RIC trace can be located and identified although this is a time consuming process. It is recommended that a column conditioning step (column at 175°C for 1-2 hours immediately before analytical cycle) be added to the GC/MS/DS method. Test runs indicate this modification should drastically reduce the extent of the contamination problem.. A better solution might be to install one of the newer type[12] capillary columns in place of the present packed column.

Assuming good mass analyzer performance, good calibration and a noncontaminating chromatography system; the offgas component analysis could be accomplished much more quickly and reliably especially if the 100 cm^3 samples can be incorporated. The INCOS system has a number of noise rejection options and the ability to accept fairly extensive command strings under a single procedure name. It is therefore possible to write a set of such procedures that would have the effect of automating the analysis so that the component identification is listed on the printer, almost coincident with the end of the acquisition. This will require expertise with the data system and manpower input.

The direct inlet results presented here are admittedly quite cursory but they do support the notion that a MS/DS facility could be useful at MSFC in a much wider context than routine offgas component identification. Even this single use of the MS/DS facility requires a greater manpower resource than is presently budgeted for the operation of this fairly sophisticated instrument. It would seem reasonable to recommend that a mass spectral analyst be added and placed in charge of the facility which really requires daily attention by a person of such expertise. The offgas analysis could then become an efficient and fairly automatic procedure, taking less machine time and less analyst time than in the present system. The machine time and expertise, required for wider applications of mass spectrometry, would thus appear to be existent by the addition of the mass spectral analyst.

A final suggestion concerns the hardware. The replacement of the entire system with a modern version would be relativly economical at MSFC because of presence of the PDP 11/45 computer system within the same group. Replacement of the Finnigan 4000 mass analyzer with a modern version from VG Analytic Co. is reasonable considering the age of the Finnigan 4000. The VG software is written to run on DEC computer systems. The current VG data system is marketed with a PDP 11/24 preprocessor. Most of the peripherals for the VG data system are already available within the existing 11/45 system. They could thus be deleted from the VG package reducing the cost. Upgrading the role of the MS/DS facility here would yield a quantum jump in the analytical and computer power in this group.

V. References

1. F. A. Mellon, Mass Spectrometry. Specialist Periodical Reports. The Royal Society of Chemistry (London), 6, 196-227, 1981.

2. The display of Figure 2 has been highly truncated in order to give visibility to the type of information available in the system. This visibility disguises the fundamental problem of working with large data sets which is the high volume of background information compared to that of analytical pertinence.

3. L. M. Weeks, "Flammability, Odor and Offgassing Requirements and Test Procedures for Materials in Environments That Support Combustion". NHB 8060.1B.

4. MSDS Finnigan/INCOS Operation Manual Revision 3, December 1978, pp. 44-47; pp.4-1 to 4-25.

5. Ivan J. Goldfarb, Eui-won Choe and Harold Rosenberg in "Organometallic Polymers", Charles E Carraher Jr., John E. Sheats and Charles U. Pittman Jr. Editors, Academic Press, New York, 1978, p.255.

6. Hans-Rolf Schulten and Robert P. Lattimer, Mass Spectrometry Reviews, 3, 231-315, 1984.

7. This sample was supplied by L. Chou whose cooperation is gratefully acknowledged.

8. William F. Gorham, "Encyclopedia of Polymer Science and Technology", Vol. 15, pp. 98-113, Interscience Publishers, New York, 1971.

9. Unpublished work of Hsing-Yeh Parker, Department of Chemistry, University of Oregon.

10. The thermogravimetric analyses were made possible through the cooperation of Dr. John G. Austin whose help was valuable in many instances of this project.

11. J. P. Critchley, G. J. Knight and W. W. Wright, "Heat Resistant Polymers", Ch 4, Plenum Press, New York, 1975.

12. Milton L. Lee, Frank J. Yang and Keith D. Bartle, "Open Tubular Column Gas Chromatography. Theory and Practice", pp. 143-148, John Wiley and Sons, New York, 1984. See also Ref. 1.

N85-22228

1984

NASA/ASEE SUMMER FACULTY RESEARCH FELLOWSHIP PROGRAM

MARSHALL SPACE FLIGHT CENTER
THE UNIVERSITY OF ALABAMA

GERMANIUM RESISTANCE THERMOMETER CALIBRATION AT SUPERFLUID HELIUM TEMPERATURES

Prepared By:	Franklin Curtis Mason, Ph.D.
Academic Rank:	Professor
University and Department:	Middle Tennessee State University Department of Chemistry and Physics
NASA/MSFC:	
Laboratory:	Space Science
Division:	Astrophysics
Branch:	Infrared Astronomy
NASA Counterparts:	Dan Ladner and Eugene Urban
Date:	August 3, 1984
Contract No.:	NASA-NGT-01-002-099 (The University of Alabama)

ACKNOWLEDGEMENTS

First of all, the author wishes to acknowledge the NASA/ASEE Summer Faculty Fellowship Program, and in particular the NASA/MSFC officials Dr. Jim Dozier and Mr. Leroy Osborn, and Dr. Mike Freeman, of the University of Alabama, who served as University Director for the program.

Dr.'s Dan Ladner and Eugene Urban are due a word of thanks for their guidance of this project.

An expression of appreciation is offered to Mr. J. O. Jolley and Mr. Dale Armstrong for their assistance in technical matters.

To Dr. Palmer Peters, Mr. Charles Sisk, and Mr. Ed Stephens, a word of gratitude is due, since they filled in during the absence of Dr.'s Ladner and Urban and Mr.'s Jolley and Armstrong, who were at Kennedy Space Center in Florida on temporary assignment for a period of about five weeks during the summer.

And this summer the typing of the final report was again by Mrs. Sue Davis, and the author wishes to express his gratitude for that invaluable service.

GERMANIUM RESISTANCE THERMOMETER CALIBRATION AT SUPERFLUID HELIUM TEMPERATURES

by

Franklin Curtis Mason
Professor of Physics
Middle Tennessee State University
Murfreesboro, TN

ABSTRACT

The rapid increase in resistance of high purity semiconducting germanium with decreasing temperature in the superfluid helium range of temperatures makes this material highly adaptable as a very sensitive thermometer. Also, a germanium thermometer exhibits a highly reproducible resistance versus temperature characteristic curve upon cycling between liquid helium temperatures and room temperature. These two factors combine to make germanium thermometers ideally suited for measuring temperatures in many cryogenic studies at superfluid helium temperatures. One disadvantage, however, is the relatively high cost of calibrated germanium thermometers. In comparison, their cost is about six hundred dollars each, to about one hundred dollars each for uncalibrated ones. In space helium cryogenic systems, many such thermometers are often required, leading to a high cost for calibrated thermometers. This project is concerned, therefore, with the construction of a thermometer calibration cryostat and probe which will allow for calibrating six germanium thermometers at one time, thus effecting substantial savings in the purchase of thermometers.

INTRODUCTION

In many space cryogenic systems where superfluid helium is the cryogen, thermometers of high sensitivity are generally required. The loss of sensitivity of ordinary metallic resistance thermometers and thermocouples at extremely low temperatures thus makes these devices unsuited for thermometers below a temperature of about 15 K. On the other hand, semiconducting germanium resistance thermometers and certain varieties of ordinary carbon resistors exhibit a rapid increase in resistance with decreasing temperature at liquid helium temperatures. Therefore, these types of thermometers find use as sensitive secondary thermometers at or below the normal boiling point of liquid helium, or 4.2 K. Carbon resistors suffer the disadvantage of unrepeatable resistance versus temperature characteristic curves, and it is necessary to calibrate a carbon resistor each time it is cycled between room temperature (or the temperature of liquid nitrogen) and the temperature of liquid helium (1). In contrast, germanium thermometers exhibit reproducible resistance-temperature characteristics, which means that one calibration suffices, and commercially produced and calibrated thermometers are available (2,3). The major drawback to purchasing a calibrated germanium thermometer is its fairly high cost of about six hundred dollars or so. Uncalibrated germanium thermometers are also available, with a cost of about one hundred dollars each. With in-house calibration capabilities, it is possible to realize a substantial savings on thermometer purchases. This is compounded when several such thermometers are required, as is frequently the case in space science applications.

OBJECTIVE

The objective of the project being discussed in this report is the construction of a cryostat and probe for the purpose of simultaneously calibrating six germanium thermometers with one transfer of liquid helium.

BACKGROUND DISCUSSION

Suitable semiconducting materials make excellent resistance thermometers at temperatures below which metallic elements become insensitive to small changes in temperature. The first semiconductors to be used as thermometers at low temperatures were carbon-black or "aquadag" films in 1938 by Giauque, Stoudt, and Clark (4). Later Clement and Quinnell (5) found in 1950 that commercial radio resistors

met most of the requirements of cryogenic thermometery. However, a high degree of reproducibility was lacking until crystals of doped germanium and silicon were investigated by Friedberg and Esterman in 1955 (6).

Illustrations of the resistance versus temperature characteristics for a carbon radio resistor and a germanium thermometer are shown in Figure I. The carbon resistor has a resistance of about 150 ohms at room temperature. The calibration data for this resistor is from research by the author in 1972 in connection with measuring the Kapitza boundary resistance for a copper-liquid helium interface (1). The germanium curve is that of the calibrated resistor being used in this project as a standard of calibration. All the germanium resistors, both the uncalibrated ones and the calibrated "standard" are by Lakeshore Cryotronics.

The construction details of a typical germanium resistance thermometer are given in Figure II. The bridge shape in this figure is cut from a single crystal of arsenic-doped germanium and four gold wires are welded to it as current and potential contacts. These wires are in turn welded to four Phosphor-bronze leads. The germanium sensing element is carefully mounted to avoid strains and piezo-electric effects.

Self heating becomes a problem with germanium thermometers if too much measuring current is applied. Generally the limits on current are; 100 microamps at or above 20 K, 10 microamps above 4.2 K, and 1-2 microamps below 4 K, with the power dissipation being limited to 0.1 microwatt at most (7). Also, because of the nature of semiconducting materials, stray high-frequency fields may cause additional self heating. And since semiconductors show a higher magneto-resistance than metals, care should be taken to minimize the presence of stray magnetic fields.

With respect to the representation of R(T) for germanium, the usual approach is to computer-fit a polynomial of the form

$$\log R = \sum_{n=0}^{m} A_n (\log T)_n \qquad (1)$$

or

$$\log T = \sum_{n=0}^{m} A_n (\log R)_n \qquad (2)$$

with an appropriate range on m for a specified temperature range (7). If the temperature range is very wide, the data may not be well represented by such an equation as given

above, and in this case the approach is to plot a correction graph showing the deviation of this formula from the measured variation of resistance with temperature (8).

EXPERIMENTAL APPARATUS

For this project the apparatus divides into three main categories: (1) the electronics, (2) the probe, and (3) the cryostat. A discussion of each of these follows.

Electronics

Two pieces of electronic apparatus are essential for cryogenic thermometer calibration, a helium bath temperature controller and a bridge for determining resistances. The latter of these can be either a direct reading bridge or a conductance bridge. In this study a conductance bridge has been chosen. Some specifics of the electronics are given below.

For temperature control of the bath, an Artronix Model 5301 temperature controller is being used (9). In conjunction with the Artronix, a resistive temperature probe and a heater of suitable size are needed. This regulator has a temperature range of 1 K to 320 K, with six ranges for sensors with positive temperature coefficients (positive TC) and six ranges for sensors with negative temperature coefficients (negative TC). The resistance of the positive TC sensors can range from 1 to 120 ohms, while the range on sensors of negative TC is from 4 to 15 kohms. The power dissipation in the sensors is limited to 10^{-6} W in all ranges. Platinum resistors are suggested as appropriate positive TC sensors, and germanium resistors, carbon resistors, and thermistors are all applicable as negative TC sensors. The power output for the regulator is in three ranges, low (0-2 V), medium (0-10 V), and high (0-50 V). The heater current is d. c. with low ripple content with a maximum output of 100 watts, short-circuit proof. The heater resistance can vary from 25 ohms and 25 kohms, depending on the average control power needed (watts = 2500/R). Other specifications for the Artronix controller are given in the instruction manual.

Instead of measuring resistances, a SHE Model PCB Potentiometric Conductance Bridge (10) for measuring conductances is being utilized for thermometer calibration. This bridge is a four terminal a. c. bridge with digital readout. Its novel low noise circuitry permits accurate, high resolution measurements at sub-picowatt sensor power levels. Measurement problems associated with thermal emfs and large temperature dependent contact resistances are effectively eliminated. These features, combined with a nominal accuracy of 0.1% make the Model PCB ideally suited for low temperature

measurements with resistance thermometers. Simply by taking the reciprocal, calibrated resistors can be converted into calibrated conductors. Since germanium resistance thermometers have increasing resistances as the temperature decreases, the constant voltage excitation of the PCB has the desirable property that the power dissipated in the sensor thus decreases as the temperature decreases, in contrast to constant current excitation. Measuring conductance rather than resistance has an advantage, since the temperature resolution is more uniform. Also temperature and conductance both increase or both decrease. An optional BCD output is available with the PCB for data logging purposes and computer controlled applications.

In association with the electronics is a switch box which allows for the connection of the Artronix regulator bridge and the SHE conductance bridge with the appropriate sensing and/or heating elements on the probe. In the switch box a rotary wafer switch permits each of the six uncalibrated resistors to be switched into the SHE bridge, with the calibrated resistor being switched into the bridge after resistors 1,4, and 6 in a cyclic manner. This allows for a quick multiple measurement of the calibrated resistor at each point in temperature during a calibration run.

The Probe

Central to the calibration of thermometers in this project is the probe, a diagram of which is given in Figure III. When oriented as in an actual calibration run, this probe consists of a vertical thin-walled stainless steel tube of 7/16 inch diameter and a length of 55 inches. Along the length of this tube are placed seven appropriately spaced radiation baffles. Through each of the six lower baffles two holes are drilled and fitted with rubber grommets to allow for protected passage of thermometer and heater leads from the top connector board to the lower connector board, spaced some 34 inches apart, and also mounted on the probe tube. Each of the connector boards consists of a set of pins mounted in breadboard fashion in identical rectangular arrays. Figure IV gives the details of these boards, along with the arrangement of thermometer and heater connections. There are a total of 33 connecting wires between the top and bottom board, four for each thermometer, three for the Artronix sensor, and two for the regulator heater. Each of these wires is about 5 feet in length, and those for the thermometers and Artronix sensor are each of Formvar-coated Manganin with a resistance of about 75 ohms. The regulator heater connecting wires are of #36 nylon coated copper wire. Also mounted on the probe are two liquid level indicators with appropriate wiring to the outside.

Approximately 1 inch above the bottom of the probe tube a circular copper plate 1/8 inch in thickness and 3 inches in diameter is mounted. A series of holes in this plate serves to mount the thermometers.

At the bottom of the probe tube the bath regulator heater is mounted. This heater consists of approximately 2.3 feet of 0.002-inch diameter Evanohm wire, for a total resistance of about 420 ohms. Since the heater wire is not insulated, the heater is wound on a specially designed coil form for the purpose of isolating the individual turns of the resulting coil. The coil form consists of a Nalgene laboratory bottle cap of approximately 2½ inches in diameter. On the periphery of this cap there are twelve protrusions originally meant to be used as finger grips for tightening and loosening the cap. Through each of these grips and tangent to the cap itself, six holes approximately 0.01 inch in diameter are drilled, the spacing of the holes being approximately 0.05 inch. The heater wire is threaded through each bottom hole, thus forming a turn. The direction of the threading is then reversed at the last bottom hole, with the next set of holes accommodating the next turn, and so on, until the heater is complete. In this way any stray magnetic field the heater might introduce is hoped to be negligible, since the magnetic fields of the individual windings cancel in pairs.

The heater coil is mounted to the bottom of the probe by a special adapter so designed to take advantage of the screw threads inside the Nalgene bottle cap for securing the heater to the probe. This adapter is made from phenolic composition board, and it includes a mount for the Artronix sensor just above the heater.

The Cryostat

A Kadel Engineering helium dewar, Model # 506, is the heart of the cryostat (11). The helium space of this dewar is a cylindrical aluminum alloy can with a volume of 25 liters. The helium is protected by a guard vacuum in conjunction with multilayered insulation. Connected to the helium can and isolating it from the top of the dewar is a thin-walled cylindrical insulating neck. The guard vacuum of this dewar has been pumped down to about 5×10^{-6} torr, after which the helium space was filled with liquid nitrogen to test the dewar capability for holding cryogenic liquids. So far the dewar is performing satisfactorily at nitrogen temperatures.

In association with the helium dewar is a pumping line, which is being readied at this time. Figure V gives the details of this line. A high-volume Welch DuoSeal vacuum

pump, Model # 1395 (12) is to provide the pumping necessary for lowering the temperature of the helium when desired. The pumping line is from 2-inch inside diameter stainless steel pipe in which are appropriate valves for regulating the pumping speed. Also in the line is a 24-inch section of vacuum bellows tube for surpressing the effect of pump vibrations on the calibration process.

The dewar is covered by a flange that is fitted with a modified "tee" joint concentric to the flange. This joint has an inside adapter for supporting the probe. Also, on top of the flange is a blank-off plate which can be removed during the transfer of liquid helium, thus allowing for the escape of the vapors. A 37-pin Deutsch Connector (13), which is mounted in the top flange, serves as the vacuum feed-through for connecting the various components of the probe to the electronics. The details of the pin arrangement for the vacuum feedthrough are given in Table 1.

CALIBRATION SCENARIO

To achieve the goal of thermometer calibration, the following scenario is essentially what must be accomplished.

First, the cryostat is readied to receive the helium after which a helium transfer of approximately 25 liters takes place. Since the calibration range of temperatures lies between 2.17 K and 1.5 K or lower, starting with helium at 4.2 K, pumping about 1/3 of the liquid away accomplishes the lambda transition, 2.17 K. After attaining this temperature, the pumping speed is set by adjusting the valves in the pumping line until the approximate temperature of a calibration point is reached, at which time the Artronix regulator keeps the temperature at the desired value. Data on the resistances of the uncalibrated thermometers are taken, along with an appropriate number of values of the resistance of the calibrated "standard thermometer". Using an average resistance of the standard, the point in temperature is precisely determined from a calibration curve. This value of temperature, along with the value of resistance for an uncalibrated thermometer constitutes a calibration datum point. From a set of such points, a calibration curve for the unknown is determined from either Eq. (1) or Eq. (2).

CONCLUSIONS AND RECOMMENDATIONS

In conclusion, a cryostat and a probe for germanium thermometer calibration are essentially complete at this time. The probe and dewar flange were constructed earlier this year by Mr. Dale Armstrong of the Infrared Astronomy Group, and the switchbox was previosuly wired by Mr. Charles Sisk, also of the Infrared Astronomy Group. The remainder of the apparatus construction was accomplished this summer

as a Summer Faculty Fellowship Project. Included are the wiring of the probe, the wiring of the Deutsch connector feedthrough, the design and construction of the Artronix heater coil form and the subsequent wiring of this coil, the design and construction of an adapter for mounting the heater coil on the probe, the installation of the Artronix sensor and the thermometers, and the layout of the pumping lines of the cryostat. Yet to be accomplished are the completion of the plumbing followed by a leak check of the system, the checkout of the probe at cryogenic temperatures, and finally, calibration runs.

As a matter of record, two construction points should be listed for future reference. These are:

1. Care must be taken when using G.E. 7031 varnish on Formvar-coated wires, since the solvent in this varnish dissolves the Formvar coating.

2. Because of the design of the Deutsch Connector, for the pins to line up between the top and bottom sockets, the top connector socket is based on a silicone rubber insert, while the bottom socket must have a Teflon insert, with all of the above components being peculiar to Deutsch Connectors.

And finally a comment on these past two summers as a NASA Summer Faculty Fellow: It is difficult to estimate the value of the re-thinking of old ideas and the additional experience gained. To be sure, the opportunity provided by the Summer Faculty Fellowship Program has given new direction to the professional career of this participant.

REFERENCES

1. Mason, Franklin C., The Kapitza Effect in He I and He II Ph.D. Dissertation (Unpublished), Ohio State University, Columbus, Ohio (1972).

2. Lakeshore Cryotronics, Inc., 64 E. Walnut St., Westerville, Ohio 43081.

3. CryoCal, Inc., 5301 Edina Industrial Blvd., Minneapolis, Minnesota 55435.

4. Giauque, W. F., Stout, J. W., and Clark, C. W., Journal of the American Chemical Society, 60, 1053 (1938).

5. Clement, J. R., and Quinnell, E. H., Review of Scientific Instruments, 23, 213 (1952).

6. Friedberg, Temperature, 2, 355 (1955).

7. White, G. K., Experimental Techniques in Low-Temperature Physics, Clarendon Press, Oxford, P. 109 (1979).

8. Rose-Innes, A. C., Low Temperature Techniques, D. Van Nostrand, C., Inc., P. 106 (1964).

9. Artronix Instrumentation, 716 Hanley Industrial Court, St. Louis, Missouri 63144.

10. S.H.E. Corporation, 414 Sorrento Valley Blvd., San Diego, California 92121.

11. Kadel Engineering, 1627 East Main Street, Danville, Indiana 46122.

12. Sargent-Welch Scientific Company, Vacuum Products Division, 7300 North Linder Avenue, Skokie, Illinois 60076.

13. Deutsch Electronic Components, Municipal Airport, Banning, California 92220.

TABLE 1. FEEDTHROUGH CONNECTOR PIN TABLE

ELECTRONICS INSTRUMENT	COMPONENT ON PROBE	FEEDTHROUGH PIN #'s
SHE BRIDGE	T_{CAL}	1, 2, 3, 4
" "	T_1	5, 6, 7, 8
" "	T_2	9, 10, 11, 12
" "	T_3	13, 14, 15, 16
" "	T_4	17, 18, 19, 20
" "	T_5	21, 22, 23, 24
" "	T_6	25, 26, 37, 28
ARTRONIX REGULATOR	HEATER	29, 30
" "	SENSOR	31, 32, 33
SHE BRIDGE	LEVEL INDICATOR 1	34, 35
" "	LEVEL INDICATOR 2	36, 37

NOTE: WITH REFERENCE TO THE SHE BRIDGE:

CONNECTORS 1, 5, 9, 13, 17, 21, AND 25 ARE I+

CONNECTORS 2, 6, 10, 14, 18, 22, AND 26 ARE I-

CONNECTORS 3, 7, 11, 15, 19, 23, AND 27 ARE V+

CONNECTORS 4, 8, 12, 16, 20, 24, AND 28 ARE V-

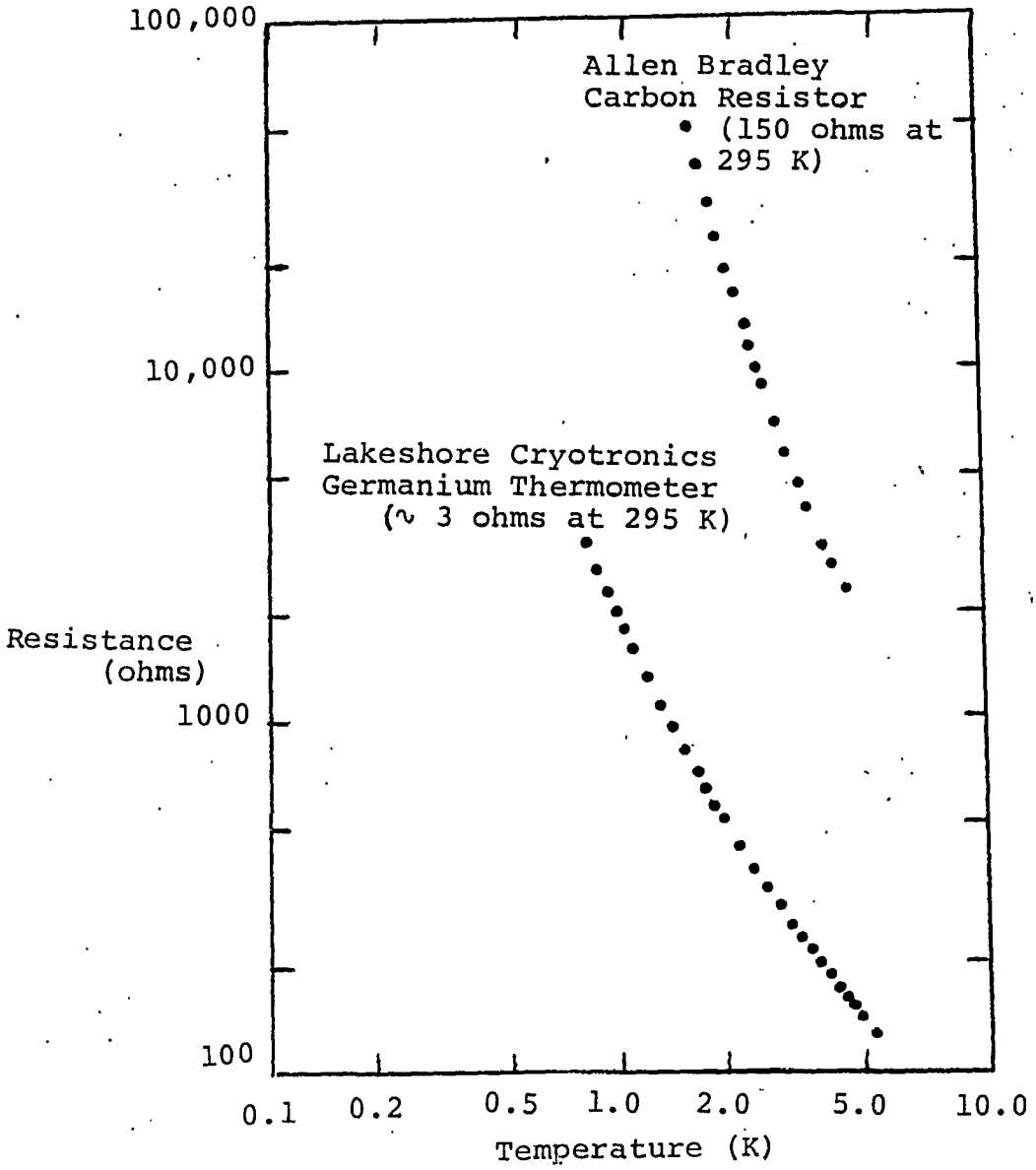

FIGURE I

THERMOMETER CHARACTERISTICS

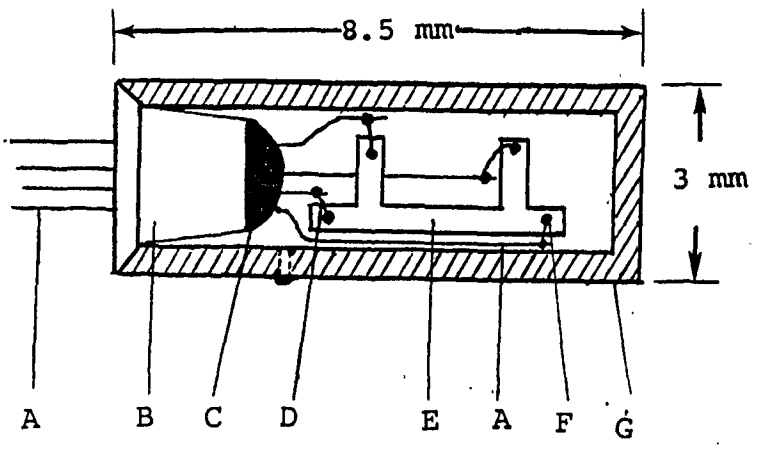

LEGEND

A-----PHOSPHOROUS-BRONZE LEADS
B-----BERYLLIUM OXIDE BASE
C-----EPOXY HEAT SINK
D-----GOLD LEADS
E-----SENSING ELEMENT
F-----SOLDERING JOINTS
G-----GOLD-PLATED COPPER CASE

FIGURE II

GERMANIUM THERMOMETER DETAILS

FIGURE III

PROBE DETAILS

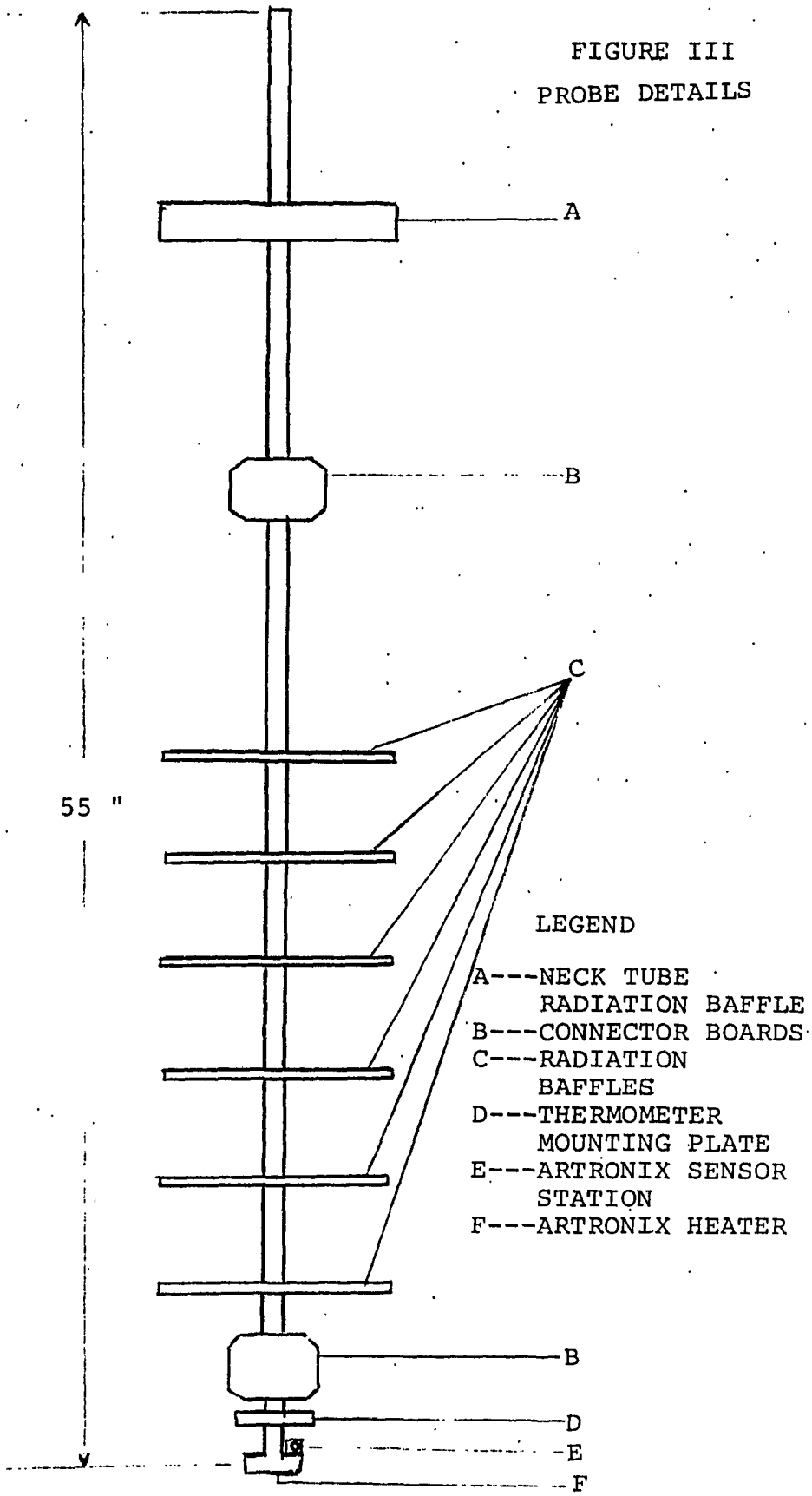

LEGEND

A---NECK TUBE RADIATION BAFFLE
B---CONNECTOR BOARDS
C---RADIATION BAFFLES
D---THERMOMETER MOUNTING PLATE
E---ARTRONIX SENSOR STATION
F---ARTRONIX HEATER

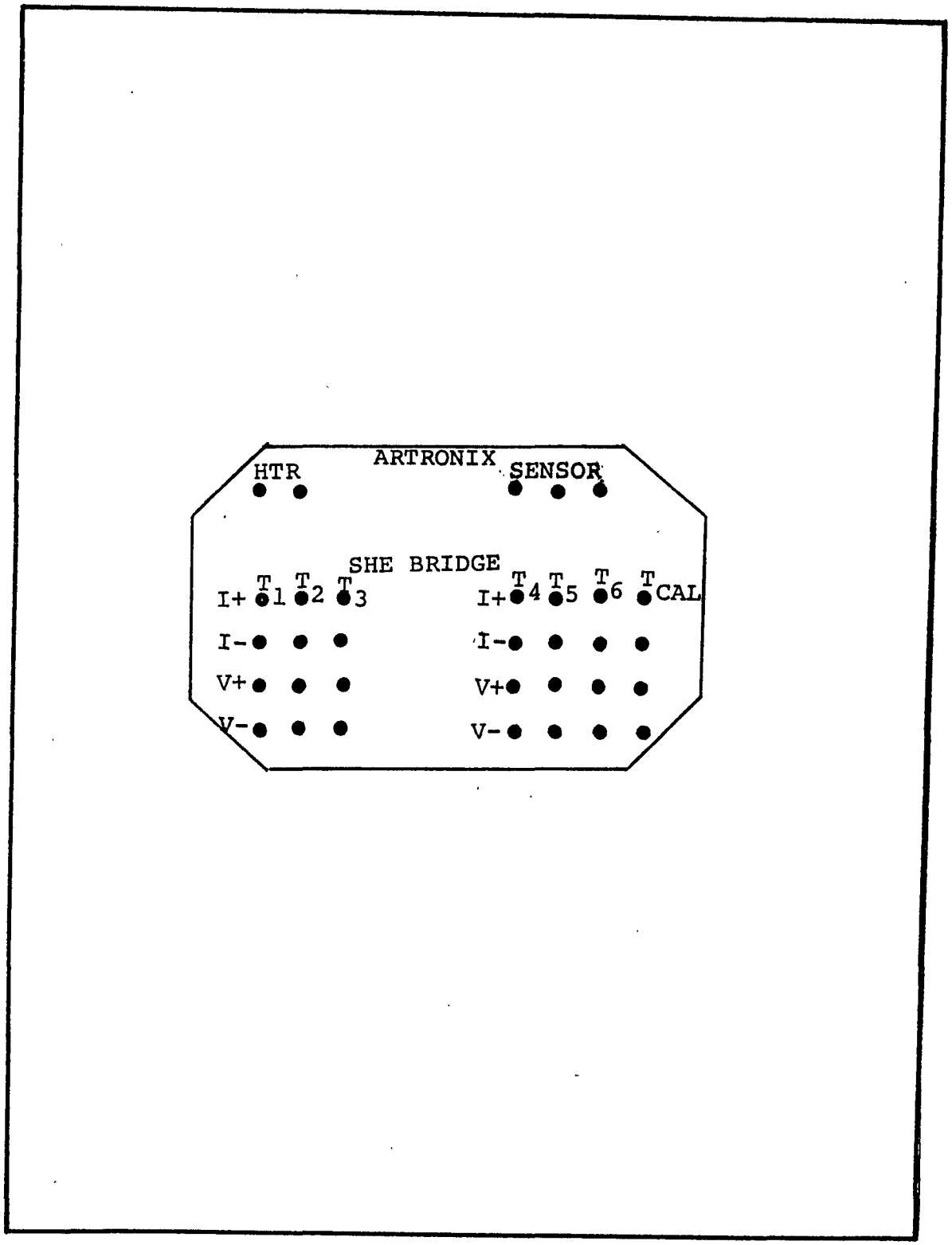

FIGURE IV

PROBE CONNECTOR BOARD DETAILS

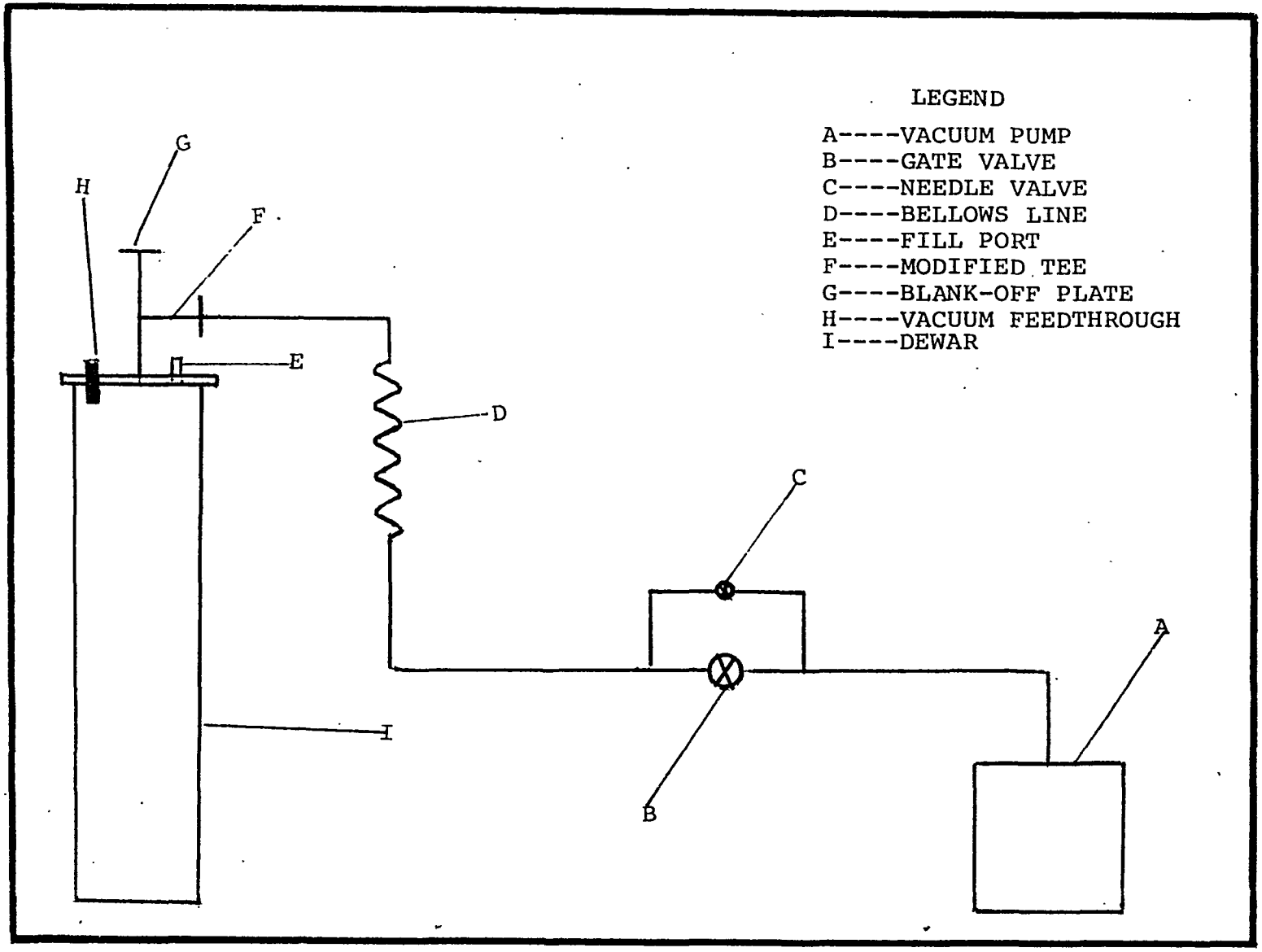

FIGURE V

THE CRYOSTAT

1984

NASA/ASEE SUMMER FACULTY RESEARCH FELLOWSHIP PROGRAM

MARSHALL SPACE FLIGHT CENTER
THE UNIVERSITY OF ALABAMA

EVALUATION OF EXPERT SYSTEMS

Prepared By:	Michael A. McAnulty
Academic Rank:	Assistant Professor
University and Department:	University of Alabama at Birmingham Department of Computer and Information Science
NASA/MSFC:	
Laboratory:	Information and Electronic Systems
Division:	Software and Data Management
Branch:	Staff
NASA Counterpart:	Audie E. Anderson
Date:	27 August 1984

NASA-NGT-01-002-099
(The University of Alabama)

Acknowledgements

Appreciation comes in many flavors. For overall mission orientation and administrative support we owe James Dozier, Leroy Osborn, and L. M. Freeman a great deal. For further elucidation of the NASA situation and requirements, as well as technical support, thanks are due to Walter Frost, Pattie Jo Miller, David Aichele, and Lyndon Stone. William Park and David Brown of SRI International, and Jonathan Bein of Martin-Marietta, were invaluable windows to the outside world. Dr. G. B. von Tiesenhausen, on very short notice, provided one of the most entertaining hours ever as well as a great deal of source material. Last, but probably foremost, thanks are due to my NASA counterpart, Audie Anderson, for his quiet sheperding of an unruly flock. If there are any bright ideas in the following, he probably had them first.

Evaluating Expert Systems - ABSTRACT

M. A. McAnulty, NASA/ASEE Fellow
NASA Contact : A. E. Anderson
Marshall Space Flight Center

The only successful applied area of artificial intelligence is that of expert systems, programs which collect and arrange information about the solution of difficult problems in a well- defined and well-circumscribed area, and are then capable of mimicking expert behavior in finding solutions to new problems. Several expert systems are now routinely outperforming experts in many areas, including CADUCEUS in internal medicine diagnosis, PROSPECTOR in geology, XCON in computer configuration, to name only a few. NASA intends to investigate the application of this technology to management and control situations in a space station environment, specifically for power,heat, communications, and attitude control, areas where much of the time human management is laborious, repetitive, and eventually error- prone.

A simple system may be controlled by a closed and precise algorithm. As the number of systems proliferates, and the number of possible conditions grows, a large layer of discrete control grows on top of the classical controllers. This is the germ of an expert system- a large collection of situational information and desired actions. To move from an existing situation to a desired situation is, at this discrete level, a graph traversal based upon a production system. The use of a human expert to add rules to the system provides heuristics, or graph-traversal shortcuts which enable a less-than exhaustive traversal.

The objective of this engagement is to identify the current and projected capabilities of the technology within the NASA framework, both in terms of expected performance and necessary technological support.

Foreword

Preliminary studies concerning automation of various space station functions, specifically power system management, communications, thermal and attitude control, have recommended the further study of expert systems as controllers. [1,2,3] This paper presents the results of a nine-week study of various aspects of expert systems, their antecedents, their possible application and implementation, and current and projected capabilities. As such, this is in no sense an original research document, rather a local consolidation of selected published and verbalized information.

There are very few cited references, as most of the assertions are in fact highly general and part of the folklore, and can be found (often along with counterassertions, such is the field) in several places in the recommended references (Appendix I).

Motivation

A classical controller senses the current state of a variable, compares it with a desired state, and directs the transition of the variable towards the desired state. In a single variable system the desired state may be a single value or one or more ranges of desirable values. For a system of many variables, however, the overall controller is not simply a collection of univariate controllers. First, the desired state specifications can not be expressed in a univariate fashion, but must be an ensemble. Second, to effect a change in one variable will affect other variables, driving them perhaps away from safe states, because they are coupled. For some systems the coupling may take a convenient functional form (convenience generally has to do with unimodality). However, even where the coupling equations can be specified, maintenance and modification are difficult and present a significant cost factor in the controller's life cycle.

More generally, control becomes a problem of situation recognition and the application of control strategies. This has been met by placing a human in the control loop, using technology to completely but concisely inform the human of current states and trends. The informing technology ranges

from meters and graphical displays to management information systems and decision support systems. The human operator applies

- o primary knowledge such as physical laws,
- o knowledge, generally incomplete, of gross interactions in the system and how it works, and
- o knowledge of what has worked in the past.

Fully automated controllers use only the first kind of knowledge, the "physics" of the system. Accumulation of the other kinds requires simulation and testing, the results of which are not easily codified. System performance can, in principle, be predicted from natural law, but the specification of desired behavior and prediction of future behavior are more directly done by sampling the state space. The accumulation of the different kinds of knowledge, which do interact to a considerable degree, constitutes expertise.

An added layer of complexity is the changing of circumstances, somewhat equivalent to adding more variables to the state space, again a job left to the human component. When resources are necessarily limited in weight, volume, and robustness, as in space operations, the attention of the human controller must necessarily be engaged more often.

Such knowledge and management, while well beyond total automation, is generally routine and tedious, and can represent a considerable and stultifying drain on a mission specialist. Currently, the only viable alternative is to exercise this control from the ground via telemetry. This is unsatisfactory as a long term solution because of the limited bandwidth of the channel and the delay of as much as two seconds for some orbits. Longer range, more unmanned and "undermanned" exercises will be essayed, and a higher form of automation will be required.

Expert systems have been proposed as a possible mechanism for exercising high level decision and control interpretations and strategies. A general overview of expert system performance and technology will be presented, to be followed by a discussion of its adaptation to space station situations.

What Expert Systems Do

The kinds of knowledge gained from simulation, experimentation, and experience go into people's memories or into books and machine memory for later use by people. The knowledge takes many forms, from the principled to the anecdotal, the latter kind often as useful as the former. Expert systems accumulate such knowledge and apply it to new situations, often with remarkable accuracy, occasionally with howling naivete. Although, as shall be described, the technology involved in informing and querying an expert system is quite laborious, expert systems have performed very well in many situations.

The most spectacular results have occurred in medical diagnosis and treatment recommendation, and are being extended to similar problems in other complex systems, primarily computers. Oversimplified, these systems make an accurate assessment of the current state of things, determine the cause of the malfunction (if any), and indicate corrective action. The criterion function is unimpressive - either a system is working correctly (desired state) or it is not. Determination of the current state, however, is impressive. A problem is presented in simple and economic terms, and the expert system determines what other things need to be known and prompts for them. The user is not burdened with entry of useless data, the system works through an inferential chain, prompting for antecedent conditions that it requires in order to proceed.

Because the diagnosis is reached via a chain of entailments, the expert system can explain, albeit primitively, the reasoning it used to arrive at a conclusion. This capability should be contrasted with that available from a purely statistical decision theoretic approach, where the basis of inference is covariance. The entailments that expert systems use, their rules, are generally stated in english words, high-level terms that, for the system, do not carry meaning but are rather symbols, but which enable a somewhat readable trace of the process to be generated. The terms are those used by the experts whose thinking has been translated into rules, and enable the correction of incorrect or poorly stated rules.

Among the most well-known of working expert systems are MYCIN, which diagnoses blood infections, and INTERNIST which diagnoses a variety of internal medicine situations and regularly outperforms the New England Journal of Medicine case

of the week. [4] Another highly successful system, PROSPECTOR, can infer the presence or absence of certain geologic features (like oil or gold) given incomplete information about a site. A more methodologically primitive system, DENDRAL, determines important aspects of chemical structure from mass spectrometry and nuclear magnetic resonance profiles, and can be fairly said to have changed forever the way certain kinds of chemistry are done.

There are at present a few hundred working expert systems at most, but the number is probably doubling every year or so. If certain aspects of an expert system's performance are temporarily ignored, primarily its speed and ease of use, then most of the current and future systems will perform as well or better than a recognized expert most of the time. In one major sense, then, it is already possible to accumulate and use highly specific and expensive knowledge and apply it using a computer.

Guises, Similarities

Expert systems grew out of research in artificial intelligence, a provenance which stigmatizes them to more traditional practitioners. On the basis of both promise and performance the stigma is unwarranted. Expert systems are more accurately and constructively viewed as extensions of both data base systems and software engineering. They serve similar objectives and use many of the same tools, as well as contributing to the general tool-kit. Further, they are neither artificial nor very intelligent except in a prerecorded sense.

Among the concerns shared with data base systems are the storage and retrieval of information, the organization of knowledge as hierachical and recursive structures, and pattern matching (any data base query is a pattern matching problem). Expert systems are able to conveniently represent things that more traditional data bases cannot, because expert systems use a looser, freer data style. Even so, constraints are easier to enforce in expert systems than in data base systems, and can be more rigorously specified. Further, data base systems are passive, in that every retrieval must be asked for explicitly, where expert systems (like information retrieval systems) are active and once started will generate and follow search paths. Thus, the

new systems represent at the least a new modality for interacting with traditional data bases.

Loading an expert system with expertise is a form of programming. The knowledge might be regarded as the data for a table driven program (this will be explicated in the next section), and this organization is much easier to manage than if the system were implemented in a traditional procedure oriented language. While standard programming problems, such as faulty logic and organization, are still nontrivial their detection and diagnosis is more direct. Expert systems appear to offer a more direct approach to the implementation of complex systems than has been heretofore available, and for this reason alone are of great importance to software engineering.

How They Do It

This section is a simple introduction to the basic operation of expert systems. Most are based on a collection of rules, or entailments, and a program that moves from one rule to the next, which is somewhat complicated by the fact that there is generally more than one next rule. A rule is of the form

IF conditions-1 THEN ASSERT conditions-2

To apply a rule, the program determines that conditions-1, which is one or more simple conditions, are all on the list of currently active conditions. If all are, then each of conditions-2 is also added, recalling that some of the new conditions may negate certain entries in the active list, as some rule may forbid their cooccurrence. Thus, the list of active conditions is changed and some new rules become applicable and others become inapplicable. Finding these rules in the rule base is a matching problem that occupies much of the program's time. The inferential chaining process halts when certain asserted conditions are recognized as 'goal' conditions. Typical systems contain on the order of 500-1500 separate rules.

This represents a fairly straightforward graph-traversal problem. The so-called 'weak methods' of artificial intelligence are aimed at reducing the number of unnecessary paths to be traversed. For example, a medical

diagnosis system that is trying to figure out pulmonary symptoms needn't spend much time in its skin disease rules. Reduction of the number of paths is effected by a number of means, including numerical estimates of success and more general techniques known as heuristics. A rule base attempts to capture these methods, essentially by including 'rules about rules', much as it is supposed experts do, in order to avoid an exhaustive traversal of irrelevant rules. Rules may also take short cuts and make huge reasoning leaps, avoiding a precise analytic step-by-step reasoning process. This tends to compact the rule-base and shorten execution time.

The foregoing description is simplified, and generic in the sense that it fully describes no particular system, but it does illustrate some central points.

- First, the executable software, often termed a production system or 'inference engine', is generally a straighforward off-the-shelf black box item. While there are several different systems in use and many improvements will be made, the performance of an expert system does not critically depend upon the particular production system used.

- Second, because performance is entirely dependent upon rules, it is possible to have inconsistent rules and infinite loops if the rule base is poorly constructed. Also, is is possible to make rules which are experientially stupid.

There are two major research areas in expert systems. The first is development of a methodology for developing rule bases, and has a number of components, including interface studies and the structuring of knowledge, which may be subsumed under the term knowledge engineering. The second area concerns systems that 'think', or ruminate, discovering their own inconsistencies and inferring missing rules. Only the first will be discussed, because the higher order cognitive processes that mimic thought are generally conspicuously absent from current expert system work.

Knowledge Engineering - A Generalist's View

There are two main issues to be addressed. The first is knowledge representation, or how experience should be represented. The second is interfacing, or how to translate

what we 'know' into that representation.

Representation in the narrow sense means what sort of data structures are required to adequately represent information. From a user's point of view this is moot, since rule structures are already so widely accepted and used. It is of some interest that an alternative approach is highly reminiscent of traditional data bases, where entities are cast as 'frames', within which are links to other frames in the data base. Frame representation 'reasons' by traveling linkages, not altogether different from following rule chains. In either case, the representation will prove adequate or it won't and will thus be modified.

Accepting some structure, such as rules, is a minor problem compared to what rules to use, and this is the more fundamental challenge in knowledge representation. This challenge involves the difference, if any, between trivial and fundamental knowledge, the differences among objects, concepts, entities, and the like, and similar such questions. Related questions include treatment of generalization and specification, a problem for data base theorists as well.

While the fundamental issue of long range interest is the structure of thought and is considered by some to be ultimately intractable, expert system technology takes a short cut. That is, anything that an expert says is probably worth remembering. Further, the order and manner in which an expert utters the idea is also important. The terms that an expert uses, as noted in an earlier section, are merely symbols in the rule base, place-markers that connect one rule to another. Their significance is whatever the expert assigns to them and, most important, their relationship to other terms as expressed in the rule base.

While a number of theoretical questions are thus bypassed in the interest of empirical adequacy (and the systems are, on this score, quite adequate), the problem of actually committing an expert's knowledge to a rule base is still substantial. In practically all cases, the informant (expert) talks with a go-between, a knowledge engineer, who knows the syntax and domain-independent semantics of the particular rule formalism being used. In the course of translating, the go-between will necessarily revise certain assumptions. For instance, a term which appeared to mean one thing turns out to mean several different things, or a particular idiom turns out to mean one thing to the expert and another to the go-between. Further, an expert's expressive competence will often prove to be lacking. What is uttered

as a chain of reasoning may turn out, upon testing of a rule base, to be quite inadequate for several reasons, implicit assumptions about the domain generally predominating.

Setting up a rule base is just a form of programming, and is liable to all the ills that other kinds of programming display. Specifications that look airtight up front turn out to be loaded with imprecision, trivial variables exert non-trivial effects, and the task of understanding is invariably sobering. It is fairly common that to create an expert system - essentially to set up the data base - is a highly protracted process, measured in months and generally more than twelve of those. Many of the reasons for this are the same ones that make a traditional systems analysis and implementation take similar amounts of time. That is, if the situation is complex (and most systems are) then the implementor must learn it in order to re-create it. This is usually a cyclic process, if prototyping (the use of trial, simplified systems within the environment) is employed. That is, a crude implementation is tested, improved, retested, and so on. Arranging the necessary rematches between the expert and the go-between is a necessarily human and traditional function that no amount of computational power can shorten in the slightest.

It appears that, for two major reasons, the function of knowledge engineer will be distinguished. First, the amount of attention already given to expert systems in the trade press suggests that a marketing niche has already been established and will be difficult to redefine. Second, and more fundamental, the style of programming employed goes well beyond the procedural paradigm embodied in the standard languages (Fortran, Cobol, and all their relations). There are at least three other paradigms recognized in addition to procedure-oriented programming, which are object-oriented, access-oriented, and rule-oriented. Persons who can adequately function in any of these are still in incredibly short supply, and working with rule-bases absolutely requires these extended skills.

If we accept the debasement of the term 'knowledge engineer' to this programming interface function, it appears that these people will be to the late eighties what programmers were to the late sixties. That is, short on methodology, short on supply, and long on mystification. That this function will be overpriced goes without saying. Other parallels predict a bleak short term future. Most good programmers will admit that there are very few 'good' programmers, most of the practitioners are uninspired hacks, and this is not generally a function of vanity as much as

frustration. Unfortunately, predicting excellence is as difficult in this field as any other except maybe baseball, so that those organizations in search of a service are at the mercy of titles and job descriptions. There isn't a foolproof certification process for doctors, programmers, or systems analysts yet, and there won't be for the next generation of similar types either.

An alternate to the gloomy scenario above can be suggested. As discussed in a previous section, expert systems require a new style of programming and are of considerable research interest for that reason alone. Among the interesting possibilities is that a new style of programming may turn out to be more accessible to a wider range of people than current styles. Many non-technical people are becoming quite proficient with software packages for personal computers, in large part because the packages are 'problem oriented' and use terms and data structures specific to the application area. As important, the personal computer environment forces people to do their own thinking, there is no staff available to push problems down to. It is conceivable that new forms of interaction and programming formalism may bring the system design closer to the end user and downplay the go-between function.

The function of go-between and its attendant difficulties is as old as contract programming, and is not radically different in kind or degree for expert system generation. Much current research in applied computer science is focused upon more facile user interfaces, and some effort has been made in the expert system field as well. Systems such as KAS (Knowledge Acquisition System), ROSIE, and HEARSAY, among others, address various overhead tasks such as reformatting (when applicable), consistency checking, and syntactic enforcement. Additionally, they augment the explanation facility which displays the actual reasoning used by a system under development, which, like a program trace, enables the implementor to correct imperfect reasoning. Because expert systems have excited so many different university and commercial groups, and so many different approaches are being tried, the expectation of some highly competent interfaces is not unreasonable.

It should be remembered, however, that even in the good old days when mathematicians and physicists did their own programming (and they are still among the best programmers in terms of productivity) they didn't get it right the first time. Even for the relatively simple systems they addressed mistakes are possible not only in transcription but in basic logic as well. Likewise, the transmission of expertise

should not be expected to be a simple exercise. Expertise, almost by definition, is that which cannot be expressed concisely or portably, and the knowledge acquisition process, whether by machine or human, will remain a significant and sobering task.

Technological Requirements

Expert systems are generally slower than expert people in coming up with an answer, and can tie up respectably sized computers in knots while reaching their conclusions. There are three main aspects of expert systems and artificial intelligence programs in general which cause this. First, a great deal of pattern matching is necessary, for which traditional machine architectures are ill-suited. Second, this sort of programming is inherently multiprocess oriented, and most available operating systems and machine architectures are graceless in this regard. Third, the basic data structures of symbolic programming are not the fixed length operands that standard machines handle well.

Pattern matching can be achieved by cleverer programming or by hardware associative memory, or a creative synthesis of both. The objective is to look at structures which are likely to match, and not waste time on those which will not. This objective is shared with data-base research and there is no prospect of exhausting the possibilities any time soon. Associative (content addressable) memories are routinely used in virtual memory systems, but are necessarily limited in size and function because they are inherently expensive. There is not likely to be an easing of the pattern match problem by a pure hardware approach. Pure software and hybrid schemes will continue to be developed and perform well in limited contexts, but a general purpose and broad- based approach is highly unlikely.

The multiprocess nature of this sort of programming arises because each current hypothesis in a reasoning structure generates more than one new hypothesis. Each new hypothesis requires the same basic program to work on slightly different, although largely shared, data. The number of processes spawned at each new step is generally an exponential function of the number of steps, although in the fortunate cases heuristics and the recognition of blind alleys lead eventually to a manageable number of

conclusions. A responsive multi-processor architecture will improve the performance of expert systems greatly, but since overall utilization statistics will be even poorer than those for pipeline and array machines [5] this will not be a cost-effective solution in the near future. Features do appear. The extended subroutine call-return instructions in the VAX architecture enable the stacking of activation records (local data for a subroutine invocation) in much fewer instruction cycles than the more traditional linkage conventions of, for example, the IBM 370 architecture, but even these advances do not generalize sufficiently to greatly ease the multiprocessing burden. Basically, even if the routine overhead is reduced, there remains the considerable burden of problem specific processing.

Finally, most non-numeric machines have been aimed at the commercial data processing market where computational speed has never been a critical issue. The non-numeric data types required by expert systems are currently simulated clumsily, although there are attempts to incorporate such types directly into high-speed architectures. The various lisp machines aim at more efficient treatment of list structures, and enhance pointer-based operations. As with pattern matching and parallel processing, the development cycle is in a steady but slow phase, and there are unlikely to be any quick fixes.

While the foregoing is not optimistic, there are some leavening factors. Most programming for expert systems, and artificial intelligence in general, is still first-generation prototyping to determine if a method will work at all. As expert systems enter the commercial sector and must compete with one another, the re-engineering of software techniques alone can be expected to bring about performance improvements of almost an order of magnitude. As re-engineering makes critical steps more apparent, relatively modest hardware improvements can capitalize upon that criticality to great effect.

Why They Work

There are three major components in the current and projected success of expert systems. The first, undoubtedly the most important, is that real knowledge is in fact stored in retrievable form. The second is that the terms used to build and query the knowledge base are at a sufficiently high and precise level that discourse with the system is an

order of magnitude more convenient than the usual run of software systems. Finally, expert systems admit imprecision and incompleteness with an ease unavailable in procedure oriented contexts.

The importance of knowledge may be indicated by the following citations: [6]

> "...human experts achieve outstanding performance because they are knowledgable. If computer programs embody and use this knowledge, then, they too should attain high levels of performance. This has proved to be true repeatedly in the short history of expert systems." (p. 4)
>
> "The power of an expert system derives from the knowledge it possesses, not from the particular formalisms and inference schemes it employs." (p.6)

Knowledge is an expensive resource, and while it is renewable maintaining it exacts a severe requirement in study and apprenticeship. Heretofore, existing computer systems have been unequal to the task of saving knowledge.

A second factor in expert system success has to do with the narrow mindedness of representative systems. They generally deal with a highly restrictive domain of experience, and deal with it in the expert's terms, or jargon. While the systems thus lack "common sense", they gain a great advantage, in that jargon tends to be very precise and unambiguous. It is, after all, expert shorthand. This cuts through a significant barrier, the difficulty of processing natural language with its inherent ambiguities.

Finally, expert systems embody within one formalism several different modes of thought and expression, from the highly analytical to the circumstantial. If a sloppy inference is truly better than no inference at all, introducing it to the rule base is no more work than for an ironclad truth. Thus, in addition to 'hard' knowledge, these systems can also assimilate intuitive hunches and short cuts which bypass a considerable amount of laborious analysis. It is this sort of information that provides the path-pruning heuristics which make expert systems work at all, albeit slowly.

Conclusions and Recommendations

The long term benefits of knowledge engineering are likely to be of more benefit to ground-based operations such as data management and planning. Long term acceptance of the technology requires some up-front success in order to win personnel commitment. While system control is an under-investigated area of application, although of great interest for reactor and refinery operations, the systems considered in the current effort appear to be soluble. They suffer, however, from a built-in bias based on time-criticality and severe resource limitations. It is highly unlikely that computer hardware capable of running an expert system will fly any time soon, and even ground-based systems are limited by telemetry constraints, so that 'important' actions are effected by other means. It would be unfortunate if the technology were to be judged too hastily on the basis of an overly hostile environment.

The software environment appears to be highly traditional and oriented towards 'classical' engineering computation. This complicates the data management and data base requirements, and blunts the introduction of newer software methodologies. Expert systems are only one area of software endeavor that are much easier to implement in a paradigm other than procedure oriented programming. It is important to note that 'easier' is quite often the difference between doable and undoable, not merely a question of convenience. The feasibility of a new methodology must include prior attitudes toward the methodology, since the best ideas in the world are worthless if no one understands them. Expert systems may be a foot in the door, but they bring their own overhead in the form of recursive languages and their inability to look and behave like traditional packages. The possible prejudice against software engineering progress should be, where possible, softened, because long term productivity gains require easier programming, not faster machines.

Appendix I - References

Cited References

[1] Boeing Aerospace Co., Final Report D180-27935-x, "Space Station Systems Technology Study", Contract NAS8-34893, February 1984

[2] Martin-Marietta Corporation, Final Report MCR-83-645, "Power System Automation Study", Contract NAS8-34938, November, 1983

[3] Martin-Marietta Corporation, Progress Reports for NAS8-34938 (extension) through June 1984

[4] D. W. Wirtschafter, personal communication

[5] Jean-Loup Baer,"Computer Systems Architecture", Chapter 10, Computer Science Press, Rockville, MD, 1980

[6] Frederick Hayes-Roth, Donald A. Waterman, and Douglas B. Lenat (eds.), Building Expert Systems , Addison-Wesley, Reading MA, 1983

Recommended References

The first book noted here is as complete a source of current information and literature citations as can be found between two covers. Like all writing on expert systems, this paper included, it is about twice as long as one would like. The second is a more local discussion of one particular (Rutgers) methodology.

The next two books (3 and 4) are of more distant import, each is a standard text on artificial intelligence. Winston's is felt to be 'experimentally oriented' and is designed to be used in connection with his Lisp book (5). Nilsson is theoretically stronger, and is the most often cited AI reference.

The periodical AI Magazine is essential to staying abreast of current activity, and I have been unable to find it in the library (RSIC). The Artificial Intelligence Report is of companion interest, and not unduly expensive as such

services go.

1. Frederick Hayes-Roth, Donald A. Waterman, and Douglas B. Lenat (eds.), Building Expert Systems , Addison-Wesley, Reading MA, 1983

2. Sholom M. Weiss and Casimir A. Kulikowski, A Practical Guide to Designing Expert Systems , Rowman and Allenheld, Totowa NJ, 1984

3. N. Nilsson, Principles of Artificial Intelligence , Tioga, Palo Alto CA, 1980

4. Patrick Henry Winston, Artificial Intelligence , Addison-Wesley, Reading MA, 1984

5. P. H. Winston and B. K. P. Horn, LISP , Addison-Wesley, Reading MA, 1981

6. "The AI Magazine"

7. Artificial Intelligence Report , Artificial Intelligence Publications, 95 First Street, Los Altos CA, 94022 ($150.00 / ann.)

APPENDIX II - Commercial Sources

The following list, almost entirely drawn from the Artificial Intelligence Report of August 1983 (see Recommended References), is non-selective and, given its age, quite incomplete. Requests for information are being made of each locatable company.

Software, Knowledge Engineering

Applied Expert Systems, Inc., Cambridge MA

Artificial Intelligence, Inc.

The Carnegie Group, Inc., 5867 Douglas St., Pittsburgh PA 15217

Cognitive Systems, Inc., New Haven CT

Computer Thought, Inc., Richardson TX

Gantech, Inc., Palo Alto CA

IntelliGenetics, Palo Alto CA

Intelligent Terminals, Ltd., Edinburgh, Scotland

ISIS, Ltd., London, England

Kestrel Institute, 1801 Page Mill Road, Palo Alto CA

SPL, Ltd., Abingdon England

SRI International, 333 Ravenswood Ave., Menlo Park CA 94025

Smart Systems Technology, 6870 Elm Street, McLean VA, 22101 (703-448-8562)

Symantec, Sunnyvale CA

Syntelligence, 800 Oak Grove Ave.- Ste. 201, Menlo Park CA 94025

Teknowledge, Palo Alto CA

Tektronix, Inc., Beaverton OR

Hardware

Lisp Machine Inc., Culver City CA

Machine Intelligence Corporation, Sunnyvale CA

Three Rivers Computer Corp., Pittsburgh PA

Symbolics, Inc.,Chatsworth CA

Xerox Corporation, Pasadena CA

1984

NASA/ASEE SUMMER FACULTY RESEARCH FELLOWSHIP PROGRAM

MARSHALL SPACE FLIGHT CENTER

THE UNIVERSITY OF ALABAMA

EVALUATION OF OMV RANGING AND DOCKING SYSTEMS

Prepared By:	Malcolm W. McDonald, Ph.D.
Academic Rank:	Associate Professor
University/Department	Berry College Department of Physics
NASA/MSFC: (Laboratory) (Division) (Branch)	 Information & Electronic Systems Computers and Communication Communications Systems
MSFC Counterpart:	E. H. Gleason
Date:	August 10, 1984
Contract Number:	NGT-01-002-099 The University of Alabama

ACKNOWLEDGEMENTS

I am very grateful to Marshall Space Flight Center, NASA, ASEE, and the University of Alabama for the opportunities provided by the Summer Faculty Research Fellowship Program. The program provides a stimulating and challenging diversion from the normal classroom duties of the academic year. It was directed in a most effective manner by the capable leadership of Dr. L. M. Freeman, Dr. James Dozier, and Mr. Leroy Osborn.

Many MSFC personnel unselfishly relinquished hours of time to support this program in discussions and seminar presentations. Their support and contributions are gratefully acknowledged.

My greatest debt of gratitude is owed to my NASA counterpart, Mr. Ed Gleason, and the NASA personnel in the Communications Systems Branch. They have all been fully supportive of the work I undertook on this project. I thank them all for their shared ideas and challenges and their universal warmness which provided for me an especially pleasurable summer research experience.

Finally, I wish to thank Ms. Margaretta Nelson for spending time decoding my handwriting and formatting the text of this report in the word processor in a splendid manner.

EVALUATION OF OMV RANGING AND DOCKING SYSTEMS

By

Malcolm W. McDonald
Associate Professor of Physics
Berry College
Mount Berry Georgia

ABSTRACT

The Orbital Maneuvering Vehicle (OMV) will serve as a shuttle-based or permanent space station-based vehicle designed to rendezvous and soft dock with various other free-flying space vehicles for purposes of inspection, support, and retrieval. This study is concerned primarily with the eventual need for the OMV to rendezvous and dock softly with the Edwin P. Hubble Space Telescope (ST).

Utilizing the available capabilities of the large microwave anechoic chamber facility at Marshall Space Flight Center for simulating docking target vehicle motions in a free-space environment, a program is being devised for benchmark testing of rendezvous and docking sensor systems proposed for use on the OMV. This report develops a testing regimen suitable for evaluating the accuracy and tracking agility in sensing range, range rate, and angle information at close ranges ($0 < R < 30m$).

LIST OF FIGURES

LIST OF TABLES

NOMENCLATURE

Symbol	Interpretation
a	Positioner Azimuth Angle
$\dot{a}$	Positioner Azimuth Angle Rate
b	Positioner Elevation (Tilt) Angle
$\dot{b}$	Positioner Elevation (Tilt) Angle Rate
C	Effective Top of Positioner Tower
$\vec{D}$	Vector From Origin to Sensor
H	Effective Positioner Tower Height
L	Target Reference Projection Distance
MAC	Microwave Anechoic Chamber
MSFC	Marshall Space Flight Center
O	Origin of MAC Coordinate System
OMV	Orbital Maneuvering Vehicle
R	Range (from Sensor to Target)
$\dot{R}$	Range Rate
RF	Radio Frequency
R/D	Rendezvous and Docking
SA	Solar Array (on ST)
ST	Edwin P. Hubble Space Telescope
T	Target Reference Point
$\vec{T}$	Vector from Origin to Point T
TMS	Teleoperator Maneuvering System
(x, y, z,)	Coordinates of Target Reference T
(X_o, Y_o, Z_o)	Coordinates of Sensor

INTRODUCTION

The Orbital Maneuvering Vehicle (OMV), originally referred to as the Teleoperator Maneuvering System (TMS), will be carried into space by the shuttle and used initially as a fetch vehicle to retrieve other free-flying target vehicles from orbit for return to the shuttle to permit inspection, service, repair, or replenishment of consumables. It would also be used to execute orbital transfer maneuvers to move objects away from the vicinity of the shuttle to other orbits. In the future the OMV will perform these tasks with the Orbiting space station serving as its home base.

One of the early assignments to be handled by the OMV will be to rendezvous and dock with the Edwin P. Hubble Space Telescope (ST) when it becomes necessary to retrieve it for service, repair, or refurbishment. This, and other rendezvous and docking (R/D) assignments, will require that the OMV be fitted with an accurate ranging sensor system to enable, during the R/D operation, a precise measurement of target range, range rate, and angular position information. These data, in conjunction with the video information available from a television camera mounted on the OMV, will enable a remotely stationed human operator to guide the OMV to a necessarily gentle docking encounter with the ST.

The thrust of the study reported in this paper is to determine and make recommendations on how a program of testing of radar ranging sensor systems proposed for use on OMV can best be effected, utilizing the available capabilities of the large microwave anechoic chamber facility at Marshall Space Flight Center (MSFC). A target mock-up, such as the aft section of the ST, mounted atop a movable tower driven by an azimuth-over-elevation positioner in the anechoic chamber can simulate the relative motions between the OMV range sensor and the ST during the docking maneuvers in a free-space environment.

This work follows earlier studies reported from this laboratory on the development and testing of a 35 gigahertz FMCW radar system for possible use on the OMV (See References 1 and 2). That ground work developed an expertise on understanding radar ranging capabilities which led to the present study.

OBJECTIVES

The objectives observed in guiding this study were the following:

1. To conduct a literature search for any available information regarding any similar testing which may have been performed and to gather ideas from any previous work,

2. To plan for making most effective use of the capabilities already available in the large microwave anechoic chamber at MSFC as a testing facility,

3. To devise a suitable program of testing the abilities of contractor-proposed candidate OMV radar ranging systems in providing the range, range rate, and angular location data needed to support the OMV-ST docking maneuver, and

4. To determine if the ranging data measurement accuracies of the candidate systems under test meet the rather stringent requirements for soft docking of the OMV with ST.

REPORT

This report is presented in four sections. The first section presents pertinent facts about the ST and the OMV with special emphasis on the docking requirements and constraints for the two vehicles. The second section includes a description of some of the pertinent features of the microwave anechoic chamber (MAC) facility. The third section is a description of a radar ranging system testing routine designed to take advantage of the properties of the MAC facility. The final section will consist of concluding remarks and recommendations.

I. OMV/ST Characteristics and Docking Requirements.

An October, 1983 Lockheed study (See Ref. 3) sets forth conditions and requirements which govern encounters and interactions between the OMV and the ST. The ST will be about 14.3 meters in length, basically cylindrical in shape with solar array and antenna appendages projecting from the main body, and having a diameter at the aft end of about 4.3 meters. Its mass will be approximately 11,600 kilograms. Consideration has been given to three optional positions of the ST at which the OMV could dock. The favored plan is for the OMV to latch on to three pins affixed to the aft shroud of the ST. This configuration prevents interference of the OMV with any deployed appendages of the ST (solar array panels or high-gain antennas) during engagements.

The OMV will be basically a disc-shaped configuration with a diameter similar to that of the aft shroud of the ST, where docking will occur. It will have a mass of approximately 3500 kilograms. The OMV will be equipped with a television camera as well as range data sensing equipment to provide necessary information to a man in the docking loop to allow for soft docking of the OMV to the ST.

The soft, or gentle, docking requirements are imposed due to designed maximum acceleration loads tolerable by the ST solar array appendages in the deployed state. There is a requirement for the OMV to be able to dock with the ST when its solar arrays are deployed. Selected data for the OMV-ST docking encounter are presented in Table I.

TABLE I. SELECTED OMV-ST DOCKING DATA

Max. ST Mass	-	11,600 Kg
OMV Mass (Approximate)	-	3,400 Kg
Max. ST Accel. (SA Deployed)	-	0.005 g (0.049 m/s^2)
Max. Impact Force	-	590 lb. (2630 N)
Max. Closing Speed	-	0.11 f/s (0.034 m/s)

In an R/D engagement between two space vehicles there seems to be a generally accepted definition that at a range of about 100 feet, or 30 meters, the rendezvous phase gives way to the docking phase. Thus, for a radar (or any other type) range sensing system to be useful in supporting the OMV-ST docking maneuver, it must have the capacity to measure target range and angle values with a high accuracy throughout zero to thirty meter OMV-ST separation distances. The system must further be capable of measuring range rate (or OMV-ST relative speed) with good reliability down in the domain of zero to three centimeters per second to insure that the OMV and ST do not suffer an impact capable of delivering an intolerable acceleration to the deployed ST solar arrays.

This section of the report has outlined the performance characteristics necessary in a ranging sensor system suitable for supporting OMV docking maneuvers with the ST. The next section will examine the capabilities of the MAC facility at MSFC for providing the simulated free-space environment and the sensor-target range motions sufficient for testing of candidate sensor systems proposed for use on the OMV.

II. Description of Microwave Anechoic Chamber (MAC) Facility.

The anechoic chamber is 120 ft (36m) long and measures 30 ft (9.1m) in width and height at the large-dimension end. Those width and height dimensions prevail over approximately forty feet of "flat floor" surface. Beyond the forty foot point the chamber symmetricaly tapers (includes floor, both walls, and ceiling) to the small width and height dimensions at the narrow end of the chamber. In the approximate middle of the flat floor area is a movable sixteen feet (4.9m) tall target or antenna tower operated by a heavy duty variable-speed motor-driven positioner (azimuth-over-elevation) mounted in the floor.

A sketch to illustrate the positioner-tower geometry is shown in Figure 1. The entire assembly can be tilted backward or forward through an angle b ($-45^{o} < b < +92^{o}$). The base and tower can be driven about the azimuth axis through an angle, a. A target can be mounted on a shaft extending through the top of the tower along the roll axis. In fact, the target can be rotated about the roll axis by a driving motor in the base, although that option is not used in the proposed testing regimen. A manual crank allows translation of the base and tower along the translation axis, which is the longitudinal axis of the base. This translation allows adjustment of the distance from the target reference (T) to the intersection of the azimuth axis with the roll axis (point C).

The effective height (H) of the tower is indicated in the figure as the distance from the intersection of the azimuth axis with the elevation axis (point O) up to point C. A transverse distance (L) is to represent the possible projection distance of the target reference (T) in front of point C.

This geometry allows a target reference point (T) to be moved about in the MAC at rates determined by the two motor-driven angular rates, $\dot{b}$ and $\dot{a}$. The target reference point (T) moves about the origin point (O) at the end of a radius vector equal in length to the hypotenuse of H and L. This motion permits range changes (measured to a static sensor positioned in the MAC) of several meters and range rates from -3 cm/sec to +3 cm/sec. The available motion also permits significant changes (dependent upon sensor placement) in angular position of the target. This scale of motion is perfectly in line with the scale of motion anticipated in am OMV-ST soft-docking encounter.

The use of the MAC facility for OMV ranging sensor testing is made even more attractive by the extreme isolation of its interior from external RF signals. This degree of isolation is desirable to simulate the empty free-space environment for OMV-ST docking. The interior of the MAC will be isolated from RF signals to an extent greater that 100 dB throughout a frequency range from 200 MHz to 100 GHz. The MAC facility will soon be supported in data handling and analysis by a Hewlett-Packard 9836C computer system.

A rigid attachment of the ST aft shroud mock-up target to a shaft extending through the top of the positioner tower would have the undesirable effect of causing large attitudinal changes in the target as seen from the ranging sensor. A reasonable maintenance of target aspect, as seen by the sensor, will be accomplished through the use of a two-axis universal yoke assembly to attach the rear of the target to the shaft at the top of the tower.

This section has examined briefly the suitable and desirable attributes of the MAC facility for serving as a testing facility for proposed candidate range sensing systems for the OMV. It has

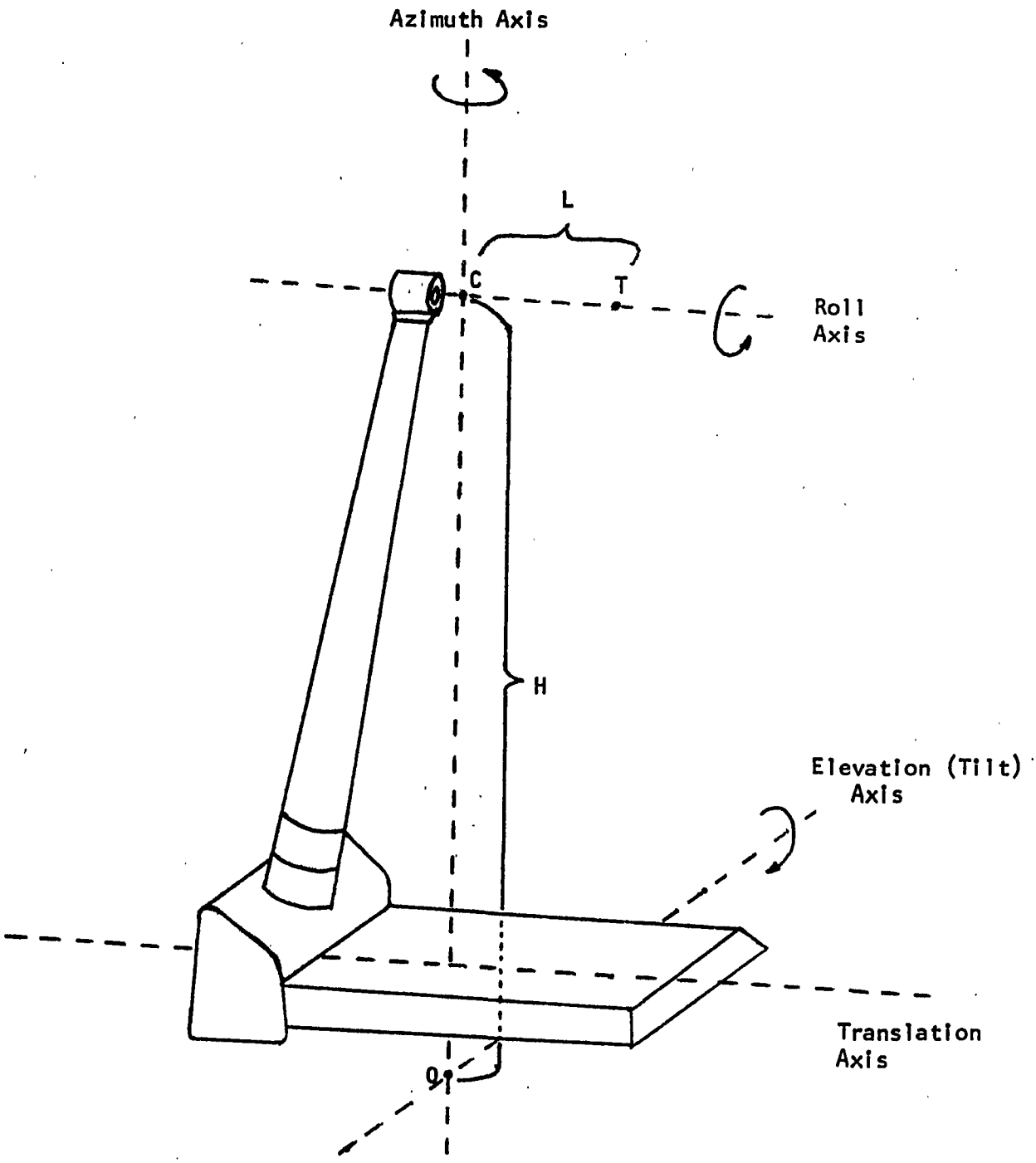

Figure 1. Target Positioner Geometry. The origin of the coordinate system used is at Point O. The effective top of the tower is Point C. A reference point on the target is at T. The transverse distance from the Azimuth Axis to Point T is distance L. The effective height of the tower is H.

been indicated that the sensor-target relative motions needed to simulate OMV-ST docking maneuvers are within the capability of the present facility. The computer needed to support the testing program in the MAC facility will soon be in place. The next section will explore a specific testing routine which will serve as an adequate test of the tracking and ranging capabilities of proposed OMV ranging and docking sensor systems.

III. Description of Radar Sensor Testing Routine.

In order to develop a range testing algorithm it was necessary first to define a reference coordinate system suitable to the interior of the MAC. A right-hand Cartesian coordinate system is defined as having its origin at point O (see preceding section). The X-axis runs horizontally and parallel to the long axis of the anechoic chamber. The Y-axis runs horizontally. The Z-axis is a vertical axis.

Figure 2 illustrates the coordinate system and useful vectors for describing the location of the target reference point (T) and the range sensor (point D). Vector $\vec{H}$ locates point C relative to the origin (point O). Vector $\vec{L}$ locates target reference point T relative to C. Therefore, a vector $\vec{T}$ for the position of the target relative to the origin can be defined by $\vec{T} = \vec{H} + \vec{L}$.

The vector $\vec{T}$ can be defined by:

$$\vec{T} = \hat{i}\,(H \sin b + L \cos b \cdot \cos a) + \hat{j}(L \sin a) + \hat{k}(H \cos b - L \sin b \cdot \cos a).$$

It can be shown easily that the vector T meets the condition for its length,

$$T^2 = H^2 + L^2.$$

Now, if the sensor is fixed in position at coordinates (X_o, Y_o, Z_o), its position is given by vector D where

$$\vec{D} = \hat{i}X_o + \hat{j}Y_o + \hat{k}Z_o.$$

Then we define the sensor-to-target range by a vector $\vec{R}$ where

$$\vec{R} = \vec{T} - \vec{D}.$$

Thus,

$$\vec{R} = \hat{i}(H \sin b + L \cos b \cdot \cos a - X_o) + \hat{j}(L \sin a - Y_o) + \hat{k}(H \cos b - L \sin b \cdot \cos a - Z_o).$$

This leads to an expression for the range R in terms of the various coordinates and parameters written as

$$R^2 = (H \sin b + L \cos b \cdot \cos a - X_o)^2 + (L \sin a - Y_o)^2 + (H \cos b - L \sin b \cdot \cos a - Z_o)^2.$$

This becomes

$$R^2 = K^2 - 2H(X_o \sin b + Z_o \cos b) - 2L(X_o \cos b \cdot \cos a + Y_o \sin a - Z_o \sin b \cdot \cos a)$$

Where the constant K^2 is a substitution defined by

$$K^2 = H^2 + L^2 + X_o^2 + Y_o^2 + Z_o^2.$$

To derive an expression for range rate one need merely take the derivative with respect to time of Equation 1. This operation yields

$$\dot{R} = (H/R)\dot{b}(Z_o \sin b - X_o \cos b) + (L/R)(X_o(\dot{b} \sin b \cdot \cos a + \dot{a} \cos b \cdot \sin a) - Y_o \dot{a} \cos a + Z_o (\dot{b} \cos b \cdot \cos a - \dot{a} \sin b \cdot \sin a)).$$

Equation 2 gives range rate in terms of elevation angle rate $\dot{b}$ and azimuth angle rate $\dot{a}$. These target positioner drive rates as well as the angles themselves can be set and monitored in the MAC facility operation. Thus the range and range rate can be computed from the two derived equations with the input of the constants, the angles b and a and their drive rates $\dot{b}$ and $\dot{a}$.

Now, to specify the direction from sensor to target let us define two angles) θ and ϕ with

θ = angle in XY plane measured from -X direction (the -X direction is the forward direction of the OMV sensor, for purposes of this test). Positive values of this angle indicate the target located to the right of the forward direction, as viewed from the sensor, while negative values indicate the target located to the left of the forward direction. This is the angle normally referred to as azimuth.

and ϕ = angle measured in vertical plane (positive values indicate target higher in elevation than sensor). This angle is normally referred to as altitude, or elevation.

These two angles are defined by

$$\tan \theta = (y - Y_o)/(X_o - x)$$

$$\text{and } \tan \phi = (z - Z_o)/(X_o - x), \text{ where } (x,y,z)$$

represents the coordinates of the target. Upon substituting for those coordinates the two previous equations become

$$\tan \theta = (L \sin a - Y_o)/(X_o - H \sin b - L \cos b \cdot \cos a)$$

$$\tan \phi = (H \cos b - L \sin b \cdot \cos a - Z_o)/(X_o - H \sin b - L \cos b \cdot \cos a).$$

If angle rates were desired, they could be obtained easily by taking the time derivatives of the latter two equations.

IV. Conclusions and Recommendations.

The four numbered equations in the preceding section yield outputs for range, range rate, and two position angles for the sensor-target system. These outputs require the input of certain available constants and the target positioner rates and angles which can be set and monitored. A test routine would involve placing the candidate sensor at a fixed location (X_o, Y_o, Z_o) in the MAC, starting the target positioner at known angular positions b_o and a_o, and sweeping either or both angular position drives at set rates $\dot{b}$ and $\dot{a}$. Then the readings yielded by the candidate system being tested could be compared for agreement with the values computed from the equations. The results of these comparisons will be a measure of the accuracy and reliability of the tested sensor system.

A first step in the testing procedure would have the sensor placed at about 30 meters range from the target, on a fixed platform in the tapered end of the MAC. A test primarily of range and range rate ability would be performed with a single driven sweep of the target in a rotation about the elevation axis from b = 0 degrees to b = 60 degrees. This will produce more than a ten percent change in range and closing range rates up to 3 cm/sec.

A second test would place the sensor down in the "flat floor" area of the MAC within a few meters of the target. Then a single sweep can produce several meters change in range, range rates from -3 cm/sec to +3 cm/sec, and significant changes in target azimuth and elevation, thus providing a test of both ranging and tracking capability of the sensor.

The equations 1-4 were programmed into a computer so simulated runs could be made to verify the range variable capabilites inherent in the MAC target positioning mechanism. Figure 2 illustrates the results of a run to explore range and range rate variable capacities in the "flat floor" region. Actual measurements on the target positioning tower assembly or review of manufacturer's specifications provided necessary constants used in the four equations. The constants are summarized in Table II.

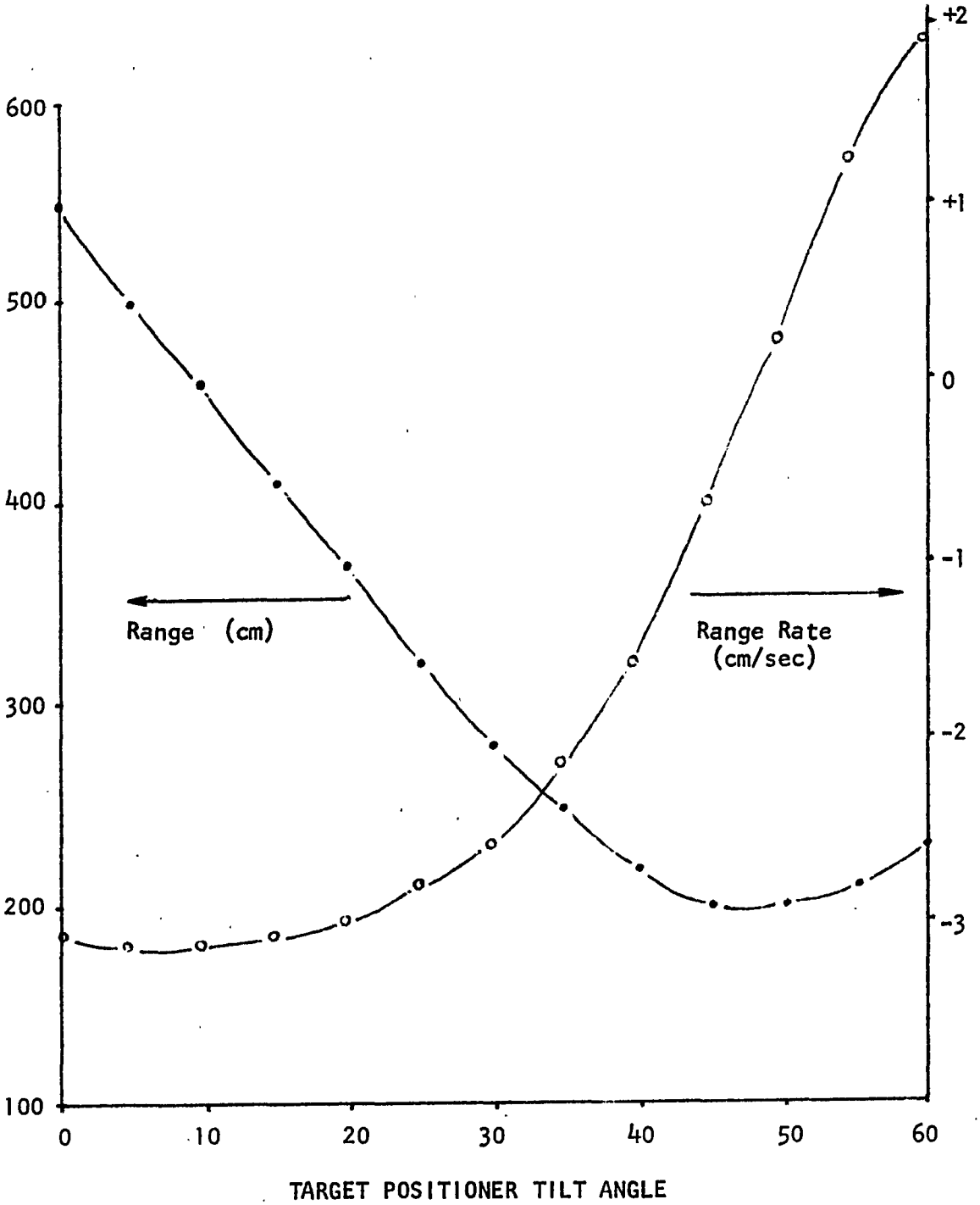

Figure 2. Range/Range Rate Capacities. This illustrates the sensor-target ranges and range rates producible in a single tilt drive from $b=0^{o}$ to $b=60^{o}$ at the maximum tilt rate. The tower azimuth is set at $a=45^{o}$, and the sensor is positioned at (X_o,Y_o,Z_o) = (600,0,400 cm).

Table II. Constants of Target Positioner

Characteristic	Value
H	531 cm.
L	Settable (100cm assumed)
$\dot{b}$ (Max)	20 degrees/min.
$\dot{a}$ (Max)	180 degrees/min.
Position Accuracy (b)	0.05 degree
Position Accuracy (a)	0.03 degree

In conclusion, it is recommended that OMV ranging sensor testing can be adequately performed with the available properties of the MAC facility at MSFC. Other simulation facilities at MSFC are more capable of simulating OMV-target vehicle docking motions. However, they are not performing in a free-space simulation environment, thereby allowing multiple path sensor signal returns from walls, ceiling, floor, etc.

It is recognized that a role reversal testing approach could be applied in the MAC facility. That is to say, the target (ST aft shroud mock-up) could be statically positioned in the MAC while the sensor system is moved about at the end of the positioner arm in the vicinity of the target. This approach was not pursued, but it might be explored as an alternative approach. This would involve derivation of a new set of equations, similar to Equations 1-4.

REFERENCES

1. McDonald, M. W., "Study of Proposals for the Correction of Errors in a Radar Ranging Device Designed to Facilitate Docking of the Teleoperator Maneuvering System", in NASA Contractor Report - 1982 - NASA/ASEE Summer Faculty Fellowship Program, edited by B. F. Barfield, et al, NASA CR-162051, August 1982.

2. McDonald, M. W., "A FMCW Radar Ranging Device for the Teleoperator Maneuvering System", in NASA Contractor Report-1983-NASA/ASEE Summer Faculty Fellowship Program, edited by G. Karr, et al, NASA CR-162051, August 1983.

3. ST-TMS REQUIREMENTS, Lockheed Missiles and Space Company, Inc., October 31, 1983. (This document is a study in response to MSFC Technical Directive TA31/233-1, dated August 1, 1983.)

D21

1984 NASA/ASEE
SUMMER FACULTY FELLOWSHIP PROGRAM

MARSHALL SPACE FLIGHT CENTER
THE UNIVERSITY OF ALABAMA

THE MODELLING OF LATITUDINAL GRADIENTS IN THE SOLAR WIND IN THE OUTER SOLAR SYSTEM

Prepared By:	Steven Nerney
University:	San Juan College Farmington, NM
NASA/MSFC Division: Branch:	 Space Science Laboratory Solar Science Branch
MSFC Counterpart:	Steve Suess
Date:	August 1, 1984
Contract No.:	NASA NGT-01-002-099 The University of Alabama

THE MODELLING OF LATITUDINAL GRADIENTS IN THE SOLAR WIND IN THE OUTER SOLAR SYSTEM

BY

Steven Nerney
Space Science Laboratory
NASA Marshall Space Flight Center
Huntsville, Alabama 35812

ABSTRACT

A steady, axisymmetric, quasi-radial, global model is developed for thermally driven stellar winds with embedded magnetic fields. The asymptotic, linear results are presented for O(1) latitudinal variations in the radial magnetic field, mass-loss rate, and radial velocity of the wind. The MHD equations are solved for the latitudinal dependence of the rotational velocity and magnetic field. They are driven by the meridional flows that develop naturally from internal magnetic stresses. Most flows open flux tubes in the star's equatorial plane, redistributing mass and magnetic flux as a function of stellar latitude. The plasma spins up to conserve angular momentum in fields and plasma.

I. Introduction

The nature of the solar wind in the outer solar system has been the subject of much theoretical work as well as observation and data analysis. Steady, axisymmetric, global modelling predicts an equatorial divergence of the wind for distances large compared with the Alfvén radius, Winge and Coleman, 1974, Suess and Nerney, 1973, and Nerney and Suess, 1975, hereafter Paper I. Fully non-linear, 3-D numerical models corroborated the linear mathematical modelling in Paper I (Pizzo, 1982), and comet tail data showed that a negative meridional velocity (an equatorial divergence), constant with heliocentric radius and varying as $\sin 2\theta$ (colatitude) was present in the analysis of aberration angles, Brandt, Harrington, and Roosen, 1973. While $\sin 2\theta$ was the only functional form which strongly reduced the residuals, the average value of v_θ still had a large spread about the mean: $v_\theta = (-2.6 \pm 1.2) \sin 2\theta$ [km/s].

Fortunately, a much longer data base is now available which allows workers to separate temporal from spatial effects. This is due to the large number of spacecraft positioned at varying distances in the solar system together with a time period that allows the subtraction of some solar cycle effects. Also, systematic studies have shown that one of the best parameters to study is the azimuthal component of the interplanetary magnetic field, $H\phi$. This is because it dominates the magnetic field structure at large distances and is least affected by fluctuations (Thomas and Smith, 1980; Burlaga et al., 1982). In particular, Slavin et al., 1984, find that the spatial gradient of $H\phi$ is proportional to $r^{-1.12 \pm .06}$ for 1 AU < r < 12 AU. This was derived from observations of Pioneers 10 and 11, and ISEE-3, and supports our earlier modelling efforts, although stream dynamics could also explain these results. Additionally, Thomas et al., 1983, further examined this spatial gradient and found that the field topology is consistent with the predicted meridional flow.

The initial results of Paper I were extended to study these latter effects and to include the corrections to the simple picture of the Archemedean spiral Interplanetary magnetic field; namely, the opening of the magnetic flux tubes in the equatorial plane in response to the equatorial divergence of the flow field, Nerney and Suess, 1975b, hereafter Paper II.

A further modification of these global solar wind models led to the inclusion of large amplitude latitudinal gradients in the radial magnetic field, mass-loss rate, and radial velocity, Nerney and Suess, 1975c, herafter Paper III. This clearly showed that even equatorial convergence can develop at large radii for a quite reasonable set of imposed latitudinally dependent boundary conditions. Moreover, Pizzo, 1982, has shown that the linear results of both Papers II and III are substantially correct for the non-linear flows that he successfully modelled. Pizzo found, as we did, that the opening of the flux tubes transports mass and magnetic flux to higher latitudes while the radial and azimuthal velocities are slightly enhanced in the equatorial plane. The linear model overestimated these effects as we ignored the dynamic relaxation of the driving forces. However, we did show that the linear effects in mass and magnetic flux redistribution grow logarithmically with heliocentric radius.

It is our purpose in this paper to complete the linear model through the inclusion of 0(1) latitudinal variations which not only drive more complicated meridional flows, but also affect the azimuthal magnetic field and velocity in new and interesting ways.

The work of Pizzo, 1982, clearly shows that the most vigorous non-radial flows and transport effects are due to stream interactions, and not these relatively smooth, axisymmetric, internally generated flows. However, these results are analytic and show explicitly how to treat the mathematics of these complicated interactions between outflow, rotation, and embedded magnetic fields. As such, they are a useful tutorial for studying internally generated flows and also allow the development of an intuitive geometrical picture of these interactive effects. We also hope that these studies will prepare the way for a more complete understanding of the fully nonlinear case. An analytic model of this latter type would allow the study of outflows from fast rotating stars, Nerney, 1980.

II. Mathematical Analysis

In what follows we refer the reader to previous papers where we discuss in detail the iterative solution through the two singularities, the multiple expansion, nonseparability of the partial differential equations, and other interesting aspects that do not affect these asymptotic results.

Following Yeh's (1970) nondimensionalization, velocity, mass density, pressure, magnetic-field intensity, and length are scaled by v_c, ρ_c, $\rho_c v_c^2$, H_c, and GM/v_c^2, respectively. The subscripts indicate evaluation at the polar sonic critical point. G is the gravitational constant, $M_\odot$ is the mass of the Sun, and $\vec{\omega} = \omega\hat{k}$ is the Sun's angular velocity. The following non-dimensional numbers appear:

$$N = GM_\odot \omega / v_c^3 , \qquad C = \frac{H_c^2}{4\pi \rho_c v_c^2} .$$

The polar critical radius is at $r_c = GM_\odot/2v_c^2$ (Yeh, 1970), and $\hat{k}$ is a unit vector along the rotation axis.

The magnetohydrodynamic (MHD) equations (in emu) with the magnetic permeability set equal to unity, in non-dimensional form, and in the corotating frame of reference, are:

$$\nabla \cdot (\rho \vec{v}) = 0 , \tag{1}$$

$$\rho\, \vec{v}\cdot\nabla\vec{v} + 2N\rho\hat{k}\times\vec{v} - \tfrac{1}{2} N^2 \rho \nabla |\hat{k}\times\vec{r}|^2 = -\nabla P + C(\nabla \times \vec{H})\times\vec{H} - \rho\hat{r}/r^2 , \tag{2}$$

$$\nabla \cdot \vec{H} = 0 , \tag{3}$$

$$\nabla \times (\vec{v} \times \vec{H}) = 0 , \tag{4}$$

$$\vec{v} \cdot \nabla\left(\frac{P}{\rho^\gamma}\right) = 0 , \quad 1 \leq \gamma \leq \frac{5}{3} , \tag{5}$$

where $\hat{r}$ is a unit vector in the radial direction and differential rotation is not included.

The previous expansion of the nonlinear MHD equations was in powers of N, but this was extended to include a multiple expansion by defining

$$\varepsilon \equiv \left\{\frac{1}{\rho_{00} r} \frac{\partial}{\partial \theta} \left(P_{00} + \frac{C}{2} H^2_{r',00}\right)\right\}_{r_c \theta_o} \tag{6}$$

where θ_o is the colatitude at which the gradient is a maximum and the subscripts are defined below. Considering ε as a second small parameter in the problem, a double expansion is made of the form

$$A = \sum_{m=0}^{\infty} \sum_{n=0}^{\infty} N^{2m} \varepsilon^n A_{mn} ,$$

$$v_\phi = N \sum_{m=0}^{\infty} \sum_{n=0}^{\infty} N^{2m} \varepsilon^n v_{\phi,mn} ,$$

$$H_\phi = N \sum_{m=0}^{\infty} \sum_{n=0}^{\infty} N^{2m} \varepsilon^n H_{\phi,mn} ,$$

where A is any of the variables besides v_ϕ or H_ϕ.

The basic equations which represent the flow to 0(1) have m=n=0, and reduce to the following form:

$$\rho_{00} v_{r,00} r^2 = M(\theta) , \tag{7}$$

$$\tfrac{1}{2} v^2_{r,00} + \frac{\gamma}{\gamma-1} \frac{P_{00}}{\rho_{00}} - \frac{1}{r} = E(\theta) , \tag{8}$$

$$H_{r,00} = \eta(\theta)/r^2 \ , \tag{9}$$

$$P_{00} = \frac{1}{\gamma} \rho^{\gamma}_{00} \ , \tag{10}$$

The O(N) equations reduced to equations (11) and (12) which are the Weber and Davis (1967) solution extended to three dimensions through the inclusion of $\sin\theta$ and written in the corotating frame. This is:

$$v_{\phi,00} = \frac{M_A^2}{r} \frac{(r^2 - r_A^2)}{1 - M_A^2} \sin\theta \ , \tag{11}$$

$$H_{\phi,00} = \frac{H_{r,00}}{v_{r,00}} v_{\phi,00} \ , \tag{12}$$

where $M^2_A = \rho_{00} v^2_{r,00}/CH^2_{r,00}$ = radial Alfvén Mach number, and r_A is the radius of the radial Alfven critical point.

The extension of the O(1) equations to include latitudinally dependent boundary conditions creates a new dependence of the O(N) azimuthal velocity on latitude. The solution is the same but

$$M^2_A = \frac{M^2(\theta)}{\eta^2(\theta)\rho_{00}(r,\theta)C} \tag{13}$$

Equations (7-10) have been discussed in many papers and will not be treated here except to say they define what we mean by a "Parker" wind.

We now focus on the m=1, n=0 solutions of the multiple expansion. The interested reader can find the details in Paper III and also in Suess and Nerney (1975). Essentially, the $v_{\theta,10}$, $v_{\phi,10}$, $H_{\phi,10}$ solutions are the largest internally generated flows driven by the sun's rotation for $r >> r_A$, and this is why they are of interest.

The meridional momentum equation reduces to the following form

$$\frac{v_{r,00}}{r}\frac{\partial}{\partial r}(rv_{\theta,10}) + I = -\frac{1}{\rho_{00}r}\frac{\partial}{\partial\theta}P_{10} - \frac{CH_{r,10}}{\rho_{00}r}\frac{\partial}{\partial\theta}H_{r,00}$$

$$+\frac{CH_{r,00}}{\rho_{00}r}\left\{\frac{\partial}{\partial r}\left(\frac{rH_{r,00}}{v_{r,00}}v_{\theta,10}\right) - \frac{\partial}{\partial\theta}H_{r,10}\right\} , \qquad (14)$$

$$I = \frac{CH_{r,00}v_{\phi,00}}{\rho_{00}v_{r,00}r\sin\theta}\frac{\partial}{\partial\theta}\left(\sin\theta\, H_{r,00}\frac{v_{\phi,00}}{v_{r,00}}\right) - \frac{r}{2}\sin 2\theta +$$

$$- v_{\phi,00}\left(v_{\phi,00}\frac{\cot\theta}{r} + 2\cos\theta\right) .$$

This is equivalent to equation (20) in Paper I, (equation (13) in Paper III) where the forcing function (I) has been generalized to include 0(1) variations in latitude (where θ measures colatitude).

The term $-\frac{CH_{r,10}}{\rho_{00}r}\frac{\partial}{\partial\theta}H_{r,00}$

should formally have been included in equation (13), Paper III, but is $0(\ell nr/r^3)$ and does not contribute asymptotically.

Equation (14) integrates to the following form:

$$v_{\theta,10}\ \overrightarrow{r\gg r_A} - \frac{n(\theta)\,C}{M(\theta)v_{r,00}(\infty,\theta)}\frac{\partial}{\partial\theta}\left(\frac{\sin^2\theta n(\theta)}{v_{r,00}(\infty,\theta)}\right) . \qquad (15)$$

This generalized form for $v_{\theta,10}$ allows a more complicated latitudinal dependence for $H_{\phi,1}$ and $v_{\phi,1}$. It was shown in Paper II that the transport of mass and magnetic flux to higher latitudes forces $H_{\phi,1}$ to be positive (the opposite sign of $H_{\phi,0}$) and this causes the plasma in the equatorial plane to spin-up. This is simply a consequence of conserving angular momentum in particles and fields. There is less angular momentum in the magnetic field near $\theta = \pi/2$ so that the particles must make up the difference.

More complicated 0(1) variations in latitude can change the "simple" picture for $H_{\phi,1}$ and $v_{\phi,1}$ through more complicated meridional flow patterns.

The derivation of the integral forms for the azimuthal quantities procedes in a similar manner to that in Paper II. In particular, equations (2), (3), and (4) therein remain the same and,

$$\frac{1}{r}\frac{\partial}{\partial r}\left[r(H_{r,00}v_{\phi,10}-v_{r,00}H_{\phi,10}+H_{r,10}v_{\phi,00}-v_{r,10}H_{\phi,00})\right] = 0 \quad (16)$$

$$\frac{\partial}{\partial r}\left[r(v_{\phi,10} - CH_{\phi,10})\right] + I_{\phi} = 0 \quad , \quad (17)$$

but I_{ϕ} has a slightly different form than previously discussed.

After some work, we show that

$$I_{\phi} = 2\frac{v_{\theta,10}}{V_{r,00}}(g+r)\cos\theta + 4L_2(\theta)\frac{Cn}{M}\frac{\partial}{\partial r}(r\,H_{\phi,00}) + \frac{v^2_{\theta,10}\,g}{r^2\sin\theta} - \frac{CH^2_{r,00}\,v_{\theta,10}\sin\theta}{\rho_{00}\,V^3_{r,00}}\frac{\partial g}{\partial\theta} \quad (18)$$

$$\text{here } g(r,\theta) = \frac{m_A^2}{r}\frac{(r^2 - r_A^2)}{1 - M_A^2} \quad (19)$$

and M_A^2 is defined in equation (13).

Asymptotically, $H_{\phi,00} \propto \frac{1}{r}$, $\frac{\partial g}{\partial\theta} \to 0$, and $g \to -r$ so that

$$I_{\phi} \xrightarrow[r>>r_A]{} -\frac{v^2_{\theta,1}}{r\sin\theta}$$

Asymptotically, the azimuthal momentum equation may be integrated to the following form:

$$v_{\phi,10} - \frac{C\eta}{M} H_{\phi,10} = \frac{v^2_{\phi,10}}{\sin\theta} \frac{\ell nr}{r} + \frac{L_4(\theta)}{r} \qquad (20)$$

where $L_4(\theta)$ is determined by passing through the Alfven radius and need not concern us for $r>>r_A$.

The induction equation, (16), integrates to:

$$H_{r,00}v_{\phi,10} - v_{r,00}H_{\phi,10} + v_{\phi,00}H_{r,00}[\rho_{10}/\rho_{00} - 4L_2(\theta)] = L_5(\theta)/r. \qquad (21)$$

which was equation (12) in Paper II.

Asymptotically,

$$H_{\phi,10} \xrightarrow[r>>r_a]{} v_{\phi,00} \frac{H_{r,00}}{v_{r,00}} \frac{\rho_{10}}{\rho_{00}} \qquad (22)$$

With some work from Paper I, we can derive the asymptotic form for ρ_{10}/ρ_{00}.

Using equations (18) and (19) therein, together with the asymptotic form for X, which is defined as $\frac{H_{r,10}}{H_{r,00}}$, derived from (15) in Paper I we find

$$\frac{\rho_{10}}{\rho_{00}} \xrightarrow[r>>r_A]{} X \longrightarrow - A(\theta)\ \ell nr \qquad (23)$$

where

$$A(\theta) = \frac{1}{\eta \sin\theta} \frac{\partial}{\partial\theta} \left(\frac{\sin\theta\ v_{\theta,10}\ \eta}{v_{r,00}}\right) \qquad (24)$$

so that

$$H_{\phi,10} \xrightarrow[r>>r_A]{} \frac{\eta A \sin\theta}{v_{r,00}(\infty,\theta)} \frac{\ell nr}{r} \qquad (25)$$

$$v_{\phi,10} \xrightarrow[r>>r_A]{} \left(\frac{v^2_{\theta,10}}{\sin\theta} + \frac{C\eta^2 A \sin\theta}{M\ v_{r,00}(\infty,\theta)}\right) \frac{\ell nr}{r} \qquad (26)$$

The sign of $v_{\phi,10}$ is determined by the competition between these two terms. The first is proportional to $v^2_{\theta,1}$ and hence is positive definite, spinning up the plasma at all latitudes. It is derived from the $j_{r,0} H_{\theta,1}$ force and is due to the latitudinal gradient in $H_{\phi,00}$.

The second term is due to the $H_{r,10} v_{\phi,00}$ electric field in the meridional direction which is derived from the opening of flux tubes near the equatorial plane. This is zero at the zero of the second Legendre polynominal. The first term dominates for large values of CN^2 causing $v_{\phi,10}$ to be positive at all latitudes (asymptotically). Weaker meridional flows allow $v_{\phi,10}$ to be negative near the poles but positive near the equator. For this latter case, $v_{\phi,10}$ follows the behavior of $H_{\phi,10}$.

III. An Analytical Example

For the case of a high-speed stream originating from the solar poles together with lower speed flow at the equator, we can consider asymptotic 0(1) variables of the following form:

$$v_{r,00}(\infty,\theta) = V(1 - C_v \sin\theta) \tag{27a}$$

$$\mathcal{M}(\theta) = M(1 + C_m \sin\theta) \tag{b}$$

$$\eta(\theta) = H(1 - C_\eta \sin\theta) \tag{c}$$

$v_{r,00}(\infty,\theta)$ is the asymptotic form of the 0(1) nondimensional radial velocity and we use $v_{r,00}(\infty,0) = 5.3$. The variables are scaled by their values at the sonic critical point so that

$$v_r(\infty,\ \theta=0) = v_c\ v_{r,00}\ (\infty,\ \theta=0) = v_c\ V \tag{28}$$

Using v_c = 126 km/s (corresponding to $r_c = 6\ r_\odot$ and $\gamma = 1.2$) gives a radial velocity of ~670km/s at the poles and choosing $C_v = \frac{1}{2}$ gives half this velocity at the equator.

$M(\theta)$ is the nondimensional mass loss rate per steradian. Choosing $M = \frac{1}{4}$ reproduces the Yeh (1970) nondimensional scheme at the poles. We choose $H = \frac{1}{4}$ so that the 0(1) nondimensional radial magnetic field is one at the polar critical point.

Strictly speaking these 0(1) latitudinal variations in the dependent variables correspond to a latitudinal variation in the input of momentum and energy and might equivalently be considered a variation of the polytropic index with latitude, $\gamma(\theta)$. This is of no consequence for these asymptotic results as the pressure gradient drops out of the equations for $r \gg r_A$. In this sense the formal solutions for $v_{\theta,10}$, $v_{\phi,10}$, and $H_{\phi,10}$ are independent of the choice of energy equation, although strongly dependent on the energy and momentum input to the wind as they affect the 0(1) variations in v_r, etc. (Suess and Nerney, 1973).

For the purposes of this study, we presume that these latitudinal variations are given (see figure 1) and ask what is then implied for the meridional flow pattern, flux tube opening (or closing), mass flux redistribution, and particle spin-up (or spin-down).

Substituting equations (27a, b, c) into equation (15) gives

$$v_{\theta,10} \xrightarrow[r>>r_A]{} \frac{C}{M}\left\{\frac{\eta^2}{v^2_{r,00}(\infty,\theta)}\sin 2\theta + \frac{\eta}{v_{r,00}(\infty,\theta)}\sin^2\theta\,\frac{\partial}{\partial\theta}\left(\frac{\eta}{v_{r,00}(\infty,\theta)}\right)\right\} \quad (29)$$

If $C_\eta = C_v$ so that $\eta(\theta) = v_{r,00}(\vartheta)$ we recover

$$v_{\theta,10} \xrightarrow[r>>r_A]{} -\frac{C\sin 2\theta}{16M(\theta)\,v^2_{r,00}}$$

which is identical to equation (15) in Paper III (we multiplied $v_{\theta,10}$ by the smallness parameter N^2, the velocity at the critical point, v_c, and set $r_c^2 = M = \frac{1}{4}$ in Paper III).

For these particular 0(1) variations, equation (29) reduces further to:

$$v_{\theta,10} = -\frac{C}{M}\frac{\eta}{v_{r,00}}\sin 2\theta\left\{\frac{\eta}{v_{r,00}} + \frac{(C_v - C_\eta)\sin\theta)}{8V(1-C_v\sin\theta)^2}\right\} \quad (30)$$

Equation (24) for $A(\theta)$ reduces to:

$$A(\theta) = -\frac{C\,\eta}{M\,v^2_{r,00}}\left\{\frac{2}{v_{r,00}}\left[(2\cos^2\theta - \sin^2\theta)\eta\right.\right.$$

$$\left. - \sin\theta\cos^2\theta\left[\frac{3}{4}C_\eta + \eta\left(\frac{C_m}{4M} - \frac{3\,VC_v}{v_{r,00}}\right)\right]\right]$$

$$+ \frac{(C_v - C_\eta)}{4V(1-C_v\sin\theta)^2}\left[\cos\theta\sin 2\theta + \sin\theta\cos 2\theta\right.$$

$$\left.\left. - \sin^2\theta\cos^2\theta\left[\frac{C_\eta}{2\eta} + \frac{C_m}{4M} - \frac{2V\,C_v}{v_{r,00}} - \frac{2\,C_v}{1-C_v\sin\theta}\right]\right]\right\} \quad (31)$$

IV. Numerical Results

Figure 2 shows the results of a high-speed stream study in which C_v was set equal to one-half and the radial velocity at the pole was set to 670 km/s ($v_{r,00} = 5.3$) and half that at the equator. N^2 was set to .04 and C was chosen to be 14 as these are reasonable numbers which also reproduce $v_\theta = -2.5 \sin 2\theta$, km/s, for $C_m = C_v = C_\eta = 0$. We then systematically varied $M(\theta)$ and $\eta(\theta)$. In case 1 we used $C_m = C_\eta = 0$, case 2 had $C_m = C_\eta = .15$, case 3 had $C_m = C_\eta = .25$, and case 4 had $C_m = C_\eta = .5$. The strongest effects are seen in the first case where there are no latitudinal variations. We also studied the effects when C_m was set to zero with $C_v = .5$. Stepping C_η through the same range of numbers produced similar curves somewhat reduced in value (about a 20% reduction, at most).

These solutions show that the dominant effects are near the equatorial plane. For these parameters, flux tubes open within about 25° of the equatorial plane and plasma spins up in this region by 1-3 km/s depending upon the latitudinal variations in the 0(1) mass loss rate and radial magnetic field intensity.

Nearer the poles the high speed stream "opens" the field lines, reducing the magnetic pressure variation in latitude, producing weak meridional flows together with small corrections to $v_{\phi,00}$ and $H_{\phi,10}$.

The character of the solution for $v_{\phi,10}$ changes as C is increased. Paper II presented the case for C = 100 but without latitudinal variations in 0(1) variables. Figure 3 therein shows that $v_{\phi,10}$ is positive at all colatitudes, showing the dominance of the first term in equation (26). The meridional velocity scales as CN^2 so that this part of the contribution to $v_{\phi,10}$ scales as C^2N^4 and is nearly fifty times larger in the earlier study than in the study reported here. Meridional flows of that magnitude, 0(10km/s), create a spin-up of the plasma at all colatitudes so that $v_{\phi,10}$ no longer follows the analytic behavior of $H_{\phi,10}$.

Figure 3 shows the results of a slow-speed wind study for the same set of parameters as those studied in figure 2. The exception is that $v_{r,00}$ was not allowed to vary in latitude but rather was set equal to 334 km/s, the value in the equatorial plane for the previous cases. Now the variations in latitude are strictly due to $M(\theta)$ and $\eta(\theta)$. We used $C_m = C_\eta = 0$ for case 5, $C_m = C_\eta = .15$ for case 6,

$C_m = C_\eta = .25$ for case 7, and $C_m = C_\eta = .5$ for case 8. Again, the dominant meridional flows were for case 5; i.e., no latitudinal variations. The effect of the variations in $M(\theta)$ and $\eta(\theta)$ is to move the region of minimum v_θ much closer to the poles than in the high speed stream study. This is, in turn, reflected in the similar nature of the $v_{\phi,10}$ and $H_{\phi,10}$ profiles. As the latitudinal variations become larger in $M(\theta)$ and $\eta(\theta)$, the region of flux tube opening and plasma spin-up is moved closer to the poles, although the overall effects are diminished.

V. Conclusions

We have completed a linear study of the MHD equations for internal generated, steady, axi-symmetric flows. The results are generally applicable to stars like the sun with thermally driven winds.

The results indicate that the usual equatorial divergence that builds up asymptotically from assumed spherically symmetric boundary conditions is modified due to O(1) latitudinal variations in the mass-loss rate, radial velocity, and radial magnetic field at the base of the model. It is possible for an equatorial convergence to develop (Paper III); however, this was not the case for the models studied herein. We found equatorial divergences limited approximately to within ±25° of the equatorial plane for quite reasonable variations in O(1) parameters. The response of the wind to these meridional flows is to open flux tubes and, generally, to spin-up the plasma near the equatorial plane.

Analytical results were derived for the latitudinal variation in v_θ as well as the corrections to v_ϕ and H_ϕ. The results show that these variations depend critically on the value of C, a nondimensional number which measures the ratio of the strength of the $\vec{j} \times \vec{H}$ force to the advection term in the momentum equation (evaluated at the sonic critical point). As C becomes large ($C > 100$), v_θ becomes large and the plasma spins up at all latitudes. This is due to the opening of flux tubes which requires spin-up of the plasma to maintain conservation of angular momentum in fields and plasma.

These analytic results do not depend on the choice of an energy equation. At large distances, the pressure gradient decouples from the equations so that the polytropic assumption is not a severe limitation. Of course, the asymptotic values for the flow field depend sensitively on the energy and momentum input at all radii and latitudes, but these formal results are still correct.

Also, it should be remembered that stellar wind studies that neglect the inherent three-dimensional nature of the interaction between outflow, rotation, and magnetic fields, may overlook important aspects of the wind structure. In fact, one cannot find an appropriate set of boundary conditions to minimize terms like $\frac{\partial v_\theta}{\partial}$ when studying the

interaction between rotation and the magnetic field. Consequences of the latitudinal gradients are of the same order of magnitude as the interactions which are to be studied, Suess and Nerney, 1973.

Solar cycle effects can severely limit the comparison of data with this model. For instance, Slavin et al., 1984, found a general increase in the interplanetary magnetic field during 1976-82 as Pioneer and Voyager spacecrafts moved farther from the sun. Without a correction for the time variation of the fields, the respective magnetic field radial gradients are underesti_mated. As the opening of flux tubes in the outer solar system will lead to a drop off in H_ϕ that is more pronounced than that predicted by the Parker model (r^{-1}), one must be careful to separate temporal from spatial field gradients. Slavin et al. find $H_\phi \propto r^{-1.12\pm.06}$ for 1 AU < r < 12 AU and this is consistent with our results for an approximate 10% correction in the Parker model $\left(N^2 \frac{H_{\phi,1}}{H_{\phi,0}} = .1\right)$. However, the analytic form for the correction is proportional to ln r which is a different analytic form than the usual power law fit to the data. As ln r is a slowly varying function, this may not be a problem. We are, however, reminded of the study of Brandt et al., 1973, where various power law fits to the latitudinal variation in v_θ derived from aberration angles were used. The residuals were finally reduced when a $\sin 2\theta$ variation was suggested from theory. Perhaps similar progress would occur for radial gradient studies if the ln r variation were included.

A final note of caution is in order as the solar wind is not axisymmetric. The most vigorous rotational velocities develop from stream-stream interactions, Pizzo, 1982, and these have been neglected in our study. However, we hope that this linear model will guide those who will attempt to analytically model the nonlinear MHD equations which describe these internally generated flows.

References

Brandt, J. C., R. S. Harrington, and R. G. Roosen, 1973, Ap. J., 184, 27.

Burlaga, L. F., R. P. Lepping, K. W. Behannon, L W. Klien, and F. M. Neubauer, 1982, J. Geophys. Res., 87, 4345.

Nerney, S. F., 1980, Astrophys. J., 242, 723.

Nerney, S. F. and S. T. Suess, 1975a, (Paper I), Astrophys. J., 196, 837.

_____, 1975b, (Paper II), Astrophys. J., 200, 503.

_____, 1975c, (Paper III, Solar Phys, 45, 255.

Pizzo, V. J., 1982, J. Geophys. Res., 87, 4374.

Slavin, J. A., E. J. Smith, and B. T. Thomas, 1984, Geophys. Res. Lett., 11, 279.

Suess, S. T. and S. F. Nerney, 1973, Ap. J., 184, 17.

_____, 1975a, Sol. Phys., 40, 487.

Suess, S. T., A. K. Richter, C. R. Winge, and S. F. Nerney, 1977, Astrophys. J., 217, 296.

Thomas, B. T. and E. J. Smith, 1980, J. Geophys. Res., 85, 6861.

Thomas, B. T., J. A. Slavin, and E. J. Smith, 1983, EOS. Trans. Amer. Geophys. Union, 64, 822.

Weber, E. J. and L. Davis., Jr., 1967, Ap. J., 148, 217.

Winge, C. R. and P. J. Coleman, 1974, Planet. and Spa. Sci., 22, 439.

Yeh, T., 1970, J. Geophys. Res., 75, 6309.

Figure Captions

1. The asymptotic nondimensional, colatitudinal variations for (a) $v_r = V(1-C_v \sin\theta)$ for $C_v = .15, .25, .5$; (b) the mass-loss rate/steradian, $M(\theta) = \frac{1}{4}(1+C_m \sin\theta)$ for $C_m = .15, .25, .5$; and (c) the radial magnetic field ($H_{r,00} = \eta(\theta)/r^2$), $\eta = \frac{1}{4}(1-C_\eta \sin\theta)$ for $C_\eta = .15, .25, .5$.

2. A high-speed stream study showing dimensional solutions for v_θ, as well as the corrections to v_ϕ and H_ϕ for $N^2=.04$, $C = 14$, $H_c = .1$ gauss at 6 $r_\odot$, and $v_c = 126$ km/s. The radial velocity at the pole is 670 km/s and half this at the equator. Case 1 has $C_m = C_\eta = 0$, case 2 has $C_m = C_\eta = .15$, case 3 has $C_m = C_\eta = .25$, case 4 has $C_m = C_\eta = .5$, and all have $C_v = .5$.

3. A slow-speed stream study for the same case studies as in figure 2 but with $C_v = 0$ and a radial velocity of 334 km/s at all latitudes. Case 5 has $C_m = C_\eta = 0$, etc.

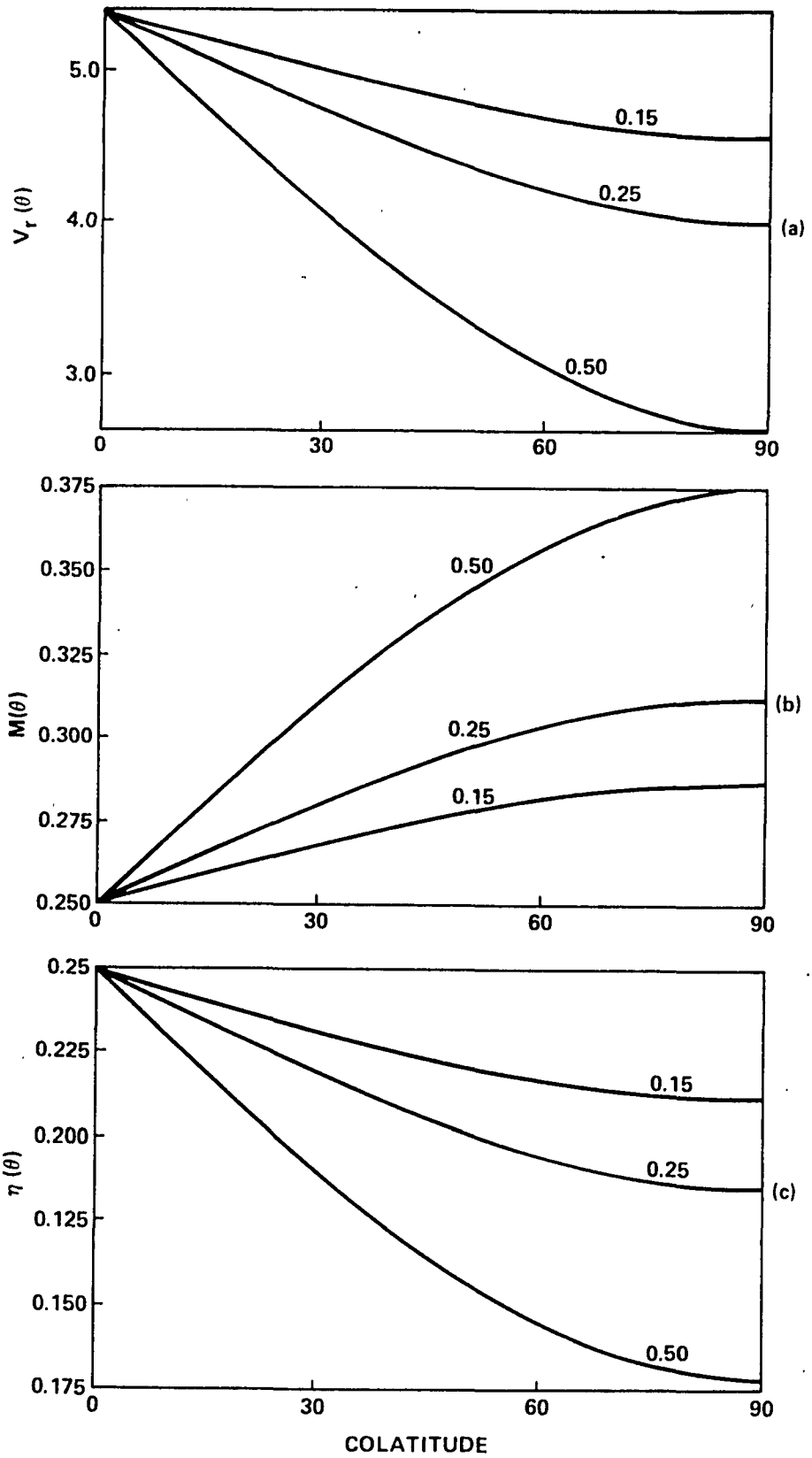
5.0
4.0
3.0
$V_r(\theta)$
0.15
0.25
0.50
(a)
0
30
60
90
0.375
0.350
0.325
0.300
0.275
0.250
$M(\theta)$
0.50
0.25
0.15
(b)
0
30
60
90
0.25
0.225
0.200
0.125
0.150
0.175
$\eta(\theta)$
0.15
0.25
0.50
(c)
0
30
60
90
COLATITUDE

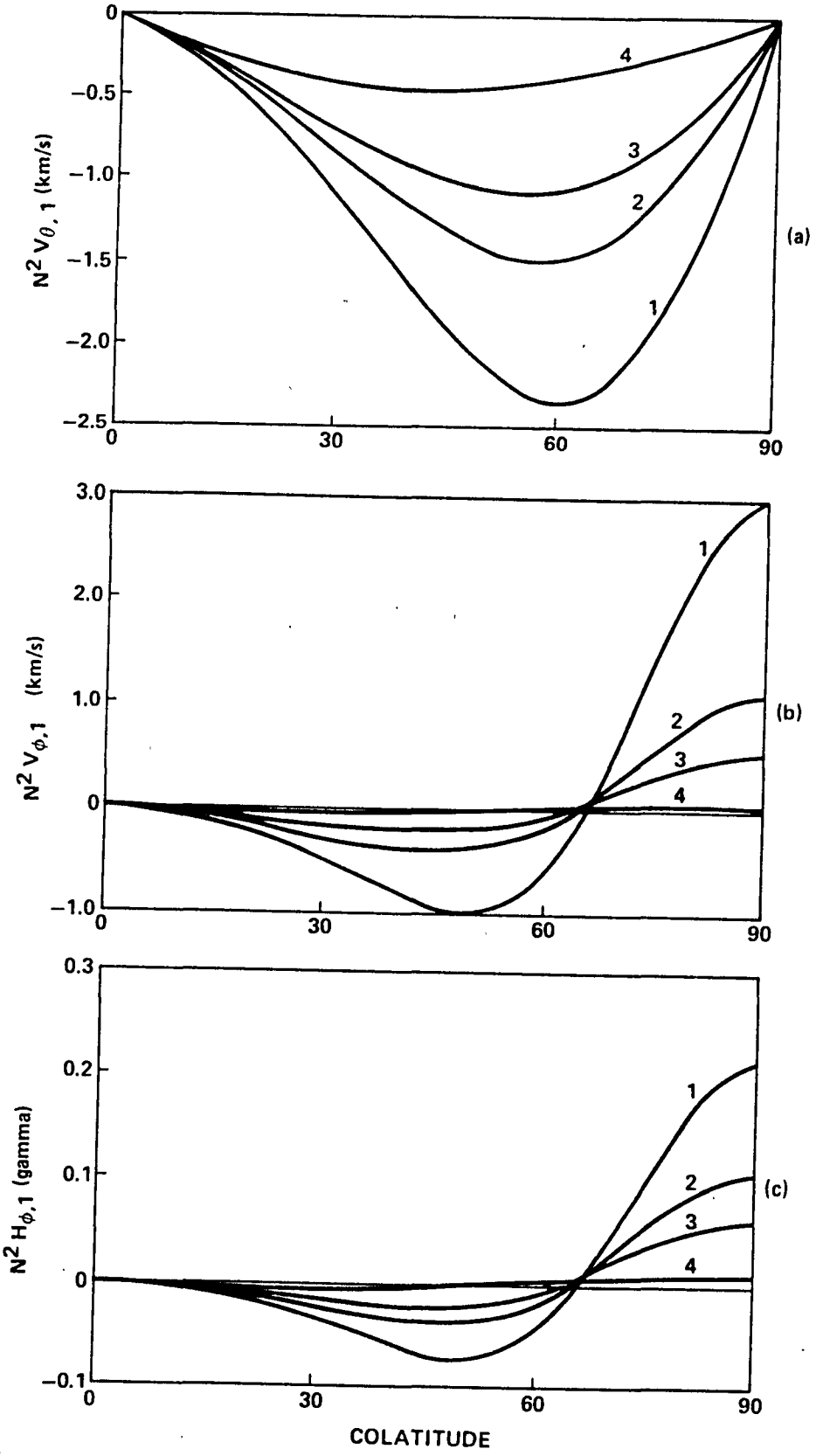
0
−0.5
−1.0
−1.5
−2.0
−2.5
$N^2 V_{\theta,1}$ (km/s)
4
3
2
1
(a)
0
30
60
90
3.0
2.0
1.0
0
−1.0
$N^2 V_{\phi,1}$ (km/s)
1
2
3
4
(b)
0
30
60
90
0.3
0.2
0.1
0
−0.1
$N^2 H_{\phi,1}$ (gamma)
1
2
3
4
(c)
0
30
60
90
COLATITUDE

SLOW–SPEED WIND STUDY (V_∞ = 334 km/s)

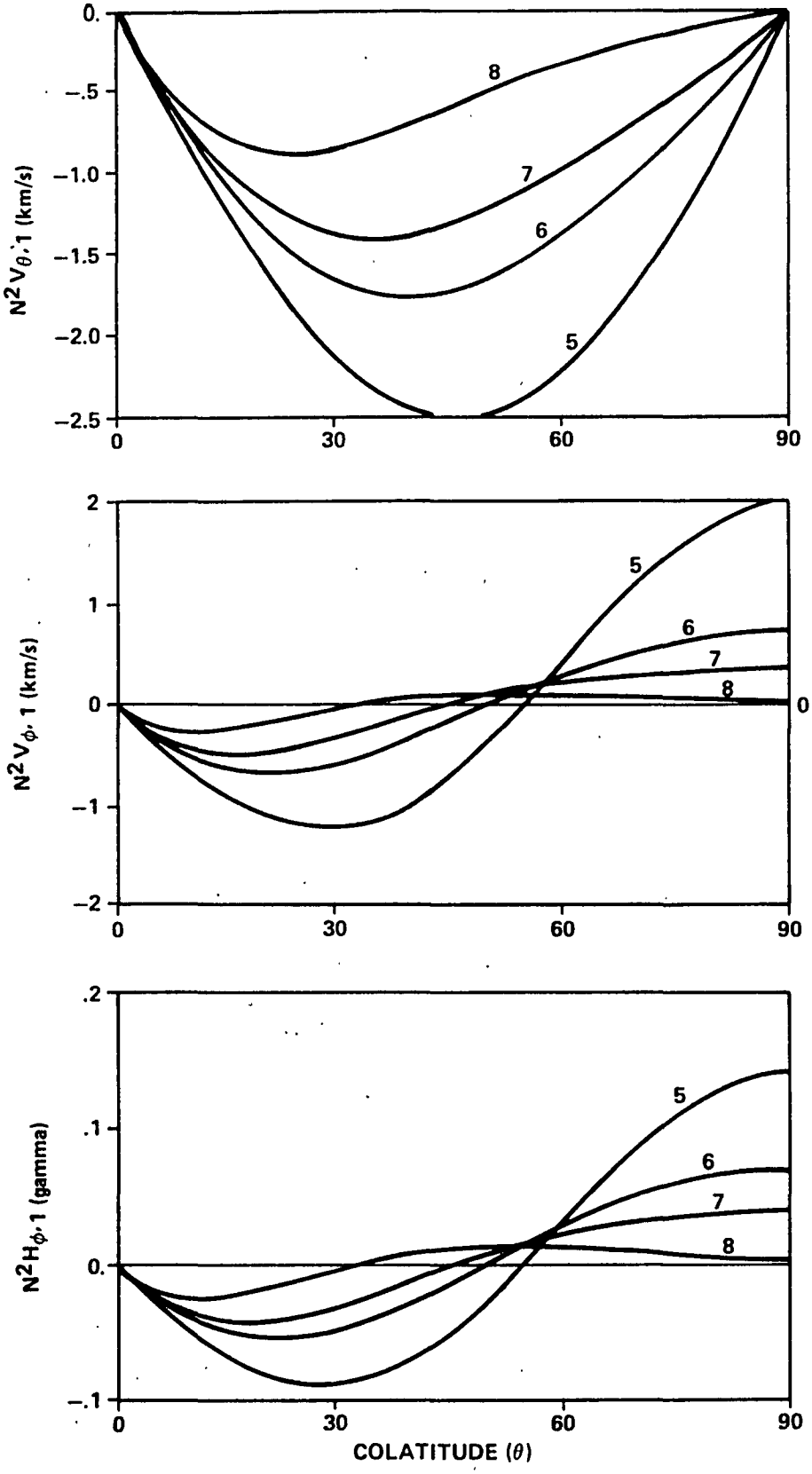

1984

NASA/ASEE SUMMER FACULTY RESEARCH FELLOWSHIP PROGRAM

Marshall Space Flight Center
The University of Alabama

A MATHEMATICAL FORMULATION OF THE PROBLEM OF OPTIMAL USE OF GROUND RESOURCES FOR FUTURE SPACE MISSIONS

Prepared By:	Meckinley Scott, Ph.D.
Academic Rank:	Professor
University and Department:	The University of Alabama Department of Mathematics
NASA/MSFC:	
Laboratory:	Program Development, Preliminary Design
Division:	Mission Analysis & Integration
Branch:	Operations Analysis
Date:	August3, 1984
Contract No.:	NASA NGT-01-002-099 The University of Alabama

ACKNOWLEDGEMENTS

I would like to express my appreciation to Mr. Gary Johnson, my counterpart at MSFC for his time, patience and efforts to help me successfully complete this project. Various useful suggestions and guidance in the preparation of this report provided me by Dr. James Steincamp, Chief, Operations Analysis Branch, are gratefully acknowledged. I would also like to thank Mr. John W. Cole, Chief, Design and Development Branch, for clarifying some of the ideas relating to this project.

A MATHEMATICAL FORMULATION OF THE PROBLEM OF OPTIMAL USE OF GROUND RESOURCES FOR FUTURE SPACE MISSIONS

By

Meckinley Scott
Professor of Mathematics
University of Alabama
Tuscaloosa, AL

ABSTRACT

In this project we propose an approximate mathematical formulation for scheduling of future space missions. Our main objective is to schedule these flights to efficiently use available ground resources. Thus, our interest is to minimize the inventory level of ground resources needed. Equivalently, our objective will be achieved if we schedule these flights to minimize the overlapping or conflicting periods during which the same types of resources are used by the various flights.

The development of the mathematical formulation of the problem takes into account the presence of a large number of sequencing and resource constraints, e.g., (i) the order in which the flights are to be launched is predetermined, and (ii) some types of resources are to be used only by certain flights. A linear objective function based on cost considerations (penalty costs for overlapping utilization of the same types of resources) is constructed and this function is minimized subject to the various constraints.

1. Introduction

This project is concerned with the problem of scheduling future space missions. The missions will typically consist of a number of payloads manifested into a Shuttle-compatible cargo, or mission. The evaluation involves flight scheduling in the most cost effective manner from the standpoint of launch site facilities and space hardware resources. The flights will use some common facilities and resources, as well as those unique to a particular class or category. For example, all flights will use a launch pad, while only Spacelab flights will require a core module and associated equipment. The scheduling problem is further complicated by different seize-release requirements for each piece of equipment (timelines) and by unique costs associated with each resource to be tracked. Therefore, the minimum overall investment cost is the objective, rather than just quantities of resources in the inventory. For this reason, cost weighting factors are used.

Timely availability of needed ground resources plays a key role in scheduling flights of these missions. Assuming that the requirement for the various resources can be met, the main objective of this project is to find a practical technique to minimize the inventory level of these resources. As one might well expect, the problem is one of considerable complexity die to the presence of a large number of variables. Also, a number of these variables may be of a stochastic nature and this would further increase the degree of complexity of the problem. Thus, at the present time it appears that any attempt to obtain a rigorous solution to the general scheduling problem will lead to a dead end. In fact, even to attempt to set up a precise

mathematic formulation of the problem seems to be a very difficult task. Currently there exists a scheduling program "GROPE" (Ground Resource Operations Program Executive) which uses heuristic procedures to schedule flights to achieve near-to-optimal solutions. Consequently, this program lacks complete mathematical justification, rigor and formality.

It is our intent in this report to build an approximate mathematical model to formulate the problem. This will be based on assumptions which describe the actual situation as closely as possible. As will be seen in the next section, most of these assumptions reflect the presence of a large number of time sequence and resource constraints in the system. As mentioned above, our main objective here is to minimize the inventory level of needed ground resources. This problem will be dealt with in an indirect manner: Instead of analyzing the problem by minimizing the inventory level of needed resources, the flights will be scheduled in such a way as to minimize the overlapping or conflicting periods during which the same types of resources are used by the various flights. Associated with each overlap for the use of the same type of resource by any pair of flights is a penalty cost which depends upon the number of units of that resource needed by these flights. The over-all objective function is assumed to be linear with respect to these penalty costs. Since the various sequencing resource constraints are also linear, the problem under consideration falls within the realm of linear programming.

2. Assumptions for the Formulation of the Problem

Basically decisions concerning scheduling of flights are based on five assumptions. These assumptions are stated below in somewhat more general context to allow us to have more flexibility for applications.

1) There are n flights to be launched during some given interval of time, $[0,T]$.

2) The order in which these flights are to be launched is predetermined.

3) Of the n flights, there are p ($<n$) specific flights where launch dates have been fixed. However, each such flight may have launch window of a certain specified length.

4) All flights utilize at least one type of ground resource from a collection of M different types.

5) Any flight that utilizes say, a type 'k' ground resource may require n_k (≥ 1) units of that resource.

3. Notation and Some Basic Definitions

Let t_i, (i=1,2,3,...,n) denote the time for launching of the ith flight and let t_{n_1}, t_{n_2}, ..., t_{n_p} be the fixed launch times for the p specific flights corresponding to assumption 3) above. Since the n flights are to take place according to some predetermined order and no two flights can occur at the same instant of time, there is a class of sequencing constraints of the form

$$0<t_1<t_2<\ldots<t_{n_1-1}<t_{n_1}<t_{n_1+1}<\ldots<t_{n_2-1}<t_{n_2}<t_{n_2+1}$$

$$<\ldots<t_{n_p-1}<t_{n_p}<t_{n_p+1}<\ldots<t_{n-1}<t_n<T.$$

Since the flights may utilize resources either before or after (or both before and after) their launch times, it is convenient to introduce the following zero-one variables. For k=1,2,3,...,M. let

δ_{ij}^{k1} = 1, if both ith and jth flights utilize a type 'k' resource and the seize times for this resource occur before their launch times t_i and t_j respectively,

= 0, otherwise (i<j).

δ_{ij}^{k2} = 1, if both ith and jth flights utilize a type 'k' resource and the seize times for this resource occur before t_i for the ith flight and after t_j for the jth flight,

= 0, otherwise (i<j).

δ_{ij}^{k3} = 1, if both ith and jth flights utilize a type 'k' resource and the seize times for this resource occur after t_i for the ith flight and before t_j for the jth flight,

= 0, otherwise (i<j).

δ_{ij}^{k4} = 1, if both ith and jth flights utilize a type 'k' resource and the seize times for this resource occur after their launch times t_i and t_j respectively,

= 0, otherwise (i<j).

For any flight i, (i=1,2,3,...,n) that utilizes a type 'k' resource before its launch time t_i, let s_i^{k1} denote the length of time in which this resource is seized before t_i, and let d_i^{k1} denote the corresponding duration for its use.

Again, for any flight i, (i=1,2,3,...,n) that utilizes a type 'k' resource after its launch time t_i, let s_i^{k2} denote the length of time in which this resource is seized after t_i, and let d_i^{k2} denote the corresponding duration for its use.

For $1 \le i < j \le n$, let us define the following "overlap" variables:

$$O_{ij}^{k1} = \text{Max } \{0, \ (t_i - s_i^{k1} + d_i^{k1}) - (t_j - s_j^{k1})\}, \ (\delta_{ij}^{k1} = 1)$$

$$O_{ij}^{k2} = \text{Max } \{0, \ (t_i - s_i^{k1} + d_i^{k1}) - (t_j + s_j^{k2})\}, \ (\delta_{ij}^{k2} = 1)$$

$$O_{ij}^{k3} = \text{Max } \{0, \ (t_i + s_i^{k2} + d_i^{k2}) - (t_j - s_j^{k1})\}, \ (\delta_{ij}^{k3} = 1)$$

$$O_{ij}^{k4} = \text{Max } \{0, \ (t_i + s_i^{k2} + d_i^{k2}) - (t_j + s_j^{k2})\}, \ (\delta_{ij}^{k4} = 1)$$

The variable O_{ij}^{k1} measures the amount of the overlapping or conflicting period of time for the utilization of a type 'k' resource by the ith and jth flights in the case where the seize times for the resource occur before their launch times. The variable O_{ij}^{k2} measures the amount of the overlapping period of time for the utilization of a type 'k' resource by the ith and jth flights in the case where the seize times for the resource ovvur before the launch time t_i for the ith flight and after t_j for the jth flight. The variables O_{ij}^{k3} and O_{ij}^{k4} are similarly interpreted: In the case of O_{ij}^{k3} the seize times for the resource occur after t_i for the ith flight and before t_j for the jth flight. In the case of O_{ij}^{k4} the seize times for the resource by both flights occur after their launch times.

4. Cost Functions and Formulation of the Problem

With each overlapping period for the utilization of the same type of resource, there is associated with it a penalty which may be measured in terms of cost per unit time. Let C_{ij}^{k1} = cost per unit time arising from the simultaneous utilization of a type 'k' resource that is associated with the variable O_{ij}^{k1}.

Similar to C_{ij}^{k1} are costs C_{ij}^{k2}, C_{ij}^{k3}, and C_{ij}^{k4} that correspond to the variables O_{ij}^{k2}, O_{ij}^{k3}, and O_{ij}^{k4} respectively, At this point, we will the assumption that the penalty cost T_{ij}^{kr} associated with the variable O_{ij}^{kr} is directly proportional to the cost per unit time, that is

$$T_{ij}^{kr} = C_{ij}^{kr}\ O_{ij}^{kr},\ (\ =1,2,3,4),$$

and the total cost T is simply the sum of such costs taking into consideration all the M types of ground resources. Thus,

$$T = \sum_{k=1}^{M} \sum_{r=1}^{4} \sum_{\{(i,j)/1\le i<j\le n,\ \delta_{ij}^{kr}=1\}} C_{ij}^{kr}\ O_{ij}^{kr}.$$

The above cost T is the objective function to be minimized subject to the various sequencing and resource constraints.

The assumption that no two flights are to be scheduled at the same instant of time leads to constraints of the type

$$t_{i+1} - t_i \ge d>0,\ (i=1,2,\ldots,\ n-1).$$

The provision that the p specific flights with launch dates fixed at times t_{n_1}, t_{n_2}, ..., t_{n_p} may, possibly, have launch windows of certain specified lengths yields constraints of the type

$$t_n \ge \underline{\ell}_i, t_n \le \bar{\ell}_i,\quad (i = 1,2,3,\ldots,p).$$

The relationship between the variables O_{ij}^{kr}, (r = 1,2,3,4; k = 1,2,..., ..,M) and the launch times t_i, (i = 1,2,....,n) given before may be re-written in the form

$$-\delta_{ij}^{kr}\ t_i + \delta_{ij}^{kr}\ t_j + \delta_{ij}^{kr}\ O_{ij}^{kr} = D_{ij}^{kr}\quad (1\le i<j\le n;\ r=1,2,3,4;\ k=1,2,\ldots,M).$$

Where

$$D_{ij}^{kr} = \delta_{ij}^{kr} d_{ij}^{kr},$$

$$d_{ij}^{k1} = d_i^{k1} - s_i^{k1} + s_j^{k1},$$

$$d_{ij}^{k2} = d_i^{k1} - s_i^{k1} - s_j^{k2},$$

$$d_{ij}^{k3} = d_i^{k2} + s_i^{k2} + s_j^{k1},$$

$$d_{ij}^{k4} = d_i^{k2} + s_i^{k2} - s_j^{k2},$$

$$0_{ij}^{kr} \geq 0.$$

5. Assumption Concerning Cost Functions and Form of the Objective Function

For any pair (i,j) such that $\delta_{ij}^{kr}=1$, (r=1,2,3,4), let n_i^{k1} and n_j^{k1} denote, respectively, the number of replicates of a type 'k' resource utilized by the ith and jth flights when the seize times for this resource occur before their launch times. n_i^{k2} and n_j^{k2} denote corresponding quantities when the seize times for the resource occur after their launch times t_i and t_j respectively. Since our objective is, in essence, to minimize the overlapping utilization of the resources by the various flights, the form of the cost functions should reflect this desired feature. Among various other possibilities, the following form appears to be an appropriate choice for the cost functions under consideration:

$$C^{k1} = \{\text{Min } (n_i^{k1}, n_j^{k1})\}\, C^{(k)} = n_{ij}^{k1}\, C^{(k)}, \text{ say}$$

$$C^{k2} = \{\text{Min } (n_i^{k1}, n_j^{k2})\}\, C^{(k)} = n_{ij}^{k2}\, C^{(k)}, \text{ say}$$

$$C^{k3} = \{\text{Min } (n_i^{k2}, n_j^{k1})\}\, C^{(k)} = n_{ij}^{k3}\, C^{(k)}, \text{ say}$$

$$C_{ij}^{k4} = \{\text{Min } (n_i^{k2}, n_j^{k2})\}\, C^{(k)} = n_{ij}^{k4}\, C^{(k)}, \text{ say}$$

where $C^{(k)}$ is the weight given to a type 'k' resource based on cost considerations relative to other types of resources in the collection. With this assumption, the objective function may be written

$$T = \sum_{k=1}^{M} C^{(k)} \sum_{r=1}^{4} \sum_{\{(i,j)/1\le i<j\le n\}} n_{ij}^{kr}\, 0_{ij}^{kr} .$$

It can easily be shown that minimizing the objective function T is equivalent to minimizing τ given by

$$\tau = \sum_{k=1}^{M} C^{(k)} \sum_{\{(i,j)/1\le i<j\le n\}} m_{ij}^{k}(t_i - t_j),$$

where

$$m_{ij}^{k} = \sum_{r=1}^{4} n_{ij}^{kr} .$$

Alternatively, τ can be rewritten in the form

$$\tau = \sum_{i=1}^{n} C_i t_i, \qquad \text{(I)}$$

Where

$$C_i = \sum_{k=1}^{M} C^{(k)} \left(\sum_{i<r\le n} m_{ir}^k - \sum_{1\le s<i} m_{si}^k \right), \quad (i=1,2,3, \ \ldots \ ,n)$$

and recall that τ is to be minimized subject to the following constraints:

$$-t_i + t_{i+1} \ge d, \quad (i = 1,2, \ \ldots \ , n-1)$$

$$t_{n_i} \ge \underline{\ell}_i,$$

$$t_{n_i} \le \bar{\ell}_i, \quad (i = 1,2, \ \ldots \ , p)$$

$$t_1 \ge 0, \ t_n \le T,$$

$$-\delta_{ij}^{kr} t_i + \delta_{ij}^{kr} t_j = \delta_{ij}^{kr} \, 0_{ij}^{kr} = D_{ij}^{kr} \ ,$$

$$0_{ij}^{kr} \ge 0, \quad (i\le i\le j\le n; \ \ r=1,2,3,4; \ k=1,2, \ \ldots \ ,M). \qquad \text{(II)}$$

We have, thus, formulated the problem as a standard linear programming problem with objective function τ and constraints as given in (II) above.

6. Notation in Matrix Form

To computerize the problem, it may be convenient to rewrite the objective function and constraints in matrix notation. Nore that there are $n+2Mn(n-1)$ variables, namely, t_1, t_2 ...,

$$t_n; \ 0_{12}^{11}, \ 0_{12}^{12}, \ 0_{12}^{13}, \ 0_{12}^{14}, \ \ldots, \ 0_{12}^{M1}, \ 0_{12}^{M2}, \ 0_{12}^{M3}, \ 0_{12}^{M4}, \ \ldots$$

$$\ldots, \ 0_{(n-1)n}^{M1}, \ 0_{(n-1)n}^{M2}, \ 0_{(n-1)n}^{M3}, \ 0_{(n-1)n}^{M4}.$$

Corresponding to the constraints

$$-t_i + t_{i+1} \ge d, \ (i = 1,2,\ldots, \ n-1)$$

$$t_{n_i} \ge \underline{\ell}_i, \quad (i = 1,2,\ldots, \ p)$$

we associate $n+p-1$ surplus variables denoted by say, U_1, U_2, ... , U_{n+p-1}.

Similarly, corresponding to the contraints

$$t_{n_i} \leq \bar{\ell}_i, \quad (i = 1,2,\ldots, p)$$

$$t_n \leq T,$$

we introduce p+1 slack variables which will be denoted by v_1, v_2, ..., v_{p+1}. The objective function τ can be written in the form $\tau = c\hat{t}$, where c is a row vector given by

$$c = (c_1, c_2, \ldots, c_n)$$

and $\hat{t}$ is the transpose of a row vector $t = (t_1, t_2, \ldots, t_n)$. In matrix form, the constraints can be written as $A\hat{\eta} = \hat{\omega}$ where A is an $\{n+2p+2Mn(n-1)\}$ X $\{2n+2p+2Mn(n-1)\}$ matrix, $\hat{\eta}$ is the transpose of a row vector η consisting of $2n+2p+2Mn(n-1)$ elements and $\hat{\omega}$ is the transpose of a row vector ω consisting of $n+2p+2Mn(n-1)$ elements.

It is convenient to decompose the vector ω into three sub-row vectors given by $W = (\underline{d}, \ell, \underline{D})$, where $\underline{d}$ is a row vector consisting of (n-1) elements, each element being equal to d. is a row vector consisting of (2p+1) elements given by $\underline{\ell} = (\underline{\ell}_1, \bar{\ell}, \underline{\ell}_2, \bar{\ell}_2, \ldots, \underline{\ell}_p, \bar{\ell}_p, T)$ and $\underline{D}$ is a new vector with $2Mn(n-1)$ elements given by

$$\underline{D} = (D_{12}^{11}, D_{12}^{12}, D_{12}^{13}, D_{12}^{14}, \ldots, D_{12}^{M4}, \ldots, D_{(n-1)n}^{M1}, D_{(n-1)n}^{M2}, D_{(n-1)n}^{M3}, D_{(n-1)n}^{M4}).$$

The vector η may be written as

$$\eta = (\underline{t}, \underline{0}, \underline{U}, \underline{V})$$

where $\underline{t}$, $\underline{0}$, $\underline{U}$, $\underline{V}$ are row vectors given by

$$\underline{t} = (t_1, t_2, \ldots, t_{n_1}, \ldots, t_{n_2}, \ldots t_{n_p}, \ldots t_{n-1}, t_n),$$

$$\underline{0} = (0_{12}^{11}, 0_{12}^{12}, 0_{12}^{13}, 0_{12}^{14}, \ldots, 0_{12}^{M4}, \ldots 0_{(n-1)n}^{M1}, 0_{(n-1)n}^{M2}, 0_{(n-1)n}^{M3}, 0_{(n-1)n}^{M4},$$

$$\underline{U} = (u_1, u_2, \ldots, u_{n+p-1}),$$

$$\underline{V} = (v_1, v_2, \ldots, v_{p+1}).$$

A, which is an $\{n+2p+2Mn(n-1)\}$ X $\{2n+2p+2Mn(n-1)\}$ matrix, can also be most easily described in terms of submatrices. Let us first partition A as follows:

$$A = \begin{bmatrix} A_1 \\ A_2 \\ A_{12} \\ A_{13} \\ A_{14} \\ \vdots \\ A_{ij} \\ \vdots \\ A_{(n-1)n} \end{bmatrix} .$$

All submatrices A_1, A_2, A_{12}, A_{13}, ... , A_{ij}, ... , $A_{(n-1)}$, have $2n + 2p + 2Mn_{(n-1)}$ columns. A_1 has (n-1) rows, A_2 has 2p+1 rows. Each of the remaining sub-matrices, (A_{ij}, $1 \le i \le j \le n$), has 4M rows.

The matrix A_1 may be written as

$$A_1 = (A_1^1,\ 0_1^1,\ A_1^2,\ 0_1^2),$$

where A_1 is an (n-1) X n matrix, 0_1^1 is an (n-1) X 2Mn(n-1) null matrix, A_1^2 is a square (n-1) X (n-1) matrix and 0_1^2 is an (n-1) X (2p+1) null matrix. The elements a_{ij} of the matrix A_1 are given by

$$\left.\begin{array}{lll} a_{ij} = & -1, & j=i \\ = & 1, & j=i+1 \\ = & 0, & \text{otherwise} \end{array}\right\} \quad , (i=1,2, \ldots , n-1).$$

The matrix

$$A_1^2 = -I,$$

Where I is an (n-1) X (n-1) identity matrix.

The matrix A_2 may be written as

$$A_2 = (A_2^1,\ 0_2^1,\ A_2^2),$$

where A_2^1 is an (2p+1) X n matrix, 0_2^1 is an (2p+1) X {(n-1)(2Mn+1)} null matrix and A_2^2 is an (2p+1) X (2p+1) diagonal matrix.

The elements a_{ij} of the matrix A_2^1 are given by

$$\left.\begin{aligned} a_{ij} &= 1, \quad i=2r-1, \ j=n_r \\ &= 1, \quad i=2r, \quad j=n_r \\ &= 1, \quad i=2p+1, \ j=n, \end{aligned}\right\} \ (r=1,2, \ \dots \ , p),$$

$$= 0, \quad \text{otherwise.}$$

The elements of the diagonal matrix A_2^2 are given by

$$a_{ii} = -1, \text{ if } i \text{ is odd and } i < 2p+1,$$

$$= 1, \text{ otherwise.}$$

The matrix A_{12} may be partitioned as

$$A_{12} = (A_{12}^1,\ A_{12}^2,\ 0_{12}^1).$$

A_{12}^1 is an 4MXn matrix. The elements being zero everywhere except for columns 1 and 2. In order, the 4M entries of column 2 are δ_{12}^{11}, δ_{12}^{12}, δ_{12}^{13}, δ_{12}^{14}, δ_{12}^{21}, ... , δ_{12}^{M1}, δ_{12}^{M2}, δ_{12}^{M3}, δ_{12}^{M4}. The elements of Column 1 are simply the negatives of the corresponding entries of Column 2. A_{12}^2 is an 4MX4M diagonal matrix. The elements in the diagonal are, in order, the same as those of Column 2 of the matrix A_{12}^1. 0_{12}^1 is an 4M X {n+2p +2Mn(n-1)-4M} null matrix. The matrix $A_{(n-1)n}$ may be partitioned as

$$A_{(n-1)n} = (A_{(n-1)n}^1,\ 0_{(n-1)n}^1,\ A_{(n-1)n}^2).$$

$A_{(n-1)n}^1$ is an 4M X n matrix. The elements being zero everywhere except for the last two columns. In order, the entries in the last column are $\delta_{(n-1)n}^{11}$, $\delta_{(n-1)n}^{12}$, $\delta_{(n-1)n}^{13}$, $\delta_{(n-1)n}^{14}$, $\delta_{(n-1)n}^{21}$, ... , $\delta_{(n-1)n}^{M1}$, $\delta_{(n-1)n}^{M2}$, $\delta_{(n-1)n}^{M3}$, $\delta_{(n-1)n}^{M4}$. Entries in the (n-1)th column are simply the negatives of the corresponding entries of the last column.

$0^1_{(n-1)n}$ is an 4M X {n+2p+2Mn(n-1)-4M} null matrix. $A^2_{(n-1)n}$ is an 4M X 4M diagonal matrix. The elements of the diagonal, in order, are the same as those of the last column of the matrix $A^1_{(n-1)n}$. The other submatrices A_{ij}, $(1<i<j<n)$ may be partitioned as

$$A_{ij} = (A^1_{ij}, 0^1_{ij}, A^2_{ij}, 0^2_{ij}).$$

A^1_{ij} is an 4M X n matrix. The entries being zero everywhere except for columns i and j. In order, the entries in column j are δ^{11}_{ij}, δ^{12}_{ij}, δ^{13}_{ij}, δ^{14}_{ij}, δ^{21}_{ij}, ... , δ^{M1}_{ij}, δ^{M2}_{ij}, δ^{M3}_{ij}, δ^{M4}_{ij}. Entries in column i are simply the negatives of the corresponding entries of column j. 0^1_{ij} is an 4M X {(2n-i)(i-1)+2(j-i-1)} 2M null matrix. A^2_{ij} is an 4M X 4M diagonal matrix. The elements of the diagonal, in order, are the same as those of column j of the matrix A^1_{ij}. Lastly, 0^2_{ij} is an 4M X {(n+2p+2Mn(n-1)-2M(2n-i)(i-1)-4(j-i)M } null matrix.

7. Concluding Remarks

In this project we have formulated the problem of optimal use of ground resources for future space missions by means of an approximating mathematical model based on assumptions which reflect the actual situation to a certain degree. With these assumptions, a linear programming problem (LPP) formulation has been developed. The results generated by this LPP will be optimal to the extent that these assumptions are a faithful representation of the "real world" scheduling problem. We are now in a situation where we will be able to compare these results with those generated by the heuristics of the existing methods. Based on this comparison, a decision will be made whether to continue using the heuristics or replace them by the proposed model.

References

1. Bellman, R., Esogbue A.O. and Naheshima, I., Mathematical Aspects of Scheduling and Applications, Pergamon Press, Oxford, 1982.

2. Rao, S.S., Optimization - Theory and Applications, Halsted Press, New Delhi, 1984.

3. Fletcher, R., Practical Methods of Optimization, Vol. 2, Wiley & Sons, Chichester, 1981.

4. Wiest, J.D., "A Heuristic Model for Scheduling Large Projects with Limited Resources", Management Science, February 1967.

5. Traver, A.E., "Investigation of the Application of Lineow Programming Techniques to Optimal Project Scheduling", Research Reports NASA-ASEE Summer Faculty Fellowship Program, 1977.

D23

1984

NASA/ASEE SUMMER FACULTY RESEARCH FELLOWSHIP PROGRAM

MARSHALL SPACE FLIGHT CENTER
THE UNIVERSITY OF ALABAMA

SENSOR CONTROL OF ROBOT ARC WELDING

Prepared by:	Fred R. Sias, Jr., Ph.D.
Academic Rank:	Associate Professor
University and Department:	Clemson University Electrical and Computer Engr.
NASA/MSFC:	
Division:	Process Engineering Division
Branch:	Metals Processing Branch, EH-42
MSFC Counterpart:	Arthur C. Nunes, Jr., Ph.D.
Date:	July 27, 1984
Contract No.:	NASA-NGT-01-002-099 (The University of Alabama)

SENSOR CONTROL OF ROBOT ARC WELDING

ABSTRACT

SENSOR CONTROL OF ROBOT ARC WELDING

by

Fred Sias
Clemson University

A basic problem in the application of robots for welding is how to guide a torch along a weld seam using sensory information. The primary motivation for this effort is to raise the quality and consistancy of certain Gas Tungsten Arc welds on the Space Shuttle Main Engine (SSME) that are too complex geometrically for conventional automation and therefore are done by hand.

Last summer the overall problem was studied with a broad perspective. This included an analysis of the particular problems associated with SSME manufacturing as well as weld-seam tracking with an emphasis on computer vision methods. A number of conclusions and recommendations were proposed.

During the past year NASA has acquired most parts of a research system to study weld-seam tracking on the SSME. That system includes an Advanced Robotics CYRO 750 robot, a computer-vision based seam-tracking system, a Digital Equipment Corporation MINC-23 general-purpose computer and special-purpose software to integrate the system. The control software for the vision subsystem and special interface software for the robot is still under development. Applications software for the MINC-23 is scheduled for future research.

The effort this summer has been to develop special interface software for the MINC computer that will allow it to be used both as a test system to check out the robot interface software and later as a development tool for further investigation of sensory systems to be incorporated in NASA welding procedures.

ACKNOWLEDGEMENTS

My two summers at the Marshall Space Flight Center have added greatly to my understanding of robotics and especially arc welding. Many persons have contributed to that understanding and have provided both background material and technical details that are included in this report. Among those responsible for my education are Mr. Bill Wilson, Mr. Clyde Jones, III, Ms. Lisa Hawkins, Ms Carolyn Kurgan, Mr. Joe Sexton, Mr. Charles Brosemer, Mr. Ernie Bayless, Mr. Sam Clark, Mr. Jeff Norris, and, of course, my NASA counterpart Dr. Arthur C. Nunes, Jr. Ms. Vanita Brown and Mr. Ken Fernandez have provided computer systems support.

While many persons have contributed to the factual material in this report, the opinions expressed are those of the author.

1.0 INTRODUCTION

1.1 OVERVIEW:

A basic problem in the application of robots for welding is how to guide a torch along a weld seam using sensory information. The primary motivation for this effort is to raise the quality and consistency of certain Gas Tungsten Arc Welds (GTAW) on the Space Shuttle Main Engine (SSME) that are too complex geometrically for conventional automation and are done by hand.

Last summer the overall problem was studied with a broad perspective. This included an analysis of the particular problems associated with SSME manufacturing as well as weld-seam tracking with an emphasis on computer-vision methods. A number of conclusions and recommendations were proposed.

During the past year NASA has acquired most parts of a research system to study weld-seam tracking on the SSME. That system includes an Advanced Robotics Cyro 750 robot, a computer-vision based seam-tracking system developed at Ohio State University, a Digital Equipment Corporation MINC-23 general-purpose computer, and special-purpose software to integrate the system. Control software for the vision subsystem and special interface software for the robot is still under development. Applications software for the MINC-23 is scheduled for future research.

The effort this summer has been to develop special interface software for the MINC computer that will allow it to be used both as a test system to check out the robot interface software and later as a development tool for further investigation of sensory systems to be incorporated in NASA welding procedures.

The hardware and software for the robot External Device Interface was delivered only three days prior to the date of this report. At that time it was discovered that some features of the interface specifications had been changed, were not completely defined, or were yet to be finished. For example, the initialization procedure to establish communication between the robot an an external device requires an exchange of several messages not completely spelled out in the Advanced Robotics External Device Specification of 27 April 1984. Several weeks prior to the date of this report, Advanced Robotics indicated that several programs in the robot systems software have not been written and will be delivered at a later date.

Based on these last-minute conditions, a new initialization routine for the MINC system has been added and is in the process of being debugged. Completion of the system must await additional programming effort.

1.2 EXPANDED ROBOT-SENSOR RESEARCH:

A robot interface to an external computer provides additional capabilities for developing new robot-sensor features. An external computer, such as a Digital Equipment Corporation MINC-23, provides various special devices including analog-to-digital converters, digital clocks, digital input and digital output interfaces that may be used to acquire sensory information suitable for controlling a robot arc welder. For example, additional vision capabilities suitable for global positioning of the robot are possible. The ability to incorporate special penetration sensors or alternative power input measurements is made possible by an additional external computer.

In addition, an external computer makes it possible to enhance several of the operating characteristics of Advanced Robotics' robot. Examples of this include off-line storage of N/C programs on MINC flexible disketts and the use of MINC peripherals for editing and printing robot control programs.

The software described in this report provides a basic system that may be used to check out various communication functions that are described in the Advanced Robotics Corporation External Device Interface Specification dated 27 April 1984. The new communication subroutines provide a foundation for further expansion of the MINC-23 for additional welding-sensor research.

2.0 OBJECTIVES

2.1 PROBLEM STATEMENT:

The overall objective of this research is to investigate techniques for enhancing robot-welding capability. The more limited problem addressed this summer may be stated as follows:

> How to program the MINC-23 computer to communicate on-line with the Cyro 750 Robot to provide both interface check-out programs and additional software modules suitable for expanding sensory-systems research.

The broad problem statement has been further subdivided to identify problems that may be associated with specific tasks that are, in turn, solved by writing specific software modules. These include:

1. How to write a routine to control user interaction with the MINC-23.

2. How to write basic communication subroutines for transferring data between the MINC-23 and the Cyro 750 robot.

3. How to include special subroutines that may be used for detecting and transmitting individual handshaking logic signals for interface checkout.

4. How to run Cyro 750 control program from the console of the MINC-23 computer.

5. How to save and retrieve robot control programs on the MINC-23 flexible diskette file storage system.

6. How to test and exercise other features offered in the Advanced Robotics External Interface Specification but not specifically used or tested by the Ohio State vision system.

7. How to incorporate the above capabilities in a system software package which may be easily modified and expanded.

8. How to facilitate future modification of the system for operation under other real-time operating systems such as RSX-11M.

3.0 DESCRIPTION OF ROBOT INTERFACE

3.1 CYRO 750 HARDWARE INTERFACE:

Communication with the Advanced Robotics Cyro 750 robot is provided by the addition of a special feature to the basic robot control computer. This interface includes both hardware and software.

The hardware specification provided by the vendor is shown diagramatically in Figure 3.1. The initial installation will provide only one connector and the individual interface switches shown are not included. Actual communication with an external device is provided by the optional DRV-11 Parallel Interface Module with the logic signal definitions shown in Figure 3.2. Preliminary specifications of the pin connect- ions in the connector attached to the Cyro 750 are shown in Figure 3.3.

3.2 PARALLEL INTERFACE HANDSHAKING PROTOCOL:

The handshaking protocol defined by Advanced Robotics is as follows:

Output from Robot -

1. Write data to port.
2. Set CSR1 (Logic level CSR1 indicates data ready.)
3. Wait for REQA to be set. (Logic level REQA from external device indicates that it has accepted data.) If not set in 5 seconds, then exit to error recovery.
4. Clear CSR1.
5. Wait for REQA to be cleared. If not cleared in 500 milliseconds, then exit to error recovery.

Input to Robot -

The REQB signal line (Logic level from the external device is used to generate an interrupt to indicate that the information is available on the port.

1. If REQB is not set, then exit to error recovery.
2. Read data from port.
3. Set CSR0. (Indicates that data has been read.)
4. Wait for REQB to be cleared. If not cleared in 500 milliseconds, then exit to error recovery.
5. Clear CSR0.

The exit to error recovery comments in the above protocol cause program control to return to the mainline program where different consequences will occur depending on the source of the error. In some cases the robot software may attempt to re-transmit a message and in other cases an error message may

EXTERNAL DEVICE INTERFACE(S) HARDWARE STRUCTURE:

ENABLE/DISABLE SWITCHES ON ROBOT FRONT PANEL:

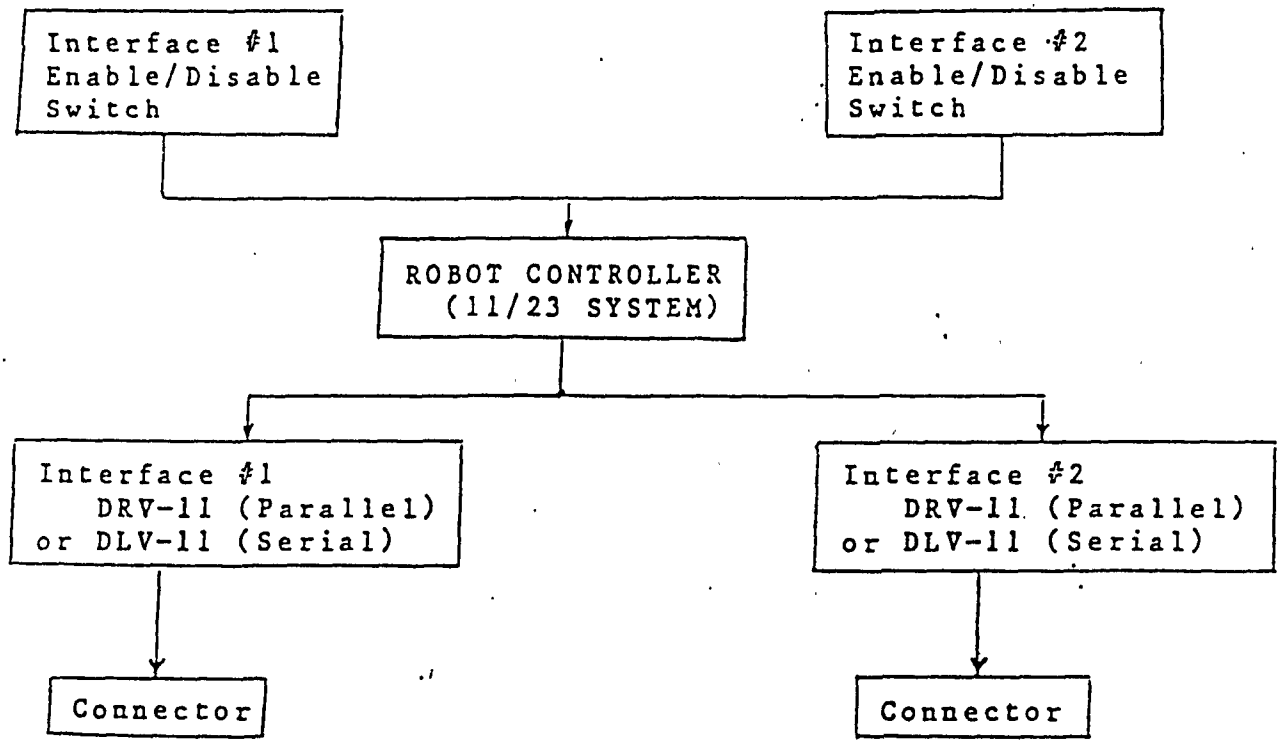

CONNECTORS LOCATED ON CONNECTOR PANEL

Figure 3.1 - External Device Interface Hardware

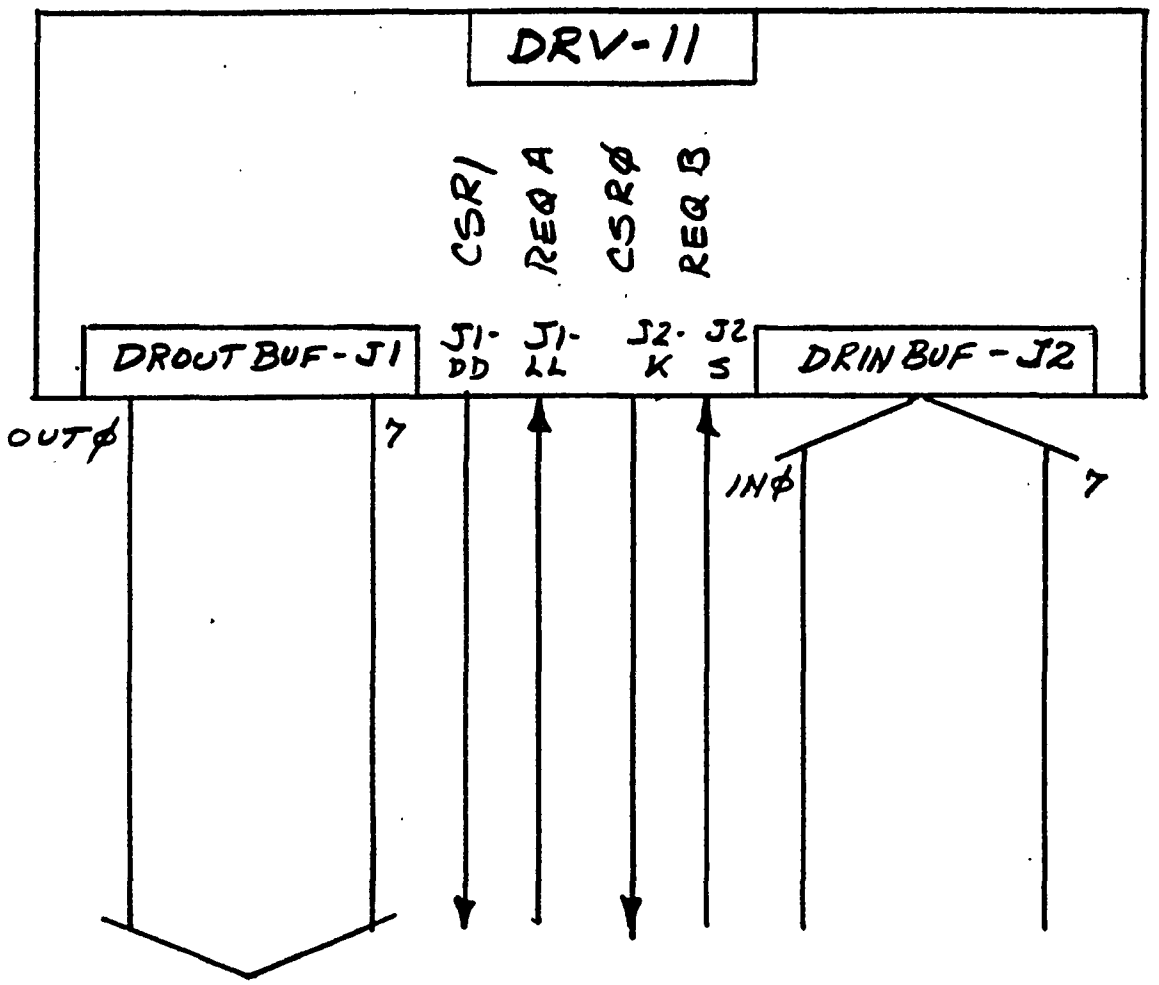

Figure 3.2 - DRV-11 Parallel Interface

PARALLEL INTERFACE

Pin #	Signal
2	IN07
4	IN06
6	IN05
8	IN04
10	IN03
12	IN02
14	IN01
16	IN00
18	NEW DATA READY
20	DATA TRANS
22	CSR1
24	CSR0
28	REQ B
30	REQ A
34	OUT07
36	OUT06
38	OUT05
40	OUT04
42	OUT02
44	OUT02
46	OUT01
48	OUT00

*Note - all odd pins are ground

Connector at Control Cabinet - combination mount Delta Ribbon Socket (3565 -1000).

Mating connector - 3M (3564 - 1001).

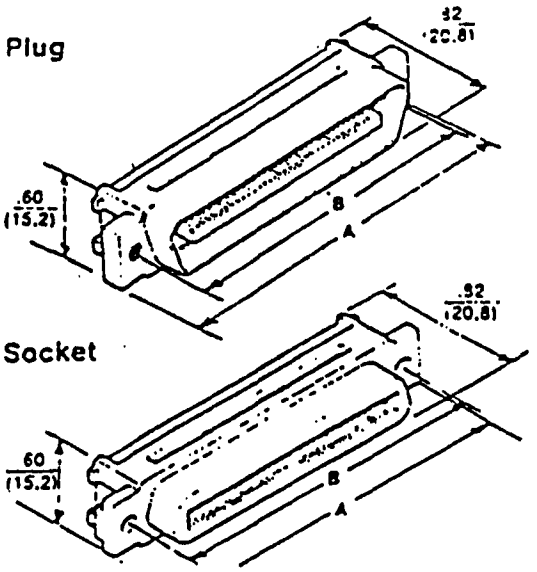

Figure 3.3 - Parallel Interface Connector

be displayed indicating that the external device is not ready to communicate with the robot.

A similar interface handshaking protocol could be written from the viewpoint of the MINC-23 computer. However, the MINC specification is merely the mirror image of the robot protocol so there is no real need to present it explicitly.

3.3 MESSAGE PROTOCOL:

Messages to and from the robot are transmitted as variable length sequences of 8-bit bytes. The entire message, along with several control bytes, is transmitted in a single burst. An acknowledge message is expected from the receiving device when the entire message has been received. Handshaking, as described in the previous section, is used to synchronize the transfer of individual bytes of data. A 100 millisecond timeout is established for the initial handshaking response from the receiver and a 1 millisecond timeout is established as the limiting waiting period for a handshaking signal between bytes of data. The following message protocol is quoted from the Advanced Robotics External Device Interface Specification:

> "Length - a byte of information is transmitted by the sender indicating the length of the type code and data portion of the message. The length of a message can range from 1 to 254 bytes.
>
> "Sequence number - a byte identifying each message. This number will be used to reference a particular message, for example, an error message may reference this number to indicate which error caused a message.
>
> "Type Code - a byte indicating the type of message that is being transmitted. This message is used to define the format of the data following, and is application dependent.
>
> "Data - 0 to 253 bytes of information that are application dependent. The number of data bytes plus the type code byte defines the length of the message.
>
> "Longitudinal Redundancy Check - a byte transmitted by the sender to verify that the type code and data were correctly received. This is a software computed check, and is unrelated to any hardware checks that may be performed. The LRC will be computer by exclusive or-ing the length with 'FF', then using the result to exclusive or with the sequence number, then using the result to exclusive or with the type code, then using the result to exclusive or with each byte of data.
>
> "The message will be complete when a byte is transmitted

by the receiver to acknowledge the correct or incorrect receipt of the message from the sender. If the LRC computed by the receiver matches the LRC sent by the sender, then the message was received correctly."

A response of 1 (binary) is transmitted by the receiver if the calculated LRC matches the received LRC. A response of 2 (binary) is returned if the LRC does not match.

3.4 MESSAGE TYPES:

Six message types are supported by the Advanced Robotics External Device Interface. These are described in detail in the APPENDIX. Data is transmitted in 8-bit bytes, however, some data represents 16-binary integers, while other data represents ASCII coded text messages. Where data represents a distance, the 16-bit integer is scaled to represent 1/128 inch (.0078) per bit. Angular information is scaled to represent 1/10th degree per bit. The message types specified in the Advanced Robotics External Device Specification (27 April 1984) are as follows:

"Messages from the robot to all devices

- Request Device Identification/Status - Type Code 1
- Program Status Mode - Type Code 2
- Welding Status Mode - Type Code 3
- Robot Positions - Type Code 4
- Special Message to Device - Type Code 5
- Error - Type Code 6
- Robot System Parameters - Type Code 7
- Device Modes - Type Code 8

"Messages from the Robot to Sensor Devices

- Sensor Set-up Parameters - Type Code 33
- Sensor Table Parameters - Type Code 34
- Sensor Position Definition - Type Code 35
- Sensor Diagnostic - Type Code 36
- Sensor Calibration - Type Code 37
- Search for seam - Type Code 38

"Messages from Robot to Computer Devices

- Load prog. from Computer Acknowledge- Type Code 65
- Save Program to Computer Acknowledge- Type Code 66
- Save Program to Computer - Type Code 67

"Messages from all Devices to the Robot

- Device Identification/Status - Type Code 129
- Set Program Mode - Type Code 130
- Set Welding Mode - Type Code 131
- Request Robot Positions - Type Code 132

- Special Message from Device - Type Code 133
- Error - Type Code 134
- Jog - Type Code 135
- Stop Jog - Type Code 136
- Move Robot - Type Code 137
- Request Robot System Parameters - Type Code 138

"Messages from Sensor Device to Robot

- Override Data - Type Code 161
- In Position Command - Type Code 162

"Messages from Computer Devices to the Robot

- Request Save Program to Computer - Type Code 193
- Request Load Program from Computer - Type Code 194
- Load Program from Computer - Type Code 195"

4.0 DESCRIPTION OF MINC-23 INTERFACE

4.0 MINC INTERFACE MODULES:

Digital communication with the MINC-23 computer is relatively straightforward. It is accomplished using standard MINC digital input modules referred to as MNCDI's and MINC digital output modules known as MNCDO's. Up to a maximum of eight of either type may be incorporated into a system. The system referred to as the "External Computer" for the Advanced Robotics system, includes two MNCDI's and two MNCDO's. Each MNCDO or MNCDI includes 16 output or 16 input lines, respectively, plus connections for strobe and reply logic signals. Figure 4.1 shows the connector blocks for the MINC digital input and output module along with notes that identify the logic signals that may be used to synchronize communication with various peripheral devices.

4.2 THE MINC-ROBOT INTERFACE:

The communication link between the MINC computer and the Advanced Robotics External Device Interface is shown in Figure 4.2. The MNCDO's and MNCDI's were determined to be suitable for communication with the robot rather than installing an additional Digital Equipment Corporation DRV11 module which would perform essentially the same function. A second pair of digital interface modules is available to perform additional communication duties such as relaying data back and forth between the MINC and an Ohio State University welding seam-tracking system that will be attached to the same robot.

The interface shown in Figure 4.2 includes some features that should be described. Although the MNCDO and MNCDI modules include logic signals for handshaking, it was determined that these inputs and outputs were designed for short-duration pulse signals rather than logic levels that remain set until answered or cleared under program control. Based on the Advanced Robotics External Interface Specification it was decided to use the circuit shown in Figure 4.2 rather than attempt to use the pulse handshaking signals which could be of such a short duration that proper sychronization between the robot and MINC would not be possible. (This problem may be explored further once the External Interface hardware and soft ware is installed in the Advanced Robotics robot controller; however, there appears to be little reason for using the regular pulse handshaking inputs rather than the configuration chosen here.)

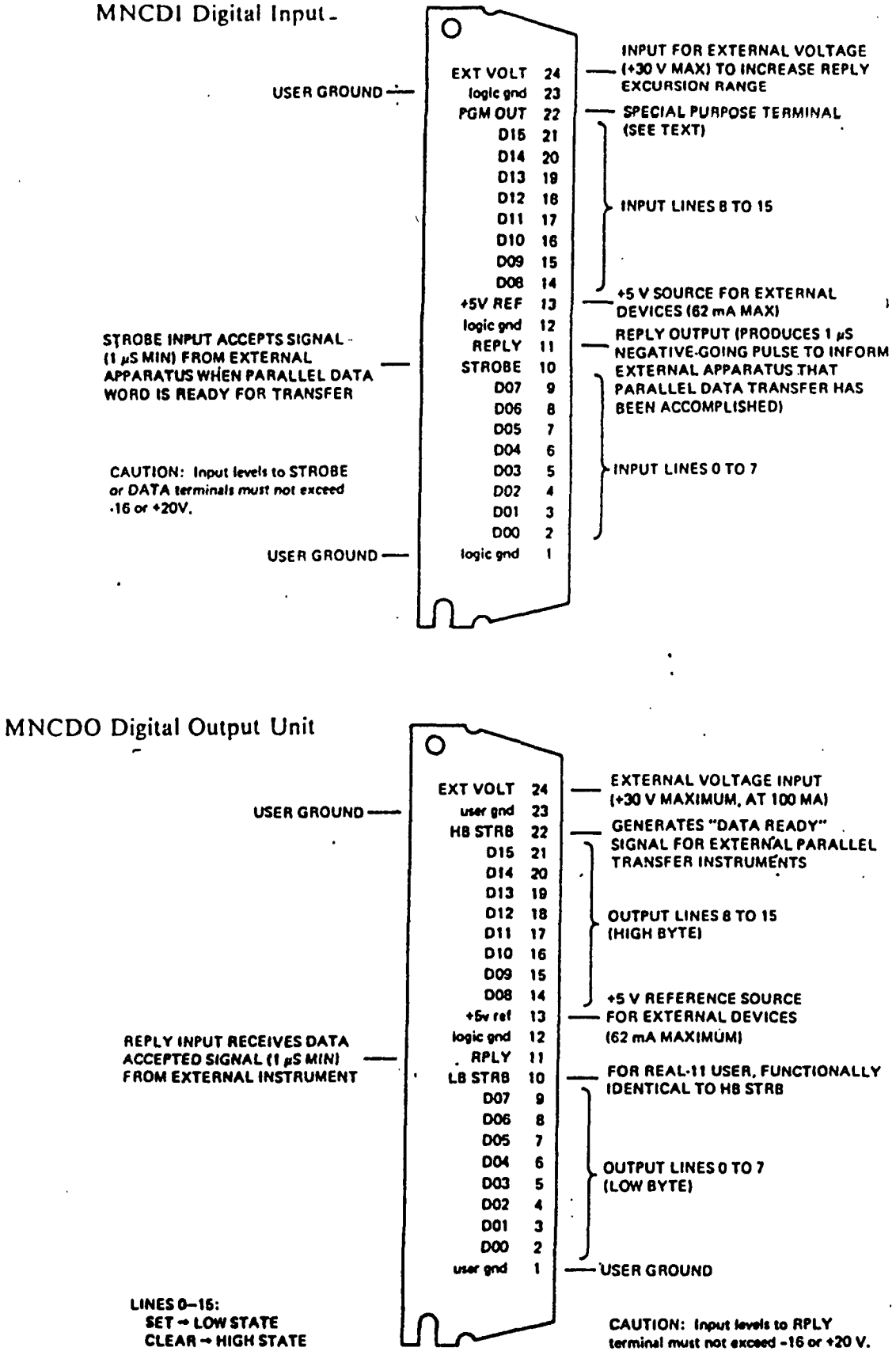

Figure 4.1 - MINC Digital I/O Terminal Blocks

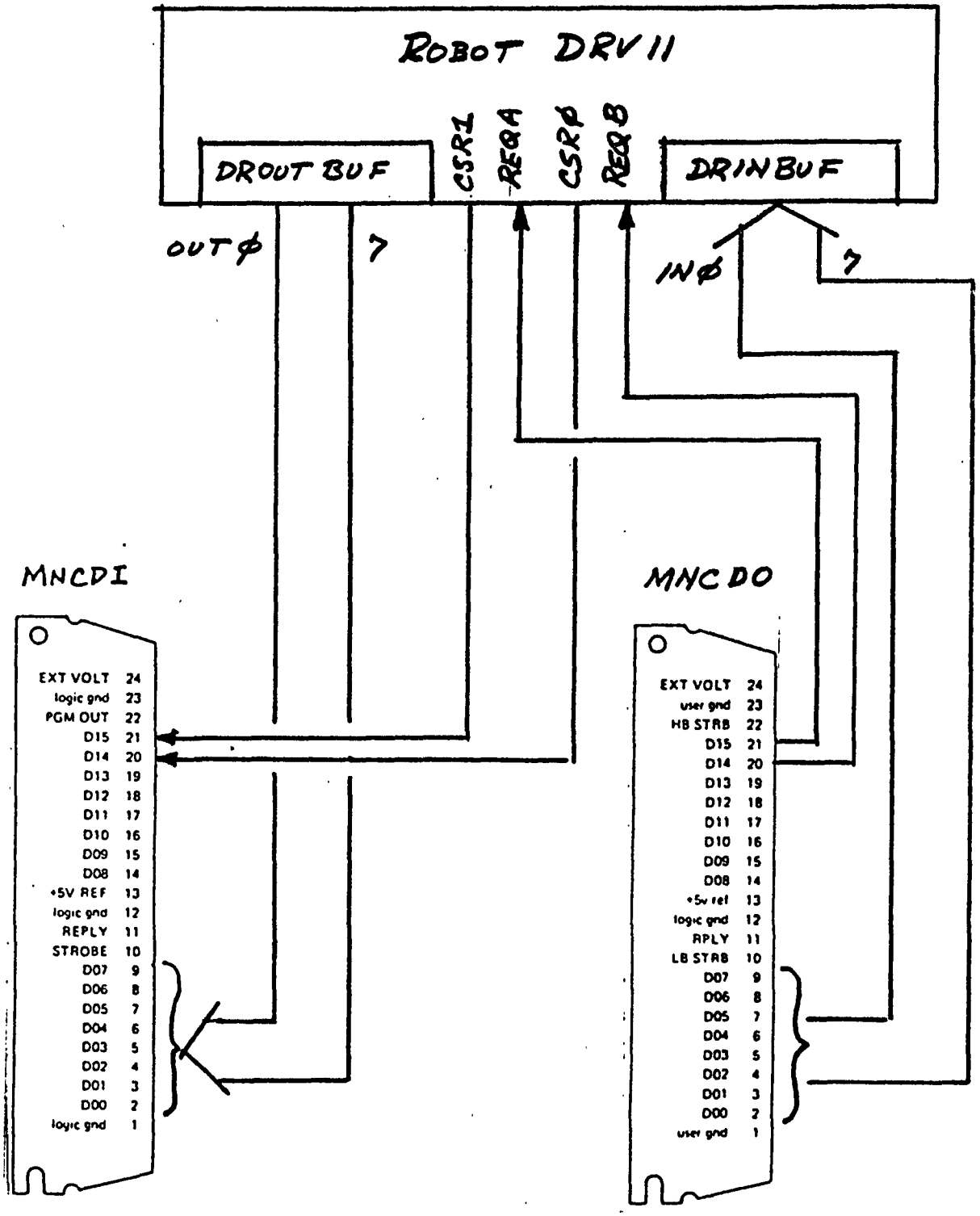

Figure 4.2 - MINC/Robot Interface Connections

The interface connections shown in Figure 4.2 utilize the high-order two bits of the digital input and digital output modules for handshaking. Since only 8-bit bytes are transferred back and forth between the two devices, the high-order 8 bits of both the input and output modules are unused for data transfer and may be used for handshaking purposes.

The software described below was designed to function in a simple polling mode; however, the MNCDI and MNCDO modules make provision for hardware interrupts. An interrupt signal may be obtained either from the pulse logic handshaking inputs or from the high order two bits on the MINC digital input module. This choice is controlled using software to appropriately set a hardware control/status register in the interface module. (Relatively slight modification is required to change the communications software from a polling configuration to an interrupt-driven system. This may be more desirable should the software be modified for applications other than the interface check-out function described in this report.)

5.0 INTERFACE TEST HARDWARE

5.1 INPUT-OUTPUT TEST REGISTERS:

Since the CYRO 750 robot interface hardware described in this report was not available for test purposes while the software was being written, it was deemed desriable to test proper handshaking and data transfer using a temporary breadboard interface. The circuit constructed for this purpose is shown in Figure 5.1. A single 8-bit dual inline switch is used to control six low order bits for data input and the two high-order switches are used to control the high-order input bits for handshaking. Unused input connections are wired to ground to simulate "zero" input levels on those input signals. A ten-bit light-emitting diode (LED) package enables one to observe all eight data output bits plus the two output handshaking signals.

The communications software described in the next section is tested by manipulating the switches in the proper order to simulate the signals transmitted by the robot to the MINC. Data and handshaking logic levels transmitted by the MINC are observed using the LED register.

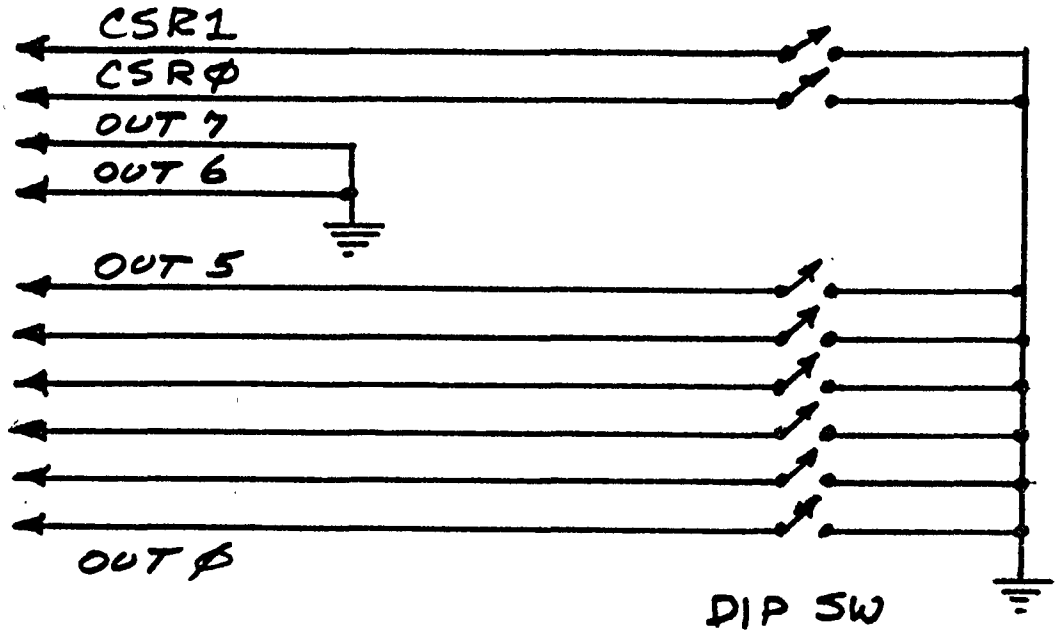

SIMULATED ROBOT OUTPUT REGISTER

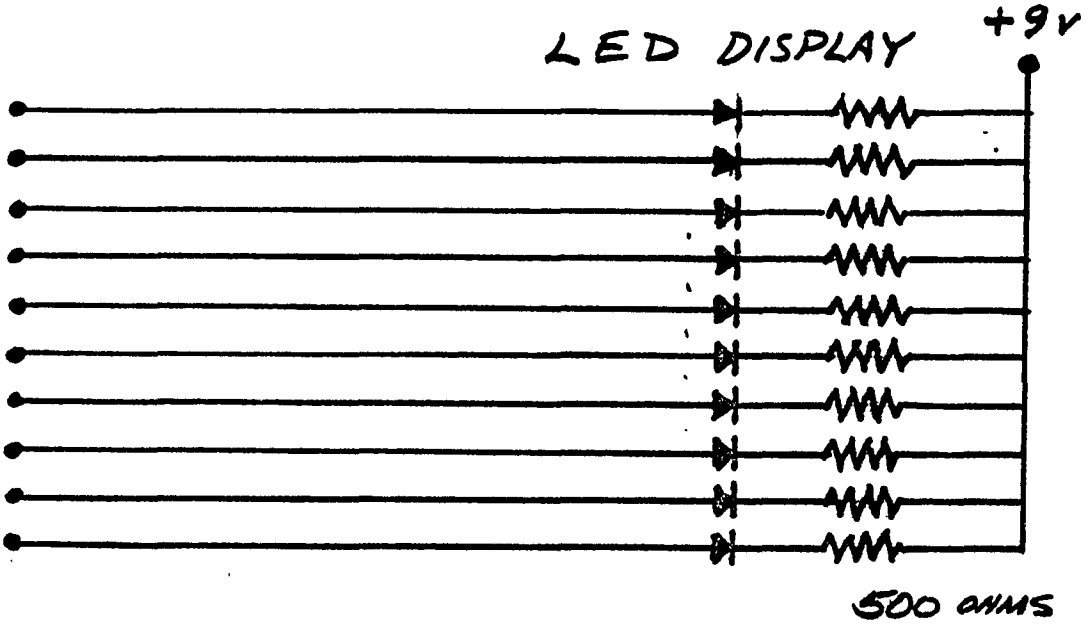

SIMULATED ROBOT INPUT REGISTER

Figure 5.1 - Robot Breadboard Simulated Interface

6.0 SOFTWARE DESCRIPTION

6.1 OVERALL DESIGN:

The software system for MINC-robot communication and checkout is called CYRO1. It is a menu driven, modular system that allows a user to communicate with the robot in three different modes:

1. Transmit and receive individual data bytes and flags.
2. Transmit and receive arrays of data prepared or displayed in Hexadecimal format.
3. Transmit and receive standard messages as defined in the Advanced Robotics External Device Interface Specification.

Control of the CYRO1 system is achieved by selecting functions by number from the following main menu that is displayed when the program is loaded:

1. MOVE robot.
2. Request robot POSITION.
3. Request robot system PARAMETERS.
4. Send IN-POSITION command.
6. SAVE program from robot.
7. LOAD program to robot.
8. RUN a program.
9. Send a MESSAGE to the robot console.
10. Single WORD I/O.
11. RECEIVE an array.
12. TRANSMIT an array.

"E" EXIT to the operating system.

Only the number and a carriage return is typed for menu selection, although additional parameters or data may be requested when the program branches to the appropriate subroutine.

Routines that interact directly with the MINC digital input and digital output interfaces are written in assembly language. In particular assembler routines DOUT and DINP permit the user to output or input a single 16-bit value to or from the MINC digital I/O modules. The transfer is a "jam" transfer to or from the I/O hardware and the subroutines perform no error chacking. Data to be handled by DINP and DOUT are manipulated by FORTRAN calling routines that handle terminal input and output and perform any required conversions between Hexadecimal and binary formats.

SEND and RECEVE (spelled as shown) are two assembler subroutines that transmit or receive complete arrays of data that are manipulated by calling FORTRAN routines. The two subroutines called SNDBYT and GETBYT could be referred to as device handlers since they handle the actual input and output

and take care of the appropriate handshaking protocol described in section 3.2 of this report. SEND and RECEVE transmit complete arrays of data and receive or return appropriate single-byte acknowledge messages.

SNDBYT and GETBYT are the only message-handling subroutines that directly affect or are affected by interface hardware. At the present time, polling techniques are used to synchronize input/output operations with handshaking flags. The system could be converted to an interrupt-driven environment by merely altering these two rather simple device handlers.

Most of the rest of the CYRO1 software package consist of a set of FORTRAN subroutines that merely prepare or accept various messages that are moved into or out of a 257 word integer array that is, in turn, processed by subroutines SEND or RECEVE that handle the actual I/O as described above.

Software listings and detailed documentation for each routine is included in the APPENDIX.

6.2 SINGLE-WORD I/O MODE

At the most basic level of operation, a user of CYRO1 can examine individual bits that are transmitted to the MINC digital input interface. This mode of operation allows one to examine flag bits and, in general, step through a basic handshaking protocol to determine whether the robot interface is functioning as described in the specifications. Single bits may be set in the output register for similar debugging purposes.

Once the general behavior of the communication link has been determined, the next level of operation at the message level may be tried. Any arbitrary message may be generated or accepted using the array handling options. All data I/O is in HEX, therefore any array of bit patterns may be created for test purposes. The complete array is transmitted or received as a message.

A selected group of messages may be chosen from the main Menu. In general, the message-handling provided in the menu is to test a number of External Device Interface functions that are either important for off-line program manipulation or will not otherwise be tested using other hardware such as the Ohio State seam-tracking system.

6.3 ASSEMBLER COMMUNICATION ROUTINES:

Four assembly language communication routines are used for passing messages between the MINC computer and the Cyro 750 robot. SNDBYT accepts a single byte from the calling program as a parameter in hardware register R0. The subroutine, after optionally masking the data, outputs the data to the digital output hardware by merely implementing the handshaking protocol described in section 3.2. GETBYT, in a similar fashion, accepts a single word from the digital input module and returns the word to the calling program in register R0. A mask parameter permits one to eliminate any desired bits from the input word.

While each I/O data transfer is handled by SNDBYT and GETBYT, the subroutines SEND and RECEVE manipulate entire arrays of data passed to or from calling programs and calculate Longitudinal Redundancy Check bytes that are used for insuring that messages are not corrupted during transmission. SEND and RECEVE are also responsible for measuring timeout periods, and sending appropriate error codes to the calling program or over the communication link. SEND does not release control until an acknowledge byte is returned from the robot or a 5-second timeout period passes without response. RECEVE is responsible for checking for LRC errors and returning the appropriate acknowledge byte to the robot before returning control to the calling program.

6.4 MESSAGE HANDLING IN FORTRAN:

All messages generated by the basic checkout routines in CYRO1 are created by the FORTRAN subroutines MOVE, POSIT, PARS, INPOS, SAVE, LOAD, RUN, and MESAGE. The names obviously indicate the correlation between the subroutines and the main menu. These routines merely use terminal I/O for user interaction and generate messages that are passed to and from the assembler routines in the 257 word integer array IDATA. FORTRAN subroutines that fill the IDATA for message transmission do not calculate the checksum. The checksum is calculated by the subroutine SEND and placed at the end of the array prior to message transmission.

The FORTRAN routines listed above also process error codes received from SEND and RECEVE. Appropriate error messages are displayed on the MINC CRT display to aid in debugging problems. Data received from the robot is formatted and displayed by the FORTRAN subroutines.

Several FORTRAN utility subroutines are included for data conversion required for some displays or keyboard data input. HEXIN accepts 16-bit integers from the MINC keyboard and converts them to simple binary integers. Subroutine ATOI converts the ASCII value of an input HEX integer to the

corresponding binary integer. HEXOUT performs corresponding conversion duties when data is displayed in HEX. Subroutine CNVDIG accepts the binary representation of the HEX digits to be displayed and converts them to the corresponding ASCII codes for transmission to the CRT display.

7.0 CONCLUSIONS AND RECOMMENDATIONS

7.1 GENERAL CONCLUSIONS:

The software described in this report is a prototype system for interfacing a general-purpose digital computer and a robot. The routines were designed to provide a general communications capability as well as test a number of specific robot control features described in the Advanced Robotics External Device Interface Specification. Each of the routines in the software package have been tested using a breadboard simulation of the robot interface since the hardware to actually attach the MINC to the Advanced Robotics Cyro 750 robot has not been installed by the vendor. The software described in this report has been written based entirely on the written interface specification and partially tested using a breadboard simulated interface.

The simulated interface makes it possible to transmit test data to the MINC computer using a manually set external register and also to visually display data being transfered out of the MINC computer. All routines have been tested using the simulated interface and the appropriate sequence of output signals were displayed and the routines responded appropriately when the proper sequence of input signals were received. Further debugging will require the actual hardware interface. Should problems occur during the actual checkout procedure, The single-word I/O routines (menu select item 10) will make it possible to examine individual data and control lines to locate any possible incorrect circuitry.

7.2 RECOMMENDATIONS:

Recommendations fall into to two categories: (1) Software checkout and (2) Future Development:

Software Checkout - Two steps are required before the software can be checked out by actually communicating with the Cyro 750 robot. First, the hardware interface must be physically installed in the robot controller. A plug will be installed on the control panel for external connections. Advanced Robotics will diverge from the 27 April 1984 since two separate plugs and enable/disable switches will not be installed. Second, a cable must be assembled to mate the robot interface plug with the MINC digital input and digital output connector blocks. Software checkout may then proceed.

It is recommended that the single-word input command be used to examine the individual signals being sent to the MINC computer when a robot transmits data on the external interface. A "Device Identification/Status" request (Type code 1) would activate output lines from the robot to the MINC. If the appropriate signal lines appear to be active, select menu selection 11 to "Receive an array." The complete message from the robot should be transferred with proper handshaking and the message in HEX will appear on the MINC CRT display. A satisfactory exit from this function will demonstrate partial reverse communication since an acknowledge byte must be transmitted to the robot and the robot control software should respond appropriately.

Once message communication has been established from the robot to the MINC, the reverse communication path may be tested by selecting a menu item such as menu selection 9 to send an ASCII message to the robot CRT display. The more complicated functions of the checkout software package may be checked once two-way communications has been demonstrated using the least complicated routines such as those mentioned above.

Future Development - The software system described in this report provides a basic system for testing MINC-robot communication. In addition, this basic software package provides useful operational software since programs can be saved from and loaded to the robot. Once loaded, programs can be executed from the MINC console and operational data can be obtained from the robot. At this point it will be possible to determine the feasiblility of obtaining robot positional data while the robot controller is actually in the process of executing a weld, for example.

The outcome of several experiments using this software package will guide future software development. Additional development falls into three categories:

1. To develop new operational features.
2. To incorporate the MINC computer in on-line control of the robot.
3. To establish the desirability and possibly convert the software to operate in an interrupt-driven mode.
4. To investigate and possibly convert the system to function under another operating system such as RSX-11M.

A number of new operational features could be easily incorporated in this checkout package. For example, off-line printing of the robot numerical control programs would be a natural extension of the program SAVE feature. Off-line program preparation and editing using the full-screen editor available on the MINC system would greatly facilitate program

preparation and modification. With some more additions the MINC system could be used to communicate with other computers and obtain dimensional information regarding parts to be welded and, with appreciable additional work, produce numerical control programs directly from computer stored drawings of the parts to be welded.

The second area of possible future system expansion would be to place the MINC within the control loop between the Ohio State University seam-tracking system. Control information could be passed through the MINC computer with a delay in the microsecond range. This would permit the MINC to either monitor corrections applied to a seam-tracking weld application or, alternatively, interpose requests for position information from the robot regarding the "true" or corrected seam path. Using this information, "fill" passes of the weld seam could be accomplished using new information rather than by applying corrections to the original penetratration pass N/C program. It is possible that fill passes will not be able to use the same visual seam-tracking algorithm that is incorporated in the Ohio State system for correcting the penetration pass.

The current MINC-robot communications system does not operate in an interrupt driven mode since only one process is executed at a time in the test mode. It is unclear whether there is any advantage in developing a system that can handle multiple processes with the attendant overhead that is incurred to service interrupts. The MINC computer is unlikely to be used for entirely independent processes, such as program development, while it is being used on-line with the robot. N/C program development will probably be handled when the system being used for automatic welding.

The most demanding environment will be when the MINC is handling simultaneous communication with the robot, the vision seam-tracking system, and possibly with off-line computers that process dimension information regarding parts that are to be welded. It is likely that the robot control system will provide the most serious constraint on the ability to control robot joint servo motors and simultaneously transmit joint position information to the MINC for multi-pass welding. Under such a circumstance the MINC may be installed within the control loop to either pick up correction information being passed to the robot from the vision system or interrogate the robot for position information between periods when data is being passed to the robot by the vision system. In either case it may be desirable to handle the communication and data collection as a single process to eliminate the overhead due to servicing interrupts. There may be no clear reason for separating the tasks that must be accomplished into several asynchronous processes. For example, data from the vision

system could be passed on to the robot and simultaneously stored in a buffer in the MINC by merely echoing incoming data on the outgoing line to the robot and then save the data in a buffer. The complete sequence of operations could probably be handled in a shorter period of time than would be required to service interrupts to switch between separate processes. Should the timing requirements be less stringent, one might find a conversion to a interrupt driven process would facilitate concomitant file manipulation. The final answers to the questions raised here will require further study and possibly experimental data obtained using the existing programs to interrogate the robot while N/C programs are being processed.

A final area for further investigation is in regard to the operating system to be used. The system provided with the MINC-23 is RT-11. This is basically a single-job or, at best, a background-foreground system with interrupt processing capability. The MINC-23 could be operated using the RSX-11M operating system which provides a much more sophisticated multiprocess operating system. A conversion to RSX-11 may involve more considerations than merely the desire to use a more sophisticated operating system. For example, support by other laboratories at NASA may be easier to obtain if the system operates under RSX-11 since the more advanced operating system is currently in use at other installations at the Marshall Flight Center. On the other hand, greater flexibility usually entails slower response times when servicing interrupts. Again the optimum choice is not clearly evident and further study and perhaps experimentation would be required to provide a final decision. The conclusion to this final question will undoubtedly require the interaction of this laboratory with other NASA laboratories.

APPENDIX

SOFTWARE LISTINGS

PROGRAM:	DESCRIPTION:
CYRO1	- Mainline FORTRAN program with menu.
SEND	- Primary communication Subprogram in Assembler.
RECEVE	- Primary communication Subprogram in Assembler.
SNDBYT	- Assembler output message handler.
GETBYT	- Assembler input message handler.
DINP	- Single word input handler in Assembler.
DOUT	- Single word output handler in Assembler.
INIT	- Fortran subr. to initialize Robot-MINC communications.
MOVE	- Fortran subroutine to move robot to a position.
POSIT	- Fortran subroutine to request robot position.
PARS	- Fortran subr. to request robot system parameters.
INPOS	- Fortran subr. to transmit "in-position" message.
SAVE	- Fortran subr. to save a robot program.
LOAD	- Fortran subr. to load a program from disk into robot.
RUN	- Fortran subr. to start execution of robot program.
MESAGE	- Fortran subr. to send message to robot console.
DEBUG	- Fortran subr. that controls single-word I/O.
ACCEPT	- Fortran subr. to display message from RECEVE.
TRNSMT	- Fortran subr. to prepare message for SEND.
HEXOUT	- Fortran utility to display byte in HEX.
HEXIN	- Fortran utility to accept byte in HEX.
DHEXIN	- Fortran utility to display integer in HEX.
DHEXIN	- Fortran utility to accept integer in HEX.
ATOI	- Fortran utility to convert ASCII to integer digits.
CNVDIG	- Fortran utility to convert integer digits to ASCII.

```
C*************************************************************************
C
      PROGRAM CYRO1
C
C     MAINLINE PROGRAM AND STUBS FOR TESTING ADVANCED ROBOTICS
C     EXTERNAL DEVICE INTERFACE OPTION
C
C     FRED R. SIAS, JR.
C     NASA/ASEE SUMMER FACULTY FELLOW FROM CLEMSON UNIVERSITY
C
C     18 MAY 1984
C
C*************************************************************************
C
C     This is the mainline program for a system that may be used to
C     communicate with the Advanced Robotics CYRO 750 Robot.
C
C     The main selection menu allows one to select one of the following
C     features:
C
C      CYRO 750 EXTERNAL DEVICE INTERFACE TEST MENU:
C
C            1.  MOVE Robot
C            2.  Request Robot POSITION
C            3.  Request Robot System PARAMETERS
C            4.  Send IN-POSITION command
C            5.  INITIALIZE System. (Reset Robot!)
C            6.  Get program from robot and SAVE
C            7.  LOAD program and verify
C            8.  RUN a program
C            9.  Send MESSAGE to robot console
C            10. Single WORD I/O
C            11. RECEIVE an array
C            12. TRANSMIT an array
C            "E" EXIT to the operating system
C
C
C     SELECT>
C
C*************************************************************************
```

```
C
C       DECLARATIONS
C
        INTEGER*2 IDATA(257),INPUT, RT, WT
        REAL X
C
C       INITIALIZATION
C
        WT=7
        RT=5
C
        WRITE (WT,100)
100     FORMAT('1',/////,
     1          '                          MANUAL CHECKOUT ROUTINE FOR',/,
     2          '                       CYRO 750 EXTERNAL DEVICE INTERFACE',///,
     3          '                              F. R. SIAS, JR.',//,
     4          '                        NASA/ASEE - CLEMSON UNIVERSITY',/,
     5          '                                  JUNE 1984',//////////,
     6          ' TO CONTINUE PRESS RETURN>'$)
C
        READ  (RT,110) X
110     FORMAT(G6.0)
C
        WRITE(WT,200)
200     FORMAT('1',//////,
     1  ' Select test mode by item number in the following menu.',/,
     2  ' Then provide requested parameters.',//,
     3  ' YOU MUST TURN ON THE MINC COMPUTER AND EXECUTE THE',/,
     4  ' INITIALIZATION PROGRAM (MENU SELECTION 5) BEFORE THE',/,
     5  ' ROBOT WILL RESPOND TO OTHER COMMANDS!  RESET THE ROBOT',/,
     6  ' AFTER MENU ITEM 5 HAS BEEN SELECTED.',//,
     7  ' Use "return" or "enter"',/,
     3  ' to terminate each entry parameter or to advance to the next',/,
     4  ' whenever the following is displayed:',//////,
     5  ' SELECT >',$)
C
        READ (RT,110) X
C
C       MAIN SELECTION MENU
C
300     CONTINUE
C
        WRITE (WT,310)
310     FORMAT('1',/////,
     1  ' CYRO 750 EXTERNAL DEVICE INTERFACE TEST MENU:',//,
     2  '       1.  MOVE Robot',/,
     3  '       2.  Request Robot POSITION',/,
     4  '       3.  Request Robot System PARAMETERS',/,
     5  '       4.  Send IN-POSITION  command',/,
     6  '       5.  INITIALIZE System. (Reset Robot.)',/,
     7  '       6.  Get a program from robot and SAVE',/,
     8  '       7.  LOAD program and verify',/,
     9  '       8.  RUN program',/,
     1  '       9.  SEND message to robot console',/,
```

```
     1   '        10. Single WORD I/O',/,
     2   '        11. RECEIVE an array',/,
     3   '        12. TRANSMIT an array',//,
     2   '        "E" EXIT TO OPERATING SYSTEM',////,
     3   ' SELECT>',$)
C
         READ  (RT,400) INPUT
400      FORMAT(A2)
C
         IF (INPUT.EQ.'1')  CALL MOVE
         IF (INPUT.EQ.'2')  CALL POSIT
         IF (INPUT.EQ.'3')  CALL PARS
         IF (INPUT.EQ.'4')  CALL INPOS
         IF (INPUT.EQ.'5')  CALL INIT
         IF (INPUT.EQ.'6')  CALL SAVE
         IF (INPUT.EQ.'7')  CALL LOAD
         IF (INPUT.EQ.'8')  CALL RUN
         IF (INPUT.EQ.'9')  CALL MESAGE
         IF (INPUT.EQ.'10') CALL DEBUG
         IF (INPUT.EQ.'11') CALL ACCEPT
         IF (INPUT.EQ.'12') CALL TRNSMT
         IF (INPUT.EQ.'E') STOP
C
         GOTO 300
C
         END
```

```
;-----------------------------------------------------------------------
;
;FILENAME SEND.MAC
;
        .TITLE SEND
        .GLOBL SEND
        .GLOBL SNDBYT
;
;       FRED R. SIAS, JR.
;       21 JUNE 1984
;       REVISED 6 JULY 1984
;
;SUBROUTINE TO SEND A MESSAGE OF VARIABLE LENGTH TO ROBOT AND
;THEN WAIT FOR A RETURN MESSAGE FROM THE ROBOT CONFIRMING THAT THE
;ORIGINAL MESSAGE WAS TRANSMITTED WITHOUT A CHECKSUM ERROR.
;
;THIS ROUTINE IS NOT INTERRUPT DRIVEN BUT IT COULD BE ALTERED.
;
;MESSAGE SUPPLIED IN ARRAY IDATA
;
;CALLING SEQUENCE: CALL SEND(IERROR,ILEN,IDATA)
;                        WHERE IDATA IS A 257 WORD ARRAY
;                        ILEN IS ACTUAL LENGTH OF DATA
;                        IERROR IS AN ERROR CODE RETURNED BY SUBR.
;
;ERROR CODES RETURNED:   0 = NORMAL EXIT
;                        1 = TIMEOUT ERROR
;                        2 = LRC ERROR RECEIVED FROM ROBOT
;
;
;       THIS ROUTINE CHANGES R0,R1,R2,R3,R4,R5
;
        DIR=171162
        DOR=171262
        REQA=100000
        REQB=040000
        CSR1=100000
        CSR0=040000
;
        JSW = 44
        .MCALL  .TTYOUT
;
;               DOR = DIGITAL OUTPUT REGISTER ADDR.
;               DIR = DIGITAL INPUT REGISTER ADDR.
;       USED WHEN TRANSMITTING TO ROBOT:
;               REQB = MASK TO TRANSMIT A REQUEST FOR SERVICE TO ROBOT
;               CSR0 = MASK TO CHECK FOR ACKNOWLEDGE FROM ROBOT
;       USED WHEN RECEIVING MESSAGE FROM ROBOT:
;               CSR1 = MASK TO CHECK FOR REQUEST FOR SERVICE FROM ROBOT
;               REQA = MASK TO ACKNOWLEDGE REQUEST FOR SERVICE FROM ROBOT
;
;-----------------------------------------------------------------------
```

```
;APPLICATION OF SUBROUTINE "SEND":
;
;       SUBROUTINE SEND IS NOT INTERRUPT DRIVEN BUT IS CALLED WHENEVER
;       COMMUNICATION WITH THE ROBOT IS DESIRED.  IT IS TO BE USED IN A
;       TEST MODE WHEN MULTIPLE PROCESSES ARE NOT APPLICABLE.  THE ROUTINE
;       SHOULD BE MODIFIED IF AN INTERRUPT-DRIVEN SYSTEM IS REQUIRED.
;
;       THIS ROUTINE IS CALLED WHENEVER A MESSAGE TO BE TRANSMITTED TO THE
;       ROBOT HAS BEEN PLACED IN THE LOW-ORDER BYTES OF THE ARRAY IDATA.
;       THE ARRAY MAY BE OF ANY LENGTH WITH THAT LENGTH INDICATED BY THE
;       COUNT IN THE FIRST ARRAY ELEMENT.
;       THE CHECKSUM IS NOT PROVIDED BY THE CALLING ROUTINE.
;       THE CONTENTS OF THE ARRAY ARE AS SPECIFIED BY THE ADVANCED ROBOTICS
;       CORPORATION "EXTERNAL DEVICE INTERFACE" SPECIFICATIONS.
;
;       THE "ILEN" PARAMETER TRANSMITTED TO THE SUBROUTINE INDICATES THE
;       NUMBER OF ELEMENTS IN "IRRAY" THAT CONTAIN DATA.  THIS IS TWO GREATER
;       THAN THE DATA IN THE FIRST ELEMENT OF THE ARRAY WHICH INDICATES THE
;       MESSAGE LENGTH AND DOES NOT INCLUDE THE BYTES INDICATING THE LENGTH,
;       SEQUENCE NUMBER, AND LONGITUDINAL REDUNDANCY CHECK BYTE.
;
;       THIS SUBROUTINE SCANS THE ARRAY AND CALCULATES THE LRC BYTE, PLACES
;       THIS BYTE IN THE NEXT ELEMENT OF THE ARRAY, AND INCREMENTS ILEN BY
;       ONE SO THAT THIS NEW NUMBER MAY BE USED AS A COUNTER TO OUTPUT THE
;       COMPLETE ARRAY INCLUDING THE CHECKSUM.
;
;       FOLLOWING TRANSMISSION OF THE COMPLETE ARRAY USING THE "SNDBYT"
;       SUBROUTINE, THIS SUBROUTINE ENTERS A LOOP TO WAIT FOR A BYTE OF
;       DATA FROM THE ROBOT THAT INDICATES WHETHER OR NOT THE DATA WAS
;       RECEIVED CORRECTLY BASED ON THE TRANSMITTED LRC BYTE AND THE LRC
;       BYTE CALCULATED BY THE RECEIVING ROUTINE IN THE ROBOT.
;       A ONE (1) INDICATES SUCCESSFUL DATA RECEPTION AND A TWO (2)
;       INDICATES A CHECKSUM ERROR.  APPROPRIATE CODES ARE RETURNED
;       TO THE CALLING PROGRAM IN IERROR.
;
;       IN ADDITION, THIS ROUTINE WAITS FOR THE CONFIRMATION BYTE ONLY
;       FOR FIVE (5) SECONDS.  IF A CONFIRMATION BYTE IS NOT RECIEVED WITHIN
;       THIS TIME PERIOD, A TIMEOUT ERROR CODE (1) IS RETURNED IN IERROR.
;
;       MESSAGE RETRANSMISSION OR OTHER ERROR-HANDLING IS PERFORMED BY THE
;       CALLING ROUTINE.
;
;-------------------------------------------------------------------------
```

```
SEND:   TST     (R5)+           ;SKIP PARAMETER COUNT
        MOV     R5,-(SP)        ;SAVE POINTER TO ERRCODE PAR ON STACK
        TST     (R5)+           ;SKIP ERROR CODE
        MOV     @(R5)+,R3       ;PUT ARRAY LENGTH IN COUNTER R3
;                               ;ARRAY DOES NOT YET CONTAIN CHECKSUM
;                               ;R5 NOW POINTS TO ADDRESS OF ARRAY
        MOV     R3,R4           ;ALSO MAKE COUNTER IN R4
        MOV     (R5),R1         ;PUT ADDRESS OF ARRAY IN R1
        MOV     #377,R2         ;SET LRC BYTE TO ALL 1'S
LOOP6:  MOV     (R1)+,R0        ;GET A BYTE FROM ARRAY
        XOR     R0,R2           ;CALULATING CHECKSUM
        DEC     R4              ;COUNT NUMBER OF ELEMENTS
        BNE     LOOP6           ;KEEP CALCULATING CHECKSUM
        MOV     R2,(R1)         ;PUT CHECKSUM AT END OF ARRAY
        ADD     #01,R3          ;INCREASE ARRAY LENGTH BY ONE
        MOV     (R5),R1         ;AGAIN PUT ADDR. OF ARRAY IN R1
LOOP7:  MOV     (R1)+,R0        ;GET A BYTE FROM ARRAY
        CALL    SNDBYT          ;TRANSMIT BYTE WITH HANDSHAKING
        BR      TMERR           ;GO TO TIMEOUT ERROR HANDLING
        .TTYOUT #103            ;DISPLAY A "C"
        DEC     R3              ;STEP THRU ARRAY
        BNE     LOOP7           ;KEEP OUTPUTTING BYTES
        MOV     (SP)+,R4        ;GET ERRCODE POINTER FROM STACK
        MOV     #0,@(R4)        ;SET ERROR CODE TO ZERO TO SHOW OK
;
;NOW WAIT FOR CONFIRMATION BYTE FROM ROBOT
;USE R3 WHICH CONTAINS ZERO (0) FOR A COUNTER
;SET R5 FOR LOOP COUNT MULTIPLIER SINCE R5 NOT NEEDED ANY MORE.
;
        MOV     #10,R5          ;MULTIPLIER FOR LOOP COUNT
LOOP8:  BIT     #CSR1,@#DIR     ;LOOK FOR ROBOT REQUEST TO SEND
        BNE     GETCFM          ;BRANCH IF REQUEST FOUND
        DEC     R3              ;OTHERWISE COUNT DOWN
        BNE     LOOP8           ;KEEP LOOPING UNTIL ZERO
        DEC     R5              ;DECREMENT OUTSIDE LOOP
        BNE     LOOP8           ;KEEP LOOPING
        MOV     #1,@(R4)        ;PUT TIMEOUT ERROR CODE IN IERROR
        RETURN
GETCFM: CALL    GETBYT          ;GO GET CONFIRMATION BYTE IN R0
        CMP     #1,R0           ;LOOK FOR A (1) IN R0
        BEQ     OK              ;RETURN WITH ZERO IN IERROR IF OK
        MOV     #2,@(R4)        ;OTHERWISE RETURN CHECKSUM ERROR CODE
OK:     RETURN
;
TMERR:  .TTYOUT #104            ;DISPLAY "D"
        MOV     (SP)+,R4        ;GET POINTER TO ERROR CODE OFF STACK
        MOV     #1,@(R4)        ;PUT TIMEOUT ERROR MESSAGE IN IT
        RETURN                  ;GO HOME
```

```
;-----------------------------------------------------------------------
;
;FILENAME RECEVE.MAC
;
        .TITLE  RECEVE
        .GLOBL  RECEVE
        .GLOBL  GETBYT
;
;       FRED R. SIAS, JR.
;       8 JUNE 1984
;       REVISED 6 JULY 1984
;
;SUBROUTINE TO RECEIVE A MESSAGE OF VARIABLE LENGTH FROM
;THE ROBOT USING MINC MODULE MNCDI UNIT 0 AND RETURN A MESSAGE
;THAT INDICATES THAT THE RECEIVED MESSAGE DID NOT HAVE A CHECKSUM ERROR.
;
;THE MESSAGE RECEIVED BY THIS SUBROUTINE IS RETURNED TO
;THE CALLING PROGRAM IN AN ARRAY OF WORDS EACH WITH THE
;HIGH-ORDER BYTE ZEROED.
;
;CALLING SEQUENCE:  CALL RECEVE(IERROR,ILEN,ICSUM,IDATA)
;                WHERE   IDATA IS A 257 WORD ARRAY.
;                        ILEN IS THE LENGTH OF THE DATA
;                        ICSUM IS THE CALCULATED CHECKSUM
;                        IERROR IS AN ERROR CODE RETURNED BY SUBR.
;
;ERROR CODES RETURNED:   0 = NORMAL EXIT
;                        1 = TIMEOUT ERROR
;                        2 = CHECKSUM ERROR
;
;       THIS ROUTINE CHANGES R0,R1,R2,R3,R4, AND R5
;
        DIR =171162
        DOR =171262
        REQA=100000
        REQB=040000
        CSR1=100000
        CSR0=040000
;
        JSW = 44                ;LOC OF JOB STATUS WORD IN SYSCOM
        .MCALL  .TTYOUT         ;SYSTEM MACRO CALL TO DISPLAY CHARACTER
        .MCALL  .TTINR          ;SYSTEM MACRO CALL FOR KEYBOARD INPUT
;
;               DIR = DIGITAL INPUT REGISTER ADDRESS
;               DOR = DIGITAL OUTPUT REGISTER ADDRESS
;       USED WHEN TRANSMITTING TO ROBOT:
;               REQB = MASK TO TRANSMIT A REQUEST FOR SERVICE TO ROBOT
;               CSR0 = MAKD TO CHECK FOR ACKNOWLEDGE FROM ROBOT
;       USED WHEN RECEIVING MESSAGE FROM ROBOT
;               CSR1 = MASK TO CHECK FOR REQUEST FOR SERVICE FROM ROBOT
;               REQA = MASK TO ACKNOWLEDGE REQUEST FOR SERVICE FROM ROBOT
;-----------------------------------------------------------------------
```

```
;APPLICATION OF SUBROUTINE "RECEVE:
;
;       SUBROUTINE RECEVE IS NOT INTERRUPT DRIVEN BUT IS CALLED WHENEVER
;       A MESSAGE FROM THE ROBOT IS EXPECTED.  IT IS TO BE USED IN A TEST
;       MODE WHEN MULTIPLE PROCESSES WILL NOT BE ACTIVE.  THE ROUTINE SHOULD
;       BE MODIFIED IF AN INTERRUPT-DRIVEN SYSTEM IS REQUIRED.
;
;       THIS SUBROUTINE IS CALLED WHENEVER A MESSAGE FROM THE ROBOT IS
;       EXPECTED; E.G. WHEN TESTING VARIOUS ROBOT MESSAGE PROTOCOLS.
;       ALL PARAMETERS SPECIFIED ARE TO RETURN VARIOUS MESSAGES OR DATA
;       TO THE CALLING PROGRAM.
;
;       IERROR RECEIVES ERROR CODES INDICATING THE FOLLOWING CONDITIONS:
;               0 = NORMAL EXIT
;               1 = TIMEOUT ERROR
;               2 = CHECKSUM ERROR
;
;       ILEN RECEIVES THE TOTAL LENGTH OF THE RECEIVED DATA INCLUDING THE
;       LENGTH TRANSMITTED BY THE ROBOT, THE SEQUENCE NUMBER, THE TYPE CODE,
;       AND THE TRANSMITTED LONGITUDINAL REDUNDANCY CHECK BYTE.
;
;       ICSUM CONTAINS THE CHECKSUM CALCULATED BY THIS ROUTINE WHICH MAY
;       DIFFER FROM THE CHECKSUM TRANSMITTED BY THE ROBOT.
;
;       IDATA, OF COURSE, CONTAINS ALL DATA RECEIVED FROM THE ROBOT.  EACH
;       BYTE RECEIVED FROM THE ROBOT IS CONTAINED IN THE LOW-ORDER BYTE
;       OF THE 16 BIT INTEGER PASSED IN IDATA.
;
;       THIS SUBROUTINE ALSO TRANSMITS A MESSAGE CONFIRMATION BYTE TO THE
;       ROBOT INDICATING WHETHER THE RECEIVED DATA PASSED AN LRC CALCULATION.
;       (1) INDICATES SUCCESSFUL DATA RECEPTION WHILE (2) INDICATES THAT
;       THE CALCULATED LRC BYTE DOES NOT AGREE WITH THE TRANSMITTED LRC BYTE.
;
;       THIS ROUTINE WAITS INDEFINITLY FOR A MESSAGE FROM THE ROBOT.  IF NO
;       MESSAGE IS RECEIVED AND THE USER WISHES TO STOP WAITING, ANY KEY MAY
;       BE PRESSED ON THE MINC KEYBOARD TO RETURN TO THE CALLING PROGRAM.
;       A TIMEOUT ERROR MESSAGE (IERROR = 2) IS RETURNED TO THE CALLING PROG.
;
;-----------------------------------------------------------------------------
```

```
RECEVE: BIS     #10000,JSW      ;SET BIT 12 IN JSW FOR IMM. RET. IN .TTYIN
        BIS     #100,JSW        ;SET BIT 6 FOR RETURN WITHOUT CHAR
LOOP7:  BIT     #CSR1,@#DIR     ;LOOK FOR ROBOT REQUEST TO SEND
        BNE     FOUND           ;GO GET DATA IF CSR1 IS SET
        MOV     #0,R0           ;MAKE SURE R0=0
        .TTINR                  ;LOOK FOR KEYBOARD CHARACTER
        CMP     #0,R0           ;ANY CHARACTER FROM KEYBOARD?
        BEQ     LOOP7           ;KEEP LOOKING FOR MESSAGE OR KEY STROKE
        TST     (R5)+           ;GET READY TO RETURN ERROR CODE; SKIP PAR CNT
        MOV     #1,@(R5)        ;SET IERROR TO TIMEOUT ERROR CODE
        BIC     #10100,JSW      ;CLEAR BIT 12 AND BIT 6 OF JSW
        RETURN                  ;GO BACK TO CALLING PROGRAM
;                               ;ERROR HANDLING IN CALLING PROGRAM
FOUND:  BIC     #10100,JSW      ;CLEAR BIT 12 AND BIT 6 OF JSW
        TST     (R5)+           ;SKIP PARAMETER COUNT
        MOV     R5,R4           ;SAVE POINTER TO ERRCODE PARAMETER
        TST     (R5)+           ;SKIP ERROR CODE
        MOV     #377,R2         ;SET LRC BYTE TO ALL 1'S
;
        CALL    GETBYT          ;FIRST BYTE IN R0 IS LENGTH OF MESSAGE
        XOR     R0,R2           ;UPDATE CHECKSUM WITH LENGTH DATA
;
        MOV     R0,@(R5)+       ;PUT LENGTH IN LENGTH PARAMETER
        TST     (R5)+           ;SKIP CHECKSUM VARIABLE
;                               ;NOW POINTS TO START OF DATA ARRAY
        MOV     R0,R3           ;SET UP DOWN COUNTER FOR LOOP
        MOV     (R5),R1         ;PUT ADDRESS OF ARRAY IN R1
        MOV     R0,(R1)+        ;PUT LENGTH OF MESSAGE IN ARRAY
        CALL    GETBYT          ;GET SEQUENCE NUMBER
        XOR     R0,R2           ;UPDATE CHECKSUM WITH SEQ. NO.
        MOV     R0,(R1)+        ;PUT IN ARRAY
;
LOOP5:
        .TTYOUT #65             ;DEBUG TYPE "5"
        CALL    GETBYT          ;GET NEXT BYTE
        MOV     R0,(R1)+        ;SAVE NEXT BYTE IN ARRAY
        XOR     R0,R2           ;UPDATE CHECKSUM
        DEC     R3              ;DECREMENT BYTE COUNTER
        BNE     LOOP5           ;KEEP READING DATA UNTIL COUNT IS ZERO
;
        CALL    GETBYT          ;GET TRANSMITTED CHECKSUM
        MOV     R0,(R1)         ;PUT TRANSMITTED CHK SUM AT END OF ARRAY
        CMP     R0,R2           ;DOES IT AGREE WITH CALC. CHECKSUM?
        BEQ     NORMAL          ;EXIT IF ALL OK
        MOV     #2,@(R4)+       ;RETURN CHECKSUM ERROR MESSAGE TO CALLING PRO(
        BR      EXIT            ;GO CLEAN UP AND RETURN
;
NORMAL: MOV     #0,@(R4)+       ;ALL OK ERROR CODE
EXIT:   TST     (R4)+           ;MOVE PAST ILEN POINTER
        MOV     R2,@(R4)        ;RETURN CALC CHECK SUM IN PARAMETER
;
;BEFORE RETURNING TO CALLING PROGRAM RETURN CONFIRMATION MESSAGE
;TO ROBOT.
;
```

```
;(1) INDICATES LRC OK WHILE (2) INDICATES LRC ERROR.
;
        CMP     R0,R2           ;AGAIN COMPARE CALC AND RECEIVED LRC
        BEQ     OK
BAD:    MOV     #2,R0           ;SET UP ERROR MESSAGE TO TRANSMIT
        CALL    SNDBYT          ;TRANSMIT CONFIRMING MESSAGE
        BR      TMERR           ;TIMING ERROR FROM SNDBYT
        RETURN
OK:     MOV     #1,R0           ;SET UP "DATA OK" MESSAGE
        CALL    SNDBYT          ;TRANSMIT CONFIRMATION
        BR      TMERR           ;TIMING ERROR FROM SNDBYT
        RETURN
;
TMERR:  MOV     #1,@(R4)+       ;RETURN TIMEOUT ERROR
        BR      EXIT
```

```
;-----------------------------------------------------------------------
;
;       MACRO SUBROUTINE SNDBYT
;
;       THIS IS THE MOST ELEMENTARY BYTE TRANSMISSION SUBROUTINE FOR
;       COMMUNICATION WITH THE ROBOT.  IT HANDLES THE HANDSHAKING FOR
;       TRANSMISSION OF A SINGLE BYTE TO THE ROBOT. NO ERROR CHECKING
;       IS HANDLED AT THIS LEVEL AS ERROR MESSAGES MUST BE RETURNED
;       FROM THE ROBOT AND ARE RECEIVED BY GETBYT.
;
;       ENTER SNDBYT SUBROUTINE WITH BYTE IN R0
;
;-----------------------------------------------------------------------
;
SNDBYT: MOV     R2,-(SP)        ;PUSH R2
        MOV     R1,-(SP)        ;PUSH R1
        BIC     R0,@#DOR        ;PLACE DATA IN OUTPUT REGISTER (7-26-84)
        BIC     #REQB,@#DOR     ;SEND TRANSMIT REQ. TO ROBOT (COMP. 7-26-84)
        MOV     #0,R1           ;CLEAR INNER COUNTER
        MOV     #10,R2          ;PUT 10 IN OUTER COUNTER
LOOP3:  BIT     #CSR0,@#DIR     ;CHECK FOR ACKNOWLEDGE
        BNE     EXIT            ;LOOP UNTIL REC. ACK. FROM ROBOT
;       TIMEOUT COUNTER IS HERE
        DEC     R1              ;DIDDLE INNER COUNTER.
        BNE     LOOP3           ;KEEP CHECKING
        DEC     R2              ;DECREMENT OUTER LOOP
        BNE     LOOP3           ;COUNT SOME MORE
TMOUT:  .TTYOUT #101            ;DISPLAY AN "A"
        MOV     (SP)+,R1        ;POP R1
        MOV     (SP)+,R2        ;POP R2
;       STACK NOW CLEARED OF TEMPORARY DATA; POINTING TO RETURN ADDR.
        RETURN                  ;ERROR RETURN TO LOC. FOLLOWING CALL
;
EXIT:   .TTYOUT #102            ;DISPLAY A "B"
        BIS     #REQB,@#DOR     ;CLEAR TRANSMIT REQUEST (COMP. 7-26-84)
LOOP4:  BIT     #CSR0,@#DIR     ;IS CSR0 CLEAR?
        BNE     LOOP4           ;WAIT FOR CSR0 TO CLEAR
        MOV     (SP)+,R1        ;POP R1
        MOV     (SP)+,R2        ;POP R2
;       STACK CLEAR AND READY TO RETURN TO 2ND LOCATION AFTER CALL
        ADD     #2,(SP) ;MOVE RET. ADDR. FWD ONE INSTRUCTION
        RETURN
        .END
```

```
;-----------------------------------------------------------------------
;
;       MACRO SUBROUTINE GETBYT
;
;       THIS IS THE MOST ELEMENTARY BYTE RECEPTION SUBROUTINE FOR
;       FOR COMMUNICATION WITH THE ROBOT.  IT HANDLES HANDSHAKING
;       AND ACCEPTS A SINGLE BYTE FROM THE ROBOT.  SINCE THIS SUBROUTINE
;       WILL WAIT FOREVER FOR A CSR1 BIT TO BE SET, THE TIMEOUT LOGIC
;       MUST BE HANDLED PRIOR TO CALLING THIS SUBROUTINE.
;
;       THIS ROUTINE RETURNS BYTE IN R0
;       ALL OTHER REGISTERS INTACT
;
;       DIR  IS ADDRESS OF DIGITAL INPUT REGISTER
;       CSR1 IS MASK SHOWING WHICH BIT SET FOR DATA READY FLAG
;       REQA IS MASK SHOWING BIT TO SET TO REQUEST DATA
;               FROM ROBOT
;
;-----------------------------------------------------------------------
;
GETBYT:
LOOP1:
        .TTYOUT #61             ;DISPLAY A "1" DURING CHECKOUT
        BIT     #CSR1,@#DIR     ;CHECK TO SEE IF FLAG IS SET
        BEQ     LOOP1           ;KEEP CHECKING UNTIL FLAG SET
        .TTYOUT #62
        MOV     @#DIR,R0        ;READ A BYTE
        BIC     #177400,R0      ;CLEAR HIGH-ORDER BYTE
        BIC     #REQA,@#DOR     ;TRANSMIT REQA TO INDICATE (7-26-84)
                                ;DATA HAS BEEN RECEIVED
        MOV     R0,-(SP)        ;PUSH   R0
LOOP2:
        .TTYOUT #63             ;DISPLAY A "3"
        BIT     #CSR1,@#DIR     ;CHECK TO SEE IF CSR1 RESET
        BNE     LOOP2           ;KEEP CHECKING
        BIS     #REQA,@#DOR     ;CLEAR REQA (COMP. 7-26-84)
        MOV     (SP)+,R0        ;POP    R0
        RETURN                  ;RETURN WITH BYTE IN R0
        .END
```

```
        .TITLE DINP
        .GLOBL DINP
;FILE NAME DINP.MAC
;DIGITAL OUTPUT ROUTINE TO CALL FROM FORTRAN
;CALL DINP(IUNIT,IMASK,IERR,INDATA)
;
;INPUTS FROM UNIT 0 ONLY AT PRESENT
;ONLY RETURNS ERROR CODE 1
;
        DIR0=171162
        DIR1=171172
        DIR2=171202
        DIR3=171212
;
DINP:   TST (R5)+       ;SKIP PARAMETER COUNT
        MOV (R5),R1     ;SAVE ADDR. OF UNIT NO. IN R1
        TST (R5)+       ;SKIP UNIT NUMBER
        MOV (R5),R2     ;SAVE ADDR. OF MASK IN R2
        TST (R5)+       ;SKIP MASK
        MOV #01,@(R5)+  ;PUT 1 IN ERROR VARIABLE
        MOV @#DIR0,R0   ;READ IN DATA TO R0
        MOV @(R2),R3    ;GET MASK
        COM R3          ;COMPLEMENT FOR BIC OPERATION
;       BIC R3,R0       ;AND MASK WITH DATA
        MOV R0,@(R5)    ;PASS BACK AS PARAMETER
        RETURN
        .END
```

```
        .TITLE DOUT
        .GLOBL DOUT
;FILE NAME DOUT.MAC
;DIGITAL OUTPUT ROUTINE TO CALL FROM FORTRAN
;CALL DOUT(IUNIT,IMASK,IERR,DATA)
;
;AT PRESENT ONLY OUTPUTS TO UNIT 0
;AND HAS NO ERROR MESSAGES, I.E. RETURNS "1"
;
        DOR0=171262
;
DOUT:   TST (R5)+       ;SKIP PARAMETER COUNT
        MOV (R5),R1     ;ADDRESS OF UNIT NO IN R1
        TST (R5)+       ;SKIP UNIT NUMBER
        MOV (R5),R2     ;SAVE ADDR OF MASK IN R2
        TST (R5)+       ;SKIP MASK
        MOV #01,@(R5)+  ;PUT 1 IN ERROR VARIABLE
        MOV @(R5),R0    ;GET OUTPUT DATA IN R0
        MOV @(R2),R3    ;GET MASK
        COM R3          ;GET MASK READY FOR BIC
;       BIC R3,R0       ;MASK OUTPUT DATA
        MOV R0,@#DOR0   ;OUTPUT DATA
        RETURN
        .END
```

```
C*************************************************************************
C
      SUBROUTINE INIT
C
C     FRED R. SIAS, JR.
C     25 JULY 1984
C
C     SUCCESSFUL COMPLETION OF THIS SUBROUTINE ESTABLISHES THAT
C     COMMUNICATION PROTOCOLS ARE WORKING PROPERLY.
C
C     THIS SUBROUTINE IS REQUESTED FROM THE MINC CONSOLE
C     PRIOR TO RESETTING THE ROBOT.
C     WHEN THE ROBOT IS RESET IT WILL REQUEST A DEVICE IDENT/STATUS
C     FROM THE MINC COMPUTER.
C           TYPE CODE = 1
C
C
C     THIS SUBROUTINE WILL RESPOND THAT THE MINC IS OPERATIONAL
C     AND WILL TRANSMIT THE APPROPRIATE CODES:
C           TYPE CODE = 129
C           DEVICE TYPE (1 BYTE) = 2   (MEANS THAT COMPUTER DEVICE)
C           DEVICE IDENT. (3 ASCII BYTES) = "MNC"
C           SYSTEM STATUD (1 BYTE)        = 1 (MEANS OPERATIONAL)
C           ASCII MESSG = "MINC OK - CYR01 V1.0"
C
C     THIS SUBROUTINE WILL CALL THE RECEVE SUBROUTINE TO WAIT FOR THE
C     INITIAL MESSAGE FROM THE ROBOT.  THE MINC WILL WAIT INDEFINITLY
C     FOR THE ROBOT TO RESPOND.  TO QUIT WAITING HIT ANY KEY ON THE MINC
C     CONSOLE AND THE PROGRAM WILL RETURN TO THE MAIN MENU.
C
C*************************************************************************
```

```
      INTEGER*2 IDATA(257),RT,WT
      BYTE INPUT
C
      RT=5
      WT=7
C
C     FIRST OUTPUT 000000 TO CLEAR DIGITAL OUTPUT REGISTER
C
      IUNIT=0
      IMASK="000000
C
      CALL DOUT(IUNIT,IMASK,IERR,IMASK)
C
10    CONTINUE
C
      WRITE (WT,50)
50    FORMAT(/,' WAITING FOR ROBOT TO RESPOND!',/,
     1          ' HIT ANY KEY TO QUIT WAITING.> ',$)
C
C-------------------------------------GET FIRST MESSAGE
C
      CALL RECEVE(IERROR,ILEN,ICSUM,IDATA)
C
C     TIME OUT ERROR
      IF (IERROR.EQ.1) GOTO 199
C
C     CHECKSUM ERROR IF IERROR = 2
      IF (IERROR.EQ.2) GOTO 2000
C
C     ILLEGAL ERROR CODE IF GREATER THAN 2
      IF (IERROR.GE.3) GOTO 3000
C
C-------------------------------------GET SECOND MESSAGE
C
      CALL RECEVE(IERROR,ILEN,ICSUM,IDATA)
C
C     TIME OUT ERROR
      IF (IERROR.EQ.1) GOTO 199
C
C     CHECKSUM ERROR IF IERROR = 2
      IF (IERROR.EQ.2) GOTO 2000
C
C     ILLEGAL ERROR CODE IF GREATER THAN 2
      IF (IERROR.GE.3) GOTO 3000
C
C-------------------------------------GET THIRD MESSAGE
C
      CALL RECEVE(IERROR,ILEN,ICSUM,IDATA)
C
C     TIMEOUT ERROR
      IF (IERROR.EQ.1) GOTO 199
C
C     CHECKSUM ERROR IF IERROR = 2
      IF (IERROR.EQ.2) GOTO 2000
```

```
C
C       ILLEGAL ERROR CODE IF GREATER THAN 2
        IF (IERROR.GE.3) GOTO 3000
C
C-----------------------------------------GET FOURTH MESSAGE
C
        CALL RECEVE(IERROR,ILEN,ICSUM,IDATA)
C
C       TIME OUT ERROR
        IF (IERROR.EQ.1) GOTO 199
C
C       CHECKSUM ERROR IF IERROR = 2
        IF (IERROR.EQ.2) GOTO 2000
C
C       ILLEGAL ERROR CODE IF GREATER THAN 2
        IF (IERROR.GE.3) GOTO 3000
C
        GOTO 5100
C
C-------------------------------------------------------------------
C
C       HERE IF TIMES OUT AT ANY TIME
C
199     CONTINUE
C
        WRITE (WT,200)
200     FORMAT(//,' NO INITIALIZATION MESSAGE FROM ROBOT',/,
     1          ' PRESS "RETURN" TO CONTINUE> ',$)
        READ  (RT,5230) INPUT
C
        RETURN
C
C       HERE TO PROCESS CHECKSUM ERROR
2000    CONTINUE
        WRITE (WT,2010)
C
2010    FORMAT(//,' CHECKSUM DOES NOT COMPUTE!',/,
     1          ' TRY AGAIN? (Y OR N)> ',$)
        READ  (RT,5230) INPUT
        IF (INPUT.EQ.'Y') GOTO 10
        RETURN
C
C       HERE TO PROCESS ILLEGAL ERROR CODE AND RETURN TO MENU
3000    CONTINUE
C
        WRITE (WT,3010)
3010    FORMAT(//,' RECEIVED AN ILLEGAL ERROR CODE FROM RECEVE',
     1          ' SUBROUTINE.',/,
     2          ' PRESS "RETURN" TO CONTINUE> ',$)
        READ  (RT,5230) INPUT
        RETURN
C
C
C       HERE TO PROCESS INCOMING MESSAGE
```

```
C5000   CONTINUE
C
C       ITYPE=IDATA(3)
C       IF (ITYPE.EQ.1) GOTO 5100
C
C
C       WRITE (WT,5010)
C5010   FORMAT(//,' WRONG TYPE CODE (',I4,') RECEIVED FROM ROBOT!',/,
C     1             ' PRESS "RETURN" TO CONTINUE> ',$)
C       READ  (RT,5230) INPUT
C       RETURN
C
5100    CONTINUE
C       HERE TO PROCESS ACCEPTABLE REQUEST
C
C       RETURN STATUS/IDENTIFICATION INFO TO ROBOT
C
        IDATA(3)=129
C
C       DEVICE TYPE = 1 I.E. THIS IS A COMPUTER
        IDATA(4)=1
C
C       DEVICE IDENTIFICATION = "MNC"
C
        IDATA(5)=77
        IDATA(6)=78
        IDATA(7)=67
C
C       SYSTEM STATUS IS OPERATIONAL
        IDATA(8)=1
C
C       SEND MESSAGE "MINC OK - CYRO1 V1.0"
        IDATA(9)=77
        IDATA(10)=73
        IDATA(11)=78
        IDATA(12)=67
        IDATA(13)=32
        IDATA(14)=79
        IDATA(15)=75
        IDATA(16)=32
        IDATA(17)=45
        IDATA(18)=32
C       CYRO1
        IDATA(19)=67
        IDATA(20)=89
        IDATA(21)=82
        IDATA(22)=79
        IDATA(23)=49
        IDATA(24)=32
C       V1.0
        IDATA(25)=86
        IDATA(26)=49
        IDATA(27)=46
        IDATA(28)=48
```

```
C
      IDATA(1)=26
C
      ILEN=28
C
C     WILL TRY TO SEND FIVE TIMES
C
      DO 5200 I=1,5
C
      CALL SEND(IERROR,ILEN,IDATA)
C
      IF (IERROR.EQ.0) GOTO 5500
C
5200  CONTINUE
C
      WRITE (WT,5210)
5210  FORMAT(//,' MINC GAVE UP AFTER 5 TRIES TO SEND!',/)
C
      WRITE (WT,5220)
5220  FORMAT(/,' PUSH "RETURN" TO CONTINUE> ',$)
      READ  (RT,5230) INPUT
5230  FORMAT(A4)
      RETURN
C
5500  CONTINUE
C     HERE IF INITIALIZATION COMPLETE AND OK
      WRITE (WT,5510)
5510  FORMAT(//,' INITIALIZATION COMPLETE AND OK!',/,
     1          ' PRESS "RETURN" TO CONTINUE> ',$)
      READ  (RT,5230) INPUT
C
      RETURN
      END
```

```
C*****************************************************************
C
      SUBROUTINE MOVE
C
C     THIS SUBROUTINE ALLOWS THE USER TO MOVE THE ROBOT TO AN ABSOLUTE
C     LOCATION IN THE ROBOT COORDINATE SYSTEM.  X,Y,Z,A, AND C COORDINATES
C     WILL BE REQUESTED ON THE CRT SCREEN.
C
C     VALUES FOR EACH COORDINATE WILL BE ENTERED AS SIGNED REAL NUMBERS
C     SPECIFIED TO THE NEAREST 128TH OF AN INCH.  EACH VALUE
C     WILL BE MULTIPLIED BY 128 AND TRANSMITTED TO THE ROBOT AS A
C     TWO-BYTE SIGNED INTEGER.
C
C     MESSAGE TO ROBOT CONSISTS OF A TYPE CODE 137 FOLLOWED BY TEN BYTES
C     OF DATA REPRESENTING SIGNED POSITIONS ON EACH OF THE FIVE AXES.
C
C*****************************************************************
C
      INTEGER*2 IDATA(257),RT,WT,INTGR,IMESSG(40)
      BYTE BYT(2),BARRAY(514)
      EQUIVALENCE (BYT(1),INTGR)
      EQUIVALENCE (BARRAY(1),IDATA(1))
C
      WT=7
      RT=5
C
      WRITE (WT,100)
100   FORMAT(//,' INPUT VALUES FOR EACH COORDINATE TO THE',/,
     1          ' NEAREST .01 INCH OR 0.1 DEGREE:',///,
     1          '        X-AXIS (INCHES):',$)
      READ  (RT,110) XAXIS
110   FORMAT(G10.0)
C
      WRITE (WT,120)
120   FORMAT(   '        Y-AXIS (INCHES):',$)
      READ  (RT,110) YAXIS
C
      WRITE (WT,140)
140   FORMAT(   '        Z-AXIS (INCHES):',$)
      READ  (RT,110) ZAXIS
C
      WRITE (WT,160)
160   FORMAT(   '        A-AXIS (DEGREES):',$)
      READ  (RT,110) AAXIS
C
      WRITE (WT,180)
180   FORMAT(   '        C-AXIS (DEGREES):',$)
      READ  (RT,110) CAXIS
C
      IXAXIS=XAXIS*128.
      IYAXIS=YAXIS*128.
      IZAXIS=ZAXIS*128.
      IAAXIS=AAXIS*10.
      ICAXIS=CAXIS*10.
```

```
C
C       LENGTH OF MESSAGE
        IDATA(1)=11
C       SEQUENCE NUMBER
        IDATA(2)=0
C       TYPE CODE
        IDATA(3)=137
C
C       NOW TRANSFER DATA ELEMENTS TO IDATA ARRAY
C       THIS PROCEDURE IS COMPLICATED DUE TO NEED
C       TO MOVE HIGH AND LOW ORDER BYTES INTO SUCCESSIVE
C       ARRAY ELEMENTS WITHOUT EXTENDING SIGN BIT INTO HIGH-ORDER
C       BYTE OF IDATA ARRAY BY THE ASSIGNMENT STATEMENT
C
        INTGR=IXAXIS
        BARRAY(7)=BYT(1)
        BARRAY(9)=BYT(2)
C
        INTGR=IYAXIS
        BARRAY(11)=BYT(1)
        BARRAY(13)=BYT(2)
C
        INTGR=IZAXIS
        BARRAY(15)=BYT(1)
        BARRAY(17)=BYT(2)
C
        INTGR=IAAXIS
        BARRAY(19)=BYT(1)
        BARRAY(21)=BYT(2)
C
        INTGR=ICAXIS
        BARRAY(23)=BYT(1)
        BARRAY(25)=BYT(2)
C
        ILEN=13
C
C       ITEST=1
C       IF (ITEST.EQ.1) CALL TEST(ILEN,IDATA)
C
        CALL SEND(IERROR,ILEN,IDATA)
C
        IF (IERROR.EQ.0) GOTO 2000
C
        WRITE (WT,1000) IERROR
1000    FORMAT(//,' ERROR CODE',I4,' RETURNED FROM SEND.',/,
     1          ' PRESS "RETURN" TO CONTINUE> ',$)
        READ  (RT,1010) INPUT
1010    FORMAT(A2)
        RETURN
2000    CONTINUE
        WRITE (WT,2010)
2010    FORMAT(//,' MESSAGE ACCEPTED BY ROBOT AND',
     1          ' ACKNOWLEDGED OK.',/,
     1          ' PRESS "RETURN" TO CONTINUE> ',$)
```

```
READ  (RT,1010) INPUT
RETURN
END
```

```
C*****************************************************************************
C
      SUBROUTINE POSIT
C
C     THIS ROUTINE REQUESTS THE CURRENT ROBOT POSITION AND
C     AND DISPLAYS ON MINC CRT.
C
C     FRED R. SIAS, JR.
C     26 JUNE 1984
C
C     THE ROUTINE TRANSMITS A REQUEST FOR ROBOT POSITIONS
C     (TYPE CODE 132) WITH THE SINGLE BYTE MESSAGE ZERO (0) THAT
C     INDICATES THAT ONLY ONE RESPONSE PER REQUEST IS DESIRED.
C     THEN THE ROUTINE WAITS FOR A RESPONSE FROM THE ROBOT WHICH
C     SHOULD INCLUDE THE TYPE CODE 4 FOLLOWED BY EIGHTEEN (18)
C     BYTES OF BINARY DATA THAT CONVEY NINE CURRENT ROBOT POSITIONS.
C     EACH POSITION CONSISTS OF TWO SEQUENTIAL BYTES, LOW-ORDER FIRST
C     FOLLOWED BY THE HIGH-ORDER BYTE.
C
C     SUBROUTINES CALLED:
C           SEND (IERROR,ILEN,IDATA)
C                 where ILEN is the total length of the data array
C                 transmitted by the SEND subroutine.
C
C                 IDATA is a 257 word array into which the data is
C                 place before the subroutine call.  Each BYTE of
C                 data is place in the low-order byte of the
C                 INTEGER*2 elements in IDATA.
C
C                 IERROR returns any error code from the SEND
C                 subroutine. The error code (0)
C                 is returned to indicate transmission is ok.
C                 Error code (1) indicates that the robot did not
C                 acknowledge the message within 5 seconds and
C                 error coded (2) indicates that the robot returned
C                 a checksum error message.
C
C           RECEVE(IERROR,ILEN,ICSUM,IDATA)
C                 where IERROR is an error code returned by the
C                 subroutine. A code of two (2) indicates a checksum
C                 error, (1) indicates that the robot never responded,
C                 while a code of zero (0) indicates correct
C                 data reception.
C
C                 ILEN is the length of the array received.
C
C                 ICSUM is the checksum calculated by RECEVE while
C                 the last element of IDATA contains the checksum
C                 transmitted by the robot.
C
C                 IDATA is a 257 element integer array that contains
C                 the entire data stream received from the robot.
C
C*****************************************************************************
```

```
C
      BYTE STRING(254)
      INTEGER*2 IDATA(257)
      LOGICAL*1 PROMT(16)
C
      RT=5
      WT=7
C
C     LENGTH OF MESSAGE
      IDATA(1)=2
C
C     SETS SEQUENCE NO. TO ZERO
      IDATA(2)=0
C
C     SETS TYPE CODE
      IDATA(3)=132
C
C     SETS RATE TO ONCE PER REQUEST
      IDATA(4)=0
C
C     NO OF BYTES TO TRANSMIT IN SEND
      ILEN=4
      CALL SEND(IERROR,ILEN,IDATA)
C
      IF (IERROR.EQ.0) GOTO 5
C
      WRITE (WT,2) IERROR
2     FORMAT(' ERROR CODE',I4,' RECEIVED FROM SUBR. SEND.')
C
5     CONTINUE
C
C     NOW WAIT FOR MESSAGE TO COME BACK WITH INFO
C
      CALL RECEVE(IERROR,ILEN,ICSUM,IDATA)
C
      IF (IERROR.EQ.2) WRITE (WT,10)
10    FORMAT(' CHECKSUM ERROR. DATA MAY BE WRONG!')
C
      WRITE (WT,12)
12    FORMAT(' PRESS RETURN TO CONTINUE> ',$)
      READ  (RT,210) INPUT
C
C     SHOULD BE MESSAGE TYPE CODE 4
C
      IF (IDATA(3).NE.4) WRITE (WT,15) IDATA(3)
15    FORMAT(' ILLEGAL TYPE CODE ',I2,' RECEIVED')
C
      IXDATA=IDATA(5)
      IXDATA=(IXDATA*256+IDATA(4))/128.
      WRITE (WT,100) IXDATA
100   FORMAT(' X-axis position is      ',I8,' inches.')
      IYDATA=IDATA(7)
      IYDATA=(IYDATA*256+IDATA(6))/128.
      WRITE (WT,110) IYDATA
```

```
110     FORMAT(' Y-axis position is      ',I8,' inches.')
C
        IZDATA=IDATA(9)
        IZDATA=(IZDATA*256+IDATA(8))/128.
        WRITE (WT,120) IZDATA
120     FORMAT(' Z-axis position is      ',I8,' inches.')
C
        ICXPOS=IDATA(11)
        ICXPOS=(ICXPOS*256+IDATA(10))/10.
        WRITE (WT,130) ICXPOS
130     FORMAT(' C positioner, X-axis is ',I8,' degrees.')
C
        ICYPOS=IDATA(13)
        ICYPOS=(ICYPOS*256+IDATA(12))/10.
        WRITE (WT,140) ICYPOS
140     FORMAT(' C positioner, Y-axis is ',I8,' degrees.')
C
C
        IDXPOS=IDATA(15)
        IDXPOS=(IDXPOS*256+IDATA(14))/10.
        WRITE (WT,150) IDXPOS
150     FORMAT(' D positioner, X-axis is ',I8,' degrees.')
C
        IDYPOS=IDATA(17)
        IDYPOS=(IDYPOS*256+IDATA(16))/10.
        WRITE (WT,160) IDYPOS
160     FORMAT(' D positioner, Y-axis is ',I8,' degrees.')
C
        WRITE (WT,200)
200     FORMAT(//,' CARRIAGE RETURN TO CONTINUE> ',$)
        READ  (RT,210) INPUT
210     FORMAT(I4)
        RETURN
        END
```

```
C*************************************************************************
C
      SUBROUTINE PARS
C
C     THIS ROUTINE REQUESTS THE CURRENT ROBOT PARAMETERS AND
C     AND DISPLAYS THEM ON MINC CRT.
C
C     FRED R. SIAS, JR.
C     27 JUNE 1984
C
C*************************************************************************
C
      BYTE STRING(254)
      INTEGER*2 IDATA(257)
      LOGICAL*1 PROMT(16)
C
      RT=5
      WT=7
C
C     SETS SEQUENCE NO. TO ZERO
      IDATA(2)=0
C
C     REQUEST CODE FOR SYSTEM PARAMETERS
      IDATA(3)=138
C
      IDATA(1)=2
C
      IDATA(4)=0
C
      ILEN=4
      CALL SEND(IERROR,ILEN,IDATA)
C
C     NOW WAIT FOR MESSAGE TO COME BACK WITH INFO
C
      CALL RECEVE(IERROR,ILEN,ICSUM,IDATA)
C
      IF (IERROR.EQ.2) WRITE (WT,10)
10    FORMAT(' CHECKSUM ERROR. DATA MAY BE WRONG!')
C
C
C     SHOULD BE MESSAGE TYPE CODE 7
C
      IF (IDATA(3).NE.7) WRITE (WT,15) IDATA(3)
15    FORMAT(' ILLEGAL TYPE CODE ',I2,' RECEIVED')
C
      IXDATA=IDATA(5)
      IXDATA=(IXDATA*256+IDATA(4))/128.
      WRITE (WT,100) IXDATA
100   FORMAT(' Torch feed rate is     ',I8,' inches per minute.')
      IYDATA=IDATA(7)
      IYDATA=(IYDATA*256+IDATA(6))/128.
      WRITE (WT,110) IYDATA
110   FORMAT(' Wire feed rate is      ',I8,' inches per minute.')
C
```

```
      IZDATA=IDATA(9)
      IZDATA=IZDATA*256+IDATA(8)
C     ONE BIT EQUALS .1 PERCENT
      IZDATA=IZDATA/10.
      WRITE (WT,120) IZDATA
120   FORMAT(' Weld level is          ',I8,' percent.')
C
      ICXPOS=IDATA(11)
      ICXPOS=ICXPOS*256+IDATA(10)
C     ONE BIT EQUALS .1 PERCENT
      ICXPOS=ICXPOS/10.
      WRITE (WT,130) ICXPOS
130   FORMAT(' AVC/ACC Setpoint Level ',I8,' percent.')
C
      IF (IDATA(12).EQ.0) WRITE (WT,140)
      IF (IDATA(12).EQ.1) WRITE (WT,150)
      IF (IDATA(12).EQ.2) WRITE (WT,160)
      IF (IDATA(12).GT.2) WRITE (WT,170) IDATA(12)
C
140   FORMAT(' No Oscillation has occured.')
150   FORMAT(' Left Oscillation has occured.')
160   FORMAT(' Right Oscillation has occured.')
170   FORMAT(' ILLEGAL OSCILLATION CODE ',I8,' RECEIVED.')
C
      WRITE (WT,200)
200   FORMAT(//,' CARRIAGE RETURN TO CONTINUE> ',$)
      READ  (RT,210) INPUT
210   FORMAT(I4)
      RETURN
      END
```

```
C*************************************************************************
C
      SUBROUTINE INPOS
C
C     THIS ROUTINE TRANSMITS AN IN-POSITION CODE TO ROBOT.
C
C     TYPE CODE 162
C
C     FRED R. SIAS, JR.
C     11 JULY 1984
C
C*************************************************************************
C
      INTEGER*2 IDATA(257)
C
      RT=5
      WT=7
C
C
      IDATA(1)=1
      IDATA(2)=0
      IDATA(3)=162
C
      ILEN=3
C
      CALL SEND(IERROR,ILEN,IDATA)
C
      IF (IERROR.EQ.2) WRITE (WT,110)
110   FORMAT(//,' CHECKSUM ERROR MESSAGE RECEIVED FROM ROBOT',/)
C
      IF (IERROR.EQ.1) WRITE (WT,120)
120   FORMAT(//,' TIMEOUT ERROR.  ROBOT NEVER RESPONDED',
     1          ' WITH ACKNOWLEDGE MESSAGE!',/)
C
      RETURN
      END
```

```
C*************************************************************************
C
      SUBROUTINE SAVE
C
C     FRED R. SIAS, JR.
C     28 JUNE 1984
C
C     THIS ROUTINE ACCEPTS A PROGRAM NUMBER TO BE SAVED FROM THE TERMINAL
C     THEN A REQUEST IS TRANSMITTED TO THE ROBOT AND THE COMPUTER
C     RECEIVES AND FILES THE PROGRAM RETURNED TO IT.
C
C     IN ADDITION TO ACCEPTING A PROGRAM NUMBER FROM THE KEYBOARD,
C     AN OPTIONAL DESCRIPTIVE COMMENT CAN BE FILED WITH THE PROGRAM.
C     THIS IS REQUESTED FROM THE USER FOLLOWING THE PROGRAM NUMBER.
C
C
C     HANDSHAKING:
C             Computer transmits Type Code 193 - REQUEST TO SAVE
C                              PROGRAM TO COMPUTER.
C             The computer waits for Type Code 66 - SAVE PROGRAM
C                              TO COMPUTER ACKNOWLEDGE.
C             When computer is ready to receive program it again
C                              transmits Type Code 193.
C             Then computer accepts and files a sequence of blocks
C                              using Type Code 193 to indicate when
C                              it is ready for each block.
C             Each block of data transmitted to the robot has a header
C                              containing the Type Code 67 followed by
C                              a sequential block number and the actual
C                              N/C program data.
C
C*************************************************************************
C
      INTEGER*2 NUMBER,IDATA(257),RT,WT,FILNO,HEADER(256)
      BYTE INPUT
C
C
      WT=7
      RT=5
C
10    CONTINUE
C
      WRITE (WT,100)
100   FORMAT(///,' Input NUMBER of Program to be saved> ',$)
      READ  (RT,110) FILNO
110   FORMAT(I1)
C
C     START TO BUILD HEADER FOR FIRST BLOCK OF PROGRAM FILE
C     HEADER(1)=PROGRAM NUMBER
C     HEADER(2)=NUMBER OF 256 WORD BLOCKS OF DATA
C     HEADER(3) TO IDATA(256) CONTAIN DESCRIPTIVE COMMENT ABOUT
C              PROGRAM STORED ONE CHARACTER PER ARRAY ELEMENT.
C
      WRITE (WT,112)
```

```
112     FORMAT(/,' Type any descriptive comment to be filed',
     1           ' with this program.',
     2           ' (Press "RETURN" to skip this feature. > ',$)
        READ  (RT,113) (HEADER(I),I=3,256)
113     FORMAT(A1)
C
        WRITE (WT,115) FILNO
115     FORMAT(//,' OPENING FILE "PCYRO',I1,'".'//)
C
C       NOW OPEN FILE "PCYRO[N]"
C
        IF (FILNO.EQ.1) OPEN (UNIT=9,NAME='PCYRO1.DAT',ERR=10)
        IF (FILNO.EQ.2) OPEN (UNIT=9,NAME='PCYRO2.DAT',ERR=10)
        IF (FILNO.EQ.3) OPEN (UNIT=9,NAME='PCYRO3.DAT',ERR=10)
        IF (FILNO.EQ.4) OPEN (UNIT=9,NAME='PCYRO4.DAT',ERR=10)
        IF (FILNO.EQ.5) OPEN (UNIT=9,NAME='PCYRO5.DAT',ERR=10)
        IF (FILNO.EQ.6) OPEN (UNIT=9,NAME='PCYRO6.DAT',ERR=10)
        IF (FILNO.EQ.7) OPEN (UNIT=9,NAME='PCYRO7.DAT',ERR=10)
        IF (FILNO.EQ.8) OPEN (UNIT=9,NAME='PCYRO8.DAT',ERR=10)
        IF (FILNO.EQ.9) OPEN (UNIT=9,NAME='PCYRO9.DAT',ERR=10)
C
        IF (FILNO.GE.9) GOTO 400
        IF (FILNO.LT.1) GOTO 400
C
        NUMBER=FILNO
        HEADER(1)=FILNO
C
120     CONTINUE
C
C       NOW TRANSMIT A "REQUEST TO SAVE" TO ROBOT
C
        CALL REQTS(NUMBER,IERROR)
C
        IF (IERROR.EQ.1) GOTO 2100
        IF (IERROR.EQ.2) GOTO 2200
        IF (IERROR.GE.3) GOTO 2300
C
C       NOW WAIT FOR SAVE ACKNOWLEDGE - TYPE CODE 66
C
200     CONTINUE
C
        CALL RECEVE(IERROR,ILEN,ICSUM,IDATA)
C
        IF (IERROR.EQ.1) GOTO 3100
        IF (IERROR.EQ.2) GOTO 3200
        IF (IERROR.GE.3) GOTO 3300
C
        ITYPE=IDATA(3)
        IACK=IDATA(4)
        IPNUM=IDATA(5)
        ISIZE=IDATA(6)+256*IDATA(7)
C
C       WRONG MESSAGE TYPE RECEIVED
C
```

```
        IF (ITYPE.NE.66) GOTO 1100
C
        IF (IPNUM.NE.NUMBER) GOTO 1200
C
C       NOT READY TO RECEIVE CODE = 0
C
        IF (IACK.EQ.0) GOTO 1300
        IF (IACK.GE.2) GOTO 1000
C
        IBLKCT=0
C
C       SENDS BLOCK NUMBER AND 252 BYTES OF DATA IN EACH BLOCK
C
C*************************************************************************
C
C       NOTE!! THIS BLOCK SIZE IS A GUESS  UNTIL WE KNOW WHAT
C       AMERICAN ROBOTICS TRANSMITTS SINCE THIS IS NOT STATED
C       IN THE SPECIFICATIONS.
C
C*************************************************************************
C
        ITOTBK=ISIZE/252
        IREM=ISIZE-ITOTBK*252
        IF (IREM.NE.0) ITOTBK=ITOTBK+1
C
        DO 300 I=1,ITOTBK
C
        CALL REQTS(NUMBER,IERROR)
C
        IF (IERROR.EQ.1) GOTO 2100
        IF (IERROR.EQ.2) GOTO 2200
        IF (IERROR.GE.3) GOTO 2300

        STARTS RECEIVING PROGRAM HERE

        CALL RECEVE(IERROR,ILEN,ICSUM,IDATA)

        IF (IERROR.EQ.1) GOTO 3100
        IF (IERROR.EQ.2) GOTO 3200
        IF (IERROR.GE.3) GOTO 3300

        ITYPE=IDATA(3)
        IF (ITYPE.EQ.67) GOTO 1100
        IBLOCK=IDATA(4)
        IF (IBLOCK.NE.IBLKCT) GOTO 4100

      PUT ARRAY ON DISK IN UNFORMATTED SEQUENTIAL FORM.
      ONLY 256 WORDS SAVED TO EFFICIENTLY USE DISK SPACE.
      THIS PRESUMES THAT ONLY 252 BYTES OF DATA WAS TRANSMITTED
      IN A GIVEN BLOCK AND THAT THESE ARE SAVED IN THE LOW-ORDER BYTES
      OF THE 256 WORD ARRAY IDATA.

      THE ARRAY ALSO CONTAINS THE LENGTH OF THE MESSAGE,
      THE SEQUENCE NUMBER, THE TYPE CODE, AND THE LOGITUDINAL
```

```
C       REDUNDANCY CHECK BYTE STORED IN THE LAST ELEMENT OF THE
C       ARRAY THAT IS RECORDED ON DISK (I.E. IDATA(256)).
C
        WRITE (9,ERR=950) (IDATA(I),I=1,256)
C
        IBLOCK=IBLOCK+1
C
300     CONTINUE
C
        CLOSE (UNIT=9,DISPOSE='KEEP',ERR=992)
C
400     WRITE (WT,402)
402     FORMAT(//,' ONLY PROGRAM NUMBERS 1-9 ACCEPTABLE.')
        GOTO 10
C
        WRITE (WT,500) IPNUM
500     FORMAT(//,' PROGRAM NO.',I4,' SUCCESSFULLY RECEIVED AND FILED',/,
     1           ' PRESS "RETURN" TO GOT MAIN MENU.> ',$)
        READ  (RT,904) INPUT
        RETURN
C
```


C-7

```
C-----------------------------------------------------------------------
C
C       ALL OF THE VARIOUS ERROR MESSAGES FOLLOW:
C
900     CONTINUE
        WRITE (WT,902)
902     FORMAT(//,' FATAL ERROR! FILE WILL BE DELETED.',/,
     1            ' PRESS "RETURN" TO GOTO MAIN MENU.> ',$)
        READ  (RT,904) INPUT
904     FORMAT(I4)
C
        CLOSE (UNIT=9,DISPOSE='DELETE',ERR=990)
C
        RETURN
C
950     WRITE (WT,952)
952     FORMAT(//,' ERROR WRITING FILE TO DISK!')
        GOTO 900
C
990     WRITE (WT,992)
992     FORMAT(//,' ERROR CLOSING FILE CONTAINING PROGRAM.',/,
     1            ' PRESS RETURN TO GOTO MAIN MENU> ',$)
        READ  (RT,904) INPUT
        RETURN
C
1000    WRITE (WT,1002)
1002    FORMAT(//,' ILLEGAL ACKNOWLEDGE CODE RECEIVED,')
        GOTO 900
C
1100    WRITE (WT,1102)
1102    FORMAT (//,' WRONG MESSAGE TYPE RECEIVED!')
        GOTO 900
C
1200    WRITE (WT,1202)
1202    FORMAT(//,' WRONG PROGRAM NUMBER RETURNED BY ROBOT!')
        GOTO 900
C
1300    WRITE (WT,1302)
1302    FORMAT(//,' ROBOT NOT READY TO RECEIVE.',
     1            ' TYPE "RETURN" TO TRY AGAIN> ',$)
        READ  (RT,904) INPUT
        GOTO 120
C
2100    WRITE (WT,2102)
2102    FORMAT(//,' TIME OUT ERROR WHILE WAITING FOR',/,
     1            ' ACKNOWLEDGE FROM ROBOT.')
        GOTO 900
C
2200    WRITE (WT,2202)
2202    FORMAT(//,' LRC ERROR MESSAGE RETURNED AFTER TRANSMISSION.')
        GOTO 900
C
2300    WRITE (WT,2302) IERROR
2302    FORMAT(//,' ILLEGAL ACKNOWLEDGE CODE',I4,' RECEIVED',
```

```
     1            ' AFTER TRANSMISSION TO ROBOT.')
3100     WRITE (WT,3102)
3102     FORMAT(//,' FIVE SECOND TIMEOUT OCCURED DURING RECEIVE.')
         GOTO 900
C
3200     WRITE (WT,3202)
3202     FORMAT(//,' CHECKSUM ERROR CALCULATION PRODUCED ERROR',
     1            ' DURING RECEIVE.')
         GOTO 900
C
3300     WRITE (WT,3302) IERROR
3302     FORMAT(//,' ILLEGAL ERROR CODE',I4,' RETURNED FROM',
     1            ' RECEIVE SUBROUTINE.')
         GOTO 900
C
4100     WRITE (WT,4102) IBLOCK,IBLKCT
4102     FORMAT(//,' BLOCK COUNT TRANSMITTED (',I4,')',
     1            ' DOES NOT MATCH EXPECTED BLOCK (',I4,').')
         GOTO 900
C
         END
```

```
C-----------------------------------------------------------------------
C
      SUBROUTINE REQTS(NUMBER,ERROR)
C
      INTEGER*2 IDATA(257),NUMBER,ERROR
C
C     SEND REQUEST TO SAVE PROGRAM [NUMBER] TO ROBOT
C
C     LENGTH OF MESSAGE
      IDATA(1)=2
C     SEQUENCE NO. SET TO ZERO
      IDATA(2)=0
C     SET TYPE CODE
      IDATA(3)=193
C     SEND PROGRAM NUMBER
      IDATA(4)=NUMBER
C
      ILEN=4
C
      CALL SEND(IERROR,ILEN,IDATA)
C
      ERROR=IERROR
C
      RETURN
      END
C
```

```
C*************************************************************************
C
      SUBROUTINE LOAD
C
C     THIS ROUTINE ALLOWS THE USER TO SELECT A PARTICULAR PROGRAM
C     TO BE LOADED.  THEN THE APPROPRIATE PROGRAM IS TRANSMITTED
C     TO THE ROBOT WITH APPROPRIATE HANDSHAKING.
C
C     FRED R. SIAS, JR.
C     13 JULY 1984
C
C     HANDSHAKING:
C             Computer transmits Type Code 194 - REQUEST TO LOAD
C                          PROGRAM FROM COMPUTER.
C             The computer waits for Type Code 65 - LOAD PROGRAM
C                          FROM COMPUTER ACKNOWLEDGE.
C             When computer is ready to transmit the program it
C                          transmits a block of code proceeded
C                          by Type Code 195.
C             Then the robot accepts and files a sequence of blocks
C                          using Type Code 65, LOAD PROGRAM FROM
C                          COMPUTER ACKNOWLEDGE, to indicate when
C                          it is ready for each block.
C
C*************************************************************************
C
      INTEGER*2 NUMBER,IDATA(257),RT,WT,FILNO,LSIZE,HSIZE
      BYTE INPUT
C
C
      WT=7
      RT=5
C
10    CONTINUE
C
      WRITE (WT,100)
100   FORMAT(///,' Input NUMBER of Program to be loaded.> ',$)
      READ  (RT,110) FILNO
110   FORMAT(I1)
C
C
      WRITE (WT,115) FILNO
115   FORMAT(//,' OPENING FILE "PCYRO',I1,'".'//)
C
C     NOW OPEN FILE "PCYRO[N]"
C
      IF (FILNO.EQ.1) OPEN (UNIT=9,NAME='PCYRO1.DAT',ERR=10)
      IF (FILNO.EQ.2) OPEN (UNIT=9,NAME='PCYRO2.DAT',ERR=10)
      IF (FILNO.EQ.3) OPEN (UNIT=9,NAME='PCYRO3.DAT',ERR=10)
      IF (FILNO.EQ.4) OPEN (UNIT=9,NAME='PCYRO4.DAT',ERR=10)
      IF (FILNO.EQ.5) OPEN (UNIT=9,NAME='PCYRO5.DAT',ERR=10)
      IF (FILNO.EQ.6) OPEN (UNIT=9,NAME='PCYRO6.DAT',ERR=10)
      IF (FILNO.EQ.7) OPEN (UNIT=9,NAME='PCYRO7.DAT',ERR=10)
      IF (FILNO.EQ.8) OPEN (UNIT=9,NAME='PCYRO8.DAT',ERR=10)
```

```
      IF (FILNO.EQ.9) OPEN (UNIT=9,NAME='PCYRO9.DAT',ERR=10)
C
      IF (FILNO.GE.9) GOTO 400
      IF (FILNO.LT.1) GOTO 400
C
      NUMBER=FILNO
C
C     NOW GET THE FIRST RECORD FROM FILE SO THAT WE CAN FIND OUT
C     THE SIZE OF THE PROGRAM TO BE LOADED
C
      READ (9,ERR=950) (IDATA(I),I=1,256)
C
C     NOW GET LENGTH OF PROGRAM FROM THIS FILE
C*************************************************************************
C
C     HAVE TO MAKE A DECISION HERE AND IN SAVE PROGRAM TO FIND A WAY
C     TO SAVE THE LENGTH OF THE PROGRAM.
C
C*************************************************************************
C
120   CONTINUE
C
C     NOW TRANSMIT A "REQUEST TO LOAD" TO ROBOT
C
      IDATA(1)=4
      IDATA(2)=0
      IDATA(3)=194
      IDATA(4)=NUMBER
      IDATA(5)=LSIZE
      IDATA(6)=HSIZE
      ILEN=4
C
      CALL SEND(IERROR,ILEN,IDATA)
C
      IF (IERROR.EQ.1) GOTO 2100
      IF (IERROR.EQ.2) GOTO 2200
      IF (IERROR.GE.3) GOTO 2300
C
C     NOW WAIT FOR LOAD ACKNOWLEDGE - TYPE CODE 65
C
200   CONTINUE
C
      CALL RECEVE(IERROR,ILEN,ICSUM,IDATA)
C
      IF (IERROR.EQ.1) GOTO 3100
      IF (IERROR.EQ.2) GOTO 3200
      IF (IERROR.GE.3) GOTO 3300
C
      ITYPE=IDATA(3)
      IACK=IDATA(4)
      IPNUM=IDATA(5)
C
C     WRONG MESSAGE TYPE RECEIVED
C
```

```
        IF (ITYPE.NE.65) GOTO 1100
C
        IF (IPNUM.NE.NUMBER) GOTO 1200
C
C       NOT READY TO LOAD CODE = 0
C
        IF (IACK.EQ.0) GOTO 1300
        IF (IACK.GE.2) GOTO 1000
C
C       FOUND IACK=1
C       REACH THIS POINT IF READY TO START SENDING PROGRAM TO ROBOT
C
        IBLKCT=0
C
C       SENDS BLOCK NUMBER AND 252 BYTES OF DATA IN EACH BLOCK
C
C*************************************************************************
C
C       NOTE!! THIS BLOCK SIZE IS A GUESS  UNTIL WE KNOW WHAT
C       AMERICAN ROBOTICS TRANSMITTS SINCE THIS IS NOT STATED
C       IN THE SPECIFICATIONS.
C
C*************************************************************************
C
C
        DO 300 I=1,ITOTBK
C
C       STARTS SENDING PROGRAM HERE
C
        CALL SEND(IERROR,ILEN,IDATA)
C
        IF (IERROR.EQ.1) GOTO 2100
        IF (IERROR.EQ.2) GOTO 2200
        IF (IERROR.GE.3) GOTO 2300
C
        IBLOCK=IDATA(4)
        IF (IBLOCK.NE.IBLKCT) GOTO 4100
C
C       PUT ARRAY ON DISK IN UNFORMATTED SEQUENTIAL FORM.
C       ONLY 256 WORDS SAVED TO EFFICIENTLY USE DISK SPACE.
C       THIS PRESUMES THAT ONLY 252 BYTES OF DATA WAS TRANSMITTED
C       IN A GIVEN BLOCK AND THAT THESE ARE SAVED IN THE LOW-ORDER BYTES
C       OF THE 256 WORD ARRAY IDATA.
C
C       THE ARRAY ALSO CONTAINS THE LENGTH OF THE MESSAGE,
C       THE SEQUENCE NUMBER, THE TYPE CODE, AND THE LOGITUDINAL
C       REDUNDANCY CHECK BYTE STORED IN THE LAST ELEMENT OF THE
C       ARRAY THAT IS RECORDED ON DISK (I.E. IDATA(256)).
C
        CALL REQTS(NUMBER,IERROR)
C
        IF (IERROR.EQ.1) GOTO 2100
        IF (IERROR.EQ.2) GOTO 2200
        IF (IERROR.GE.3) GOTO 2300
```

```
C
      READ (9,ERR=950) (IDATA(I),I=1,256)
C
      IBLOCK=IBLOCK+1
C
300   CONTINUE
C
      CLOSE (UNIT=9,DISPOSE='KEEP',ERR=992)
C
C
      WRITE (WT,500) IPNUM
500   FORMAT(//,' PROGRAM NO.',I4,' SUCCESSFULLY LOADED',/,
     1           ' PRESS "RETURN" TO GOT MAIN MENU.> ',$)
      READ  (RT,904) INPUT
      RETURN
C
400   WRITE (WT,402)
402   FORMAT(//,' ONLY PROGRAM NUMBERS 1-9 ACCEPTABLE.')
      GOTO 10
C
```

```
C-----------------------------------------------------------------------
C
C       ALL OF THE VARIOUS ERROR MESSAGES FOLLOW:
C
900     CONTINUE
        WRITE (WT,902)
902     FORMAT(//,' FATAL ERROR! FILE WILL BE DELETED.',/,
     1          ' PRESS "RETURN" TO GOTO MAIN MENU.> ',$)
        READ  (RT,904) INPUT
904     FORMAT(I4)
C
        CLOSE (UNIT=9,DISPOSE='DELETE',ERR=990)
C
        RETURN
C
950     WRITE (WT,952)
952     FORMAT(//,' ERROR READING FILE FROM DISK!')
        GOTO 900
C
990     WRITE (WT,992)
992     FORMAT(//,' ERROR CLOSING FILE CONTAINING PROGRAM.',/,
     1          ' PRESS RETURN TO GOTO MAIN MENU> ',$)
        READ  (RT,904) INPUT
        RETURN
C
1000    WRITE (WT,1002)
1002    FORMAT(//,' ILLEGAL ACKNOWLEDGE CODE RECEIVED,')
        GOTO 900
C
1100    WRITE (WT,1102)
1102    FORMAT (//,' WRONG MESSAGE TYPE RECEIVED!')
        GOTO 900
C
1200    WRITE (WT,1202)
1202    FORMAT(//,' WRONG PROGRAM NUMBER RETURNED BY ROBOT!')
        GOTO 900
C
1300    WRITE (WT,1302)
1302    FORMAT(//,' ROBOT NOT READY TO LOAD PROGRAM.',
     1          ' TYPE "RETURN" TO TRY AGAIN> ',$)
        READ  (RT,904) INPUT
        GOTO 120
C
2100    WRITE (WT,2102)
2102    FORMAT(//,' TIME OUT ERROR WHILE WAITING FOR SEND',/,
     1          ' ACKNOWLEDGE FROM ROBOT.')
        GOTO 900
C
2200    WRITE (WT,2202)
2202    FORMAT(//,' LRC ERROR MESSAGE RETURNED AFTER TRANSMISSION.')
        GOTO 900
C
2300    WRITE (WT,2302) IERROR
2302    FORMAT(//,' ILLEGAL ACKNOWLEDGE CODE',I4,' RECEIVED',
```

```
     1            ' AFTER TRANSMISSION TO ROBOT.')
3100     WRITE (WT,3102)
3102     FORMAT(//,' FIVE SECOND TIMEOUT OCCURED DURING RECEIVE.')
         GOTO 900
C
3200     WRITE (WT,3202)
3202     FORMAT(//,' CHECKSUM ERROR CALCULATION PRODUCED ERROR',
     1            ' DURING RECEIVE.')
         GOTO 900
C
3300     WRITE (WT,3302) IERROR
3302     FORMAT(//,' ILLEGAL ERROR CODE',I4,' RETURNED FROM',
     1            ' RECEIVE SUBROUTINE.')
         GOTO 900
C
         END
```

```
C*************************************************************************
C
      SUBROUTINE RUN
C
C     FRED R. SIAS, JR.
C     10 JULY 1984
C
C     THIS ROUTINE IS USED TO START ANY PROGRAM STORED IN THE ROBOT.
C     THE PARTICULAR PROGRAM IS SELECTED BY NUMBER WHICH IS REQUESTED
C     BY THIS PROGRAM AND PASSED TO THE ROBOT AS PART OF THE MESSAGE.
C
C     THE LOAD PROGRAM IN THE MINC MAY BE USED TO TRANSFER A PROGRAM
C     FROM THE MINC DISC TO THE ROBOT MEMORY PRIOR TO STARTING THE
C     PROGRAM USING THIS RUN ROUTINE.
C
C     THE ACTUAL MESSAGE TRANSMITTED BY THIS ROUTINE IS THE
C     "SET PROGRAM MODE" MESSAGE.  THIS MUST BE TRANSMITTED WHILE THE
C     ROBOT IS IN THE "NO-ACTIVITY STATE" OTHERWISE IT WILL BE IGNORED.
C     THE PROGRAM MUST ALREADY BE STORED IN THE ROBOT CONTROLLER MEMORY.
C
C     THE KEYSWITCH ON THE ROBOT MUST BE ENABLED FOR THIS MESSAGE TO
C     FUNCTION.
C
C     MESSAGE TYPE CODE = 131
C
C*************************************************************************
C
      INTEGER*2 WT,RT,IDATA(257),INDATA
      INTEGER*2 ILEN,IERROR
C
      WT = 7
      RT = 5
C
10    CONTINUE
      WRITE (WT,100)
100   FORMAT(//,' PLEASE TYPE PROGRAM NUMBER SELECTED',
     1          ' AND A CARRIAGE RETURN> ',$)
      READ  (RT,110,ERR = 10) INDATA
110   FORMAT(I4)
      IF (INDATA.LT.1.OR.INDATA.GT.9) GOTO 10
C
C     LENGTH OF MESSAGE TO TRANSMIT
      IDATA(1) = 3
C     SET SEQUENCE NUMBER TO 0
      IDATA(2) = 0
C     SET TYPE CODE TO 131
      IDATA(3) = 131
C     SET PROGRAM STATUS TO "RUN"
      IDATA(4) = 1
C     TRANSMIT PROGRAM NUMBER
      IDATA(5) = INDATA
C
      ILEN = 5
C
```

```
      CALL SEND (IERROR,ILEN,IDATA)
C
      IF (IERROR.EQ.0) WRITE (WT,1010)
      IF (IERROR.EQ.1) WRITE (WT,1020)
      IF (IERROR.EQ.2) WRITE (WT,1030)
      IF (IERROR.GE.3) WRITE (WT,1040)
C
      WRITE (WT,1050)
      READ  (RT,1060) INPUT
C
1010  FORMAT(//,' MESSAGE ACKNOWLEDGED!')
1020  FORMAT(//,' TIMEOUT ERROR - MESSAGE NOT ACKNOWLEDGED!')
1030  FORMAT(//,' LRC ERROR MESSAGE RETURNED FROM ROBOT!')
1040  FORMAT(//,' UNKNOWN ERROR MESSAGE RETURNED FROM SUBROUTINE SEND!')
1050  FORMAT(//,' DO YOU WISH TO HALT THE PROGRAM? (Y OR N) ',$)
1060  FORMAT(A4)
C
      IF (INPUT.EQ.'Y') GOTO 2000
C
      RETURN
C
2000  IDATA(4) = 2
C
      CALL SEND (IERROR,ILEN,IDATA)
C
      IF (IERROR.EQ.0) WRITE (WT,1010)
      IF (IERROR.EQ.1) WRITE (WT,1020)
      IF (IERROR.EQ.2) WRITE (WT,1030)
      IF (IERROR.GE.3) WRITE (WT,1040)
      WRITE (WT,1070)
1070  FORMAT(//,' PRESS "RETURN" TO CONTINUE> ',$)
      READ  (RT,1060) INPUT
C
      RETURN
      END
```

```
C*************************************************************************
C
      SUBROUTINE MESAGE
C
C     THIS ROUTINE ACCEPTS A MESSAGE FROM COMPUTER KEYBOARD
C     AND TRANSMITS TO ROBOT FOR DISPLAY ON CONSOLE
C
C     FRED R. SIAS, JR.
C     25 JUNE 1984
C
C*************************************************************************
C
      BYTE STRING(254)
      INTEGER*2 IDATA(257),RT,WT,INPUT
      LOGICAL*1 PROMT(16)
C
      DATA PROMT /'I','N','P','U','T',' ','M',
     1          'E','S','S','A','G','E',':',' ',00/
      RT=5
      WT=7
C
      WRITE (WT,10)
10    FORMAT(' INPUT SEQUENCE NUMBER: ',$)
      READ  (RT,15) IDATA(2)
15    FORMAT(I3)
C
      IDATA(3)=133
C
C
      CALL GTLIN(STRING,PROMT)
C
      LENGTH=LEN(STRING)
C
      ILEN=LENGTH+3
      DO 100 I=4,ILEN
      IDATA(I)=STRING(I-3)
100   CONTINUE
      IDATA(1)=LENGTH+1
C
      CALL SEND(IERROR,ILEN,IDATA)
C
      IF (IERROR.EQ.2) WRITE (WT,110)
110   FORMAT(//,' CHECKSUM ERROR. DATA MAY BE WRONG.')
      IF (IERROR.EQ.1) WRITE (WT,120)
120   FORMAT(//,' TIMEOUT ERROR. ROBOT DID NOT RESPOND.')
      WRITE (WT,130)
130   FORMAT(/,' TYPE "RETURN" TO CONTINUE> ',$)
      READ  (RT,140) INPUT
140   FORMAT(I4)
C
      RETURN
      END
```

```
C*************************************************************************
C
      SUBROUTINE DEBUG
C
C     THIS ROUTINE PERMITS CONTROL OF INDIVIDUAL WORDS TRANSMITTED TO
C     OR RECEIVED FROM THE EXTERNAL DEVICE INTERFACE.
C
C     FRED R. SIAS, JR.
C     24 MAY 1984
C
C*************************************************************************
C
C     DECLARATIONS
C
      INTEGER*2 INPUT,RT,WT
C
      RT=5
      WT=7
C
C     COMMAND INTERPRETER
C
100   CONTINUE
      WRITE (WT,110)
110   FORMAT('1',//////,
     1       ' COMMANDS:',/,
     2       '    A = Accept WORD and display in HEX',/,
     3       '    T = Transmit WORD (HEX input will be requested',/,
     6       '    E = Exit to main menu',/,
     7       '    Carriage return alone to display this menu')
C
120   CONTINUE
      WRITE (WT,125)
125   FORMAT(//////////,
     1       ' COMMAND >',$)
C
      READ (RT,130) INPUT
130   FORMAT(A2)
C
      IF (INPUT.EQ.'') GOTO 100
      IF (INPUT.EQ.'A') GOTO 1000
      IF (INPUT.EQ.'T') GOTO 2000
      IF (INPUT.EQ.'E') RETURN
C
      WRITE (WT,140)
140   FORMAT(//,' NO SUCH COMMAND! TRY AGAIN.')
      GOTO 100
C
C-------------------------------------------------------------------------
C
1000  CONTINUE
C
C     ACCEPT COMMAND ROUTINE - ACCEPTS WORD FROM ROBOT AND
C     DISPLAYS IT IN HEX ON THE CRT
C
```

```
        IMASK="177777
        IUNIT=0
        CALL DINP(IUNIT,IMASK,IERR,INDATA)
        WRITE (WT,1010) INDATA
1010    FORMAT(' ','INDATA FROM DINP= ',I10)
        IF (IERR.NE.1) GOTO 1900
        WRITE (WT,1100) IUNIT
1100    FORMAT(' INPUT DATA FROM UNIT ',I1,' WAS ',$)
        CALL DHEXOU(INDATA)
        GOTO 120
1900    CONTINUE
C
C       ERROR PRINTING ROUTINE FOR DIGITAL INPUT DEVICE
C
        WRITE (WT,1910) IUNIT,IERR
1910    FORMAT(' ERROR CODE ',I3,' RETURNED WHEN READING UNIT ',I1,',')
        GOTO 120
C
C-------------------------------------------------------------------------
C
2000    CONTINUE
C       TRANSMIT COMMAND ROUTINE - REQUESTS DATA FROM KEYBOARD AND
C       TRANSMITS TO ROBOT.
C
        IMASK="177777
        IUNIT=0
        WRITE (WT,2100)
2100    FORMAT(' INPUT 16-BIT PATTERN TO TRANSMIT TO ROBOT IN HEX: ',$)
        CALL DHEXIN(INPUT)
        CALL DOUT(IUNIT,IMASK,IERR,INPUT)
        IF (IERR.NE.1) GOTO 2900
        GOTO 120
2900    CONTINUE
C
C       ERROR PRINTING ROUTINE FOR DIGITAL INPUT DEVICE
C
        WRITE (WT,2910) IUNIT,IERR
2910    FORMAT(' ERROR CODE ',I3,' RETURNED WHEN SENDING BY UNIT ',I1,',')
        GOTO 120
C
        END
```

```
C*************************************************************************
C
      SUBROUTINE ACCEPT
C
C     ROUTINE FOR RECEIVING A MESSAGE FROM THE ROBOT AND
C     DISPLAYING THE DATA TRANSMITTED AS AN ARRAY IN HEX.
C
C     FRED R. SIAS, JR.
C     NASA/ASEE SUMMER FACULTY FELLOW FROM CLEMSON UNIVERSITY
C
C     12 JULY 1984
C
C*************************************************************************
C
C     DECLARATIONS
C
      INTEGER*2 IDATA(257),INPUT, RT, WT
C
C     INITIALIZATION
C
      WT=7
      RT=5
C
3000  CONTINUE
C
      WRITE (WT,3100)
3100  FORMAT(//,'      ************WAITING************',///,
     1          ' Press RETURN to give up!) ',$)
C
C     COMMAND TO RECEIVE AN ARRAY AND DISPLAY IN HEX
C
      CALL RECEVE(IERROR,ILEN,ICSUM,IDATA)
C
      WRITE (WT,3001) IERROR,ILEN,ICSUM
3001  FORMAT(' '//,' IERROR=',I8,' ILEN=',I8,' ICSUM=',I8)
C
      WRITE (WT,3002) IDATA(3)
3002  FORMAT(//,' TYPE CODE RECEIVED: ',I2)
C
      IF (IERROR.EQ.0) GOTO 3030
      IF (IERROR.EQ.1) GOTO 3060
      IF (IERROR.EQ.2) GOTO 3010
C
3004  CONTINUE
      WRITE (WT,3005) IERROR
3005  FORMAT(/,' ILLEGAL ERROR CODE',I4,' RECEIVED')
      GOTO 3030
3010  CONTINUE
      WRITE (WT,3011)
3011  FORMAT(/,' CHECKSUM ERROR!')
C
3020  FORMAT(A2)
C-------------------------------------------------------------------
C
```

```
C       THIS IS NORMAL PATH TO DISPLAY ARRAY
C
3030    CONTINUE
        LENGTH=IDATA(1)+3
        DO 3040 I=1,LENGTH
        IBYTE=IDATA(I)
        CALL HEXOUT(IBYTE)
3040    CONTINUE
        WRITE (WT,3050)
3050    FORMAT(//,' PRESS RETURN TO CONTINUE> ',$)
        READ (RT,3020) INPUT
        RETURN
C-------------------------------------------------------------------
C
3060    CONTINUE
        WRITE (WT,3065)
3065    FORMAT(/,' TIMEOUT ERROR CODE RECEIVED!')
        GOTO 3040
        END
```

```
C*************************************************************************
C
      SUBROUTINE TRNSMT
C
C     SUBROUTINE FOR TRANSMITTING AN ARRAY TO THE ROBOT.
C
C     FRED R. SIAS, JR.
C     NASA/ASEE SUMMER FACULTY FELLOW FROM CLEMSON UNIVERSITY
C
C     12 JULY 1984
C
C*************************************************************************
C
C     DECLARATIONS
C
      INTEGER*2 IDATA(257),INPUT,RT,WT
C
C     INITIALIZATION
C
      WT=7
      RT=5
C
4000  CONTINUE
C
C     COMMAND TO ACCEPT ELEMENTS AND TRANSMIT A TEST ARRAY
C
      WRITE (WT,4010)
4010  FORMAT(' INPUT SEQUENCE NUMBER IN DECIMAL> ',$)
      READ (RT,4020) INPUT
4020  FORMAT(I4)
      IDATA(2)=INPUT
      WRITE (WT,4030)
4030  FORMAT(' INPUT TYPE CODE IN DECIMAL> ',$)
      READ (RT,4020) INPUT
      IDATA(3)=INPUT
      WRITE (WT,4040)
4040  FORMAT(' INPUT HEX DATA BYTES EACH FOLLOWED BY "RETURN":',/,
     1       ' TYPE "X" TO TERMINATE DATA INPUT')
C
      ICOUNT=0
      DO 4050 I=1,253
      CALL HEXIN(INPUT)
      IF (INPUT.EQ.999) GOTO 4060
      IDATA(I+3)=INPUT
      ICOUNT=ICOUNT+1
4050  CONTINUE
4060  CONTINUE
C     MESSAGE LENGTH INCLUDES LENGTH, SEQ. NO. AND TYPE CODE
      ICOUNT=ICOUNT+3
      IDATA(1)=ICOUNT
      CALL SEND(IERROR,ICOUNT,IDATA)
C
      IF (IERROR.EQ.1) WRITE (WT,4100)
      IF (IERROR.EQ.2) WRITE (WT,4150)
```

```
      IF (IERROR.EQ.0) WRITE (WT,4160)
C
      WRITE (WT,4200)
4100  FORMAT(/,' TIMEOUT ERROR CODE RETURNED!')
4150  FORMAT(/,' LRC CHECK BYTE ERROR CODE RETURNED FROM ROBOT!')
4160  FORMAT(/,' DATA TRANSMITTED AND ACKNOWLEDGED BY ROBOT!')
4200  FORMAT(//,' PRESS RETURN TO CONTINUE> ',$)
      READ  (RT,4020) INPUT
C
      RETURN
      END
C
```

```
C*************************************************************************
C
      SUBROUTINE HEXOUT(IOHEX)
C
C     SUBROUTINE TO CONVERT INTEGER*2 TO HEX AND DISPLAY ON CRT
C
C     FRED R. SIAS, JR.
C     24 MAY 1984
C
C*************************************************************************
C
      INTEGER*2 IDATA,RT,WT
      BYTE IBYTE(2)
      EQUIVALENCE (IDATA,IBYTE(1))
C
      RT=5
      WT=7
      MSD=IOHEX/16
      LSD=IOHEX-(16*MSD)
C
C     WRITE (WT,50) ' (',MSD,'/ ',LSD,'/ ',MSD,'/ ',LSD,')'
C50   FORMAT(' ',I4,I4,A1,A1)
      CALL CNVDIG(MSD)
      IF (MSG.EQ.99) GOTO 10
      IBYTE(1)=MSD
      CALL CNVDIG(LSD)
      IF (LSD.EQ.99) GOTO 10
      IBYTE(2)=LSD
      WRITE (WT,100) IDATA
100   FORMAT(' ',A2)
C
10    RETURN
      END
C
```

```
C*************************************************************************
C
      SUBROUTINE HEXIN(INHEX)
C
C     SUBROUTINE TO ACCEPT TWO HEX DIGITS FROM KEYBOARD AND
C     CONVERT TO INTEGER*2
C
C     FRED R. SIAS, JR.
C     24 MAY 1984
C
C*************************************************************************
C
C     DECLARATIONS
C
      BYTE DIGIT(2)
      INTEGER*2 INHEX,INPUT,RT,WT
      EQUIVALENCE (INPUT,DIGIT(1))
C
      RT=5
      WT=7
C
10    CONTINUE
      READ (RT,100) INPUT
100   FORMAT(A2)
      IF (INPUT.EQ.'X') GOTO 150
C
C     WRITE (WT,120) DIGIT(1),DIGIT(2)
C120  FORMAT (' ',A1,A1)
C
      IDIGIT=DIGIT(1)
      CALL ATOI(IDIGIT)
      IF (IDIGIT.EQ.99) GOTO 10
      INHEX=16*IDIGIT
C
      IDIGIT=DIGIT(2)
      CALL ATOI(IDIGIT)
      IF (IDIGIT.EQ.99) GOTO 10
      INHEX=INHEX+IDIGIT
      RETURN
C
150   CONTINUE
      INHEX=999
      RETURN
      END
C
```

```
C*************************************************************************
C
      SUBROUTINE DHEXIN(INHEX)
C
C     SUBROUTINE TO ACCEPT FOUR HEX DIGITS FROM KEYBOARD AND
C     CONVERT TO INTEGER*2
C
C     REVISION OF TWO DIGIT ROUTINE
C
C     FRED R. SIAS, JR.
C     22 JUNE 1984
C
C*************************************************************************
C
C     DECLARATIONS
C
      BYTE INPUT(4),TABLE(8)
      INTEGER*2 INHEX,INDATA(4),RT,WT
      INTEGER*4 INP
      EQUIVALENCE (INDATA(1),TABLE(1))
      EQUIVALENCE (INP,INPUT(1))
C
      RT=5
      WT=7
C
10    CONTINUE
      READ (RT,100) INP
100   FORMAT(A4)
C
      TABLE(2)=0
      TABLE(4)=0
      TABLE(6)=0
      TABLE(8)=0
      TABLE(1)=INPUT(1)
      TABLE(3)=INPUT(2)
      TABLE(5)=INPUT(3)
      TABLE(7)=INPUT(4)
C
      DO 200 I=1,4
      CALL ATOI(INDATA(I))
C
      IF (INDATA(I).EQ.99) GOTO 10
200   CONTINUE
      INHEX=INDATA(1)*4096
      INHEX=INHEX+256*INDATA(2)
      INHEX=INHEX+16*INDATA(3)
      INHEX=INHEX+INDATA(4)
C
      RETURN
      END
C
```

```
C*************************************************************************
C
      SUBROUTINE DHEXOU(IOHEX)
C
C     SUBROUTINE TO CONVERT INTEGER*2 TO 4 DIGIT HEX AND DISPLAY ON CRT
C
C     MODIFIED FROM HEXOUT
C
C     FRED R. SIAS, JR.
C     22 JUNE 1984
C
C*************************************************************************
C
      INTEGER*2 RT,WT,IOHEX,IDIGIT,IDATA(2),ITEMP
      BYTE IBYTE(2),IBITE(4),IOUT(4)
      EQUIVALENCE (ITEMP,IBYTE(1))
      EQUIVALENCE (IBITE(1),IDATA(1))
C
      RT=5
      WT=7
      ITEMP=IOHEX
      IBITE(2)=0
      IBITE(4)=0
      IBITE(1)=IBYTE(2)
      IBITE(3)=IBYTE(1)
C     WRITE (WT,111) IDATA(1)
C     WRITE (WT,111) IDATA(2)
111   FORMAT(I8)
      IDIGIT=IDATA(1)/16
      CALL CNVDIG(IDIGIT)
      IOUT(1)=IDIGIT
      IDIGIT=IDATA(1)-((IDATA(1)/16)*16)
      CALL CNVDIG(IDIGIT)
      IOUT(2)=IDIGIT
C
      IDIGIT=IDATA(2)/16
      CALL CNVDIG(IDIGIT)
      IOUT(3)=IDIGIT
      IDIGIT=IDATA(2)-((IDATA(2)/16)*16)
      CALL CNVDIG(IDIGIT)
      IOUT(4)=IDIGIT
C
      WRITE (WT,150) (IOUT(I),I=1,4)
150   FORMAT(' ',4A1)
C
10    RETURN
      END
```

```
C*************************************************************************
C
      SUBROUTINE ATOI(IDIGIT)
C
C     SUBROUTINE TO CONVERT ASCII VALUE OF HEX DIGIT TO AN INTEGER
C
C*************************************************************************
C
      INTEGER*2 RT,WT
      RT=5
      WT=7
C
C
      IF (IDIGIT.EQ.48) IDIGIT=0
      IF (IDIGIT.EQ.49) IDIGIT=1
      IF (IDIGIT.EQ.50) IDIGIT=2
      IF (IDIGIT.EQ.51) IDIGIT=3
      IF (IDIGIT.EQ.52) IDIGIT=4
      IF (IDIGIT.EQ.53) IDIGIT=5
      IF (IDIGIT.EQ.54) IDIGIT=6
      IF (IDIGIT.EQ.55) IDIGIT=7
      IF (IDIGIT.EQ.56) IDIGIT=8
      IF (IDIGIT.EQ.57) IDIGIT=9
      IF (IDIGIT.EQ.65) IDIGIT=10
      IF (IDIGIT.EQ.66) IDIGIT=11
      IF (IDIGIT.EQ.67) IDIGIT=12
      IF (IDIGIT.EQ.68) IDIGIT=13
      IF (IDIGIT.EQ.69) IDIGIT=14
      IF (IDIGIT.EQ.70) IDIGIT=15
C
C     WRITE (WT,100) IDIGIT
C
C     ERROR TRAP FOR NON HEX DIGIT
C     COULD FAKE IT OUT BY TYPING ASCII CONTROL CODES 0-15
C
      IF (IDIGIT.GT.15) GOTO 500
      IF (IDIGIT.LT.0)  GOTO 500
C
      RETURN
C
500   WRITE (WT,510)
510   FORMAT(///,' ILLEGAL DIGIT PLEASE REENTER DATA.',//)
      IDIGIT=99
      RETURN
      END
C
```

```
C*************************************************************************
C
      SUBROUTINE CNVDIG(INTHEX)
C
C     ROUTINE TO CONVERT BINARY-CODED INTEGER TO ASCII
C
C*************************************************************************
C
      INTEGER*2 RT,WT
      RT=5
      WT=7
C
      IF (INTHEX.LT.0) GOTO 500
      IF (INTHEX.GE.16) GOTO 500
      IF (INTHEX.EQ.0)  INTHEX=48
      IF (INTHEX.EQ.1)  INTHEX=49
      IF (INTHEX.EQ.2)  INTHEX=50
      IF (INTHEX.EQ.3)  INTHEX=51
      IF (INTHEX.EQ.4)  INTHEX=52
      IF (INTHEX.EQ.5)  INTHEX=53
      IF (INTHEX.EQ.6)  INTHEX=54
      IF (INTHEX.EQ.7)  INTHEX=55
      IF (INTHEX.EQ.8)  INTHEX=56
      IF (INTHEX.EQ.9)  INTHEX=57
      IF (INTHEX.EQ.10) INTHEX=65
      IF (INTHEX.EQ.11) INTHEX=66
      IF (INTHEX.EQ.12) INTHEX=67
      IF (INTHEX.EQ.13) INTHEX=68
      IF (INTHEX.EQ.14) INTHEX=69
      IF (INTHEX.EQ.15) INTHEX=70
C
200   CONTINUE
      RETURN
500   CONTINUE
      WRITE (WT,510)
510   FORMAT(' NOT A LEGAL HEX DIGIT FOR OUTPUT')
      INTHEX=99
      RETURN
      END
```

```
      IDATA(1)=46
C
      ILEN=48
C
C     WILL TRY TO SEND FIVE TIMES
C
      DO 5200 I=1,5
C
      CALL SEND(IERROR,ILEN,IDATA)
C
      IF (IERROR.EQ.0) GOTO 5500
C
5200  CONTINUE
C
      WRITE (WT,5210)
5210  FORMAT(//,' MINC GAVE UP AFTER 5 TRIES TO SEND!',/)
C
      WRITE (WT,5220)
5220  FORMAT(/,' PUSH "RETURN" TO CONTINUE> ',$)
      READ  (RT,5230) INPUT
5230  FORMAT(A4)
      RETURN
C
5500  CONTINUE
C     HERE IF INITIALIZATION COMPLETE AND OK
      WRITE (WT,5510)
5510  FORMAT(//,' INITIALIZATION COMPLETE AND OK!',/,
     1          ' PRESS "RETURN" TO CONTINUE> ',$)
      READ  (RT,5230) INPUT
C
      RETURN
      END
```

```
5000    CONTINUE
C
        ITYPE=IDATA(3)
        IF (ITYPE.EQ.1) GOTO 5100
C
        WRITE (WT,5010)
5010    FORMAT(//,' WRONG TYPE CODE (',I4,') RECEIVED FROM ROBOT!',/,
     1           ' PRESS "RETURN" TO CONTINUE> ',$)
        READ  (RT,5230) INPUT
        RETURN
C
5100    CONTINUE
C       HERE TO PROCESS ACCEPTABLE REQUEST
C
C       RETURN STATUS/IDENTIFICATION INFO TO ROBOT
C
        IDATA(3)=129
C
C       DEVICE TYPE = 1 I.E. THIS IS A COMPUTER
        IDATA(4)=1
C
C       DEVICE IDENTIFICATION = "MNC"
C
        IDATA(5)=77
        IDATA(6)=78
        IDATA(7)=67
C
C       SYSTEM STATUS IS OPERATIONAL
        IDATA(8)=1
C
C       SEND MESSAGE "MINC OK - CYRO1 V1.0"
        IDATA(9)=77
        IDATA(10)=73
        IDATA(11)=78
        IDATA(12)=67
        IDATA(13)=32
        IDATA(14)=79
        IDATA(15)=75
        IDATA(16)=32
        IDATA(17)=45
        IDATA(18)=32
C       CYRO1
        IDATA(19)=67
        IDATA(20)=89
        IDATA(21)=82
        IDATA(22)=79
        IDATA(23)=49
        IDATA(24)=32
C       V1.0
        IDATA(25)=86
        IDATA(26)=49
        IDATA(27)=46
        IDATA(28)=48
C
```

```
      INTEGER*2 IDATA(257),RT,WT
      BYTE INPUT
C
      RT=5
      WT=7
C
10    CONTINUE
C
      WRITE (WT,50)
50    FORMAT(/,' WAITING FOR ROBOT TO RESPOND!',/,
     1           ' HIT ANY KEY TO QUIT WAITING.> ',$)
C
      CALL RECEVE(IERROR,ILEN,ICSUM,IDATA)
C
C     NORMAL EXIT WITH IERROR=0
      IF (IERROR.EQ.0) GOTO 5000
C
C     CHECKSUM ERROR IF IERROR = 2
      IF (IERROR.EQ.2) GOTO 2000
C
C     ILLEGAL ERROR CODE IF GREATER THAN 2
      IF (IERROR.GE.3) GOTO 3000
C
C     FALLS THRU TO HERE IF TIME OUT (IERROR=1)
C
      WRITE (WT,200)
200   FORMAT(//,' NO INITIALIZATION MESSAGE FROM ROBOT',/,
     1           ' PRESS "RETURN" TO CONTINUE> ',$)
      READ  (RT,5230) INPUT
C
      RETURN
C
C     HERE TO PROCESS CHECKSUM ERROR
2000  CONTINUE
      WRITE (WT,2010)
C
2010  FORMAT(//,' CHECKSUM DOES NOT COMPUTE!',/,
     1           ' TRY AGAIN? (Y OR N)> ',$)
      READ  (RT,5230) INPUT
      IF (INPUT.EQ.'Y') GOTO 10
      RETURN
C
C     HERE TO PROCESS ILLEGAL ERROR CODE AND RETURN TO MENU
3000  CONTINUE
C
      WRITE (WT,3010)
3010  FORMAT(//,' RECEIVED AN ILLEGAL ERROR CODE FROM RECEVE',
     1           ' SUBROUTINE.',/,
     2           ' PRESS "RETURN" TO CONTINUE> ',$)
      READ  (RT,5230) INPUT
      RETURN
C
C
C     HERE TO PROCESS INCOMING MESSAGE
```

```
C*************************************************************************
C
      SUBROUTINE INIT
C
C     FRED R. SIAS, JR.
C     25 JULY 1984
C
C     SUCCESSFUL COMPLETION OF THIS SUBROUTINE ESTABLISHES THAT
C     COMMUNICATION PROTOCOLS ARE WORKING PROPERLY.
C
C     THIS SUBROUTINE IS REQUESTED FROM THE MINC CONSOLE
C     PRIOR TO RESETTING THE ROBOT.
C     WHEN THE ROBOT IS RESET IT WILL REQUEST A DEVICE IDENT/STATUS
C     FROM THE MINC COMPUTER.
C           TYPE CODE = 1
C
C
C     THIS SUBROUTINE WILL RESPOND THAT THE MINC IS OPERATIONAL
C     AND WILL TRANSMIT THE APPROPRIATE CODES:
C           TYPE CODE = 129
C           DEVICE TYPE (1 BYTE) = 2   (MEANS THAT COMPUTER DEVICE)
C           DEVICE IDENT. (3 ASCII BYTES) = "MNC"
C           SYSTEM STATUD (1 BYTE)        = 1 (MEANS OPERATIONAL)
C           ASCII MESSG = "MINC OK - CYR01 V1.0"
C
C     THIS SUBROUTINE WILL CALL THE RECEVE SUBROUTINE TO WAIT FOR THE
C     INITIAL MESSAGE FROM THE ROBOT.  THE MINC WILL WAIT INDEFINITLY
C     FOR THE ROBOT TO RESPOND.  TO QUIT WAITING HIT ANY KEY ON THE MINC
C     CONSOLE AND THE PROGRAM WILL RETURN TO THE MAIN MENU.
C
C*************************************************************************
```

```
     1   '        10. Single WORD I/O',/,
     2   '        11. RECEIVE an array',/,
     3   '        12. TRANSMIT an array',//,
     2   '        "E" EXIT TO OPERATING SYSTEM',////,
     3   ' SELECT)',$)
C
      READ  (RT,400) INPUT
400   FORMAT(A2)
C
      IF (INPUT.EQ.'1')  CALL MOVE
      IF (INPUT.EQ.'2')  CALL POSIT
      IF (INPUT.EQ.'3')  CALL PARS
      IF (INPUT.EQ.'4')  CALL INPOS
      IF (INPUT.EQ.'5')  CALL INIT
      IF (INPUT.EQ.'6')  CALL SAVE
      IF (INPUT.EQ.'7')  CALL LOAD
      IF (INPUT.EQ.'8')  CALL RUN
      IF (INPUT.EQ.'9')  CALL MESAGE
      IF (INPUT.EQ.'10') CALL DEBUG
      IF (INPUT.EQ.'11') CALL ACCEPT
      IF (INPUT.EQ.'12') CALL TRNSMT
      IF (INPUT.EQ.'E') STOP
C
      GOTO 300
C
      END
```

```
C
C       DECLARATIONS
C
        INTEGER*2 IDATA(257),INPUT, RT, WT
        REAL X
C
C       INITIALIZATION
C
        WT=7
        RT=5
C
        WRITE (WT,100)
100     FORMAT('1',/////,
     1          '                                MANUAL CHECKOUT ROUTINE FOR',/,
     2          '                            CYRO 750 EXTERNAL DEVICE INTERFACE',//,
     3          '                                    F. R. SIAS, JR.',//,
     4          '                              NASA/ASEE - CLEMSON UNIVERSITY',/,
     5          '                                         JUNE 1984',//////////,
     6          ' TO CONTINUE PRESS RETURN>'$)
C
        READ  (RT,110) X
110     FORMAT(G6.0)
C
        WRITE(WT,200)
200     FORMAT('1',//////,
     1  ' Select test mode by item number in the following menu.',/,
     2  ' Then provide requested parameters.',//,
     3  ' YOU MUST TURN ON THE MINC COMPUTER AND EXECUTE THE',/,
     4  ' INITIALIZATION PROGRAM (MENU SELECTION 5) BEFORE THE',/,
     5  ' ROBOT WILL RESPOND TO OTHER COMMANDS!  RESET THE ROBOT',/,
     6  ' AFTER MENU ITEM 5 HAS BEEN SELECTED.',//,
     7  ' Use "return" or "enter"',/,
     3  ' to terminate each entry parameter or to advance to the next',/,
     4  ' whenever the following is displayed:',//////,
     5  ' SELECT >',$)
C
        READ (RT,110) X
C
C       MAIN SELECTION MENU
C
300     CONTINUE
C
        WRITE (WT,310)
310     FORMAT('1',/////,
     1  ' CYRO 750 EXTERNAL DEVICE INTERFACE TEST MENU:',//,
     2  '       1.  MOVE Robot',/,
     3  '       2.  Request Robot POSITION',/,
     4  '       3.  Request Robot System PARAMETERS',/,
     5  '       4.  Send IN-POSITION  command',/,
     6  '       5.  INITIALIZE System. (Reset Robot.)',/,
     7  '       6.  Get a program from robot and SAVE',/,
     8  '       7.  LOAD program and verify',/,
     9  '       8.  RUN program',/,
     1  '       9.  SEND message to robot console',/,
```

```
C*************************************************************************
C
      PROGRAM CYRO1
C
C     MAINLINE PROGRAM AND STUBS FOR TESTING ADVANCED ROBOTICS
C     EXTERNAL DEVICE INTERFACE OPTION
C
C     FRED R. SIAS, JR.
C     NASA/ASEE SUMMER FACULTY FELLOW FROM CLEMSON UNIVERSITY
C
C     18 MAY 1984
C
C*************************************************************************
C
C     This is the mainline program for a system that may be used to
C     communicate with the Advanced Robotics CYRO 750 Robot.
C
C     The main selection menu allows one to select one of the following
C     features:
C
C      CYRO 750 EXTERNAL DEVICE INTERFACE TEST MENU:
C
C            1.  MOVE Robot
C            2.  Request Robot POSITION
C            3.  Request Robot System PARAMETERS
C            4.  Send IN-POSITION command
C            5.  INITIALIZE System. (Reset Robot!)
C            6.  Get program from robot and SAVE
C            7.  LOAD program and verify
C            8.  RUN a program
C            9.  Send MESSAGE to robot console
C            10. Single WORD I/O
C            11. RECEIVE an array
C            12. TRANSMIT an array
C            "E" EXIT to the operating system
C
C
C     SELECT>
C
C*************************************************************************
```

D24

1984

NASA/ASEE SUMMER FACULTY RESEARCH FELLOWSHIP PROGRAM

MARSHALL SPACE FLIGHT CENTER

THE UNIVERSITY OF ALABAMA

DEBRIS IMPACT ON EARTH-ORBITING SPACECRAFT

Prepared By:	Dallas G. Smith, Ph.D
Academic Rank:	Professor
University and Department:	Tennessee Technological University Department of Civil Engineering
NASA/MSFC:	
Laboratory:	Structures and Propulsion
Division:	Structures
Branch:	Structural Development
MSFC Counterpart:	Erich E. Engler
Date:	August 3, 1984
Contract No.:	NASA-NGT-01-002-099 (The University of Alabama)

DEBRIS IMPACT ON EARTH-ORBITING SPACECRAFT

BY

Dallas G. Smith
Professor of Civil Engineering
Tennessee Technological University
Cookeville, Tennessee

ABSTRACT

The accumulation in recent years of Earth-orbiting space debris leads to some important new design considerations. Some 5,000 orbiting objects, many of them explosion fragments, are currently being tracked. Many objects too small to track are known to exist. Future collision of these objects with each other is predicted. These collisions will occur at high velocities in the neighborhood of 10 km/s. Consequently, each collision will be explosive, ejecting thousands, perhaps millions, of new orbiting objects, in turn increasing the frequency of future collisions. The debris population may thus become "self-regenerative," and the future flux of orbiting debris will exceed that of meteoroids. As a result, a large space structure in earth-orbit for several years has a significant probability of impact by debris objects. As a design problem, debris impact is significantly different from meteoroid impact. Past meteoroid calculations involved particles of low mass, on the order of 10^{-2} gm. Orbiting debris objects are much larger, on the order of several centimeters in size. Protection against such large objects may require severe structural measures. Thus debris impact could be one of the prime considerations in the design of large, earth-orbiting spacecraft. Curbing the addition of man-made objects by international agreement could help solve the problem.

ACKNOWLEDGEMENTS

The author acknowledges the support of the NASA/ASEE Summer Faculty Fellowship Program which made this research possible.

Appreciation is extended to the scholars and scientists whose work was used in the preparation of this report. B. G. Cour-Palais and D. J. Kessler, as well as many others mentioned in the Introduction, have written with great clarity, imagination and foresight on the space debris problem. Their work is prophetic.

The author is grateful to several members of the Structures Division of the Structures and Propulsion Laboratory. Erich Engler, counterpart and Structural Development Branch Chief, offered support and hospitality throughout the summer. Clyde Nevins, Division Chief provided information and guidance based on his considerable knowledge of the meteoroid impact problem. Linda Hillis, an efficient and good-humored secretary, typed this report with skill and patience.

INTRODUCTION AND OBJECTIVES

A growing number of scientists are becoming aware of the space debris issue. Early on, Brooks[1] expressed concern over the debris impact hazard. He noted that an order of magnitude increase in structural resistance to penetration failed to produce a corresponding decrease in penetration probability. Kessler and Cour-Palais[2] in 1978 introduced the notion that collisions among satellites could generate fragments which could impact other satellites. Kessler et al[3] continued to publize the hazard. In 1981 Kessler[4] coined the phase "self-regenerative" to denote the self propagating nature of the debris. Finally, in 1981, an AIAA position paper[5] called for corrective action and an international dialog to recommend policy. An orbital debris workshop[6], and recent papers by Reynolds, Fischer and Rice[7] and by Chobotov[8] reflect the growing concern. But, the recent report by Johnson[9] shows, the debris population continues to grow.

Some of the results on the accumulation of space debris of those mentioned above will be reviewed. The implications of those results in the design of a large space station will be considered. The main objective will be to call attention to the menance posed by space debris.

OBSERVED DEBRIS

Some 5000 objects in earth-orbit are currently tracked by NORAD.[5,8] Only abour 5 percent of these are active satellites.[9] About half of the observed population is attributed to some 80 fragmentations of satellites.[9] Some of these fragmentation events were produced by anti-satellite tests, some by accidental explosions of rocket motors (the U. S. Delta rocket for example). Half of the fragmentations remain unexplained.

The observed objects display a variety of orbits and directions. Their spatial density in objects per unit volume of space is random in longitude.[2] The spatial density varies in latitude but not by more than about a factor of 2 from the average.[2] Because of this Kessler has dealt with the average at a given altitude.

Since the objects display a variety of directions and orbits, a given spacecraft is subject to impact from many directions at many relative velocities. The direction and relative velocity of impact upon a given spacecraft depends upon the orbit inclination of that spacecraft. Chobotov[8], however, has shown that, regardless of the inclination, the mean relative velocity of impact would be near 10 km/s and that the mean direction of the object would be about 90° to that of the spacecraft. Thus on average, a spacecraft is subjected to impact of a cross tracking space object at a relative impact velocity of about 10 km/s. Since this impact is in the hypervelocity regime, penetration, and other structural damage is possible, even from objects as small as 1 mm.

Figure 1 shows the debris flux expressed in impacts per unit area per unit time as computed by Kessler.[4] Two curves are shown; one is the observed curve, the other is a corrected curve which accounts for objects too small to observe. The probability, p_i, of a spacecraft sustaining impact by any of the objects is given by[8]

$$p_i = 1-e^{-FAt} \qquad (1)$$

where F is the space debris flux given in Figure 1; A is the spacecraft's area, usually taken to be the average cross-sectional area for debris calculations; and t is the exposure time.

To illustrate a case discussed by others, consider the probability of impact on a large space station. Specifically, assume a space station having an average diameter of 100m, on orbit for 10 years at an altitude of 500 km. Figure 1 shows that the flux for that altitude is about $6X10^{-7}$ impacts/m^2-yr. The space station cross sectional area is $\frac{\pi}{4}(100)^2$ or 7853m^2. Therefore,

$$FAt = 6X10^{-7}\ (7853)\ (10) = 0.047 \text{ impacts,}$$

so that

$$p_i = 1-e^{-0.047} \approx 0.05.$$

Thus a 5 percent probability exists that the space station would be struck by an observed object in a period of 10 years. This is the probability based on the presently observed flux and does not include the effects of future growth in flux and does not include objects smaller than 4 cm in diameter. (A 4 cm impacting object is very large, capable of penetrating several inches of aluminum. Past meteoroid calculations involved particles on the order of 10^{-2} grams.)

Many debris objects tracked by NORAD are explosion fragments. Since explosions produce many fragments smaller than 4 cm, a vast number of fragments exist in orbit but escape detection. Indeed, in one special test NORAD temporarily lowered the sensitivity threshold of a North Dakota facility and were able to see several times the number of objects previously seen.[9] Thus the actual debris flux is much greater than that actually observed.

Based on the number of fragments produced by an earth explosion of an Atlas rocket (1337 fragments) Kessler[4] made an approximate correction to the observed flux. This produced the upper curve in Figure 1. If this curve is used, the flux at 500 km is increased to near $1X10^{-6}$ impacts/m^2-yr. The probability of impact on the space station in the above example now becomes about 8 percent. An impact probability near 10 percent for a large space station has been noted before.[1,3,4] Future growth of the debris population will increase the probability.

It should be noted that the impact probability on small spacecraft remains small. For example, a spacecraft with a 10m diameter on orbit for 1 year still has an impact probability on the order of only 10^{-4}. A significant probability occurs specifically for large spacecraft exposed several years.

GROWTH OF DEBRIS

The historical growth of orbiting debris is well documented. The number of observed objects has increased at 300 to 500 objects per year.[3,4] Past growth has been in large part due to explosions. Some of these were accidental (e.g. the Delta rocket) and have since been corrected by redesign. Others were intentional military tests, which could either stop or continue in the future.

Even without further input from man, however, the growth of the debris population may continue. The source will be ejecta particles resulting from intercollisions of presently existing objects.[4] The probability of intercollision of any two objects is proportional to the square of the number of objects in orbit. Thus the probable time-to-collision can be calculated. In 1981 Kessler[4] estimated that the first intercollision would occur in 17 years. Subsequent collisions would occur more frequently so that by 1998 the collision frequency would be increased to 0.24 to 1 collisions per year.

Such collisions are matters of probability and there is some evidence that the first collision has already occurred. The Soviet satellite Cosmos 954 suffered a sudden loss of pressure, possibly due to impact, which resulted in an uncontrolled reentry over Canada.[3] The U. S. Pageos ballon suddenly broke up on a region of high collision probability after nine year in orbit.[3] On Geos 2 a section of solar panel was damaged, apparently by impact.[3]

Intercollisions of orbiting objects will occur at hyper velocities, capable of creating many ejecta particles. The number of ejecta particles depends on the size, shape, and composition of the two colliding bodies. Estimates vary. Kessler[4] indicates that a 4 to 40 cm object colliding with a 3 to 4m payload or rocket motor produces $1.4X10^4$ objects greater than 1 cm and $3.5X10^6$ objects greater than 1 mm. Johnson[9] refers to one particular earth test conducted with a projectile of 235 gm at a velocity of 6 km/s which produced 10^4 fragments in the size range 1-25 mm. While the precise number varies and depends upon the nature of the colliding bodies, it seems that a collision will produce tens of thousands, perhaps millions, of ejected fragments.

Each collision produces a large number of orbiting objects. This reduces the time to the next collisions, which in turn produces more objects, reducing the time to the next collision and so on. Thus the number of objects will increase at an accelerating rate.

Orbital decay from atmospheric drag acts to reduce the number of objects. The rate at which objects are removed by this action depends upon the mass and orbit of the objects. Significant cleansing may take tens, hundreds or thousands of years.[9] If the number of fragments produced by intercollisions exceeds the clearing of orbital decay, then a net increase in the debris population will occur. In Kessler's

words[4] the debris will become "self-regenerative."

Cour-Palais[10] has estimated the future debris flux. His projection, prepared for Space Station Program Customer Services Handbook, is shown in Figure 2. It can be seen that the debris flux at the 500 km altitude exceeds the meteoroid flux for particles larger than about 0.2 cm. Moreover the presumed density of the debris objects is about 2.8 gm/cm^3 whereas that for meteoroids is 0.5 gm/cm^3. The impact velocity is 9 km/s for a space station in a 30^o inclination orbit and 10 km/s for a 60^o inclination orbit at a 500 km altitude. Cour-Palais estimates the uncertainity in Figure 2 to be factor of 3 for the 1 cm flux and a factor of 10 for the 1 mm flux.

IMPLICATIONS FOR A SPACE STATION

The hazard of debris impact on large, long-duration space structures has been discussed by Kessler et al.[3,4] Some example numbers help illustrate the problem. By use of the projected flux in Figure 2, it is possible to estimate the wall thickness required to insure a given probability of penetration protection.

The probability, p_o of zero impact by an object of a given diameter or greater is given by

$$p_o = e^{-FAt} \tag{2}$$

where F is the flux corresponding to the given object diameter. One selects a desired probablity of zero penetration. Then for a spacecraft of known cross sectional area, A, and duration, t, the flux, F, is calculated from equation (2). This flux is used in Figure 2 to determine the corresponding object diameter. This is the object size which the spacecraft wall must be designed to defeat.

To determine the wall thickness required one uses an equation for "threshold penetration" or "ballistic limit." The equation currently in use for meteoroid impact is[11, 22]

$$t = k_1 \, m^{0.352} \, \rho^{1/6} \, V^{0.875} \tag{3}$$

where k_1 is a constant for a given wall material, approximately equal to 0.57 for aluminum; m is the projectile mass in grams; ρ is the projectile density in grams/cm^3; V is the projectile velocity in km/s; and t is the threshold thickness, the minimum plate thickness which will prevent penetration.

Equations (2) and (3), together with Figure 2, were applied to three example space stations having average cross-sectional diameters of 100m, 50m, and 25m. For each, the required wall thickness was determined so as to insure a penetration protection reliability of 0.99, 0.95, and 0.90 during a 10 year exposure time. The meteoroid flux was neglected.

Results are shown in Table 1. One can see that for 0.99 zero-penetration probability excessive single wall thicknesses are required: 686, 48, and 11 cm for the 100, 50, and 25m diameter space stations respectively. Lowering the protection reliability to 0.95 results in single wall thicknesses of 35, 8.2, and 3.3 cm respectively. Finally lowering the reliability to 0.90 results in 14, 4.4, and 2.5 cm wall thicknesses. Even the last case (0.90 reliability, 25m diameter space station) requires a 1-inch (2.5 cm) thick wall. A probablity of zero penetration higher than 0.90 is desirable. By way of comparison, Skylab was designed for a protection probability (against meteoroid penetration) of 0.995. In view of the projected debris flux it appears practically impossible to achieve such a high degree of reliability for a large, long-duration space structure.

The use of double wall construction (placing a shield or bumper outboard of the main wall) substantially lowers the required total wall thickness. The precise efficiency of such a system depends upon the velocity of impact, wall spacing, shield thickness, etc., but the total thickness will be on the order of 1/5 of the single wall thickness.[13] This value is shown in the last column of Table 1. Even for a double wall construction, the required wall thickness for all but the smallest space station and the two lowest reliability requirement are on the order of an inch or greater. As noted before, resulting structures may be too heavy and expensive to be practical. To achieve high, even modest, levels of reliability it may be necessary to explore new methods of protection: triple-wall construction, and composite materials for example. Impact testing of proposed designs will be necessary. Even with these measures, high reliability may still not be possible.

The alternatives to providing protection is to accept higher risk or alter the debris environment. To alter the environment by debris collection and removal would require propulsion enough to chase and catch thousands of objects. This is not feasible with present propulsion technology.[7]

It seems that the least expensive solution is to curb the addition of man made objects in space. Payloads can be designed to reenter the atmosphere at the end of their useful life for example.[5] Military explosions can be halted. This solution requires international agreements and legislative action.

CONCLUSIONS AND RECOMMENDATIONS

A substantial number of debris objects are presently observed in near-earth space. Many of these are fragments of explosions. Evidence indicates a large population of objects too small to observe. The number of objects is expected to grow as a result of ejecta from intercollisions. Military operations in space can accelerate the growth. The growth in number may exceed the natural cleaning effect of orbital decay so that the debris population will continue to grow, become "self-regenerative." Near earth space may become virtually impossible to use.[7]

Spacecraft collisions with debris objects will be catastrophic, occurring at hyper velocities near 10 km/s. The present probability of impact to small spacecraft on short missions is negligibly small. The probability of impact on a large space station, however, is of the order of 10 per cent. Impact protection for such structures is a prime design consideration; the expense of high penetration protection reliability may be prohobitive.

Once debris is in orbit it is expensive, if not impossible, to recover.[7] Therefore, it is important to slow the growth now before too much accumulates. To solve the problem, the manner in which space is used can be altered.[1] The addition of man-made objects can be curbed by means of international agreements and legislative action.

REFERENCES

1. Brooks, D. R., "A Comparison of Spacecraft Penetration Hazards Due to Meteoroids and Manmade Earth-orbiting Objects," NASA TM X-73978, November 1976.

2. Kessler, D. J. and Cour-Palais, B. G., "Collision Frequency of Artificial Satellites: The Creation of a Debris Belt," Journal of Geophysical Research, Vol. 83, No. A6, June 1978, pp. 2637-2646.

3. Kessler, D. J, et al, "Collision Avoidance in Space," IEEE Spectrum, Vol. 17, June 1980, pp. 37-41.

4. Kessler, D. J., "Sources of Orbital Debris and the Projected Environment for Future Spacecraft," Journal of Spacecraft, Vol. 18, No. 4, July - August 1981, pp. 357-360.

5. Anonymous, "Space Debris, An AIAA Position Paper," American Institute of Aeronautics and Astronautics, New York, 1981.

6. Kessler, D. J., "Summary of Orbital Debris Workshop," International Astronautical Federation, International Astronautical Congress, 33rd, Paris, France, Sept. 27 - Oct. 2, 1982, Paper 82-254.

7. Reynolds, R. C., Fischer, N. H., and Rice, E. E., "Man-Made Debris in Low Earth Orbit - A threat to Future Space Operations," Journal of Spacecraft, Vol. 20, No. 3, May - June 1983, pp. 279-285.

8. Chobotov, V.A., "Classification of Orbits with Regard to Collision Hazard in Space," Journal of Spacecraft, Vol. 20, No. 5, Sept. - Oct. 1983, pp. 484-490.

9. Johnson, N. L., "History and Consequences of On-Orbit Break-Ups,' Presented at XXV COSPAR, Graz, Austria, June 29, 1984.

10. Cour-Palais, B. G., Private Communication, July 9, 1984, of a section prepared by him for a Space Station Customer Services Handbook being compiled by the Goddard Space Center.

11. Cour-Palais, B. G., "Meteoroid Environment Model - 1969 (Near Earth to Lunar Surface)," NASA SP-8013, March 1969.

12. Frost, V. C., "Meteoroid Damage Assessment," NASA SP-8042, May 1970.

13. Frost, V. C., "Aerospace Meteoroid Environment and Penetration Criterion," Aerospace Corporation, TOR-269 (4560-40)-2, August 1964.

TABLE 1. WALL THICKNESS REQUIRED FOR LARGE SPACE STRUCTURE SUBJECTED TO DEBRIS IMPACT

P_0 PROBABILITY OF ZERO PENETRATION	d, SPACE STATION AVERAGE DIAMETER, (m)	F, DEBRIS FLUX $(\frac{\text{Impacts}}{m^2\text{-yr.}})$	D, DEBRIS OBJECT DIAMETER, (cm)	m, DEBRIS OBJECT MASS (g)	t, SINGLE WALL THICKNESS (cm)	t/5 DOUBLE WALL THICKNESS (cm)
0.99	100	$1.28X10^{-7}$	100	$1.47X10^{6}$	686	137
	50	$5.12X10^{-7}$	8	750	48	9.6
	25	$2.05X10^{-6}$	2	11.7	11	2.2
0.95	100	$6.53X10^{-7}$	6	317	35	7.0
	50	$2.61X10^{-6}$	1.5	5.0	8.2	1.6
	25	$1.05X10^{-5}$	0.64	0.38	3.3	0.66
0.90	100	$1.34X10^{-6}$	2.5	22.9	14	2.8
	50	$5.36X10^{-6}$	0.84	0.87	4.4	0.88
	25	$2.14X10^{-5}$	0.49	0.17	2.5	0.50

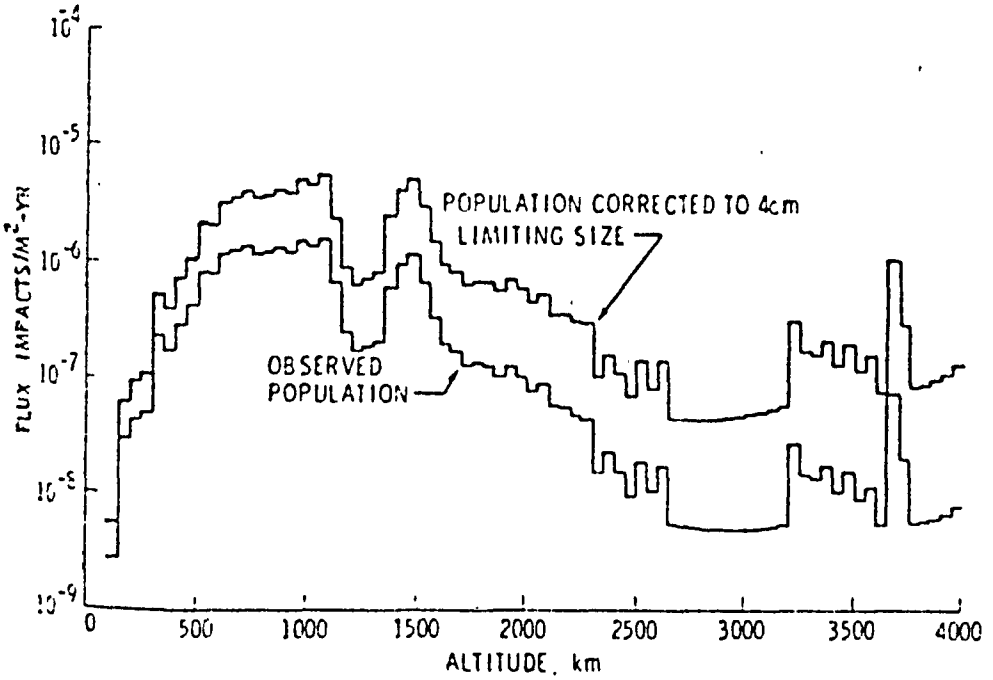

FIGURE 1. Spatial Density of Debris Objects (from Reference 4).

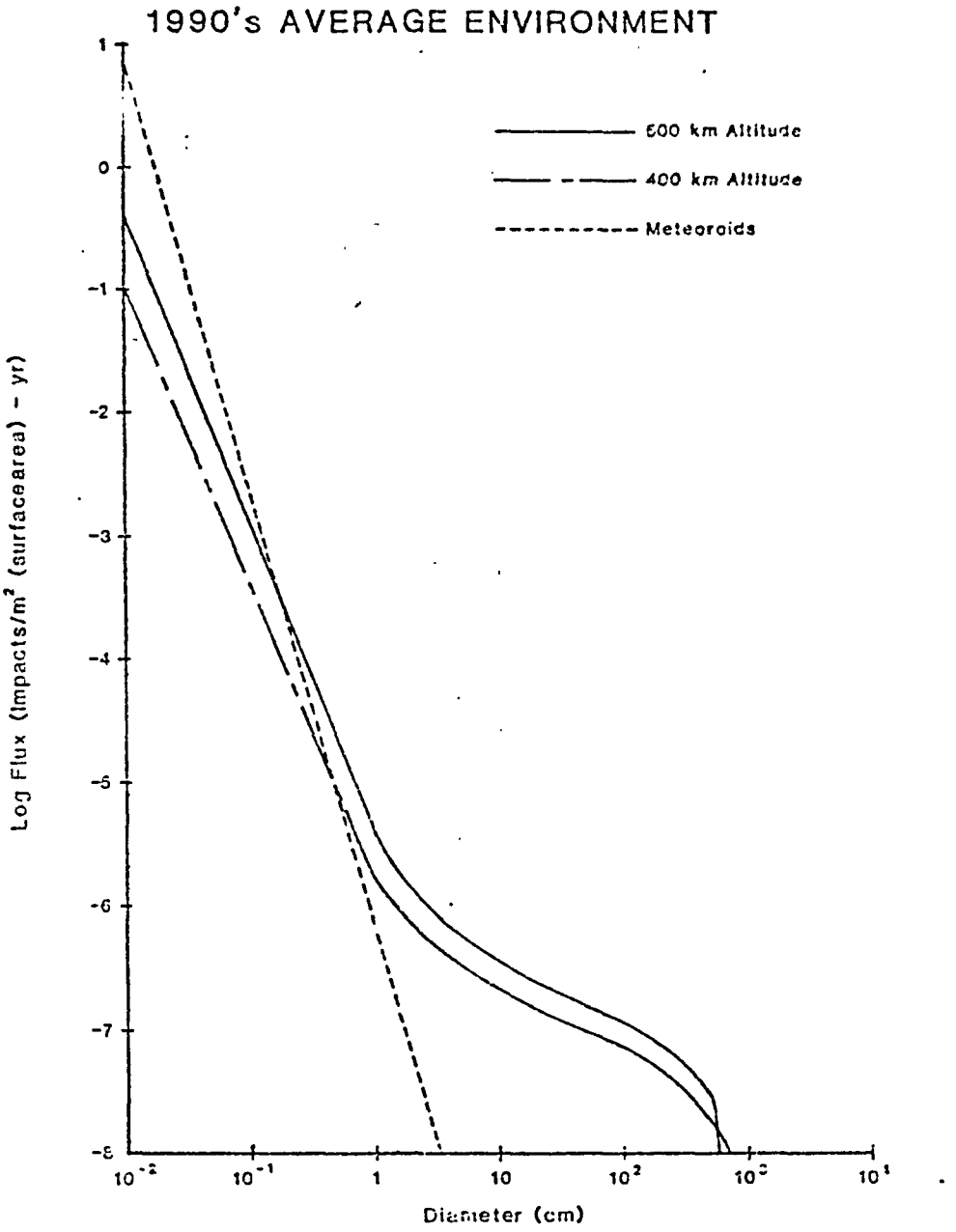

FIGURE 2. Projected Debris Flux for 1990's (from Reference 10).

1984

NASA/ASEE SUMMER FACULTY RESEARCH FELLOWSHIP PROGRAM

MARSHALL SPACE FLIGHT CENTER
THE UNIVERSITY OF ALABAMA

EXPERIMENTAL DETERMINATION OF SYSTEMS SUITABLE FOR STUDY AS MONOTECTIC BINARY METALLIC ALLOY SOLIDIFICATION MODELS

Prepared By:	James E. Smith, Jr., PhD
Academic Rank:	Assistant Professor
University and Department:	University of Alabama in Huntsville Department of Mechanical Engineering/Chemical Engineering Program
NASA/MSFC:	
(Laboratory)	Space Science Laboratory
(Division)	Space Processing
(Branch)	Solidification Process Branch
MSFC Counterparts:	Donald O. Frazier, PhD
Date:	August 10, 1984
Contract No.:	NASA-NGT-01-002-099 The University of Alabama

EXPERIMENTAL DETERMINATION OF SYSTEMS SUITABLE FOR STUDY AS MONOTECTIC BINARY METALLIC ALLOY SOLIDIFICATION MODELS

By

James E. Smith, Jr.
Assistant Professor of Chemical Engineering
University of Alabama in Huntsville
Huntsville, Alabama 35899

ABSTRACT

Transparent binary metallic alloy solidification models have become increasingly more important in attempts to understand the processes causing liquid-liquid and solid-liquid phase transformations in metallic alloy systems. These models permit visual observation of the phase transformation and the processes preceding solidification. There is a need to experimentally expand the number of these transparent monotectic binary models to distinguish between the unique and general phenomena observed using the limited number of model systems currently available. The objective of this study was to expand the number of accurately determined monotectic phase diagrams of model systems, while contributing to a data base for eventual use with UNIFAC group contribution methods.

The phase diagrams of the model systems were measured using a light scattering technique developed in the preceding study. Systems studied included: succinonitrile (SN) - anhydrous ethanol, SN - axeotropic ethanol and water, SN - deuterium oxide (D_2O), SN - cyclohexanol, SN - benzene and SN - 20°C neutrally buoyant mixture of D_2O and H_2O.

INTRODUCTION

Generally, attempts to solidify immiscible mixtures to make binary alloys in situ have yielded poorly dispersed composites. If a binary homogeneous melt is cooled into a immiscible region, the newly formed second phase will generally have a density different from the bulk phase and will separate readily by sedimentation in unit gravity. Unless the system is quenched extremely rapidly, which can only be accomplished using very small samples, phase separation will be virtually complete when the melt solidifies. Therefore, it is not possible to make alloys of finely dispersed composites with systems having liquid phase immiscibility regions using standards casting techniques [1]. To date, more than 500 metallic systems have been found to exhibit this liquid phase immiscibility region [2] which is characteristic of all binary monotectic systems. Uses for monotectic metallic alloys, solidified in microgravity enviroment to reduce sedimentation effects, have been suggested by Gelles [3] and include lower-cost electrical contact materials and composites with unique electrical and super conductive properties.

Transparent binary metallic alloy solidification models have become incresingly more important in attempts to understand the processes causing liquid-liquid and solid-liquid phase trasnformations in metallic alloy systems. Until the discovery of these transparent alloy models [4], sectioning after solidification, followed by metallography, was the only way to study metal castings. Today, one can use a transparent alloy solidification model, which produces similar casting patterns and observe directly those processes which produce the pattern. Further, since most of the important organic model systems' phase changes take place at lower temperatures (-50 to 150°C) they are generally safer, easier, and more economically studied than their metallic counterpart. There is a need to experimentally expand the number of these transparent monotectic binary model to distinguish between the unique and general phenomena observed using the limited number of model systems currently available.

The temperature versus composition phase diagam has always been the most important tool for understanding and identifying the solidification morphologies in metallurgical studies and is equally as important in transparent model investigations. Correlation of solidified and sectioned alloy casting patterns with their binary phase diagram have yielded a fair amount of information with respect to single phase solid solutions, eutectics, and now monotectic transformations. Since the advent of transparent models, considerably more information has become available, particularly though the eutectic studies of Hunt and Jackson [5] and monotectic work by Hellawell et.al. [6] and Frazier and coworkers [1].

Monotectic systems are characterized by a region at liquid phase immiscibility commmonly referred to as the miscibility gap. These systems contain in their phase diagrams a regine where two liquid phases are in equilibrium having an upper critical solution point at a critical temperature T_c and composition x_c. This point is called the critical point, above which only a homogeneous liquid can exist. The lower boundary of a monotectic systems resides at the monotectic temperature (T_m). At this temperature one of the liquid phases decomposed into a solid phase and the other liquid phase. It is very important to accurately know both the shape of the two phase region as well as its thermal bounndaries.

The objective of this study was to expand the number of accurately determined monotectic phase diagrams of specific model systems, while supporting directional solidification, critical wetting, and interfacial phenomena studies currently being conducted at the MSFC. Additionally, these phase diagrams will contribute to a data base for eventual use with UNIFAC group contribution methods [7]. This method, with revised interaction parameters, will permit the estimation of phase behavior of various binary pairs without the use of time consuming and expensive screening experiments.

This study examined the phase behavior of succinonitrile (SN)-ethanol and SN-azeotropic ethanol-water mixtrure to determine why a KC-135 critical wetting experiment produced an interface which disappeared below the expected homogeneous temperature. SN-benzene was investigated since it is nonhydroscopic and produces large morphological features at the interface. This system had also been measured by Kaukler, et.al. [8] using both thermal and spectroscopic methods. Due to the suspected carcinogenic nature of benzene, the SN-toluene system was investigated as a possible substitute for the benzene system. The SN-cyclohexanol phase diagram was measured to verify a previous measurement [8] and was of interest since both components are model materials. Finally, SN-deuterium oxide (D_2O) and SN-20°C mutally buoyant mixture of D_2O and water was measured to support the directional solidification and critical wetting studies [1].

EXPERIMENTAL

The experimental apparatus was the same developed and used in the previous study [7] which employs a light scattering technique to determine the phase boundaries. The procedures followed were virtually the same with the exception of one additional step. Prior to loading the vessel with succinonitrile, the system was assembled, heated to 60°C and outgased to remove atmospheric air and moisture from the mixer, thermocouple, tubing and the o-ring seal. This step was found to reduce the running time of the

experiment and prevent contamination of the SN initial charge.

RESULTS AND DISCUSSION

SN-Ethanol and SN-Azeotropic Ethanol and Water

Tables 1 and 2 show the experimental phase equilibria data obtained for the two systems. Figure 1 shows the phase diagram of SN-ethanol (200 proof), using care to prevent contamination with atmospheric air. The monotectic temperature was found to be 14.775°C with a composition of 25.80 wt% ethanol. These and all further reported values were obtained by curve fitting the region around the point in question, using least squares techniques, and taking either the derivative of the function or solving two function with the consolute temperature for the monotectic and eutectic compositions.

Figure 2 shows the phase diagram of the pseudo binary SN-azeotropic ethanol-water mixture which was 95.602 wt% ethanol and 4.398 wt% water. The monotectic was found to be at 12.289°C and 24.19 wt% solution. The critical point was lowered to 25.80°C at 51.00 wt% solution. This small addition of water resulted in a depression of the critical temperature of 21.1% and a shift in the critical composition by 8.4%. The monotectic temperature was depressed 16.83% with only a change of 6.24% in composition.

The KC-135 critical wetting experiment examined a SN-anhydrous ethanol solution. The initial solutions were made up from previously opened bottles of anhydrous ethanol. When these solutions were taken through their phase transformation it was found that the transition temperature was well below the expected temperature. If the anhydrous ethanol were absorbing water from the air, upon mixing with SN, it would have a reduced phase diagram. The temperature when this solution would become homogeneous would now be well below the expected anhydrous transformation temperature. Subsequent experiments on anhydrous ethanol show that it does absorb water quite rapidly when exposed to the atmosphere.

SN-Benzene and SN-Toluene

Table 3 presents the phase equilibria data for SN-benzene. Figure 3 show the phase diagram for the same system. The monotectic was found to be 11.45°C at 36.90 wt% benzene, with a eutectic at -2.14°C and 93.30 wt% benzene. Critical temperature was 39.83°C at 66.83 wt% benzene. The triangles shown indicate the thermal findings of Kaukler et.al. [8] while the squares show the UV spectroscopy results of the same study. Possible causes for the differences can be attributed to the purity of the chemicals and the visual method used for thermal analysis. Kaukler et.al. [8] used

Fisher reagent grade benzene (b.p. 79.8-80.2°C) while this study used Aldrich Gold Label spectroscopic grade benzene with a purity of 99+% and boiling point of 80.2°C. The boiling point range given by Fisher indicates that this benzene was quite impure. Further, this study used triply distilled and zone refined succinonitrile while Kaukler et.al. [8] used double distilled SN.

SN-toluene was investigated as a possible replacement for benzene due to the suspected carcinogenic hazards associated with benzene. Toluene was considered because it is a safer compound and favors benzene in its chemical behavior. Table 4 and Figure 4 show the limited results obtained using SN-toluene. The phase diagram was not completed because the relative volatility of the toluene cause a refluxing in the neck of the experimental vessel. This refluxing caused a shift in the bulk concentration above about 70°C making it impossible to accurately know the compositon. Of particular interest is the monotectic temperature which is well above room temperature at 30.46°C at a composition of 21.98 wt% toluene. This high monotectic temperature makes this system a very good candidate for growth rate experiments and directional solidification with larger thermal gradients than is currently possible due to cold bath temperature limitations. Further, a relatively high temperature monotectic alloy will permit studies without the need of refrigeration.

SN-Cyclohexanol

The phase diagram for this system is shown in Figure 5 with the tabulated equilibria data given in Table 5. This system was of interest since both the components are model materials. This system had been previously measured by Kaukler et.al. [8] who visually observed the cloud point. The results of this work are shown by the triangles on Figure 5. The data are in fair agreement with this study, except in the regions where the minority phase is in low concentration. In this region, a visual observation of the cloud point is not possible until one has cooled well into the immicible region.

SN-Deuterium Oxide (D_2O)-Water

This system was investigated because it is possible to adjust succinonitrile-water system to a neutral density configuration with the addition of D_2O. Initially it was decided to examine SN-D_2O to see just how much difference existed between the SN-D_2O and SN-H_2O. Table 6 and Figure 6 show the results obtained for this system. The monotectic temperature for the SN-D_2O system was 20.67°C which exceed that of SN-H_2O (18.82°C) by 9.8% [9]. The monotectic composition of 9.38 wt% D_2O was shifted only 3.6% from that of the H_2O system (9.41 wt% H_2O). The critical temperature for the D_2O system was 59.7°C at a composition of 48.1 wt% D_2O. This is 3.5°C higher than that determined for the SN-H_2O system. The eutectic temperature for the D_2O system was found at 2.59°C

while that of the H_2O system was previously determined at -1.24°C. A difference of 3.8°C. Finally, the freezing point of the two pure components D_2O (3.82°C) and H_2O (0°C) differ by about the same 3.8 degree margin. This final difference is attributed to the isotope effects which allows D_2O to form stronger hydrogen bonds. The stronger hydrogen bonds results in a specific heat increase of 10%, a viscosity increase of 30%, a density increase of 10%, and a vapor pressure decrease by 7% compared to that of water [10]. These property variations contribute to the observed differences between the two systems.

A 20°C mutually buoyant mixture at SN-D_2O-H_2O was examined. The solution required a mixture of 13.44 wt% D_2O and 85.56 wt% H_2O to assure neutral buoyancy at this temperature. Table 7 and Figure 7 show the results using this mixture. Figure 8 shows all three phase diagrams plotted together. This figure more clearly shows the behavior of the neutrally buoyant mixture. As can be seen, this mixture behaves more like SN-D_2O on the left side of the phase diagram (succinonitrile rich) and like SN-H_2O on the water rich side of the phase diagram. This must be due to the D_2O preferentially interacting with the SN, causing a rejection of H_2O and a redistribution of the SN from the SN rich phase. This finding indicates that the addition of D_2O to the SN-H_2O system results in a redistribution of the three components which produces the neutral buoyancy condition.

These data are of current interest in the directional solidification and critical wetting studies currently being conducted at the MSFC and reviewed in reference 1.

CONCLUSIONS

This study has investigated many new monotectic systems as well as redetermined, with greater accuracy, some that were previously known. It has shown the potential problem which can result from using hydroscopic materials (ethanol) as well as very volatile components such as toluene in transparent studies. Finally it has improved our understanding of the processes taking place in the neutrally bouyant mixtures.

These data will contribute to a data base, which may eventually be used to develop a new UNIFAC group interaction matrix for use with model systems. Further work, using a different experimental apparatus, will be required to complete the SN-toluene phase diagram.

References

1. Frazier, D. O., Facemire, B. R., Kaukler, W. F., Witherow, W. K., and Fanning, U., "Separation Processes During Binary Monotectic Alloy Production," NASA TM-82579, April 1984.

2. Reger, J. L., "Study of Processing Immiscible Materials in Zero-Gravity-Interim Report," Contract NAS8-28267, May 1973.

3. Gelles, S. H., Markworth, A. J., Oldfield, W. and Duga, J., "Investigation of Immiscible Systems and Potential Applications," Contract NAS8-29748, Final Report, April 1975.

4. Timmerman, J. J. Chem. Phys., 35, 3312 (1938).

5. Jackson, K. A. and Hunt, J. D., Acta. Met., 13, 1212 (1965).

6. Hellawell, A. and Grugel, R. N., Met. Trans., 12A, 669 (1981).

7. Smith, Jr., J. E., "Determination of Systems Suitable for Study as Monotectic Binary Metallic Alloy Solidification Models," NASA/ASEE Summer Faculty Fellowship Program, Contract NGT 01-008-021, (1983).

8. Kaukler, W., Frazier, D. O., and Facemire, B., "Determination of the Succinonitrile-Benzene and Succinonitrile-Cyclohexanol Phase Diagrams by Thermal and UV Spectroscopic Analysis," NASA TM-82581, April 1984.

9. Smith, Jr., J. E., Frazier, D. O., and Kaukler, W. F., "A Redetermination of the Succinonitrile-Water Phase Diagram," Scripta Met., 18, 677 (1984).

10. Franks, F., "Water A Comprehensive Treaties," Plenum Press, New York (1972).

Table 1

Succinonitrile-Ethanol
Phase Equilibria Data

Composition Weight Percent EtOH	Temperature (°C)	Mototectic Temperature (°C)
0.000	58.090	
2.040	54.674	
5.530	44.976	
9.350	35.683	
11.400	31.333	
14.669	25.325	14.751
19.090	19.500	
21.396	17.750	14.800
24.253	16.225	
27.644	18.725	
32.391	25.663	14.775
36.130	29.122	
38.209	29.841	
41.884	31.310	
46.489	32.402	
48.806	32.524	
50.455	32.573	
51.604	32.683	
53.709	32.707	
59.784	32.683	
62.689	32.610	
66.299	32.512	
70.410	31.964	
75.247	30.013	
78.523	28.378	
82.72	24.524	

Table 2

Succinonitrile-(95.602wt% EtOH, 4.398wt% Water)
Phase Equilibria Data

Composition Weight Percent Solution	Temperature (°C)	Mototectic Temperature (°C)
0.000	58.091	
2.607	51.395	
5.133	44.679	
8.707	34.571	
15.641	21.088	
20.772	15.425	
25.072	14.250	12.268
33.776	22.049	12.310
45.635	25.775	
51.090	25.800	
55.525	25.650	
61.453	25.350	
66.479	24.829	
70.370	24.950	
74.267	23.100	
78.808	19.563	
83.786	15.000	
88.674	8.692	

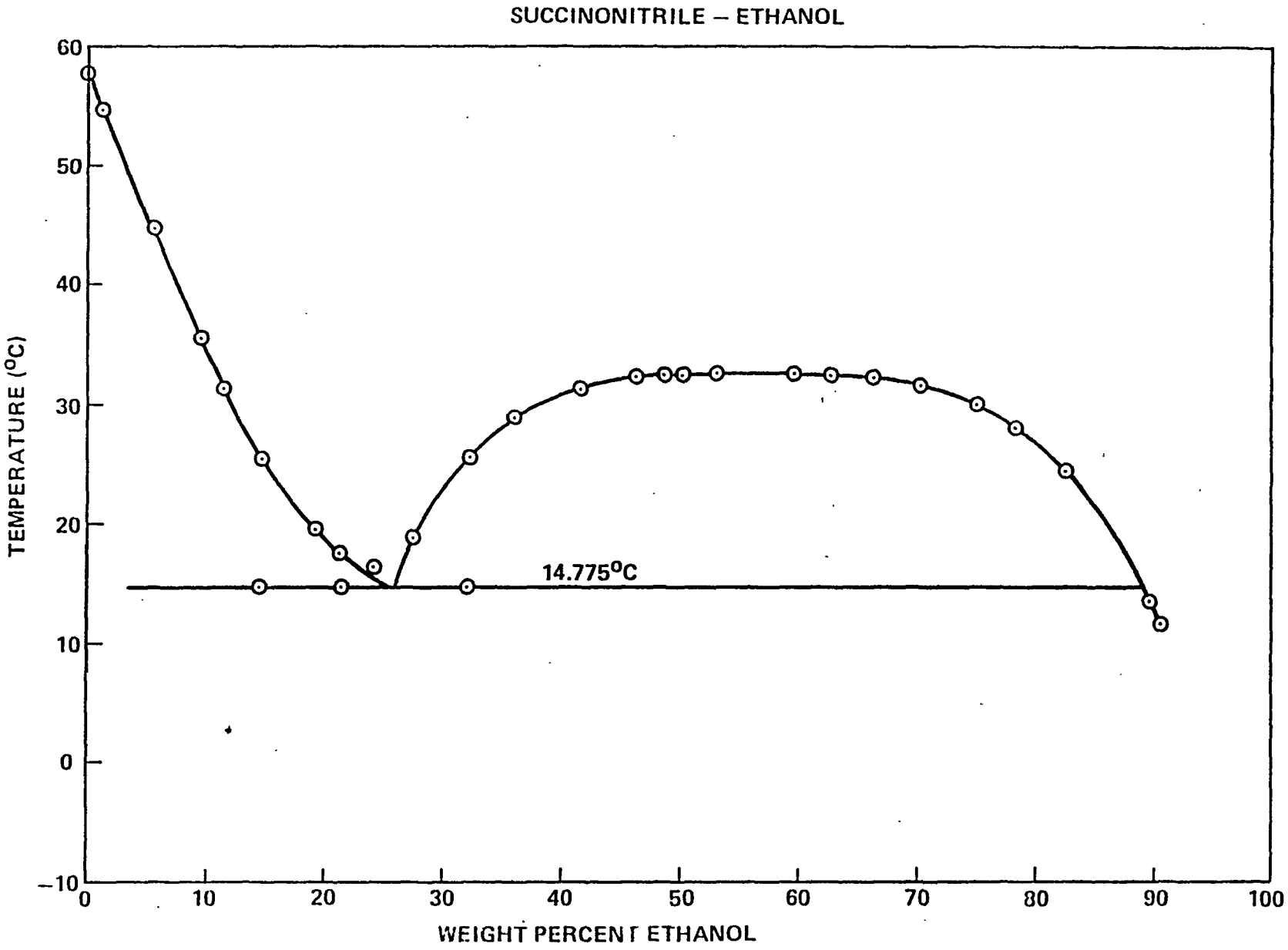

Figure 1. Phase Diagram of Succinonitrile - Ethanol

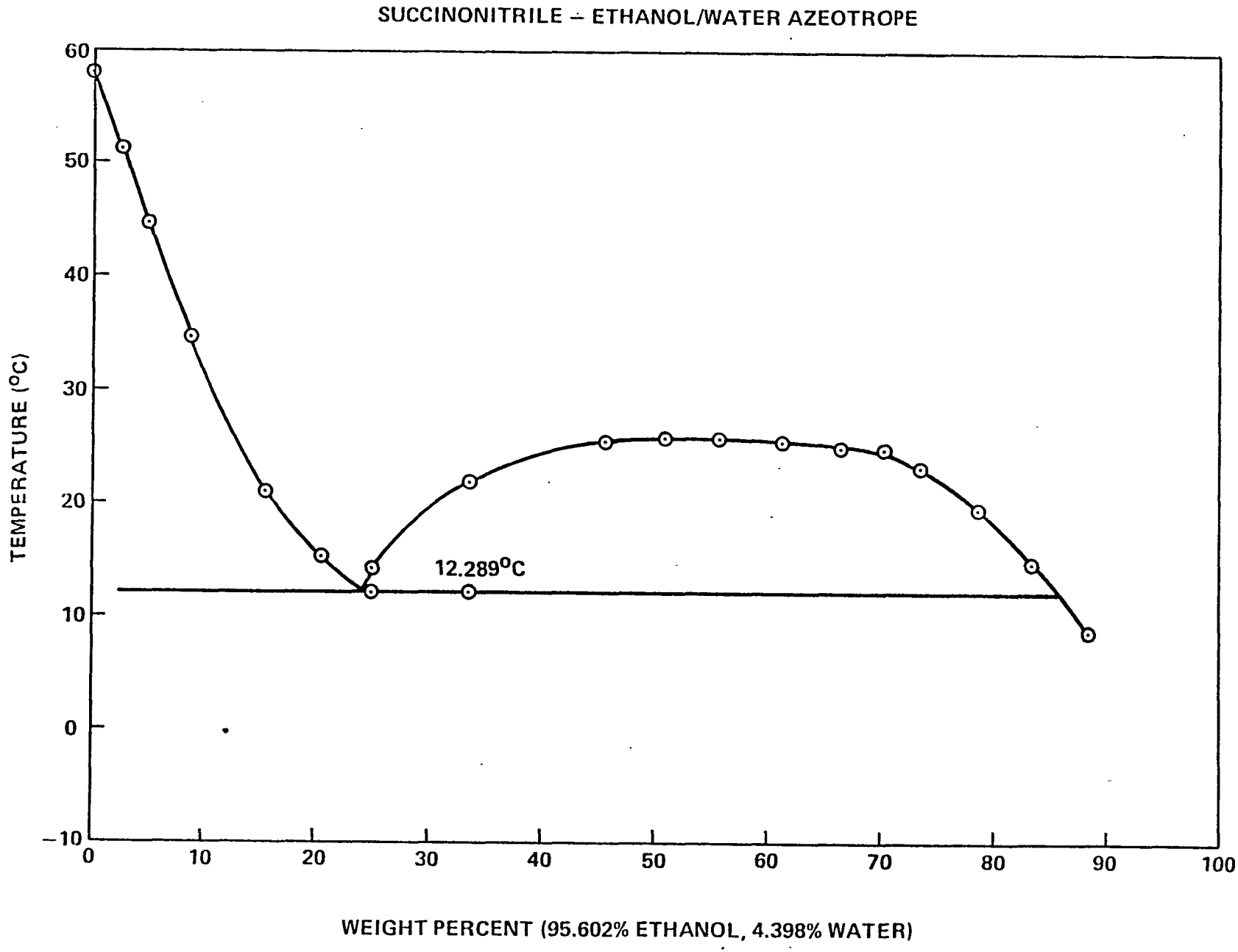

Figure 2. Phase Diagram of Succinonitrile Azeotropic Ethanol-Water Mixture

Table 3

Succinonitrile-Benzene
Phase Equilibria Data

Concentration Weight Percent Benzene	Temperature (°C)	Monotectic Temperature (°C)	Eutectic Temperature (°C)
0.000	58.082		
3.484	52.223		
6.896	47.314		
10.879	39.607		
15.384	33.073		
20.194	26.037		
24.995	20.781		
30.840	15.375	11.450	
33.982	13.564		
38.063	14.364		
41.945	21.163	11.453	
45.651	25.800		
50.505	31.032		
56.101	35.740		
63.113	38.674		
66.809	39.821		
70.708	39.643		
72.234	39.502		
76.339	39.071		
79.414	38.134	11.480	
83.830	33.160		
86.045	28.110		
89.334	18.025		
92.305	5.808		-2.141
94.505	1.051		
95.969	2.658		
96.992	3.615		

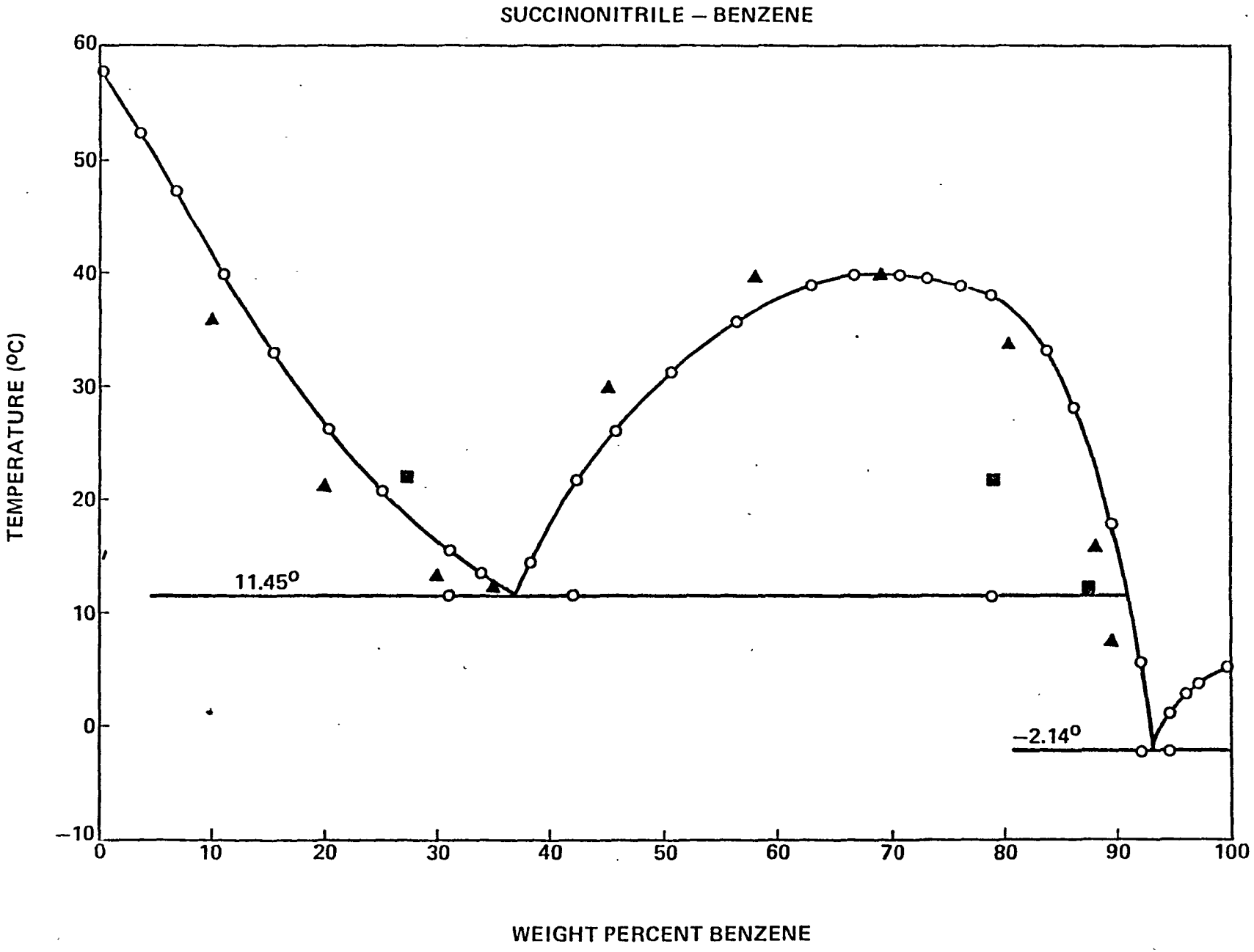

Figure 3. Phase Diagram of Succinonitrile-Benzene

Table 4

Succinonitrile-Toluene
Phase Equilibria Data

Composition Weight Percent Toluene	Temperature (°C)	Mototectic Temperature (°C)
0.000	58.088	
1.197	54.988	
3.694	51.302	
5.652	46.833	
9.426	41.893	
12.054	39.464	
14.896	36.238	
18.017	32.793	30.488
21.981	30.793	30.463
26.363	50.244	
30.818	64.557	

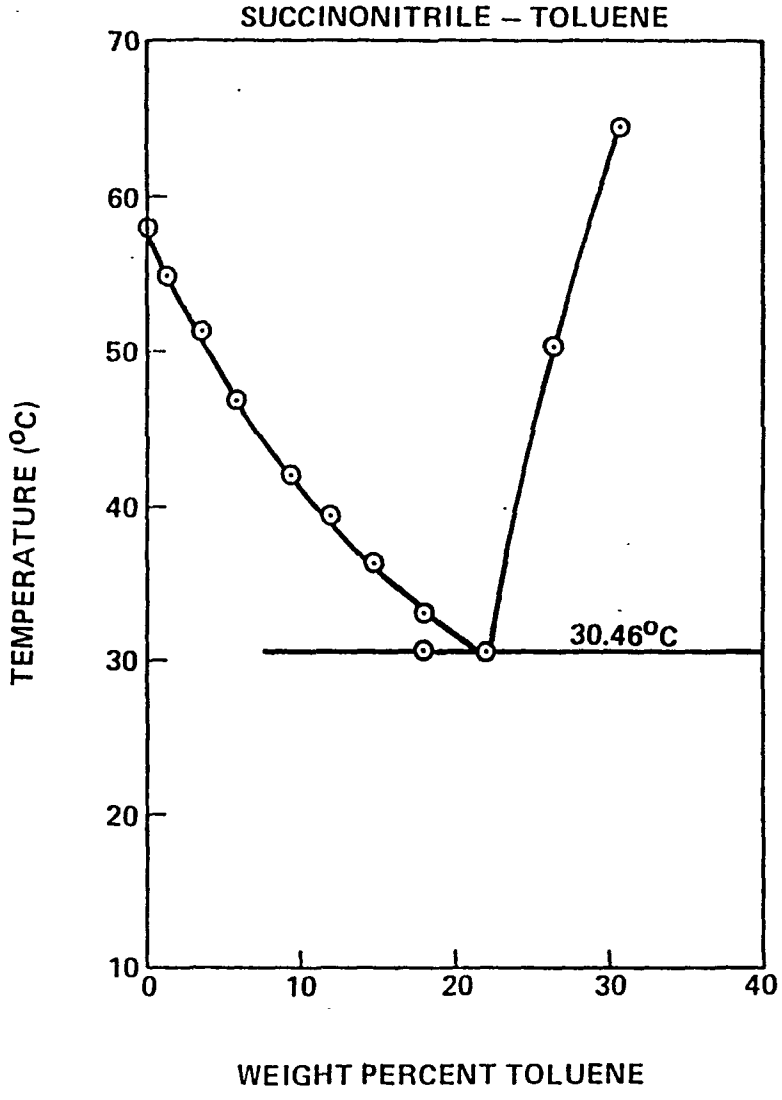

Figure 4. Partial Phase Diagram of Succinonitrile-Tuluene

Table 5

Succinonitrile-Cyclohexnol
Phase Equilibria Data

Composition Weight Percent Cyclohexnol	Temperature (°C)	Monotectic Temperature (°C)	Eutectic Temperature (°C)
0.000	58.084		
1.204	56.453		
2.825	53.942		
4.602	51.249		
6.227	48.779		
7.878	46.786		
9.220	45.035		
11.576	42.895	40.810	
13.854	48.452	40.881	
16.535	55.545		
19.494	62.742		
23.044	68.189		
28.991	74.568		
35.282	78.120		
41.482	79.473		
47.554	80.171		
52.791	80.389		
58.221	80.556	40.952	
64.733	80.451		
69.116	80.216		
73.358	79.900		
76.698	79.600		
84.222	75.833		
90.179	69.102		
92.509	64.795		
94.699	55.364	40.952	
96.086	47.105		17.288
96.862	40.071		
97.952	34.071		
98.317	28.010		17.150
98.742	20.390		

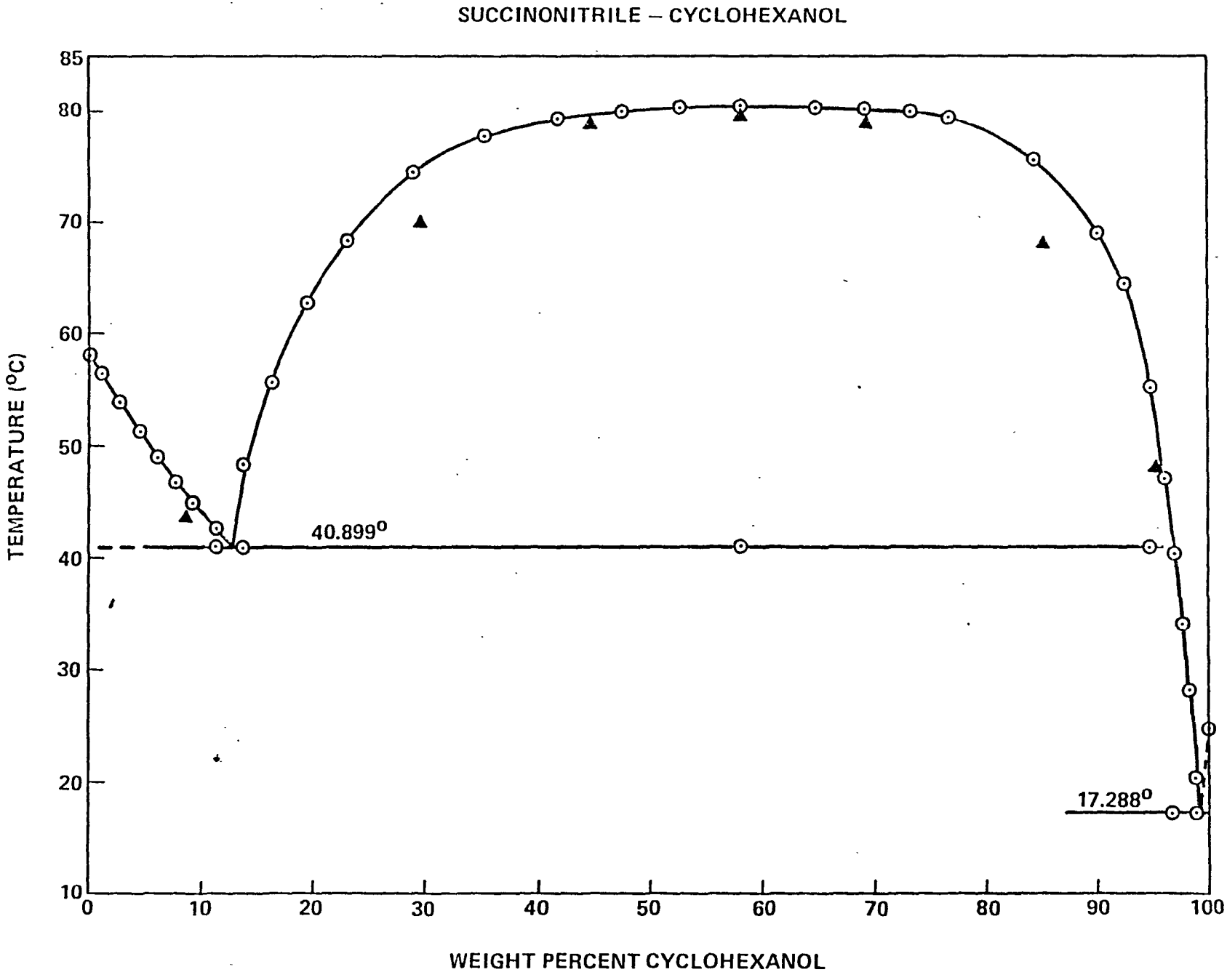

Figure 5. Phase Diagram of Succinonitrile-Cyclohexanol

Table 6

Succinonitrile-Deuterium Oxide (D_2O)
Phase Equilibria Data

Composition Weight Percent D_2O	Temperature (°C)	Monotectic Temperature (°C)	Eutectic Temperature (°C)
0.000	58.090		
0.562	53.919		
1.171	49.545		
2.325	41.917		
3.934	33.596		
5.540	27.756		
7.475	23.425	20.671	
9.336	26.032	20.634	
11.088	31.143		
14.603	40.452		
28.029	55.636		
37.198	58.334		
43.834	59.341		
48.024	59.698		
49.836	59.622		
55.076	59.640		
61.534	59.407	20.683	
64.690	58.909		
71.409	57.101		
77.305	52.472		
83.055	44.650		
87.830	33.505		
90.089	25.642	20.672	
91.250	20.878		
93.110	15.717		
94.903	5.128		2.564
96.316	3.321		
97.341	3.647		2.615
98.463	3.769		
100.000	3.820		

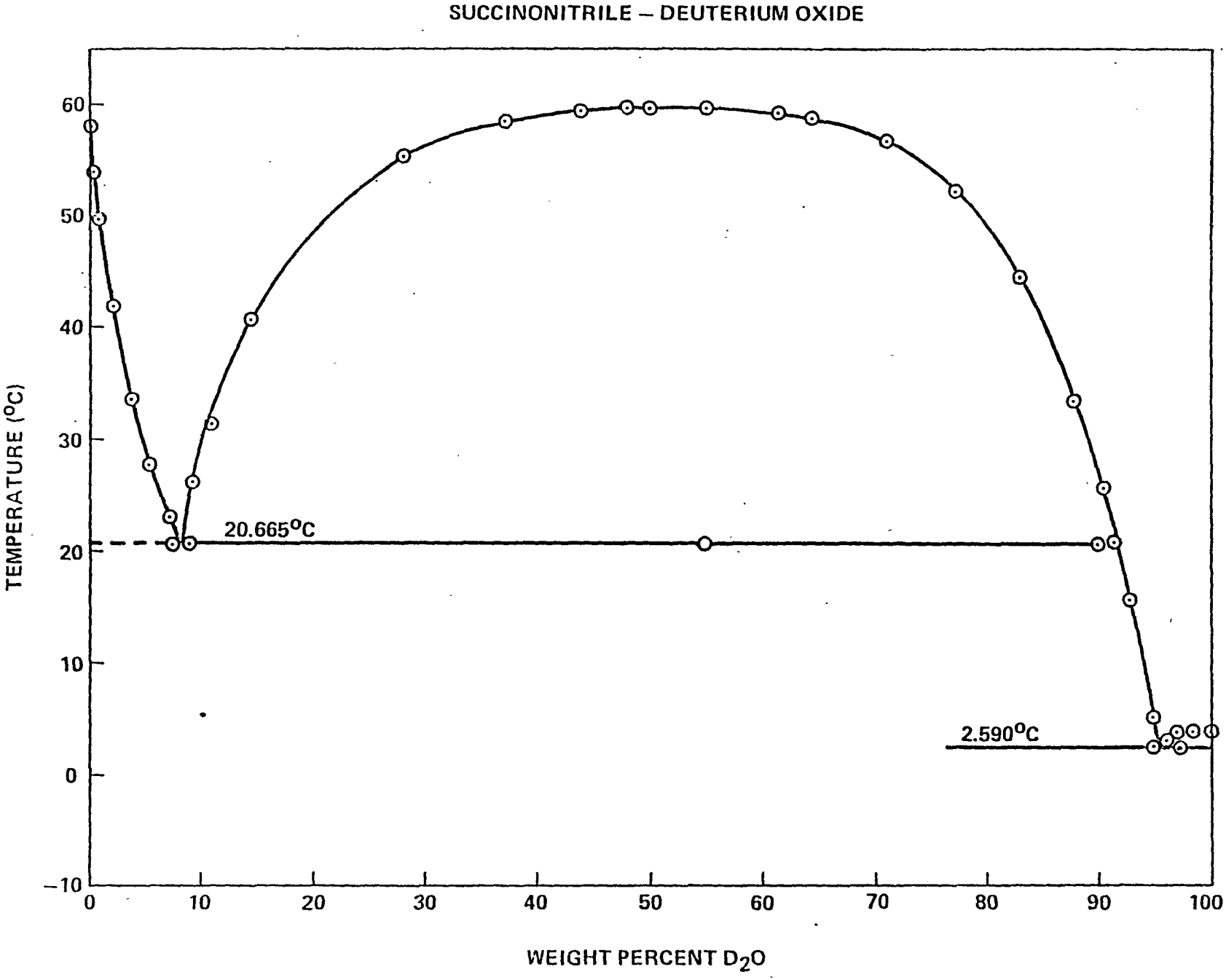

Figure 6. Phase Diagram of Succinonitrile-Deuterium Oxide

Table 7

Succinonitrile-20°C Mutually Bouyant D_2O-H_2O Mixture
Phase Equilibria Data

Composition Weight Percent Toluene	Temperature (°C)	Mototectic Temperature (°C)
0.000	58.084	
1.809	46.071	
3.671	34.667	
6.199	24.976	
7.618	22.073	
9.115	24.244	18.925
11.361	30.683	19.000
16.551	43.286	
29.085	54.616	
34.015	55.864	
38.545	55.886	
43.956	56.058	
48.546	56.198	
55.640	56.151	19.050
65.439	55.318	
74.027	50.756	
80.260	44.191	
84.876	34.440	
88.847	24.475	
92.253	15.775	

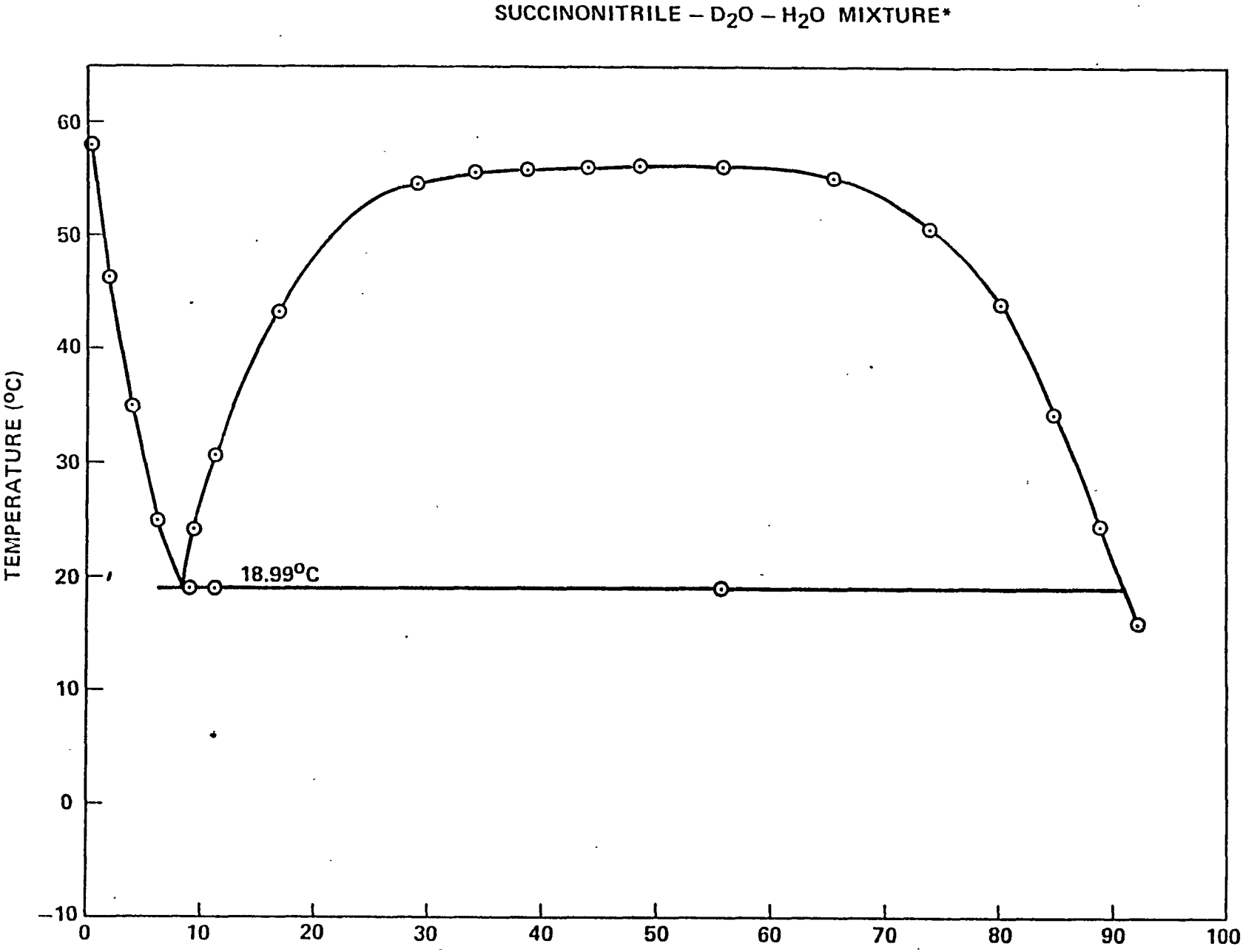

Figure 7. Phase Diagram of Succinonitrile-20°C Neutrally Buoyant D_2O-H_2O Mixture

*13.44% D_2O AND 86.56% H_2O BY WEIGHT

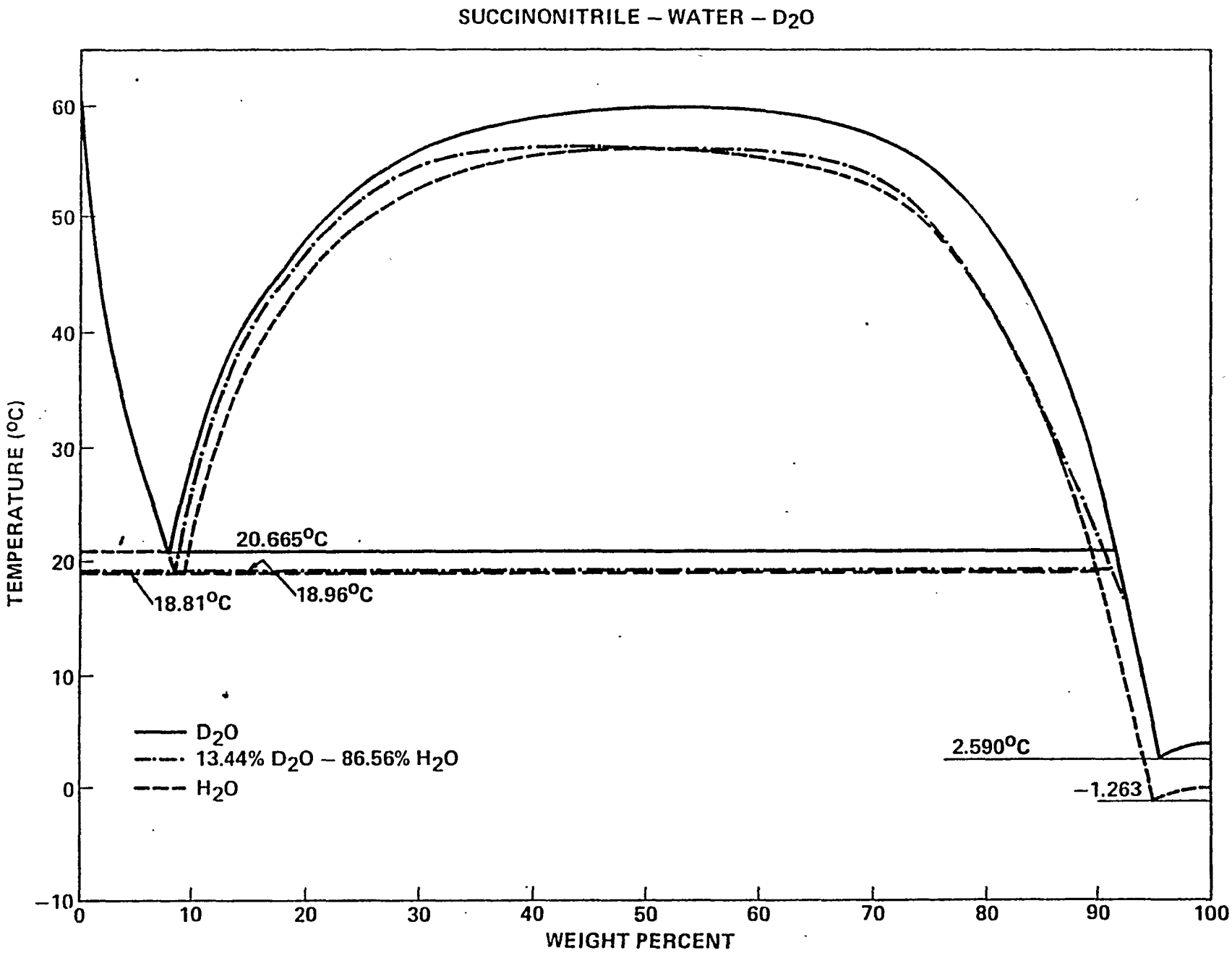

Figure 8. Comparison of Various Succinonitrile-Water-Deuterium Oxide Phase Diagrams

D26

1984

NASA/ASEE SUMMER FACULTY FELLOWSHIP PROGRAM

MARSHALL SPACE FLIGHT CENTER
THE UNIVERSITY OF ALABAMA

NEW RESULTS ON THE PLL FALSE LOCK PHENOMENON

Prepared By:	John L. Stensby
Academic Rank:	Assistant Professor
University and Department:	The University of Alabama Department of Electrical and Computer Engineering
NASA/MSFC:	
Laboratory:	Information and Electronics
Division:	Computer and Communications
Branch:	Communication Systems
NASA Counterpart:	Bill Reed
Date:	August 3, 1984
Contract No.	NASA-NGT-01-002-099 (The University of Alabama)

NEW RESULTS ON THE PLL FALSE LOCK PHENOMENON

BY

John Stensby
Assistant Professor
Electrical and Computer Engineering
The University of Alabama in Huntsville
Huntsville, Alabama

ABSTRACT

A necessary condition, based on the multipliers of a linear differential equation with periodic coefficients, for the occurrence of false lock in a phase lock loop (PLL) is given. Next, two new and powerful algorithms are presented for computing ω_{fl}, the frequency difference between the reference and voltage controlled oscillator when the loop is false locked. Both algorithms employ the necessary condition mentioned above, and neither requires linearization of the differential equation describing the loop. The first algorithm expresses ω_f^{-1} as a power series in the closed loop gain. The second algorithm expresses ω_f^{-1} as part of a solution to a nonlinear algebraic system of equations which can be solved by numerical methods. The power of both algorithms is illustrated by applying them and comparing the results to data found in the literature. The material should be of interest to users of the phase lock principle as well as researchers seeking new methods to detect and/or avoid the false lock phenomenon.

I. INTRODUCTION

It is possible for a phase lock loop (PLL) to false lock. Under this condition, frequency search halts, and the loop appears to lock at a frequency that bears no obvious relation to the reference frequency. The frequency error in a false locked loop is a small fraction of the reference frequency in most practical applications.

There are two distinct mechanisms of practical interest which cause false lock in PLLs. False lock can occur naturally given the proper closed loop dynamics[1,2,3]. New results on this so called "excess-time delay" false lock mechanism are presented in this report. Secondly, false lock can be induced by modulation on the reference [4,5]. This so called "data-related" false lock mechanism is not considered here.

The existence of stable false lock points in practical, high order loops is to be expected if no precautions are taken to prevent them. In practical applications it is often difficult to determine that a loop is false locked because most commonly used lock indicators will show that a false locked PLL is correctly locked. Also, noise within the loop can disguise the fact that a loop is false locked. Hence, the false lock phenomenon is often a very disturbing and difficult problem to solve in practice.

The "excess-time delay" false lock mechanism mentioned above is so named because most PLLs will false lock if a small pure time delay is added to the loop filter. Alternatively, loops containing high-order loop filters with significant phase shift often have stable false lock points. This is the case in narrow bandwidth, highly sensitive, phase lock receivers employing the long loop principle [1]. These receivers often fall victim to the "excess-time" false lock mechanism because they usually employ a narrow-band filter with significant phase shift in the loop's intermediate frequency (IF) amplifier. Also, this type of false lock is often introduced in practical PLLs by limitations inherent in the loop's components and/or by stray wiring capacitances.

Figure 1 depicts the classical PLL used in the analysis of the "excess time-delay" false lock problem. The loop filter F(s) should include the effects of any unwanted in-loop filtering in addition to the desired loop filter. Long loops can be modeled in this manner by using low-pass equivalents for their band-pass IF sections.

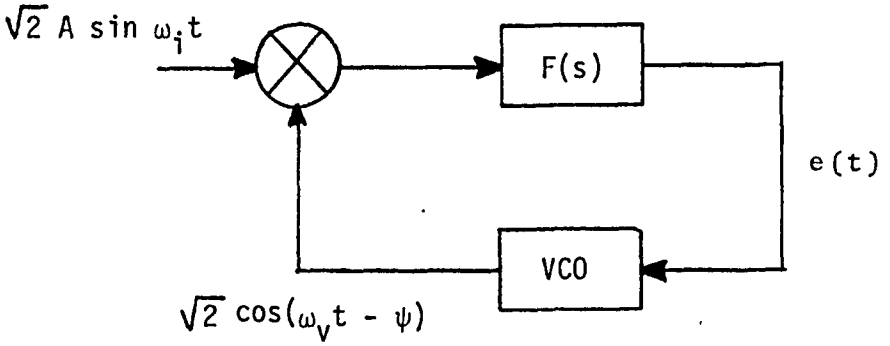

ω_0 Denotes the VCO Center Frequency(VCO freq. with e=0)

K_m Denotes The Multiplier Gain

K_v Denotes The VCO Gain

$\delta \triangleq K_m K_v A$ Represents a DC gain Term

$\omega f = \omega_i - \omega_v$

$$F(s) = \frac{s^M + a_{M-1}s^{M-1} + \ldots + a_0}{s^N + b_{N-1}s^{N-1} + \ldots + b_0}$$

Figure 1: A simple model of the phase locked loop.

The loop depicted by Figure 1 can be described by a nonlinear differential equation with periodic coefficients. The fundamental frequency of the equation's coefficients is equal to ω_f which is defined as the difference between the reference frequency ω_i and ω_V, the frequency of the voltage controlled oscillator (VCO). The quantity Ψ, the dependent variable in the equation, is periodic with a fundamental frequency equal to that of the equations coefficients when the loop is false locked.

That the PLL depicted by Figure 1 can, for proper F(s), false lock is a direct consequence of the nonlinearity inherent in the phase detector. A stable false lock condition in this PLL corresponds to a limit cycle of the above mentioned nonlinear differential equation. Equivalently, a stable false lock condition in this PLL corresponds to an asymptotically stable periodic solution of the nonlinear equation. It is possible to show that the "linearized" version of this equation has no such solution (it is often possible to obtain quantative information on the frequency error in the false locked loop from an analysis of this linear equation).

It is possible to determine the (exact) permissible value(s) of ω_f, denoted ω_{fl}, at which the PLL depicted by Figure 1 false locks by examining certain stability properties of the above-mentioned nonlinear equation. Unfortunately, this approach is not trivial; such an analysis, even for relatively simple special cases, has not been published.

To avoid mathematical difficulties in the analysis of the false lock phenomenon, several authors [1,2,3] have invoked simplifying assumptions and have obtained some quantitative results. The assumptions often employed are:

A) the frequency error in the false locked loop is very large compared to the closed loop gain;
B) the nonlinear problem can be linearized, and
C) all frequency components in Ψ beyond the fundamental can be ignored.

Unfortunately, it is not always clear whether or not methods based on these assumptions (which are not independent) apply in a particular application.

The above-mentioned assumptions are not required below in the development of two new algorithms for determining the frequency error in a false locked loop. Both algorithms are based on a condition given below which is necessary for false lock to occur. The material should be of interest to users of the phase lock principle as well as researchers seeking new methods to detect and/or avoid the false lock

phenomenon.

The above-mentioned necessary condition for false lock is discussed in Section III. The condition is stated in terms of the multipliers [7] of a linear differential equation with periodic coefficients.

The first new algorithm, described in Section VI, expresses ω_{fl}^{-1}, reciprocal of the frequency error in the false locked loop, as a power series in the closed loop gain. The second new algorithm, described in Section VII, expresses ω_{fl}^{-1} as part of the solution of a nonlinear algebraic system of equations which can be solved by numerical methods. The new methods are illustrated by example and the results are compared to data found in the literature.

II. OBJECTIVES

The principal investigator's main objective while participating in the 1984 NASA/ASEE Summer Faculty Fellowship Program was to finish the initial phase of his research effort on the PLL false lock phenomenon. This initial phase has taken approximately one and one-half years of effort on a part-time basis.

This report outlines some new results on the false lock phenomenon found by the PI. These results should help the communication systems engineer better understand a troublesome and perplexing problem which is often encountered in practical communication systems. They will serve as the basis of a technical paper submitted to the IEEE Transactions on Communications.

III. A CONDITION NECESSARY FOR FALSE LOCK

A necessary condition is given below for false lock to occur in the PLL depicted by Figure 1. It employs the fact that only discrete values of frequency error are permitted in a false locked loop. The condition is given in terms of the multipliers [7] of a linear differential equation with periodic coefficients. The necessary condition is used in two algorithms described below for computing the frequency error in a false locked PLL.

The equation describing Ψ in the PLL depicted by Figure 1 is given by

$$\left[\frac{d^N}{dt^N} + b_{N-1}\frac{d^{N-1}}{dt^{N-1}} + \ldots + b_0\right] \cdot \left[\omega_i - \omega_o - \frac{d\Psi}{dt}\right] \qquad \text{(III-1)}$$
$$= \delta\left[\frac{d^M}{dt^M} + a_{M-1}\frac{d^{M-1}}{dt^{M-1}} + \ldots + a_0\right] \mathrm{SIN}(\omega f \cdot t + \Psi)$$

This nonlinear differential equation with periodic coefficients is obtained by substituting $\omega f \cdot t + \Psi$ for the phase error term in the standard loop equation given in the literature [8]. The quantity δ represents a closed loop gain factor which will be used as a perturbation parameter in the analysis appearing below. The quantities a_k, $0 \leq k \leq M-1$ and b_k, $0 \leq k \leq N$, are parameters in the loop filter.

Define $x_1 = \Psi$, $x_2 = d\Psi/dt$, ... , $x_{N+1} = d^N\Psi/dt^N$ and the vector

$$X = \left[x_1 \;\; x_2 \;\; \ldots \;\; x_{N+1}\right]^T \qquad \text{(III-2)}$$

Equation (III-1) can be written as

$$\frac{dX}{dt} = F(t\ ,\ X\ ;\ \delta)$$
$$F(t\ ,\ X\ ;\ \delta) = F(t + T\ ,\ X\ ;\ \delta) \qquad \text{(III-3)}$$
$$T = 2\pi/\omega f$$

The quantity $F(t, X ; \delta)$ is a vector-valued nonlinear function of the state vector X, and the independent variable t. The vector F becomes linear in X when $\delta = 0$; that is,

$$F(t , X ; 0) = C X \qquad \text{(III-4)}$$

and $$F(t, X ; \delta) = C X + \delta \tilde{F}(t , X)$$

where C is an (N+1) × (N+1) matrix.

First, it is advantageous to consider PLLs with loop filters F(s) having no poles at the origin of the complex plane (the more complicated case corresponding to loop filters with poles at the origin is discussed later). Note that matrix C has one eigenvalue at the origin under this assumption; the remaining eigenvalues of C are assumed to be in the left half of the complex plane in what follows. Equivalently, Equation (III-3), with $\delta = 0$, has one multiplier [7] at unity; the remaining multipliers are assumed to be within the complex plane's unit circle.

Assume that the PLL described by (III-3) false locks for all values of loop gain δ in some neighborhood of the origin. Of course, the frequency error in the false locked loop, denoted $\omega fl (\delta)$, will be a function of δ. Equation (III-3) has a $T = 2\pi/\omega fl$ periodic vector solution, denoted $XP(t;\delta)$, which corresponds to this false lock condition.

The equation of first variation [9] for (III-3) with respect to $XP(t ; \delta)$ is written by using (III-4) as

$$\frac{dQ}{dt} = \left[C + \delta \tilde{F}_X (t , XP) \right] Q \qquad \text{(III-5)}$$

where $\tilde{F}_X$ denotes the Jacobian of $\tilde{F}$ with respect to vector X. Equation (III-5) is a <u>linear</u> differential equation with periodic coefficients. A necessary condition, given in terms of the multipliers of (III-5), for false lock to occur is discussed next. The necessary condition is based, in part, on the observation that only discrete values of frequency error are permitted in a false locked PLL.

Equation (III-5) has one multiplier at $\lambda = 1$ when $\delta = 0$. This multiplier must remain at unity for δ in some neighborhood of the origin if the PLL is false locked for these values of δ. The multiplier cannot move outside of the unit

circle as δ assumes small nonzero values since $XP(t, \delta)$ is stable [9]. It cannot move inside the unit circle since only discrete values of frequency error are permitted in a false locked loop. To see this, suppose that the multiplier leaves unity for a position inside the unit circle for arbitrarily small (but fixed) δ and the loop is false locked with a frequency error of $\omega f1(\delta)$. Under these conditions, all the multipliers of (III-5) are within the unit circle (for sufficiently small δ) and (III-3) has a unique, asymptotically stable, $T = 2\pi/\omega f$ periodic solution $\tilde{X}p(t;\omega f)$ (δ is fixed and ωf is a variable parameter) which is a continuous function of ωf for ωf in some neighborhood of $\omega f1(\delta)$; also, $\tilde{X}P(t;\omega f1(\delta)) = XP(t;\delta)$ [9]. This implies that the frequency error in the false locked loop could take on a continuum of values in some neighborhood containing $\omega f1(\delta)$. This cannot happen, and the necessary condition is established.

The above necessary condition is used below in the development of two algorithms for computing the frequency error in a false locked loop. The algorithms are applied to two examples to show their utility and provide data illustrating the necessary condition.

IV. SERIES EXPANSION OF $\omega f1^{-1}(\delta)$ AND $XP(t;\delta)$

The periodic vector $XP(t;\delta)$ and $\omega f1^{-1}(\delta)$, the reciprocal of the frequency error in the false locked loop, are given formal power series representations in this section. This material is used in Section VI to obtain an explicit formula which approximates the frequency error in a false locked second-order PLL with imperfect integrator.

The quantities $XP(t;\delta)$ and $\omega f1^{-1}(\delta)$ are represented in the analysis below as

$$XP(t;\delta) = X_0 + X_1(t)\delta + X_2(t)\delta^2 + \cdots\cdots$$

$$\omega f1^{-1} = \tilde{\omega}_0 + \tilde{\omega}_1\delta + \tilde{\omega}_2\delta^2 + \cdots\cdots \qquad \text{(IV-1)}$$

The vector X_0 is constant and has zero as its second through (N+1)th entry. The constant in the first entry of X_0 represents a DC component in Ψ and does not affect $\omega f1$. This can be seen from a close examination of (III-1). Any DC component added to Ψ represents a simple phase shift (or simple translation in the time variable) in (III-1) and does not affect the stability properties of this equation.

An algorithm for computing the coefficients in (IV-1) is presented in Section VI where it is used to approximate the frequency error $\omega f1$ as a function of δ for a false locked second-order loop with imperfect integrator. These results are compared with exact results obtained by a second method for computing $\omega f1$ which is presented in Section VII.

V. SECOND ORDER LOOP WITH IMPERFECT INTEGRATOR

A model for a second-order PLL with imperfect integrator is presented in this section. The material is used in Section VI to illustrate a method of calculating the coefficients in (IV-1). In Section VII this material is used to illustrate a new and powerful numerical method for finding the exact frequency error in a false locked loop.

The second order PLL with imperfect integrator has a loop filter given by

$$F(s) = \frac{s + a}{s + b} \qquad \text{(V-1)}$$

This loop has been studied by Viterbi[8] and others who have shown with analog computer techniques that a stable limit cycle (which corresponds to a false lock condition) exists as a possible loop response to a reference of constant frequency.

A nonlinear time-varying first-order system describing the above-mentioned loop is

$$\frac{dX}{d\tau} = \omega_f^{-1} Y$$

$$\frac{dY}{d\tau} = - b \cdot \omega_f^{-1} Y - \delta \left[\cos(\tau + X) + \omega_f^{-1} \left\{ \cos(\tau + X)\, Y + a \sin(\tau + X) \right\} \right] \qquad \text{(V-2)}$$

$$- b \left[1 - \omega_f^{-1} (\omega_i - \omega_0) \right]$$

This equation was obtained from (III-1) by 1) setting $b_1 = b$ and $a_1 = a$, 2) writing the system in phase variable canonical form with $x(t) = \Psi(t)$ and $y(t) = d\Psi/dt$, and 3) setting $\tau = \omega_f t$.

VI. FIRST ALGORITHM

An algorithm for calculating the coefficients in (IV-1) is illustrated below by applying it to the second-order PLL described in Section V. The approximation to $\omega f1$ described here is compared with exact values for this variable which are computed by the new numerical algorithm presented in Section VII.

An Overview

Assume that the PLL described by (V-2) false locks for all values of δ in some interval containing the origin. The reciprocal of the frequency error in the false locked loop, and the periodic solutions of (V-2) which correspond to this false locked condition, are given the expansions

$$\omega f1^{-1} = \tilde{\omega}_0 + \tilde{\omega}_1 \delta + \tilde{\omega}_2 \delta^2 + \ldots.$$

$$x = x_0 + x_1 \delta + x_2 \delta^2 + \ldots. \qquad \text{(VI-1)}$$

$$y = y_0 + y_1 \delta + y_2 \delta^2 + \ldots.$$

The coefficients in (VI-1) are calculated by solving a recursive system of linear differential equations with constant coefficients obtained by
1) substituting (VI-I) into (V-2),
2) expanding the nonlinear term $\cos(\tau + \sum_{K=0}^{\infty} x_k \delta^k) =$

$$= \mathrm{COS}(\tau + x_0) - x_1 \mathrm{SIN}(\tau + x_0)\,\delta$$

$$- \left[\tfrac{1}{2} x_1^2 \mathrm{COS}(\tau + x_0) + x_2 \mathrm{SIN}(\tau + x_0)\right] \delta^2 \qquad \text{(VI-2)}$$

$$- \left[x_1 x_2 \mathrm{COS}(\tau + x_0) + (x_3 - x_1^3/6)\mathrm{SIN}(\tau + x_0)\right] \delta^3 + \ldots.$$

with a similar expansion for $\sin(\tau + x)$ and,
3) equating equal powers in δ. Note that the constant x_0

represents a phase shift and enters the recursive system of linear differential equations through $\cos(\tau + x_0)$ and $\sin(\tau + x_0)$.

The periodic coefficients x_k and y_k in (VI-1) are, for $k \geq 0$, solutions of the kth-order equation (obtained by equating terms involving δ^k) in the above-mentioned recursive system. The quantity x_k is defined up to an additive constant c_k of integration, for $k \geq 1$, respectively, and both x_k and y_k, $k \geq 1$, are defined up to the phase shift constant x_0 by the requirement that they satisfy this recursive system. The integration constants and the coefficients in the expansion of ωfl^{-1}, are interrelated and need to be computed in pairs as described in this section.

The coefficients $\tilde{\omega}_0$, $\tilde{\omega}_1$, and $\tilde{\omega}_2$, in (VI-1) are calculated directly from the zeroth, first, and second order equations, respectively, in the recursive system. This is accomplished below without knowledge of any integration constants. The coefficients $\tilde{\omega}_{k+2}$ and constants c_k must be determined in pairs $(\tilde{\omega}_{k+2}, c_k)$ for $k \geq 1$.

The pairs (ω_{k+2}, c_k), $k \geq 1$, are calculated so that
1) the k+2th order equation in the recursive system has a periodic solution, and
2) the necessary condition of Section III is satisfied.
A method of satisfying these constraints and calculating $\tilde{\omega}_{k+2}$ and c_k, $k \geq 1$, is illustrated below.

First Algorithm: Generating and Using the Recursive System

The algorithm outlined above was used to write the first five equations (corresponding to δ^0 through δ^4) in the recursive sequence. The first three equations are given below. These equations are used to produce $\tilde{\omega}_0$, $\tilde{\omega}_1$ and $\tilde{\omega}_2$; these coefficients are used to obtain a very good small gain (second order in δ) approximation to the frequency error in the false locked loop under consideration. The two equations corresponding to δ^3 and δ^4 are long and cumbersome (but obtained in a straight forward manner) and are not given here. However, they were used to produce $\tilde{\omega}_3$ and $\tilde{\omega}_4$ for a fourth-order approximation of ωfl. In Section VIII this approximation is compared to both the second order approximation mention above and exact results obtained by the numerical method given in Section VII.

The equation obtained by equating terms of order δ° in the above-mentioned procedure is given as

$$\frac{dX}{d\tau}_0 = \tilde{\omega}_0 Y_0$$

$$\frac{dY}{d\tau}_0 = - b \tilde{\omega}_0 Y_0 - b \left[1 - \tilde{\omega}_0 \{\omega_i - \omega_0\}\right] \qquad \text{(VI-3)}$$

If (VI-3) is to have a periodic solution the quantity $\tilde{\omega}_0$ must be chosen as

$$\tilde{\omega}_0 = \{\omega_i - \omega_0\}^{-1} . \qquad \text{(VI-4)}$$

The variable Y_0 in (VI-3) must be zero; as expected, (VI-3) imposes no constraints on the phase shift constant X_0.

Equation (VI-4) implies that the frequency error in the false locked loop approaches the frequency difference between the reference and zero-input VCO as the closed loop gain approaches zero. This follows intuitively since the DC output of the multiplier approaches zero as the closed loop gain does.

The first order equation for X_1 and Y_1 is given as (with $Y_0 = 0$)

$$\frac{dX}{d\tau}1 = \tilde{\omega}_0 Y_1$$

$$\frac{dY}{d\tau}1 = -b \tilde{\omega}_0 Y_1 - \text{COS}(\tau + X_0) - a \tilde{\omega}_0 \text{SIN}(\tau + X_0) \qquad \text{(VI-5)}$$

$$+b \{\omega_i - \omega_0\} \tilde{\omega}_1$$

If (VI-5) is to have a periodic solution the quantity $\tilde{\omega}_1$ must be identically zero. The general periodic solution of (VI-5) is given as

$$X_1 = \tilde{\omega}_0 \left[A_1 \text{SIN}(\tau + X_0) - B_1 \text{COS}(\tau + X_0)\right] + c_1$$

$$Y_1 = A_1 \text{COS}(\tau + X_0) + B1 \text{SIN}(\tau + X_0) \qquad \text{(VI-6)}$$

where

$$A1 = \left[\frac{(a - b)}{1 + b^2\tilde{\omega}_0^2}\right]\tilde{\omega}_0 \qquad B1 = -\left[\frac{1 + a\,b\,\tilde{\omega}_0^2}{1 + b^2\tilde{\omega}_0^2}\right]$$

and c_1 is a constant of integration which is determined below.

The conclusion that $\omega_1 = 0$ is not unexpected. The simplified linear analysis discussed in Section I and the numerical method presented in Section VII suggest that the frequency error in the false locked loop under consideration is an even function of closed loop gain. This would require that the expansion of ωfl contain only even powers of δ; this requirement is supported by the observation that $\tilde{\omega}_1 = 0$.

The second order equation for X_2 and Y_2 is given as (with $Y_0 = 0$ and $\tilde{\omega}_1 = 0$)

$$\frac{dX_2}{d\tau} = \tilde{\omega}_0 Y_2$$

$$\frac{dY_2}{d\tau} = -b\,\tilde{\omega}_0 Y_2 + \left[\mathrm{SIN}(\tau + X_0) - a\,\tilde{\omega}_0\,\mathrm{COS}(\tau + X_0)\right] X_1 \qquad \text{(VI-7)}$$

$$- \tilde{\omega}_0\,\mathrm{COS}(\tau + X_0)\, Y_1 + b\,\{\omega_i - \omega_0\}\,\tilde{\omega}_2 .$$

The constant c_1 in X_1 must be evaluated before (VI-7) can be solved for a periodic solution. Before accomplishing this, $\tilde{\omega}_2$ is determined directly from (VI-7) and (VI-6).

The DC component in Y_2 must be zero if (VI-7) is to have a periodic solution. If (VI-6) is substituted into (VI-7), and the DC component in Y_2 is equated to zero, one obtains

$$\tilde{\omega}_2 = -\tfrac{1}{2}\left[\frac{a\,B1}{b(\omega_i - \omega_0)^3}\right] \qquad \text{(VI-8)}$$

The formula

$$\omega f1^{-1} \cong \tilde{\omega}_0 + \tilde{\omega}_2 \delta^2$$

where $\tilde{\omega}_0$ and $\tilde{\omega}_2$ are given by (VI-4) and (VI-8), respectively, provides a good small loop gain approximation to the frequency error in the false locked loop under consideration. This second-order formula, and a fourth order one discussed below, are compared in Section VIII with exact values for $\omega f1$ obtained from the numerical method presented in Section VII.

The fourth order approximation to $\omega f1$ cannot be generated until the integration constants c_1 and c_2 (c_2 is added to X_2) are determined. These integration constants are calculated below by a method based on the necessary condition of Section III.

First Variation and the Necessary Condition of Section III

The equation of first variation for (V-2) with respect to 2π periodic X and Y is

$$\frac{d}{d\tau}\begin{bmatrix} z_1 \\ z_2 \end{bmatrix} = \begin{bmatrix} 0 & \sum_{K=0}^{\infty} \tilde{\omega}_k \delta^k \\ f_x & f_y \end{bmatrix} \begin{bmatrix} z_1 \\ z_2 \end{bmatrix} \qquad \text{(VI-9)}$$

where

$$F_x = \delta\left[1 + \left(\sum_{K=0}^{\infty} \tilde{\omega}_k \delta^k\right)\left(\sum_{K=0}^{\infty} Y_k \delta^k\right)\right] \mathrm{SIN}\left(\tau + \sum_{K=0}^{\infty} X_k \delta^k\right)$$

$$- a\,\delta\left(\sum_{K=0}^{\infty} \tilde{\omega}_k \delta^k\right) \mathrm{COS}\left(\tau + \sum_{K=0}^{\infty} X_k \delta^k\right)$$

$$F_y = -\left[\delta \mathrm{COS}\left(\tau + \sum_{K=0}^{\infty} X_k \delta^k\right) + b\right]\left(\sum_{K=0}^{\infty} \tilde{\omega}_k \delta^k\right)$$

This linear 2π-periodic first order system can be written as

$$\frac{dZ}{d\tau} = \left[K_0 + \sum_{K=0}^{\infty} B_k \delta^k\right] Z \qquad \text{(VI-10)}$$

if the sin and cos terms are given the expansions suggested by (VI-2). For example, the quantities Z, K_0, B_1, and B_2 in (VI-10) are (with $\tilde{\omega}_1 = Y_0 = 0$)

$$Z = \begin{bmatrix} z_1 \\ z_2 \end{bmatrix} \qquad K_0 = \begin{bmatrix} 0 & \tilde{\omega}_0 \\ 0 & -b\tilde{\omega}_0 \end{bmatrix}$$

$$B_1 = \begin{bmatrix} 0 & 0 \\ (\mathrm{SIN} - a\tilde{\omega}_0\mathrm{COS}) & -\tilde{\omega}_0\mathrm{COS} \end{bmatrix} \qquad \text{(VI-11)}$$

$$B_2 = \begin{bmatrix} 0 & \tilde{\omega}_2 \\ (X_1\,\mathrm{COS} + \tilde{\omega}_0(Y_1+aX_1)\mathrm{SIN}) & (\tilde{\omega}_0 X_1 \mathrm{SIN} - b\tilde{\omega}_2) \end{bmatrix}$$

where $\mathrm{COS} \triangleq \mathrm{COS}(\tau + X_0)$ and $\mathrm{SIN} \triangleq \mathrm{SIN}(\tau + X_0)$.

Terms B_k, $k > 2$, can be readily calculated. However, they rapidly grow in complexity with k.

Since K_0 has a zero eigenvalue, (VI-10) has a characteristic exponent [7] $\lambda(\delta)$ with the property that $\lambda(\delta) \to 0$ as $\delta \to 0$. This characteristic exponent can be expressed as

$$\lambda(\delta) = \lambda_1 \delta + \lambda_2 \delta^2 + \ldots \qquad \text{(VI-12)}$$

for δ in some neighborhood of the origin. The coefficients λ_k, $k \geq 1$, can be calculated by a well-known method [7]. These coefficients must be zero if the necessary condition of Section III is to be satisfied.

The method outlined in the Overview subsection above for determining $\tilde{\omega}_{k+2}$ and c_k, $k \geq 1$, can be clarified by using the material contained in this subsection. For $k \geq 1$, the coefficient $\tilde{\omega}_{k+2}$ and the integration constant c_k are calculated so that

1) the (k+2)th order linear differential equation in the above-mentioned recursive system has a periodic solution and,
2) λ_{k+2} , as calculated by the well known method presented in Yakubovich [7], is zero.

The coefficients λ_1 and λ_2 , as calculated by the previous referenced method, are zero independent of ω_{k+2} and c_k , $k \geq 1$. For each $k \geq 1$, the above two requirements produce two equations which can be solved for the unknowns $\tilde{\omega}_{k+2}$ and c_k .

The pairs $\tilde{\omega}_3$, c_1 and $\tilde{\omega}_4$, c_2 were computed as outlined above. The results of these calculations were used to produce a fourth order approximation to $\omega f1^{-1}$. The results of these calculations are sumarized in Section VIII. The details of the calculations are not included here since the work involves a considerable amount of tedious computation and consumes considerable space.

The quantity $\tilde{\omega}_3$ is identically equal to zero as expected. This is consistent with the fact that $\omega f1(\delta)$ is an even function of δ.

VII. NUMERICAL DETERMINATION OF ωfl

A new and powerful numerical method for determining the frequency error in a false locked loop is presented in this section. This method can produce very accurate results (limited only by machine precision). The method uses the necessary condition of Section III and the dynamical equations describing the loop to formulate a system of nonlinear algebraic equations which can be solved by numerical methods. The frequency error ωfl in the loop is part of the solution of these equations. The method is illustrated by applying it to the second order loop presented in Section V.

Assume that the PLL described by (V-2) with fixed parameters a, b, and δ is false locked. The necessary frequency error ωfl in the loop is such that both X and Y are $T = 2\pi/\omega fl$ periodic and the necessary condition of Section III is satisfied.

The periodicity requirement on X and Y implies that initial values X(0), Y(0) and frequency error ωf be selected when integrating (V-2) so that

$$F_1(X(0),Y(0),\omega f) = X(0) - X(2\pi) = 0$$

$$F_2(x(0),Y(0),\omega f) = Y(0) - Y(2\pi) = 0 \qquad \text{(VII-1)}$$

Equation (VII-1) represents a system of two nonlinear algebraic equations in three unknowns. A third independent equation results from the necessary condition of Section III.

The necessary condition of Section III can be formulated as

$$F_3(X(0),Y(0),\omega f) = a_1 + a_2 + 1 = 0., \qquad \text{(VII-2)}$$

The quantities a_1 and a_2 are coefficients in the characteristic polynomial

$$\lambda^2 + a_1\lambda + a_2 = 0 \qquad \text{(VII-3)}$$

of the monodromy matrix [7] for the equation of first variation of (V-2) with respect to X and Y. Constraint (VII-2) is both necessary and sufficient for the polynomial (VII-3) to have a root at $\lambda = 1$.

The quantities F_1 , F_2 , and F_3 can be computed by numerically integrating (V-2) and its first variation over one 2π period. The integration process starts with initial conditions $X(0)$, $Y(0)$ and selected value of ωf . The well-known fourth-order Rung-Kutta technique [12] was used to produce the results presented in Section VIII.

The numerical algorithm for computing $\omega f1$ involves solving the nonlinear algebraic system (VII-1) and (VII-3). This can be accomplished by using the routine ZSPOW in the widely available IMSL software package [10]. This routine uses a variation of the well-known Newton-Ralphson technique [11] with the Jacobian computed by a finite difference scheme. Results of these computations are given in Section VIII.

VIII. COMPUTATIONAL RESULTS

Computational results from the algorithm presented in Section VI and VII are given in this section. Results from these algorithms are compared below with data from the PLL literature.

Table (VIII-1) contains approximations to $\omega f1$ for several values of δ. This data was obtained from the second and fourth order (in δ) approximations to $\omega f1^{-1}$ which were described in Section VI. These approximate values of $\omega f1$ are compared below to extremely accurate values computed by the numerical algorithm of Section VII. The loop filter parameters used in obtaining this data were a = 5 and b = 1; the initial (with $\delta = 0$) frequency offset between the reference and VCO was $\omega_i - \omega_0 = 35$ radians/second.

Very accurate values of $\omega f1$ for comparison with the above-mentioned approximate values are given in Table (VIII-2). These values were computed by using the algorithm outlined in Section VII.

The parameters NSIG and FNORM from ZSPOW (used in the algorithm of Section VII) are listed in Table (VIII-2). NSIG, which is supplied by the user, denotes the number of digits of accuracy desired in the computed root. A root of the system (VII-1), (VII-2) is accepted by ZSPOW if two successive iterations of the root finding algorithm produce roots having components which do not differ in the NSIG most significant digits. FNORM is computed by ZSPOW and it is an indication of how well the routine converged. Denote the (approximate) root of (VII-1) and (VII-2) found by ZSPOW as $(X_0', Y_0', \omega f')$. Then

(VIII-1)

$$FNORM = F_1(X_0', Y_0', \omega f')^2 + F_2(X_0', Y_0', \omega f')^2 + F_3(X_0', Y_0', \omega f')^2$$

VALUE OF GAIN	SECOND ORDER	FOURTH ORDER
1.	34.92848	34.92817
2.	34.71568	34.71071
3.	34.36672	34.34208
4.	33.88979	33.81417
5.	33.29570	33.11806
6.	32.59728	32.24616
7.	31.80875	31.19467
8.	30.94502	29.96601
9.	30.02113	28.57062
10.	29.05173	27.02784

Table VIII-1: Approximate frequency error in the false locked loop of Section V as computed by the algorithm of Section VI. The loop parameters used are a=5, b=1, and $\omega_i - \omega_0 = 35$. Results for the second and fourth order (in δ) approximation are given.

VALUE OF GAIN	FREQUENCY ERROR IN THE FALSE LOCKED PLL	NSIG	FNORM
1.	34.9282	4	.2623E-16
2.	34.7112	4	.5169E-16
3.	34.3439	4	.1557E-15
4.	33.8173	4	.4623E-15
5.	33.1168	4	.3059E-12
6.	32.2206	4	.7681E-13
7.	31.0946	4	.5813E-11
8.	29.6836	4	.1600E-12
9.	27.8898	4	.1164E-10
10.	25.5071	4	.2878E-11

TABLE VIII-2: Very accurate values for the frequency error in the false locked loop of Section V as computed by the numerical algorithm of Section VII. The loop parameters used are a=5, b=1, and $\omega_i - \omega_0 = 35$.

IX. CONCLUSIONS

A new condition necessary for false lock was discovered during this phase of the research effort which ends with the conclusion of the 1984 ASEE/NASA Summer Faculty Fellowship program. This necessary condition is given in Section III. The condition involves certain eigenvalues of a matrix obtained from the dynamical equations describing the loop.

The necessary condition was used in Section VI to develop a new algorithm for computing the frequency error in a false locked loop. The new algorithm expresses the frequency error as a power series in the PLL's closed loop gain. The algorithm was applied to the second order loop with imperfect integrator introduced in Section V. The results of these computations are given in Table (VIII-1) of Section VIII.

A second new algorithm for computing the frequency error in a false locked loop was introduced in Section VII. This algorithm must be implemented on a computer and it requires no laborious hand calculations. The algorithm gives results limited in accuracy only by machine precision. The algorithm formulates the false lock problem as a system of nonlinear algebraic equations which are solved by a standard routine in the IMSL package. The algorithm was applied to the PLL of Section V and the results are listed in Table (VIII-2) of Section VII.

The above mentioned algorithms will help communication system engineers in their efforts to "design around" or to avoid the false lock problem since the algorithms provide powerful methods for determining the false lock properties of systems employing the phase lock principle.

C-8

REFERENCE

1. F.M. Gardner, Phaselock Techniques, 2nd ed. Wiley, New York, 1971.

2. Develet, J., "The Influence of Time Delay on Second-Order Phase Lock Loop Acquisition Range," Int. Telem. Conf., pp 432-437, London, 1963.

3. Tausworthe, R., "Acquisition and False-Lock Behavior of Phase-Locked Loops with Noisy Inputs," JPL SPS 37-46, Vol. IV, pp 226-234, Jet Propulsion Laboratory, Pasadena, CA, August 31, 1967.

4. Hedin, G., Homes, J., and Lindsey, W., "Theory of False Lock in Costas Loops," IEEE Trans. on Comm., Vol. COM-26, No. 1, Jan. 1978.

5. Homes, J., Spread Spectrum. John Wiley, New York, 1982.

6. Lindsey, W., Synchronization Systems in Communication and Control. Prentice Hall, Englewood Cliffs, NJ, 1972.

7. Yakubovich, V. and Starzhinskii, V., Linear Differential Equations with Periodic Coefficients Vol. 1. Wiley, New York, 1975.

8. Viterbi, A., Principles of Coherent Communication. McGraw Hill, New York, 1966.

9. Coddington, E.,and Levinson, N., Theory of Ordinary Differential Equations. McGraw-Hill, New York, 1955.

10. International Mathematics and Scientific Library, IMSL Library Edition 9, NBC Building, 7500 Bellaire Boulevard, Houston, Texas.

11. Luenberger, D., Optimization By Vector Space Methods. John Wiley, New York, 1968.

12. Kreyszig, E., Advanced Engineering Mathematics, Fifth Edition. John Wiley, New York, 1983.

13 Stensby, J., "On The PLL Spectral Purity Problem", IEEE Trans. on Cir. and Sys., Vol. CAS-30, No. 4, p248-251, April 1983.

1984 NASA/ASEE SUMMER RESEARCH FACULTY FELLOWSHIP PROGRAM

MARSHALL SPACE FLIGHT CENTER
THE UNIVERSITY OF ALABAMA

A COMPUTER CONTROLLED MASS SPECTROMETER SYSTEM FOR INVESTIGATING THE DECOMPOSITION OF NON-METALLIC MATERIALS UNDER ATMOSPHERIC CONDITIONS

Prepared by:	James M. Thompson, Ph.D
Academic Rank:	Associate Professor
University and Department	Alabama A & M University Normal, Alabama 35762
NASA/MSFC:	
Laboratory:	Materials and Processing
Division:	Nonmetallic Materials
Branch:	Analytical and Physical Chemistry
MSFC Counterpart	John G. Austin, Jr.
Date:	August 3, 1984
Contract No.:	NASA NGT-01-002-099 The University of Alabama

ACKNOWLEDGEMENTS

My second summer at NASA has been equally as fulfilling and intellectually stimulating as the first summer, mainly due to the generous hospitality and assistance of Dr. John G. Austin, Jr. For this I am grateful.

I also wish to extend appreciation to Dr. L. M. Freeman and other members of the 1984 NASA/ASEE coordinating team for selecting me to participate for a second year in this excellent program.

These summer fellowships have broadened my knowledge in the area of quadrupole mass spectrometry and have enabled me to acquire a second research interest which I expect to continue with in future years.

A COMPUTER CONTROLLED MASS SPECTROMETER SYSTEM FOR INVESTIGATING THE DECOMPOSITION OF NON-METALLIC MATERIALS UNDER ATMOSPHERIC CONDITIONS

By

James M. Thompson
Associate Professor of Chemistry
Alabama A & M University
Normal, Alabama 35762

ABSTRACT

A PDP 11/23 - quadrupole mass spectrometer system has been coupled to a non-discriminating gas inlet system permitting gases at atmospheric pressure to be admitted into a high vacuum chamber containing the ion source of the mass spectrometer without separation of the gaseous components.

The resolution of related software problems has resulted in a convenient computer-mass spectrometer system capable of generating masses, relative intensities and related data on the gaseous products resulting from the atmospheric thermal decomposition of non-metallic materials.

LIST OF ILLUSTRATIONS

LIST OF TABLES

INTRODUCTION

In a previous paper, we reported the interfacing of a Balzer quadrupole mass spectrometer (QMG 511) with a PDP 11/23 desktop computer, as well as a description of the computer-mass spectrometer system and the advantages derived therefrom.[1] Recently, we have sought to extend the capability of the computer-quadrupole mass spectrometer by coupling the system with a non-discrimination gas inlet valve, permitting gases at atmospheric pressure to be admitted into the high vacuum chamber of the mass spectrometer without separating the gaseous components.

In addition, the incompatability of certain related software problems has been resolved and modification made which now permits the rapid acquisition, processing, analysis and display of electrometer values, mass spectrograms, mass numbers and corresponding intensities, all under programmed control.

The hardware enhancement, software resolutions and modifications have resulted in a convenient computer-mass spectrometer system that provides for the rapid acquisition and processing of mass spectral data relating to the thermal decomposition of non-metallic materials related to the National Space Exploration Program. Furthermore, the system is also capable of automatically setting and reading the parameters of the spectrometer for optimization and measurement in a "closed loop" operation.

OBJECTIVES

The objectives of this project are:

1. To assemble a computer-mass spectrometer system capable of permitting the investigation of the atmospheric thermal decomposition of non-metallic materials.

2. To resolve certain software problems, thus enhancing the capabilities of the computer-mass spectrometer system such that data pertaining to the thermal decompositions of non-metallic materials are rapidly acquired, processed, analyzed and hard copies of the data generated.

DESCRIPTION OF THE NON-DISCRIMINATION GAS INLET MASS SPECTROMETER SYSTEM

In these laboratories, we are interested in decompositions studies in both high vacuum systems and under atmospheric conditions. To meet the latter requirement, a non-discrimination gas inlet system has been coupled to a computer-quadrupole mass spectrometer as shown in Figure 1.

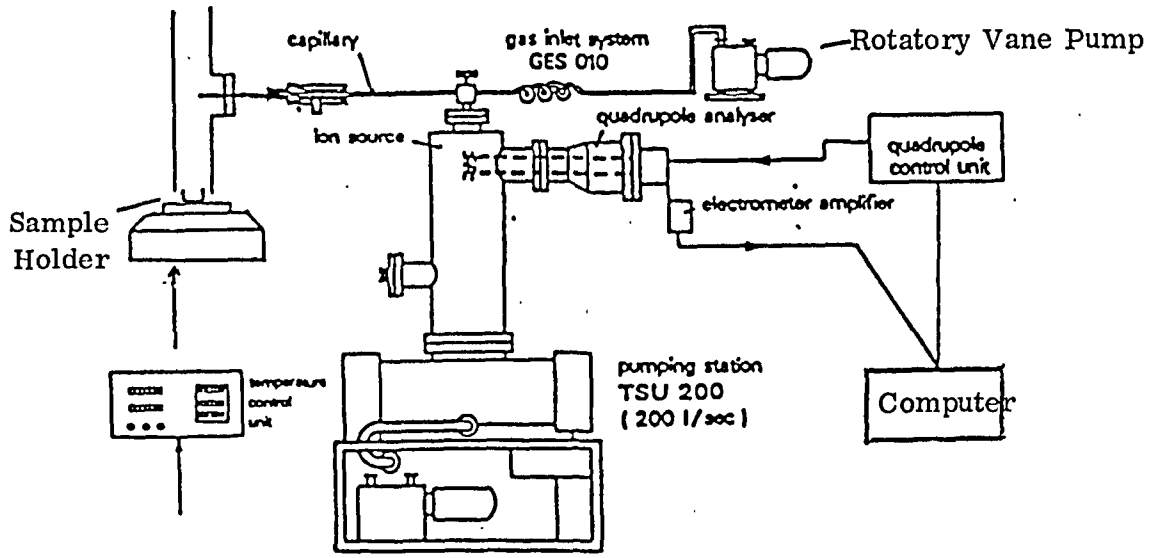

Figure 1. Schematic Diagram of the Non-Discrimination Gas Inlet/Mass Spectrometer Coupling*.

Thermal decompositions in vacuum systems such as with a mass spectrometer-thermal analyzer provide important information relative to weight changes during decomposition, partial pressure changes and mass spectral data. However, such systems do not always lend themselves to decomposition studies in air or in other gaseous systems. For investigations of the latter type, a pressure reduction gas inlet valve must be inserted between the sample and the mass spectrometer. In addition, if accurate qualitative results are required, the inlet valve must meet the following requirements:

---

*The non-discrimination gas inlet system is manufactured by Balzer High Vacuum and Components, Hudson, N.H.

1. The ratio of the gaseous components must not change as they enter the spectrometer.

2. There must be a short response time between sample decomposition and the time the volatile components enter the spectrometer.

3. There must be no condensation of gaseous components as they travel to the vacuum chamber of the spectrometer.

The non-discrimination gas inlet system described herein meets the requirements enumerated above.[2]

As indicated in Figure 1, the non-metallic material is placed in the sample holder, which is attached to the non-discrimination inlet valve by a .15 mm x 1 mm stainless steel capillary tube. Thermal decomposition of the sample is carried out, preferably under controlled temperature. The volatile components released during decomposition enter the capillary in laminar flow.** These components are pumped off, still in laminar flow by a rotary vane pump, attached to the inlet valve (Figures 1 and 2), whereupon a small portion of the gaseous components enters the high vacuum chamber of the spectrometer through an artificial leak, consisting of a fritted stainless steel poral filter. As the gases enter the vacuum chamber, they are converted to molecular flow.** A schematic diagram of the inlet valve is shown in Figure 2.

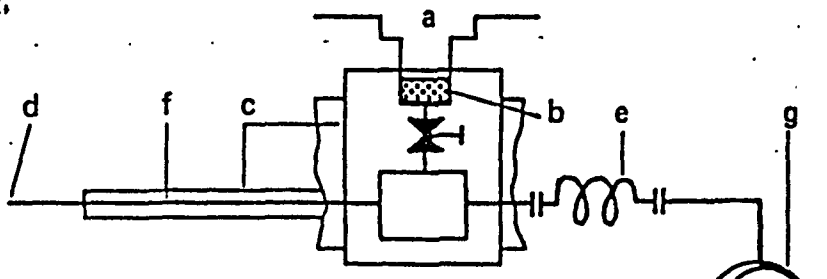

Figure 2. A Schematic Diagram of the Non-Discrimination Gas Inlet System.

** For laminar flow, the mean free path of the gaseous atoms or molecules is small compared to the diameter of the vacuum line. Whereas in molecular flow the path is large relative to the vacuum line or pores of the artificial leak.

The intermediate pressure of the inlet valve's body is dependent upon the pumping speed of the rotary vane pump. At a pumping speed of at least 1 m^3/h, this pressure is approximately 0.75 Torr. Both the valve's body and the capillary tube may be heated by coils up to a maximum temperature of 200 °C, making possible the measurement of condensable gases.

As the volatile components enter the vacuum chamber of the ion source, they are ionized by electron impact. The positive ions are accelerated into the quadrupole mass filter and analyzed. In thermal decomposition investigations, a greater accuracy is attained if the background gases in the vacuum chamber of the mass spectrometer are low and their concentration constant. This may be accomplished, to some extent, by evacuating the chamber to pressures of at least 10^{-6} Torr. Especially is it important to reduce and stablize the concentrations of the common components of air such as H_2O, CO, and CO_2. Using a 200 liters/sec turbomolecular pump and metal sealing on the high vacuum part, the QMG 511 mass spectrometer in this laboratory has been evacuated to approximately 10^{-7} Torr. The system also has degassing capabilities, making it possible to reduce background gases even further.

Information on mass numbers and intensities as well as information from the various units of the spectrometer is digitally transferred to the buffer of the QMG 511 over a defined data path. This information is available as output to the PDP 11/23 computer through an asynchronous dialogue.[1], All parameters and controls of the spectrometer (except power) is accessible through the buffer.

Data transfer between the buffer and the computer occurs on a high speed balanced line transmission, which consists of a general purpose 16 bit parallel line interface (DRV-11, by Digital Equipment) and an LT-511 line tranceiver (by Balzer). The latter is a pc board containing the electrical circuits necessary for converting transistor-transistor logic (TTL) to constant output current on twisted pair lines leading to the buffer and vice versa[1].

OTHER GAS INLET SYSTEMS FOR QMG 511 QUADRUPOLE MASS SPECTROMETER COUPLING

Descriptions of specialized gas inlet systems for investigating the thermal decomposition of non-metallic materials have been reported by several workers.[3,4,5]. In most of these instances, the quadrupole mass spectrometer is coupled to the vacuum system of a thermal analyzer (TA) and thermal decompositions usually conducted at pressures not exceeding 10^{-4} Torr. Beyond this pressure, the proportionality between ion current and sample concentration is no longer valid and linearity is lost. However, if only qualitative information is desired, the pressure limitations need not be strictly adhered to.

In Figure 3, is shown a gas inlet system that may be coupled to the QMG 511 quadrupole mass spectrometer for investigating decompositions both under atmospheric pressure and under high vacuum.[5]. In this system, a modified Mettler thermal analyzer (TA-1) is coupled with a water cooled diffusion pump using polyphenylether as the pump fluid (convalex 10 or Santovac 5). It is reported that low gas backgrounds are easily attained, thereby facilitating trace analyses. For high vacuum decompositions, the Butterfly-valve and TA furnace must be open.

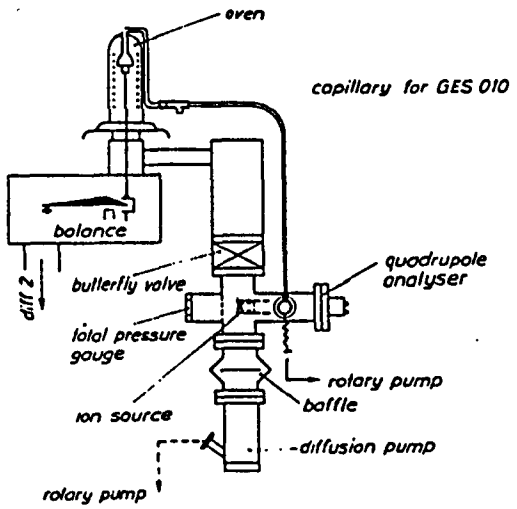

Figure 3. An Example of a Thermal Analyzer/Mass Spectrometer System for Investigating Decompositions at Atmospheric Pressure and Under High Vacuum.

In cases where one or more of the decomposition products condense at 100 °C or above, the specialized dual stage pressure reduction valve shown in Figure 4, may be used.[5] In this valve, which is constructed of quartz glass, the orifice inlet is located within the heating zone of a modified TA-heater. As a result, the orifice is heated to about the same temperature as the sample crucible. It is reported that temperatures up to 800 °C may be attained with the system, however, the valve is limited to investigations of thermal decompositions under vacuum conditions.

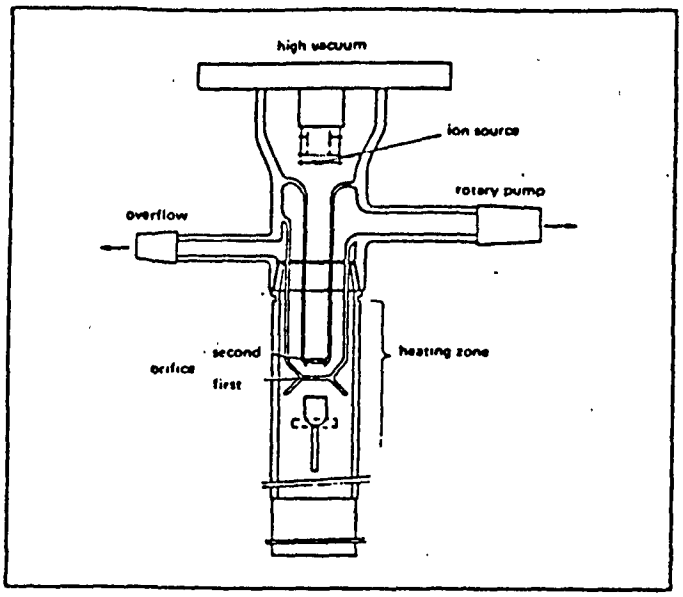

Figure 4. A Specialized Quartz Glass Inlet System for Investigating Highly Condensable Gases.

For investigating solid and liquids samples with low vapor pressures under vacuum conditions, there is available a direct inlet system (DIS 100, by Balzer).[6] In this system, which is shown in Figure 5, the sample under study is introduced directly into the vacuum chamber of the spectrometer. According to Balzer, the valve system is designed to study solids and low vapor liquids such as pump fluids.

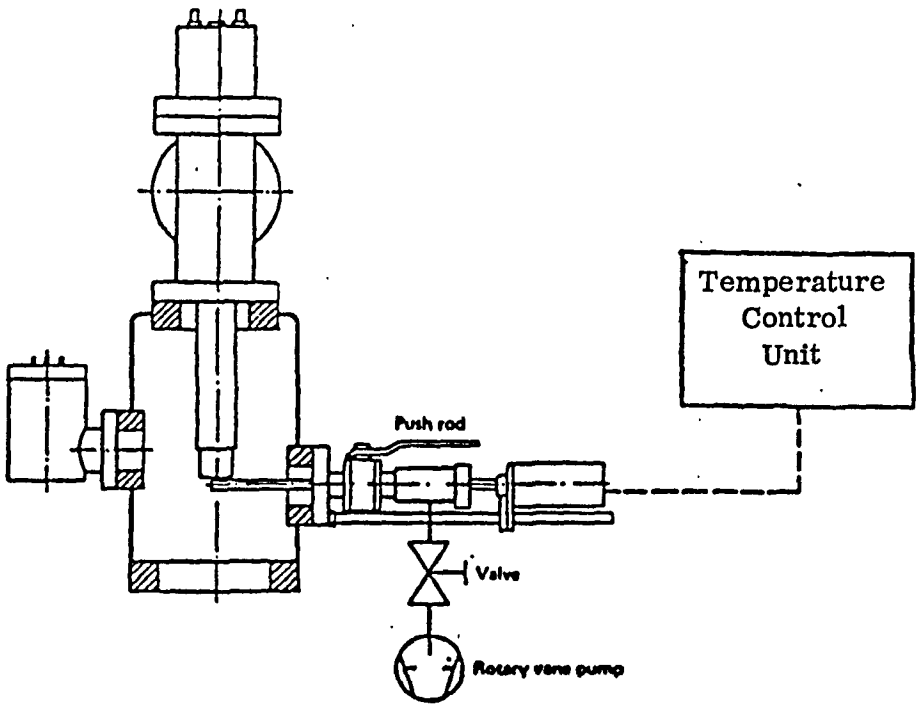

Figure 5. Schematic Diagram of a Direct Solid Sample Inlet System for the GMG 511 Mass Spectrometer.

The direct sample inlet valve consists of a push rod containing the sample block, a vacuum lock and a temperature control unit. The sample is deposited either in a glass, platinum or gold crucible and inserted into the vacuum chamber. The push rod is designed such that the sample is introduced into the vacuum chamber without venting. With the temperature control unit, the sample may be heated from room temperature to 400 °C in 1-2 °C increments. A cooling unit is also integrated into the block for rapid sample cooling.

RESOLUTION OF SOFTWARE PROBLEMS

After successfully interfacing the PDP 11/23 computer with the QMG 511 and coupling the system with the GES 100 non-discrimination inlet valve, it remained necessary to resolve certain related software problems. Previously, problems involving missing globals had been resolved. As a result, several QMG FORTRAN subroutines were complied and linked, resulting in executable programs. One of which automatically sets and reads 21 parameters of the mass spectrometer for optimization and measurement in a "closed loop" operation as shown in Table 1 and 2. Other programs resulted in the generation of unnormalized mass spectral data such as mass numbers and corresponding ion currents.

To meet the software requirements necessary to facilitate the acquisition, processing and analysis of data from the thermal decompositions, a single program capable of performing a number of operations was needed. Specifically, a program that would:

1. Test if the QMG 511 is on line

2. Automatically switch on the filament and place all front panel parameters under computer control.

3. Initalize the buffer of the mass spectrometer and set certain defined consol parameters, such as voltage, electrometer filter, magnifier, polarity and RF.

4. Allow the operator to enter certain other parameters such as scan speed, resolution, electrometer current, SEM voltage, beginning mass and ending mass.

5. Generate mass numbers and corresponding ion current in ampers.

6. Generate mass numbers and corresponding relative intensities.

7. Produce a mass spectrogram where relative intensities are plotted against mass numbers.

8. Direct the above data to both the CRT and the line printer.

Rather than attempt to write a program that would satisfy the software requirements, it was decided to modify an existing FORTRAN program that had been obtained from Balzer. On previous occassions, repeated attempts to compile the program had been unsuccessful. It appeared that the program in question had initially been compiled using an older version of the RT-11 operating System and undoubtly there existed some differences between the two compilers that caused the problem. Furthermore, the program in question was written to transfer data to the CRT only. The final resolution of the problem required that the programe line:

```
Call SSEM(ISEM,0)
```

be changed to:

```
Call SSEM(ISEM)
```

Even though the program modification was simple, it proved preplexing and required considerable effort in arriving at the solution. After making the indicated changes, write commands were added in order to transfer data to the line printer. The program was then compiled and linked without difficulty to give an executable program that resulted in generating the desired mass spectral data. The program, which is called SCAN12, is listed in its entirety in Table 6 and Tables 4 and 5 show examples of the data obtained from it execution.

Table 1. Examples of the Parameters of the OMG 511 Mass Spectrometer Automatically Set and Read Under Programmmed Control.

```
CONSOLE PARAMETER  1 =     0
CONSOLE PARAMETER  2 =    54
CONSOLE PARAMETER  3 =    10
CONSOLE PARAMETER  4 =    48
CONSOLE PARAMETER  5 =   250
CONSOLE PARAMETER  6 =     7
CONSOLE PARAMETER  7 =     1
CONSOLE PARAMETER  8 =     0
CONSOLE PARAMETER  9 =     0
CONSOLE PARAMETER 10 =     0
CONSOLE PARAMETER 11 =     0
CONSOLE PARAMETER 12 =   111
CONSOLE PARAMETER 13 =     9
CONSOLE PARAMETER 14 =     0
CONSOLE PARAMETER 15 =     0
CONSOLE PARAMETER 16 =     0
CONSOLE PARAMETER 17 =     0
CONSOLE PARAMETER 18 =     0
CONSOLE PARAMETER 19 =     0
CONSOLE PARAMETER 20 =     0
CONSOLE PARAMETER 21 =     1
CONSOLE PARAMETER 22 =     0
```

Table 2. Explanation of the Parameters of the Mass Spectrometer Automatically Set and Read Under Programmed Control.

ParameterCode	Parameters
1	Mass Numbers
2	Fraction
3	Scan Width
4	Resolution
5	SEM Voltage
6	Scan speed
7	Single/Manual/Repeat
8	Integral/Spectrum
9	RF On/Off
10	Electrometer Range
11	Polarity
12	Magnifier
13	Filter
14	SEM Switch
15	Filameter Switch On/Off
16	Normal/Degas
17	Electron Energy
18	Display
19	Auto Control Channel
20	Auto Control/Operation
21	Autocontrol On/Off
22	Autocontrol Set/Not Set

Table 3. Mass Numbers and Ion Currents Generated Using the SCAN12 Program.

MASS(AMU)	ION CURRENT(AMPS)
10	-0.144E-07
11	-0.280E-08
12	-0.112E-06
13	-0.760E-08
14	-0.728E-06
15	-0.764E-07
16	-0.528E-06
17	-0.160E-05
18	-0.536E-05
19	-0.384E-07
20	-0.356E-07
21	-0.168E-07
22	-0.440E-08
23	-0.440E-08
24	-0.840E-08
25	-0.124E-07
26	-0.152E-07
27	-0.128E-05
28	-0.520E-05
29	-0.136E-06
30	-0.424E-07
31	-0.168E-06
32	-0.932E-06
33	-0.760E-08
34	-0.400E-08
35	-0.112E-07
36	-0.156E-07
37	-0.360E-08
38	-0.560E-08
39	-0.560E-08
40	-0.520E-07
41	-0.188E-07
42	-0.220E-07
43	-0.356E-06
44	-0.436E-06
45	-0.360E-08
46	-0.680E-08
47	-0.136E-07
48	-0.360E-08
49	-0.400E-08
50	-0.268E-07

Table 4. Mass Numbers and Relative Intensities Generated Using the SCAN12 Program.

MASS(AMU)	RELATIVE INTENSITY(PERCENT)
10	0.27
11	0.05
12	2.09
13	0.14
14	13.58
15	1.43
16	9.85
17	29.85
18	100.00
19	0.72
20	0.66
21	0.31
22	0.08
23	0.08
24	0.16
25	0.23
26	0.28
27	23.88
28	97.01
29	2.54
30	0.79
31	3.13
32	17.39
33	0.14
34	0.07
35	0.21
36	0.29
37	0.07
38	0.10
39	0.10
40	0.97
41	0.35
42	0.41
43	6.64
44	8.13
45	0.07
46	0.13
47	0.25
48	0.07
49	0.07
50	0.50

Table 5. The Final Version of the SCAN12 Program.

```
C THIS PROGRAM SCANS A SINGLE MASS SPECTRUM AND GIVES AN UN-
C NORMALIZED TABULATED SPECTRUM, OR NORMALIZED TABULATED
C SPECTRUM, OR A NORMALIZED BAR GRAPH PRESENTATION. ALL SCAN
C PARAMETERS ARE SET BY THE PROGRAM, EXCEPT THOSE CONTAINED
C IN THE OPERATOR QUERY. BUFFERED DATA ACQUISITION IS USED.
C
 DIMENSION MASBUF(64),SIGBUF(511)
C
C SET UP STANDARD SCAN CONDITIONS
C
C ASSIGN PRINTER
C
 CALL ASSIGN(6,'LP:')
 CALL STRT
 CALL SDSP(0) !MASS
 CALL SSCW(1) ! 1 AMU WIDTH
 CALL SMOD(0,1,1) !SINGLE,SPECTRUM,RF ON
 CALL SELE(1,0,0) !FIL ON,NORM,EE V1
 CALL SPOM(-1,111) !NEG.,AUTORANGE
 CALL SSSW(1)  !SEM ON
C
C QUERY OPERATOR FOR OTHER SCAN PARAMETERS
C
920 TYPE 100
 WRITE (6,100)
100 FORMAT(1X,'SCAN SPEED(0,1,2,...)=',$)
 ACCEPT 200,ISPED
 TYPE 101
 WRITE(6,101)
101 FORMAT(1X,'RESOLUTION(0-63)=',$)
 ACCEPT 200,IRES
 TYPE 102
       WRITE (6,102)
102 FORMAT(1X,'ELECTROMETER RANGE(-5,-7,-9,OR -11)=',$)
 ACCEPT 200,IELEC
 TYPE 103
       WRITE (6,103)
103 FORMAT(1X,'SEM HIGH VOLTAGE(0-355)=',$)
 ACCEPT 200,ISEM
 TYPE 104
       WRITE (6,104)
104 FORMAT(1X,'START MASS(1-511)=',$)
 ACCEPT 200,IFMAS
 TYPE 105
       WRITE (6,105)
105 FORMAT(1X,'LAST MASS(1-511)=',$)
 ACCEPT 200,ILMAS
200 FORMAT(I3)
C
C SET OPERATOR ENTERED PARAMETERS
 CALL SFMA(IFMAS,0)
 CALL SSSP(ISPED)
 CALL SRES(IRES)
 CALL SFIL(ISPED)
 CALL SELR(IELEC)
 CALL SSEM(ISEM)
C  WAIT FOR OPERATOR TO INITIATE START
 TYPE 106
       WRITE (6,106)
106 FORMAT(1X,'TYPE 1 AND RETURN TO START SCAN',$)
 ACCEPT 200,IDUMY
C
C DATA ACQUISITION AND DETERMINATION OF MAXIMUM IN EACH AMU.
C
910 DO 300 MASS=IFMAS,ILMAS
 CALL SFMA(MASS,0)
 CALL ELCR(MASBUF,64)
 SIGMAX=0.0
 DO 301 J=2,64
 CALL RBEC(MASBUF(J),SIGNAL)
 IF(ABS(SIGNAL)-ABS(SIGMAX)) 301,311,311
311 SIGMAX=SIGNAL
301 CONTINUE
 SIGBUF(MASS)=SIGMAX
300 CONTINUE
```

```
C
C CHOOSE DATA OUTPUT FORMAT
 TYPE 350
       WRITE (6,350)
350 FORMAT(1X,'CHOOSE DATA FORMAT:---')
 TYPE  351
       WRITE (6,351)
351 FORMAT(1X,'FOR UNNORMALIZED TABULATED SPECTRUM- TYPE 0')
 TYPE 352
       WRITE (6,352)
352 FORMAT(1X,'FOR NORMALIZED TABULATED SPECTRUM-TYPE 1')
 TYPE 353
       WRITE (6,353)
353 FORMAT(1X,'FOR NORMALIZED BAR GRAPH SPECTRUM-TYPE 2')
 TYPE 354
       WRITE (6,354)
354 FORMAT(1X,'FOR ALL THREE - TYPE 3')
 ACCEPT 200,IFORM
 IF(IFORM-1) 400,500,600
C 400=UNNORMALIZED TABULATED
C 500=NORMALIZED  TABULATED
C 600=NORMALIZED BAR GRAPH OR ALL 3
600 IF(IFORM-3) 700,400,400
C 700=NORMALIZED BAR GRAPH ONLY
C
C DATA OUTPUT--UNNORMALIZED TABULATED
400 TYPE 401
       WRITE (6,401)
401 FORMAT(//,1X,'UNNORMALIZED TABULATED MASS SPECTRUM',/)
 TYPE 402
       WRITE (6,402)
402 FORMAT(//,1X,'MASS(AMU)',5X,'ION CURRENT(AMPS)',/)
 DO 410 I=IFMAS,ILMAS
410 TYPE 403,I,SIGBUF(I)
       WRITE (6,403)I,SIGBUF(I)
403 FORMAT(4X,I3,12X,E10.3)
 IF(IFORM-3) 800,500,800
C 500=GO TO NORMALIZED TABULATED
C 800=GO OUT OF DISPLAY ROUTINES
C
C DATA OUTPUT--NORMALIZED TABULATED
500 TYPE 501
       WRITE (6,501)
501 FORMAT(//,1X,'NORMALIZED TABULATED MASS SPECTRUM',/)
 TYPE 502
       WRITE (6,502)
502 FORMAT(//,1X,'MASS(AMU)',5X,'RELATIVE INTENSITY(PERCENT)',/)
C
C DETERMINE SIGNAL MAXIMUM
 SIGMAX=0.0
 DO 510 I=IFMAS,ILMAS
 IF(ABS(SIGBUF(I))-ABS(SIGMAX)) 510,520,520
520 SIGMAX=SIGBUF(I)
510 CONTINUE
C
C NORMALIZE DATA
 DO 530 I=IFMAS,ILMAS
 SIGION=(SIGBUF(I)*100.0)/SIGMAX
530 TYPE 535,I,SIGION
       WRITE (6,535)I,SIGION
535 FORMAT(4X,I3,14X,F6.2)
 IF(IFORM-3) 800,700,800
C 700=GO TO NORMALIZED BAR GRAPH
C 800=GO OUT OF DISPLAY ROUTINES
```

```
C
C DATA OUTPUT--NORMALIZED BAR GRAPH
700 TYPE 701
        WRITE (6,701)
701 FORMAT(//,1X,'NORMALIZED BAR GRAPH MASS SPECTRUM',/)
 TYPE702
        WRITE (6,702)
702 FORMAT(/,3X,'0%',46X,'50%',46X,'100%',/)
C DETERMINE MAXIMUM SIGNAL
 SIGMAX=0.0
 DO 710 I=IFMAS,ILMAS
 IF(ABS(SIGBUF(I))-ABS(SIGMAX)) 710,720,720
720 SIGMAX=SIGBUF(I)
710 CONTINUE
C NORMALIZE DATA AND CALCULATE POINTS FOR GRAPH
 DO 730 I=IFMAS,ILMAS
 IPNT=INT(((SIGBUF(I)*100.0)/SIGMAX)+0.5)
 TYPE 740,I
        WRITE (6,740)I
740 FORMAT(1X,I3,$)
 IF(IPNT-1) 795,790,790
790 CONTINUE
 DO 750 J=1,IPNT
750 TYPE 760
        WRITE (6,760)
760 FORMAT(1X,'X',$)
795 TYPE 770
        WRITE (6,770)
770 FORMAT(1X)
730 CONTINUE
 TYPE 780
        WRITE (6,780)
780 FORMAT(///)
C
C QUERY FOR MORE SCANS
800 CONTINUE
 TYPE 801
        WRITE (6,801)
801 FORMAT(1X,'FOR ANOTHER SCAN WITH:--')
 TYPE 802
        WRITE (6,802)
802 FORMAT(1X,'THE SAME SCAN PARAMETERS - TYPE 1')
 TYPE 803
        WRITE (6,803)
803 FORMAT(1X,'DIFFERENT SCAN PARAMETERS - TYPE 2')
 TYPE 804
        WRITE (6,804)
804 FORMAT(1X,'FOR NO MORE SCANS - TYPE 0')
 ACCEPT 200,IAGAN
 IF(IAGAN-1) 900,910,920
900 CONTINUE
        CALL EXIT
 END
```

Recommendations and Conclusions

Efforts to assembly a computer-mass spectrometer system, capable of investigating the atmospheric thermal decompositions of non-metallic materials has been successful. The resolution of certain software problems has enhanced the system further, making the rapid acquisition, processing and analyses of mass spectral data possible.

It is proposed that a solid sample inlet system such as the DIS 100 (Figure 5) be coupled to the the mass spectrometer. This would expand the capability of the system, allowing investigations of solid and low vapor liquids under high vacuum conditions.

REFERENCES

1. Thompson, J.M., Laboratory Automation of a Quadrupole Mass Spectrometer, Faculty Fellowship Program, NASA Contractor Report No. 170342, December 1983.

2. Balzer Data Sheet, A 41-0948e, 2nd Edition, May, 1983.

3. Giovanoli, R. and H.G. Wiedemann, Helvetia Chemica Acta, vol. 51, p. 1134-1143.

4. Aspinal, M.L., Thermal Analyses, vol. 1, Proceedings of the 3rd International Congress on Thermal Analyses (ICTA), Davos, 1971.

5. Dunner, W. and H. Eppler, Advanced Coupling Systems for Thermoanalyzers With Quadrupole Mass Spectrometers, The 4th International Congress on Thermal Analyses (ICTA), Budapest, July, 1974.

6. Balzer Data Sheet, BK 800 095 BE, 1st Edition, May, 1982.

1984

NASA/ASEE SUMMER FACULTY RESEARCH FELLOWSHIP PROGRAM

MARSHALL SPACE FLIGHT CENTER
THE UNIVERSITY OF ALABAMA

SOLID ROCKET MOTOR CASE (SRMC) DYNAMIC SENSITIVITY TO CHANGES IN COMPOSITE PROPERTIES

Prepared By:	R. Noel Tolbert, Ph.D., P.E.
Academic Rank:	Associate Professor
University and Department:	Tennessee Technological University Civil Engineering Department
NASA/MSFC Division: Branch:	 Structural Dynamics Systems Analysis
MSFC Counterparts:	Robert S. Ryan Tulon Bullock
Date:	August 10, 1984
Contract No.:	NASA-NGT-01-002-099 The University of Alabama

ACKNOWLEDGEMENTS

There were several NASA employees that contributed to the work in this report and to the author's NASA/ASEE summer program. A few are singled out for their especially valuable contributions. Dr. John Admire, Mr. Edward Ivey, Mr. Rocky Stephens, Mr. Frank Bugg, and Mr. Larry Kiefling provided assistance for using the NASA computers and associated terminals. I am especially grateful to Mr. Bugg for providing an orientation to NASTRAN and to Mr. Kiefling for a similar orientation to SPAR. Ms. Carol Lee cordially and competently typed the report. Mr. Tulon Bullock and Mr. Robert Ryan provided excellent program support and project leadership. The author extends his appreciation to all of these.

SRMC DYNAMIC SENSITIVITY TO CHANGES IN COMPOSITE PROPERTIES

by

R. Noel Tolbert
Associate Professor of Civil Engineering
Tennessee Technological University
Cookeville, Tennessee

ABSTRACT

Traditional composite lamination theory was used to compute the constitutive matrices using a potential range of lamina properties. Sensitivity of vibrational frequencies was examined for variations in constituent materials and geometric properties. The material component interactions examined were the lamina longitudinal and transverse Young's modulus, the lamina Poisson's ratio, and the shear modulus. Fiber and resin properties were related to the frequency response through lamina properties. Geometric properties examined were void ratio and helical wind angle. In addition, capabilities and applications of the SPAR and NASTRAN computer codes were examined for laminated cylindrical shells.

INTRODUCTION

Experimental testing of scaled test articles are often used to predict behavior for full-scale structures for obvious reasons of economy, speed, and availability of adequate test facilities. The need for mathematical models to accurately predict structural behavior is an integral part of such a test program. NASA is currently conducting such a program for epoxy-graphite, filament wound, solid rocket motor cases (SRMC). A lack of agreement when comparing experimental test results to values calculated from computer analysis indicated the need for a thorough examination of contractor provided stiffness properties and analytical modeling verification. A previous study by the author[1] provided applicable micromechanical equations for graphite-epoxy composites as well as lamination theory and computer codes for computing filament wound, cylinder properties. Also, a sensitivity study was conducted of both the micromechanical and macromechanical properties as related to the SRMC extensional and bending stiffness properties. In this study, the analytical models used for computing static and dynamic behavior were reviewed, and sensitivities of micromechanical and macromechanical properties were related to dynamic responses.

OBJECTIVES

The objectives of this study were as follows: (1) To review the analytical models used for static and dynamic response of laminated cylindrical shells and (2) to determine the sensitivity of micromechanical and macromechanical properties to dynamic responses.

ANALYTICAL MODELS

Marshall Space Flight Center (MSFC) has conducted four in-house, static and dynamic tests of cylindrical, filament wound, case segments. A COSMIC version of the NASTRAN computer code[2] was used to analytically model the test articles. Material properties for the filament wound test articles were provided by Hercules, a NASA subcontractor. Errors made in computing and providing these data as well as inconsistencies in physical measurements of weight and geometry frustrated analytical modeling efforts by MSFC. In an effort

to resolve differences in the analytical model and test results, extensive efforts have been made to improve the accuracy and consistency of material properties. It was also important to verify the analytical modeling procedure to ascertain the solution quality. In this regard, the NASTRAN code was examined for applicability of element type, convergence of solution with element size, influence of aspect ratio, and the effect of changes in model parameters. Test article data provided by Hercules for DV 36-26(3) were used in all analyses reported in this study.

First, the element type used for the cylindrical models was examined. The NASTRAN quadrilateral plate and membrane element, CQUAD2, had been selected as the appropriate finite element. This element provided capability for both extensional and bending stiffness. Material property matrices, [A] and [D] normalized for thickness, were required as input data. Coupling between extensional and bending action was not permitted and thus the [B] matrix was not required. The [A], [B], and [D] matrices are computed using lamination theory and are described in composite texts(4, 5), as well as by this author(1). This coupling effect was later examined using the SPAR(6) code.

Now, focusing on the CQUAD2 element, the NASTRAN Theory Manual(7) indicated the element should not be used on sharply curved surfaces but rather recommended that the triangular element, CTRIA2, be used. The manual did not define a sharply curved surface. Thus, the triangular element was used to analyze the same cylinder, DV 36-26, using the same 312 joints, same boundary conditions, and loads. The results showed almost identical results for both finite elements. The CTRIA2 element gave static deflections only 0.05 percent higher than the CQUAD2 element. Similarly, the difference in dynamic results was also very small. When comparing the cyclic frequencies, using modal shapes 2, 2a, 3, and 3a as reported by Bugg(8) and shown in Figure 1, the largest difference was 0.37 percent in mode 3a. The different direction of the various frequencies was not consistent, and when comparing differences in summations of all four modes, only 0.06 percent existed. From this, it was concluded that the CQUAD2 element would provide essentially equivalent results as the CTRIA2 element. Thus, the restrictions on CQUAD2, as pertaining to sharply curved surfaces, was not applicable in this case as long as other precautions were exercised.

Next, to continue the examination of the NASTRAN code and its CQUAD2 element, the same model, DV 36-26, with the same 288 element grid was analyzed using SPAR with a similar quadrilateral element, E43. The coupled option for element E43 was used which permits the input of the [A], [B], and [D] laminate matrices. Uncoupled comparisons can be made by setting all values in [B] matrix equal to zero. This zero [B] matrix corresponds to a laminate that is symmetrical with respect to its plate middle surface. Since coupling between bending and axial deformation does not occur for this type of laminate, this capability would not be required. However, all test articles were to some degree unsymmetrically wound due to a thin initial cloth winding. Later test articles, such as DV 36-26, had unsymmetrical winding patterns. Thus, the NASTRAN element was deficient in this regard. Since the SPAR element E43 could accommodate coupling, it was used for both coupled and uncoupled solutions to determine the coupling significance.

When comparing the NASTRAN DV 36-26 solution to its equivalent uncoupled SPAR solution, the SPAR static results yielded deflections that were slightly unsymmetrical, while the NASTRAN results were symmetrical. This SPAR deflection was 0.46 percent lower than the NASTRAN solution. Since the lack of SPAR symmetry of solution indicated a small round off error, the SPAR problem was rerun using double precision. The round off problem was corrected with resulting symmetrical deflections. However, the SPAR deflection values were now 1.84 percent larger than the NASTRAN values. The SPAR double precision dynamic frequencies were progressively lower for each mode examined (2, 2a, 3, 3a) and averaged a reduction of 1.38 percent. The static and dynamic comparisons were consistent, in that both indicated a more flexible stiffness when using the SPAR E43 element with double precision.

Next, the coupling effect was examined using the SPAR shell element E43. For test article DV 36-26, inclusion of the coupling matrix increased deflections 0.81 percent and decreased vibrational frequencies by an average of 0.48 percent. Again, the increase in deflections and decrease in vibrational frequencies indicated increased flexibility. It should be noted that DV 36-26 was very nearly a symmetrical laminate and a large coupling effect was not expected. However, both Whitney[9] and Jones[10] reports that coupling can result in significantly decreased vibrational frequencies.

Solution convergence based on grid size was next examined using the same SPAR finite element on cylinder DV 36-26. Solutions for 32, 128, and 288 elements indicated that a 288 element grid should be used. When comparing the 32 element grid to the 128 element grid, a static deflection difference of 4.56 percent resulted along with an average dynamic frequency difference of 5.07 percent. Comparing the 128 element grid to the 288 element grid, the static centerline deflections were equal to the three significant digits provided by the output, while the average frequency change was 0.61 percent. The frequency changes were not consistent, in that of the four examined, two increased and two decreased. A smaller number of elements could possibly be used by increasing the size of the element dimensions along the cylinder length. An increase in the aspect ratio (longest element dimension divided by shortest element dimension) from approximately 1 to 1.5 in the SPAR yielded an increase of 1.0 percent in the static deflection and a 0.07 percent increase in the average dynamic frequencies.

Another item to note was the variation in the SPAR computed weight that occurred with variations in the circumferential griding. This resulted from using a series of flat plates to approximate the cylindrical surface.

The accuracy of the cylinder's weight improved with additional circumferential divisions. The eight divisions of the 48 element solution resulted in a 2.27 percent lower weight than the 24 division, 288 element solution. If a constant mass is desirable regardless of grid size, the SPAR input value of weight per surface area can be modified to offset the modeling error. This may be of particular interest in dynamic analysis.

SENSITIVITY ANALYSIS

The sensitivity results reported in this study were based on the epoxy-graphite laminated cylinder, DV 36-26, as described by Hercules[3]. The cylinder winding and layer geometry conforms to the sample output of a modified version of COMP[1] as given along with its FORTRAN code in Appendix I. The sensitivities of its laminate properties were examined using the computer code LAM developed by Tolbert[1] with the results shown in Table 1.

A small percentage change of the fiber longtitudinal modulus had a large carryover effect to the laminate. A change in this property resulted in a carryover effect of 84 percent for the laminate Ex, 81 percent for Ey, 91 percent for Gxy and 13 percent for μxy. The effects of other fiber and resin parameters were very small and are shown as ratios to the fiber's longitudinal stiffness to show its dominance. The larger the tabular value, the less its significance. The only other variable of even modest significance was the resin Young's modulus. Since the resin is isotropic, the effect on the laminate is compounded by a corresponding increase in the resin shear modulus.

Next, the effect on dynamic cyclic frequencies was examined for variations in lamina properties. Frequency variations for changes in E_1, the lamina longitudinal modulus; E_2, the lamina transverse modulus; G_{12}, the lamina principal shear modulus; and μ_{12}, the principal Poisson's ratio were analyzed for modal shapes as described by Bugg[8] and numbered 2, 2a, 3, and 3b. The starting or baseline lamina values were taken from Hercules generated data. These lamina and corresponding laminate values are duplicated in the output of COMP as listed in Appendix I. The percentage change in the dynamic frequency for a 10 percent change in each lamina variable is given in Table 2. When comparing values in Table 2, E_1 appears to be the dominant property with the other lamina variables of much less importance. However, it is probable that a much larger error may exist in these other lamina variables. Data exist that indicates E_2 may be much larger than the 0.3×10^6 psi, Hercules value. In fact, a value near 0.9×10^6 psi, a 300 percent increase, appears to be more logical. Thus, when examined in this light as shown in Table 3, only the lamina Poisson's ratio is of minor importance. The ± values shown in Table 3 are the average changes for the positive and negative increments.

Also, examined was the effect of the helical winding angle on dynamic frequency. A 10 percent increase in the wind angle increased the average dynamic cyclic frequency 4.29 percent, while a 10 percent decrease resulted in an average frequency reduction of 2.01 percent. Small manufacturing tolerances in the winding angle of less than 0.5 degrees would thus have negligible effects on the dynamic frequencies.

Another variable examined was the void ratio. If a layer (lamina) of hoop or helical winding uses a specific weight of fiber and resin, voids can be determined from physical measurements of the cylinder. Voids dispersed in the laminate will create an increase in its thickness. As an example, the theoretical thickness of DV 36-26 based on the laminate being void free was 0.3164 inches. However, measurements of the fabricated test article as recorded by Hercules indicated the thickness to be 0.331 inches. This

difference in thicknesses could be accounted for by computing a void ratio of 4.61 percent. This percentage was similar to other void ratio percentages reported by Hercules in previous tests. The effect on the lamina stiffness values would be to reduce them by the product of the reciprocal of "one plus the void ratio." The layer thicknesses would be increased by the product inverse of the previous relationship. The net effect will be a modest increase in bending stiffness as represented by the [D] matrix, and no change in axial stiffness as represented by the [A] matrix. The computer code COMP was used to calculate these matrix values for use in the NASTRAN finite element model. As indicated, the [A] matrix was unchanged and the [D] matrix was modestly increased. The NASTRAN analysis of DV 36-26 with void ratios of 2, 4, and 6 percent yielded increases in frequencies for the modal shapes shown in Figure 1 of 1.99, 4.03, and 5.95 percent, respectively. For this test article, the frequency percentage increases were almost equal to the void ratio percentages. An important item to note when gathering data for analytical modeling is that both a change in layer stiffness and layer thickness must be accommodated to account for voids. If not careful, only the thickness may be included in the analytical model. In addition, changes in void ratios and physical dimensions require corrections to model density. The NASTRAN code was used to test the effect of an error in density on the dynamic frequencies. A density increase of 10 percent in DV 36-26 reduced vibrational frequencies 4.65 percent.

CONCLUSIONS AND RECOMMENDATIONS

The NASTRAN code is suitable for modeling epoxy-graphite laminated models that are balanced and symmetric. For unsymmetric laminates, increased flexibility results from coupling between bending and axial deformation. If coupling is neglected, static deflections are under predicted and dynamic frequencies are over predicted. For test article DV 36-26, disregarding coupling resulted in an error of less than one percent for both static deflection and vibrational frequencies. The NASTRAN quadrilateral element, CQUAD2, was compared to the triangular element, CTRIA2, and found to yield almost identical results for both static and dynamic behavior. In addition, both NASTRAN elements yielded similar results when compared to the SPAR quadrilateral element, E43.

The SPAR element, E43, is more suitable for laminated composites and provides several options for material property characterization. While the element permits a laminate, layer by layer data input, the computer code COMP can be used to develop the laminate properties, and then the coupled option can be used for the material property description. However, the SPAR code needs modifications to provide output of laminate properties for an intermediate solution check. A weakness of SPAR is its tendency to produce results with unacceptable round off error. This was particularly true for the solutions encountered in this study that had approximately 1800 degrees of freedom (kinematic unknowns). This problem was corrected by using the double precision

option on selected processors. Users of SPAR should be particularly careful by providing some type of solution verification for SPAR solutions that do not use double precision. For the DV 36-26 test article using identical finite element grids and uncoupled material properties, the SPAR as compared to NASTRAN deflections were 1.84 percent larger and the vibrational frequencies were 1.38 percent lower. This indicates that the SPAR model was more flexible than the NASTRAN model. Also, SPAR executed more rapidly and the required data input was easier to execute. However, the NASTRAN User's Manuals were better written and easier to follow than SPAR's.

Other modeling items of concern, irrespective of the particular computer code, includes the finite element size and shape (aspect ratio). Convergence should be checked by varying the grid size, preferable by subdividing previous grids. Also, the aspect ratio should be maintained near unity. For dynamic analysis, care should be exercised in matching the appropriate density to the other geometric data input.

In reviewing the micromechanical sensitivity results, attention is focused on the dominance of longitudinal fiber properties in lamina stiffness description. Nevertheless, improvements are needed in micromechanical models to better predict lamina stiffness values. In this regard, data on the transverse properties of the AS4W-12K Hercules graphite fibers are needed. While extensive test attention has been provided for the fiber's longitudinal Young's modulus, data are needed for the corresponding transverse modulus to verify and improve micromechanical models. For instance, the relationship, if any, between the fiber's shear modulus and the fiber's transverse Young's modulus is not understood.

An examination of lamina sensitivities on vibrational frequencies indicated two items of particular importance. One item was the direct effect of a lamina stiffness variation on vibrations and the other was the range of potential error in the computed lamina property. While the lamina sensitivity E_1 was the dominant sensitivity, its expected range of potential error was smallest. On the other hand, E_2 had a low sensitivity but had the highest potential error based on using the Hercules initial value of E_2.

Now turning specifically to means of matching analytical results with experimental results, large reductions in lamina stiffness E_1 values would be required to substantially reduce predicted vibrational frequencies. Correcting E_2 to a more logical value would increase the predicted frequencies. Using E_1 to achieve a 10 percent frequency reduction requires an E_1 reduction of 26 percent. Rather than varying lamina values to match data, improvements in modeling may help to account for some discrepancies. The dynamic SPAR solution was 1.38 percent lower than the NASTRAN solution. Coupling reduced frequencies an additional 0.48 percent. In addition, correcting input densities may further reduce frequencies. In conclusion, it is essential that accurate manufacturing information be available for accurate analytical modeling to succeed.

TABLE 1

SENSITIVITY RATIOS IN LAMINATE PROPERTIES OF DV 36-26

Ratio of ΔE_{f_L} to	Laminate			
	E_x	E_y	G_{xy}	μ_{xy}
$\Delta \mu_f$	586	1768	119	7
ΔE_{f_T}	60	31	70	7
ΔG_f	44	38	31	5
$\Delta \mu_m$	31	29	43	2
ΔE_m	7	6	15	1
ΔE_{f_L}	1	1	1	1

TABLE 2

PERCENTAGE CHANGE IN DYNAMIC CYCLIC FREQUENCY RESULTING FROM A 10 PERCENT INCREASE IN THE LAMINA VARIABLE DV 36-26

Mode Shape Number	Lamina Variables			
	E_1	G_{12}	E_2	12
2	+3.71	+0.392	+0.122	+0.033
2a	+3.98	+0.352	+0.086	+0.009
3	+3.71	+0.388	+0.121	+0.033
3a	+3.86	+0.372	+0.099	+0.019

TABLE 3

PERCENTAGE CHANGE IN DYNAMIC CYCLIC FREQUENCY
RESULTING FROM A POTENTIAL CHANGE IN THE
LAMINA VARIABLE OF DV 36-26

Mode Shape Number	Lamina Variables and Potential Change			
	±10% E_1	±50% G_{12}	+300% E_2	±50% ν_{12}
2	±3.78	±1.96	+3.61	±0.167
2a	±4.06	±1.76	+2.54	±0.045
3	±3.78	±1.94	+3.59	±0.166
3a	±3.93	±1.87	+2.95	±0.094

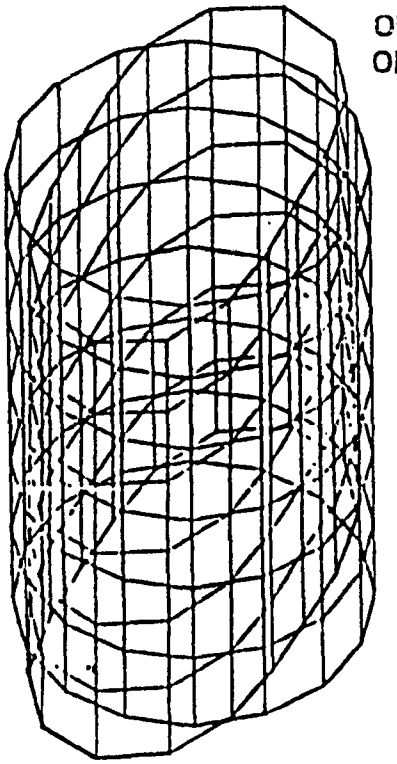

n = 2

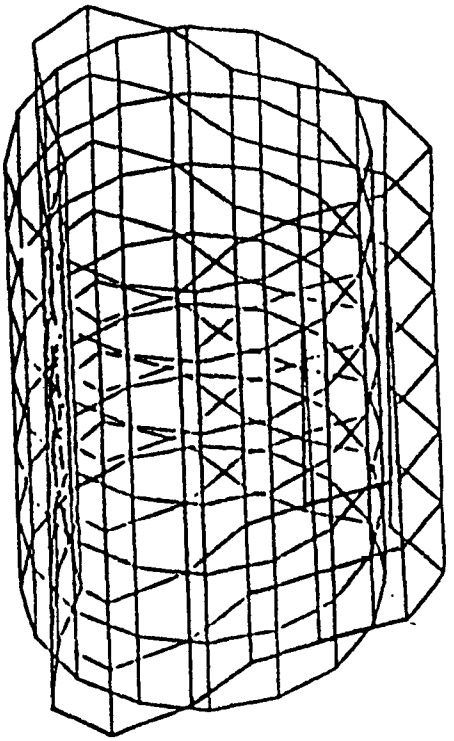

n = 3

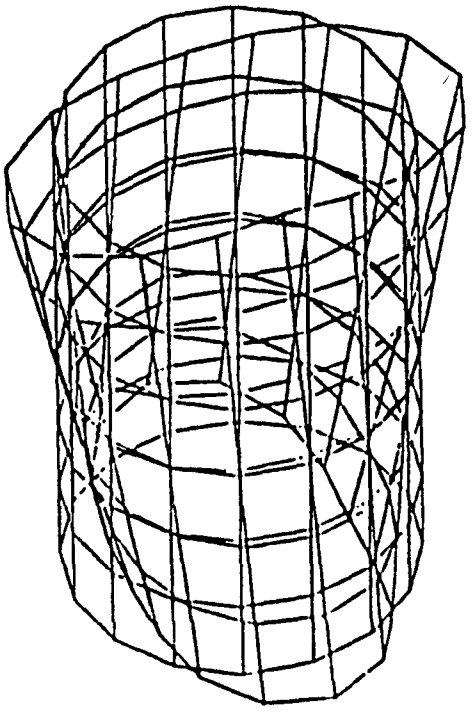

n = 2 a

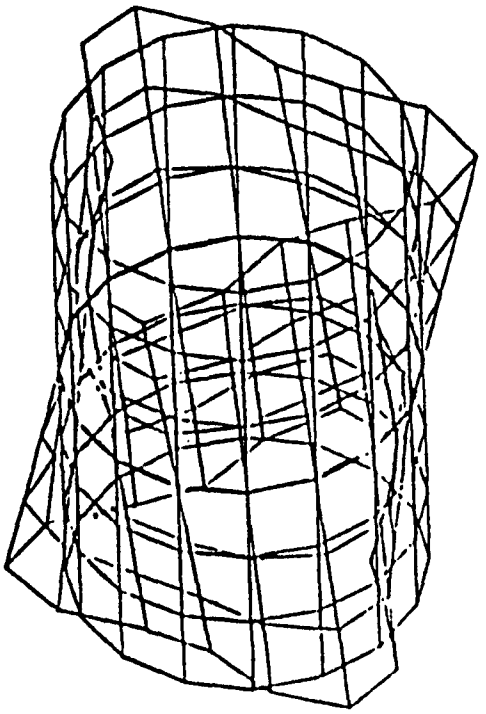

n = 3 a

Figure 1. NASTRAN Modes for DV 36-26

REFERENCES

1. Tolbert, Robert N: Stiffness Properties for Dynamic Modeling of Composite Graphite-Epoxy Cylindrical Orthotropic Shells. NASA-NTG-01-008-021, August 1983.

2. The NASTRAN User's Manual, NASA SP-222(06), September 1983.

3. Hercules, Inc., Bacchus Works: Data Package (DV-36-26 STA Junior) for NASA, Report. Magna, Utah, December 8, 1983.

4. Jones, Robert M.: Mechanics of Composite Materials. Scripta Book Company, Washington, D.C. 1975.

5. Agarwal, Bhagwan D. and Broutman, Lawrence J.: Analysis and Performance of Fiber Composites. Wiley and Sons, New York, NY, 1980.

6. SPAR Structural Analysis System Reference Manual, Vol. 1, NASA CR 158970-1, December 1978.

7. The NASTRAN Theoretical Manual, NASA SP-221(06), January 1981.

8. Bugg, Frank M.: MSFC In-house FWC Tests, Report. Huntsville, AL, April 1984.

9. Whitney, J. M. and Lessa, A. W.: Analysis of Heterogeneous Anisotropic Plates. ASME Transactions, Journal of Applied Mechanics, June 1969, pp. 261-266.

10. Jones, Robert M. and Morgan, Harold S.: Buckling and Vibration of Cross-Ply Laminated Circular Cylindrical Shells. AIAA Journal, May 1975, pp. 664-671.

APPENDIX A

"COMP"

```
 1:@FREE PF.
 2:@DELETE,C PF.
 3:@ASG,UP PF.,F/1/POS/5
 4:@FREE PF.
 5:@EXTEND PF.8
 6:@ASG,A PF.
 7:@BRKPT PRINT8/PF
 8:@USE F,SYS$IMSFCFOR8
 9:@F.FOR,IS MAIN,MAIN
10:C ************************** INPUT OF DATA **************************
11:C THIS PROGRAM CAN ACCEPT 25 LAMINA TYPES AND 100 LAYERS.  A CHANGE
12:C IN THE DIMENSION STATEMENTS WOULD PERMIT LARGER LAMINATES.
13:C 1ST LINE....PROVIDE A TITLE FOR PROGRAM
14:C 2ND LINE....ALLOWS FOR A SUBTITLE--LEAVE BLANK LINE IF NOT USED
15:C 3RD LINE....TYPE IN DATE: MONTH-DAY-YEAR
16:C NEXT.........NUMBER OF LAMINA LAYER TYPES?
17:C NEXT.........EXPRESS THE VOID RATIO AS A DECIMAL. (5% VOIDS = .05)
18:C NEXT.........ONE LINE OF DATA FOR EACH TYPE OF LAMINA.  GIVE E1,
19:C              E2,G12, AND U12, RESPECTIVELY.
20:C NEXT.........NUMBER OF LAYERS?
21:C THEN.........ONE LINE OF DATA FOR EACH LAYER GIVING THE THICKNESS,
22:C              WINDING ANGLE, AND LAMINA TYPE.  THE LAMINA TYPE FOR
23:C              EACH LAYER MUST MATCH THE PREVIOUS DATA.
24:C ***********************************************************************
25:C
26:       DIMENSION TK(100),AN(100),Q11B(100),Q12B(100),Q16B(100),Q22B(100)
27:       DIMENSION Q66B(100),Z(101),Q26B(100),T(9,3),TD(9,3)
28:       DIMENSION IE(100),EL(25),ET(25),GLT(25),ULT(25)
29:       READ(5,85)T1,T2,T3,T4,T5,T6,T7,T8,T9
30:       READ(5,85)S1,S2,S3,S4,S5,S6,S7,S8,S9
31:       READ(5,85)D1,D2,D3
32: 85    FORMAT(9A6)
33:       WRITE(6,86)T1,T2,T3,T4,T5,T6,T7,T8,T9
34:       WRITE(6,87)S1,S2,S3,S4,S5,S6,S7,S8,S9
35:       WRITE(6,84)D1,D2,D3
36: 84    FORMAT(10X,'DATE= ',3A6)
37: 86    FORMAT(/10X,'TITLE= ',9A6)
38: 87    FORMAT(10X,'SUBTITLE= ',9A6)
39:       READ(5,52)NLT
40:       READ(5,52)VR
41:       VR=VR+1.
42: 52    FORMAT()
43:       DO 5 I=1,NLT
44:       READ(5,52)EL(I),ET(I),GLT(I),ULT(I)
45:       EL(I)=EL(I)/VR
46:       ET(I)=ET(I)/VR
47: 5     GLT(I)=GLT(I)/VR
48:       READ(5,52)NL
49:       DO 4 I=1,NL
50:       READ(5,52)TK(I),AN(I),IE(I)
51: 4     TK(I)=TK(I)*VR
52: 30    DO 17 I=1,NL
53:       J=IE(I)
54:       AM=1/(EL(J)-ET(J)*ULT(J)**2)
55:       Q11=AM*EL(J)**2
56:       Q22=AM*EL(J)*ET(J)
57:       Q12=ULT(J)*Q22
```

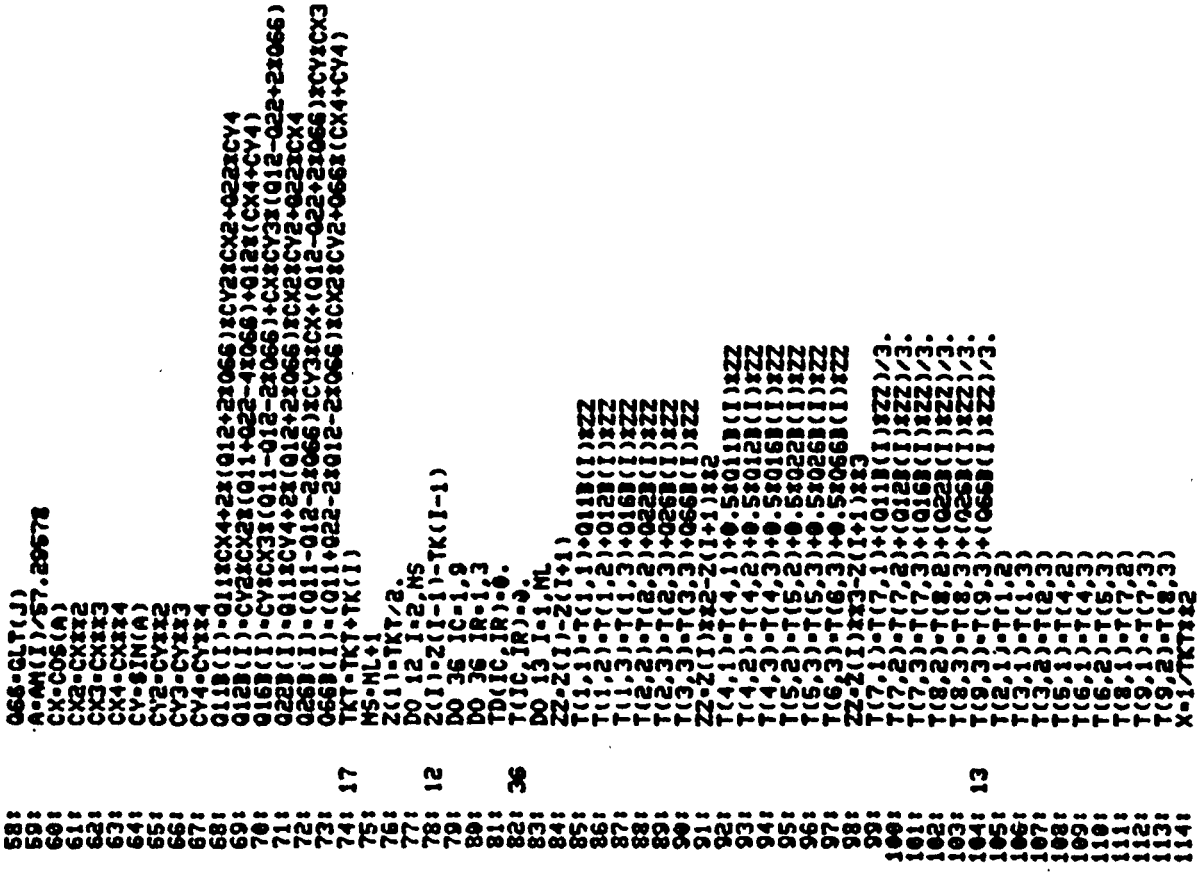

```
      XX=12/TKT**3
      DO 38 IR=1,3
      DO 38 IC=1,3
38    TD(IR,IC)=T(IR,IC)/TKT
      DO 39 IR=4,6
      DO 39 IC=1,3
39    TD(IR,IC)=T(IR,IC)*XX
      DO 40 IR=7,9
      DO 40 IC=1,3
40    TD(IR,IC)=T(IR,IC)*XXX
      WRITE(6,51)
51    FORMAT(//' ***** DATA FOR EACH LAYER *****')
      WRITE(6,72)
      WRITE(6,73)
72    FORMAT(/' LAYER     THICKNESS     ANGLE OF PLY      LAYER')
73    FORMAT(' COUNT     (INCHES)       (DEGREES)        TYPE')
      DO 9 I=1,NL
9     WRITE(6,74)I,TK(I),AN(I),IE(I)
      WRITE(6,86)T1,T2,T3,T4,T5,T6,T7,T8,T9
      WRITE(6,87)S1,S2,S3,S4,S5,S6,S7,S8,S9
      WRITE(6,84)D1,D2,D3
      WRITE(6,70)NL,TKT
      VRR=(VR-1.)*100
      WRITE(6,288)VRR
288   FORMAT(29X,'VOID RATIO=',F5.2,'%')
70    FORMAT(/' ** NUMBER OF LAYERS=',I3,5X,'LAMINATE THICKNESS='
     1,F6.4,' IN. **')
74    FORMAT(I4,F13.4,F15.2,I10)
      WRITE(6,67)
67    FORMAT(/' ** LAMINA PROPERTIES FOR LAYER TYPES **')
      WRITE(6,68)
68    FORMAT(5X,'TYPE',8X,'E1',10X,'E2',10X,'G12',9X,'U12'/)
      DO 8 I=1,NLT
8     WRITE(6,50)I,EL(I),ET(I),GLT(I),ULT(I)
50    FORMAT(I8,4X,4F12.4)
37    WRITE(6,75)
75    FORMAT(//' THE MODULUS AND MATRIX VALUES ARE TO BE MULTIPLIED')
      WRITE(6,76)
76    FORMAT('      BY 10 TO THE SIXTH, STIFFNESS UNITS ARE PSI.'/)
      WRITE(6,89)
      DO 41 IR=1,9
      WRITE(6,77)T(IR,1),T(IR,2),T(IR,3),TD(IR,1),TD(IR,2),TD(IR,3)
      IF (IR .EQ. 3) WRITE (6,78)
41    IF(IR .EQ. 6) WRITE(6,79)
      EX=TD(1,1)-TD(1,2)**2/TD(2,2)
      EY=TD(2,2)-TD(1,2)**2/TD(1,1)
      UNXY=TD(1,2)/TD(2,2)
      EXF=TD(7,1)-TD(7,2)**2/TD(8,2)
      EYF=TD(8,2)-TD(7,2)**2/TD(7,1)
      WRITE(6,93)
      WRITE(6,94)
      WRITE(6,95)
93    FORMAT(//1X,'LAMINATE STIFFNESS PROPERTIES')
94    FORMAT(' AVERAGE AXIAL',40X,'FLEXURAL')
95    FORMAT(5X,'EX',11X,'EY',11X,'GXY',10X,'NUXY',9X,'EX',11X,'EY')
      WRITE(6,96)EX,EY,TD(3,3),UNXY,EXF,EYF
      WRITE(6,86)T1,T2,T3,T4,T5,T6,T7,T8,T9
```

```
      WRITE(6,87)S1,S2,S3,S4,S5,S6,S7,S8,S9
      WRITE(6,84)D1,D2,D3
96    FORMAT(6F13.6//)
80    FORMAT(//' THE A MATRIX',89X,'THE A DIVIDED BY TK MATRIX'//)
77    FORMAT(3F12.6,8X,3F12.6)
78    FORMAT(//' THE B MATRIX',29X,'THE B/(TK**8) MATRIX'//)
79    FORMAT(//' THE D MATRIX',29X,'THE 12*D/(TK**3) MATRIX'//)
      END
@MAP,IS SYM,ABS
LIB F.
@XQT ABS
DV 36-26,USING HERCULES DEC. 8, 1983 PROPERTIES
FROM DATA PACKAGE -STA JUNIOR-
JULY 26, 1984
3
0.
19.55,.30,.67,.267
18.75,.30,.67,.267
6.63,2.01,.76,.285
19
.0105,0,3
.0105,90,3
.0170,33.55,2
.0170,-33.55,2
.0132,90,1
.0170,33.55,2
.0170,-33.55,2
.0132,90,1
.0170,33.55,2
.0170,-33.55,2
.0132,90,1
.0297,33.55,2
.0297,-33.55,2
.0132,90,1
.0170,33.55,2
.0170,-33.56,2
```

SAMPLE SOLUTION LISTING FOR DV 36-26

```
267:
268:          TITLE- DU 36-26,USING HERCULES DEC. 8, 1983 PROPERTIES
269:          SUBTITLE- FROM DATA PACKAGE -STA JUNIOR-
270:          DATE- JULY 26, 1984
271:
272:
273: ****** DATA FOR EACH LAYER ******
274:
275: LAYER     THICKNESS     ANGLE OF PLY      LAYER
276: COUNT     (INCHES)       (DEGREES)        TYPE
277:    1         .0105             .00          3
278:    2         .0105           90.00          3
279:    3         .0170           33.55          2
280:    4         .0170          -33.55          2
281:    5         .0132           90.00          1
282:    6         .0170           33.55          2
283:    7         .0170          -33.55          2
284:    8         .0132           90.00          1
285:    9         .0170           33.55          2
286:   10         .0170          -33.55          2
287:   11         .0132           90.00          1
288:   12         .0170           33.55          2
289:   13         .0170          -33.55          2
290:   14         .0132           90.00          1
291:   15         .0297           33.55          2
292:   16         .0297          -33.55          2
293:   17         .0132           90.00          1
294:   18         .0170           33.55          2
295:   19         .0170          -33.55          2
296:
297:          TITLE- DU 36-26,USING HERCULES DEC. 8, 1983 PROPERTIES
298:          SUBTITLE- FROM DATA PACKAGE -STA JUNIOR-
299:          DATE- JULY 26, 1984
300:
301: ** NUMBER OF LAYERS- 19      LAMINATE THICKNESS- .3164 IN. **
302:                              VOID RATIO-  .00%
303:
304: ** LAMINA PROPERTIES FOR LAYER TYPES **
305:      TYPE          E1             E2             G12          U12
306:
307:         1        19.5500          .3000          .6700        .2670
308:         2        18.7500          .3000          .6700        .2670
309:         3         6.6300         2.0100          .7600        .2850
310:
311:
312: THE MODULUS AND MATRIX VALUES ARE TO BE MULTIPLIED
313:      BY 10 TO THE SIXTH, STIFFNESS UNITS ARE PSI.
314:
```

```
297:          TITLE- DU 36-26,USING HERCULES DEC. 8, 1983 PROPERTIES
298:          SUBTITLE- FROM DATA PACKAGE -STA JUNIOR-
299:          DATE- JULY 26, 1984
300:
301: ** NUMBER OF LAYERS- 19      LAMINATE THICKNESS- .3164 IN. **
302:                              VOID RATIO-  .00%
303:
304: ** LAMINA PROPERTIES FOR LAYER TYPES **
305:     TYPE          E1            E2            G12          U12
306:
307:       1         19.5500         .3000         .6700        .2670
308:       2         18.7500         .3000         .6700        .2670
309:       3          6.6300        2.0100         .7600        .2850
310:
311:
312: THE MODULUS AND MATRIX VALUES ARE TO BE MULTIPLIED
313:     BY 10 TO THE SIXTH, STIFFNESS UNITS ARE PSI.
314:
315:
316: THE A MATRIX                                THE A DIVIDED BY TK MATRIX
317:
318:    2.334853      .825941      .000000          7.379434     2.610433     .000000
319:     .825941     1.957924      .000000          2.610433     6.188129     .000000
320:     .000000      .000000     1.003797           .000000      .000000    3.172558
321:
322:
323: THE B MATRIX                                THE B/(TK**2) MATRIX
324:
325:    -.014261     -.008453      .013284          -.142455     -.084438     .132694
326:    -.008453      .002481      .006514          -.084438      .024784     .065070
327:     .013284      .006514     -.009747           .132694      .065070    -.097362
328:
329:
330: THE D MATRIX                                THE 12*D/(TK**3) MATRIX
331:
332:     .019799      .006694     -.000633          7.501108     2.536054    -.239683
333:     .006694      .013647     -.000310          2.536054     5.170410    -.117535
334:    -.000633     -.000310      .008059          -.239683     -.117535    3.053345
335:
336:
337: LAMINATE STIFFNESS PROPERTIES
338: AVERAGE AXIAL                                              FLEXURAL
339:     EX            EY            GXY          MUXY          EX           EY
340:   6.27824       5.26470       3.17256        .42185       6.25719      4.31299
341:
342:
343:
344:          TITLE- DU 36-26,USING HERCULES DEC. 8, 1983 PROPERTIES
345:          SUBTITLE- FROM DATA PACKAGE -STA JUNIOR-
346:          DATE- JULY 26, 1984
```

D29

N85-22239

1984
NASA/ASEE SUMMER FACULTY RESEARCH FELLOWSHIP PROGRAM

MARSHALL SPACE FLIGHT CENTER
THE UNIVERSITY OF ALABAMA

ELECTRICAL PERFORMANCE OF SEMICONDUCTOR DEVICES AT CRYOGENIC TEMPERATURES

Prepared by:	Carl A. Ventrice, Ph.D
Academic Rank:	Professor
University and Department:	Tennessee Technological University Electrical Engineering Department
NASA/MSFC:	
Laboratory:	Information & Electronic Systems
Division:	Electrical
Branch:	Electrical/Electronic Parts
NASA Counterpart:	Robert DeHaye
Date:	August 17, 1984
Contract No:	NASA NGT-01-002-099 University of Alabama

ELECTRICAL PERFORMANCE OF SEMICONDUCTOR DEVICES AT CRYOGENIC TEMPERATURES

Carl A. Ventrice
Electrical Engineering Department
Tennessee Technological University
Cookeville, Tennessee 38505

ABSTRACT

The electrical performance of semiconductor devices is examined over the temperature range from 300 to 1.4K. Special emphasis is given to the design, fabrication, and tesing of p-channel MOSFET's with the ultimate objective of developing a device that will perform satisfactorily in the temperature range from 4.2 to 1.4K. The current-voltage characteristics of the device are obtained as a function of temperature for varying channel lengths and channel dopant levels. MOSFET's with average channel lengths of 3.27, 5.68, 8.37, and 11.39 microns are examined. Initial results indicate that the devices with the shorter channel lengths perform better in the 4 to 20K range than those with the longer channel lengths. Additional testing will be done down to 1.4K and with different channel dopant levels.

INTRODUCTION

In man's quest to obtain more information about the universe, he has ventured deeper and deeper into space. This venture has been effected by means of earth-bound and satellite deep-space probing systems. The deeper these systems probe into space, the weaker are the information bearing signals that must be detected and processed. Noise, therefore, becomes of major concern owing to the fact that it has a degrading effect on the system's ability to detect and process these signals. There are numerous sources of noise that can affect system performance. A major source of noise is thermal, or Johnson, noise which is generated by the detector and the associated electronic signal processing subsystems. Thermal noise increases approximately in direct proportion to the temperature of the detector and the associated electronics. By lowering the temperature of the detector and the associated electronics, one can lower system noise and, therefore, increase the signal-to-noise ratio (SNR) of the incoming signal.

Primary motivation for the present investigation stems from the effort in infrared astronomy which is being conducted by the astronomy group here at the Marshall Space Flight Center (MSFC). In this effort, infrared radiation in the wavelength range from 8 to 40 micrometers is observed from distant galaxies in order to learn more about the mechanism of star formation. Thus, the signals which are received at the focal plane of the IR telescope are extremely weak. In order to get a SNR 1, the detector must be cooled down to liquid helium temperatures (T 4.2K). At present, the detector is maintained at a temperature of 1.4K. The detector being used is a Ge:Ga bolometer. An array of 20 detectors (4 x 5 array) is used in order to minimize the sky scanning time.

The signal from the detector is fed to a preamplifier, then to the signal processing electronics. Owing to the high input impedance of the preamplifier, it is necessary to cool it down in order to lower the introduction of Johnson noise onto the signal. At present, the preamplifier is cooled down to a temperature between 60 and 80K. In an effort to improve the SNR of the receiving system, the astronomers would like to adjoin the preamplifier to the detector and operate it at the same temperature as the detector. The semiconductor devices used in the preamplifier are designed to operate effectively at room temperature. These devices, however, are observed to perform very well down to approximately 60K. Unfortunately, the performance of these devices degrades rapidly below this temperature. This degradation can be attributed to carrier freezeout. A description of how carrier freezeout affects the electrical properties of semiconductor materials will be given in the body of the report. The present investigation is concerned with the performance of semiconductor devices at cryogenic temperatures, with special emphasis given to the temperature range from 1.4 to 4.2K.

OBJECTIVE

The primary objective in this investigation is to attempt to develop semiconductor devices that will perform effectively in the temperature range from 4.2 to 1.4K. This will entail the design, fabrication, and testing of p-channel metal-oxide-semiconductor field-effect transistor (MOSFET) devices. The design parameters that will be considered are the channel geometry (length and width) and the channel dopant level. Device testing will entail the determination of the I-V characteristics of the device at various temperatures. From these characteristics the transconductance and threshold voltage can be determined.

THE MOSFET DEVICE

If a highly conductive electrode is placed in close proximity to a surface of a lightly doped semiconductor substrate, a voltage applied to the electrode relative to the substrate can have a pronounced effect on the electronic properties of the semiconductor surface. If n-type silicon is used as the substrate material, the application of a negative voltage to the electrode will repel electrons from the surface, and the region near the surface will become totally depleted of mobile charge. Nonmobile positive charge will remain in the form of the ionized donor-type impurities. If the magnitude of the applied negative voltage is increased, mobile positive charges (holes), which are the minority carriers within the n-type silicon, will be attracted to the surface, forming a conducting layer in which the holes will be the majority carriers. In this case, the silicon surface is said to be inverted. Similarly, if the silicon substrate is p-type, the application of a positive voltage to the electrode will form a surface inversion layer in which electrons will be the majority carriers. The phenomenon described above is referred to as the surface field effect and is the underlying principle behind the operation of MOSFET devices.

There are two distinctly different types of MOSFET devices: n-channel and p-channel. The n-channel MOSFET's operate by means of surface conduction of electrons under the influence of a transverse applied electric field, while the charge carriers that give rise to current flow in a p-channel device are holes. The cross-sectional structure of a p-channel MOSFET is shown in Figure 1. The device consists of two closely spaced, degenerately doped p^+ regions, the "drain" and the "source," which have been diffused into a lightly doped n-type silicon substrate. Typically, the distance separating the two diffused regions (channel length) varies from sub-micrometers up to tens of micrometers. A thin insulating

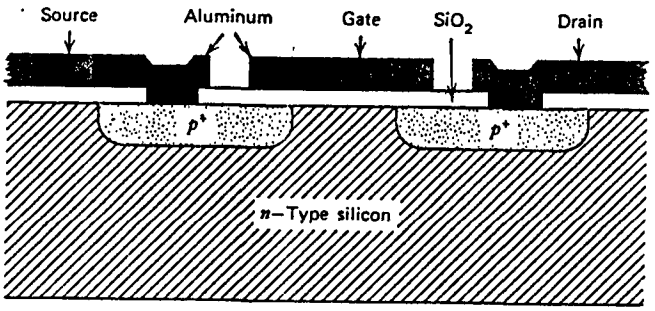

Figure 1. Cross-sectional view of a p-channel MOSFET device.

layer of silicon dioxide (approximately 1000 Angstroms thick) is formed directly above the channel region by oxidizing the surface of the silicon at high temperatures in an oxygen-rich ambient. Metal contacts, usually aluminum, are made to both diffused regions, and a "gate" electrode is positioned directly over and completely covering the channel region. The structure of an n-channel MOSFET device is similar to that shown in Figure 1 except that n^+ regions are diffused into a p-type silicon substrate. Typical current-voltage characteristics of a p-channel MOSFET are shown in Figure 2.

Most p-channel MOSFET's are usually enhancement-type devices: there will be no current flow between the drain and source when a negative voltage is applied to the drain, with respect to the source, and the applied gate-to-source voltage V_G is set equal to zero. However, if a large negative voltage is applied to the gate, a p-type surface inversion layer will form in the silicon directly below the gate, providing a conducting channel between the drain and the source which results in appreciable current flow between the two regions. The gate-to-source voltage which is required to achieve surface inversion and, as a result, conduction between the drain and source regions, is defined as the threshold voltage V_T.

In general, the three-terminal electrical characteristics of MOSFET's can be divided into three regions. At values of applied drain voltage which are sufficiently small as to be very much less than the magnitude of V_G-V_T, the drain current at constant V_G is found to increase linearly with increasing drain voltage, and the characteristics of the device are like those of a voltage-variable resistor, with the drain-to-source resistance decreasing steadily with increasing values of V_G. Under these conditions, the MOSFET is said to be operating in the variable-resistance region. As the applied drain-to-source voltage V_D is increased and becomes larger than V_G-V_T, the drain current tends to saturate and becomes relatively constant and independent of V_D. Under such conditions, the device is said to be operating in the region of saturated current flow. At very large values of V_D, avalanche breakdown of the drain diode occurs, and the drain current begins to increase extremely rapidly with increasing V_D. At this time, the device is said to be operating in the avalanche breakdown region.

EXPERIMENTAL ARRANGEMENT AND PROCEDURES

The fabrication of the MOSFET's was performed in Clean Room B-126 in building 4487. Both (1,0,0) and (1,1,1) plane silicon wafers, 1.5 inches in diameter, and 8 to 10 mils in thickness were used. Approximately 100 chips were produced from a single wafer. On each chip, four MOSFET's of varying channel lengths were fabricated. The average channel lengths were 3.27, 5.68, 8.37, and

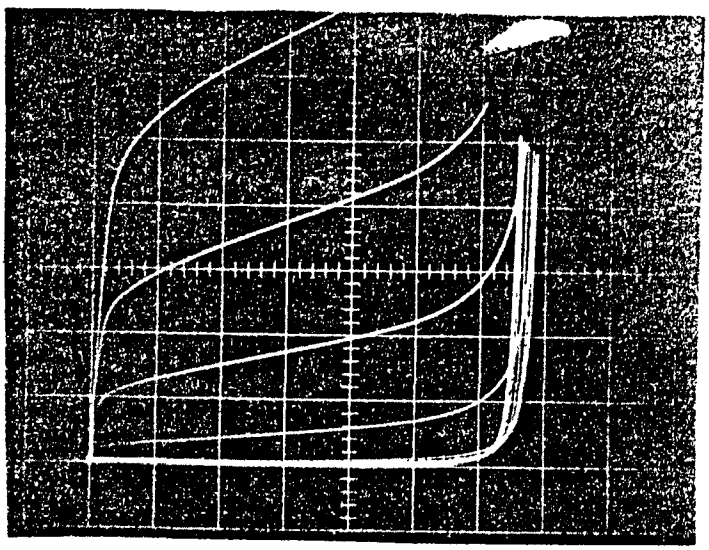

Figure 2. I-V characteristics of a typical p-channel MOSFET. Vertical scale: drain current: -1 mA/div.; horizontal scale: drain voltage: -10V/div.; gate voltage: 0 to -8V, in -1V steps.

11.39 micrometers. Figure 3 shows a typical chip magnified 25 times. The four MOSFET devices are shown at the bottom half of the photograph. The device with the narrowest channel length is shown at the left, and the one with the longest is shown at the right. Connections to the external circuitry were made by bonding 1 mil gold wire to the interconnecting pads, shown at the bottom of the photograph.

The experimental arrangement used in collecting the data is shown in Figure 4. The test chip and silicon temperature sensing diode were mounted in the test insertion device. The insertion device was lowered into a helium dewar. Rubber O-rings were used to maintain a vacuum seal at the top of the dewar. The chip was electrically connected to a type 576 Tektronix curve tracer. The temperature sensing diode was electrically connected to a Model DRC 80C Lake Shore Cryotronics temperature controller. I-V characteristics were obtained for V_G varying in 1 volt increments down to -10 volts. Temperatures between 4.2 and 77K were obtained by heating the chip by means of a resistor placed in close proximity to the chip. Temperatures below 4.2K were obtained by lowering the pressure in the dewar by means of a vacuum pump.

RESULTS

In the first test run, p-channel enhancement mode, MOSFET's were tested over the temperature range from 296K down to 4.3K. These devices were fabricated on a (1,1,1,) plane silicon wafer that was doped with phosphorus to a dopant level of 2.5×10^{16} cm^{-3}. The p^+ wells were formed from boron diffusion. Figures 5 through 8 show the I-V characteristics at various temperatures. From Figure 5, one can see that the characteristics are better at 80.6K than at room temperature. This can be attributed to the increase in carrier mobility with the decrease in temperature. One can see from Figures 6, 7, and 8 that as the temperature decreases, the degradation in the characteristics increases. The onset of degradation appears to have started at approximately 60K. In addition, it appears that the transconductance is decreasing with decreasing temperature.

More devices are being fabricated and will be tested at a later date.

CONCLUSIONS AND DISCUSSION

Little data has been taken so far in this project. Most of the time has been spent planning, constructing, and testing the apparatus and developing procedural techniques for acquiring data. Numerous tests are planned for the future. The technique for fabricating

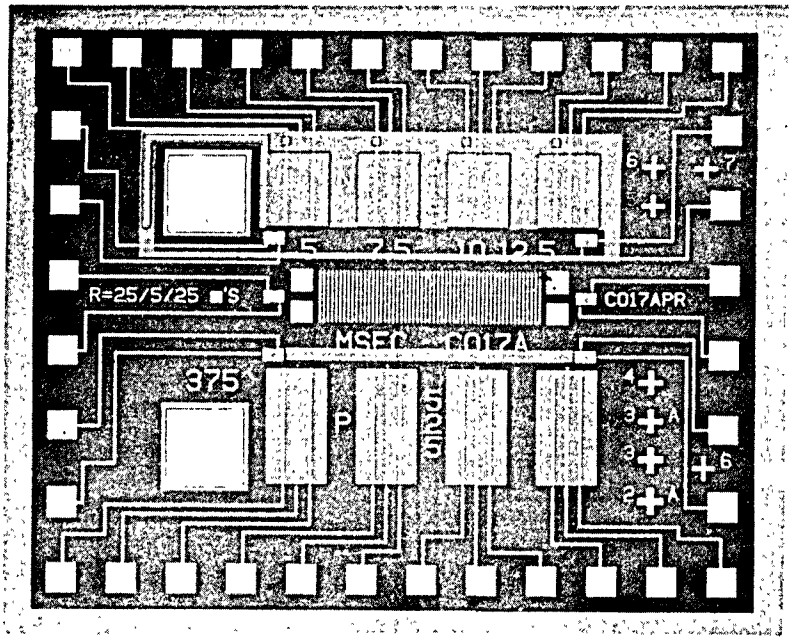

Figure 3. Photograph of test chip with 25X magnification.

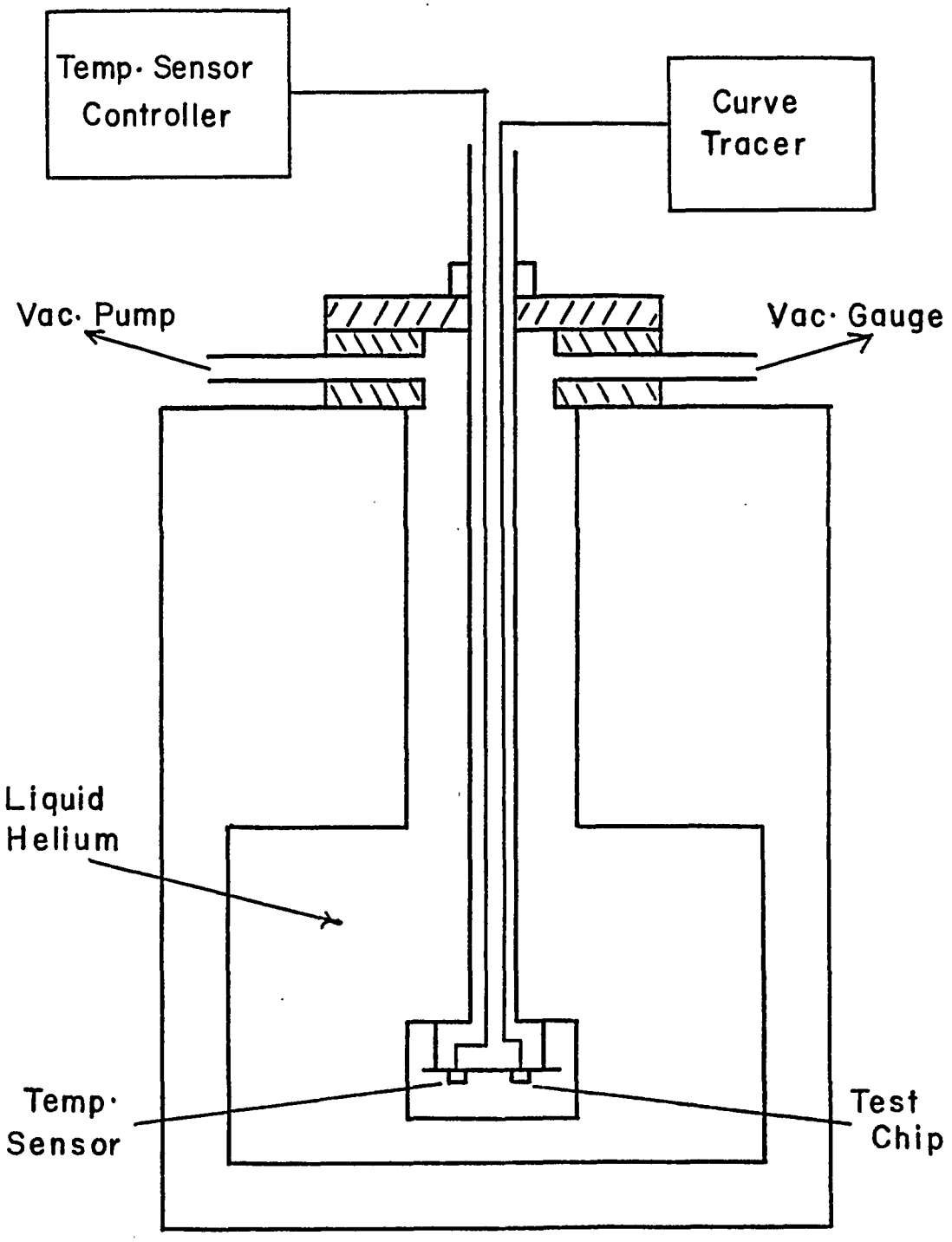

Figure 4. Schematic diagram of experimental arrangement used for obtaining I-V characteristics.

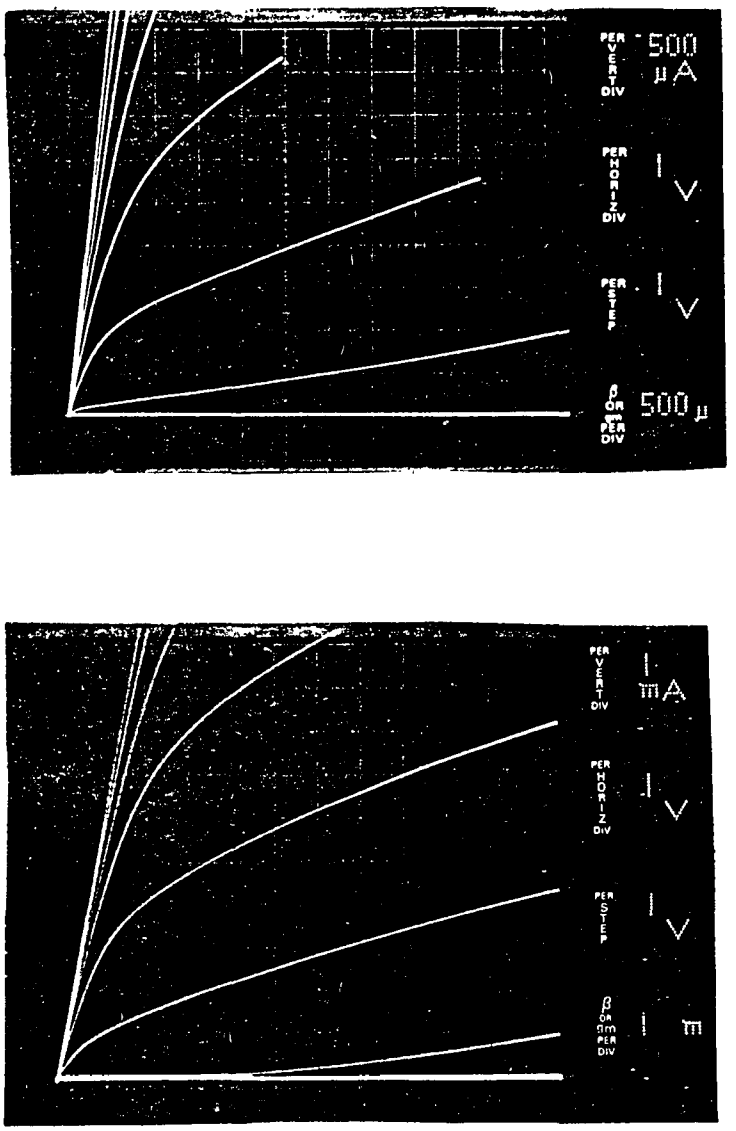

Figure 5. I-V characteristics of a p-channel MOSFET at T = 296K (upper) and T = 80.6K (lower).

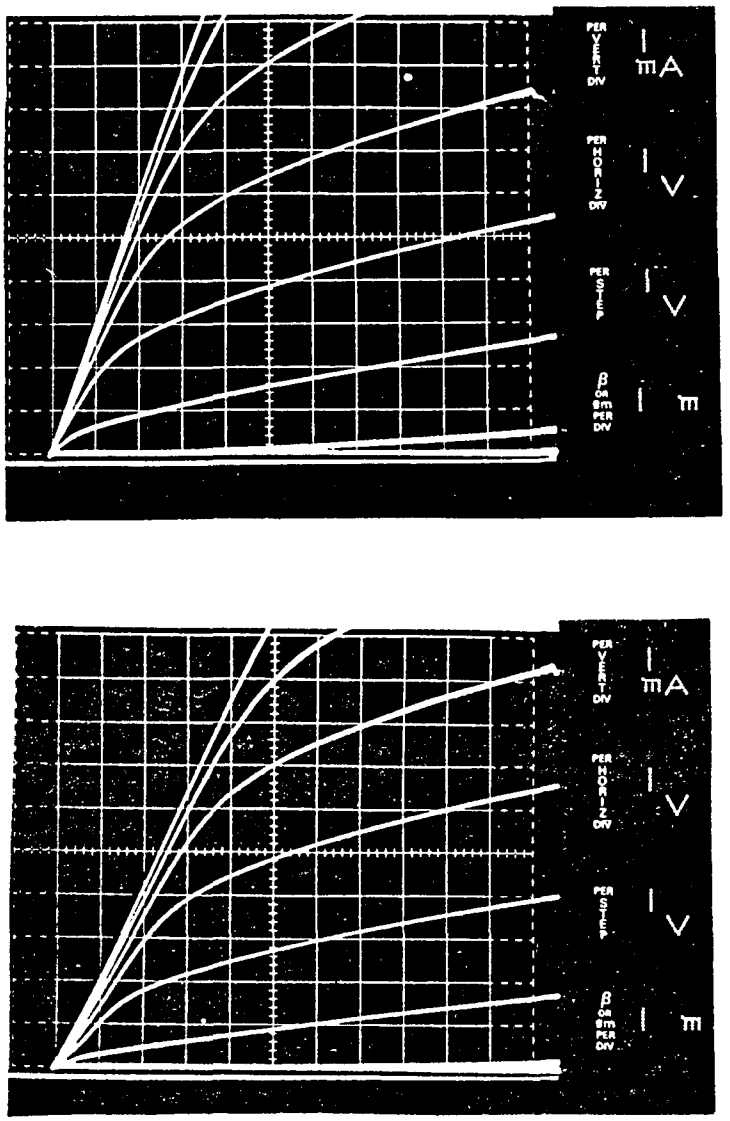

Figure 6. I-V characteristics of a p-channel MOSFET at T = 46.4K (upper) and T = 30.5K (lower).

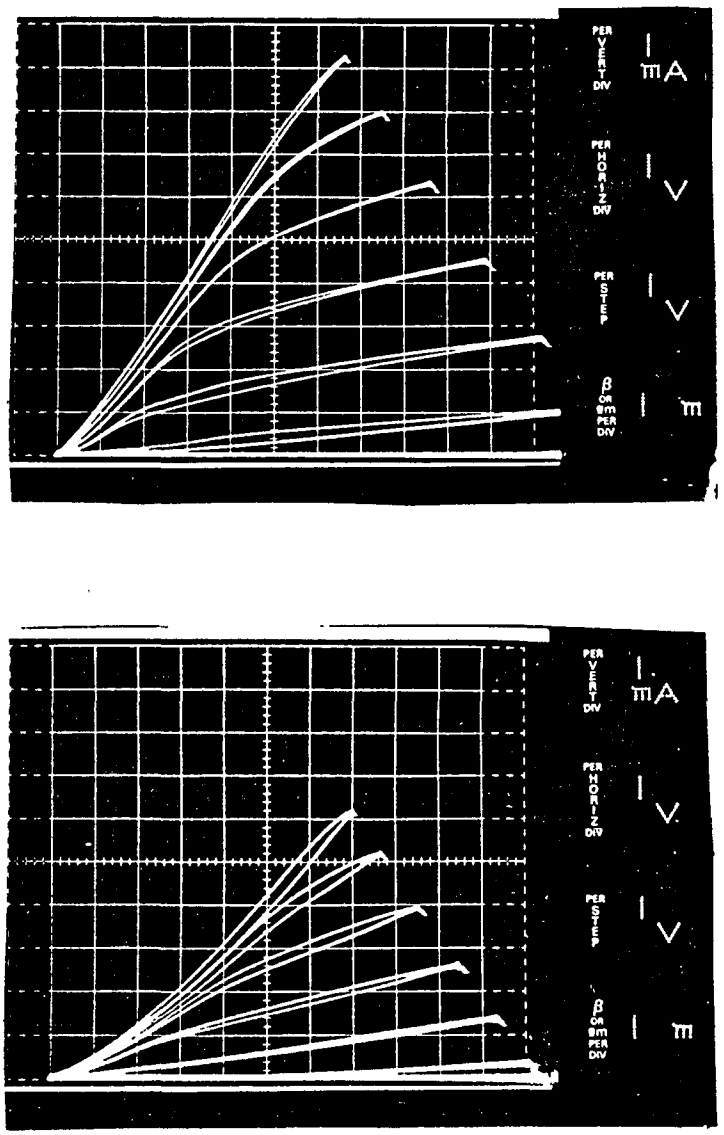

Figure 7. I-V characteristics of a p-channel MOSFET at T = 19K (upper) and T = 10K (lower)

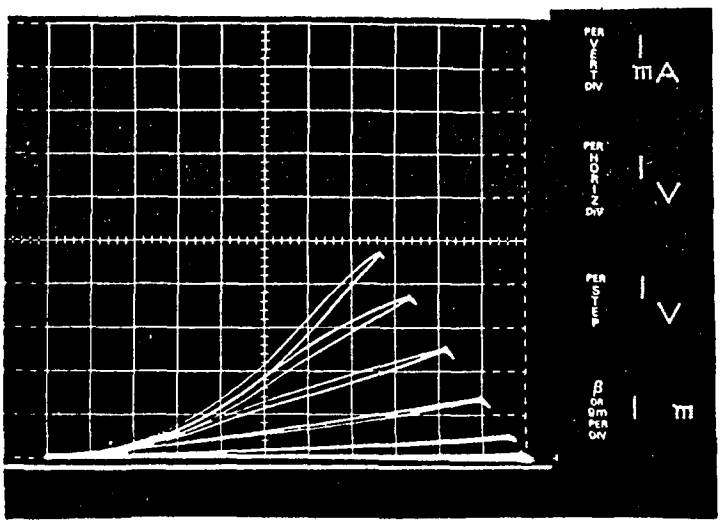

Figure 8. I-V characteristics of a p-channel MOSFET at T = 4.3K.

the devices and the procedure for testing these devices has been proven to be very sound. The initial data confirms that degradation in performance does occur in conventional MOSFET's at temperatures below 60K. This degradation is attributed to carrier freezeout. One can gain some incite into this phenomenon by considering the energy level diagram for silicon shown in Figure 9. The energy gap between the valence band and the conduction band is approximately 1.1 eV. For pure silicon (intrinsic), the conduction electron concentration n will equal the hole concentration p. These concentrations are a function of temperature. At room temperature (296K), $n = p = 1.38 \times 10^{16}/m^3$. Both conduction electrons and holes contribute to current flow; thus, the conductivity of intrinsic silicon at room temperature is 4×10^{-4} mhos/m, which means that intrinsic silicon is a very poor conductor. Now, suppose that one part per million of phosphorus was added to the silicon. Phosphorus has five valence electrons; four of these electrons form covalent bonds with the neighboring silicon atoms, the fifth electron is loosely bound to the system. The energy level of this fifth electron lies approximately .04 eV below the bottom of the conduction band. At room temperature, thermal excitation is sufficient to ionize almost 100% of these "donor" atoms, thus, raising the fifth electron up to the conduction band. This forms an extrinsic semiconductor with $n = 5.1 \times 10^{22}/m^3$ and $p = 3.7 \times 10^{9}/m^3$. Electrons are the majority carriers and holes are the minority carriers. The conductivity increases to a value of 1.1×10^{3} mhos/m. Suppose that instead of phosphorus being added, boron were added, again at one part per million. Boron has three valence electrons. These electrons will form covalent bonds with the neighboring silicon atoms. The boron atom will have an affinity for attracting an electron to complete the missing bond. The energy level for this fourth electron will be at approximately .04 eV above the top of the valence band. At room temperature, thermal excitation is sufficient to raise electrons from the valence band to this "acceptor" level; thus ionizing almost 100% of the boron atoms. In this case, $p = 5.1 \times 10^{22}/m^3$ and $m = 3.7 \times 10^{9}/m^3$. Holes are the majority carriers, and electrons are the minority carriers. The conductivity increases to a value of 410 mhos/m. One can see that, in both cases, the introduction of a small amount of an impurity can cause drastic changes in the electrical properties of a semiconductor. Now, as the temperature is lowered, the number of impurity atoms that are ionized will decrease. As the material approaches very low temperatures, very few impurity atoms will ionize, thus, causing the material to revert back to its intrinsic properties. This reversion has a degrading effect on device performance.

As one increases the impurity concentration in the silicon, the donor and acceptor levels split and form bands (see Figure 9).

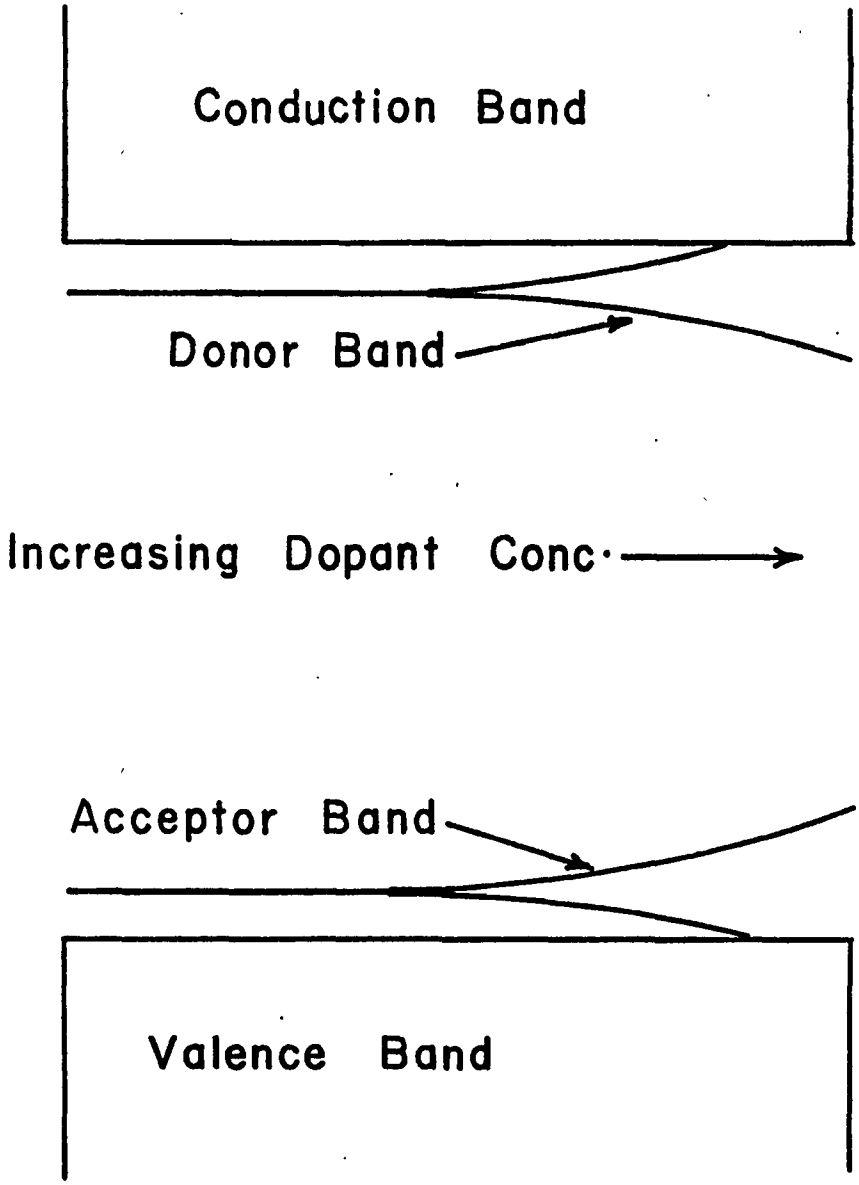

Figure 9. Energy level diagram for a semiconductor showing broadening of donor and acceptor bands with increasing dopant level.

When forming the p^+ wells in a MOSFET, the acceptor impurity concentration is of such a value that the acceptor band overlaps with the valence band. Under such a condition, freezeout is no longer possible. P-channel MOSFET's are being fabricated on a p-type wafer, for which the acceptor concentration in the substrate is of such a value that the gap between the acceptor band and the valence band is much less than .04 eV. Such devices will not operate at room temperature, but may operate at very low temperatures through the aid of partial freezeout. Testing on these devices will occur in the near future.

D30

1984 NASA/ASEE
SUMMER FACULTY FELLOWSHIP PROGRAM

Marshall Space Flight Center
The University of Alabama

EVALUATION OF 'PHOENICS' AS A DESIGN ANALYSIS TOOL FOR SSME

Prepared By: M. B. Ventrice, Ph.D.

Academic Rank: Associate Professor

University and Department: Tennessee Technological University
Department of Mechanical Engineering

NASA/MSFC
Laboratory: Systems Dynamics
Division: Atmospheric Sciences
Branch: Fluid Dynamics

NASA Counterpart: Warren Campbell

Date: August 17, 1984

Contract No.: NASA-NGT-01-002-099
The University of Alabama

ACKNOWLEDGEMENTS

The author's thanks are extended to Dr. Warren Campbell who selected the problems and offered extensive guidance in carrying it out. Dr. Campbell's enthusiasm and intellectual curiousity made participation in the NASA/ASEE Summer Faculty Fellowship Program an outstanding experience. Thanks are also extended to the other members of the Fluid Dynamics Branch for their friendship, hospitality and technical guidance. The assistance of the people of CHAM of North America was important to the success of the project, as was the help of Karen Parker of the Atmospheric Sciences Division's Research Computing Center.

Thanks are expressed to NASA and ASEE for sponsoring the program, to the people of Marshall Space Flight Center for making it a challenging, informative and rewarding experience, and to Dr. Mike Freeman of The University of Alabama for running the program smoothly and efficiently. Everyone's efforts combined well to create a very rewarding professional experience.

EVALUATION OF "PHOENICS"[1] AS A DESIGN ANALYSIS TOOL FOR SSME

Marie B. Ventrice
Associate Professor of Mechanical Engineering
Tennessee Technological University
Cookeville, Tennessee

Abstract

It has been proposed by the Atmospheric Sciences Division of the Systems Dynamics Laboratory of NASA's Marshall Space Flight Center that the computational fluid dynamics computer code PHOENICS be used as a design analysis tool for improving the Space Shuttle Main Engines (SSME). PHOENICS is a general-purpose computer code for the simulation of fluid-flow, heat-transfer, mass-transfer and combustion processes arising in engineering, scientific research and the environment. It is capable of analysis of one- or two-phase flows, in one, two, or three dimensions.

Since the code is complex and extensive, as are the SSME, it was necessary to apply the code to simpler problems, prior to application to the SSME, in order to develop expertise in, and insight into, effective use of the code. The object of this work was to apply PHOENICS to the evaluation of the performance of high-pressure gaseous-hydrogen filters. To demonstrate the usefulness of the code and to illustrate the ability of the code to handle successively more complex features of the device being modeled, and to develop the expertise of the user, several filter design were analysed.

The work comfirmed the applicability and usefulness of the code.

---

[1] PHOENICS (Parabolic, Hyperbolic or Elliptic Numerical Integration Code Series) is a computer code copyrighted by CHAM Limited (Concentration Heat and Momentum Limited) of London, England -- D. Brian Spalding, managing director.

INTRODUCTION

The performance of the Space Shuttle Main Engines (SSME) has not as yet met the original design criteria. It has been proposed by the Fluid Dynamics Branch of the Atmospheric Science Division of the Systems Dynamics Laboratory of NASA's Marshall Space Flight Center that the computational fluid dynamics computer code PHOENICS* be used as a design analysis tool for improving the SSME. PHOENICS is a general purpose computer code for the simulation of fluid-flow, heat-transfer, mass-transfer and combustion processes arising in engineering, scientific research and the environment. It is capable of analysis of one- or two-phase flows, in one, two, or three dimensions.

Since PHOENICS is complex and extensive, as are the SSME, it is appropriate to apply the code to simpler problems, prior to application to the SSME, in order to develop expertise in, and insight into, effective use of the code. The object of this work was to apply PHOENICS to the evaluation of the performance of a high-pressure gaseous-hydrogen filter. The parameters of the problem were suggested by the Materials and Processes Laboratory and were taken from blueprints of a high-pressure gaseous-hydrogen filter [1] designed by that laboratory. The second object was to evaluate the code itself as to its ease of use and appropriateness for SSME analyses.

THE FILTER

Fig. 1 is a schematic diagram of the actual filter from which the problem analysed by PHOENICS was derived. Gaseous-hydrogen at ambient temperature and a maximum pressure of 34.5 MPa (10,000 lbf /in.^{2}) enters through a 5.16×10^{-3}m (0.203 in.) inside diameter cylindrical passageway at the top and flows through a series of fourteen 2.54×10^{-3}m (0.100 in.) diameter laterial holes, and the end of the passageway, into the filter media (shown in the figure as dotted shading). The hydrogen exits the filter through twelve 3.18×10^{-3}m (0.125 in.) diameter lateral holes and four axial holes of the same diameter. It then proceedes through various clear passageways to the bottom of the device and passes out through a 5.16×10^{-3}m (0.203 in.) inside diameter exit at the bottom. The maximum permissible pressure drop across the filter is 34.5 MPa (5,000 lbf/in.^{2}). Twenty-mesh screen is located at the entrances to and the exits from the filter media. The filter media consists

---

*PHOENICS (Parabolic, Hyperbolic or Elliptic Numerical Integration Code Series) is a computer code copyrighted by CHAM Limited (Concentration Heat And Momentum Limited) of London, England -- D. Brian Spalding, managing director.

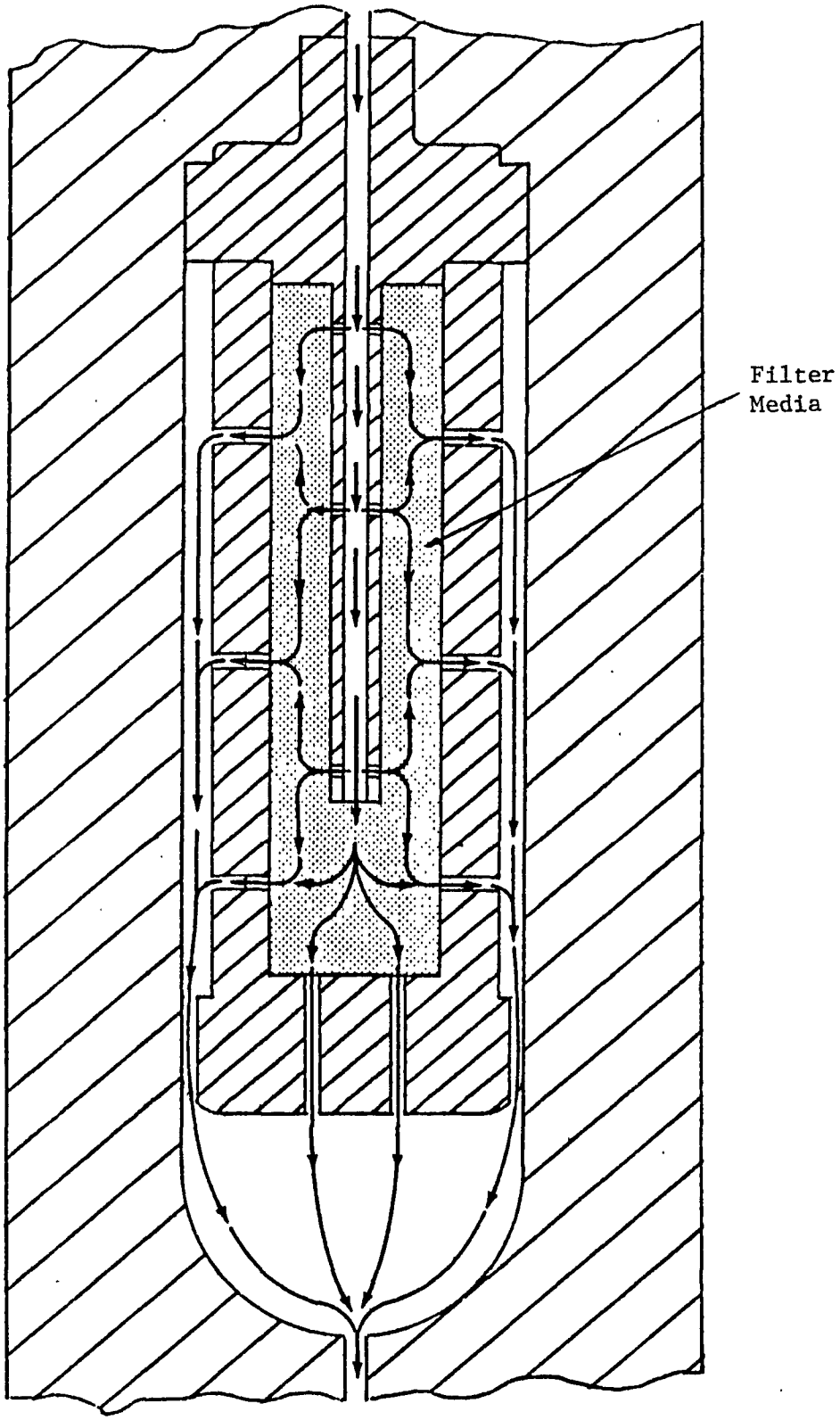

Figure 1. Schematic Diagram of a High-Pressure Hydrogen Filter Illustrating the General Pattern of Flow.

of equal parts by volume of activated alumina, activated charcoal and molecular sieve having an overall average diameter of 2.44×10^{-3}m (0.096 in.).

Originally the object was to analyse the filter described above. The characteristics of the filter were to be coded into PHOENICS and then various parametric studies were to be carried out. Of interest were the mass flow rates associated with various pressure drops across the filter. Also of interest were the predicted patterns of flow through the filter and identification of any limitations or problems that might be predicted to exist.

To carry out the task it was planned to start with a very simple geometry. The flow in the simple model would include the features of the more complex flow -- compressibility, functional dependence of enthalpy on both temperature and pressure, pressure losses due to the filter media, screens and orifaces, and any other significant characteristics. Due to lack of time, ana analysis of only the simple geometry consisted of a 0.10 m (3.94 in.) diameter cylinder having a 0.01 m (0.394 in.) diameter entrance and a 0.02 m (0.787 in.) diameter exit. Its length was 0.15 m (5.906 in.). Screens were placed at the inlet and exit and the filter was packed with equal parts by volume of activated alumina, activated charcoal and molecular sieve. The inlet and exit areas of the simple filter corresponded approximately to the inlet and exit areas of the actual filter. The remainder of the paper deals with analysis of the simple filter and suggestions for how to extend the work to analysis of the actual filter.

FLUID DYNAMICS OF THE FILTER

The flow through the filter must satisfy the steady-state conservation of mass, momentum and energy equations. For this case the conservation of mass equation is

$$\text{div } (\rho \vec{u}) = 0$$

where ρ is the density and $\vec{u}$ the velocity. The x-direction momentum equation is

$$\text{div } (\rho \vec{u} u) = \text{div } (\mu \text{ grad } u) - \frac{\partial p}{\partial x} + B_x + V_x$$

where μ is the viscosity, p is the pressure, B_x is the x-direction body force per unit volume, and V_x includes the viscous terms other than div (μ grad u). Similar equations could be written for the other two dimentions. The last three terms could be combined and called S since they are all source or sinh of momentum terms. The energy equation is

$$\text{div } (\rho \vec{u} h) = \text{div } (\frac{k}{c} \text{ grad } h) + S_h$$

where h is the specific enthalpy, k is the thermal conductivity, c is the constant-pressure specific heat and S_h is the volumetric rate of heat generation.

To solve the above equations, appropriate property values and an equation of state are needed, as well as information about pressure gradients, body forces, viscous terms and heat generation. Property values were taken from reference 2 for the conditions of the problem:

$C = 15$ kJ/kg-K

$M = 9.5 \times 10^{-6}$ kg/m-s

Fitting an emperical equation to the property data in reference [2], in the range of interest, results in the equation

$$T = 15.24 - 4.029 \times 10^{7}p + (.0681 - 1.74 \times 10^{-11}p)h$$

where T is in degrees kelvin, p is in pascals and h is in kilojoules per kilogram. The equation of state selected was the the compressibility equation

$$\rho = p/zRT$$

where R is the gas constant, which for hydrogen is 4123.5 N-m/kg-K, T the absolute temperature and z the compressibility which, for hydrogen within the range of pressures and temperatures of the problem, is a function of both T and P:

$$z = -0.50800 + 1.1337 \times 10^{-2}\ T - 2.0867 \times 10^{-5}T^2$$

$$+ (8.183 \times 10^{-8} - 5.456 \times 10^{-10}T + 0.969 \times 10^{-12}T^2)P$$

$$+ (-5.604 \times 10^{-16} + 5.833 \times 10^{-18}T - 0.819 \times 10^{-20}T^2)P^2$$

where, again, T is in degrees kelvin and p is in pascals.

For the filter, the term $-\partial p/\partial x$ is the drop in pressure due to the resistance to flow created by the filter media. Pressure drops also occur due to the screens at the entrance and exit. In the actual filter pressure drops due to sudden expansions, bends in the flow path and other frictional losses would also need to be considered.

Jones and Krier [3] have expressed the pressure drop due to filter material as a function of a friction factor F_v,

$$\frac{\Delta P}{L} = F_v \frac{\mu V_{ave}}{Db^2} \left(\frac{1-\phi}{\phi}\right)^2$$

where ϕ is the porosity of the filter media, D_b is the average particle diameter and V_{ave} is the average gas velocity determined from the mass flow, $\dot{m}$.

$$V_{ave} = \frac{\dot{m}}{\rho A_p \phi}$$

where A_p is the cross-sectional area of the filter. Jones and Krier's experimentally determined equation for the friction factor is

$$F_v = 150 + 3.89\ (Re')^{.87}$$

where Re′ is a modified Reynolds number and is defined as

$$Re' = \rho V_{ave} D_b \phi/\mu(1-\phi)$$

For the filter being considered, the first term in the equation for F_v is negligible compared to the second.

Perry's Chemical Engineers' Handbook [4] gives an equation for the loss Δh through screens which, when expressed as a pressure loss, becomes

$$\Delta p = 0.5001 \quad (\frac{n}{c^2})(\frac{1-\alpha^2}{\alpha^2})\rho V$$

where Δp is in pascals; n is the number of screens; c is the screen discharge coefficient, dimensionless and constant at 1.5 for large values of Reynolds number; α is the fractional free projected area of screen, dimensionless and equal to 0.438 for 20-mesh screens; ρ is the density in kg/m^3 and V is the superficial velocity ahead of the screen, m/s. Expressing the superficial velocity in terms of the average velocity through the screens, $V = \alpha V_{ave}$, and using the above values for the constants, the pressure loss for one screen becomes

$$\Delta p = 0.1794 \rho V_{act}^2$$

PHOENICS

PHOENICS is a system of computer codes having three elements. 'EARTH' is the control equation solver which solves the fluid mechanics problem specified by means of an appropriate 'SATELLITE' and 'GROUND-STATION'. EARTH solves the conservation of mass, momentum and energy equations after first expressing them in finite domain form. The EARTH code is not accessible to the user.

Appendix A is a copy of the SATELLITE code with appropriate information for solution of the simple filter problem coded into it. As can be seen by examination of Appendix A, SATELLITE contains instructions for how to implement its various features. Further information is contained in the PHOENICS instruction manual [5]. The purpose of SATELLITE is to specify as much of the information about the problem as is possible in a simple format. It prompts the user to specify information about the coordinate system, problem geometry, dependent variables to be solved for, density and viscosity, boundary conditions, initial fields, solution convergence and termination, and variables to be printed out.

Special information situations not adequately dealt with by SATELLITE are specified by means of FORTRAN statements written into GROUND. Appendix B is a copy of the GROUND-STATION code, including the appropriate information for a solution of the simple filter problem initiated in Appendix A. For the filter, the pressure loss due to the filter material and the screens, the equation for density, and property information (i.e. the equation for temperature as a function of enthalpy and pressure) were formulated in GROUND. Again, GROUND itself contains information as to its use, with further information given in the PHOENICS handbook.

FILTER PROBLEM RESULTS

The problem solution obtained by PHOENICS is available in two forms -- tables of values, and plots generated by a special PHOENICS graphics subroutine in conjunction with Tektronix Plot 10 computer graphics software. Table 1 shows the results of the filter problem specified in Appendices A and B. Fig. 2 illustrates the velocity field and Fig. 3 is a plot of the pressure field, both drawn by the PHOENICS GRAFFICS program. Fig. 4 is a perspective view of the velocity field shown in Fig. 2. Fig. 5 is a perspective view of the velocity vectors at constant-z planes located at z = 0.05 L, 0.50 L and 0.95 L where L is the length of the filter; L=0.15 m. PHOENICS GRAFFICS is capable of generating various views of the vector and scalar fields of the problem solution.

The inlet mass flow rate per unit area specified in SATELLITE is high, 21,000 kg/m^2-s. Table 1 lists the inlet density as 31.17 kg/m^3; hence, the inlet velocity determined from the solution is about 674 m/s. The decrease in pressure across the filter is 16.0 MPa, which is well below the 34.5 MPa value specified as the maximum permissible pressure loss.

TABLE 1. Continuity Errors, Velocity Components, Pressure and Density Fields After 100 Sweeps

```
ISW=100 CONTINUITY ERROR: NET= 4.642E-02 ABS/RESREF(1)= 4.644E-02
CONTINUITY ERRORS FOR EACH IZ DURING SWEEP  100
  7.559E-06  -3.338E-06  -1.842E-05   1.377E-05   8.106E-06  -1.104E-05   8.177E-06  -9.332E-06   3.792E-06  -5.715E-06
             5.643E-06   2.410E-06  -3.278E-06   5.066E-06   1.050E+00
3D PP'S 1ST DIFMAX=  3.338E+01    ITER= 21    DIFMAX=  6.113E-02
FIELD VALUES OF V1
  IY= 5   0.000E+00   0.000E+00   0.000E+00   0.000E+00   0.000E+00   0.000E+00   0.000E+00   0.000E+00   0.000E+00   0.000E+00
  IY= 4   9.940E+00   1.939E+01   1.664E+01   9.745E+00   4.506E+00   1.699E+00   4.875E-01   2.106E-02  -2.289E-01  -6.197E-01
  IY= 3   1.922E+01   5.152E+01   4.067E+01   2.236E+01   9.702E+00   3.418E+00   9.966E-01   2.548E-02  -4.183E-01  -1.140E+00
  IY= 2   5.601E+01   1.090E+02   6.951E+01   3.493E+01   1.425E+01   4.618E+00   1.087E+00   2.096E-03  -4.619E-01  -1.257E+00
  IY= 1   2.738E+02   1.813E+02   8.306E+01   3.656E+01   1.413E+01   4.227E+00   8.489E-01  -2.390E-02  -3.017E-01  -7.640E-01
  IZ=         1           2           3           4           5           6           7           8           9          10
  IY= 5   0.000E+00   0.000E+00   0.000E+00   0.000E+00   0.000E+00
  IY= 4  -1.555E+00  -3.750E+00  -8.466E+00  -1.793E+01  -3.258E+01
  IY= 3  -3.018E+00  -7.825E+00  -1.901E+01  -4.154E+01  -8.177E+01
  IY= 2  -3.541E+00  -1.003E+01  -2.657E+01  -6.368E+01  -2.018E+02
  IY= 1  -2.145E+00  -5.977E+00  -1.504E+01  -3.209E+01  -1.082E+02
  IZ=        11          12          13          14          15
FIELD VALUES OF W1
  IY= 5   8.838E+00   2.608E+01   4.091E+01   4.968E+01   5.387E+01   5.561E+01   5.628E+01   5.655E+01   5.660E+01
  IY= 4   5.112E+00   2.722E+01   4.317E+01   5.134E+01   5.471E+01   5.593E+01   5.640E+01   5.665E+01   5.681E+01
  IY= 3   2.149E+01   4.809E+01   5.524E+01   5.662E+01   5.665E+01   5.649E+01   5.653E+01   5.675E+01   5.714E+01
  IY= 2   1.521E+02   1.269E+02   9.088E+01   6.944E+01   6.025E+01   5.720E+01   5.657E+01   5.680E+01   5.747E+01
  IY= 1   5.754E+02   3.209E+02   1.655E+02   9.377E+01   6.602E+01   5.787E+01   5.643E+01   5.673E+01   5.759E+01
  IZ=         1           2           3           4           5           6           7           8           9
  IY= 5   5.631E+01   5.518E+01   5.208E+01   4.475E+01   2.893E+01
  IY= 4   5.690E+01   5.625E+01   5.408E+01   4.769E+01   3.276E+01
  IY= 3   5.777E+01   5.833E+01   6.049E+01   6.240E+01   6.193E+01
  IY= 2   5.890E+01   6.249E+01   7.225E+01   9.833E+01   1.644E+02
  IY= 1   5.939E+01   6.397E+01   7.631E+01   1.071E+02   1.732E+02
  IZ=        10          11          12          13          14
FIELD VALUES OF P1
  IY= 5   3.916E+07   3.916E+07   3.911E+07   3.899E+07   3.882E+07   3.863E+07   3.843E+07   3.823E+07   3.803E+07   3.783E+07
  IY= 4   3.917E+07   3.917E+07   3.913E+07   3.900E+07   3.882E+07   3.863E+07   3.843E+07   3.823E+07   3.803E+07   3.783E+07
  IY= 3   3.917E+07   3.928E+07   3.924E+07   3.904E+07   3.883E+07   3.863E+07   3.843E+07   3.823E+07   3.803E+07   3.782E+07
  IY= 2   3.891E+07   3.997E+07   3.949E+07   3.911E+07   3.884E+07   3.863E+07   3.843E+07   3.823E+07   3.803E+07   3.782E+07
  IY= 1   3.850E+07   4.102E+07   3.946E+07   3.908E+07   3.883E+07   3.862E+07   3.842E+07   3.823E+07   3.803E+07   3.782E+07
  IZ=         1           2           3           4           5           6           7           8           9          10
  IY= 5   3.764E+07   3.745E+07   3.728E+07   3.717E+07   3.713E+07
  IY= 4   3.763E+07   3.743E+07   3.726E+07   3.712E+07   3.706E+07
  IY= 3   3.762E+07   3.740E+07   3.718E+07   3.692E+07   3.662E+07
  IY= 2   3.760E+07   3.736E+07   3.703E+07   3.639E+07   3.450E+07
  IY= 1   3.760E+07   3.734E+07   3.693E+07   3.627E+07   3.450E+07
  IZ=        11          12          13          14          15
FIELD VALUES OF RHO1
  IY= 5   2.522E+01   2.522E+01   2.519E+01   2.513E+01   2.504E+01   2.493E+01   2.482E+01   2.471E+01   2.460E+01   2.449E+01
  IY= 4   2.523E+01   2.523E+01   2.521E+01   2.514E+01   2.504E+01   2.493E+01   2.482E+01   2.471E+01   2.460E+01   2.449E+01
  IY= 3   2.523E+01   2.529E+01   2.526E+01   2.516E+01   2.504E+01   2.493E+01   2.482E+01   2.471E+01   2.460E+01   2.449E+01
  IY= 2   2.508E+01   2.566E+01   2.540E+01   2.519E+01   2.505E+01   2.493E+01   2.482E+01   2.471E+01   2.460E+01   2.448E+01
  IY= 1   3.117E+01   2.624E+01   2.539E+01   2.518E+01   2.504E+01   2.493E+01   2.482E+01   2.471E+01   2.460E+01   2.448E+01
  IZ=         1           2           3           4           5           6           7           8           9          10
  IY= 5   2.433E+01   2.428E+01   2.419E+01   2.412E+01   2.410E+01
  IY= 4   2.438E+01   2.427E+01   2.417E+01   2.409E+01   2.406E+01
  IY= 3   2.437E+01   2.425E+01   2.413E+01   2.398E+01   2.382E+01
  IY= 2   2.436E+01   2.423E+01   2.404E+01   2.368E+01   2.262E+01
  IY= 1   2.436E+01   2.422E+01   2.402E+01   2.362E+01   2.262E+01
  IZ=        11          12          13          14          15
```

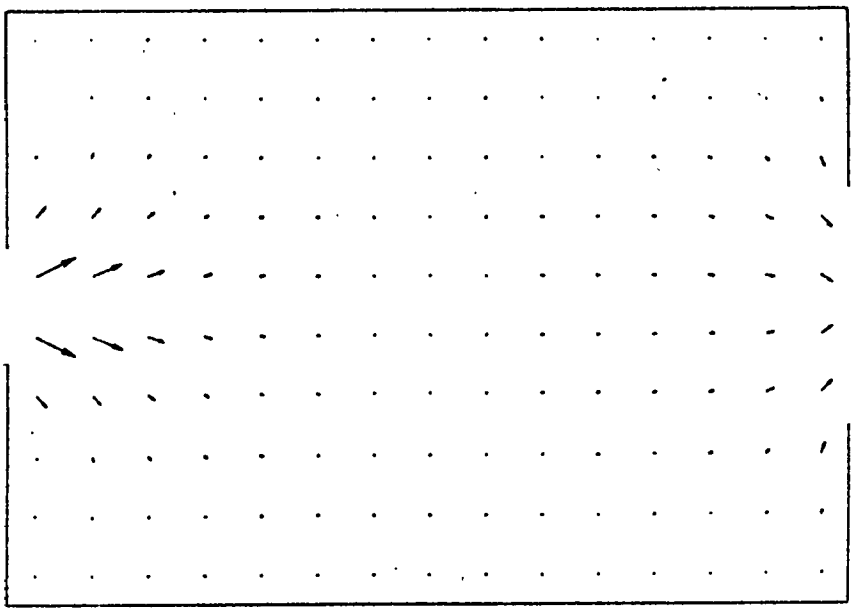

Figure 2. Velocity Field for Simple Filter; Inlet Mass Flow Rate, ρV = 21,000 kg/m^2-s. (Drawn by PHOENICS GRAFFICS)

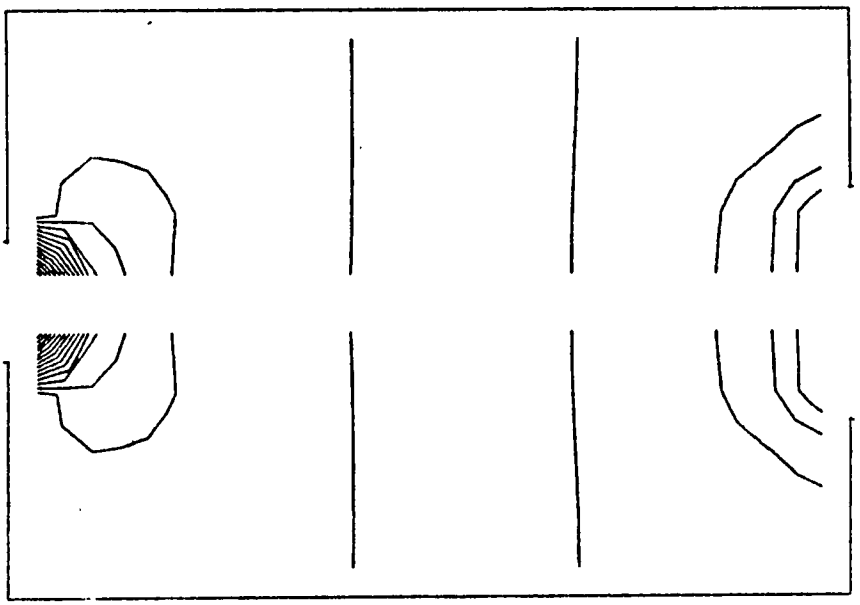

Figure 3. Pressure Field for Simple Filter; Inlet Pressure = 50.5 MPa, Outlet Pressure = 34.5 MPa, Contour Lines are Lines of Equal Pressure at Intervals of 0.8 MPa (Drawn by PHOENICS GRAFFICS).

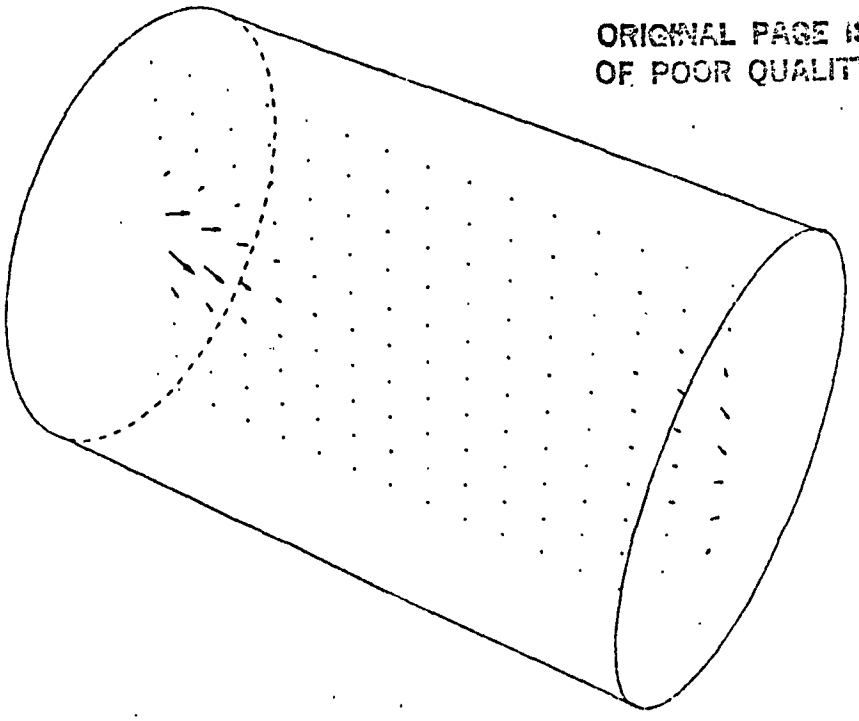

Figure 4. Perspective View of the Velocity Field Shown in Fig. 2.(Drawn by PHOENICS GRAFFICS).

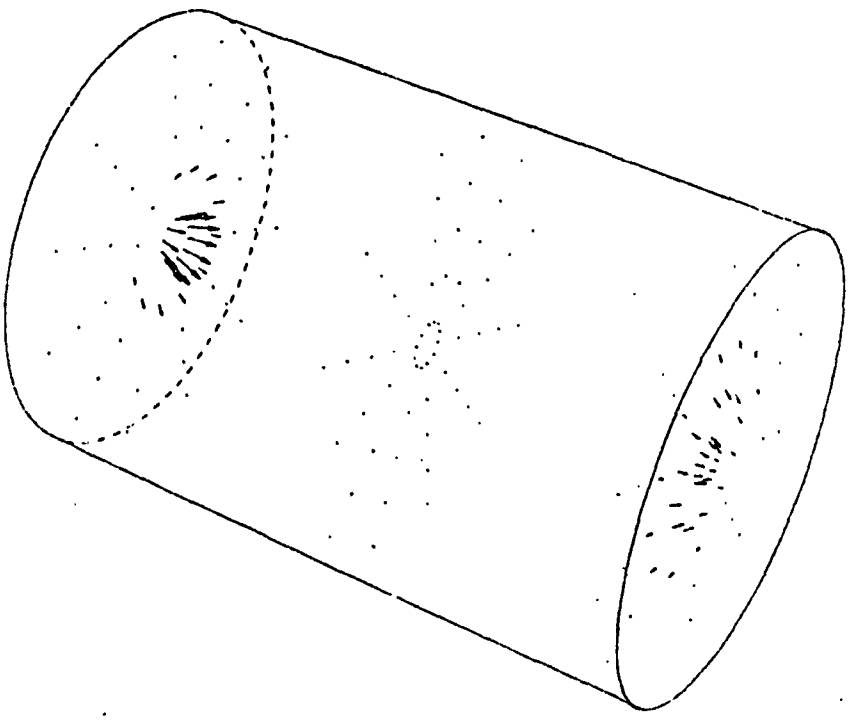

Figure 5. Perspective View of the Velocity Vectors in the Constant Z Planes Located at Z = 0.05 L, 0.50 L and 0.95 L where L is the Length of the Filter. (Drawn by PHOENICS GRAFFICS).

DISCUSSION

The Filter

The results shown previously are an initial step in the solution of the actual filter problem. The characteristics of the solution appear to have the correct trends. Before proceeding to the solution of the real filter, parametric studies should be carried out on the simple to establish the affect on the solution of such things as the grid spacing and rate of convergence.

The solution of the real filter will require the use of a fine grid and expressions for the losses associated with such things as bends in the flow path and sudden expansions, in addition to the type losses specified in the simple filter. It would be useful if ultimately the solution generated by PHOENICS could be compared to experimental results.

PHOENICS

Inital use of PHOENICS is difficult due to the organization of the instruction manual. Some of the instructions are for a previous version of the code, and information about specific features is not consolidated. Once initial work is done with the code so as to give the user some understanding of the general features of the code and the location of information in the instruction manual, a more sophisticated ability to use the code should develop relatively rapidly.

Use of the code requires significant knowledge of fluid dynamics and an understanding of the problem being formulated since this is what the use is specifying in SATELLITE and GROUND -- a PHOENICS generated solution can only be as good as the user's ability to specify the problem. The fact that EARTH is a "black box" can hinder error tracing. But the wide selection of information that the computer can be directed to print out concerning intermediate values of variables during solution partially overcomes such problems. Initial work with the code indicates that it is quite versitile and has good potential for use as an analysis tool for the SSME.

A fringe benefit of using PHOENICS is that it is challenging and enjoyable to use.

APPENDIX A

SATELLITE

```
$BATCH
C$DIRECTIVE**SATLIT
C     *FILE NAME: MODSTL.FTN
C     *ABSTRACT: SATELLITE MODEL MAIN PROGRAM.
C     *DOCUMENTATION: PHOENICS INSTRUCTION MANUAL (SPRING 1983).
C     *AUXILIARY SUBROUTINES (TAPES, ETC.) ARE IN SATELLITE LIBRARY
C      SERVICEU, WHICH MUST BE INCLUDED IN LINK EDIT TO RUN.
CXXXXXXXXXXXXXXXXXXXXXXXXXXXXXXXXXXXXXXXX STANDARD SECTION 1 STARTS:
C-----------------------------------------------------------------
CHAPTER 1   COMMON BLOCKS AND USER'S DATA.
C-----------------------------------------------------------------
$INCLUDE 9,CMNGUSSI.FTN/G
$INCLUDE 9,GUSSEQUI.FTN/G
$INCLUDE 9,CMNGRFIC.FTN/G
      COMMON/CPI/IPWRIT,IDUM(243)
      DIMENSION GDTAPE(3),DFAULT(4)
      DIMENSION ARRAY1(309),ARRAY2(194),ARRAY3(421)
      LOGICAL ARRAY1,LSPDA,WRT,RD,NAMLST
      INTEGER ARRAY2,XPLANE,YPLANE,ZPLANE
      INTEGER P1,PP,U1,U2,V1,V2,W1,W2,R1,R2,RS,EP,H1,H2,H3,C1,C2,
     &C3,C4
      REAL NORTH,LOW
      EQUIVALENCE (ARRAY1(1),CARTES),(ARRAY2(1),NX)
      EQUIVALENCE (ARRAY3(1),SPARE1(1)),(M1,R1),(M2,R2)
      EQUIVALENCE (LSTRUN,INTGR(12)),(NAMLST,LOGIC(88))
CXXXXXXXXXXXXXXXXXXXXXXXXXXXXXXXXXXXXXXXX STANDARD SECTION 1 ENDS.
CXXXXXXXXXXXXXXXXXXXXXXXXXXXXXXXXXXXXXXXX USER SECTION 1 STARTS:
C     GRAFFIC ARRAYS DIMENSIONED AS NEEDED...
      COMMON/GRAF1/PHI1(450)/GRAF2/ PHI2(3213)
C     POROSITY & SPECIAL DATA ARRAYS DIMENSIONED AS NEEDED...
      DIMENSION PE(1,5,15),PN(1,5,15),PH(1,5,15),PC(1,5,15)
      DIMENSION LSPDA(1),ISPDA(1),RSPDA(1)
C     USER PLACES HIS VARIABLES, ARRAYS, EQUIVALENCES ETC. HERE.
      DATA NLSP,NISP,NRSP/1,1,1/
C     USER PLACES HIS DATA STATEMENTS HERE.
CXXXXXXXXXXXXXXXXXXXXXXXXXXXXXXXXXXXXXXXX USER SECTION 1 ENDS.
CXXXXXXXXXXXXXXXXXXXXXXXXXXXXXXXXXXXXXXXX STANDARD SECTION 2 STARTS:
C-----------------------------------------------------------------
CHAPTER 2   SET CONSTANTS, AND ARRANGE FILE MANIPULATIONS.
C-----------------------------------------------------------------
C     PLEASE DO NOT ALTER, OR RE-SET, ANY OF THE REMAINING
C     STATEMENTS OF THIS CHAPTER.
      DATA CELL,EAST,WEST,NORTH,SOUTH,HIGH,LOW,VOLUME/
     & 0.,1.,2.,3.,4.,5.,6.,7. /
      DATA P1,PP,U1,U2,V1,V2,W1,W2,R1,R2,RS,KE,EP,H1,H2,H3,C1,C2,
     &C3,C4/1,2,3,4,5,6,7,8,9,10,11,12,13,14,15,16,17,18,19,20/
      DATA FIXFLU,FIXVAL,ONLYMS,WALL/1.E-10,1.E10,0.0,-10.0/
      DATA IPLANE,XPLANE,YPLANE,ZPLANE/0,1,2,3/
      DATA WRT,RD,DFAULT/.TRUE.,.FALSE.,4HDEFA,4HULT.,4HDTA/,1HG/
      DATA GDTAPE/4HGUSI,4HE1.D,2HTA/
      DATA NLDATA,NIDATA,NRDATA/309,194,421/
      DATA NLCREG,NTCVRG/60,350/
      CALL TAPES(10,GDTAPE,3,1,4*NRDATA)
C-----------------------------READ DEFAULT FILE IF BLOCKDATA ABSENT
          IF(INTGR1(29).NE.10) GO TO 2
      CALL WRIT40(40HDATA ESTABLISHED IN BLOCK DATA.          )
      GO TO 3
    2 CALL TAPES(1,DFAULT,4,2,4*NRDATA)
      CALL DATAIO(RD,1)
      CALL WRIT40(40HDATA TAKEN FROM DEFAULT.DTA ON GROUP A/C)
    3 CALL WRIT40(40HFILE MODSTL.FTN IS THE SATLIT USED.      )
```

```
      LOGIC(89) = .TRUE.
C-----------------------------------------------------------------
CHAPTER 3   DEFINE DATA FOR NRUN RUNS.
C-----------------------------------------------------------------
CXXXXXXXXXXXXXXXXXXXXXXXXXXXXXXXXXXXXXXX STANDARD SECTION 2 ENDS.
CXXXXXXXXXXXXXXXXXXXXXXXXXXXXXXXXXXXXXXX USER SECTION 2 STARTS:
C---  GROUP  41 MULTI-RUNS : RUN(1-30)<.T.,29*.F.>
C
      DO 410 II=1,1
  410 RUN(II)=.TRUE.
CXXXXXXXXXXXXXXXXXXXXXXXXXXXXXXXXXXXXXXX USER SECTION 2 ENDS.
CXXXXXXXXXXXXXXXXXXXXXXXXXXXXXXXXXXXXXXX STANDARD SECTION 3 STARTS:
        DO 10 IRUN=1,30
          IF(.NOT.RUN(IRUN)) GO TO 10
      NRUN=NRUN+1
      LSTRUN=IRUN
   10 CONTINUE
        DO 999 IRUN=1,LSTRUN
          IF(.NOT.RUN(IRUN)) GO TO 999
      INTGR(11) = IRUN
CXXXXXXXXXXXXXXXXXXXXXXXXXXXXXXXXXXXXXXX STANDARD SECTION 3 ENDS.
CXXXXXXXXXXXXXXXXXXXXXXXXXXXXXXXXXXXXXXX USER SECTION 3 STARTS:
C---  ALL INTEGER VARIABLES ARE DEFAULTED TO 0, AND REAL VARIABLES
C     TO 0.0, UNLESS OTHERWISE INDICATED.
C     E.G. BY VARIABLE<10>, OR <10.0> AS APPROPRIATE.
C     THE DEFAULT SETTINGS OF ALL LOGICAL VARIABLES ARE ALWAYS
C     INDICATED, E.G. VARIABLE<.T.>, OR  VARIABLE<.F.>.
C
C---  RUN1
C-----------------    ---------------    -------------------
C---  GROUP 1. FLOW TYPE :
C     PARAB<.F.>,CARTES<.T.>,ONEPHS<.T.>
      CARTES = .FALSE.
C-----------------    ---------------    -------------------
C---  GROUP 2. TRANSIENCE :
C     STEADY<.T.>,ATIME,LSTEP<1>,FSTEP<1>
C     TLAST<1.E10>,TFRAC(1-30)<30*1.>
C     SERVICE SUBROUTINE FOR 'NT' POWER-LAW TIME STEPS:
C     CALL GRDPWR(0,NT,TLAST,POWER)
C-----------------    ---------------    -------------------
C---  GROUP 3. X-DIRECTION :
C     NX<1>,XULAST<1.0>,XFRAC(1-30)
C     SERVICE SUBROUTINE FOR POWER-LAW GRID:
C     CALL GRDPWR(1,NX,XULAST,POWER)
C-----------------    ---------------    -------------------
C---  GROUP 4. Y-DIRECTION :
C     NY<1>,YVLAST<1.0>,YFRAC(1-30),RINNER,SNALFA
C     SERVICE SUBROUTINE FOR POWER-LAW GRID:
C     CALL GRDPWR(2,NY,YVLAST,POWER)
      NY = 5
      CALL GRDPWR(2,NY,.05,1.0)
C-----------------    ---------------    -------------------
C---  GROUP 5. Z-DIRECTION :
C     NZ<1>,ZWLAST<1.0>,ZFRAC(1-30)
C     SERVICE SUBROUTINE FOR POWER-LAW GRID:
C     CALL GRDPWR(3,NZ,ZWLAST,POWER)
      NZ = 15
      CALL GRDPWR(3,NZ,.15,1.0)
C-----------------    ---------------    -------------------
C---  GROUP 6. MOVING GRID :
C     MGRID,IZW1,IZW2,AZW2,BZW2,CZW2,PINT,ZW2M1T
C-----------------    ---------------    -------------------
C---  GROUP 7. BLOCKAGE: BLOCK<.F.>,IPLANE,IPWRIT
C    *SET CONSTANT POROSITIES OVER SUB-DOMAINS USING:
C     CALL CONPOR(IR,TYPE,VALUE,IXF,IXL,IYF,IYL,IZF,IZL), WHERE:
C     IR=RUN SECTION NUMBER, E.G. 1 FOR RUN1 SECTION; 'TYPE'= EAST,
```

```
C      WEST, NORTH, SOUTH, HIGH, LOW & CELL. 'VALUE'=WANTED POROSITY
C      OVER REGION IXF,...IZL.
C     *DIMENSION ARRAYS PE(NX,NY,NZ), PN(NX,NY,NZ), PH(NX,NY,NZ), &
C      PC(NX,NY,NZ) ABOVE.
C     *FOR FULLY-BLOCKED CELLS (IE. 'VALUE'= 0.0) USER NEED SET ONLY
C      THE 'CELL' POROSITY (TO ZERO), AS CELL-FACE AREAS ARE THEN
C      AUTOMATICALLY ZEROED.
C     *FOR SATELLITE PRINTOUT OF ALL POROSITIES IN DOMAIN, 'IPLANE'=
C      XPLANE YPLANE OR ZPLANE, FOR DESIRED CROSS-SECTION DIRECTION.
C     *FOR EACH 'TYPE' A MAXIMUM OF 10 CALLS TO CONPOR IS ALLOWED,
C      BUT IF REQUIREMENTS EXCEED THIS PROVISION SET BLOCK=.T. &
C      IPWRIT=-1, AND SET POROSITY ARRAYS EXPLICITLY HERE AS WANTED.
C      IN THIS CASE, THE USER  M U S T   SET  A L L  ELEMENTS OF
C      ARRAYS PE, PN, PH, PC (MANY MAY BE 0.0 OR 1.0). HE MAY USE:
C      CALL CR(PARRAY,VALUE,IXF,IXL,IYF,IYL,IZF,IZL,NX,NY,NZ)
C      ANY NUMBER OF TIMES, TO SET 'PARRAY' (= PE, ETC.) TO
C      'VALUE' OVER RANGE IXF TO IXL, IYF TO IYL, IZF TO IZL.
C     *CONPOR  M U S T  N O T  BE USED IN CONJUNCTION WITH EXPLICIT
C      SETTINGS OF THE ARRAYS (INCLUDING SETTINGS VIA CR).
       BLOCK = .TRUE.
       IPWRIT = -1
C
       DO 700 IY = 1,5
       DO 700 IZ = 1,15
       PE(1,IY,IZ) = 0.6
       PN(1,IY,IZ) = 0.6
       PH(1,IY,IZ) = 0.6
 700   PC(1,IY,IZ) = 0.5
C------------------    --------------    ------------------
C---   GROUP 8.DEPENDENT VARIABLES TO BE SOLVED FOR OR STORED :
C      SOLVAR(1-25)<25*.F.>,STOVAR(1-25)<25*.F.>,CONC1(1-4)<4*.T.>
C      USE FOLLOWING NAMED INTEGERS FOR ARRAY ELEMENTS 1-20:
C      P1,PP,U1,U2,V1,V2,W1,W2,M1,M2,RS,KE,EP,H1,H2,H3,C1,C2,C3,C4.
       SOLVAR(P1) = .TRUE.
       SOLVAR(PP) = .TRUE.
       SOLVAR(V1) = .TRUE.
       SOLVAR(W1) = .TRUE.
       SOLVAR(H1) = .TRUE.
C------------------    --------------    ------------------
C---   GROUP 9. VARIABLE LABELS :
C      TITLE(1-25)<2HP1,2HPP,2HU1,2HU2,2HV1,2HV2,2HW1,2HW2,2HR1,
C      2HR2,2HRS,2HKE,2HEP,2HH1,2HH2,2HH3,2HC1,2HC2,
C      2HC3,2HC4,2HRX,2HRY,2HRZ, 2*4H****>
       TITLE(2) = 4HRH01
C------------------    --------------    ------------------
C---   GROUP 10 PROPERTIES:
C      IRHO1<1>,IRHO2<1>,RHO1<1.0>,RHO2<1.0>,
C      ARHO1<1.0>,BRHO1<1.0>,CRHO1<1.0>
C      IEMU1<1>,EMU1<1.0>,EMULAM<1.E-10>
C      IHSAT,H1SAT,H2SAT,PSATEX<1.0>
C      SIGMA(1-25)<1.0,2.0,1.,1.E10,1.,1.E10,1.,1.E10,
C      4*1.0,1.314,1.0,1.E10,10*1.0>
       IRHO1 = -1
       RHO1 = 30.
       IEMU1 = 1
       EMULAM = 95.E-7
C------------------    --------------    ------------------
C---   GROUP 11 INTER-PHASE TRANSFER PROCESSES :
C      ICFIP,CFIPS,IMDOT,CMDOT,CA1I<1.E6>,CA2I<1.E6>
C------------------    --------------    ------------------
C---   GROUP 12 SPECIAL SOURCES :
C      ISPCSO(1-25),AGRAVX,AGRAVY,AGRAVZ,ABUOY,HREF
C------------------    --------------    ------------------
C---   GROUP 13 INITIAL FIELDS :
C      FIINIT(1-25)<25*1.E-10>
       FIINIT(P1) = 3.45E7
```

```
      FIINIT(V1) = 1.
      FIINIT(W1) = 1.
      FIINIT(H1) = 4500
C-------------------    ---------------    -------------------
C---  GROUP 14 BOUNDARY/INTERNAL CONDITIONS :
C     ILOOP1,ILOOPN,XCYCLE<.F.>,PBAR,REGION(1-10)<10*.T.>
C    *N.B. ALL 10 REGIONS ARE DEFAULTED .TRUE..  THE USER SHOULD
C     SET REGION(I)=.FALSE. FOR UNUSED REGIONS 'I'.
      DO 140 I = 6,10
  140 REGION(I) = .FALSE.
C-------------------    ---------------    -------------------
C---  GROUP 15 TO 24; REGIONS 1 TO 10
C---  ONLY THOSE REGIONS ARE ACTIVE WHICH ARE SPECIFIED BY THE
C     USER, PREFERABLY BY WAY OF:-
C     CALL PLACE(IREGN,TYPE,IXF,IXL,IYF,IYL,IZF,IZL) &
C     CALL COVAL(IREGN,VARBLE,COEFF,VALUE)
C-----------------------------------------------------------
C     CONSTANT INLET FLOW
      WIN = 1000.
      CALL PLACE(1,LOW,1,NX,1,1,1,1)
      CALL COVAL(1,M1,FIXFLU,21.0*WIN)
      CALL COVAL(1,V1,ONLYMS,0.0)
      CALL COVAL(1,W1,ONLYMS,WIN)
C     CALL COVAL(1,KE,ONLYMS,.02)
C     CALL COVAL(1,EP,ONLYMS,.02)
      CALL COVAL(1,H1,ONLYMS,4500.)
C-----------------------------------------------------------
C     CONSTANT OUTLET PRESSURE
      CALL PLACE(2,HIGH,1,NX,1,2,NZ,NZ)
      CALL COVAL(2,M1,FIXVAL,3.45E7)
C-----------------------------------------------------------
C     WALL FRICTION, CYLINDRICAL BOUNDARY
      CALL PLACE(3,NORTH,1,NX,NY,NY,1,NZ)
      CALL COVAL(3,W1,WALL,0.0)
C     CALL COVAL(3,KE,WALL,0.0)
C     CALL COVAL(3,EP,WALL,0.0)
C-----------------------------------------------------------
C     WALL FRICTION, INLET WALL
      CALL PLACE(4,LOW,1,NX,2,NY,1,1)
      CALL COVAL(4,V1,WALL,0.0)
C     CALL COVAL(4,KE,WALL,0.0)
C     CALL COVAL(4,EP,WALL,0.0)
C-----------------------------------------------------------
C     WALL FRICTION, EXIT WALL
      CALL PLACE(5,HIGH,1,NX,3,NY,NZ,NZ)
      CALL COVAL(5,V1,WALL,0.0)
C     CALL COVAL(5,KE,WALL,0.0)
C     CALL COVAL(5,EP,WALL,0.0)
C-----------------------------------------------------------
C     FRICTION DUE TO FILTER MATERIAL
C     CALL PLACE(6,VOL,1,NX,1,NY,1,NZ)
C     CALL COVAL(6,W1,1.0,0.0)
C     CALL COVAL(6,V1,1.0,0.0)
C-------------------    ---------------    -------------------
C---  GROUP 25 GROUND STATION :
C     GROSTA<.F.>,NAMLST<.F.>
C    *NAMLST ACTIVATES NAMELIST IN GROUND.
C-------------------    ---------------    -------------------
C---  GROUP 26 SOLUTION TYPE AND RELATED PARAMETERS :
C     WHOLEP<.F.>,SUBPST<.F.>,DONACC<.F.>
C-----------------------------------------------------------
      WHOLEP = .TRUE.
C-------------------    ---------------    -------------------
C---  GROUP 27 SWEEP AND ITERATION NUMBERS :
C     FSWEEP<1>,LSWEEP<1>,LITHYD<1>,LITC<1>,LITKE<1>,LITH<1>,
C     LITER(1-25)<9*1,-1,15*1>
```

```
C      IVELF<1>,NVEL<1>,IVELL<10000>,
C      IKEF<1>,NKE<1>,IKEL<10000>,
C      IENTF<1>,NENT<1>,IENTL<10000>,
C      ICNCF<1>,NCNC<1>,ICNCL<10000>,
C      IRHO1F<1>,NRHO1<1>,IRHO1L<10000>,
C      IRHO2F<1>,NRHO2<1>,IRHO2L<10000>
C-----------------------------------------------------------------
       LSWEEP = 100
       LITER(PP) = 20
C--------------------    ---------------    --------------------
C---   GROUP 28 TERMINATION CRITERIA :
C      ENDIT(1-25)<9*1.E-10,0.5,15*1.E-10>
C--------------------    ---------------    --------------------
C---   GROUP 29 RELAXATION  :
C      RLXP<1.>,RLXPXY<1.>,RLXPZ<1.>,RLXRHO<1.>,RLXMDT<1.>,
C      DTFALS(3-25)<23*1.E10>
C-----------------------------------------------------------------
       DTFALS(V1) = 2.E-2
       DTFALS(W1) = 2.E-2
C      DTFALS(KE) = 2.E-3
C      DTFALS(EP) = 2.E-3
       DTFALS(H1) = 2.E-3
C--------------------    ---------------    --------------------
C---   GROUP 30 LIMITS :
C      VELMAX<1.E10>,VELMIN<-1.E10>,RHOMAX<1.E10>,RHOMIN<1.E-10>,
C      TKEMAX<1.E10>,TKEMIN<1.E-10>,EMUMAX<1.E10>,EMUMIN<1.E-10>,
C      EPSMAX<1.E10>,EPSMIN<1.E-10>,AMDTMX<1.E10>,AMDTMN<-1.E10>
C--------------------    ---------------    --------------------
C---   GROUP 31 SLOWING DEVICES : SLORHO<1.>,SLOEMU<1.>
C--------------------    ---------------    --------------------
C---   GROUP 32 PRINT-OUT OF VARIABLES :
C      PRINT(1-25)<.T.,.F.,23*.T.>,SUBWGR<.F.>
C
C      PRINT VALUES OF RHO1
C
       PRINT(2) = .TRUE.
C
C--------------------    ---------------    --------------------
C---   GROUP 33 MONITOR PRINT-OUT :
C      IXMON<1>,IYMON<1>,IZMON<1>,NPRMON<1>,NPRMNT<1>
C-----------------------------------------------------------------
       IXMON = 1
       IYMON = 2
       IZMON = 10
       NPRINT = 20
C--------------------    ---------------    --------------------
C---   GROUP 34 FIELD PRINT-OUT CONTROL :
C      NPRINT<100>,NTPRIN<100>,NXPRIN<1>,NYPRIN<1>,NZPRIN<1>,
C      IZPRF<1>,ISTPRF<1>,IZPRL<10000>,ISTPRL<10000>
C      NUMCLS<10>,KOUTPT
C
C      PRINT OUT INITIAL FIELDS OF ALL VARIABLES SOLVED FOR
C
       KOUTPT = -1
C--------------------    ---------------    --------------------
C---   GROUP 35 TABLE CONTROL :
C      TABLES<.F.>,NTABLE,NTABVR,LINTAB,NPRTAB,NMON,
C      ITAB(1-8),MTABVR(1-8)
C--------------------    ---------------    --------------------
C      GROUP 36-38 ARE NOT DOCUMENTED IN THE INSTRUCTION
C      MANUAL AND ARE INTENDED FOR MAINTENANCE PURPOSES ONLY
C---   GROUP 36 DEBUG PRINT-OUT SLAB AND TIME-STEP :
C      IZPR1<1>,IZPR2<1>,ISTPR1<1>,ISTPR2<1>
C--------------------    ---------------    --------------------
C---   GROUP 37 DEBUG SWEEP AND SUBROUTINES :
C      KEMU,KMAIN,KINDEX,KGEOM,KINPUT,KSODAT,KCOMPF,KSORCE,
```

```
C      KSOLV1,KSOLV2,KSOLV3,KCOMPP,KADJST,KFLUX,KSHIFT,KDIF,
C      KCOMPU,KCOMPV,KCOMPW,KCOMPR,KWALL,KDBRHO<-1>,KDBEXP,KDBMDT
C      KDBGEN
C------------------    --------------    ------------------
C---   GROUP 38 MONITOR,TEST,AND FLAG :
C      MONITR<.F.>,FLAG<.F.>,TEST<.T.>,KFLAG<1>
C      END OF MAINTENANCE-ONLY SECTION
C------------------    --------------    ------------------
C---   GROUP 39 ERROR AND RESIDUAL PRINT-OUT :
C      IERRP<1000>,RESREF(1,3-24)<25*1.>,RESMAP<.F.>,
C      RESID(1-25)<2*.F.,23*.T.>,KOUTPT
       RESMAP = .TRUE.
C------------------    --------------    ------------------
C---   GROUP 40 SPECIAL DATA : LOGIC(1..10),INTGR(1..10),RE(21..30),
C      NLSP<1>,NISP<1>,NRSP<1>,SPDATA<.F.>,LSPDA(1),ISPDA(1),RSPDA(1)
C      USE FIRST 10 ELEMENTS OF ARRAYS LOGIC & INTGR AND 21ST
C      TO 30TH OF ARRAY RE FOR TRANSFERRING SPECIAL DATA FROM
C      SATELLITE TO GROUND, BUT IF REQUIREMENTS EXCEED THIS
C      PROVISION SET SPDATA = .T., AND DIMENSION ARRAYS LSPDA,
C      ISPDA, RSPDA ABOVE AND IN GROUND AS NEEDED, AND SET HERE
C      NLSP, NISP, NRSP TO DIMENSION VALUES.
       RE(21) = 777.
       RE(22) = .1794
C------------------    --------------    ------------------
C---   GROUP 42 RESTARTS AND DUMPS : SAVEM<.F.>,RESTRT<.F.>,KINPUT
      SAVEM = .TRUE.
C------------------    --------------    ------------------
C---   GROUP 43 GRAFFIC :
C      GRAPHS<.F.>,ORTHOG<.T.>,ANTSYM,NPRT<1>,ITITL<5*4H****>
C---   FOR A GRAFFIC RUN, DIMENSION PHI1 & PHI2 AS FOLLOWS:
C      PHI1(NX*NY*NZ*NM)
C      PHI2((NX+2)*(NY+2)*(NZ+2)*(NM+IBLK)) , WHERE
C      NM=NO. OF VARIABLES STORED + DENSITY(-IES)
C      IBLK=0 IF BLOCK=.FALSE.,=4 IF A 3D RUN,
C      =3 IF A 2D.YZ RUN.
       GRAPHS = .TRUE.
C------------------    --------------    ------------------
           IF(IRUN.EQ.1) GO TO 900
C---   RUN2
           IF(IRUN.EQ.2) GO TO 900
C---   RUN3
           IF(IRUN.EQ.3) GO TO 900
C---   RUN4
           IF(IRUN.EQ.4) GO TO 900
C---   RUN5
           IF(IRUN.EQ.5) GO TO 900
C---   RUN6
           IF(IRUN.EQ.6) GO TO 900
C---   RUN7
           IF(IRUN.EQ.7) GO TO 900
C---   RUN8
           IF(IRUN.EQ.8) GO TO 900
C---   RUN9
           IF(IRUN.EQ.9) GO TO 900
C---   RUN10
           IF(IRUN.EQ.10) GO TO 900
C---   RUN11
           IF(IRUN.EQ.11) GO TO 900
C---   RUN12
           IF(IRUN.EQ.12) GO TO 900
C---   RUN13
           IF(IRUN.EQ.13) GO TO 900
C---   RUN14
           IF(IRUN.EQ.14) GO TO 900
C---   RUN15
           IF(IRUN.EQ.15) GO TO 900
```

```
C---  RUN16
          IF(IRUN.EQ.16) GO TO 900
C---  RUN17
          IF(IRUN.EQ.17) GO TO 900
C---  RUN18
          IF(IRUN.EQ.18) GO TO 900
C---  RUN19
          IF(IRUN.EQ.19) GO TO 900
C---  RUN20
          IF(IRUN.EQ.20) GO TO 900
C---  RUN21
          IF(IRUN.EQ.21) GO TO 900
C---  RUN22
          IF(IRUN.EQ.22) GO TO 900
C---  RUN23
          IF(IRUN.EQ.23) GO TO 900
C---  RUN24
          IF(IRUN.EQ.24) GO TO 900
C---  RUN25
          IF(IRUN.EQ.25) GO TO 900
C---  RUN26
          IF(IRUN.EQ.26) GO TO 900
C---  RUN27
          IF(IRUN.EQ.27) GO TO 900
C---  RUN28
          IF(IRUN.EQ.28) GO TO 900
C---  RUN29
          IF(IRUN.EQ.29) GO TO 900
C---  RUN30
          IF(IRUN.EQ.30) GO TO 900
  900 CONTINUE
C---  ALL RUNS
CXXXXXXXXXXXXXXXXXXXXXXXXXXXXXXXXXXXXXXXX USER SECTION 3 ENDS.
CXXXXXXXXXXXXXXXXXXXXXXXXXXXXXXXXXXXXXXXX STANDARD SECTION 4 STARTS:
C-------------------------------------------------------------
C  WRITE GENERAL DATA ON TO THE GUSIE1.DTA TAPE, ETC...
          IF(SPDATA) CALL WRTSPC(LSPDA,NLSP,ISPDA,NISP,RSPDA,NRSP)
          IF(BLOCK) CALL WRTPOR(PE,PN,PH,PC,NX,NY,NZ,IPLANE)
C      OLD PRACTICES RETAINED FOR REFERENCE:
C          IF(SPDATA) CALL SPCDAT(IRUN)
C          IF(BLOCK) CALL PORDAT(IRUN)
           IF(GRAPHS) CALL SORT(IRUN)
           IF(RESTRT) GO TO 902
         DO 901 INDVAR=1,25
           IF(IFIX(FIINIT(INDVAR)+0.1).NE.10101) GO TO 901
      CALL FLDDAT(IRUN)
      GO TO 902
  901 CONTINUE
  902 CALL DATAIO(WRT,10)
          IF(MONITR) CALL DATAIO(WRT,-6)
  999 CONTINUE
      STOP
      END
```

APPENDIX B

GROUND-STATION

```
$BATCH
C$DIRECTIVE**MAIN
C     *FILE NAME: MODGRD.FTN
C     *INCLUDED SUBROUTINES: THE MODELS OF MAIN, GROUND & STRIDE.
C     *DOCUMENTATION: PHOENICS INSTRUCTION MANUAL (SPRING 1983).
C     *SATELLITE FILE NAME: MODSTL.FTN
      COMMON/ISHIFT/III(57),NFMAX
C SET F-ARRAY DIMENSION AS NEEDED, & SET NFMAX ACCORDINGLY.
      COMMON F(15000)
      NFMAX=15000
      CALL MAIN1
      STOP
      END
C$DIRECTIVE**GROUND
      SUBROUTINE GROUND(IRN,ICHAP,ISTP,ISWP,IZED,INDVAR)
$INCLUDE 9,CMNGUSSI.FTN/G
$INCLUDE 9,GUSSEQUI.FTN/G
C$INCLUDE 9,NMLIST.FTN/G
CXXXXXXXXXXXXXXXXXXXXXXXXXXXXXXXXXXXXXXXX STANDARD SECTION 1 STARTS:
C-----------------------------------------------------------------
C+++++MEANING OF SUBROUTINE ARGUMENTS:
C     IRN=RUN NUMBER; ICHAP=CHAPTER CALLED; ISTP=TIME STEP;
C     ISWP=SOLUTION SWEEP; IZED=Z-SLAB; INDVAR: SEE CHAPTERS BELOW.
C+++++USER-INTRODUCED VARIABLES & ARRAYS:
C     TO AVOID CONFLICT WITH VARIABLE NAMES USED IN COMMON, ALL
C     VARIABLES INTRODUCED BY THE USER SHOULD HAVE NAMES STARTING
C     WITH 'G' IF REAL, 'J' IF INTEGER, AND 'G' OR 'J' IF LOGICAL.
C     THUS GDZ(IZ) MIGHT BE A Z-INTERVAL ARRAY;
C     GW1(IY,IX) A 2-D ARRAY FOR AXIAL VELOCITY; ETC.
C     USER-GENERATED SUBROUTINES SHOULD BE NAMED CORRESPONDINGLY,EG
C     SUBROUTINE GVISC(GTEMP,GCNC,GVSC), FOR COMPUTING VISCOSITY
C     FROM CONCENTRATION & TEMPERATURE.
C+++++GROUND-TO-EARTH CONNECTING SUBROUTINES:
C    *USE GET(NAME,GARRAY,NY,NX) TO PUT VALUES OF VARIABLE NAMED
C     'NAME' INTO ARRAY 'GARRAY' DIMENSIONED GARRAY(NY,NX).
C    *USE SET(NAME,IXF,IXL,IYF,IYL,GARRAY,NY,NX) TO SET VARIABLE
C     'NAME' TO GARRAY(IY,IX) OVER THE REGION: IXF-IXL & IYF-IYL.
C    *USE PRNSLB(NAME) TO PRINT VARIABLE 'NAME' OVER X-Y PLANE.
C    *USE ADD(NAME,IXF,IXL,IYF,IYL,TYPE,CM,VM,CVAR,VVAR,NY,NX)
C     TO ADD SOURCE TO VARIABLE NAMED 'NAME' (SEE CHAPTER 5).
C    *USE READIZ(IZED) IN CHAPTERS 1, 2, 8, & 9 TO ACCESS P1,...DM
C     & VOL,...AHDZ. (SEE FOOTNOTE TO LEGALITY TABLE)
C    *USE GET1D(NAME,GARRAY,NDIM) TO PUT VARIABLE NAMED 'NAME' IN
C     ONE-D ARRAY 'GARRAY' DIMENSIONED NDIM, THUS:
C     CALL GET1D(NAME,GNX,NX) FOR XG,...DXG & DIMENSION GNX(NX);
C     CALL GET1D(NAME,GNY,NY) FOR YG,...RV & DIMENSION GNY(NY);
C     CALL GET1D(NAME,GNZ,NZ) FOR ZG,...WGRID & DIMENSION GNZ(NZ).
C+++++LEGALITY TABLE FOR USE OF EARTH-CONNECTING SUBROUTINES:
C     ENTRIES IN TABLE GIVE CHAPTERS IN WHICH SUBROUTINES CAN BE
C     USED FOR VARIABLES IN LEFT-HAND COLUMN. (SUBROUTINE
C     STRIDE IS REGARDED AS BEING IN CHAPTER 3)
C     ---------------------------------------------------------
C     : VARIABLE:: GET &   :   SET  : ADD    : READIZ : GET1D :
C     :          ::  PRNSLB :       :        :        :       :
C     ---------------------------------------------------------
C     :P1 - RZ   ::    ALL   :  6 & 7 :   5    : 1,2,8,9:  NONE :
C     :P10 - RZH::3-7, 10-16:    3    :  NONE  :  NONE  :  NONE :
C     :VOL -AHDZ::    ALL   :    3    :  NONE  : 1,2,8,9:  NONE :
C     :D1DP      ::   NONE   :   10    :  NONE  :  NONE  :  NONE :
C     :D2DP      ::   NONE   :   11    :  NONE  :  NONE  :  NONE :
```

```
C      :MU1,MU1H :: 5,13-16  :   12    :  NONE  :  NONE  :  NONE  :
C      :EXCO(L,H)::     NONE  :   13    :  NONE  :  NONE  :  NONE  :
C      :CFP      ::      5    :   14    :  NONE  :  NONE  :  NONE  :
C      :MDT      ::      5    :   15    :  NONE  :  NONE  :  NONE  :
C      :HST1,HST2::  5 & 15   :   16    :  NONE  :  NONE  :  NONE  :
C      :XG -WGRID::     NONE  :  NONE   :  NONE  :  NONE  :  ALL   :
C      ------------------------------------------------------------
C      NOTES ON ABOVE TABLE:
C     *IN CHAPTERS 1, 2, 8, & 9 VARIABLES P1...DM & GEOMETRY
C      VOL...AHDZ CAN BE ACCESSED BUT ONLY IN CONJUNCTION WITH
C      USE OF READIZ, THUS:
C      DO 1 IZED=1,NZ
C      CALL READIZ(IZED)
C    1 CALL GET(... AS REQUIRED..)
C     *GEOMETRY ACCESSED BY READIZ IS THAT AT INITIAL TIME.
C     *D1DP & D2DP ONLY ACCESSIBLE IN UNSTEADY FLOWS.
C+++++GROUND SERVICE SUBROUTINES:
C     *USE CONTUR(NAME,IPLANE,ILOC,NINT,I1,I2,J1,J2,GARRAY,NDIM) FOR
C      LINE-PRINTER PLOTS OF CONTOURS. 'NAME' = U1,...C4;
C      'IPLANE'= XPLANE, YPLANE, OR ZPLANE; ILOC SETS IX, IY, OR
C      IZ LOCATION OF IPLANE; I1, I2, J1, & J2 SET FIRST & LAST
C      CELLS IN HORIZ. & VERT. ON PLOT; GARRAY IS 1-D WORKING ARRAY
C      OF DIMENSION NX*NY, NX*NZ, OR NY*NZ DICTATED BY IPLANE; &
C      NDIM SETS VALUE OF DIMENSION OF GARRAY.
C     *USE FLD2DA(TITLE,GARRAY,NY,NX) TO PRINT ANY ARRAY DIMENSIONED
C      GARRAY(NY,NX); SET 'TITLE' TO REQUIRED NAME ( 4 HOLLERITH
C      CHARACTERS ONLY).
C     *USE FLD3DA(TITLE,GARRAY,NX,NY,NZ,IPLANE,ILOC) TO PRINT ANY
C      ARRAY DIMENSIONED GARRAY(NX,NY,NZ) IN PLANE SPECIFIED BY
C      'IPLANE' & 'ILOC' AS FOR CONTUR ABOVE; SET 'TITLE' AS FOR
C      FLD2DA.
C      VARIABLE NAMES FOR USE IN GROUND:
       COMMON/TYPE/CELL,EAST,WEST,NORTH,SOUTH,HIGH,LOW,VOLUME,WALL
       COMMON/VAR/P1,PP,U1,U2,V1,V2,W1,W2,R1,R2,RS,
      &KE,EP,H1,H2,H3,C1,C2,C3,C4,RX,RY,RZ,S1,S2
       COMMON/VAROLD/P10,PP0,U10,U20,V10,V20,W10,W20,R10,R20,RS0,
      &KE0,EP0,H10,H20,H30,C10,C20,C30,C40,RX0,RY0,RZ0,S10,S20
       COMMON/VARLOW/P1L,PPL,U1L,U2L,V1L,V2L,W1L,W2L,R1L,R2L,RSL,
      &KEL,EPL,H1L,H2L,H3L,C1L,C2L,C3L,C4L,RXL,RYL,RZL,S1L,S2L
       COMMON/VARHI/P1H,PPH,U1H,U2H,V1H,V2H,W1H,W2H,R1H,R2H,RSH,
      &KEH,EPH,H1H,H2H,H3H,C1H,C2H,C3H,C4H,RXH,RYH,RZH,S1H,S2H
       COMMON/GMTRY/VOL,VOLO,AEAST,ANORTH,AHIGH,AEDX,ANDY,AHDZ
       COMMON/PROP/D1,D2,D1DP,D2DP,MU1,MU1LAM,EXCO,CFP,MDT,HST1,HST2
       COMMON/PRPOLD/D10,D20
       COMMON/PRPLOW/D1L,D2L,EXCOL
       COMMON/PRPHI/D1H,D2H,MU1H,EXCOH
       COMMON/VARNX/XG,XU,DXU,DXG
       COMMON/VARNY/YG,YV,DYV,DYG,R,RV
       COMMON/VARNZ/ZG,ZW1,DZW,DZG,WGRID
       COMMON/GDMSCI/XPLANE,YPLANE,ZPLANE,ITNO
       COMMON/GDMSCL/LSLAB,MSLAB,HSLAB,LAMMU
       DIMENSION GV1(5,1),GW1(5,1),GD1(5,1)
       DIMENSION GP1(5,1),GH1(5,1),GT1(5,1)
       REAL NORTH,LOW
       INTEGER    P1,PP,U1,U2,V1,V2,W1,W2,R1,R2,RS,
      &EP,H1,H2,H3,C1,C2,C3,C4,RX,RY,RZ,S1,S2
       INTEGER    P10,PP0,U10,U20,V10,V20,W10,W20,R10,R20,RS0,
      &EP0,H10,H20,H30,C10,C20,C30,C40,RX0,RY0,RZ0,S10,S20
       INTEGER    P1L,PPL,U1L,U2L,V1L,V2L,W1L,W2L,R1L,R2L,RSL,
      &EPL,H1L,H2L,H3L,C1L,C2L,C3L,C4L,RXL,RYL,RZL,S1L,S2L
       INTEGER    P1H,PPH,U1H,U2H,V1H,V2H,W1H,W2H,R1H,R2H,RSH,
      &EPH,H1H,H2H,H3H,C1H,C2H,C3H,C4H,RXH,RYH,RZH,S1H,S2H
       INTEGER VOL,VOLO,AEAST,ANORTH,AHIGH,AEDX,ANDY,AHDZ
       INTEGER D1,D1DP,D2,D2DP,EXCO,CFP,HST1,HST2
       INTEGER D10,D20,D1L,D2L,EXCOL,D1H,D2H,EXCOH
       INTEGER XG,XU,DXU,DXG,YG,YV,DYV,DYG,R,RV,ZG,ZW1,DZW,
```

```
      &DIG,WGRID
       INTEGER XPLANE,YPLANE,ZPLANE
       LOGICAL LSLAB,MSLAB,HSLAB,LAMMU,LSPDA
       EQUIVALENCE (H1,R1),(M2,R2)
C      SATLIT-EQUIVALENT IRUN:
       EQUIVALENCE (IRUN,INTGR(11))
CXXXXXXXXXXXXXXXXXXXXXXXXXXXXXXXXXXXXXXX STANDARD SECTION 1 ENDS.
CXXXXXXXXXXXXXXXXXXXXXXXXXXXXXXXXXXXXXXX USER SECTION 1 STARTS:
C      ARRAYS ( DIMENSIONED NY,NX ) FOR USE WITH 'ADD':
       DIMENSION CVAR(5,1),VVAR(5,1),CM(5,1),VM(5,1),ZERO(5,1)
C      SPECIAL-DATA ARRAYS DIMENSIONED & DIMENSION VALUES SET HERE:
       DIMENSION LSPDA(1),ISPDA(1),RSPDA(1)
C      USER PLACES HIS VARIABLES, ARRAYS, EQUIVALENCES ETC. HERE.
       DATA NLSP,NISP,NRSP/1,1,1/
       DATA CVAR/5*0./,VVAR/5*0./,CM/5*0./,VM/5*0./,ZERO/5*0./
C      USER PLACES HIS DATA STATEMENTS HERE.
CXXXXXXXXXXXXXXXXXXXXXXXXXXXXXXXXXXXXXXX USER SECTION 1 ENDS.
CXXXXXXXXXXXXXXXXXXXXXXXXXXXXXXXXXXXXXXX STANDARD SECTION 2 STARTS:
C      PLEASE DO NOT ALTER, OR RE-SET, ANY OF THE REMAINING
C      STATEMENTS OF THIS SECTION.
           IF(SPDATA)
      &CALL RDSPC(IRN,INTGR(12),LSPDA,NLSP,ISPDA,NISP,RSPDA,NRSP)
       CALL GRDUTY(IRN,ICHAP,IZED,INDVAR)
           IF(ICHAP.EQ.-5) GO TO 10
           IF(ICHAP.LE.0.OR.ICHAP.GT.16) RETURN
       GO TO (100,200,300,400,500,600,700,800,900,1000,1100,1200,
      &1300,1400,1500,1600),ICHAP
       RETURN
CXXXXXXXXXXXXXXXXXXXXXXXXXXXXXXXXXXXXXXX STANDARD SECTION 2 ENDS.
CXXXXXXXXXXXXXXXXXXXXXXXXXXXXXXXXXXXXXXX USER SECTION 2 STARTS:
C-----------------------------------------------------------------
C      CHAPTER 0: MODIFY SATLIT DATA, AT START OF EACH IRN.
C-----------------------------------------------------------------
   10 CONTINUE
C          IF(.NOT.NAMLST) RETURN
C          IF(IRN.EQ.NRUN) DATFIL=.FALSE.
C---   READ SATLIT DATA NAMELIST HERE
C      CALL WRIT40(40HENTER NAMELIST DATA FOR GROUPS 1 TO 24  )
C      READ(20,G1G24)
C      CALL WRIT40(40HENTER NAMELIST DATA FOR GROUPS 25 TO 42 )
C      READ(20,G25G42)
       RETURN
C-----------------------------------------------------------------
C      CHAPTER 1: CALLED AT THE START OF EACH TIME STEP.
C      SET 'DT' HERE WHEN TLAST SET NEGATIVE IN BLOCK DATA.
C      'ATIME + DT' GIVES THE END TIME OF THE CURRENT TIME STEP.
C      NOT ACCESSED IF STEADY,OR PARABOLIC.
C-----------------------------------------------------------------
  100 CONTINUE
       RETURN
C-----------------------------------------------------------------
C      CHAPTER 2: CALLED AT THE START OF EACH SWEEP.
C-----------------------------------------------------------------
  200 CONTINUE
       RETURN
C-----------------------------------------------------------------
C      CHAPTER 3: CALLED AT THE START OF EACH SLAB;
C      NOT ACCESSED IF PARABOLIC, BUT 'STRIDE' IS.
C-----------------------------------------------------------------
  300 CONTINUE
       RETURN
C-----------------------------------------------------------------
C      CHAPTER 4: CALLED AT THE START OF EACH RE-CALCULATION OF
C      VARIABLES P1,...C4 AT CURRENT SLAB. ITNO= ITERATION NUMBER.
C-----------------------------------------------------------------
  400 CONTINUE
```

```
      RETURN
C-----------------------------------------------------------------
C     CHAPTER 5: GROUND CALLED WHEN SOURCE TERM IS COMPUTED.
C     INDVAR GIVES DEPENDENT VARIABLE IN QUESTION IE. U1,...C4.
C     TO ADD SOURCE TO DEPENDENT VARIABLE C1(SAY) FOR IX=IXF,IXL
C     AND IY=IYF,IYL INSERT STATEMENT:
C     IF(INDVAR.EQ.C1)
C    &CALL ADD(INDVAR,IXF,IXL,IYF,IYL,TYPE,CM,VM,CVAR,VVAR,NY,NX)
C     NOTES ON 'ADD':
C    *SOURCE= (CVAR(IY,IX)+AMAX1(0.0,MASFLO))*(VVAR(IY,IX)-PHI),
C     WHERE 'PHI' IS IN-CELL VALUE OF VARIABLE IN QUESTION.
C    *'MASFLO'= CM(IY,IX)*(VM(IY,IX)-P),
C     WHERE 'P' IS THE IN-CELL PRESSURE.
C    *FOR INDVAR= M1, OR =M2, SOURCE ADDED IS 'MASFLO' ONLY,
C     EXCEPT FOR ONEPHS=.F. & MASFLO < 0.0 (IE. OUTFLOW) WHEN
C     CM(IY,IX) IS MULTIPLIED BY R1*D1 (FOR M1) & R2*D2 (FOR M2).
C    *BOTH 'CVAR' & 'CM' ARE MUTLIPLIED BY CELL-GEOMETRY QUANTITY
C     DICTATED BY SETTING OF 'TYPE' (=CELL, EAST AREA,..VOLUME).
C    *TYPE-SPECIFIED AREAS ARE CALCULATED AS IF BLOCKAGE ABSENT,
C     BUT 'VOLUME' WITH ACCOUNT FOR ITS PRESENCE.
C    *FOR ALL SOLVED VARIABLES, INCLUDING M1 ( & M2 WHEN ONEPHS=F),
C     IF 'CM'> 0.0 CALL 'ADD'; FOR M1 & M2 ALTHOUGH 'CVAR' & 'VVAR'
C     HAVE NO SIGNIFICANCE THEY MUST BE ENTERED AS ARGUMENTS.
C    *'CVAR', 'VVAR', 'CM' & 'VM' MUST BE DIMENSIONED NY,NX.
C-----------------------------------------------------------------
  500 CONTINUE
C
C  ADD SINK TERMS TO REGION OF POROUS MEDIA
C
      IF(INDVAR .EQ. V1) GO TO 505
      IF(INDVAR .EQ. W1) GO TO 505
      RETURN
  505 CALL GET(V1,GV1,NY,NX)
      CALL GET(W1,GW1,NY,NX)
      CALL GET(D1,GD1,NY,NX)
      CAY = RE(21)
      DO 510 IY=1,NY
        GV = SQRT(GV1(IY,1)**2 + GW1(IY,1)**2)
        CM(IY,1) = 0.
        VM(IY,1) = 0.
        CVAR(IY,1) = CAY * ((GD1(IY,1)*GV)**.87)
        VVAR(IY,1) = 0.
  510 CONTINUE
      CALL ADD(INDVAR,1,NX,1,NY,VOLUME,CM,VM,CVAR,VVAR,NY,NX)
      IF(IZED .NE. 15) GO TO 530
      CAY2 = RE(22)
      DO 520 IY = 1,2
        GV = SQRT(GV1(IY,1)**2 + GW1(IY,1)**2)
        CVAR(IY,1) = 1.E-10
        VVAR(IY,1) = -CAY2 * GD1(IY,1) * (GV**2) * 1.E10
  520 CONTINUE
      CALL ADD(INDVAR,1,NX,1,2,HIGH,CM,VM,CVAR,VVAR,NY,NX)
      RETURN
  530 IF(IZED .NE. 1) RETURN
        GV = SQRT(GV1(1,1)**2 + GW1(1,1)**2)
        CVAR(1,1) = 1.E-10
        VVAR(1,1) = -CAY2 * GD1(1,1) * (GV**2) * 1.E10
      CALL ADD(INDVAR,1,1,1,1,LOW,CM,VM,CVAR,VVAR,NY,NX)
      RETURN
      RETURN
C-----------------------------------------------------------------
C     CHAPTER 6: CALLED AT THE END OF EACH VARIABLE-RECALCULATION
C     CYCLE COMMENCED AT CHAPTER 4. ITNO = ITERATION NUMBER.
C-----------------------------------------------------------------
  600 CONTINUE
      RETURN
```

```
C-----------------------------------------------------------------
C     CHAPTER 7: CALLED AT END OF EACH SLAB-WISE CALCULATION.
C-----------------------------------------------------------------
  700 CONTINUE
      RETURN
C-----------------------------------------------------------------
C     CHAPTER 8: CALLED AT THE END OF EACH SWEEP;
C     NOT ACCESSED IF PARABOLIC.
C-----------------------------------------------------------------
  800 CONTINUE
      RETURN
C-----------------------------------------------------------------
C     CHAPTER 9: CALLED AT THE END OF EACH TIME STEP;
C     NOT ACCESSED IF PARABOLIC.
C-----------------------------------------------------------------
  900 CONTINUE
      RETURN
C-----------------------------------------------------------------
C     CHAPTER 10: SET PHASE 1 DENSITY HERE WHEN IRHO1=-1 IN DATA.
C     SET CURRENT-Z 'SLAB' DENSITY, D1, IF MSLAB=.T.,
C     EG.  IF(MSLAB) CALL SET(D1,1,NX,1,NY,GD1,NY,NX).
C     SET NEXT LARGER-Z 'SLAB' DENSITY, D1H, IF MSLAB=.T. & PARAB=F
C     EG.  IF(MSLAB) CALL SET(D1H,1,NX,1,NY,GD1H,NY,NX).
C     SET D(LN(D1))/DP (IE. D1DP) FOR UNSTEADY FLOW,
C     EG.  IF(MSLAB) CALL SET(D1DP,1,NX,1,NY,GD1DP,NY,NX).
C-----------------------------------------------------------------
 1000 CONTINUE
C
C      CALCULATE DENSITY
C
      IF(MSLAB) GO TO 1004
      JP1 = P1H
      JH1 = H1H
      JD1 = D1H
      GO TO 1006
 1004 JP1 = P1
      JH1 = H1
      JD1 = D1
 1006 CALL GET(JP1,GP1,NY,NX)
      CALL GET(JH1,GH1,NY,NX)
      DO 1010 IX = 1,NX
      DO 1010 IY = 1,NY
      GT1(IY,IX) = ( 15.2446 - .40292 * GP1(IY,IX)*1.E-6 )
     $     + ( .068112 - 1.74E-5 * GP1(IY,IX)*1.E-6) * GH1(IY,IX)
C1010 GD1(IY,IX) = ((2.425E-4)*(GP1(IY,IX)))/((1.3)*(GT1(IY,IX)))
 1010 GD1(IY,IX) = ( (2.425E-4) * (GP1(IY,IX)) ) / (((-.508
     $ +1.1337E-2 * GT1(IY,IX) - 2.0867E-5 * GT1(IY,IX)**2)
     $ + (5.642E-4 - 3.762E-6 * GT1(IY,IX) + 6.68E-9 *GT1(IY,IX)**2)
     $ * (GP1(IY,IX) / 6894.76) + (-2.664E-8 + 2.0773E-10*GT1(IY,IX)
     $ -3.8933E-13 * GT1(IY,IX)**2) * (GP1(IY,IX) / 6894.76)**2)
     $ * (GT1(IY,IX)))
      CALL SET(JD1,1,NX,1,NY,GD1,NY,NX)
      RETURN
C-----------------------------------------------------------------
C     CHAPTER 11: SET PHASE 2 DENSITY HERE WHEN IRHO2=-1 IN DATA.
C     SET CURRENT-Z 'SLAB' DENSITY, D2, IF MSLAB=.T.,
C     EG.  IF(MSLAB) CALL SET(D2,1,NX,1,NY,GD2,NY,NX).
C     SET NEXT LARGER-Z 'SLAB' DENSITY, D2H, IF MSLAB=.T. & PARAB=F
C     EG.  IF(MSLAB) CALL SET(D2H,1,NX,1,NY,GD2H,NY,NX).
C     SET D(LN(D2))/DP FOR UNSTEADY FLOW,
C     EG.  IF(MSLAB) CALL SET(D2DP,1,NX,1,NY,GD2DP,NY,NX).
C-----------------------------------------------------------------
 1100 CONTINUE
      RETURN
C-----------------------------------------------------------------
C     CHAPTER 12: SET PHASE 1 VISCOSITY HERE WHEN IEMU1=-1 IN DATA.
```

```
C     SET CURRENT-Z 'SLAB' VISCOSITY (MU1), IF MSLAB=.T.,
C     EG.  IF(MSLAB) CALL SET(MU1,1,NX,1,NY,GVISC,NY,NX).
C     SET NEXT LARGER-Z 'SLAB' VISC. (MU1H), IF HSLAB=.T. & PARAB=F
C     EG.  IF(HSLAB) CALL SET(MU1H,1,NX,1,NY,GVSCH,NY,NX).
C
C     CHAPTER ALSO ACCESSED WHEN EMULAM=-1.0 IN DATA, SO THAT THE
C     LAMINAR VISCOSITY WHICH APPEARS IN WALL FUNCTIONS & IN THE
C     KE-EP TURBULENCE MODEL (IEMU1=2) MAY BE SET NON-CONSTANT.
C     SET CURRENT-Z 'SLAB' VALUE (MU1LAM) WHEN LAMMU=.T.,
C     EG.  IF(LAMMU) CALL SET(MU1LAM,1,NX,1,NY,GVSCL,NY,NX).
C-----------------------------------------------------------------
 1200 CONTINUE
      RETURN
C-----------------------------------------------------------------
C     CHAPTER 13: SET EXCHANGE COEFFICIENT (E.C.) FOR VARIABLE
C     INDVAR WHEN SIGMA(INDVAR)=-1.0 IN DATA.
C     SET CURRENT-Z 'SLAB' E.C. (EXCO) IF MSLAB=.T.,
C     EG.  IF(MSLAB) CALL SET(EXCO,1,NX,1,NY,GEXCO,NY,NX).
C     SET NEXT SMALLER-Z 'SLAB' E.C. (EXCOL) IF LSLAB=.T.,
C     EG.  IF(LSLAB) CALL SET(EXCOL,1,NX,1,NY,GEXCOL,NY,NX).
C     SET NEXT LARGER-Z  'SLAB' E.C. (EXCOH) IF HSLAB=.T.,
C     EG.  IF(HSLAB) CALL SET(EXCOH,1,NX,1,NY,GEXCOH,NY,NX).
C     NOTE: FOR MSLAB, INDVAR=U1,..C4; FOR LSLAB, INDVAR=U1L,..C4L
C     & FOR HSLAB, INDVAR=U1H,..C4H. IF PARAB=.T. SET MSLAB ONLY.
C-----------------------------------------------------------------
 1300 CONTINUE
      RETURN
C-----------------------------------------------------------------
C     CHAPTER 14: SET INTER-PHASE FRICTION COEFFICIENT (CFP) HERE
C     WHEN ICFIP = -1 IN DATA; ITS UNITS = FORCE / (CELL * RELATIVE
C     SPEED OF PHASES).
C-----------------------------------------------------------------
 1400 CONTINUE
      RETURN
C-----------------------------------------------------------------
C     CHAPTER 15: SET INTER-PHASE MASS-TRANSFER RATE PER CELL (MDT)
C     HERE WHEN IMDOT = -1 IN DATA.
C-----------------------------------------------------------------
 1500 CONTINUE
      RETURN
C-----------------------------------------------------------------
C     CHAPTER 16: SET HERE PHASE 1 & 2 SATURATION ENTHALPIES
C     ( HST1 & HST2) WHEN IHSAT = -1 IN DATA.
C-----------------------------------------------------------------
 1600 CONTINUE
      RETURN
      END
C$DIRECTIVE**STRIDE
      SUBROUTINE STRIDE(IZSTEP,IGOTO,IRN)
C-----------------------------------------------------------------
C     USE THIS SUBROUTINE TO SPECIFY THE GEOMETRY
C     OF THE FORWARD STEP IN PARABOLIC CALCULATIONS.
C     IZSTEP IS THE CURRENT FORWARD STEP, & NZSTP IS THE LAST
C     FORWARD STEP (FOR PARAB=.T. EARTH SETS NZ=1 ).
C     THE COMMON VARIABLE 'ZWL' GIVES THE DISTANCE OF THE
C     PREVIOUS STEP FROM THE ORIGIN.
C-----------------------------------------------------------------
$INCLUDE 9,CMNGUSSI.FTN/G
$INCLUDE 9,GUSSEQUI.FTN/G
CXXXXXXXXXXXXXXXXXXXXXXXXXXXXXXXXXXXXXXXX STANDARD SECTION 1 STARTS:
C     SATLIT-EQUIVALENT IRUN:
      EQUIVALENCE (IRUN,INTGR(11))
CXXXXXXXXXXXXXXXXXXXXXXXXXXXXXXXXXXXXXXXX STANDARD SECTION 1 ENDS.
CXXXXXXXXXXXXXXXXXXXXXXXXXXXXXXXXXXXXXXXX USER SECTION 1 STARTS:
C     USER PLACES HIS VARIABLES, ARRAYS, EQUIVALENCES ETC. HERE.
C     USER PLACES HIS DATA STATEMENTS HERE.
```

```
CXXXXXXXXXXXXXXXXXXXXXXXXXXXXXXXXXXXXXXXX USER SECTION 1 ENDS.
CXXXXXXXXXXXXXXXXXXXXXXXXXXXXXXXXXXXXXXXX STANDARD SECTION 2 STARTS:
      GO TO (10,20,30,40,50,60),IGOTO
CXXXXXXXXXXXXXXXXXXXXXXXXXXXXXXXXXXXXXXXX STANDARD SECTION 2 ENDS.
CXXXXXXXXXXXXXXXXXXXXXXXXXXXXXXXXXXXXXXXX USER SECTION 2 STARTS:
C-----------------------------------------------------------------
C     SECTION 1: SET FORWARD STEP SIZE DZ FOR IZSTEP>1 WHEN
C     ZWLAST < 0. IN DATA.
C     AT IZSTEP=1 EARTH SETS DZ = ABS(ZWDIST(1)*ZWLAST)
C-----------------------------------------------------------------
   10 CONTINUE
C*****USER SETS DZ HERE...
      RETURN
C-----------------------------------------------------------------
C     SECTION 2: SET X-WIDTH (XULAST) OF GRID FOR IZSTEP > 1
C     WHEN XULAST < 0. IN DATA.
C     AT IZSTEP=1 EARTH SETS XULAST = ABS(XULAST)
C-----------------------------------------------------------------
   20 CONTINUE
C*****USER SETS XULAST HERE...
      RETURN
C-----------------------------------------------------------------
C     SECTION 3: SET Y-WIDTH (YVLAST) OF GRID FOR IZSTEP > 1
C     WHEN YVLAST < 0 IN DATA.
C     AT IZSTEP=1 EARTH SETS YVLAST = ABS(YVLAST)
C-----------------------------------------------------------------
   30 CONTINUE
C*****USER SETS YVLAST HERE...
      RETURN
C-----------------------------------------------------------------
C     SECTION 4: SET INNER RADIUS (RINNER) OF GRID FOR IZSTEP > 1
C     WHEN RINNER < 0 IN DATA.
C     AT IZSTEP=1 EARTH SETS RINNER = ABS(RINNER)
C-----------------------------------------------------------------
   40 CONTINUE
C*****USER SETS RINNER HERE...
      RETURN
C-----------------------------------------------------------------
C     SECTION 5: SET SLOPE (SNALFA) OF INNER EDGE OF GRID FOR
C     IZSTEP > 1  WHEN SNALFA> 1, & CARTES = .FALSE.
C     AT IZSTEP=1 EARTH SETS SNALFA = SNALFA-2.
C-----------------------------------------------------------------
   50 CONTINUE
C*****USER SETS SNALFA HERE...
      RETURN
C-----------------------------------------------------------------
C     SECTION 6: SET MEAN PRESSURE (PBAR) AT NEXT FORWARD STEP
C     WHEN PBAR < 0. IN DATA.
C     FOR UNCONFINED FLOWS WITH IMPRESSED NON-ZERO
C     PRESSURE GRADIENTS SET PBAR HERE; FOR CONFINED
C     FLOWS EARTH AUTOMATICALLY COMPUTES PRESSURE REQUIRED.
C-----------------------------------------------------------------
   60 CONTINUE
C*****USER SETS PBAR HERE...
      RETURN
      END
```

REFERENCES

1. Forbes, J.C., Blueprints for High Pressure H_2 Filter, NASA-MSFC, EH23-092, 093, 097, 098, 099, 101, 102, (1984).

2. McCarty, Robert D., "Hydrogen Technological Survey - Thermophysical Properties", NASA SP-3089, (1975).

3. Jones, D.P. and H. Krier, "Gas Flow Resistance Measurements Through Packed Beds at High Reynolds Numbers", Journal of Fluids Engineering, vol. 105, (June 1983).

4. Perry, R.H., C.H. Chilton and S.D. Kirkpatrick, editors, Perry's Chemical Engineers Handbook, 4th edition, McGraw-Hill Book Company, Inc. New York, (1963).

5. Gunton, M.C., H.I. Rosten, D.B. Spalding, and D.G. Tatchell, "PHOENICS: An Instruction Manual", CHAM Report TR/75, (1983).

N85-22241 D31

1984

NASA/ASEE SUMMER FACULTY RESEARCH FELLOWSHIP PROGRAM

MARSHALL SPACE FLIGHT CENTER
THE UNIVERSITY OF ALABAMA

THEORETICAL INTERPRETATION OF THERMAL ARREST DATA FROM DIFFERENTIAL THERMAL ANALYSIS MEASUREMENTS

Prepared By:	Jai-Ching Wang
Academic Rank:	Associate Professor
University and Department:	Alabama A&M University Department of Physics
NASA/MSFC:	
(Laboratory)	Space Science Laboratory
(Division)	Space Processing
(Branch)	Solid State Devices
MSFC Counterparts:	S. L. Lehoczky, F. R. Szofran
Date:	August 3, 1984
Contract No.:	NASA-NGT-01-002-099 The University of Alabama

ACKNOWLEDGEMENTS

I would like to express my sincere appreciation to Dr. S.L. Lehoczky and the NASA/ASEE Summer Faculty Program for providing me the opportunity to participate in this program. Special thanks goes to Drs. S.L. Lehoczky, F.R. Szofran and Mrs. E. Cothran for their valuable information and suggestions. Discussions with Dr. Larry Holland were very valuable and helpful. Appreciation goes to Ms. Shirley Buford for typing this report.

THEORETICAL INTERPRETATION OF THERMAL ARREST DATA FROM DIFFERENTIAL THERMAL ANALYSIS MEASUREMENTS

by

Jai-Ching Wang, Ph.D.
Associate Professor of Physics
Alabama A&M University
Normal, Alabama

ABSTRACT

A theory has been developed to interpretate the thermal arrest data of HgCdTe system from differential thermal analysis measurements. A non-linear regression program is used to model fit the data. The purpose is to obtain a set of parameters which will give the information about average radiation coefficient, latent heat of fussion, and specific heat of the HgCdTe system at various compositions. The liquidus and solidus at various compositions can also be obtained. In this model we consider the heat radiation from the furnace, heat radiation from the system, heat capacity from both the system and the quartz tube and the heat of fussion of the system but neglect heat transfer through conduction and convection.

C-9

INTRODUCTION

Solid solution semiconducting alloy HgCdTe is a good infrared detecting material. Its material properties such as energy band gap depend on alloy composition Such alloys produced under unidirectional solidification technique show compositional segregation in both axial and radialy directions. The system has curved solid-liquid interface shape during solidification. Accurate informations about phase diagram, the specific heat, and latent heat of fussion of the system should help in understanding the cause of curved solid-liquid interface shape and the compositional segregations.

A theory has been developed to analyze the thermal arrest data from differental thermal analysis measurements obtained by S.L. Lehoczky and Frank Szofran. A non-linear regression program is then used to model fit the data to obtain a set of parameters which will give the values of heat radiation coefficient of the system, the specific heat, the latent heat of fussion, as well as the solidus temperature of the system at various compositions. The work has not been completed at this stage. In §2 the theory will be described. In §3 the detail calculations and a set of estimated parameters will be given. Finally we will give the discussion and recommendation.

OBJECTIVES

The objectives of this study is to obtain the information of the specific heat, the latent heat of fussion and the solidus temperatures of various $Hg_{1-x}Cd_xTe$ system. The method is to develop a theory to model fit the thermal arrest data from differental thermal analysis measurements by using a non-linear regression program.

THEORY

The following figure gives a rough set up of the experiment.

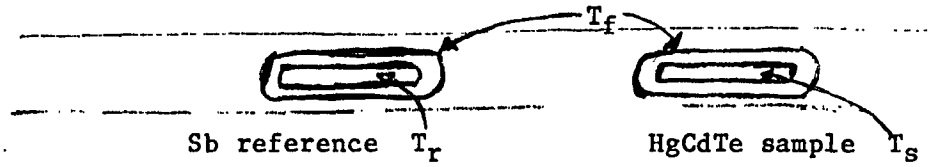

Considering radiation heat transfer and neglecting heat transfer by conducting and convecting. The heat balance at the outer wall of the sample ampule yields.

$$\int_{t_o}^{t} BT_f^4 dt = \int_{t_o}^{t} BT_s^4 dt + \int_{t_o}^{t} M_s C_s \frac{dt_s}{dt} dt + \int_{t_o}^{t} M_q C_q \frac{dT_s}{dt} dt + \int_{t_o}^{t} H \frac{dM_\ell}{dt} dt \qquad (1)$$

where

$$B = 2\pi\gamma_s \ell_s \frac{\sigma}{\frac{1}{\varepsilon_s} + \frac{A_s}{A_f}\left(\frac{1}{\varepsilon_f} - 1\right)} \simeq 2\pi\gamma_s \ell_s \sigma^{1}$$

with

γ_s = radius of sample
ℓ_s = length of sample
σ = Stefan-Boltzmann constant
ε_s, ε_f = emissivities of sample and furnace
A_s, A_f = radiating surface areas of the sample and the furnace respectively
M_s, M_q = masses of sample and quartz tube
C_s, C_q = specific heat of sample and quartz tube
t_o, t = beginning and ending times
T_f, T_s = temperature of furnace, sample
H= latent heat of fussion of sample
$\frac{dM_\ell}{dt}$ = time rate of change of the mass of sample in the melt.

The heat balance at the outer wall of the Sb reference ampule yields.

$$\int_{t_o}^{t} CT_f^4 dt = \int_{t_o}^{t} CT_r^4 dt + \int_{t_o}^{t} M_r C_r \frac{dT_r}{dt} dt + \int_{t_o}^{t} M_q C_q \frac{dT_r}{dt} dt \qquad (2)$$

where

$$C = 2\pi\gamma_r \ell_r \frac{\sigma}{\frac{1}{\varepsilon_r} + \frac{A_r}{A_f}\left(\frac{1}{\varepsilon_f} - 1\right)} \simeq 2\pi\gamma_r \ell_r \sigma$$

with

γ_r, ℓ_r = radius and length of Sb reference
ε_r, ε_f = emissivities of reference and furnace
A_r, A_f = radiating surface areas of the Sb reference and the furnace
M_r, M_q = masses of reference, quartz tube
C_r, C_q = specific heat of reference, quartz tube

Dividing eq (1) by B, eq (2) by C, then find the difference, we have

$$0 = \int_{t_o}^{t} (T_s^4 - T_r^4)\, dt + \int_{t_o}^{t} \frac{M_s C_s + M_q C_q}{B} \frac{dT_s}{dt}\, dt$$

$$- \int_{t_o}^{t} \frac{M_r C_r + M_q C_q}{C} \frac{dT_r}{dt}\, dt + \int_{t_o}^{t} \frac{H}{B} \frac{dM_\ell}{dt}\, dt \qquad (3)$$

Let $T_s = T_r - f(T_r)$
where $f(T_r)$ is the differential temperature between the sample and the reference then we have

$$\frac{dT_s}{dt} = \frac{dT_r}{dt} - \frac{df(T_r)}{dt} \qquad (4)$$

and using the approximation

$$T_s^4 - T_r^4 = \left|T_r - f(T_r)\right|^4 - T_r^4 \propto - 4T_r^3 f(T_r) \qquad (5)$$

substitute eq (4) and eq (5) into eq (3) we get

$$0 = -4\int_{t_o}^{t} f(T_r) T_r^3 dt + \int_{t_o}^{t} \frac{M_s C_s + M_q C_q}{B} \left(\frac{dT_r}{dt} - \frac{df(T_r)}{dt} \right) dt$$

$$- \int_{t_o}^{t} \frac{M_r C_r + M_q C_q}{C} \frac{dT_r}{dt}\, dt + \int_{t_o}^{t} \frac{H}{B} \frac{dM_\ell}{dt}\, dt \qquad (6)$$

After rearranging terms, we have

$$\frac{M_s C_s + M_q C_q}{B} \int_{t_o}^{t} \frac{df(T_r)}{dt}\, dt = \int_{t_o}^{t} \left[\frac{M_s C_s + M_q C_q}{B} - \frac{M_r C_r + M_q C_q}{C} \right] \frac{dT_r}{dt}\, dt$$

$$+ \int_{t_o}^{t} \frac{H}{B} \frac{dM_\ell}{dt}\, dt - 4 \int_{t_o}^{t} f(T_r) T_r^3 dt \qquad (7)$$

Assume at $t = t_o$ $\quad T_r = T_o$ solidus temperature
$t = t$ $\quad Tr = t_r$
Let $\frac{dT_r}{dt} = R$ reference and furnace heating up rate

then

$$\frac{d}{dt} = \frac{d}{dT_r} \frac{dT_r}{dt} = R \frac{d}{dT_r}$$

$$dt = \frac{dt}{dT_r} dT_r = \frac{1}{R} dT_r$$

substitute the above into eq (7), after dividing the equation by $(M_s C_s + M_q C_q)/B$ and carry out integrations. We get

$$f(T_r) = f(T_o) + \left[\frac{B(M_r C_r + M_q C_q)}{C(M_s C_s + M_q C_q)} - 1\right](T_o - T_r) + \frac{H}{M_s C_s + M_q C_q}\left[M_\ell(T_r) - M_\ell(T_o)\right] - \frac{4B}{R(M_s C_s + M_q C_q}\int_{T_o}^{T_r} f(T_r) T_r^3 dT_r \tag{8}$$

Here we have assumed that it is temperature dependent. Noting that $M(T_o) = 0$ and writing $M(T) = M_s M(T)$ that is from here on $M(T)$ would represent the percentage of the melt and let

$$P = \frac{B(M_r C_r + M_q C_q)}{C(M_s C_s + M_q C_q)} - 1 \ , \quad F = \frac{HM_s}{M_s C_s + M_q C_q}$$
$$K = \frac{4B}{R(M_s C_s + M_q C_q)} \ , \quad T = T_r \tag{9}$$

We can rewrite eq (8) as

$$f(T) = f(T_o) - P(T - T_o) + F\, M_\ell(T) - K\int_{T_o}^{T} f(T)\, T^3 dT \tag{10}$$

Let

$$g(T) = f(T_o) - P(T - T_o) + F\, M_\ell(T) \tag{11}$$

$$A = \int_{T_o}^{T} f(T) T^3 dT \tag{12}$$

then we have

$$f(T) = g(T) - KA \tag{13}$$

We may approximate A as following

$$A = \int_{T_o}^{T} f(T) T^3 dT$$
$$= \int_{T_o}^{T} [g(T) - KA]\, T^3 dT$$
$$= \int_{T_o}^{T} g(T) T^3 dT - K\int_{T_o}^{T} AT^3 dT \tag{14}$$

$$A \simeq \int_{T_o}^{T} g(T) T^3 dT - \frac{KA}{4}(T^4 - T_o^4) \tag{15}$$

$$A = \frac{\int_{T_o}^{T} g(T)T^3dT}{1 + \frac{K}{A}(T^4-T_o^4)} \tag{16}$$

Substitute eq (12) to eq (16) into eq (13) we have

$$f(T) = f(T_o) - P(T-T_o) + FM_\ell(T) - \frac{\int_{T_o}^{T} g(T)T^3dT}{1 + \frac{K}{4}(T^4-T_o^4)} \tag{17}$$

$\int_{T_o}^{T} g(T)T^3dT$ can be calculated as

$$\begin{aligned}\int_{T_o}^{T} g(T)T^3dT &= \int_{T_o}^{T} \left[f(T_o) - P(T-T_o) + FM_\ell(T)\right]T^3dT \\ &= \frac{f(T_o)}{4}(T^4-T_o^4) + \frac{PT_o}{4}(T^4-T_o^4) - \frac{P}{5}(T^5-T_o^5) \\ &\quad + \frac{F}{8}\,\mathrm{Imt3}\end{aligned} \tag{18}$$

where Imt3 is approximated as

$$\begin{aligned}\mathrm{Imt3} &= \int_{T_o}^{T} M_\ell(T)T^3dT \\ &\approx \sum_i \left[M_\ell(T_{i+1}) + M_\ell(T_i)\right](T_{i+1}^4 - T_i^4)\end{aligned} \tag{19}$$

Let $D = 1 + \frac{K}{4}(T^4-T_o^4)$ (20)

we have

$$\begin{aligned}f(T) = f(T_o) &- P(T-T_o) + FM_\ell(T) \\ &-K\left[\frac{f(T_o) + PT_o}{4} - \frac{P}{5}(T^5-T_o^5) + \frac{F}{8}\,\mathrm{Imt3}\right]/D\end{aligned} \tag{21}$$

CALCULATION AND ESTIMATION OF PARAMETERS

There are 8 sets of experimental output of thermal arrest data from thermal differential analysis measurements each with composition x = 0.1, 0.2, 0.3, 0.4, 0.6, 0.7, 0.8 and 0.9 in the $Hg_{1-x}Cd_xTe$ system. A program "TJ84D2" was developed to convert these output to give the reference temperatures and differential temperatures. The data are stored in data file "DATAD2".

We have then used the expressions

$$x^S(T) = C_1 \mathrm{Sin}(\tfrac{\pi}{2}T^*) + C_2 \mathrm{Sin}(\tfrac{\pi}{2}T^{*\frac{1}{2}}) + C_3 \log_{10}(\frac{9T-5618^oC}{412^oC}) + C_4 T^{*\frac{1}{2}}$$

$$x^L(T) = D_1 T^* + D_2 T^{*2} + D_3 T^{*3} + D_4 T^{*4}$$

$$\text{with } T^* = (T-670^oC)/412^oC$$

which are given by S.L. Lehoczky and F. Szofran for the estimation of the solid composition $x^S(T)$ and liquid composition $x^L(T)$ at temperature T to calculate the percentage of melt at various temperature.

The constants Ci and Di are

i	Ci	Di
1	0.380857	0.607640
2	0.086277	0.077209
3	1.200139	0.696167
4	-0.66231	-0.381683

The percentage of melt is given by

$$M_\ell(T) = \frac{X^S(T) - C_o}{X^S(T) - X^L(T)}$$

where Co is the overall composition of the system. The results for the melt percentage at various temperature are stored in data file "DATAMP"

The integration $\int_{T_o}^{T} M_\ell(T)T^3\,dT$ is approximated by $\sum_1 \frac{1}{2}\left[M_\ell(T_{i+1})+M_\ell(T_i)\right]\frac{1}{4}\left[T_{i+1}^4 - T_i^4\right]$. The program used to perform this calculation is "MPIMT3" and the results are stored in data file "DAIMT3".

Before we estimate the parameters

$$P = \frac{B(M_rC_r + M_qC_q)}{C(M_sC_s + M_qC_q)} - 1,\quad F = \frac{HM_s}{M_sC_s + M_qC_q},\quad K = \frac{4B}{R(M_sC_s + M_qC_q)} \quad \text{and } T_o$$

we have to estimate the relevant values of B, C, M_r, M_s. M_q, C_r, C_s, C_q, H and T.

The outer and inner diameter of the quartz ampules are 10mm and 5mm for both the sample and reference systems. The density of quartz is 2.202 g/cm^3. The mass of 1cm long of the quartz tube M_q is

$$M_q = \frac{\pi}{4}\left[\frac{(10)^2 - (5)^2}{100}\right] \times 1 \times 2.202 = 1.297\text{g}$$

The specific heat of quartz is

$C_q = 0.25 \times 4.186 = 1.0464$ J/gk

The density of reference is $\frac{121.75}{18.287} = 6.658$ g/cm$_3$

The mass of reference (Sb) M_r is

$$M_r = \frac{\pi}{4}(0.5)^2 \times 1 \times 6.658 = 1.307 \text{ g}$$

The specific heat of reference C_r is

$$C_r = \frac{3 \times 8.3143}{121.75} = 0.20487 \text{J/gk}$$

A program "MASMCT" was developed to estimate the density, the mass, and the specific heat of $Hg_{1-x}Cd_xTe$ systems at various composition x. The results are given in the following table.

Composition x in $Hg_{1-x}Cd_xTe$	density g/mole	mass g	specific heat J/gk
0.1	319.38	1.5295	.163833
0.2	320.56	1.4873	.168486
0.3	301.74	1.445	.17341
0.4	292.92	1.4028	.17863
0.6	275.28	1.3183	.19008
0.7	266.46	1.2761	.19637
0.8	257.64	1.2338	.20309
0.9	248.82	1.1916	.210293

Furnace and reference heating up rate

$= 2\text{K/min} = 1/30$ K/sec

$\sigma = 5.67 \times 10^{-12}$ J/cm^2 K^4 sec

$\varepsilon = 0.6$

$B = C = 2\pi\gamma\ell\varepsilon\sigma$

$= 2\pi \times 0.1 \times 1 \times 0.6 \times 5.67 \times 10^{-12}$

$= 1.069 \times 10^{-11}$ J/K^4 sec

The four parameters for sample 1 are estimated to be

$$P = \frac{B(M_r C_r + M_q C_q)}{C(M_s C_s + M_q C_q)} - 1$$

$$\simeq \frac{1.3087 \times 0.20487 + 1.297 \times 1.0465}{1.529 \times 0.1640 + 1.297 \times 1.0465} - 1$$

$$= 0.12954$$

$$F = \frac{HM_s}{M_s C_s + M_q C_q}$$

$$= \frac{H \times 1.5295}{1.5295 \times 0.1640 + 1.297 \times 1.0465}$$

The estimated value of H and F for various composition are

Composition x in $Hg_{1-x}Cd_xTe$	H	F
0.1	118.103	112.33
0.2	122.476	116.486
0.3	126.850	120.646
0.4	131.223	124.805
0.6	139.970	133.125
0.7	144.344	137.284
0.8	148.717	141.444
0.9	153.091	145.604

$$K = \frac{4B}{R(M_s C_s + M_q C_q)}$$

$$= \frac{4 \times 1.069 \times 10^{-11}}{\frac{1}{30}(1/5295 \times 0.1640 + 1.297 \times 1.0465}$$

$$\approx 7.977 \times 10^{-10}$$

The soludus temperature T_o at various composition are estimated to be

Composition x	Soludus Temperature T_o	Composition x	Soludus Temperature T_o
0.1	690	0.6	810
0.2	706	0.7	850
0.3	727	0.8	904
0.4	748	0.9	950

The data files "DATAD2", "DATAMP", DAIMT3" and the appropriate parameters are then read and/or input into a "NONLINEAR REGRESSION PROGRAM" which includes "JSTART" and JNONLI" to do model fitting. Till the end of this summer program we have not obtained a good fitting with physically reasonable parameters.

DISCUSSION

We feel that the theory is a resonable one. There may be some error in obtaining the data for melt percentage and the IMT3 integration. Although so far we have not obtained a good fitting with physically reasonable parameters; we do obtain many fittings with good structures. We strongly beleive that with closer to true value initial parameters and accurate data for "DATAMP" to DAIMT3" we should be able to obtain a good fitting. We have plans to do so.

REFERENCES

1. Ozisik, M. Necat, "Basic Heat Transfer", Mcgraw-Hill Book Company, New York, NY, p. 373-374.

2. Lehoczky, S.L. and Szofran, F.R., "Advanced Methods for Preparation and Characterization of Infrared Detector Materials", NASA8-33107, September 1980. The detail description of the experimental setup is in this report.

D32

1984

NASA/ASEE SUMMER FACULTY RESEARCH FELLOWSHIP PROGRAM

MARSHALL SPACE FLIGHT CENTER
THE UNIVERSITY OF ALABAMA

THE INTELLIGENT DATABASE MACHINE

PREPARED BY:	KENNETH E. YANCEY, PH.D.
ACADEMIC RANK:	PROFESSOR
UNIVERSITY AND DEPARTMENT:	LAMBUTH COLLEGE DEPT. OF MATHEMATICS AND COMPUTER SCIENCE
NASA/MSFC:	
LABORATORY:	INFORMATION & ELECTRONIC SYSTEMS
DIVISION:	COMPUTERS & COMMUNICATIONS
BRANCH:	MISSION COMPUTER SYSTEMS
NASA COUNTERPART:	DOUGLAS T. THOMAS
DATE:	JULY 30, 1984
CONTRACT NO.:	NASA-NGT-01-002-099 (THE UNIVERSITY OF ALABAMA)

ACKNOWLEDGEMENTS

The author wishes to express appreciation to the National Aeronautics and Space Administration for support received during this study. To Douglas Thomas, my thanks for quickly integrating me into the group and for allowing me to work at my own pace. Thanks go to Tish Hall, Dave Peters, and Barry Lee for contributing to my understanding of the MSFC data base management system. Thank you Lucy Thompson for typing this paper.

The Intelligent Database Machine

by

Kenneth E. Yancey
Professor of Physics and Computer Science
Lambuth College
Jackson, Tennessee

ABSTRACT

The object of this study is to determine if the database IDM 500 would better serve the needs of the MSFC data base management system than the database Oracle. Britton Lee provided a comparative study of the two and a performance study of the IDM. Oracle provided consultants. Within the limitations of the data the conclusions indicate what implementations would work best on which database. The choice is left to the database administrator.

INTRODUCTION AND OBJECTIVE

The Mission Computers group for whom this study was done is building a data base management system (DBMS) to support the orbital spacecraft. The DBMS will receive sensor data from the orbiting spacecraft, catalog the data, and store the data in an archive for future use by scientists and engineers. Figure 1 is a diagram of the DBMS.

The data will have a 512 bit header that describes the data and the source. It will be stored in the archive on optical disks (VAX 3 is host) and the header will be stored in the database. The database is presently Oracle with VAX 1 as host. See Figure 2 for the header configuration.

At the present time the headers are cataloged in Oracle. The object of this study is to see if the database IDM 500 made by Britton Lee would better serve the system as a catalog. One major limitation that now exists in the DBMS is the inability to catalog incoming sensor data at very high rates and make the data available to the user in near real time.

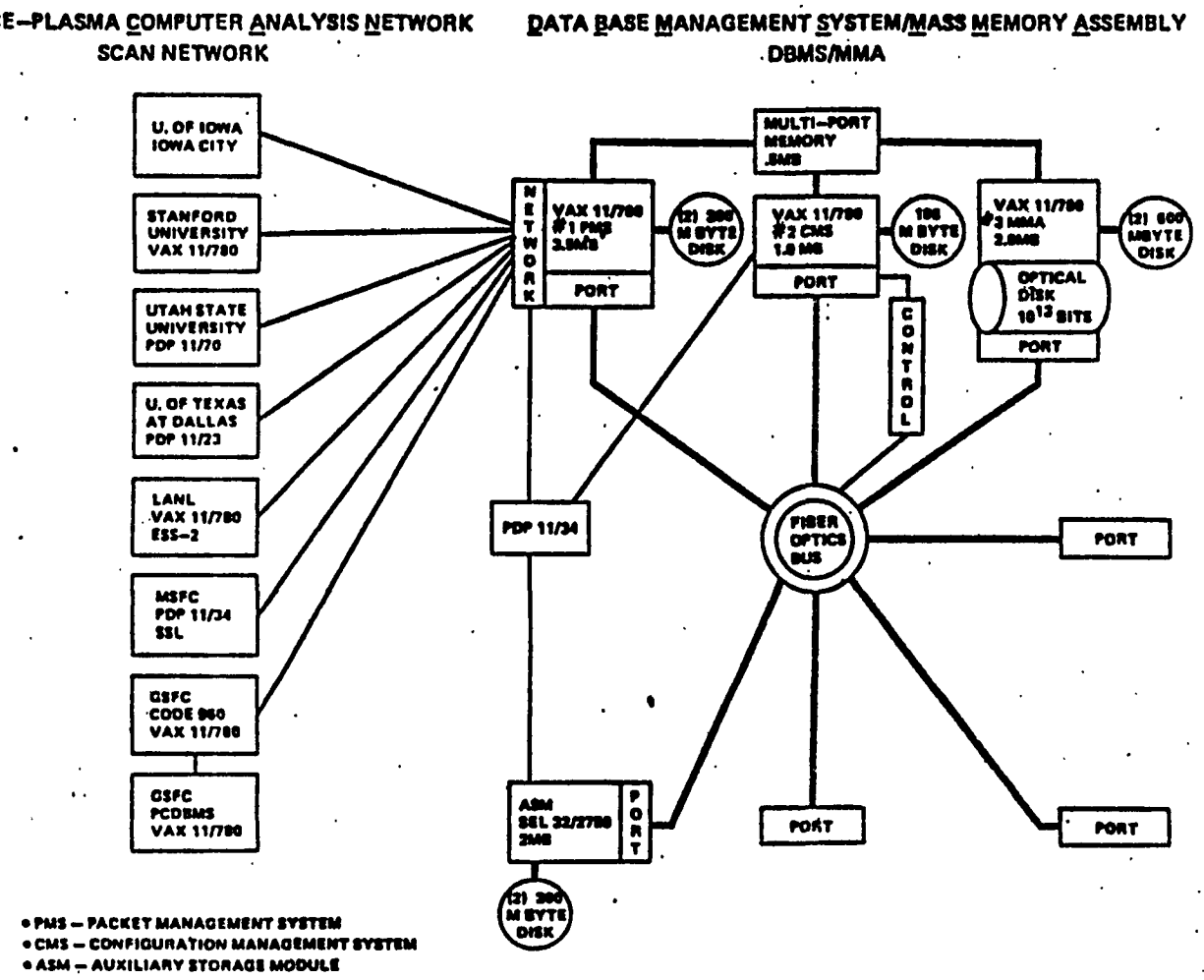

FIGURE 1

DBMS PACKET FORMAT

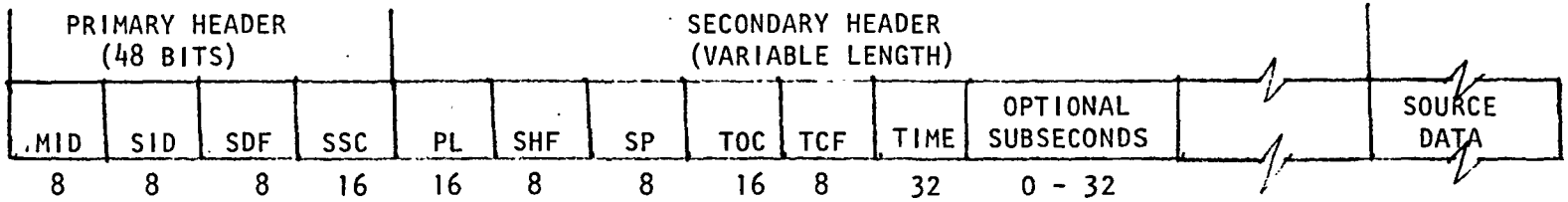

MID - MISSION ID

SID - SOURCE ID

SSC - SOURCE SEQUENCE CONTROL

BITS 15 - 14: SEGMENT FLAGS
BITS 13 - 0: SOURCE SEQUENCE COUNT

PL - PACKET LENGTH (NUMBER OF 16 BIT WORDS IN THE PACKET - 1. THIS LENGTH DOES NOT INCLUDE THE PRIMARY HEADER)

SDF - SOURCE DATA FORMAT. THIS FIELD IS USED TO IDENTIFY THE INTERNAL FORMAT OF THE DATA WHICH IS CONTAINED IN THE SOURCE DATA FIELD OF THE PACKET.

SHF - SECONDARY HEADER FORMAT. THIS FIELD SPECIFIES BY WAY OF AN EXTERNAL LOOK-UP PROCEDURE THE FORMAT AND LENGTH OF THE SECONDARY HEADER.

SP - SPARE FIELD

TOC - TABLE OF CONTENTS. THIS FIELD IS USED BY IAS AS A SERIES OF 1-BIT FLAGS TO INDICATE THE EXISTENCE OF, OR CHANGE IN, THE 16 PARAMETERS OF THE SECONDARY HEADER FOLLOWING THE TIME FIELD. IN USER GENERATED PACKETS, THIS FIELD MAY BE USED FOR OTHER PURPOSES.

FIGURE 2
XXXII-3

INTRODUCTION TO THE IDM

The cost of the IDM 500/1 is $69,500 while the cost of the IDM 500/2 (includes database accelerator) is $99,500. The software drives for VAX/VMS is $15,000. This includes the IDM-host interface, the library for Fortran, and the database administration utilities. Installation is included.

For support the Digital Equipment Corporation does maintenance on the hardware and the disks. For a $2,400 subscription Britton Lee provides telephone assistance, new releases, and instructional classes for two people.

We begin with a survey of some Intelligent Database Machine (IDM) functions. These are not meant to go in depth. The transaction facilities guarantee integrity of the data. The term integrity refers to correctness or validity. To maintain integrity all UPDATES and INSERTS must be checked for form and range. Security involves ensuring that users have a permit to do what they are doing. Integrity involves ensuring the correctness of what users are doing. The security features eliminate unauthorized access to information. The Data Dictionary helps keep a record of what information is contained in the database. If one thinks of the headers stored in the database as a table with 4 columns, each header is a row. The Data Dictionary keeps a table of information about the header-table, automatically.

A user need not understand IDM in order to use it. A high-level query language called the Intelligent Database Language (IDL) makes it easy to access and update information. The query language SQL, used on Oracle, may also be used. More than one user can have access to the same data at the same time, even during updating. If a sequence of query language commands are being used to update, then BEGIN and END delimeters may be used so the sequence will be treated as one. The update does not appear to a second user until after the END delimeter.

The transaction log is used in recovery from both a soft crash like a power failure or a hard crash due to a magnetic head coming into contact with a disk. The Database Administration causes the IDM to automatically set checkpoints at regular intervals then the recovery begins from the first readable checkpoint on the log rather than the beginning of the transaction log.

There are three models of the Britton Lee database. The IDM 500/0 is for smaller jobs. The IDM/1 can handle 4000 users, 16 disk drives, with over 10 gigabytes capacity. IDM 500/2 includes the database accelerator. Britton Lee claims the accelerator improves overall performance by more than a factor of two and increases response time to some querries by more than a factor of ten. The basic IDM modular designs consists of five PC boards that plug into a central high-speed bus. Respectively these boards are a disk control

module, a memory module, a memory timing and control module, a database processor module, and a host interface module. This one function per board modular design allows for easier maintenance.

The IDM 500 models can expand to include eight host interface boards that support sixty-four host computers, four disk controllers to support 16 SMD disks of any capacity, one tape controller with eight tape drives, six megabytes of IDM memory, and the database accelerator board.

The user can get complete package systems from Britton Lee. These include the host interface, user software, date entry facilities, and application programmer facilities. The IDM is designed for PDP-11 users running UNIX and DEC VAX users running VMS or UNIX operating systems.

Communication between the host and the IDM will be discussed later in the paper. They communicate over an RS-232 serial interface or an IEEE-488 parallel interface. The serial interface has programmable baud rates up to 19,200. The parallel interface has a maximum data rate of 170K bytes per second. When there is a high rate of transactions between the IDM and hosts, separate parallel interfaces can be assigned to each host.

What does the Database Accelerator do for the IDM? It improves overall system performance and improves response time of the IDM to some querries by up to a factor of ten. The Database Accelerator is a very high speed ten MIPS processor designed especially to do relational database functions. When a request is made to IDM the accelerator can search a page of disk memory by the time the page is completely transferred from disk to IDM memory. Much of the time-consuming work is done by the accelerator under the direction of the Database Processor module. The IDM Disk Controller module moves data between IDM memory and disks. This module works with the accelerator to process data at the speed it is read on the disk. When new SMD disks with increased storage capacity become available, they will be accommodated by the IDM. Monitoring the system and performing remote diagnostics can be done through two RS232 ports. The maintenance port can be used by the Britton Lee Service Department to remotely talk to the IDM. The IDM power supply can provide DC power to complete a 'write' in the event of power failure. If the IDM finds that it can no longer function, it will report which board should be replaced.

Database consistency means that if two users access the database with commands that affect the same data, the result will appear as if only one user had been using the database at a time. For example, user 1 at terminal 1 might issue two commands to the database. If, in between these commands, a record user from terminal 2 issue a command to change the data, the user 1 says he sees an inconsistency in the database.

The solution to this problem is for user 1 to surround his commands with transaction-delimeter commands begin transaction and end transaction. Then the database being accessed is locked; it can only be changed by user 1 until the transaction is ended or aborted.

A database or a 2K-byte block is read-locked while it is read. Multiple users can read the same data concurrently. After those who hold read-locks have completed their transactions, a user can change the data and it is write-locked. The IDM will delay a writer until all readers have finished, even if new readers begin. The Database Administration can set a pre-determined waiting time beyond which no new readers can lock out a writer.

A problem that can arise is deadlock. This occurs when two users get locked out each waiting for the other. If this occurs the IDM aborts one of the transactions.

Recovery requires the use of the IDM transaction log. Transaction here means any query language command or sequence of query language commands located between delimeters. The transaction log has a record of the changes that have been made in the database. It also knows the time the changes were made and the ID number of the user making the changes. Periodically the log should be written to another device such as another disk on the IDM or a tape. This dump empties the log and puts the record of transactions on the dump device.

The database LOAD command will take the previous database dump and bring the database to what is was when the dump was made. In the event of a disk crash the logs are LOADED and then the ROLL FORWARD command brings the database up to date. This procedure requires that the entire database be dumped periodically and that the transaction log be dumped more frequently. These dumps can be made to the database and the frequency of these dumps depends on how dynamic the database is. Dumps of the database takes the database offline but the logs can be dumped while the database is in full use. In summary to restore a database one will LOAD the last database dump, then LOAD and ROLL FORWARD all transaction log dumps since the full dump. An ad-hoc system allows the user to type in query language commands, such as IDL or SQL, and thereby manipulate the IDM database. In this case the host interface translates the statements while looking for errors, calls the host operating system to send these commands to IDM, and displays the results.

When a sequence of commands are repeated continually, pre-planned commands are convenient to use. The simpliest implementation of a pre-planned command is a subroutine library containing the commands already translated into the

IDM internal form. In this case a query language will be embedded in a high level programming language. An embedded query command is one in a program of another language such as Fortran.

If the query language IDL is embedded in Fortran, then the host system must have a pre-processor to read the Fortran program, find the embedded IDL statements, and send them to the IDL translator. The translator or parser produces Fortran calls to run-time subroutines that interface IDM and puts them in the place of the IDL commands. Then the Fortran program is compiled. It is even more effective to have the pre-processor/IDL translator create stored commands for the IDL commands. These are discussed next.

The IDM can store sequence of IDL commands within the IDM. Then when the commands are to be run, the host computer supplies a code for the commands and the necessary parameters to IDM. Not only is there less information to be transmitted but the commands are pre-processed to save time when executed. Stored commands save IDM execution time and host/IDM transmission time.

In order to embed IDL or SQL in Fortran or some other host language one must have a pre-processor that locates the IDL statements and translates them into the host language. The pre-processor can easily find the IDL commands if each line containing one begins with a special symbol such as a dollar sign, $. This makes it easier to modify the pre-processor so it will work with other languages such as Pascal or C. When the IDL commands are found they are then translated and checked for syntax errors. Each one is then sent to the IDM as a stored command. The IDM returns a 4-byte number or code that will cause the stored command to run or be executed. The IDL commands in the program are replaced with the code.

This process works when updating, say, the twelfth entry in the header, but is more complicated when data from the IDM is placed in variables or parameters defined in the program. The pre-processor can be obtained from Britton Lee.

Britton Lee has provided the results from some measurements they made on their IDM. One was on the time required to make simple retrieves depending on the number of users. An observation is that the rate at which the system does work (thruput) increases as the number of users increases. For example, the time for a retrieve with one user was 12.1 seconds and 7.167 seconds with two users. Figure 3 shows the linear relationship between time for a retrieve and the number of users.

Another performance test demonstrates the performance of the IDM doing retrieves on relations of different sizes. The

results differed drastically depending upon the access type use: lenear search or no index, clustered index, and non-clustered index. The latter two types use a B *-tree but the non-clustered does not sort the relation and is slower. The data is graphed in Figures 4 and 5. In all three cases the IDM works faster when the Database Accelerator (DAC) is used. Figures 3, 4, and 5 were provided by Britton Lee.

Appendix B: graphing the results

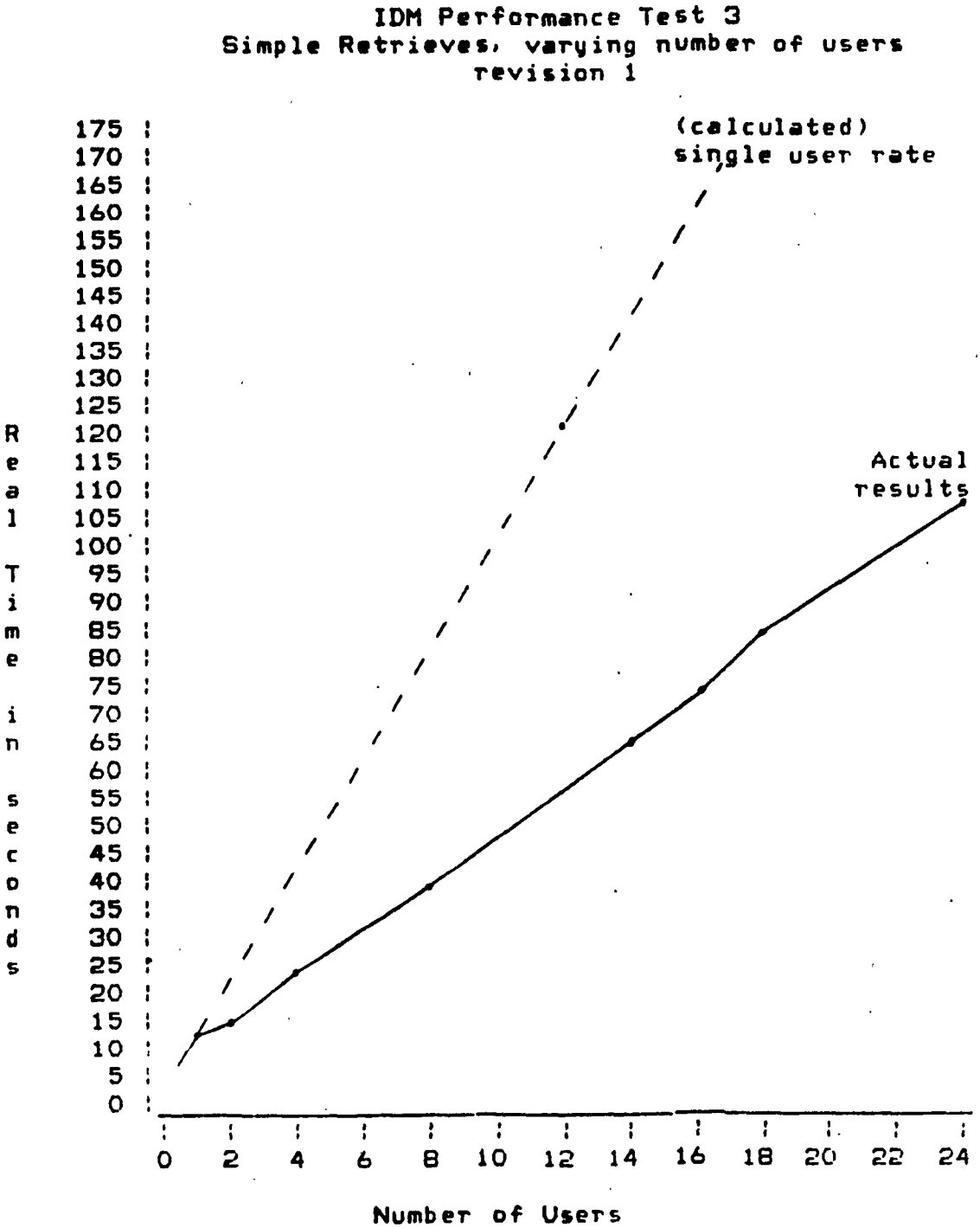

FIGURE 3

IDM Performance Test
Simple Retrieves, varying relation size
revision 0

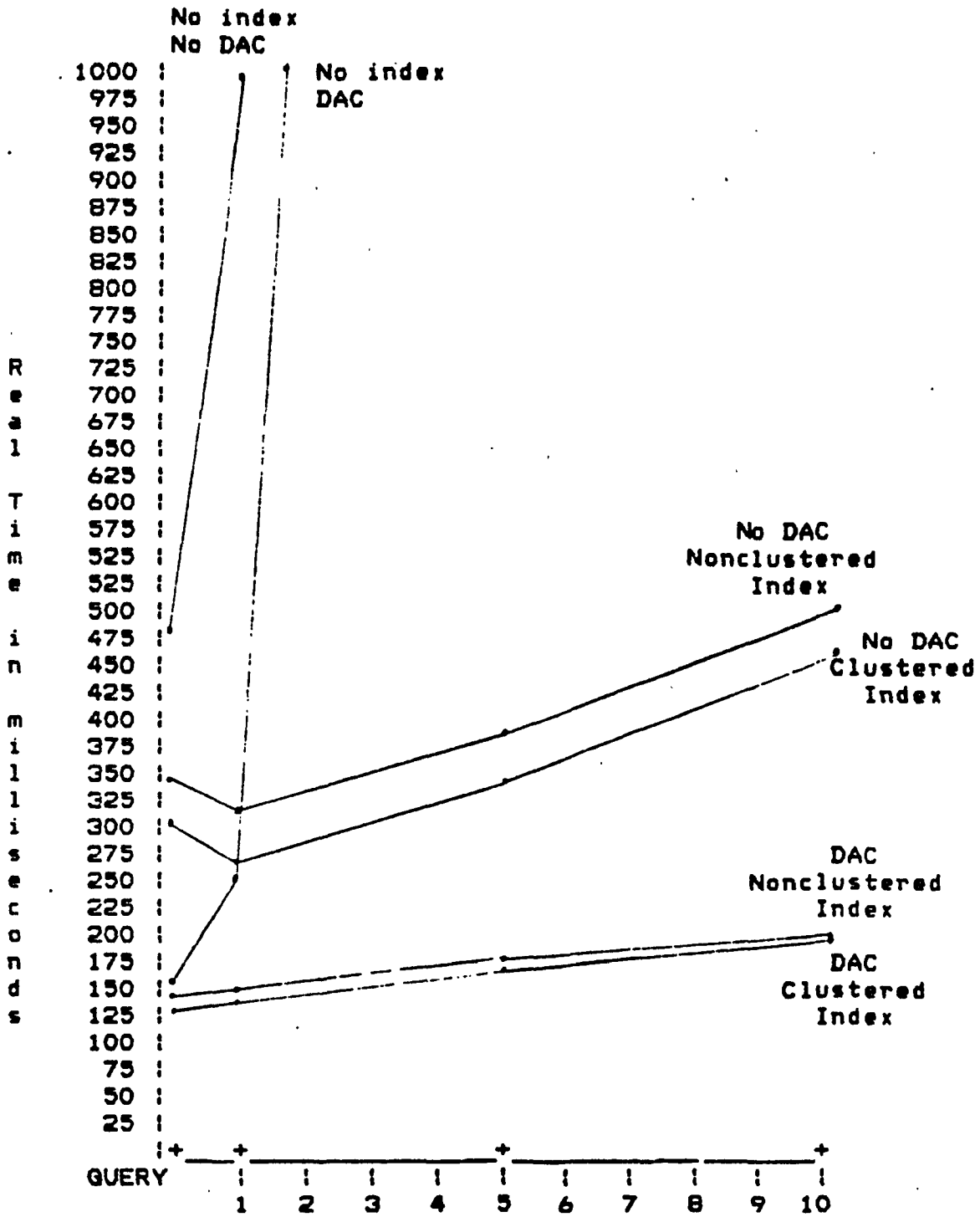

FIGURE 4
XXXII-10

Appendix A: graphing the results

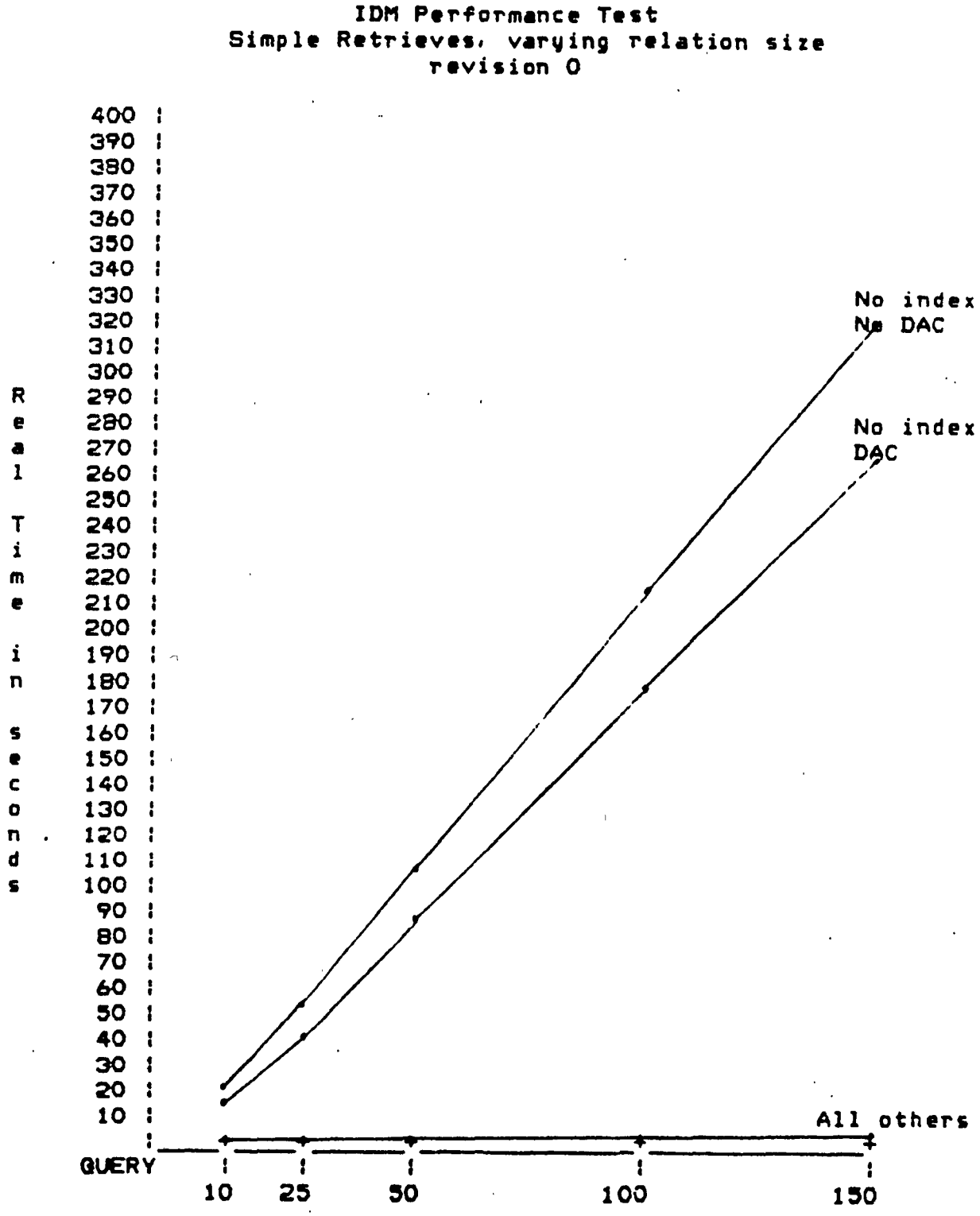

FIGURE 5

COMPARE ORACLE WITH IDM

Britton Lee has provided a benchmark to compare the database Oracle with the Intelligent Database Machine (IDM). These databases are both relational and operate under VAX/VMS. The IDM uses a language query called IDL while Oracle uses SQL. One must have some question about the tests since the database runs were made at two different sites on two different computers. The IDM tests were done by Britton Lee on a VAX 11/750 with 1 MByte of memory while the Oracle tests were done on a VAX 11/780 with 3 MBytes of memory. Texas Eastern Transmission Co. did the Oracle tests. Texas Eastern wrote the queries in SQL for their tests and Britton Lee hand-translated them into IDL. The queries were:

(1) This is an unqualified retrieve on a single relation. All columns in the relation were returned. The accelerator would not help much here.

(2) This is a qualified retrieve on a single relation. There are two qualifications. One of the columns has a clustered index. The other has no index.

(3) Unrestricted retrieve on a single relation. It sorts the returned records on an indexed field producing 700 rows.

(4) Unrestricted retrieve on a single relation. The records are sorted on a non-indexed field producing 700 rows.

(5) This is a join of two tables, a simple restriction, and a sort command. The query returns 1154 rows.

(6) This is a three table join, a restriction, and a sort command. The query returns 637 rows.

(7) This query only returns 8 wide rows. It is a three table join, two single restrictions, and a sort command.

(8) This query returns 188 rows. It is a four table join, two restrictions, and a sort command.

(9) This is a five table retrieve with one restriction. It returns 1104 rows.

See the comparative results of these nine queries on the two databases in Figures 6, 7, and 8. These figures were provided by Britton Lee in documentation sent to the author.

In all fairness it should be pointed out again that these tests were run on databases with different host computers. The Britton Lee Engineering Staff estimates that the throughput (rate at which system does work) for the Oracle host was about four times that of the IDM host. And the user memory of the Oracle host was approximately six times that of the IDM host.

The results seem to say that for all nine queries the IDM, with and without the database accelerator, responded faster than the Oracle. IDM with the database accelerator ran only slightly faster than the IDM without it except in query 9. One will probably never have a five table retrieve on the MSFC system like the one in query nine. With queries five through nine the Oracle responds significantly slower than the IDM. All of these but nine involve a join of two or more tables (relations) with a sort. The MSFC system may not use this kind of query in its operations. It depends on how the database is implemented. In queries three, four, five, six, and nine the accelerator improved performance of the IDM 500/2 over the IDM 500/1 by several percent. These involve the return of from 600 to 1100 rows (tuples). Probably, the MSFS will not need to return this many rows. It depends on how large the implementation is.

Oracle and Britton Lee were both asked by phone how many headers their respective databases could receive and store per second. Based on experiments run with 100 byte tuples, Oracle engineers estimate between 10 and 30. Britton Lee did not respond.

Documentation is an important consideration for a database. A good database with poor documentation is not worth much. Documentation for both Oracle and the IDM was excellent from the point of view of the user who wants to get the job done and doesn't care what the database is doing. Britton Lee, also, gives a good explanation of what the database is doing and how it interacts with the host computer.

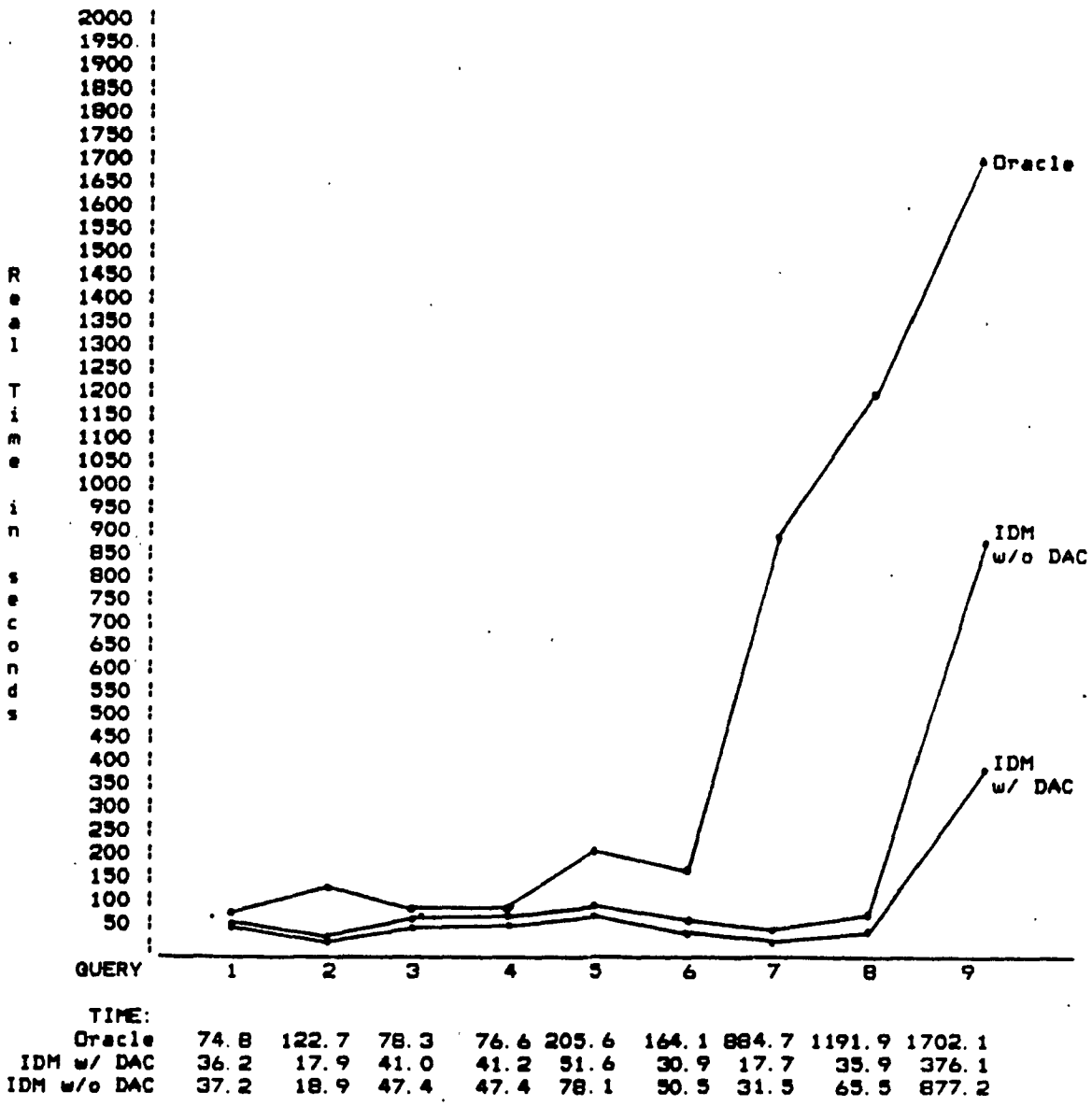

TIME:									
Oracle	74.8	122.7	78.3	76.6	205.6	164.1	884.7	1191.9	1702.1
IDM w/ DAC	36.2	17.9	41.0	41.2	51.6	30.9	17.7	35.9	376.1
IDM w/o DAC	37.2	18.9	47.4	47.4	78.1	50.5	31.5	65.5	877.2

FIGURE 6

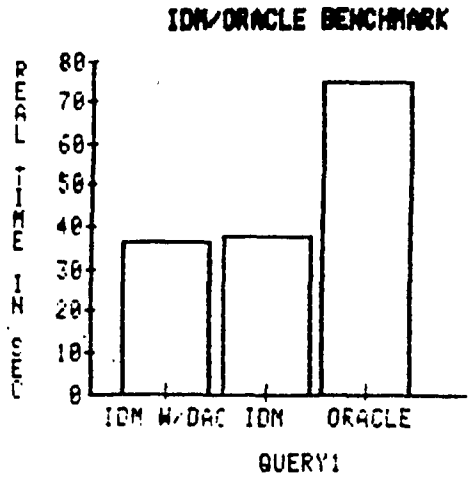

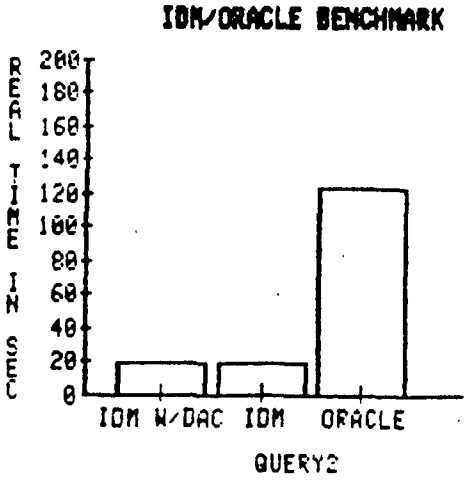

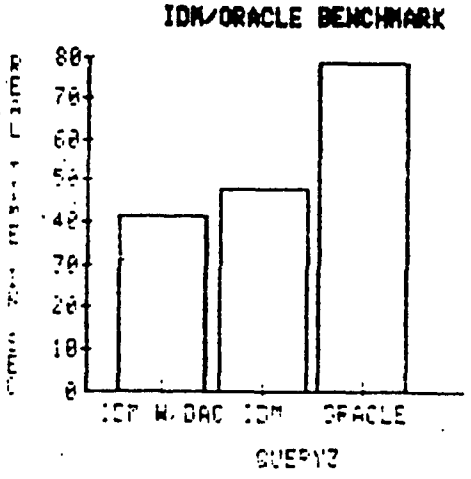

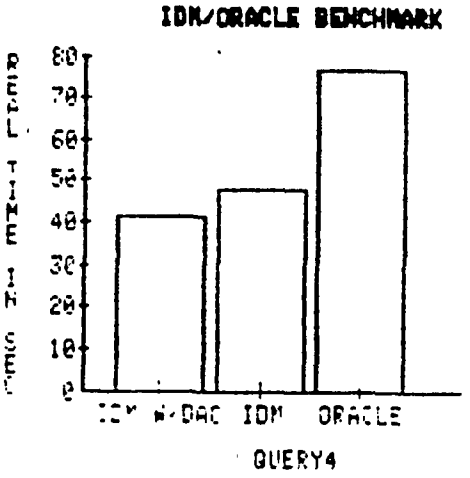

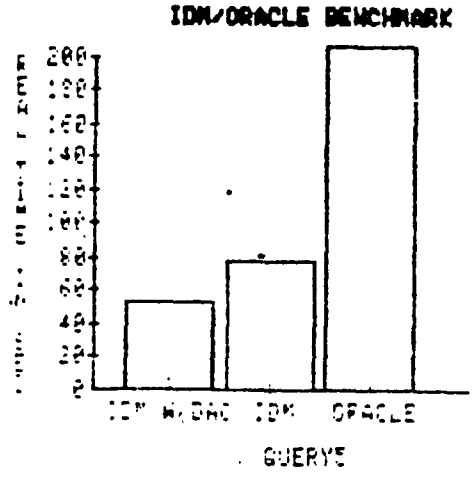

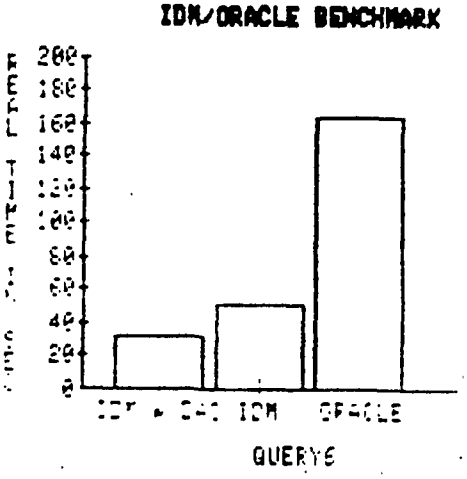

FIGURE 7

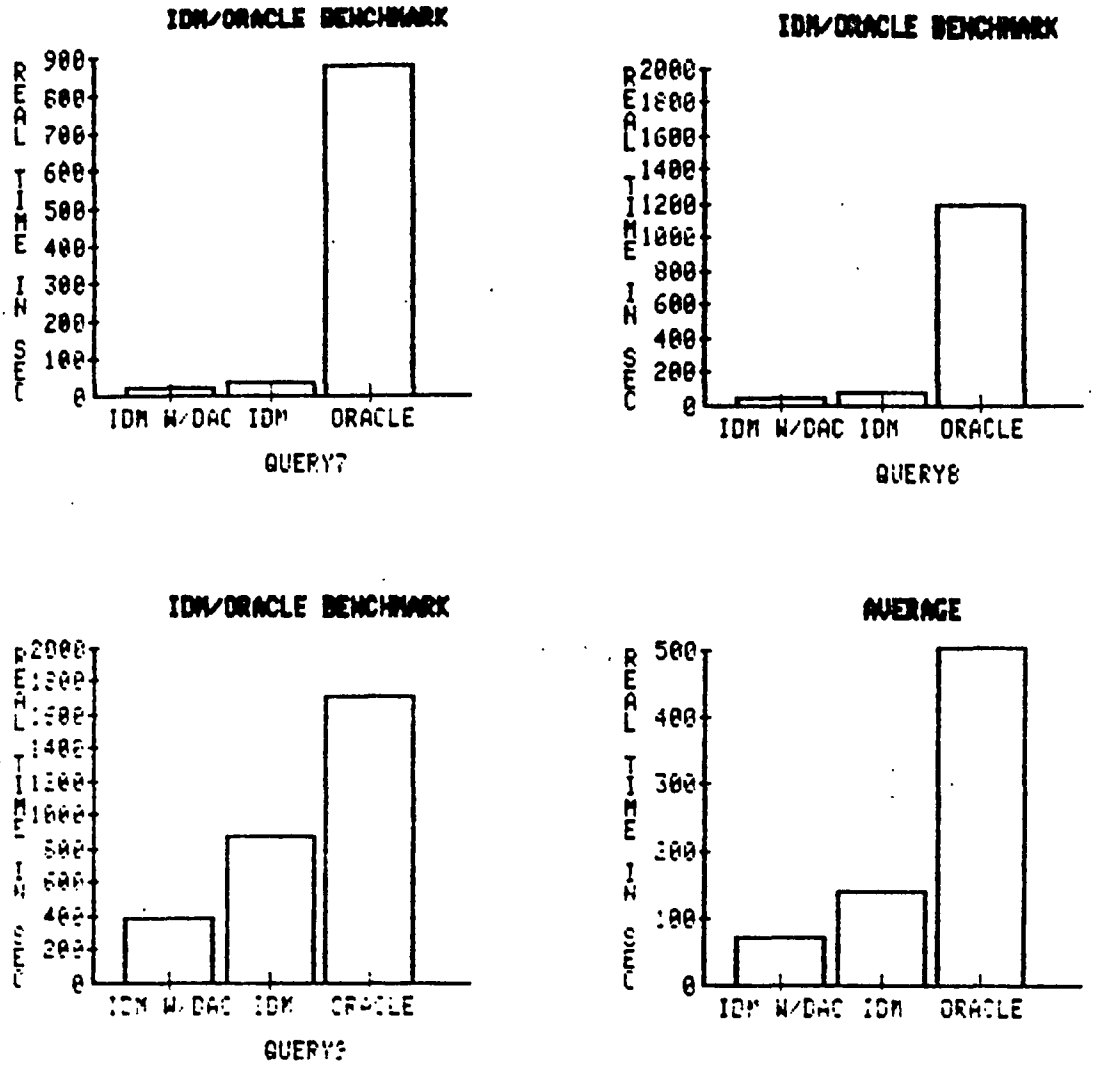

FIGURE 8

RECOMMENDATIONS AND CONCLUSION

The benchmark comparison of Oracle and the IDM was made using the same nine queries for both databases. The obvious observation is that the IDM was faster in all cases. While version 4.0 documentation for Oracle is not yet available at MSFC, information about version 4.0 indicates that it might reduce Oracle's response time by 1/2 to 1/5. This would make Oracle comparable to the IDM for simple queries like 1, 2, 3, and 4.

Queries five through nine involve more than one table and the IDM does a lot better than Oracle. There are at least two cases where this kind of retrieve might not be necessary for the MSFC database. In case 1 there would only be one big table with 4 to 12 columns and each row would be for a different source data packet. With only one table in the database, multiple table retrieves would not be used. In case 2 each user could have one or more tables with a row containing information about one packet of source data. If each table contained information about a particular type of data, there might not be any need to retrieve information from more than one table at a time.

If MSFC decides to use the IDM in its DBMS then the decision of whether or not to get an accelerator arises. The cost of the database accelerator is $30,000. The graphs in Figure 4 show that in retrieving a single row (tuple) the database accelerator (DAC) response is better than the IDM without it by a factor of two. Actually, as the size of the table goes up to 10,000 rows, it is faster by more than a factor of two. If the table or tables in the MSFC system will be large, then the database accellerator (DAC) will improve response time.

In Figures 7 and 8 one observes that the IDM with the database accelerator (IDM w/DAC) had a better response time than the plain IDM for queries 3, 4, 5, 6, and 9. These queries require that the database return between 248 and 1154 rows. This indicates that users requiring the returns of a large number of rows would benefit by having the database accelerator.

In an attempt to determine how fast the IDM will receive headers, look at the data for making simple appends. With the DAC, the IDM can make an append in between 116 and 277 milliseconds. This yields an answer of no better than 10 headers per second. The IDM works anywhere from 1.7 to 4.1 times faster with the DAC.

BIBLIOGRAPHY

C. J. Date. A Database Primer. Addison-Wesley: Reading, MA (1983)

C. J. Date. An Introduction to Database Systems. Addison-Wesley: Reading, MA (1982).

Relational Software Incorporated. Application Designers Guide-Version 2.33 (1983).

Relational Software Incorporated. Database Administrator's Guide (1983).

Britton Lee. IDM Product Description (1983).

Britton Lee. IDM Software Reference Manual Version 1.4 (1983).

Lindsay R. Peat. Pratical Guide to DBMS Selection. Walter de Gruyter: New York (1982).

J. W. Schmidt and M. L. Brodie. Relational Database Systems: Analysis and Comparison. Springer-Verlag: New York (1983).

Relational Software Incorporated. Terminal Users Guide (1983).

Britton Lee. A Benchmark: Oracle vs. The Intelligent Database Machine.

☆U.S. GOVERNMENT PRINTING OFFICE 1985—544—048/10098